(12)

AFWAL-TR-85-3069

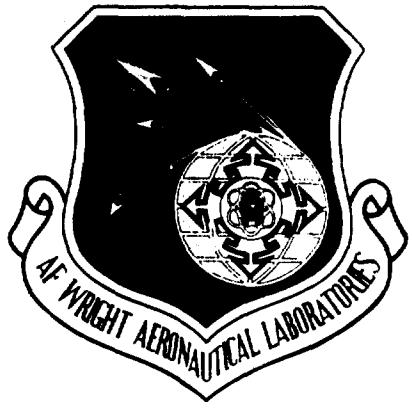

BUCKLING OF LAMINATED COMPOSITE PLATES AND SHELL PANELS

Arthur W. Leissa

The Ohio State University
Research Founation
1314 Kinnear Road
Columbus, Ohio 43212

June 1985

Final Report for the Period November 1980 - January 1985

Approved for public release; distribution unlimited.

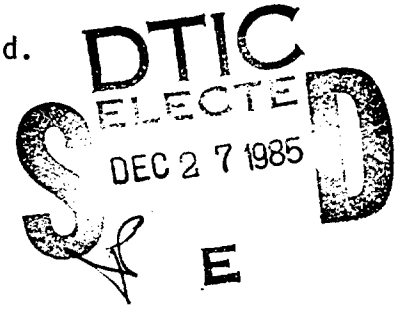

Prepared for

FLIGHT DYNAMICS LABORATORY
Air Force Wright Aeronautical Laboratories
Air Force Systems Command
Wright-Patterson Air Force Base, Ohio 45433

NOTICE

When Government drawings, specifications, or other data are used for any purpose other than in connection with a definitely related Government procurement operation, the United States Government thereby incurs no responsibility nor any obligation whatsoever; and the fact that the government may have formulated, furnished, or in any way supplied the said drawings, specifications, or other data, is not to be regarded by implication or otherwise as in any manner licensing the holder or any other person or corporation, or conveying any rights or permission to manufacture use, or sell any patented invention that may in any way be related thereto.

This report has been reviewed by the Office of Public Affairs (ASD/PA) and is releasable to the National Technical Information Service (NTIS). At NTIS, it will be available to the general public, including foreign nations.

This technical report has been reviewed and is approved for publication.

Narendra S. Khot

NARENDRA S. KHOT
Project Engineer
Design & Analysis Methods Group

Fred A. Picchioni

FREDERICK A. PICCHIONI, Lt Col, USAF
Chief, Analysis & Optimization Branch

FOR THE COMMANDER

James J. Olsen, Jr.

ROGER J. HEGSTROM, Col, USAF
Chief, Structures & Dynamics Div.

"If your address has changed, if you wish to be removed from our mailing list, or if the addressee is no longer employed by your organization please notify AFWAL/FIBRA, W-PAFB, OH 45433 to help us maintain a current mailing list".

Copies of this report should not be returned unless return is required by security considerations, contractual obligations, or notice on a specific document.

UNCLASSIFIED

SECURITY CLASSIFICATION OF THIS PAGE

AD-A162 723

REPORT DOCUMENTATION PAGE

1a. REPORT SECURITY CLASSIFICATION Unclassified	1b. RESTRICTIVE MARKINGS
2a. SECURITY CLASSIFICATION AUTHORITY	3. DISTRIBUTION/AVAILABILITY OF REPORT Approved for public release; distribution unlimited.
2b. DECLASSIFICATION/DOWNGRADING SCHEDULE	
4. PERFORMING ORGANIZATION REPORT NUMBER(S) 762513/713464	5. MONITORING ORGANIZATION REPORT NUMBER(S) AFWAL-TR-85-3069
6a. NAME OF PERFORMING ORGANIZATION The Ohio State University Sponsored Programs Adm. — 6b. OFFICE SYMBOL (If applicable)	7a. NAME OF MONITORING ORGANIZATION Flight Dynamics Laboratory (AFWAL/FIBRA)
6c. ADDRESS (City, State and ZIP Code) 1314 Kinnear Road Columbus, Ohio 43212	7b. ADDRESS (City, State and ZIP Code) Wright-Patterson AFB OH 45433-6553
8a. NAME OF FUNDING/SPONSORING ORGANIZATION — 8b. OFFICE SYMBOL (If applicable)	9. PROCUREMENT INSTRUMENT IDENTIFICATION NUMBER F33615-81-K-3203
8c. ADDRESS (City, State and ZIP Code)	10. SOURCE OF FUNDING NOS. PROGRAM ELEMENT NO.: 61102F — PROJECT NO.: 2307 — TASK NO.: N1 — WORK UNIT NO.: 15
11. TITLE (Include Security Classification) *	
12. PERSONAL AUTHOR(S) Arthur W. Leissa	
13a. TYPE OF REPORT Final	13b. TIME COVERED FROM 11/20/80 TO 1/20/85 — 14. DATE OF REPORT (Yr., Mo., Day) June 1985 — 15. PAGE COUNT 454
16. SUPPLEMENTARY NOTATION	

17. COSATI CODES		
FIELD	GROUP	SUB. GR.
11	04	

18. SUBJECT TERMS (Continue on reverse if necessary and identify by block number)
buckling, vibrations, instability, plates, shells, panels, composite materials

19. ABSTRACT (Continue on reverse if necessary and identify by block number)

* BUCKLING OF LAMINATED COMPOSITE PLATES AND SHELL PANELS

This work summarizes the technical literature dealing with buckling and post-buckling behavior of laminated composite plates and shell panels. Emphasis is given to modern materials used in the aerospace industry having fiber-matrix constituents (e.g., glass-epoxy, boron-epoxy, graphite-epoxy, boron-aluminum), but other applications are also considered (e.g., plywood, paperboard). Geometric configurations taken up are either flat (plates) or cylindrically curved (shells), and have rectangular planform. All possible types of loading conditions and edge constraint conditions are considered. Both symmetrically and unsymmetrically laminated configurations are included, with symmetrical laminates represented by orthotropic or anisotropic plate or shell theory.

(continued)

20. DISTRIBUTION/AVAILABILITY OF ABSTRACT UNCLASSIFIED/UNLIMITED ☒ SAME AS RPT. ☐ OTIC USERS ☐	21. ABSTRACT SECURITY CLASSIFICATION UNCLASSIFIED
22a. NAME OF RESPONSIBLE INDIVIDUAL N. S. KHOT	22b. TELEPHONE NUMBER (Include Area Code) (513) 255-6992 — 22c. OFFICE SYMBOL AFWAL/FIBRA

DD FORM 1473, 83 APR — EDITION OF 1 JAN 73 IS OBSOLETE.

UNCLASSIFIED

SECURITY CLASSIFICATION OF THIS PAGE

Block 19 (Abstract) - Continued

Complicating effects dealt with include: internal holes, shear deformation, sandwich plates with soft cores, local instability, inelastic materials, hygrothermal effects and stiffeners. Approximately 400 references are used. Extension numerical results are presented in graphical and tabular form. Both theoretical and experimental results are summarized. Keywords: vibrations; unsymmetric laminates

FOREWORD

This final technical report was prepared by A. W. Leissa, Department of Engineering Mechanics, The Ohio State University, Columbus, Ohio, 43212 for the Flight Dynamics Laboratory, Air Force Wright Aeronautical Laboratories, Air Force Systems Command, Department of the Air Force, Wright-Patterson Air Force Base, Ohio 45433 under Contract No. F33615-81-K-3203, Project 2307, Work Unit 2307N115. The Air Force Program Monitor was Dr N. S. Khot, AFWAL/FIBRA.

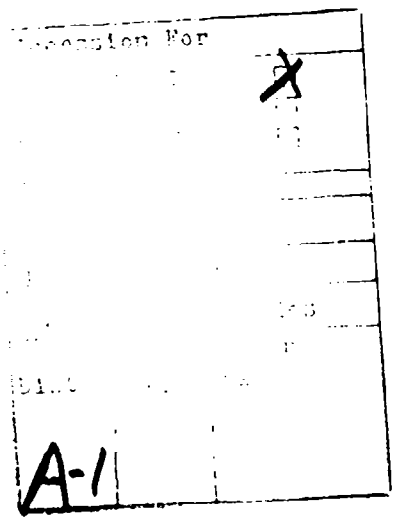

TABLE OF CONTENTS

LIST OF FIGURE TITLES

CHAPTER I. INTRODUCTION

Laminated composite plate and shell panels are becoming increasingly used in aerospace and other technical applications. The accurate knowledge of critical buckling loads, mode shapes and postbuckling behavior is essential for reliable and lightweight structural design.

The buckling of isotropic, homogeneous plate and shell panels is in itself a vast, complicated and somewhat disordered subject. Theoretical solutions to problems began nearly a century ago with the classical paper of Bryan [1], and have continued at a rapid rate since that time, yielding at least 2000 publications dealing with plate buckling in the technical literature. The best available textbooks dealing with the subject of plate buckling are those by Timoshenko and Gere [2] and by Volmir [3,4]. Other useful textbooks dealing generally with the concepts of buckling include ones by Ziegler [5], Simitses [6] and Brush and Almroth [7]. Handbooks summarizing substantial parts of the plate buckling literature and, particularly, numerical results for critical buckling loads, include Part I of the series by Gerard and Becker [8], the specialized monograph by Bulson [9], and the voluminous work of the Column Research Council of Japan [10]. In addition, a review paper by Johns [11] summarized references dealing with shear buckling, and one by the present writer [12] discussed more recent research.

A major factor responsible for the large amount of literature in plate buckling is the great variety of shapes, edge conditions and loading conditions which are considered. Thus, for example, one encounters references dealing with rectangular, circular, elliptical and parallelogram (skew) plates. The plates may have holes (cutouts) of various shapes. Simple edge conditions such as clamped, simply supported or free arise, as well as the more complicated ones of elastic

and discontinuous constraint. Point supports, either internal or along the edges, as well as line supports may be considered. Inplane loadings may be uniaxial, biaxial, uniform shear, or other, more complicated cases. The plates may have stiffeners, either along their edges or internally. Complicating effects such as an elastic foundation, variable thickness, shear deformation, and inplane heterogeneity may also be treated.

Laminated composite plates are made up of plies (layers), each ply being composed of straight, parallel fibers (e.g., glass, boron, graphite) embedded in and bonded together by a matrix material (e.g., epoxy resin). Each ply may be considered as a homogeneous, orthotropic material having a value of Young's modulus (E) considerably greater in the longitudinal direction than in the transverse directions. Adjacent plies will have longitudinal axes usually not parallel. Cross-ply laminated plates arise in the special case when the longitudinal axes of adjacent plies are perpendicular, whereas angle-ply laminates occur when adjacent layers are alternately oriented at angles of $+\theta$ and $-\theta$ with respect to the edges of the plate.

Equations governing the buckling of laminated composite plates are available in several textbooks [13-18], as well as in technical papers (e.g., [19]). A short derivation of these equations, partly for purposes of defining the notation used in this work, is given in the Appendix. From there it is seen that the complexity of the governing equations varies greatly, depending upon the stacking sequence of the plies.

For symmetrical laminates (i.e., when the plies and their orientations are identical on either side of the midplane of the plate) the governing equations are the same as those for a homogeneous, anisotropic plate. Such configurations are also called "balanced laminates" in the

literature, although this phrase is also used to indicate a stacking sequence which eliminates the bending-twisting coupling, as well as the bending-stretching coupling. At a typical point on the plate one may always determine a set of coordinate axes aligned with the principal directions for the material (i.e., directions of maximum and minimum stiffness, which are orthogonal to each other. With respect to these axes the material is orthotropic. However, if the buckling problem is stated and solved in terms of another set of more conveniently oriented axes (e.g., the edge directions for a rectangular plate), the differential equation of equilibrium for a buckling mode becomes more complicated, with bending-twisting coupling appearing by means of additional terms (see terms containing D_{16} and D_{26} in Equation A.23 in the Appendix). In this case the plate will be called "anisotropic" in the present work, in accordance with long tradition. When the principal axes of material orthotropy are aligned with the orthogonal axes of the problem, the plate will accordingly be called "orthotropic", and Equation A.24 governs. In the literature of laminated composite plate buckling one occasionally sees the term "specially orthotropic" applied to an orthotropic plate, and even "generally orthotropic" applied to an anisotropic plate. This terminology will not be used in the present work.

For an unsymmetrically laminated plate, coupling exists between bending and stretching of the midplane. This phenomenon was demonstrated in the theoretical paper by Reissner and Stavsky [20] in 1961. The coupling between bending and stretching is similar to that encountered in isotropic shell deformation problems, the order of the system of governing differential equations is similarly increased from four (for an anisotropic plate) to eight, the number of boundary conditions that must be specified is increased from two to four for each edge, and the buckling problems are correspondingly more difficult to solve.

Orthotropic plate buckling analysis apparently was first applied a half-century ago to deal with stiffened isotropic plates (e.g. [21-23]), and subsequently became extensively used to study plywood plates (cf. [24-26]). However, the publication rate of research results increased rapidly beginning two decades ago as fibrous composite panels were being to be analyzed for aircraft applications. Several literature surveys on the buckling of composite plates have been written [27-31], and related design manuals have been written (cf., [32]).

Plate buckling may be discussed in terms of a plot of inplane loading force (P) versus the transverse displacement (w) measured at a representative point on the plate. Classical buckling theory yields the bifurcation behavior depicted by branches I, II and III of the curves depicted in Figure 1.1. That is, with increasing P, the curve follows the ordinate (I) upwards, showing no displacement with increased load until a critical force (P_{cr}) is reached. At this bifurcation point the curve theoretically may continue up the ordinate (II), or may follow a buckling path, which is horizontal (III) for the linear idealization, but of increasing slope (IV) for a nonlinear (large displacement) analysis. The latter curve (IV) is also called a "postbuckling curve", for it depicts the behavior of the plate after the buckling load (P_{cr}) is reached. This behavior is very important for, typically, plates are able to carry loads far in excess of P_{cr} before they collapse. Finally, it must be noted that no plate is initially perfectly flat, and that if initial deviation from flatness exists (usually called a "geometric imperfection" or "imperfection", although other types of imperfections may also exist), the P-w curve of Figure 1.1 will follow a path similar to V. As the imperfection magnitude is decreased, curve V becomes increasingly kinked in the vicinity of P_{cr}. For this type of analysis, no clear buckling phenomenon may be defined.

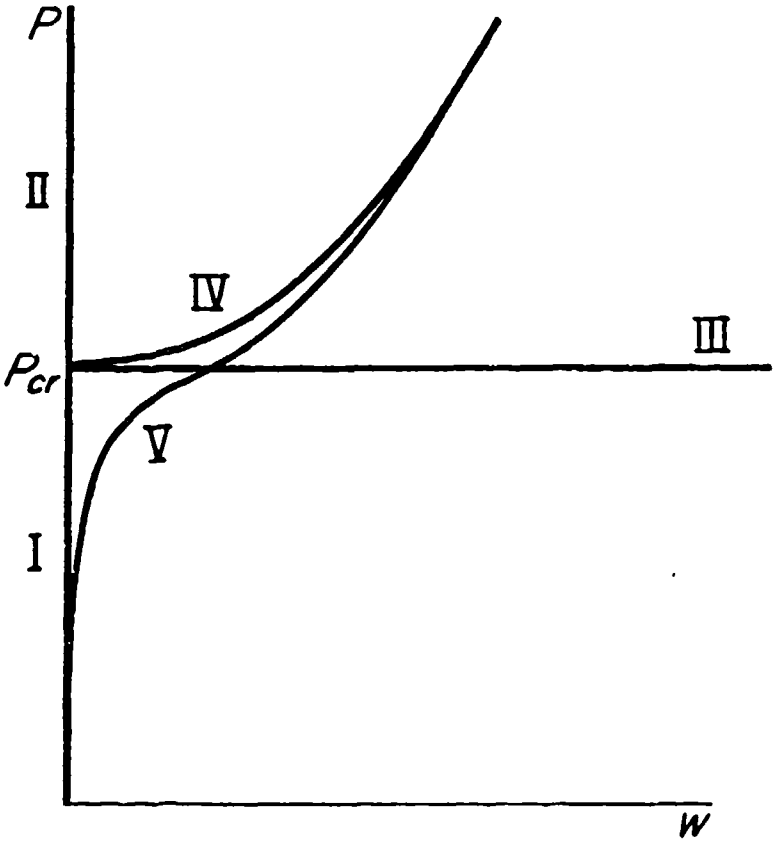

Figure 1.1. Representative curves of load versus transverse displacement.

The standard procedure for determining theoretical values of buckling loads is to solve a mathematical eigenvalue problem; that is, a problem governed by differential equations and boundary condi
of which are homogeneous (i.e., the independent variables do
plicitly appear in the equations). In a relatively few cases
be done exactly. In most cases approximate procedures such as the Ritz, Galerkin series (superposition), finite element or finite difference methods are used. The latter procedures, if properly used, will approach the exact solutions as closely as desired as the sufficient terms (or degrees of freedom) are retained in the solution, although the roots of very large determinants may be required.

Critical loads obtained by the procedures described above may be regarded as the proper values of inplane forces required to keep a plate in a position of neutral equilibrium in buckled mode shapes having infinitesimal amplitudes. The linear eigenvalue problem will typically yield more than a single buckling load for a given plate and loading. The lowest (i.e., critical) one is usually the only one sought, although higher ones may be of interest if they approach the lower ones as parameters are changed. Other ways of theoretically determining buckling loads are: (1) from the free vibration problem (finding values of natural frequencies which approach zero as inplane loadings are increased), and (2) from static or dynamic transverse loading solutions in the presence of inplane forces (transverse displacements approaching infinity, no matter how small the transverse loads).

Before the buckling eigenvalue problem is solved it is usually necessary to determine the initial state of inplane stress throughout the interior of the plate. For most buckling situations which are analyzed, this is a trivial step (e.g., uniform or linearly varying stress distributions). For others, it may require solving an anisotropic plane elasticity problem by approximate methods.

Chapters 2 through 7 of the present work are devoted to the linear, bifurcation buckling of laminated composite plates of rectangular shape, beginning with the most simple analysis of symmetrically laminated plates (Chapters 2 through 4) - problems characterized by classical, orthotropic plate theory. The case when all four edges are simply supported (SSSS) has received considerable attention and is therefore singled out for Chapter 2. The large amount of interest in this case is, no doubt, mostly due to the fact that exact, closed form solutions exist for uniform uniaxial and biaxial loading. Chapter 3 treats the other 5 sets of edge conditions existing when two opposite edges are simply supported; that is, SCSC, SCSS, SCSF, SSSF and SFSF, where C, S and F denote clamped, simply supported and free edges, respectively, and the edges are labeled in clockwise sequence around the boundary, beginning with the left edge. Thus, an SCSF plate is depicted in Figure 1.2. For such cases, as well as those when one or both of the other two edges are elastically supported, exact solutions for the buckling loads and mode shapes still exist for uniform uniaxial and biaxial loading; however, the eigenvalues (nondimensional buckling loads) are not given by explicit formulas, and must be evaluated as the roots of second or fourth order determinants.

The problems of Chapter 4 have no exact solutions. These comprise the remaining 15 cases of rectangular, orthotropic plates having "simple" boundary conditions (i.e., C, S or F), including the important CCCC case, as well as all other conceivable support conditions for orthotropic plates, such as elastic constraints, discontinuous boundary conditions and point supports. Chapter 5 generalizes the problem to the equivalent anisotropic plate representation. Although this class of problems is more general (requiring at least one additional parameter) than the orthotropic cases of the preceding three chapters, relatively little has been done with these configurations. This is, no doubt, partly because virtually no exact solutions exist, and solutions are relatively long and tedious, obtained by approxiamte methods.

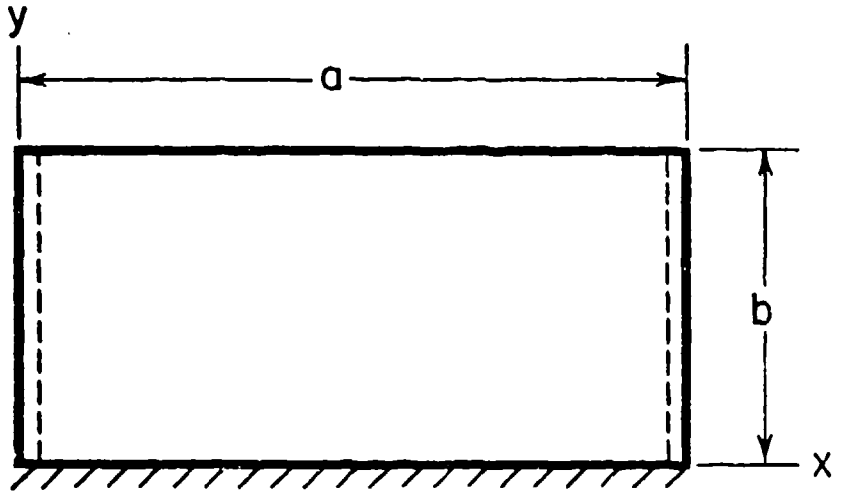

Figure 1.2. SCSF plate.

Unsymmetrically laminated plates are studied in Chapter 6. Some important progress has been made on these relatively complicated buckling problems, involving coupling between bending and midplane stretching during a buckling deformation. Chapter 7 takes up all other complicating effects encountered in linear, bifurcation buckling theory. Among the factors considered are: shear deformation, sandwich panels (e.g., fibrous composite face sheets with honeycomb cores), variable thickness, nonlinear stress-strain equations, inelastic material behavior (plastic or creep buckling), local instabilities (e.g., individual plies) and hygrothermal effects.

Chapter 8 deals with the postbuckling behavior of laminated composite plates, as well as the effects of initial imperfections, and a large number of references are found to relate to these problems. While the writer was tempted to separate these considerations into two, separate chapters, both deal with nonlinear analyses of a similar nature, the only essential difference being whether or not the imperfection amplitude is zero. Chapter 9 is a perfunctory attempt to deal with laminated plates having discrete stiffeners attached. Readers desiring additional detailed information will have to seek out those references of interest among the numerous ones listed.

Relatively little was found for the buckling of curved, composite panels. These are typically of cylindrical curvature, and may be analyzed by shell theory. What has been found is summarized in Chapter 10.

This summary is limited to composite plate and shell panels of rectangular planform. Although one can find a few references dealing with circular, elliptic and parallelogram (skew) plates having rectangular orthotropy, they are deemed of not sufficient interest to justify the

major broadening of the scope of this monograph which would be required. For similar reasons, problems having curvilinear orthotropy have been omitted, notably circular plates having polar orthotropy. It is possible that future design optimization will include the layout of fibers in curvilinear patterns with varying spacing (i.e., inplane heterogeneity) [33], and that curvilinear orthotropic plates of this type will require inclusion in some future summary.

Finally, although primary attention is given to theoretical results, particularly those available in nondimensional form, in this monograph, experimental results are also presented. The primary problems with all experimental results are: the care which went into the fabrication of the specimens, the successful accomplishment of the desired test (e.g., Were the clamped edges actually clamped ? Were the loads uniformly applied ?) and the definitive specification of all parameters affecting the problem. The writer has attempted to include considerable experimental results which appeared to be properly obtained and presented.

CHAPTER II. RECTANGULAR ORTHOTROPIC PLATES - ALL EDGES SIMPLY SUPPORTED

Consider first composite plates whose bifurcation buckling is governed by the differential equation (see Appendix)

$$D_{11}\frac{\partial^4 w}{\partial x^4} + 2(D_{12} + 2D_{66})\frac{\partial^4 w}{\partial x^2 \partial y^2} + D_{22}\frac{\partial^4 w}{\partial y^4} = h\left(\sigma_x \frac{\partial^2 w}{\partial x^2} + 2\tau_{xy}\frac{\partial^2 w}{\partial x \partial y} + \sigma_y \frac{\partial^2 w}{\partial y^2}\right) \tag{2.1}$$

This is the classical equation for the buckling of a plate having rectangular orthotropy. It is applicable to parallel-fiber composite plates in the following cases:

(1) A single layer.
(2) A cross-ply plate having multiple layers which are symmetrically arranged with respect to the midplane of the plate (i.e., a symmetrical laminate; see Appendix).

In the present chapter (as well as in Chapters III and IV) it is assumed that the axes of material orthotropy are parallel to the edges of the rectangular plate. In the composite plates literature this orientation is sometimes called "specially orthotropic".

The potential energy of an orthotropic plate undergoing buckling is given by

$$V = V_B + V_L \tag{2.2}$$

where V_B is the internal strain energy due to bending stored within the plate, given by

$$V_B = \frac{1}{2} \iint_A \left[D_{11} \left(\frac{\partial^2 w}{\partial x^2} \right)^2 + 2D_{12} \frac{\partial^2 w}{\partial x^2} \frac{\partial^2 w}{\partial y^2} + D_{22} \left(\frac{\partial^2 w}{\partial y^2} \right)^2 + 4D_{66} \left(\frac{\partial^2 w}{\partial x \partial y} \right)^2 \right] dA \tag{2.3}$$

and V_L is the potential energy of the inplane forces, given by

$$V_L = -\frac{1}{2} \iint_A h \left[\sigma_x \left(\frac{\partial w}{\partial x} \right)^2 + 2\tau_{xy} \frac{\partial w}{\partial x} \frac{\partial w}{\partial y} + \sigma_y \left(\frac{\partial w}{\partial y} \right)^2 \right] dA \tag{2.4}$$

and the integrals in both expressions are taken over the area of the plate (see Appendix). V_L is the negative of the work done by the in-plane forces during buckling.

For a rectangular plate of dimensions axb, having its edges x = 0,a and y = 0,b simply supported, the boundary conditions for the problem are (see Appendix):

Along $x = 0,a$: $w = M_x = 0$ (2.5a)

Along $y = 0,b$: $w = M_y = 0$ (2.5b)

where M_x and M_y are the bending moments applied to the edges, which for an orthotropic plate are given by (see Appendix):

$$M_x = -\left(D_{11} \frac{\partial^2 w}{\partial x^2} + D_{12} \frac{\partial^2 w}{\partial y^2} \right)$$
$$M_y = -\left(D_{12} \frac{\partial^2 w}{\partial x^2} + D_{22} \frac{\partial^2 w}{\partial y^2} \right) \tag{2.6}$$

Because w = 0 along an edge implies that all derivatives of w taken tangent to the edge are also zero, Equations 2.5 reduce to:

Along $x = 0,a$: $w = \frac{\partial^2 w}{\partial x^2} = 0$

Along $y = 0,b$: $w = \frac{\partial^2 w}{\partial y^2} = 0$ (2.7)

2.1. UNIFORM UNIAXIAL LOADING

Consider first the case of a simply supported plate subjected to uniaxial loading which yields constant inplane stresses; i. e., σ_x = constant, $\sigma_y = \tau_{xy} = 0$. This occurs when two opposite edges are subjected to uniform and equal compressive stresses (see Figure 2.1).

The boundary conditions given by Equations 2.7 are exactly satisfied by assuming the buckling mode shapes

$$w_{mn} = c_{mn} \sin \frac{m\pi x}{a} \sin \frac{n\pi y}{b} \quad (m, n = 1, 2...) \tag{2.8}$$

where c_{mn} is an arbitrary (but small) amplitude coefficient. Substituting Equation 2.8 into 2.1 (or setting $V_B = -V_L$, using Equations 2.3 and 2.4) yields the critical buckling stress resultant:

$$N_x = \sigma_x h = -\pi^2 \left[D_{11} \left(\frac{m}{a}\right)^2 + 2\left(D_{12} + 2D_{66}\right) \left(\frac{n}{b}\right)^2 + D_{22} \left(\frac{n}{b}\right)^4 \left(\frac{a}{m}\right)^2 \right] \tag{2.9}$$

This value is clearly a minimum when the buckled mode shape has only one half-sine wave in the y-direction (i.e., n = 1). Therefore, the critical value of stress resultant is

$$\sigma_x h = -\pi^2 \left[D_{11} \left(\frac{m}{a}\right)^2 + 2\left(D_{12} + 2D_{66}\right)\left(\frac{1}{b}\right)^2 + D_{22} \left(\frac{1}{b}\right)^4 \left(\frac{a}{m}\right)^2 \right] \tag{2.10}$$

Equation 2.10 may be put into different forms using various nondimensional buckling load parameters. One parameter is consistent with the one most frequently used in isotropic plate buckling analysis (cf. [2]). Let

$$K_x \equiv -\frac{N_x b^2}{D_{22}} = -\frac{\sigma_x h b^2}{D_{22}} \tag{2.11}$$

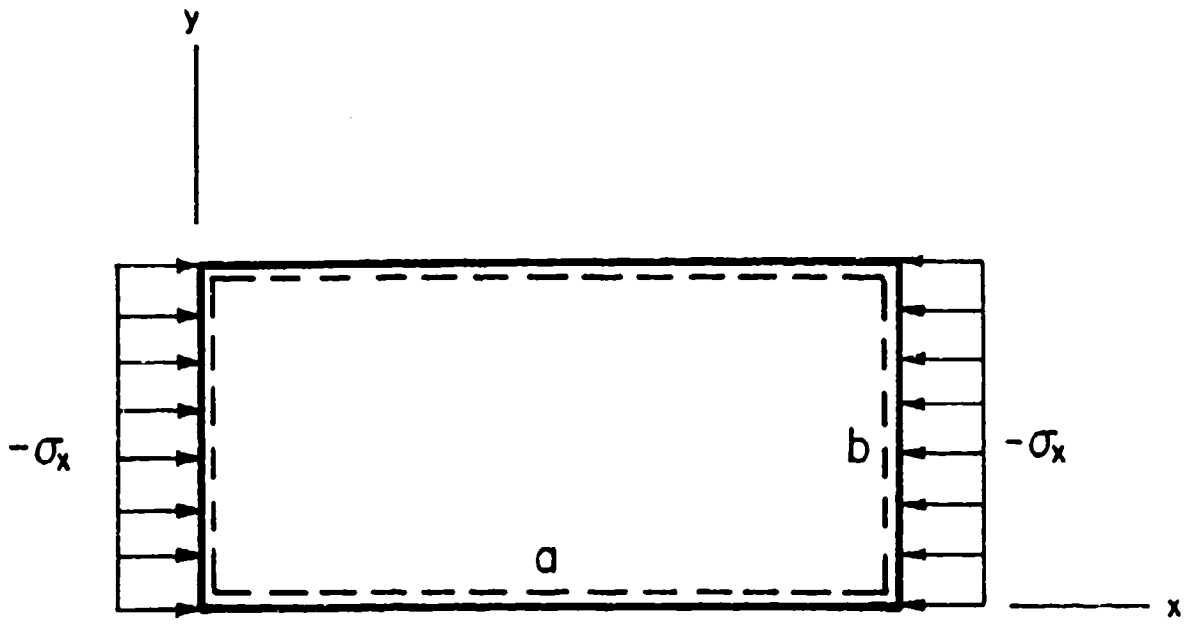

Figure 2.1. SSSS plate with uniform, uniaxial stress.

Then Equation 2.10 becomes

$$\frac{K_x}{\pi^2} = \frac{D_{11}}{D_{22}}\left(\frac{b}{a}\right)^2 m^2 + 2\left(\frac{D_{12}}{D_{22}} + 2\frac{D_{66}}{D_{22}}\right) + \left(\frac{a}{b}\right)^2 \frac{1}{m^2} \qquad (2.12)$$

Another nondimensional parameter is more consistent with the Euler buckling load of one-dimensional beam theory:

$$K_x^* \equiv -\frac{N_x a^2}{D_{22}} = -\frac{\sigma_x h a^2}{D_{22}} \qquad (2.13)$$

Then Equation 2.10 becomes

$$\frac{K_x^*}{\pi^2} = \frac{D_{11}}{D_{22}} m^2 + 2\left(\frac{D_{12}}{D_{22}} + 2\frac{D_{66}}{D_{22}}\right)\left(\frac{a}{b}\right)^2 + \left(\frac{a}{b}\right)^4 \frac{1}{m^2} \qquad (2.14)$$

Other buckling parameters may be defined using, for example, D_{11} instead of D_{22} in Equations 2.11 and 2.13.

A plot of Equation 2.12 is seen in Figure 2.2 for $(D_{12}+2D_{66})/D_{22} = 1$ and for three values of D_{11}/D_{22} (10, 1 and 0.1). The value $D_{11}/D_{22} = 1$ corresponds to the isotropic case, whereas 10 and 0.1 correspond to representative orthotropic plates which are stiffer in the loaded and unloaded directions, respectively. From the curves it is observed that the fundamental buckled mode shape may have any number of half waves in the loaded direction, depending upon the aspect ratio (a/b) and the stiffness ratio (D_{11}/D_{22}) of a particular plate. Thus, for example, for a/b = 2, the mode shape will have m = 1, 2 and 4 half-waves for $D_{11}/D_{22} = 10$, 1 and 0.1, respectively.

More understanding of the curves generated by Equation 2.12 can be had by rewriting it as

$$\frac{K_x}{\pi^2} = \frac{C_1}{r^2} + 2C_2 + r^2 \qquad (2.15)$$

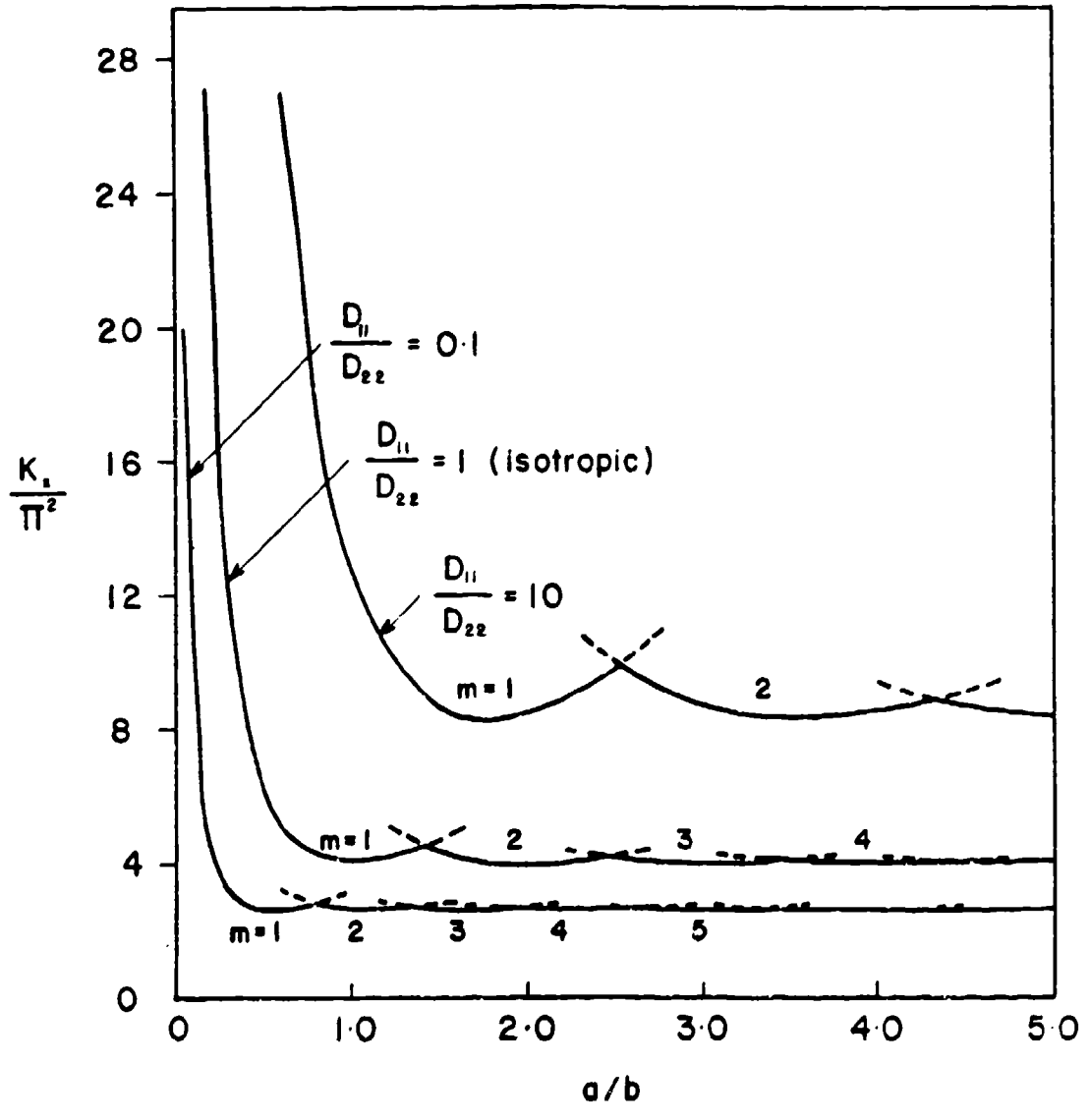

Figure 2.2. Uniaxial buckling stress ($\sigma_y/\sigma_x = 0$) of SSSS plates with various D_{11}/D_{12}, for $(D_{12}+2D_{66})/D_{22} = 1$.

where

$$r \equiv \frac{a}{mb} \quad , \quad C_1 \equiv \frac{D_{11}}{D_{22}} \quad , \quad C_2 \equiv \frac{D_{12}+2D_{66}}{D_{22}} \tag{2.16}$$

One observes from Equation 2.15 that the shapes of the curves of Figure 2.2 are affected by C_1, whereas C_2 is only a constant which shifts the curves vertically but does not change their shapes. Minimizing Equation 2.15 by setting its derivative with respect to r equal to zero, one finds that the minimum of each curve occurs at

$$\frac{a}{b} = m \sqrt[4]{C_1} \tag{2.17}$$

and that the corresponding minimum values are given by

$$\min \frac{K_x}{\pi^2} = 2\left(\sqrt{C_1} + C_2\right) \tag{2.18}$$

Thus, for example, for $C_1 = 0.1$ and $C_2 = 1$, minimum values of $K_x/\pi^2 = 2.632$ occur at a/b = 0.562, 1.125, 1.687, ..., as shown by the bottom curve of Figure 2.2. One physical interpretation of Equation 2.17 is that, for a given value of the stiffness ratio (C_1), there exists a unique plate aspect ratio (a/b) for which the plate buckles with a minimum uniaxial stress into a mode shape which is the product of single half-sine waves in each direction. The same minimum stress then exists for aspect ratios which are integer multiples (m) of the aforementioned a/b, having corresponding m half-sine waves in the x-direction. The resulting node lines x = constant which exist for m > 1 duplicate the boundary conditions at the edge of a simply supported plate; hence, each area of positive and negative displacement in the mode shape deforms as if it were a single plate having the aforementioned a/b ratio.

The intersections of buckling parameter curves as seen in Figure 2.2 identify aspect ratios for which a plate can buckle equally easy in either

of two mode shapes with the same uniaxial compressive stress. Indeed, the resulting buckled mode shape may then have any linear superposition of the two simple mode shapes, with no symmetry (or antisymmetry) of the mode being required in the x-direction. The curve intersection points may be determined by equating the right-hand-side of Equation 2.12 with another right-hand-side obtained by replacing m by m + 1. Solving the resulting equation for a/b yields

$$\left(\frac{a}{b}\right)^2 = m(m+1)\sqrt{C_1} \tag{2.19}$$

with a critical buckling parameter value of

$$\frac{K_x}{\pi^2} = \left(\frac{m}{m+1} + \frac{m+1}{m}\right)\sqrt{C_1} + 2C_2 \tag{2.20}$$

Thus, for example, for $C_1 = 0.1$ and $C_2 = 1$, intersections of the bottom curves shown in Figure 2.2 are found at a/b = 0.795, 1.377, 1.948, ... with corresponding values of $K_x/\pi^2 = 2.790$, 2.685, 2.659, ..., which approach the minimum value of $K_x/\pi^2 = 2.632$ as m and m + 1 increase.

The useful formulas presented above may also be found in the classic work of Lekhnitskii [17](see pp. 445-452). There, numerical results for $C_2 = 1.307$, and $C_1 = 12.1$ or $1/12.1 = 0.0826$, corresponding to a 3-layer birch plywood plate bonded by bakelite glue, loaded on either two sides, were presented. Because of their similarity to Figure 2.2, they will not be repeated here.

In Equation 2.15 it was seen that the buckling load parameter K_x was expressed as a function of the aspect ratio r and the two stiffness ratios C_1 and C_2. While these ratios are physically meaningful, it is interesting to note that, mathematically, it is possible to choose another form of load parameter which is a function of only two para-

meters, instead of the aforementioned three. Multiplying through Equation 2.10 by $b^2/\pi^2\sqrt{D_{11}D_{22}}$ yields

$$-\frac{\sigma_x h b^2}{\pi^2\sqrt{D_{11}D_{22}}} = B_1 + \frac{1}{B_1} + B_2 \tag{2.21a}$$

where $$B_1 \equiv \left(\frac{mb}{a}\right)^2\sqrt{\frac{D_{11}}{D_{22}}} \tag{2.21b}$$

$$B_2 = \frac{2(D_{12}+2D_{66})}{\sqrt{D_{11}D_{22}}} \tag{2.21c}$$

A number of investigators obtained experimental results for uniaxial buckling loads of SSSS orthotropic plates [34-39]. Mandell [34,35] in 1968 made a set of tests on graphite, glass and boron fiber reinforced, laminated composite plates. This work has been widely used by others for comparison with theoretical results. A description of the plates tested is given in Table 2.1. Plate identification numbers given are those used in [34,35]. "Thornel" plates were made of graphite-epoxy. The ply layup 5(0,90) indicates that the stacking sequence is 0°, 90°, 0°, 90°, 0° with respect to the load direction (i.e., the x-axis), and 20(90) indicates, for example, 20 plies all oriented at 90° with respect to the load. Bending stiffnesses for the plates are presented in Table 2.2. They were calculated from the constituent properties by various theoretical methods of micromechanics, which are explained in [34,35]. The load was applied statically by means of individually acting, spring loaded pistons to insure that it was evenly distributed. The widely used Southwell [40] method was used to determine critical loads.

Table 2.3 lists the experimental buckling loads for the plates described in Table 2.1. The critical buckling load for all plates was observed in the (1,1) mode, except for plates 207 and 405, which buckled

Table 2.1. Description of orthotropic plates tested by Mandell

Plate no.	Material	% Fiber by volume	Layup of plies	Dimensions (in)
201	Thornel-25	40.0	(0,90,90,0)	10 x 10 x 0.055
202	" "	"	9(0,90)	10 x 10 x 0.121
204	Thornel-40	60.0	5(0,90)	10 x 10 x 0.043
205	" "	"	5(90,0)	"
206	" "	"	(0,90,90,0)	10 x 10 x 0.034
207	" "	"	(90,0,0,90)	"
404	Boron	57.2	20(0)	11 x 11 x 0.096
405	"	"	20(90)	"

Table 2.2. Bending stiffnesses (lb.in) for Mandell's orthotropic plates

Plate no.	D_{11}	D_{12}	D_{22}	D_{66}
201	127	4.45	30.2	6.88
202	1065	47.5	611	73.4
204	129	1.90	38.8	4.42
205	38.8	1.90	129	4.42
206	70.1	0.94	12.9	2.18
207	12.9	0.94	70.1	2.18
404	2562	67.3	328	81.2
405	328	67.3	2562	81.2

Table 2.3. Buckling loads ($-N_x$, lb/in) for Mandell's SSSS orthotropic plates

Plate no.	Experimental	Theoretical
201	21.7	19.1
202	189	204
204	15.5	18.7
205	16.3	18.7
206	6.69	8.72
207	5.65	7.44
404	271	292
"		285*
"		299**
405	251	223
"		210*
"		226**

* obtained by Galerkin method
** obtained by Ritz method

first in the (1,2) mode. Also listed are theoretical values obtained by utilizing Equation 2.9 and by two approximate methods using the stiffness data given in Table 2.2, and the Galerkin and Ritz methods, as applied by Chamis [41] and Ashton [42], respectively. The Galerkin and Ritz methods should both give critical loads equal to or greater than the values obtained from Equation 2.9, depending upon the trial functions chosen to represent the buckled mode displacement.

It is interesting to note that the theoretical values for the uniaxial buckling loads for cross-ply, symmetrically laminated, square plates are the same regardless of whether the load is applied to one set of parallel edges or to the other set, and irrespective of the ply thickness or stacking sequence, provided that the plate buckles in the mode having $m = n = 1$. This statement even includes the special case when all plies have parallel fiber directions. This fact is seen by observing Equation 2.21 in Section 2.2, where clearly the same result is obtained whether $\sigma_x = 0$ or $\sigma_y = 0$, and is demonstrated in Table 2.3 by plates 204 and 205. The latter plates are identical 5(0,90) plates loaded in the two different directions. However, the experimental loads for the two loading cases are seen to be approximately 5 per cent different.

Buckling of uniaxially loaded SSSS orthotropic plates is discussed by many other writers [43-56], typically as part of a more complete investigation involving other loadings or boundary conditions.

2.2. UNIFORM BIAXIAL LOADING

In this case the problem of Section 2.1 is generalized to include both components of normal stress - that is, both constant, but not necessarily equal - but no inplane shear stress. A representative

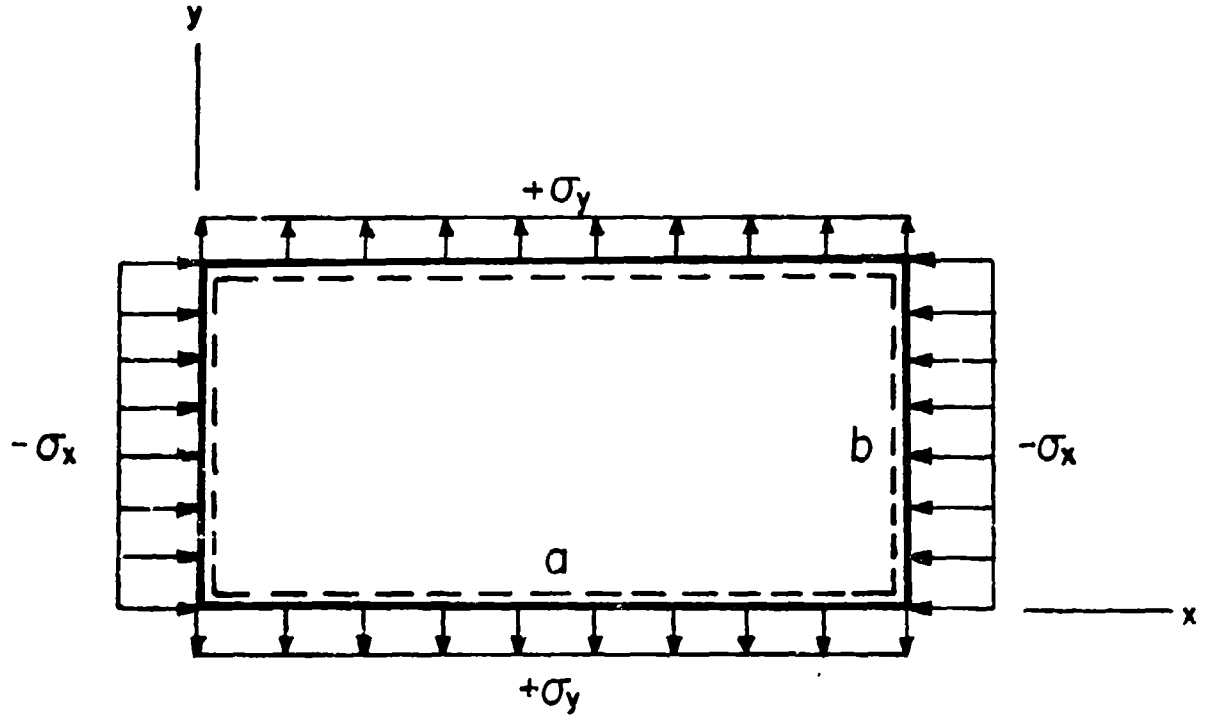

Figure 2.3. SSSS plate with uniform, biaxial stresses.

loading is shown in Figure 2.3, where one of the normal stresses (σ_x) is compressive, and the other (σ_y) is tensile. For buckling to occur, at least one of the stresses must be compressive.

Taking once again the assumed displacement function given by Equation 2.8 and substituting it into Equation 2.1, retaining both σ_x and σ_y, one obtains the following generalization of Equation 2.9:

$$\sigma_x h\left(\frac{m}{a}\right)^2 + \sigma_y h\left(\frac{n}{b}\right)^2 = -\pi^2\left[D_{11}\left(\frac{m}{a}\right)^4 + 2\left(D_{12}+2D_{66}\right)\left(\frac{m}{a}\right)^2\left(\frac{n}{b}\right)^2 + D_{22}\left(\frac{n}{b}\right)^4\right] \tag{2.22}$$

Solving Equation 2.22 for the critical stress resultant in terms of the biaxial stress ratio σ_y/σ_x, there results:

$$\sigma_x h = \frac{-\pi^2\left[D_{11}\left(\frac{m}{a}\right)^2 + 2\left(D_{12}+2D_{66}\right)\left(\frac{n}{b}\right)^2 + D_{22}\left(\frac{n}{b}\right)^4\left(\frac{a}{m}\right)^2\right]}{1+\left(\frac{\sigma_y}{\sigma_x}\right)\left(\frac{a}{b}\right)^2\left(\frac{n}{m}\right)^2} \tag{2.23}$$

Unlike the previous case of uniaxial stress (Section 2.1), the critical buckling load need not necessarily occur for n = 1 (or m = 1), so both integers must be retained in general form. In terms of the parameter defined by Equation 2.11 the nondimensional buckling stress becomes

$$\frac{K_x}{\pi^2} = \frac{\frac{D_{11}}{D_{22}}\left(\frac{b}{a}\right)^2 m^2 + 2\left(\frac{D_{12}}{D_{22}} + 2\,\frac{D_{66}}{D_{22}}\right)n^2 + \left(\frac{a}{b}\right)^2\frac{n^4}{m^2}}{1+\left(\frac{\sigma_y}{\sigma_x}\right)\left(\frac{a}{b}\right)^2\left(\frac{n}{m}\right)^2} \tag{2.24}$$

where a negative value of σ_y/σ_x is used to denote a tensile stress

acting in the y-direction, simultaneously with the compressive stress in the x-direction.

In addition to the case of uniaxial compression ($\sigma_y/\sigma_x = 0$) already discussed, at least two other important special cases exist. The first of these is hydrostatic compression, where the biaxial normal stresses in x, y and all directions are equal ($\sigma_y/\sigma_x = 1$). A plot of K_x/π^2 versus a/b for this case is shown in Figure 2.4 for the same ratios of elastic moduli used previously in Figure 2.2. As expected, a plate subjected to hydrostatic compressive stress buckles under less stress than one carrying only uniaxial stress. Unlike the case of uniaxial loading, the smallest value of K_x/π^2 always occurs for $m = n = 1$, and K_x/π^2 decreases monotonically with increasing a/b. Comparing Figure 2.4 with Figure 2.2, one can see that for an isotropic plate, the minimum value of K_x/π^2 is 1, compared with 4 for the case of the uniaxially loaded plate.

Another special case of uniform biaxial stress loading is worthy of special attention. Here $\sigma_y/\sigma_x = -1$; that is, the normal stress in the y- direction is tensile, and equals the normal compressive stress in the x-direction in magnitude. In this case all planes making a 45 degree angle with both the x and y axes are in pure shear. A plot of K_x/π^2 versus a/b for this case is shown in Figure 2.5 for the same ratios of elastic moduli used previously in Figures 2.2 and 2.4. As expected, the presence of uniform tensile stress serves to stiffen a plate. Comparing Figure 2.5 with Figure 2.2, it is seen that for an isotropic plate, the minimum value of K_x/π^2 is 8, compared with 4 for the case of the uniaxially loaded plate. Furthermore, while the minimum buckling load occurs with $n = 1$ for both loading cases, comparing Figure 2.5 with 2.2, it is observed that tension-compression buckling mode shapes tend to have more half-waves in the x-direction than the uniaxial buckling modes.

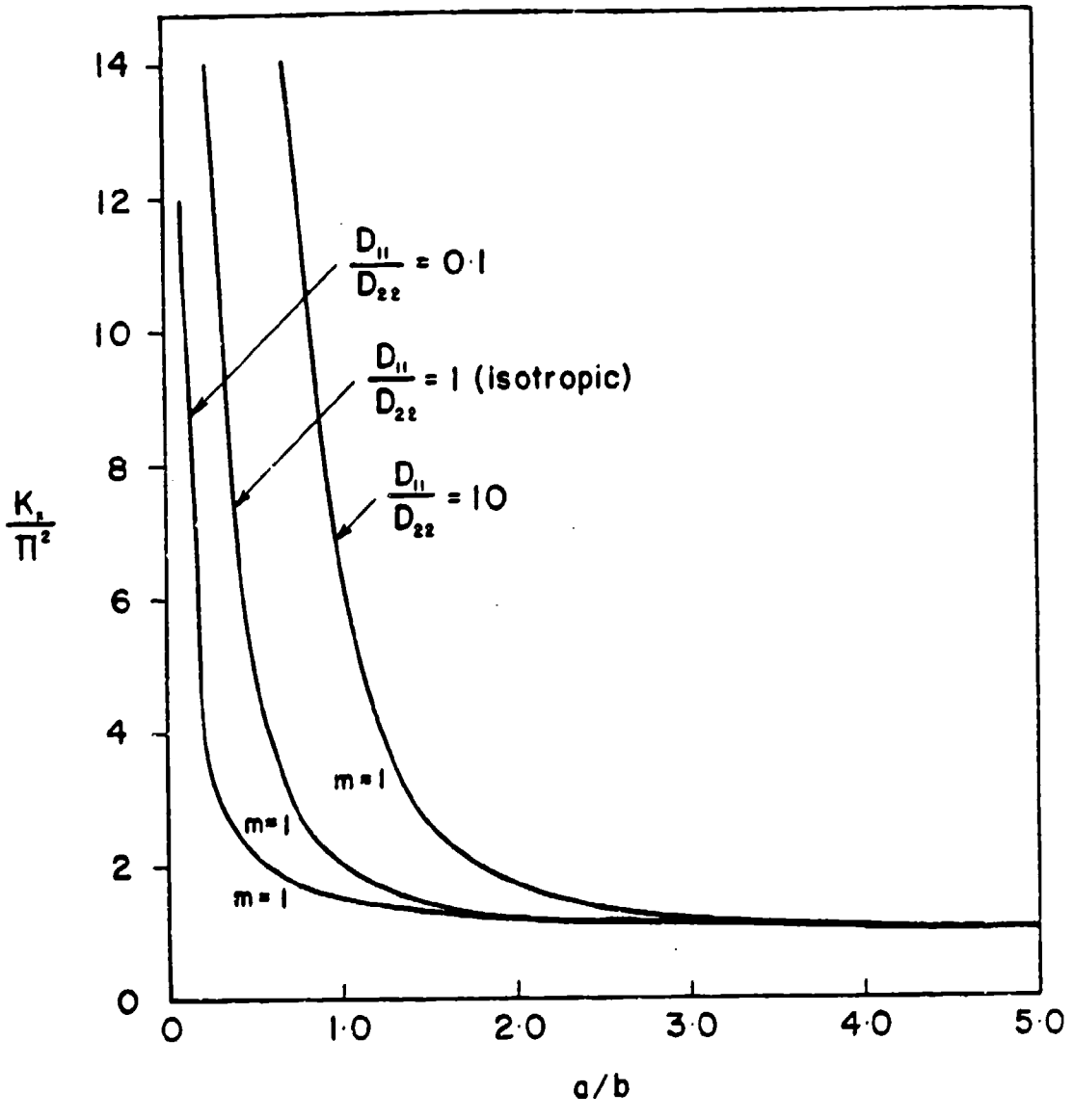

Figure 2.4. Hydrostatic stress buckling ($\sigma_y/\sigma_x = 1$) of SSSS plates with various D_{11}/D_{22}, for $(D_{12}+2D_{66})/D_{22} = 1$.

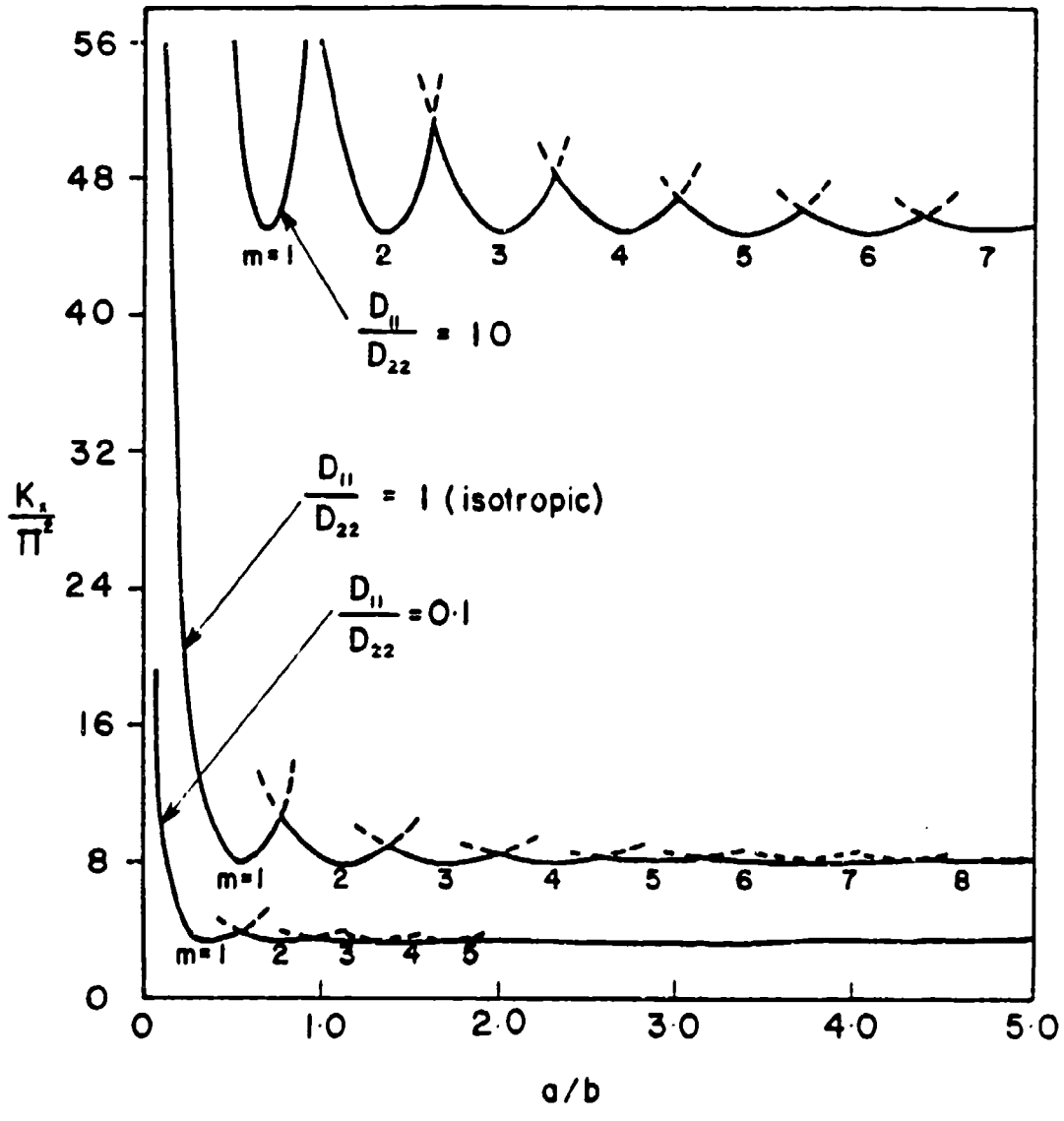

Figure 2.5. Tension-compression buckling ($\sigma_y/\sigma_x = -1$) of SSSS plates with various D_{11}/D_{22}, for $(D_{12}+2D_{66})/D_{22} = 1$.

From Equation 2.22 it is seen that for σ_x negative and σ_y positive, the smallest value of K_x always occurs when n = 1. Lekhnitskii [17] showed that in this case, for any given value of σ_y, the lowest value of buckling load is given by

$$\min \frac{K_x}{\pi^2} = 2\left[\sqrt{C_1\left(1+\frac{\sigma_y b^2}{\pi^2 D_{22}}\right)} + C_2\right] \tag{2.25}$$

where σ_y, as before, is a positive number when the plate is in tension, and that this minimum occurs where

$$\frac{a}{b} = \frac{m}{\sqrt{\frac{1}{C_1}+\frac{\sigma_y b^2}{\pi^2 D_{11}}}} \tag{2.26}$$

He showed further that the intersections of buckling parameter curves occur at

$$\frac{a}{b} = \frac{\sqrt{m(m+1)}}{\sqrt{\frac{1}{C_1}+\frac{\sigma_y b^2}{\pi^2 D_{11}}}} \tag{2.27}$$

The validity of Equations 2.25, 2.26 and 2.27 is verified by Figure 2.5 for the case when $\sigma_y/\sigma_x = -1$.

In Equation 2.24 it is seen that the buckling load parameter K_x is a function of the biaxial stress ratio (σ_y/σ_x), three stiffness ratios (D_{11}/D_{22}, D_{12}/D_{22}, D_{66}/D_{22}), the plate aspect ratio (a/b), and the half-wave numbers m and n. Thus a careful numerical study of Equation 2.24 would require plotting large numbers of curves for, say, K_x versus a/b (or mb/a), for various values of the aforementioned ratios.

Wittrick [57] showed that for small values of σ_y/σ_x, specifically, for

$$\frac{\sigma_y}{\sigma_x} < \frac{\pi^2}{K_x} \tag{2.28}$$

Equation 2.24 may be written as

$$k = \left(\frac{m}{\lambda} + \frac{\lambda}{m}\right)^2 \tag{2.29}$$

where m is the number of half sine waves in the x-direction, as before, and k and λ are defined as:

$$k = 2 - \frac{\left[\frac{\sigma_x hb^2}{\pi^2} + 2(D_{12} + 2D_{66})\right]}{\left[D_{11} D_{22}\left(1 + \frac{\sigma_y hb^2}{\pi^2 D_{22}}\right)\right]^{1/2}} \tag{2.30}$$

$$\lambda = \frac{a}{b}\left[\frac{D_{22}}{D_{11}}\left(1 + \frac{\sigma_y hb^2}{\pi^2 D_{22}}\right)\right]^{1/4} \tag{2.31}$$

where, as Wittrick [57] proved, the minimum value of K_x occurs for n = 1 when inequality (2.28) is satisfied. Equation 2.29 is seen to have the same form as the well-known formula for the uniaxial buckling of an isotropic plate (cf., Timoshenko and Gere [2], page 352), except that in the latter case, k and λ are simply K_x/π^2 and a/b, respectively, and the critical buckling loads are determined from a single curve. Thus, Equations 2.29-2.31 permit the representation of all SSSS orthotropic plate biaxial buckling loads as a single curve, rather than requiring many families of curves. This single curve is the middle curve of Figure 2.2 (i.e., isotropic), with K_x/π^2 and a/b replaced by k and λ of Equations 2.29-2.31, respectively. Results corresponding to Equations 2.29-2.31 were subsequently derived by Brunelle and Oyibo [58,59] for this problem in the special case when $\sigma_y = 0$ (i.e., uniaxial loading).

Several additional references may be found which deal with the buckling of biaxially loaded SSSS orthotropic plates [32,44,45,46,60].

2.3. UNIFORM SHEAR LOADING

A rectangular plate having dimensions axb, subjected to uniform shear stresses throughout, is depicted in Figure 2.6. The buckling of orthotropic plates due to shear loading received considerable attention by Bergmann & Reissner [21], Schmieden [22,61] and Seydel [62-65] a half century ago. Brief histories of these early contributions may be found in the works of Lekhnitskii [17] and Stavsky and Hoff [66].

The case of the <u>infinite</u> orthotropic plate (i.e., $a/b = \infty$) loaded in pure shear has an exact solution for its critical buckling stresses and mode shapes. This was determined by Bergmann & Reissner [21] following the same procedure used previously by Southwell and Skan [67] for isotropic plates. This solution is applicable for long plates (say $a/b > 4$), regardless of the edge conditions at $x = 0,a$.

Taking Equation 2.1 with $\sigma_x = \sigma_y = 0$, an exact solution may be found in the form

$$w(x,y) = f(y)e^{i\kappa\frac{x}{b}} \tag{2.32}$$

where $i = \sqrt{-1}$, b is the plate width and κ is a wave-length constant to be determined. Substituting Equation 2.32 into Equation 2.1 yields the ordinary differential equation

$$D_{22}f^{IV} - 2(D_{12}+2D_{66})\left(\frac{\kappa}{b}\right)^2 f'' + i\tau_{xy}\left(\frac{\kappa}{b}\right) f' + D_{11}\left(\frac{\kappa}{b}\right)^4 f = 0 \tag{2.33}$$

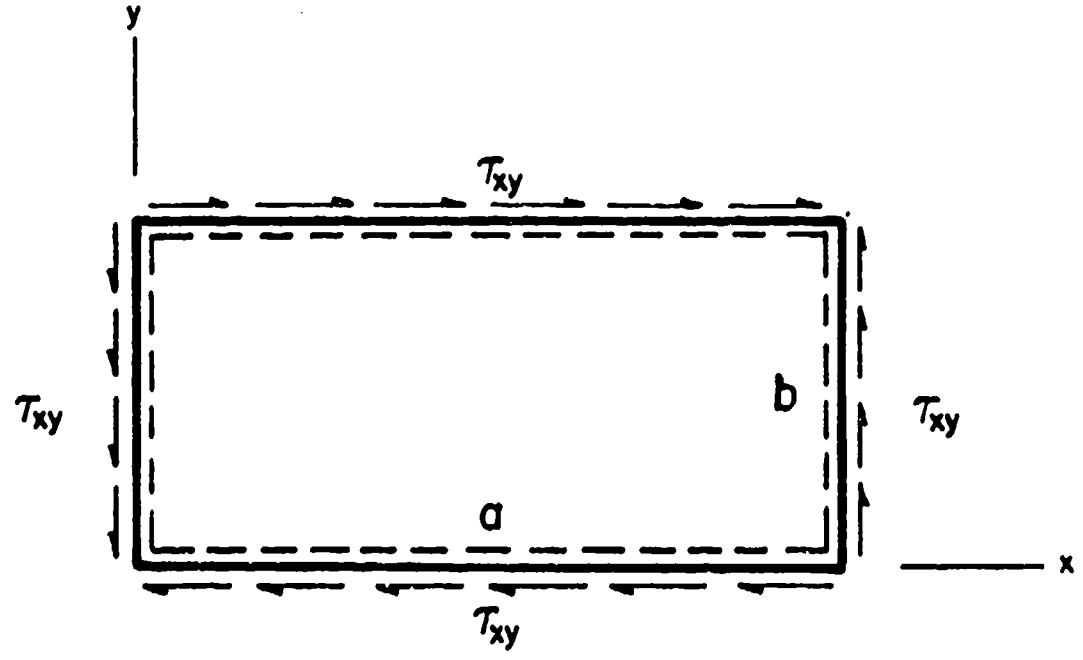

Figure 2.6. SSSS plate with uniform shear stress.

where the primes denote differentiation with respect to x. The solution of Equation 2.33 takes the form

$$f(y) = A_1 e^{i\beta_1 \frac{y}{b}} + A_2 e^{i\beta_2 \frac{y}{b}} + A_3 e^{i\beta_3 \frac{y}{b}} + A_4 e^{i\beta_4 \frac{y}{b}} \tag{2.34}$$

where $\beta_1, \ldots, \beta_4$ are the roots of a fourth degree polynomial equation arising from Equation 2.33. Substituting Equations 2.32 and 2.34 into the four simply-supported boundary conditions which exist at y = 0,b Equations 2.7, one obtains a fourth order characteristic determinant containing both κ and τ_{xy}. For each value of κ there exists at least one value of τ_{xy}. The critical value of τ_{xy} is the lowest one which can be found. It can be shown that the solution range is determined by the parameter $\sqrt{C_1/C_2}$, where C_1 and C_2 are as given by Equations 2.16. For $1 \leq \sqrt{C_1/C_2} \leq \infty$, the critical values of τ_{xy} and κ are determined from

$$K_s = \frac{\tau_{xy} hb^2}{D_{22}} = k_1 \sqrt[4]{C_1} \tag{2.35a}$$

$$\kappa = k_2 b \sqrt[4]{C_1} \tag{2.35b}$$

where k_1 and k_2 are given in Table 2.4. For $0 \leq \sqrt{C_1/C_2} \leq 1$, the values are determined from

$$K_s = k_3 \sqrt{C_2} \tag{2.36a}$$

$$\kappa = k_4 b \sqrt{C_2} \tag{2.36b}$$

where k_3 and k_4 are given in Table 2.5.

For an isotropic material ($C_1 = C_2 = 1$), the results obtained from Equations 2.35 and 2.36 agree with those of Southwell and Skan [67], viz.

Table 2.4. Coefficients k_1 and k_2 for the buckling parameters of a SS-SS infinite strip loaded in shear.

$\frac{\sqrt{C_1}}{C_2}$	k_1	k_2
1	52.68	2.49
2	43.2	2.28
3	39.8	2.16
5	37.0	2.13
10	35.	2.08
20	34.	-
30	-	2.05
40	33.0	-
∞	32.50	-

Table 2.5. Coefficients k_3 and k_4 for the buckling parameters of a SS-SS infinite strip loaded in shear.

$\frac{\sqrt{C_1}}{C_2}$	k_3	k_4
0	46.84	-
0.05	-	1.92
0.2	47.2	1.94
0.5	48.8	2.07
1	52.68	2.49

$$K_s = 52.68, \quad \kappa = 2.49b \tag{2.37}$$

The buckled mode shape for the isotropic case is shown in Figure 2.7. It is observed that the half-wave length of the mode in the x-direction is $\kappa/2 = 1.24b$, which slightly exceeds the plate width. For comparison, the infinite strip subjected to uniform uniaxial stress in the x-direction buckles when $-\sigma_x hb^2/D_{22} = 4\pi^2 = 39.48$ with a half-wave length of b (see Section 2.1).

For an orthotropic plate having $C_1 = 10$, $C_2 = 1$ (e.g., a single layer with fibers parallel to the infinite length), Equations 2.35 and Table 2.4 combine to yield

$$\begin{aligned} K_s &= 39.6 \times 1.78 = 70.4 \\ \kappa &= 2.16b \times 1.78 = 3.85b \end{aligned} \tag{2.38}$$

whereas if $C_1 = 0.1$, $C_2 = 1$ (e.g., fibers perpendicular to the infinite length), Equations 2.36 and Table 2.5 yield

$$\begin{aligned} K_s &= 47.8 \times 1 = 47.8 \\ \kappa &= 1.95b \times 1 = 1.95b \end{aligned} \tag{2.39}$$

Thus, infinite strips having fibers parallel to the two simply supported edges buckle with larger critical shear stress and longer wave length than strips having the fibers perpendicular to the edges.

The case of the SSSS plate of finite dimensions subjected to uniform shear stress has no exact solution for the buckling problem, although one may obtain solutions to any degree of accuracy needed by various approximate methods.

Perhaps the most commonly used method of solving the problem is to assume a displacement function (w) to represent the buckling mode, pre-

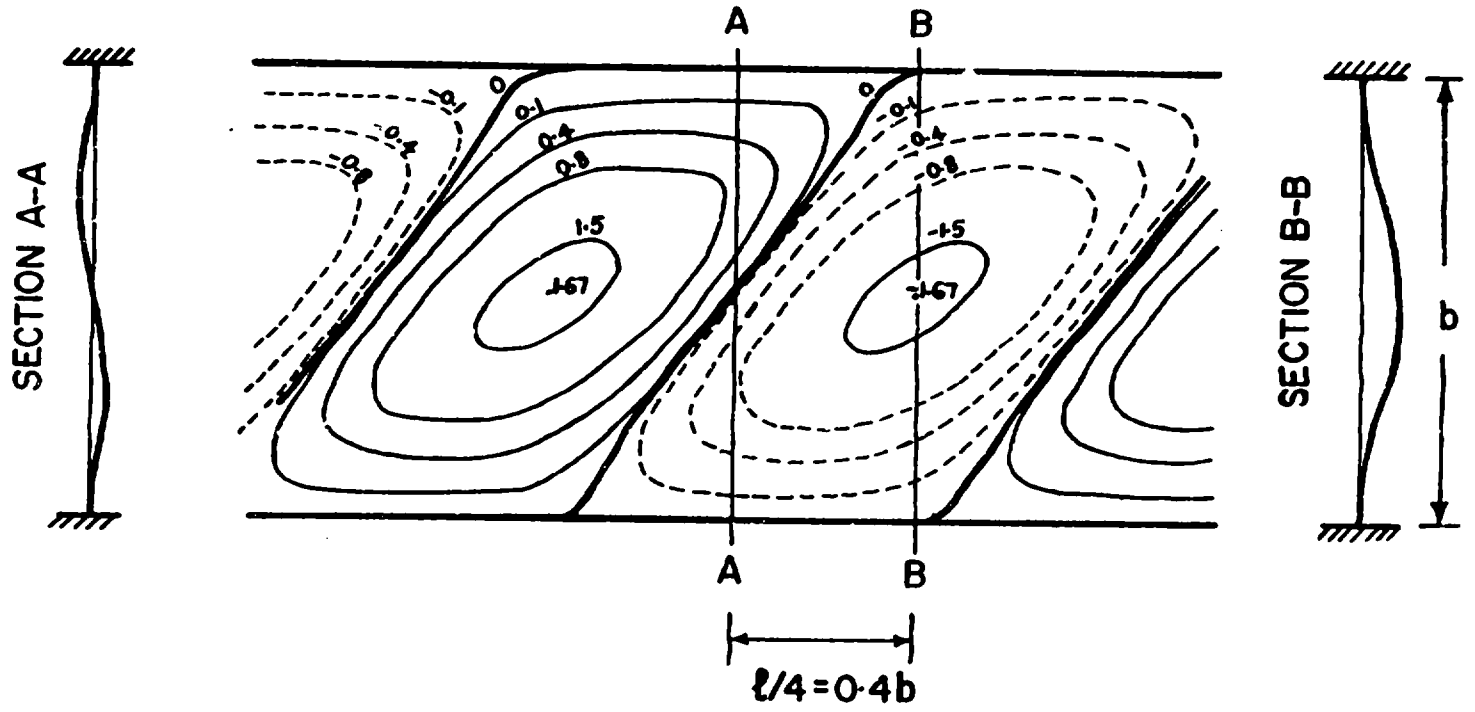

Figure 2.7. Buckled mode shape of an infinite, isotropic strip loaded in shear.

ferably one which satisfies all the boundary conditions, and equate the work done by the external forces during buckling ($-V_L$), Equation 2.4, to the bending strain energy, Equation 2.3. This allows one to solve directly for the critical value of τ_{xy}, which will be an upper bound to the exact value.

More accurate upper bound results may be obtained by choosing displacement functions with additional degrees of freedom, represented by arbitrary amplitude coefficients, and minimizing the total potential energy of the system with respect to the coefficients. For example, one function w which satisfies the SSSS boundary conditions exactly, is

$$w = \sum_{m=1}^{M} \sum_{n=1}^{N} c_{mn} \sin \frac{m\pi x}{a} \sin \frac{n\pi y}{b} \tag{2.40}$$

which is seen to be a generalization of the simple function representing the buckling of a uniformly or biaxially loaded plate, Equation 2.8. Substituting Equation 3.23 into Equations 2.3 and 2.4, the minimizing equations for the total potential, Equation 2.2, take the form

$$\frac{\partial V}{\partial c_{mn}} = 0 \qquad (m = 1,2,\ldots,M;\ n = 1,2,\ldots N) \tag{2.41}$$

This procedure yields a set of M x N homogeneous, linear, simultaneous equations in the unknown c_{mn}. The solution is the standard eigenvalue problem obtained by setting determinant of the coefficient matrix equal to zero. The resulting M x N eigenvalues are upper bound approximations to the possible buckling loads, and the smallest one is the critical one. The corresponding buckled mode shapes are found by returning to the homogeneous set of equations and solving for the amplitude ratios c_{mn}/c_{11} in the standard manner.

An extensive set of results was obtained by Housner and Stein [68, 69], using another approximate method. A finite difference approach was followed; however, trigonometric rather than the conventional polynomial central finite differences were used, which take advantage of the sinusoidal form of the buckle pattern to achieve converged solutions with fewer degrees of freedom, hence reducing computer time. As in the case of uniaxial loading, it is possible to express a shear buckling parameter completely in terms of two independent, nondimensional parameters involving the aspect ratio and the orthotropic bending stiffnesses (see Equation 2.21). The parameters utilized in [68,69] were θ and B, defined by

$$\theta = \frac{\sqrt{D_{11}D_{22}}}{D_{12}+2D_{66}}, \quad B = \frac{b}{a}\sqrt[4]{\frac{D_{11}}{D_{22}}} \tag{2.42a}$$

Values of the nondimensional shear buckling parameter k_s are listed in Table 2.6, where k_s is defined by

$$k_s = \frac{\tau_{xy} hb^2}{\pi^2 \sqrt{D_{11}D_{22}}^3} \tag{2.42b}$$

should be noted that $\theta = 1$ implies an isotropic plate.

A more detailed set of results for the same problem was presented by Fogg [32], taken from [70]. These are seen in the curves of Figure 2.8. There the same parameters are plotted (k_s versus B and θ), except that the scale for θ is given in terms of $k = 1/\theta$. Changes in mode shape for the critical load with changing B are indicated by the cusps which appear on the curves. There would be additional cusps (an infinite number) for small values of B, but they become difficult to identify. Each curve of Figure 2.8 arises from <u>two</u> curves of the theoretical

Table 2.6. Shear buckling parameters k_s for SSSS orthotropic plates (see Equations 2.40 for definitions).

θ	B	k_s	θ	B	k_s
0.2	1.0	26.28	1.25	1.0	8.43
	0.8	21.43		0.8	7.08
	0.6	17.33		0.6	6.38
	0.5	15.36		0.4	5.75
	0.4	13.77		0.2	5.09
	0.2	11.55		0.1	5.05
	0	10.87		0	4.96
0.4	1.0	15.78	1.667	1.0	7.54
	0.8	12.98		0.8	6.37
	0.6	10.86		0.6	5.85
	0.5	9.93		0.4	5.26
	0.4	9.29		0.2	4.72
	0.2	8.21		0.1	4.68
	0	7.72		0	4.60
0.6	1.0	12.21	2.5	1.0	6.65
	0.8	10.11		0.8	5.66
	0.6	8.67		0.6	5.32
	0.5	8.09		0.4	4.77
	0.4	7.73		0.2	4.32
	0.2	6.71		0.1	4.33
	0	6.53		0	4.17
0.8	1.0	10.40	5.0	1.0	5.74
	0.8	8.66		0.8	4.94
	0.6	7.57		0.6	4.78
	0.5	7.10		0.4	4.27
	0.4	6.80		0.2	3.90
	0.2	6.02		0.1	3.86
	0	5.79		0	3.75
1.0	1.0	9.31	∞	1.0	4.83
	0.8	7.60		0.8	4.22
	0.6	6.91		0.6	4.25
	0.4	6.22		0.4	3.76
	0.2	5.49		0.2	3.47
	0	5.33		0	3.30

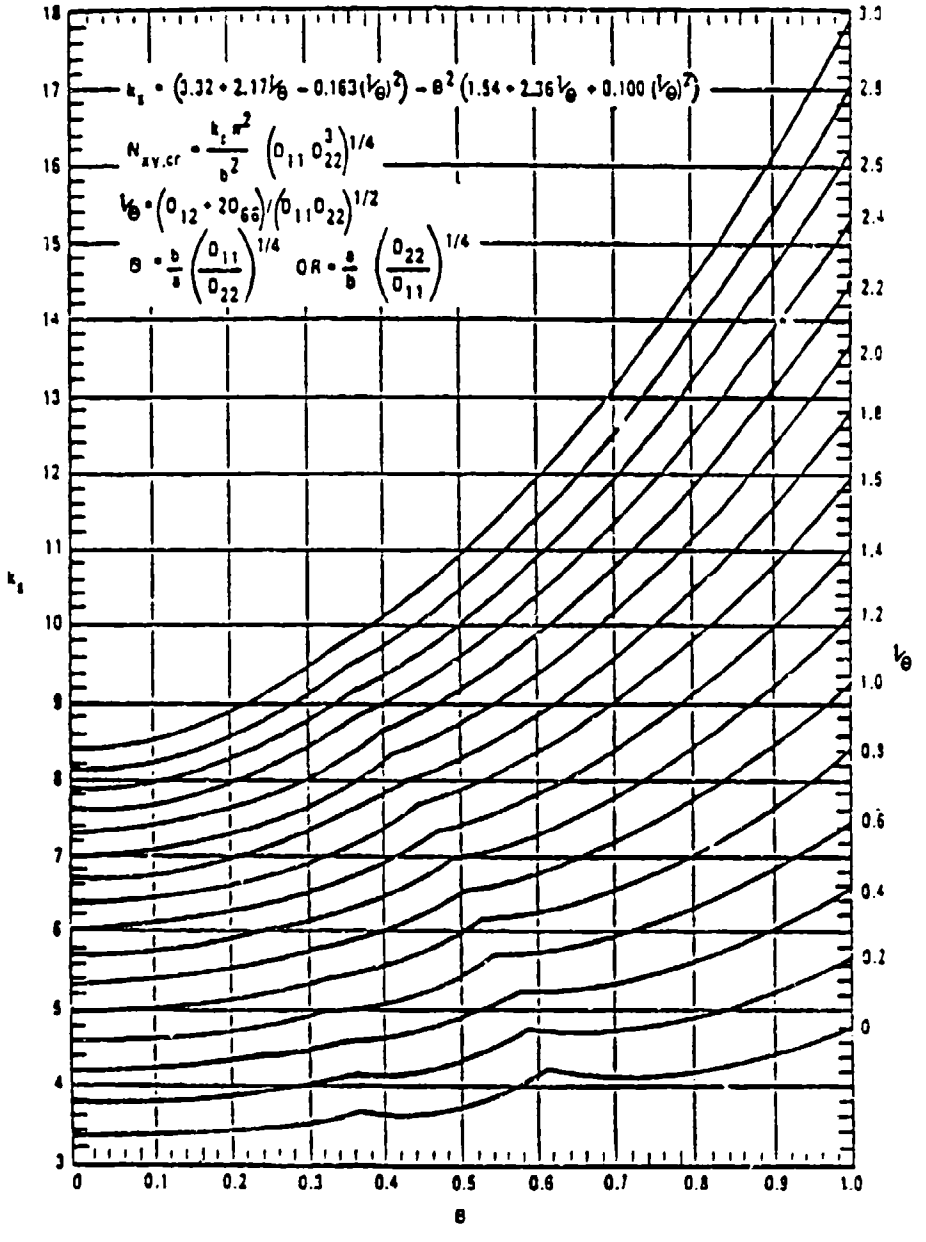

Figure 2.8. Shear buckling parameters for SSSS orthotropic plates

solution. These two curves cross and re-cross each other infinitely many times as one begins with B = 1 (where the two curves would have the same value) and moves towards B = 0. Each curve of Figure 2.8 is therefore the envelope (i.e., lowest values) of two curves

Buckling of orthotropic plates due to shear loading has received attention from a number of others in the technical literature, [45,46, 58,59,71-76].

2.4. COMBINED COMPRESSION AND SHEAR LOADING

Chamis [43,44] used the Galerkin method with displacements assumed in the form of Equation 2.40 to analyze the buckling of SSSS orthotropic plates subjected to combinations of compression and shear loading. The plates were assumed to be made up of plies having the material properties given in Table 2.7, resulting in the bending stiffnesses listed in Table 2.8. Fibers were either parallel to the x ($\theta = 0$) or y ($\theta = 90^{o}$) directions. Data for aluminum plates of the same thickness are given for comparison. Numerical results were obtained by setting M = N = 5 in Equation 2.32, yielding determinants of order 25 from which the approximate buckling eigenvalues were found.

Table 2.9 presents critical values of buckling loads for the plates described by Tables 2.7 and 2.8. Three sizes of rectangular plates were used, being 10.0 inches in one dimension, and either 5.0, 10.0 or 20.0 inches in the other dimensions. Various combinations of compressive and shear loadings are listed for each plate. Difficulties with the computer program logic required having a small value of the compressive stress resultant N_x present when a pure shear (N_{xy}) loading was desired. It is observed in Table 2.9 that the composite plates have buckling loads which are comparable to those of the aluminum plates;

Table 2.7. Material properties for plates analyzed by Chamis

Material	Modulus, $lb/in^2 \times 10^6$			ν_{12}
	E_{11}	E_{22}	G_{12}	
Fiber-matrix	32.9	1.8	0.88	0.24
Aluminum	10.0	10.0	3.83	0.30

Table 2.8. Bending stiffnesses (lb.in) for Chamis' orthotropic plates

Fiber angle θ(deg)	D_{11}	D_{12}	D_{16}	D_{22}	D_{26}	D_{66}
0	2438	32.3	0	134.8	0	64.8
90	134.8	32.3	0	2438	0	64.8
Alum.	810.1	243.1	0	810.1	0	283.5

Table 2.9. Buckling loads N_{cr}(lb/in) for Chamis' SSSS orthotropic plates

Plate dimensions (in)	Loading condition			Buckling load, N_{cr}		
	$\frac{N_x}{N_{cr}}$	$\frac{N_y}{N_{cr}}$	$\frac{N_{xy}}{N_{cr}}$	$\theta=0$	$\theta=90^\circ$	Alum.
5.0x10.0	-1	0	0	998	145	500
"	0	-1	0	581	581	1279
"	-1	-1	0	465	116	400
"	-1	0	1	948	114	479
"	0	-1	1	619	395	998
"	-1	-1	1	446	113	389
"	-0.001	0	1	2185	700	2104
10.0x10.0	-1	0	0	286	145	320
"	0	-1	0	145	286	320
"	-1	-1	0	116	116	160
"	-1	0	1	246	136	277
"	0	-1	1	136	246	277
"	-1	-1	1	111	136	153
"	-0.001	0	1	531	531	752
"	-1	-0.75	0	145	122	183
"	-1	-0.50	0	191	129	213
"	-1	-0.25	0	229	137	256
"	-1	0.25	0	381	155	426
"	-1	0.50	0	572	166	571
"	-1	1.00	0	1330	194	666
"	-1	-0.50	0.25	190	129	212
"	-1	0.50	0.25	549	165	562
"	-1	-0.50	0.50	187	127	209
"	-1	0.50	0.50	496	163	539
20.0x10.0	-1	0	0	145	145	320
"	0	-1	0	36	249	125
"	-1	-1	0	29	116	100
"	-1	0	1	99	155	250
"	0	-1	1	35	237	120
"	-1	-1	1	28	111	97
"	-0.001	0	1	175	491	528

furthermore, the densities of the composite material and aluminum were 0.06 and 0.09 lb/in , respectively [43].

Sandorff [77] discussed a procedure for modelling stiffened isotropic plates subjected to combined compression and shear by equivalent orthotropic plate theory, and applied it to the case when all edges are simply supported.

2.5. OTHER LOADINGS

For the buckling of <u>isotropic</u> plates one finds considerable results for loading cases where σ_x, σ_y and τ_{xy} are not everywhere constant (cf. [2,8,9,10]). This is particularly true for plate models of webs of beams or girders carrying bending moment and transverse shear. Buckling solutions also exist for isotropic plates subjected to in-plane point loads or partial edge loads. However, relatively little has been done for orthotropic plates carrying these more complicated loadings.

One important case of linearly varying inplane stresses may be considered as a superposition of constant inplane stresses and linearly varying stresses which arise from an inplane bending moment. Let the inplane bending stress variation be expressed as (see Figure 2.9):

$$\sigma_x = -\sigma_o \left(1-\alpha \frac{y}{b}\right) \tag{2.43}$$

when $\alpha = 0$, the stress is uniformly compressive ($-\sigma_o$). When $\alpha = 1$, the compressive stress varies from a maximum at one edge to zero at the other. When $\alpha = 2$, the tensile stress ($+\sigma_o$) at $y = b$ is the same in magnitude as the compressive stress ($-\sigma_o$) at $y = 0$, which is the case of pure inplane bending. For $\alpha > 2$, the resultant inplane force is tensile even though one part of the plate is in compression.

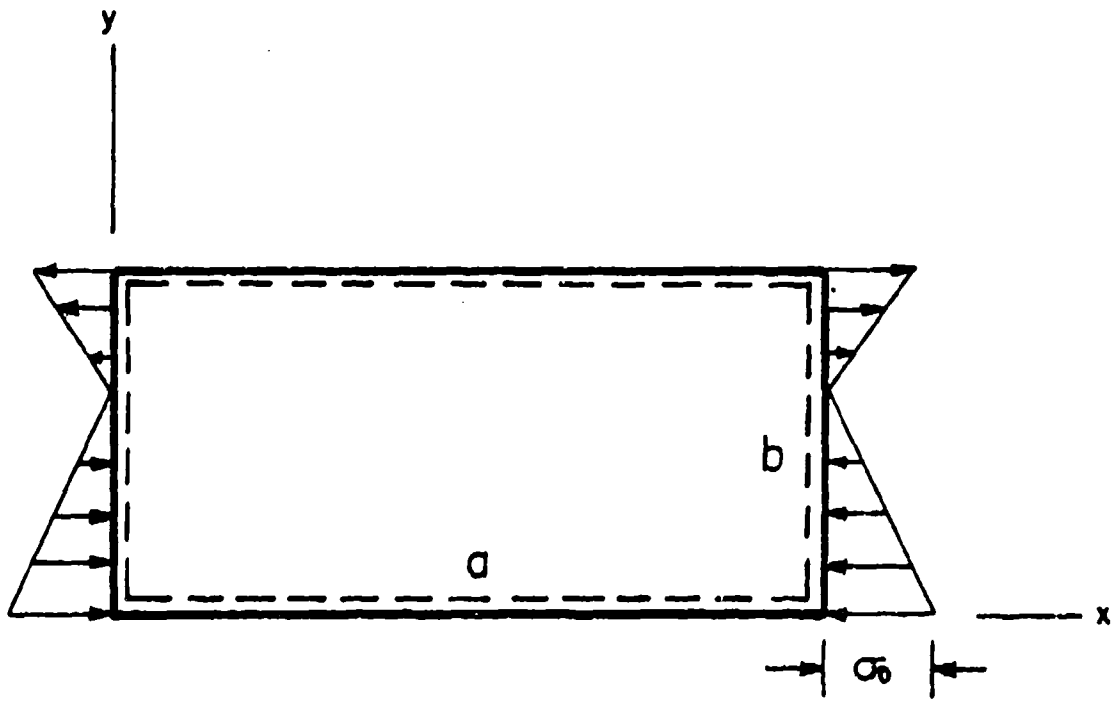

Figure 2.9. SSSS plate with linearly varying inplane stresses.

Lekhnitskii [17] solved the problem in two ways. First, he assumed the simple, one-term sinusoidal function given by Equation 2.8 with n = 1, and equated the negative of the work done by the inplane forces, Equation 2.4, to the strain energy in the plate, Equation 2.3 and arrived at the following approximate expression for the compressive stress σ_o:

$$\frac{\sigma_o hb^2(1-0.5\alpha)}{\pi^2 D_{\ell}} = \frac{C_1}{r^2} + 2C_2 + r^2 \tag{2.44}$$

where C_1, C_2 and r are defined as in Equations 2.16. It is seen that for $\alpha = 0$, Equation 2.44 reduces to the exact form for uniaxial compression Equation 2.15. Equation 2.44 should only be used for small α.

A more accurate approximation was also obtained by Lekhnitskii [17], taking two terms in the y-direction; i.e.,

$$w = \left(A_1 \sin\frac{\pi y}{b} + A_2 \sin\frac{2\pi y}{b}\right) \sin\frac{m\pi x}{a} \tag{2.45}$$

The critical buckling stress was found by minimizing the total potential energy of the system with respect to the coefficients A_1 and A_2. This yields the more accurate (but still approximate) result

$$\frac{\sigma_o hb^2}{\pi^2 D_{11}}\left[\left(1-\frac{\alpha}{2}\right)^2 - \left(\frac{16\alpha}{9\pi^2}\right)^2\right] = \frac{1}{2}\left(1-\frac{\alpha}{2}\right)(a_1+a_2) \pm \sqrt{\frac{1}{4}\left(1-\frac{\alpha}{2}\right)^2 (a_1-a_2)^2 + \left(\frac{16\alpha}{9\pi^2}\right)^2 a_1 a_2} \tag{2.46}$$

where

$$a_1 \equiv \frac{C_1}{r^2} + 2C_2 + r^2$$

$$a_2 \equiv \frac{C_1}{r^2} + 8C_2 + 16r^2 \tag{2.47}$$

with C_1, C_2 and r defined by Equations 2.16, and where the quantity $16\alpha/9\pi^2$ has been squared in both places (unlike in [17]) to make Equation 2.46 consistent with further results given below.

For the case of <u>pure inplane bending</u> ($\alpha = 2$), Lekhnitskii [17] gave the critical stress in the two corners to be

$$\sigma_o = \frac{9\pi^4 D_{22}}{32b^2h}\sqrt{a_1 a_2} \tag{2.48}$$

He also determined the minima of the various curves which would be obtained by plotting σ_o versus a/b for various m (see Section 2.1 for a similar study with uniform stress), and they occur at

$$\frac{a}{b} = 0.707m\sqrt[4]{C_1} \tag{2.49}$$

with corresponding minimum values of buckling parameters being

$$\min \frac{\sigma_o hb^2}{\pi^2 D_{22}} = 11.1\ (1.25\sqrt{C_1} + C_2) \tag{2.50}$$

Thus, for example, for $C_1 = 0.1$ and $C_2 = 1$, minimum values of $\sigma_o hb^2/\pi^2 D_{11} = 15.49$ occur at a/b = 0.398, 0.795, 1.193, ... These minima are 5.89 times as large as the corresponding values for uniform stress (see Section 2.1) and occur more frequently as a/b increases. Lekhnitskii [17] also found the curve intersection points (where a plate may buckle with equal likelihood into m or m + 1 waves in the x-direction) to occur for $\alpha = 2$ at

$$\left(\frac{a}{b}\right)^2 = \frac{1}{2}\, m(m+1)\sqrt{C_1} \tag{2.51}$$

(compare with Equation 2.19).

The same linearly varying stress situation was analyzed by Brunnelle and Oyibo [58,59] for the case of pure inplane bending ($\alpha = 2$). The buckling parameter k_o is shown plotted versus a/b in Figure 2.10, where

$$k_o = \frac{\sigma_o h b^2}{\pi^2 \sqrt{D_{11} D_{22}}} \tag{2.52}$$

In using this parameter, it was shown [58,59] that all results could be determined by a single parameter D*, defined by

$$D^* = \frac{D_{12}+2D_{66}}{\sqrt{D_{11} D_{22}}} \tag{2.53}$$

which, it may be noted, is the reciprocal of the parameter θ defined by Equation 2.41a. Thus, $D^* = 1$ corresponds to an isotropic plate. The minimum values of k_o which are shown in Figure 2.10 are listed in Table 2.10.

The same curves shown in Figure 2.10 are also available in the report by Zahn and Romstad [78] who were investigating the buckling of plywood plates. There one may also find similar curves for $\alpha = 0$, 0.5, 1.0 and 1.5, as well. A method for analyzing the buckling of orthotropic plates subjected to complicated edge loads was developed by Thierauf [79].

Extensive theoretical and experimental results for the buckling of SSSS plywood plates were published by Dekker, Kuipers et al [37] for the case of linearly varying edge stresses.

Buckling of an infinitely long orthotropic plate due to thermal stresses variable across its width was studied by Knoepke [80]. The case of the plate loaded by point loads was examined by Nowacki [81].

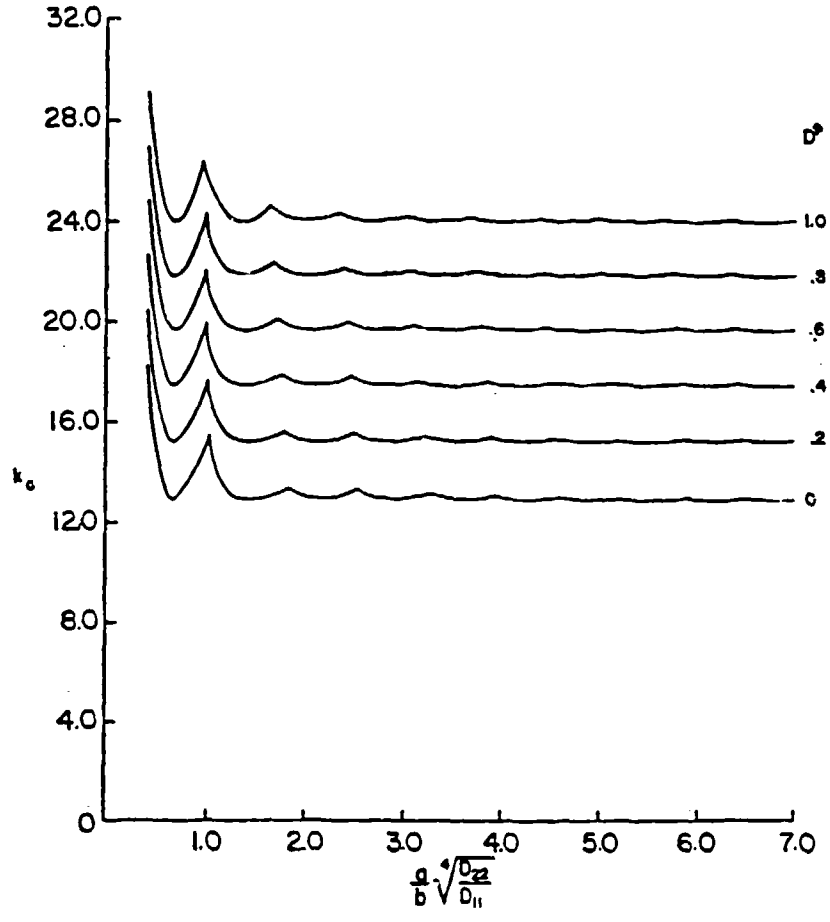

Figure 2.10. Buckling parameter for linearly varying edge load.

Table 2.10. Minimum values of k_o shown in Fig. 2.10

D*	$(k_o)_{min}$
0	12.87
0.2	15 15
0.4	17.39
0.6	19.59
0.8	21.76
1.0	23.90

CHAPTER III. RECTANGULAR ORTHOTROPIC PLATES - TWO OPPOSITE EDGES SIMPLY SUPPORTED

For a rectangular plate having two opposite edges simply supported, with the remaining two edges either clamped, simply supported or free, there exist six possible independent configurations:

1. SCSC
2. SCSS
3. SCSF
4. SSSS
5. SSSF
6. SFSF

Configuration 4 was the subject of Chapter II for, as it was seen in Sections 2.1 and 2.2, there exist simple, explicit solutions for the buckling parameters in the case of uniform inplane normal stresses. For the remaining five configurations listed above, there also exist exact solutions for the buckling loads in the case of uniform inplane normal stresses. The solutions are not simple, nor are they in explicit form. Rather, as will be seen, they are the eigenvalues of characteristic determinants which are of fourth or second order. Nevertheless, although somewhat complicated, these problems and their solutions deserve special attention in this separate chapter because accurate results can be found with relative ease compared with the remaining problems, which are taken up in Chapter IV.

3.1. EXACT SOLUTION OF THE EQUILIBRIUM EQUATION

An exact and general solution of Equation 2.1 is possible if N_x and N_y are constants and if $N_{xy} = 0$. Using the notation of Equations 2.16, Equation 2.1 is first rewritten as

$$C_1 \frac{\partial^4 w}{\partial x^4} + 2C_2 \frac{\partial^4 w}{\partial x^2 \partial y^2} + \frac{\partial^4 w}{\partial y^4} = \frac{\sigma_x h}{D_{22}} \frac{\partial^2 w}{\partial x^2} + \frac{\sigma_y h}{D_{22}} \frac{\partial^2 w}{\partial y^2} \tag{3.1}$$

If one assumes a solution to Equation 3.1 in the form

$$w(x,y) = \bar{Y}_m(y) \sin \frac{m\pi x}{a} \qquad (m = 1,2\ldots) \tag{3.2}$$

where $\bar{Y}_m(y)$ is a function of y, then simply supported boundary conditions along the edges x = 0 and a, as given by Equations 2.5a, are exactly satisfied. Substituting Equation 3.2 into 3.1 yields

$$\bar{Y}_m^{IV} - \frac{1}{b^2}\left[\frac{\sigma_y}{\sigma_x}\frac{\sigma_x hb^2}{D_{22}} + 2C_2\, m^2\pi^2\left(\frac{b}{a}\right)^2\right]\bar{Y}_m^{II} + \frac{1}{b^4}\left[\frac{\sigma_x hb^2}{D_{22}}\, m^2\pi^2\left(\frac{b}{a}\right)^2 + C_1\, m^4\pi^4\left(\frac{b}{a}\right)^4\right]\bar{Y}_m = 0 \tag{3.3}$$

where $\bar{Y}_m^{II} \equiv d^2\bar{Y}_m/dy^2$ and $\bar{Y}_m^{IV} \equiv d^4\bar{Y}_m/dy^4$. Using the nondimensional parameters K_x and r as defined previously in Equations 2.11 and 2.16, substituting the nondimensional variable $\eta = y/b$, and replacing $\bar{Y}_m(y)$ by $Y_m(\eta)$, Equation 3.3 becomes

$$Y_m^{IV} - A\, Y_m^{II} - B\, Y_m = 0 \tag{3.4a}$$

$$A \equiv 2C_2\pi^2r^2 - \left(\frac{\sigma_y}{\sigma_x}\right)K_x \tag{3.4b}$$

$$B \equiv \pi^2r^2\left[K_x - C_1\pi^2r^2\right] \tag{3.4c}$$

Equation 3.4a is a fourth order differential equation with constant coefficients A and B. Its solution can take various forms, depending upon the algebraic signs and relative magnitudes of A and B. For example, Equation 3.4c shows that B remains positive provided $K_x > C_1\pi^2r^2$. The value of K_x depends upon the boundary conditions existing along the remaining two edges ($\eta = 0,1$), yet to be prescribed.

Results for SSSS plates already shown in Figures 2.2, 2.4 and 2.5 for $0.1 \leq C_1 \leq 10$ and $0 \leq a/b \leq 5$ indicate that, at least for this set of boundary conditions, A and B are <u>typically</u> positive for every possible combination of C_1, C_2, a/b, m, n and N_y/N_x. It is known that for other boundary conditions A and/or B may be negative, and therefore all possible solution forms to Equation 3.4a should be considered.

The solution of Equation 3.4a may be written as

$$Y_m(\eta) = a_1 e^{s_1 \eta} + a_2 e^{-s_1 \eta} + a_3 e^{s_2 \eta} + a_4 e^{-s_2 \eta} \tag{3.5}$$

where s_1 and s_2 are the roots of the auxiliary equation

$$s^4 - As^2 - B = 0 \tag{3.6}$$

given by

$$s_1^2 = \frac{1}{2}\left(A + \sqrt{A^2+4B}\right), \quad s_2^2 = \frac{1}{2}\left(A - \sqrt{A^2+4B}\right) \tag{3.7}$$

However, Equation 3.5 is not a practical solution form for two reasons: (1) it does not straightforwardly recognize the presence of symmetric and antisymmetric buckling modes which will exist for symmetric boundary conditions and loadings, and (2) the roots s_1 and/or s_2 may be real, imaginary or complex. It is therefore better to rewrite Equation 3.5 using trigonometric and/or hyperbolic functions, considering the possible types of roots. The solution forms for the roots s_1 will be taken up below. Corresponding forms for the roots s_2 may be easily written and added to the s_1 forms to obtain the complete solutions, each having four independent constants of integration, $a_1 \ldots a_4$.

Case I. s_1^2 is a positive, real number

$$Y_m(\eta) = a_1 \sin s_1\eta + a_2 \cos s_1\eta \tag{3.8}$$

Case II. s_1^2 is a negative, real number

$$Y_m(\eta) = a_1 \sinh \bar{s}_1 \eta + a_2 \cosh \bar{s}_1 \eta \tag{3.9}$$

where $$\bar{s}_1^2 = -s_1^2 \tag{3.10}$$

In addition, s_1^2 and s_2^2 may be complex (4B is negative, and greater than A^2 in magnitude). In this case the solution of Equation 3.3 is more complicated, involving the products of trigonometric and hyperbolic functions. These cases are the ones having significant practical value. The case $s_1^2 = 0$ arises only in very special circumstances. It yields repeated roots and a solution form $Y_m(\eta) = a_1 + a_2\eta$ which can be approached as closely as desired in numerical computations with the forms given by Equations 3.8 or 3.9. Similarly, the case when s_2 (but not s_1) is a pure imaginary number requires $A = 0$, which can also arise only for certain special combinations of parameters, and may be approached as closely as desired by taking small values of A with the solution forms given above.

As already mentioned, no proofs are known to exist which enable one to determine a priori the correct solution form for a particular problem. For example, it is well known for isotropic plates (i.e., $C_1 = C_2 = 1$) that the complete solution form

$$Y_m(\eta) = a_1 \sin s_1 \eta + a_2 \cos s_1 \eta + a_3 \sinh \bar{s}_2 \eta + a_4 \cosh \bar{s}_2 \eta \tag{3.11}$$

$(\bar{s}_2^2 = -s_2^2)$ is applicable to a wide range of problems. However, to be certain that this solution is correct for a particular set of parameters, one must verify that s_1^2 and s_2^2 are both positive after the eigenvalues (nondimensional buckling parameters) for the problem are found.

3.2. SCSC

A plate having two opposite edges simply supported (S) and the remaining two clamped (C) is shown in Figure 3.1. The important case of uniform biaxial loading (σ_x, σ_y constant, $\tau_{xy} = 0$) is depicted in Figure 3.1, although more general stress distributions are possible. For boundary conditions and inplane stress distributions which possess two-fold symmetry, as in the present case, it is convenient to use the xy-coordinate system shown, whereupon the boundary conditions become:

$$\text{Along} \quad x = 0,a \; : \quad w = M_x = 0 \tag{3.12a}$$

$$\text{Along} \quad y = \pm b/2 \; : \quad w = \frac{\partial w}{\partial y} = 0 \tag{3.12b}$$

All buckling modes will be either symmetric or antisymmetric with respect to the symmetry axes of the plate. Thus, the solution form shown previously in Equation 3.11 may be separated, and the displacement functions may be written as:

$$\text{Symmetric modes:} \quad w(x,y) = \left(a_2 \cos \frac{s_1 y}{b} + a_4 \cosh \frac{\bar{s}_2 y}{b}\right) \sin \frac{m\pi x}{a} \tag{3.13a}$$

$$\text{Antisymmetric modes:} \quad w(x,y) = \left(a_1 \sin \frac{s_1 y}{b} + a_3 \sinh \frac{\bar{s}_2 y}{b}\right) \sin \frac{m\pi x}{a} \tag{3.13b}$$

Substituting Equations 3.13 into Equations 3.12b yields, for nontrivial solutions:

$$\text{Symmetric modes:} \quad \begin{vmatrix} \cos \frac{s_1}{2} & \cosh \frac{\bar{s}_2}{2} \\ -s_1 \sin \frac{s_1}{2} & \bar{s}_2 \sinh \frac{\bar{s}_2}{2} \end{vmatrix} = 0 \tag{3.14a}$$

$$\text{Antisymmetric modes:} \quad \begin{vmatrix} \sin \frac{s_1}{2} & \sinh \frac{\bar{s}_2}{2} \\ s_1 \cos \frac{s_1}{2} & \bar{s}_2 \cosh \frac{\bar{s}_2}{2} \end{vmatrix} = 0 \tag{3.14b}$$

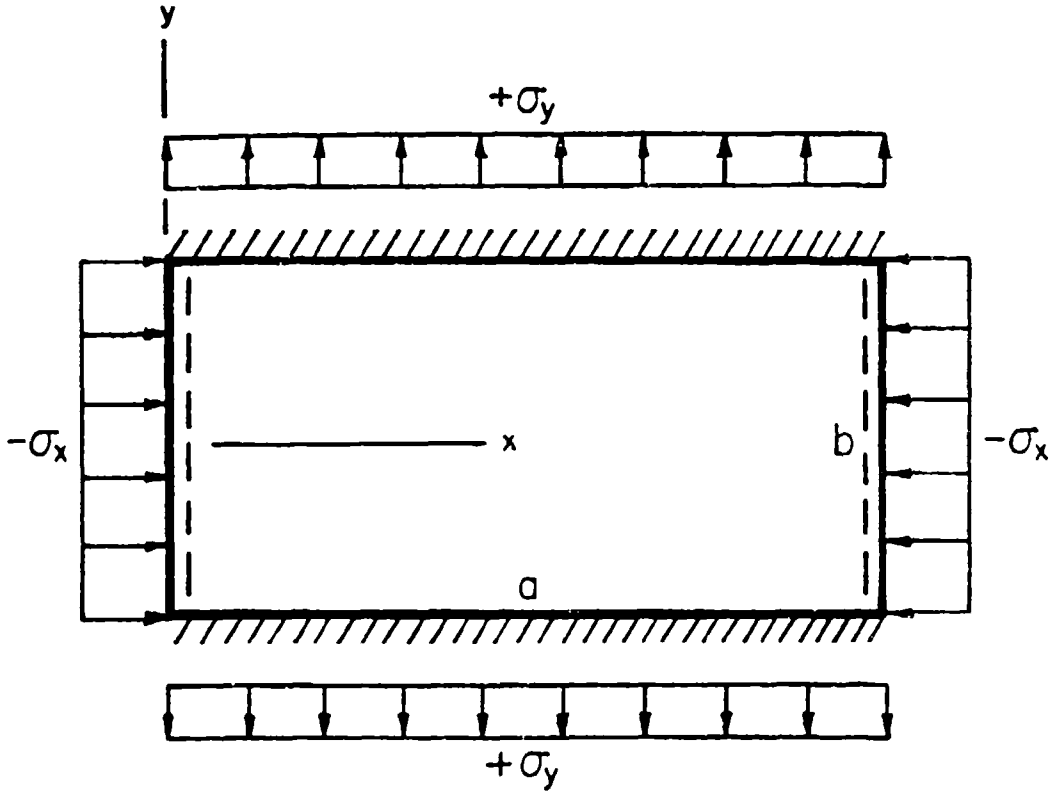

Figure 3.1. SCSC plate with uniform, biaxial stresses.

Expanding the determinants given by Equations 3.14 yields the characteristic equations:

Symmetric modes:
$$s_1 \tan \frac{s_1}{2} + \bar{s}_2 \tanh \frac{\bar{s}_2}{2} = 0 \qquad (3.15a)$$

Antisymmetric modes:
$$s_1 \tanh \frac{\bar{s}_2}{2} - \bar{s}_2 \tan \frac{s_1}{2} = 0 \qquad (3.15b)$$

The roots of these equations are the eigenvalues (nondimensional buckling stresses) K_x obtained by using Equations 3.4 and 3.7 (with $\bar{s}_2^2 = -s_2^2$).

One procedure frequently followed in the literature does not take advantage of the symmetries of the buckling modes (cf., [14,17]). If, for example, one uses a general solution for the displacement which is a superposition of Equations 3.13a and 3.13b, and applies clamped boundary conditions at $y = 0$ and $y = b$, one obtains a fourth order characteristic determinant, instead of the two second order determinants given by Equations 3.14. Expanding this determinant yields the characteristic equation

$$\sin s_1 \sinh \bar{s}_2 = \frac{2 s_1 \bar{s}_2}{\bar{s}_2^2 - s_1^2} (\cos s_1 \cosh \bar{s}_2 - 1) \qquad (3.16a)$$

Equation 3.16a may be factored into Equations 3.15a and 3.15b. It may also be written as:

$$(\cos s_1 - \cosh \bar{s}_2)^2 + (\sin s_1 - \frac{s_1}{\bar{s}_2} \sinh \bar{s}_2)(\sin s_1 + \frac{\bar{s}_2}{s_1} \sinh \bar{s}_2) = 0 \qquad (3.16b)$$

Wittrick [57] showed if the ratio σ_y/σ_x is sufficiently small, as given by the inequality (2.28), Equation 3.3 is analogous to that of an isotropic plate loaded in the same manner, and the results for SCSC isotropic plates may therefore be applied to orthotropic plates. He thus reasoned that if the parameter k is plotted versus λ, as defined in Equations 2.30 and 2.31, respectively, all results can be exhibited

by a single curve. This is shown as curve (b) of Figure 3.2, which corresponds to the ends x = 0,a being clamped and the sides y = 0,b being simply supported, with σ_x = constant and $\sigma_y = \tau_{xy} = 0$. For the case with the ends x = 0,a being simply supported and loaded, and the sides y = 0,b being clamped (i.e., as shown in Figure 3.1), but not loaded, Wittrick [57] presented curve (c) of Figure 3.2. However, for this case k is defined not by Equation 2.30, but by

$$k = \frac{\sigma_x h b^2}{\pi^2 \sqrt{D_{11} D_{22}}} + C \left[1 - \frac{2(D_{12}+2D_{66})}{\sqrt{D_{11} D_{22}}} \right] \tag{3.17}$$

with C = 2.4, and λ is defined by Equation 2.31 with σ_y set equal to zero.

Brunelle and Oyibo [58,59] solved the problem of the uniaxially loaded (σ_x = constant, $\sigma_y = \tau_{xy} = 0$) SCSC orthotropic plate, and expressed the buckling parameter

$$k_o = -\frac{\sigma_x h b^2}{\pi^2 \sqrt{D_{11} D_{22}}} \tag{3.18}$$

in terms of a reduced aspect ratio parameter and a single orthotropic stiffness parameter D*, as defined in Equation 2.53. This relationship is plotted in Figure 3.3.

Lekhnitskii [17] used the energy method to obtain an approximate, explicit formula for the critical buckling stress of a SCSC plate loaded by uniaxial stress along the two simply supported edges (σ_x constant, $\sigma_y = \tau_{xy} = 0$). Assuming a buckling mode shape

$$w = \left(1 - \cos \frac{2n\pi y}{b}\right) \sin \frac{m\pi x}{a} \qquad (m,n = 1,2\ldots) \tag{3.19}$$

results in the clamped boundary conditions at $y = \pm b/2$, as well as the

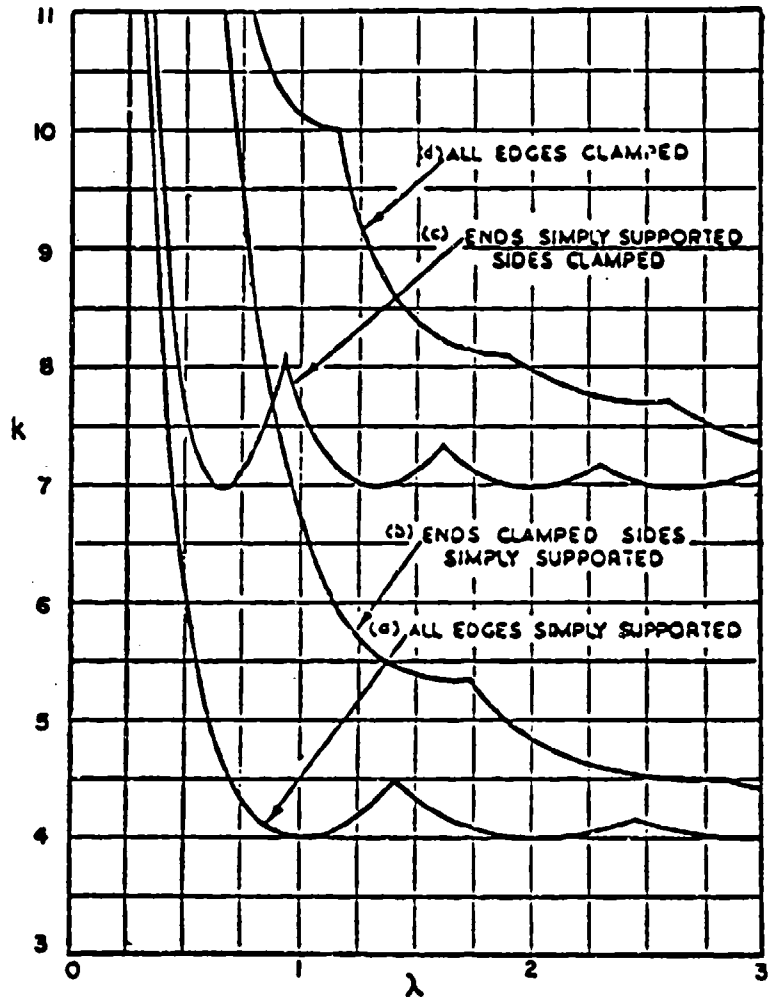

Figure 3.2. Single parameter buckling curves for uniaxial and biaxial loading, as determined by Wittrick

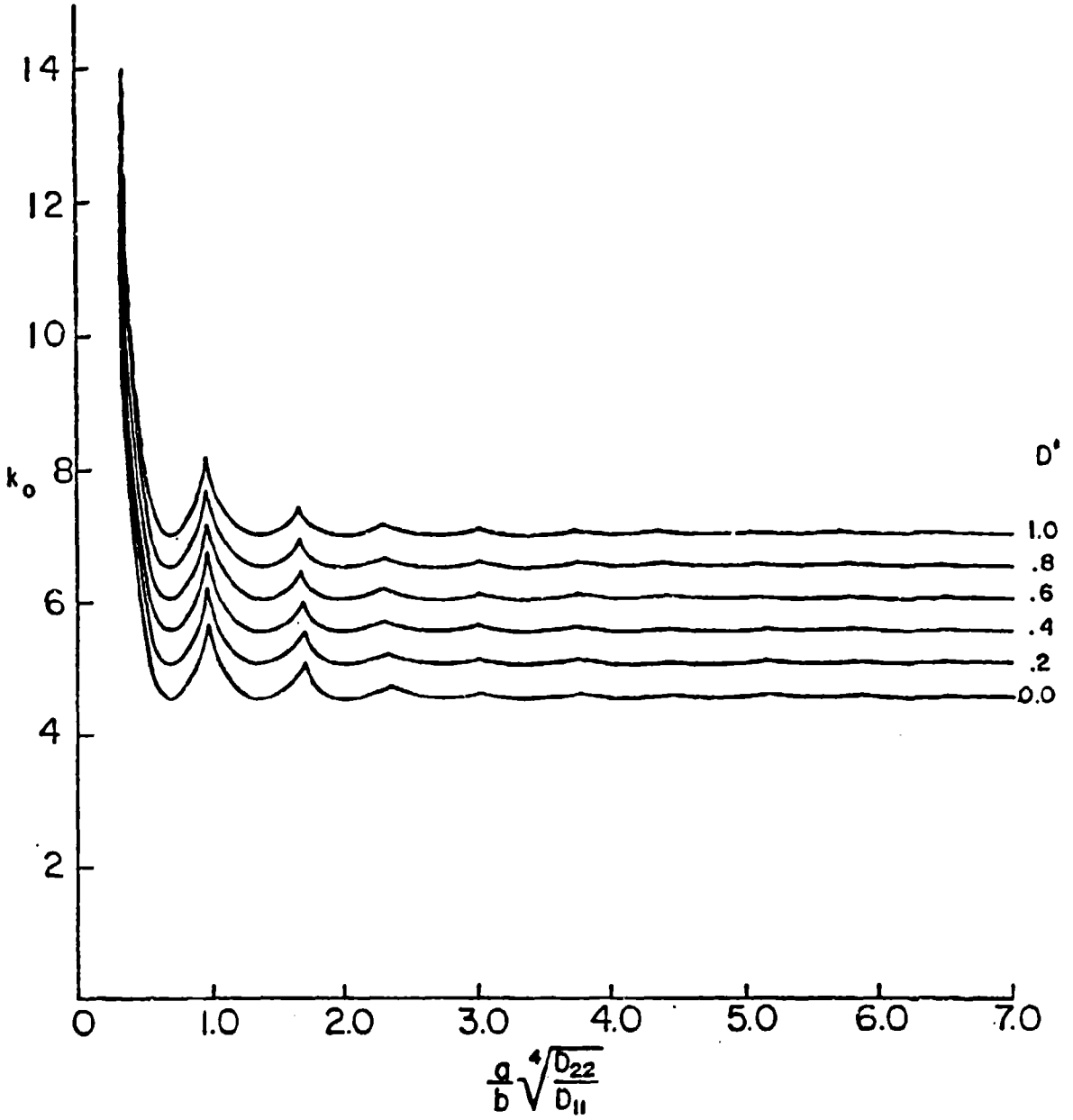

Figure 3.3. Uniaxial buckling parameters for SCSC orthotropic plates.

simply supported ones at x = 0,a, being satisfied exactly. Setting the work done by the external forces during the buckling displacements, $(-V_L)$, Equation 2.4, equal to the bending strain energy within the plate, Equation 2.3, yields

$$\sigma_x h = \frac{-\pi^2 D_{22}}{b^2}\left[\frac{C_1}{r^2} + \frac{8}{3} n^2 C_2 + \frac{16}{3} n^4 r^2\right] \tag{3.20}$$

where C_1, C_2 and r are given by Equations 2.16. Rewriting Equation 3.20 in terms of the nondimensional buckling parameter given in Equation 2.11, and recognizing that the critical buckling stress occurs for n = 1, one obtains

$$\frac{K_x}{\pi^2} = \frac{C_1}{r^2} + \frac{8}{3} C_2 + \frac{16}{3} r^2 \tag{3.21}$$

This form is similar to the exact solution presented earlier in Equation 2.15 for the SSSS plate. Differentiating Equation 3.21 with respect to r, and setting it equal to zero, one finds that the minimum value of K_x occurs at

$$\frac{a}{b} = m\sqrt[4]{\frac{3}{16} C_1} \tag{3.22}$$

and that the corresponding minimum values are given by

$$\min \frac{K_x}{\pi^2} = \frac{8}{\sqrt{3}}\sqrt{C_1} + \frac{8}{3} C_2 \tag{3.23}$$

Comparing Equations 3.22 and 3.23 with Equations 2.17 and 2.18 one observes that for the SCSC plate, not only are the minimum values of K_x greater, as expected, but that compared with the SSSS plate, they occur more frequently as a/b is increased. Further, the values of a/b at the transition points where the buckling load is the same for mode shapes having either m or m + 1 half-waves in the x-direction are given by

$$\frac{a}{b} = m(m+1)\sqrt[4]{\frac{3}{16}\,C_1} \tag{3.24}$$

which may be compared with Equation 2.19. The same result was obtained by Brukva [82] by means of the Galerkin method.

For a long isotropic plate ($a/b \to \infty$, $C_1 = C_2 = 1$) the approximate value of K_x/π^2 is found from Equation 3.21 to be 7.29, an error of approximately 4 per cent when compared to the exact value of 7 obtained from Equations 3.15 or 3.16 [17].

The case when the loaded edges ($x = 0,a$) are clamped and the unloaded loaded ones ($y = 0,b$) are simply supported (σ_x = constant, $\sigma_y = \tau_{xy} = 0$) was also treated by Brukva [82]. He used the Galerkin method along with the displacement function

$$w = \left(\cos\frac{m-1}{a}\pi x - \cos\frac{m+1}{a}\pi x\right)\sin\frac{\pi y}{b} \tag{3.25}$$

to determine the approximate buckling parameter for $m = 1$ (one half-wave) to be

$$\frac{K_x}{\pi^2} = 4C_1\left(\frac{b}{a}\right)^2 + 2C_2 + 0.75\left(\frac{a}{b}\right)^2 \tag{3.26}$$

whereas, for $m = 2,3,\ldots$

$$\frac{K_x}{\pi^2} = \frac{(m-1)^4+(m+1)^4}{(m-1)^2+(m+1)^2}\left(\frac{b}{a}\right)^2 C_1 + 2C_2 + \frac{2}{(m-1)^2+(m+1)^2}\left(\frac{a}{b}\right)^2 \tag{3.27}$$

The transition from one to two half-waves in the critical mode shape occurs wher $a/b = 1.67\sqrt[4]{C_1}$. In general, the transition from m to m + 1 half-waves (for $m \neq 1$) occurs when

$$\frac{C_1(m^4 + 6m^2 + 1) + (a/b)^4}{m^2+1} = \frac{C_1\left[(m+1)^4 + 6(m+1)^2 + 1\right] + (a/b)^4}{(m+1)^2+1} \tag{3.28}$$

Thus, the transition from 2 to 3 half-waves occurs when $a/b = 2.72\sqrt[4]{C_1}$.

A large number of other researchers also analyzed the buckling of SCSC orthotropics loaded uniaxially along either the simply supported or clamped edges [32,37,46,55,57,58,59,72,83-93].

Buckling load parameters for SCSC plates loaded in shear (τ_{xy} = constant, $\sigma_x = \sigma_y = 0$) are shown in Figure 3.4 [83]. Here the load parameter k_s (see Equation 2.42b) is plotted versus the stiffness and aspect ratio parameters, $1/\theta$ and B, respectively (see Equation 2.42a) for the case when the edges x = 0,a are clamped and y = 0,b are simply supported. The results shown are valid for $a/b > 1$ (short edges clamped, long edges simply supported).

Garashchuk, Zamula and Prikazchikov [94] used finite differences to analyze the buckling of a SCSC plate load by a combination of inplane bending (see Equation 2.43) and uniform shear (τ_{xy} = constant). Numerical results were given for a particular plate having $a/b = 0.334$ and $D_1/D_2 = 154$.

3.3 SCSS

An SCSS plate is depicted in Figure 3.5. The boundary conditions are given by:

$$\text{Along } x = 0,a: \quad w = M_x = 0 \tag{3.29a}$$

$$\text{Along } y = 0: \quad w = \frac{\partial w}{\partial y} = 0 \tag{3.29b}$$

$$\text{Along } y = b: \quad w = M_y = 0 \tag{3.29c}$$

Equations 3.29a are exactly satisfied by Equation 3.2. Substituting Equation 3.11 into Equations 3.29b and 3.29c results in a fourth order

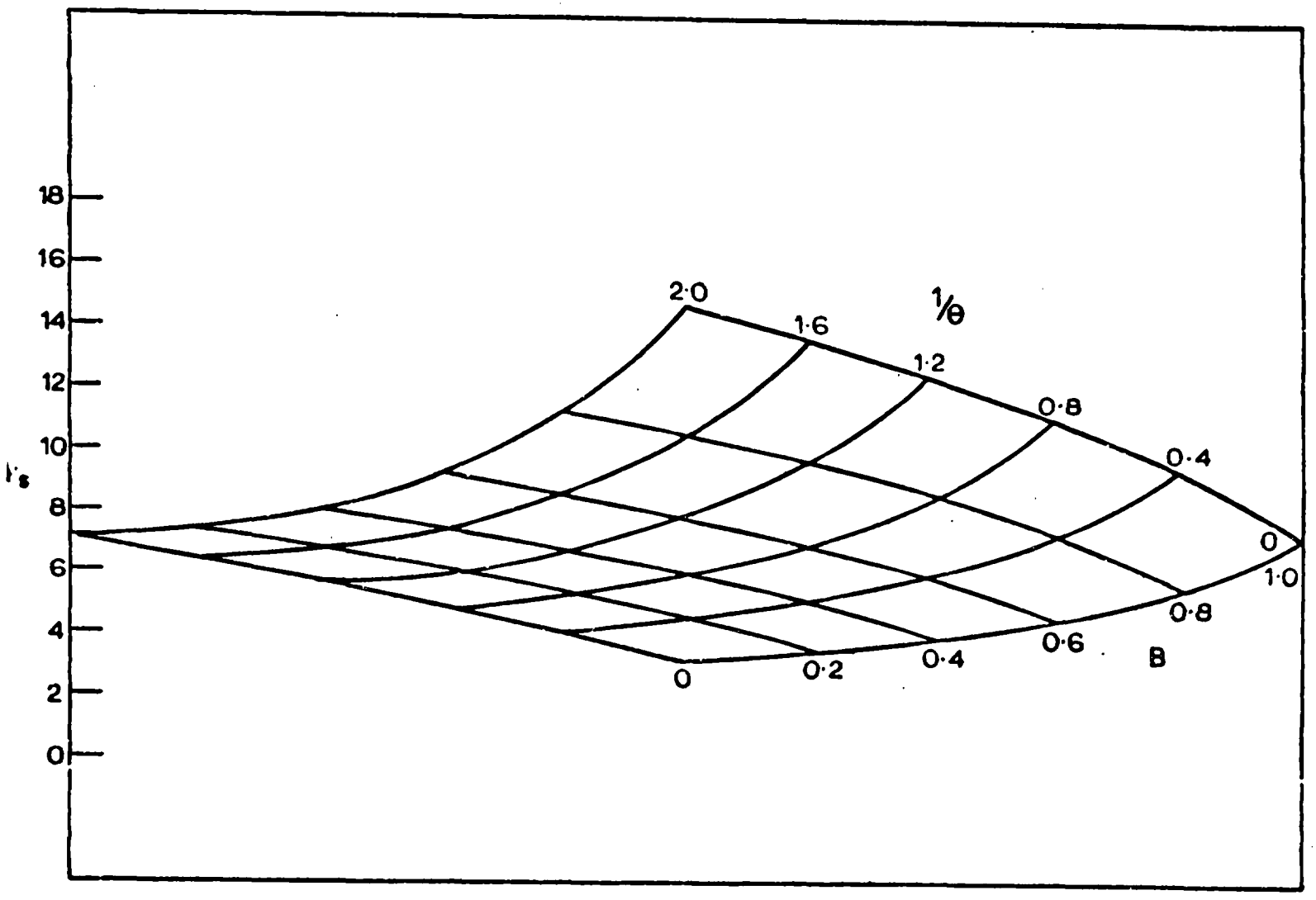

Figure 3.4. Buckling parameter k_s for CSCS plates loaded in shear.

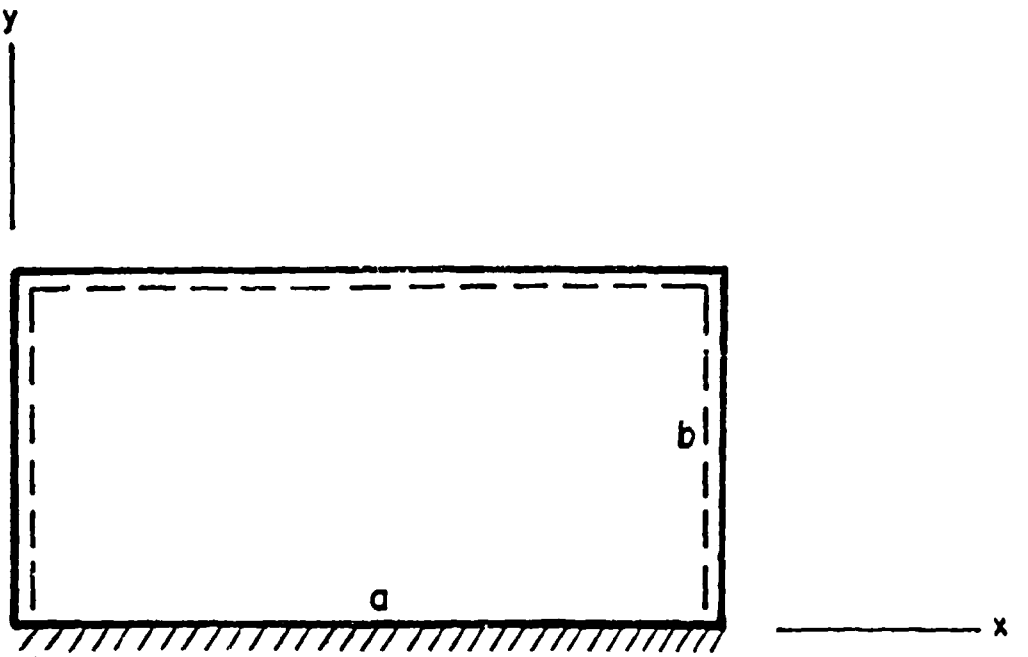

Figure 3.5. SCSS plate.

characteristic determinant which, when expanded, yields the characteristic equation [88]

$$\bar{s}_2 \tan s_1 = s_1 \tanh \bar{s}_2 \tag{3.30}$$

where s_1 and $\bar{s}_2$ are parameters which are functions of D_{11}/D_{22}, $(D_{12}+2D_{66})/D_{22}$, a/mb, σ_y/σ_x and the buckling parameter K_x, and are defined by Equations 3.4 and 3.7, with $\bar{s}_2^2 = -s_2^2$. It is also seen to be the same as Equation 3.15b for the antisymmetric buckling modes of an SCSC plate, for the antisymmetry conditions along the axis y = b/2 of an SCSC plate are identical to the simply supported boundary conditions for the SCSS plate. Finally, it may be observed that Equation 3.30 is the same form which arises for the free vibrations of an SCSS plate [95].

Brunelle and Oyibo [58,59] solved the problem of the uniaxially loaded (σ_x = constant, $\sigma_y = \tau_{xy} = 0$) SCSS orthotropic plate, and expressed the buckling parameter k_o (see Equation 3.18) in terms of a reduced aspect ratio parameter and a single orthotropic stiffness parameter and a single orthotropic stiffness parameter D* (see Equation 2.53). This relationship is plotted in Figure 3.6.

SCSS orthotropic plates having the loaded edges both simply supported (σ_x = constant, $\sigma_y = \tau_{xy} = 0$) were analyzed by Brukva [82]. The Galerkin method was used along with the displacement function

$$w = \sin \frac{m\pi x}{a} \sum_{n=1,2}^{N} A_n \left(\cos \frac{2n-1}{2b} \pi y - \cos \frac{2n+1}{2b} \pi y\right) \tag{3.31}$$

which satisfies simply supported conditions at x = 0,a and clamped conditions at y = 0,b exactly. A first approximation obtained by taking only one term of the summation (i.e., N = 1) yielded for the buckling parameter K_x (see (Equation 2.11):

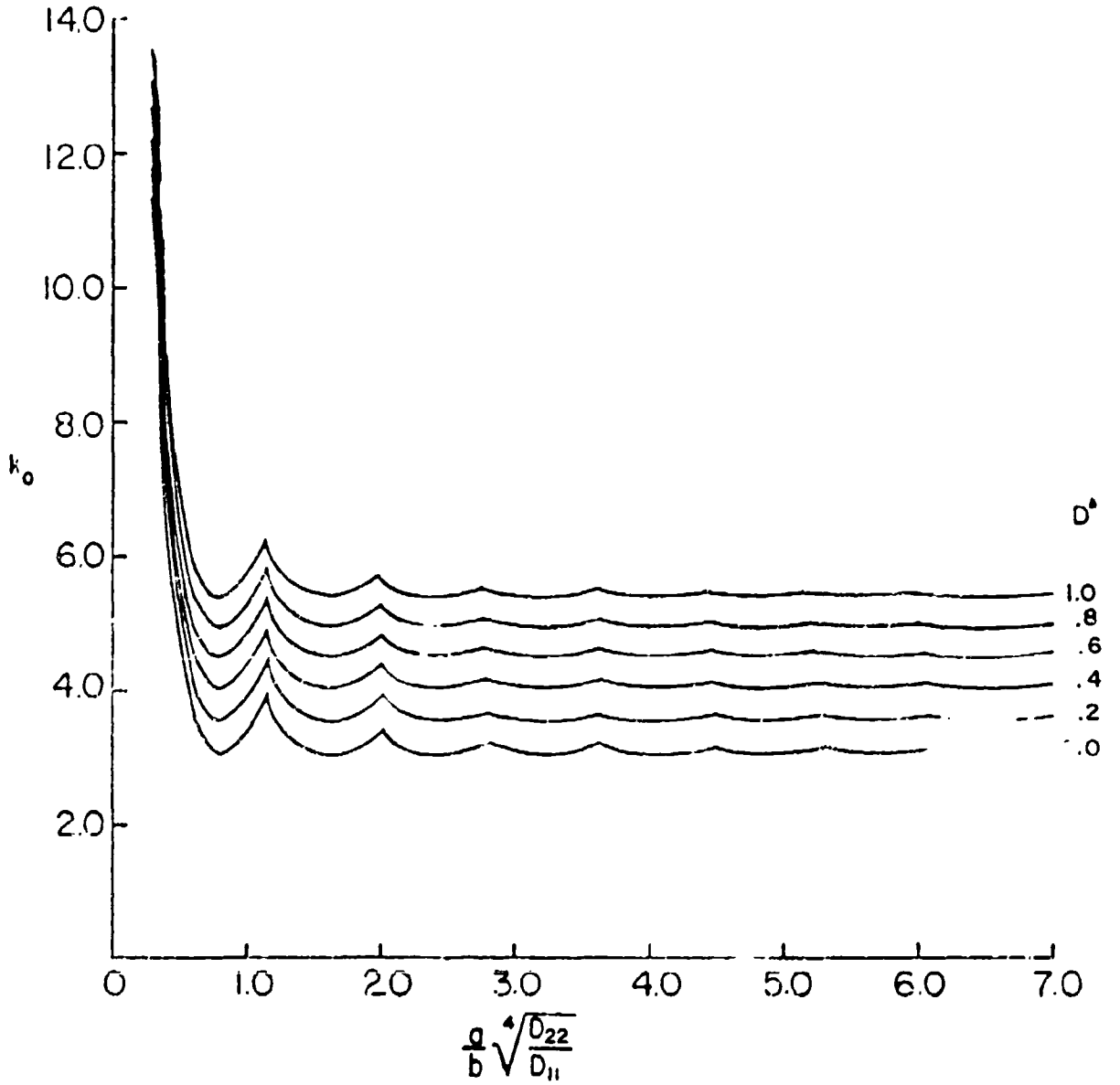

Figure 3.6. Uniaxial buck ing parameters for SCSS orthotropic plates.

$$\frac{K_x}{\pi^2} = \frac{C_1}{r^2} + 2.5\ C_2 + 2.56\ r^2 \tag{3.32}$$

It was determined that the minimum values of K_x occur at

$$\frac{a}{b} = 0.788\ m\sqrt[4]{C_1} \tag{3.33}$$

with corresponding values of K_x:

$$\min \frac{K_x}{\pi^2} = 3.2\sqrt{C_1} + 2.5\ C_2 \tag{3.34}$$

Transition points for buckling modes having m or m + 1 half-waves occur at

$$\frac{a}{b} = 0.788\sqrt{m(m+1)}\sqrt[4]{C_1}$$

The results described above may be compared with similar (but exact) expressions describing the buckling curves for an SSSS plate (see Section 2.1). An improved, second approximation was also obtained [82] by setting N = 2 in Equation 3.31. The Galerkin method then yields an eigenvalue determinant of second order.

The case when one of the loaded sides is clamped (x = 0) and the opposite one (x = a) is simply supported) (σ_x = constant, $\sigma_y = \tau_{xy} = 0$) was also treated by Brukva [82]. The Galerkin method was used along with the displacement function

$$w = \left(\cos\frac{2m-1}{2a}\pi x - \cos\frac{2m+1}{2a}\pi x\right)\sin\frac{\pi y}{b} \tag{3.35}$$

which determined the approximate buckling parameter to be (correcting a misprint):

$$\frac{K_x}{\pi^2} = 0.25\,\frac{(2m-1)^4+(2m+1)^4}{(2m-1)^2+(2m+1)^2}\left(\frac{b}{a}\right)^2 C_1 + 2C_2 + \frac{8}{(2m-1)^2+(2m+1)^2}\left(\frac{a}{b}\right)^2 \quad (3.36)$$

The ranges of aspect ratio having one or two half-waves in the critical mode shape were found to be:

$$\frac{a}{b} < 1.54\sqrt[4]{C_1} \quad , \text{ for } m = 1$$

$$1.54\sqrt[4]{C_1} < \frac{a}{b} < 2.50\sqrt[4]{C_1} \quad , \text{ for } m = 2$$

Shuleshko [96] also developed an approximate formula for determining the buckling loads of uniaxially loaded SCSS orthotropic plates. This problem was also studied by Soni and Amba Rao [90] and by Massey [97].

3.4. SCSF

As SCSF plate is depicted in Figure 3.7. The boundary conditions are given by:

Along $x = 0,a$: $\quad w = M_x = 0$ (3.37a)

Along $y = 0$: $\quad w = \frac{\partial w}{\partial y} = 0$ (3.37b)

Along $y = b$: $\quad M_y = V_y = 0$ (3.37c)

Equations 3.29a are exactly satisfied by Equation 3.2. Substituting Equation 3.11 into Equations 3.37b and 3.37c yields the characteristic determinant [80]

$$\left(\bar{s}_2^2\,\frac{B}{A} - s_1^2\,\frac{A}{B}\right)\sinh \bar{s}_2 \sin s_1 = s_1\bar{s}_2\left(\frac{B}{A} + \frac{A}{B}\right)\cosh \bar{s}_2 \cos s_1 + 2s_1\bar{s}_2 \quad (3.38)$$

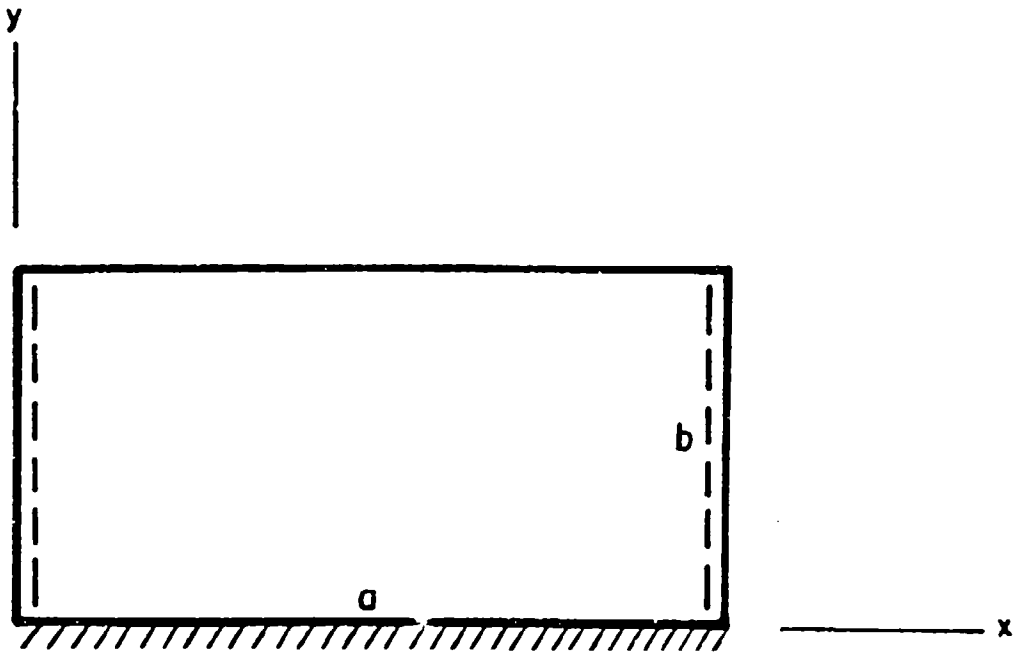

Figure 3.7. SCSF plate.

where $$A = \bar{s}_2^2 - \left(\frac{mb}{a}\right)^2 \frac{\pi^2 D_{11}}{D_{12}+2D_{66}} \nu_y \tag{3.39a}$$

$$B = s_1^2 + \left(\frac{mb}{a}\right)^2 \frac{\pi^2 D_{11}}{D_{12}+2D_{66}} \nu_y \tag{3.39b}$$

ν_y is Poisson's ratio of the contraction of the orthotropic plate in the y-direction due to σ_x, and s_1 and $\bar{s}_2$ are as used previously (see Sections 3.1 and 3.3).

Brunelle and Oyibo [58,59] solved the problem of the uniaxially loaded (σ_x = constant, $\sigma_y = \tau_{xy} = 0$) SCSF orthotropic plate, and expressed the buckling parameter k_o (see Equation 3.18) in terms of a reduced aspect ratio parameter and two orthotropic stiffness parameters, D^* and ε, where D^* is defined by Equation 2.53 and ε by

$$\varepsilon = \frac{D_{12}}{D_{12}+2D_{66}} \tag{3.40}$$

Plots of k_o are shown in Figures 3.8 and 3.9 for $\varepsilon = 0.2$ and 0.3, respectively.

This problem was also considered by Soni and Amba Rao [90] as part of a free vibration analysis of uniaxially loaded SCSF plates in the special case when the frequency becomes zero.

3.5. SSSF

An SSSF plate is depicted in Figure 3.10. The boundary conditions along the edges x = 0,a are satisfied exactly by Equation 3.2. The remaining conditions are:

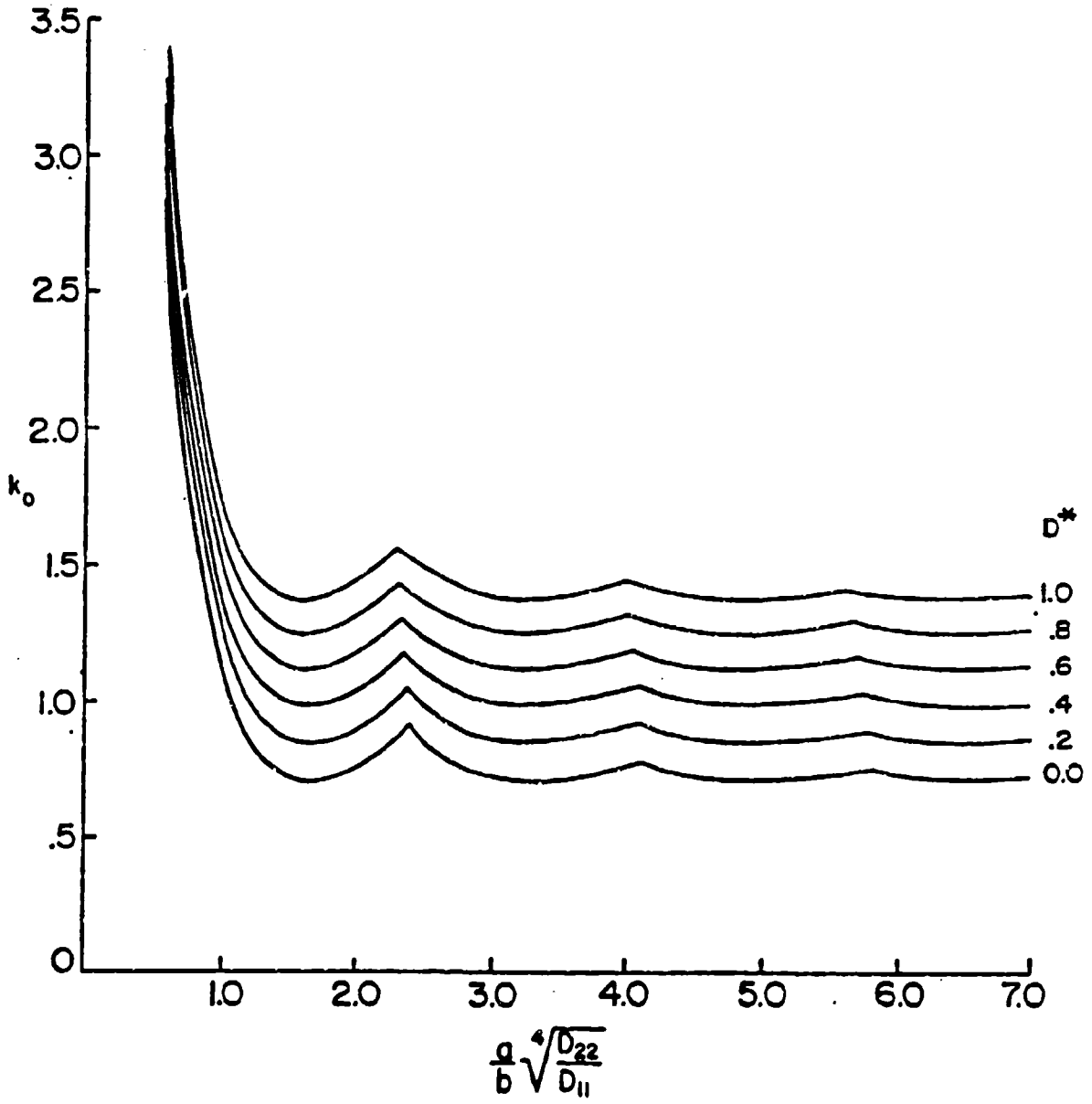

Figure 3.8. Uniaxial buckling parameters for SCSF orthotropic plates ($\varepsilon = 0.2$).

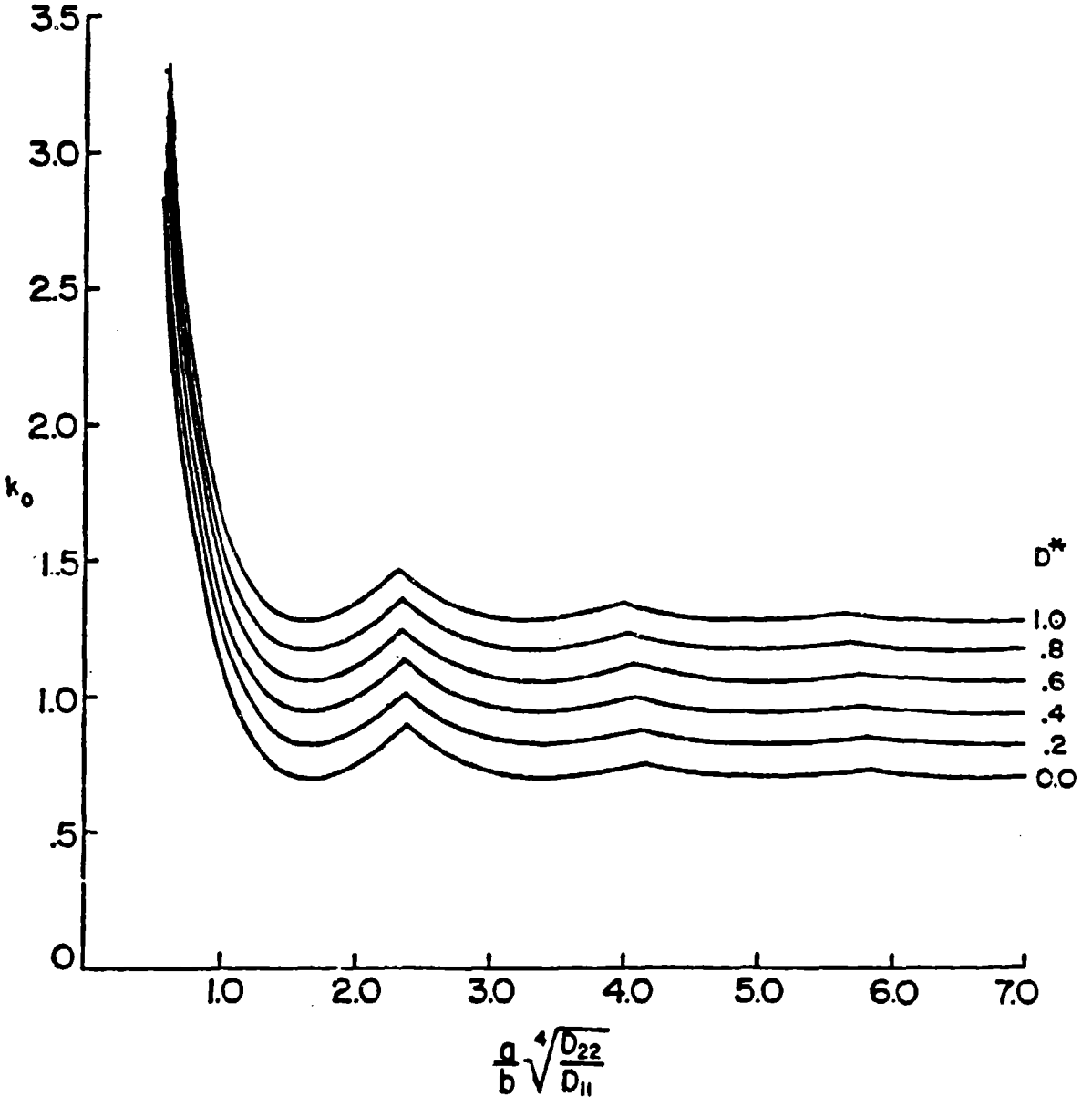

Figure 3.9. Uniaxial buckling parameters for SCSF orthotropic plates ($\varepsilon = 0.3$).

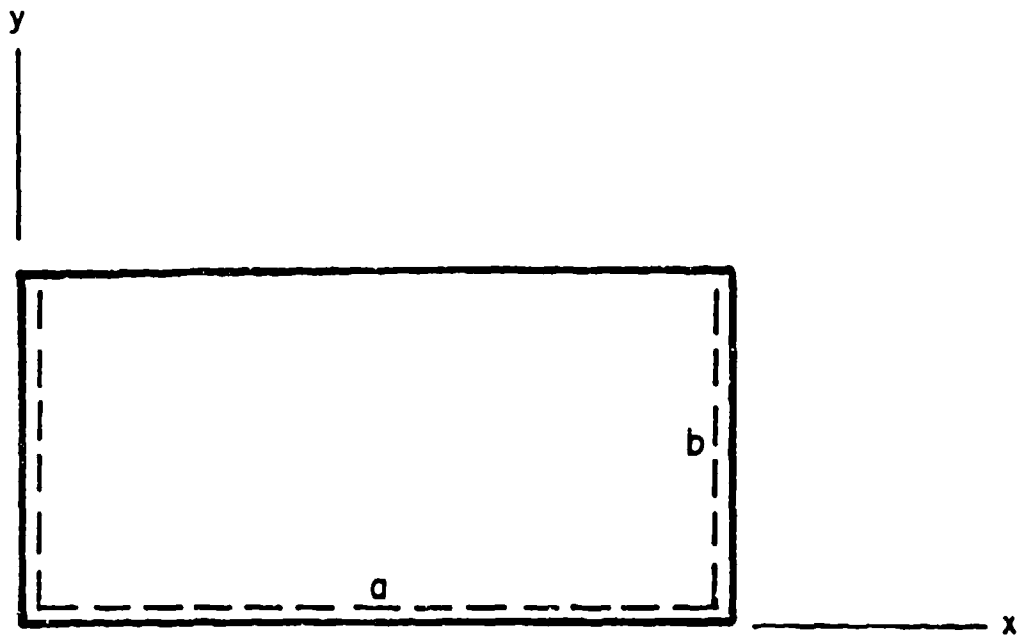

Figure 3.10. SSSF plate.

Along $y = 0$: $w = M_y = 0$ (3.41a)

Along $y = b$: $M_y = V_y = 0$ (3.41b)

Substituting Equation 3.11 into Equations 3.41a and 3.41b yields the characteristic equation [88]

$$\bar{s}_2 \frac{B}{A} \tan s_1 = s_1 \frac{A}{B} \tanh \bar{s}_2 \tag{3.42}$$

(see Section 3.4 for notation).

Brunelle and Oyibo [58,59] solved the problem of the uniaxially loaded (σ_x = constant, $\sigma_y = \tau_{xy} = 0$) SSSF orthotropic plate, and expressed the buckling parameter k_o (see Equation 3.18) in terms of a reduced aspect ratio parameter and two orthotropic stiffness parameters, D^* and ε (see Equations 2.53 and 3.40, respectively). Plots of k_o are shown in Figures 3.11 and 3.12 for $\varepsilon = 0.2$ and 0.3, respectively.

Holston [98] derived a special solution to Equation 3.1 for the case σ_x = constant, $\sigma_y = 0$ which is valid in the particular case when

$$K_x = -\frac{\sigma_x h b^2}{D_{22}} = \left(\frac{m\pi b}{a}\right)^2 \frac{D_{11}}{D_{22}} \tag{3.43}$$

It has a form containing constant and linear terms in y, as well as hyperbolic functions. He also used the energy method to develop an approximate formula for the buckling loads, and pointed out an error in two other relevant references [99,100].

This problem has also received some minor attention elsewhere [32,90].

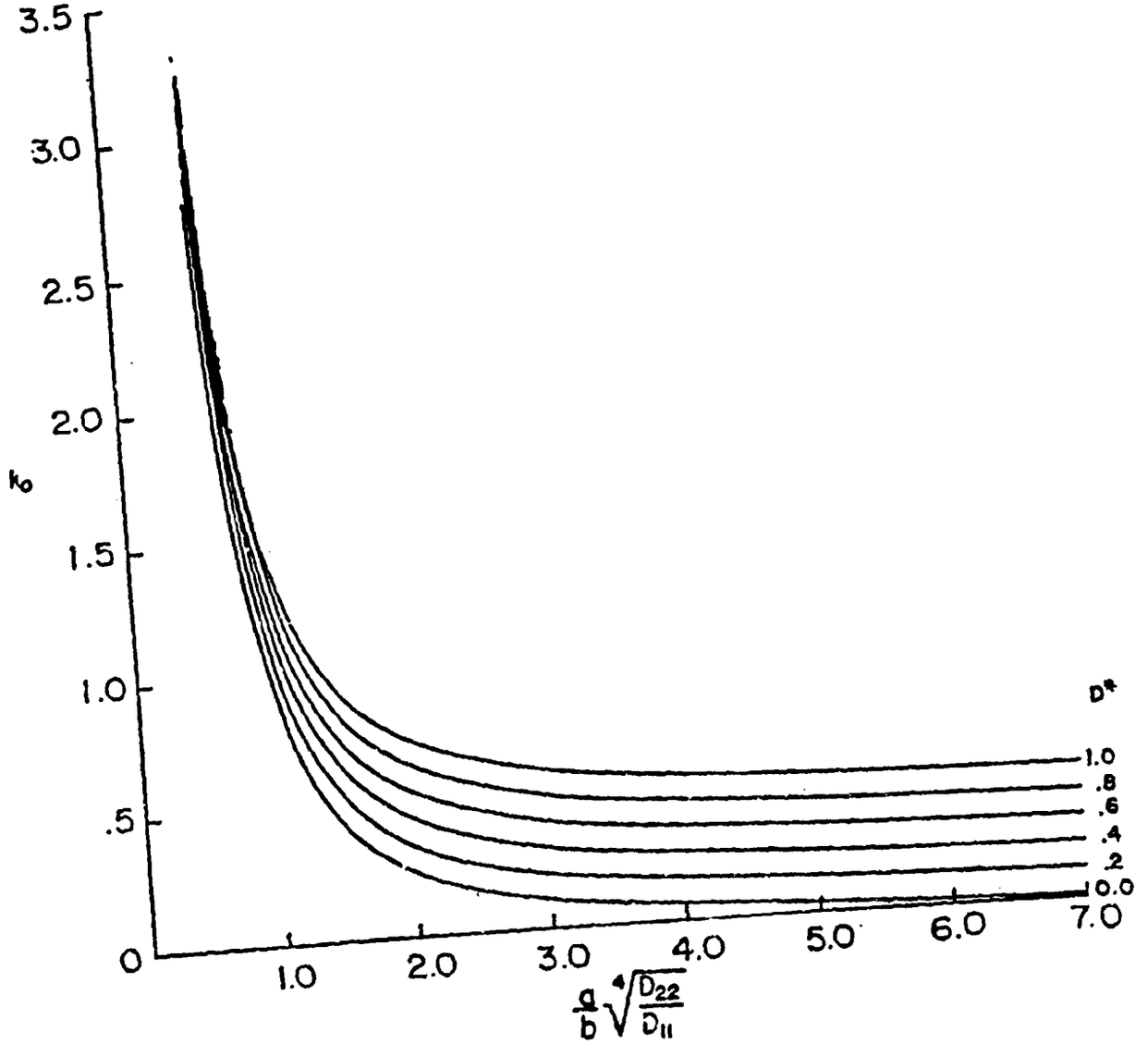

Figure 3.11. Uniaxial buckling parameters for SSSF orthotropic plates ($\varepsilon = 0.2$).

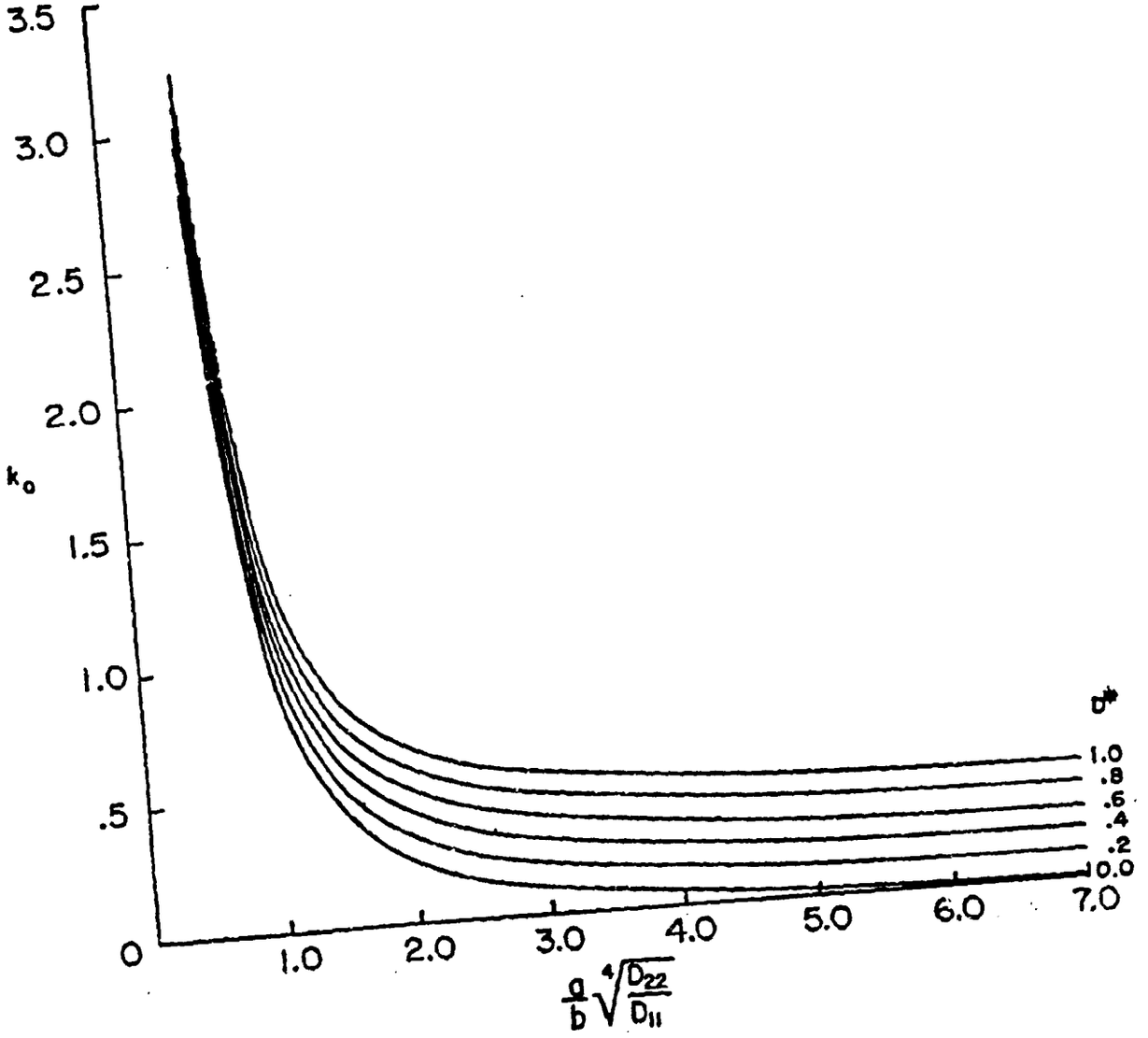

Figure 3.12. Uniaxial buckling parameters for SSSF orthotropic plates ($\varepsilon = 0.3$).

3.6. SFSF

An SFSF plate is depicted in Figure 3.13. The boundary conditions along the edges x = 0,a are satisfied exactly by Equation 3.2. The remaining conditions are:

$$\text{Along} \quad y = 0,b : \quad M_y = V_y = 0 \tag{3.44}$$

Substituting Equation 3.11 into Equations 3.44 yields a characteristic equation which may be factored into the following two equations, for symmetric and antisymmetric modes (with respect to y = b/2), respectively [88]:

$$s_1 A^2 \sin s_1 \cosh \bar{s}_2 = s_1 B^2 \sinh \bar{s}_2 \cos s_1 \tag{3.45a}$$

$$s_1 A^2 \cos s_1 \sinh \bar{s}_2 = s_1 B^2 \cosh \bar{s}_2 \sin s_1 \tag{3.45b}$$

(see Section 3.4 for notation). Equations 3.45 may also be derived by separating beforehand Equation 3.11 into its symmetric and antisymmetric components, as was done for SCSC plates in Section 3.2. Particular care must be taken in using Equations 3.45, for they are only valid for quite restricted ranges of σ_y/σ_x (see Section 3.1).

In Table 3.1 are listed the experimental buckling loads obtained by Mandell [34,35] for SFSF orthotropic plates having the simply supported edges subjected to uniaxial loading. The plates are those described previously in Section 2.2 (Tables 2.1-2.3). Theoretical results in all cases were calculated on the assumption that the plate bends as a simply supported <u>beam</u>; that is the buckling mode displacement was taken to be

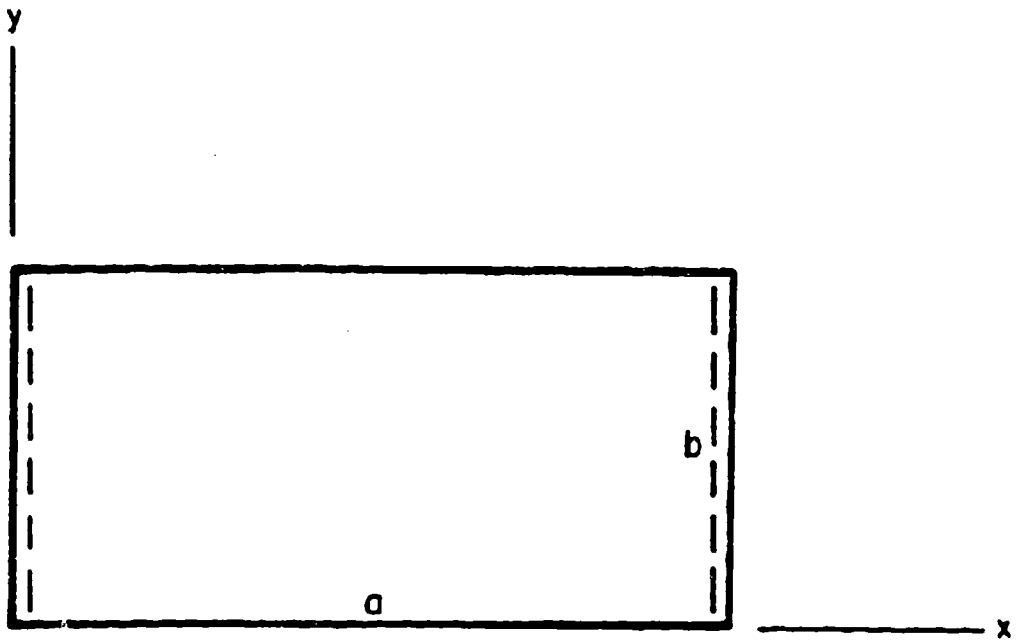

Figure 3.13. SFSF plate.

Table 3.1. Buckling loads ($-N_x$, lb/in) for Mandell's SFSF orthotropic plates

Plate no.	Experimental	Theoretical
201	11.3	12.5
202	84.9	105
204	10.8	12.7
205	2.74	3.83
206	5.26	6.92
207	0.848	1.29
404	199	215
"		216**
405	23.3	23.7
"		23.6**

** obtained by Ritz method

$$w = c_m \sin \frac{m\pi x}{a} \tag{3.46}$$

In this case the plate is assumed to have no transverse curvature or twist in the buckled mode, and the differential equation of equilibrium (2.1) reduces to

$$D_{11} \frac{\partial^4 w}{\partial x^4} = N \frac{\partial^2 w}{\partial x^2} \tag{3.47}$$

Substituting Equation 3.46 into 3.47 yields the critical load as

$$N_x = \sigma_x h = -\frac{\pi^2 D_{11}}{a^2} \tag{3.48}$$

which always occurs for m = 1. Results obtained using the Ritz method developed by Ashton [42] are also given for two plates in Table 3.1.

Viswanathan, Soong and Miller [93] tested a computer program designed for more general buckling analysis on plates 404 and 405 listed in Table 1. The program uses the exact solution procedure described at the beginning of this section, leading to Equations 3.45. Theoretical values of $-N_x$ of 206.5 and 22.6 were found, compared to the experimental values of 199 and 23.3, respectively, given in Table 3.1.

Baharlou [101] used the Ritz method with 25 algebraic polynomial terms to solve the problem of the uniaxially loaded SFSF plate having the following parameters: a/b = 1, $D_{11}/D_{22} = 10$, $(D_{12}+2D_{66})/D_{22} = 1$. This yielded $-N_x a^2/D_{11} = 0.9846\pi^2$, which is a close upper bound to the exact solution and which may be compared with the value of π^2 which is given in Equation 3.48 by beam theory.

3.7. Elastic Edge Constraints

Consider a plate with uniaxial loading (σ_x = constant, $\sigma_y = \tau_{xy} = 0$) having three sides simply supported, with the fourth side (y = b) elastically constrained against rotation (SSSE). Along y = b, the conditions to be satisfied are:

$$w = 0, \quad M_y = k_r \frac{\partial w}{\partial y} \tag{3.49}$$

where k_r is the rotational spring stiffness per unit length of edge. Following the same procedure described in the preceding sections, Shuleshko [88] showed that the following characteristic equation results:

$$(s_1^2 + \bar{s}_1^2) \sin s_1 \sinh \bar{s}_2 = \frac{4k_r b}{D_{22}} (s_1 \cos s_1 \sinh \bar{s}_2 - \bar{s}_2 \sin s_1 \cosh \bar{s}_2) \tag{3.50}$$

For the case of a uniaxially loaded plate having two sides (x = 0,a) simply supported, one (y = 0) free and the fourth (y = b) elastically restrained against rotation (SFSE), Shuleshko [88] derived the characteristic equation:

$$(s_1^2 + \bar{s}_2^2)\left(\bar{s}_2 \frac{B}{A} \sin s_1 \cosh \bar{s}_2 - s_1 \frac{A}{B} \sinh \bar{s}_2 \sin s_1\right) \tag{3.51}$$
$$= \frac{4k_r b}{D_{22}} \left[\left(\frac{A}{B} + \frac{B}{A}\right) s_1 \bar{s}_2 \cosh \bar{s}_2 \cos s_1 + 2 s_1 \bar{s}_2 - \left(\bar{s}_2^2 \frac{B}{A} - s_1^2 \frac{A}{B}\right) \sinh \bar{s}_2 \sin s_1\right]$$

(after changing the sign of the $2s_1\bar{s}_2$ term and adding a bracket to make the equation consistent with Equation 3.38).

The SCSE plate yields the characteristic equation [88]:

$$\frac{s_1^2+\bar{s}_2^2}{s_1\bar{s}_2}\left(s_1\cos s_1\sinh \bar{s}_2 - \bar{s}_2\sin s_1\cosh \bar{s}_2\right) \tag{3.52}$$

$$= \frac{4k_r b}{D}\left[\left(\cos s_1 - \cosh \bar{s}_2\right)^2 + \left(\sin s_1 - \frac{s_1}{\bar{s}_2}\sinh \bar{s}_2\right)\left(\sin s_1 + \frac{\bar{s}_2}{s_1}\sinh \bar{s}_2\right)\right]$$

The SESE plate subjected to uniaxial loading (σ_x = constant, $\sigma_y = \tau_{xy} = 0$) was studied by Libove [72]. The exact solution procedure described above was used to obtain the following formula for the buckling loads:

$$\frac{-\sigma_x hb^2}{\pi^2(D_{12}+2D_{66})} = \left(\frac{mb}{a}\right)^2\frac{D_{11}}{D_{12}+2D_{66}} + 2 + f_1 \tag{3.53}$$

where f_1 is a function of the spring stiffness parameter $k_r b/D_{22}$ and the parameter $(a/mb)^2 D_{22}/(D_{12}+2D_{66})$, and is plotted in Figure 3.14. Several others have also examined this problem [102-105].

Sakata [106] used the reduction method to analyze the buckling of continuous orthotropic rectangular plates having the edges x = 0,a simply supported, y = 0,b elastically supported with intermediate supports located at lines y = constant. Along the supports the condition w = 0 is prescribed. The problem is solved using exact solution functions given by Equations 3.2 and 3.11, with continuity of displacement, slope and moment enforced across the supports. Numerical buckling results for uniaxial and biaxial loading conditions were calculated for the case of SSSS edge conditions, with a/b = 0.5, $(D_{12}+2D_{66})/D_{22}$ = 0.25 and intermediate supports located at y = 0.3b and 0.7b (see Figure 3.15). These are displayed in Table 3.2, where the variation of K_x/π^2 (Equation 2.11) with $\sigma_y hb^2/\pi^2 D_{22}$ and D_{11}/D_{22} are seen. This problem was also dealt with by Nowacki [107].

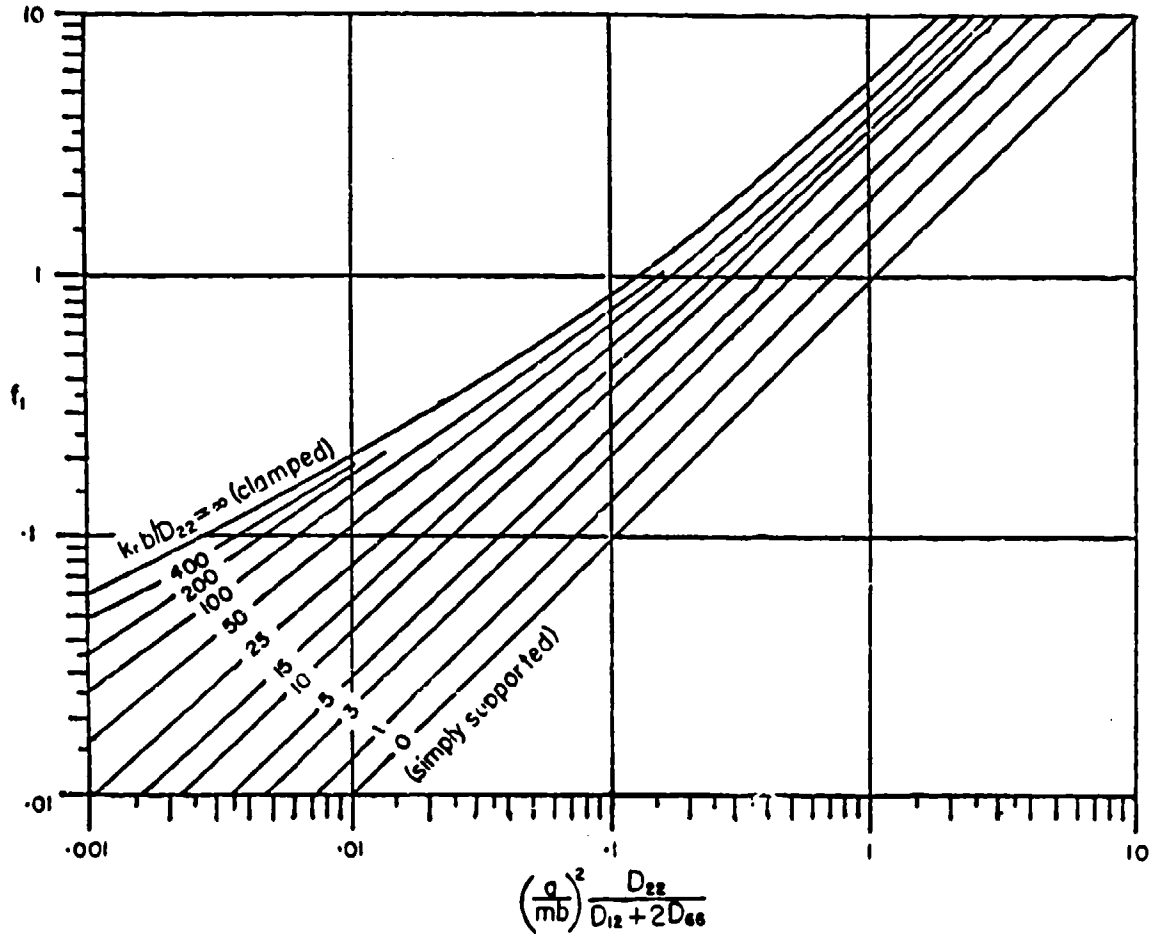

Figure 3.14. The function f_1 to be used in Equation 3.53 for the uniaxial buckling of SESE orthotropic plates.

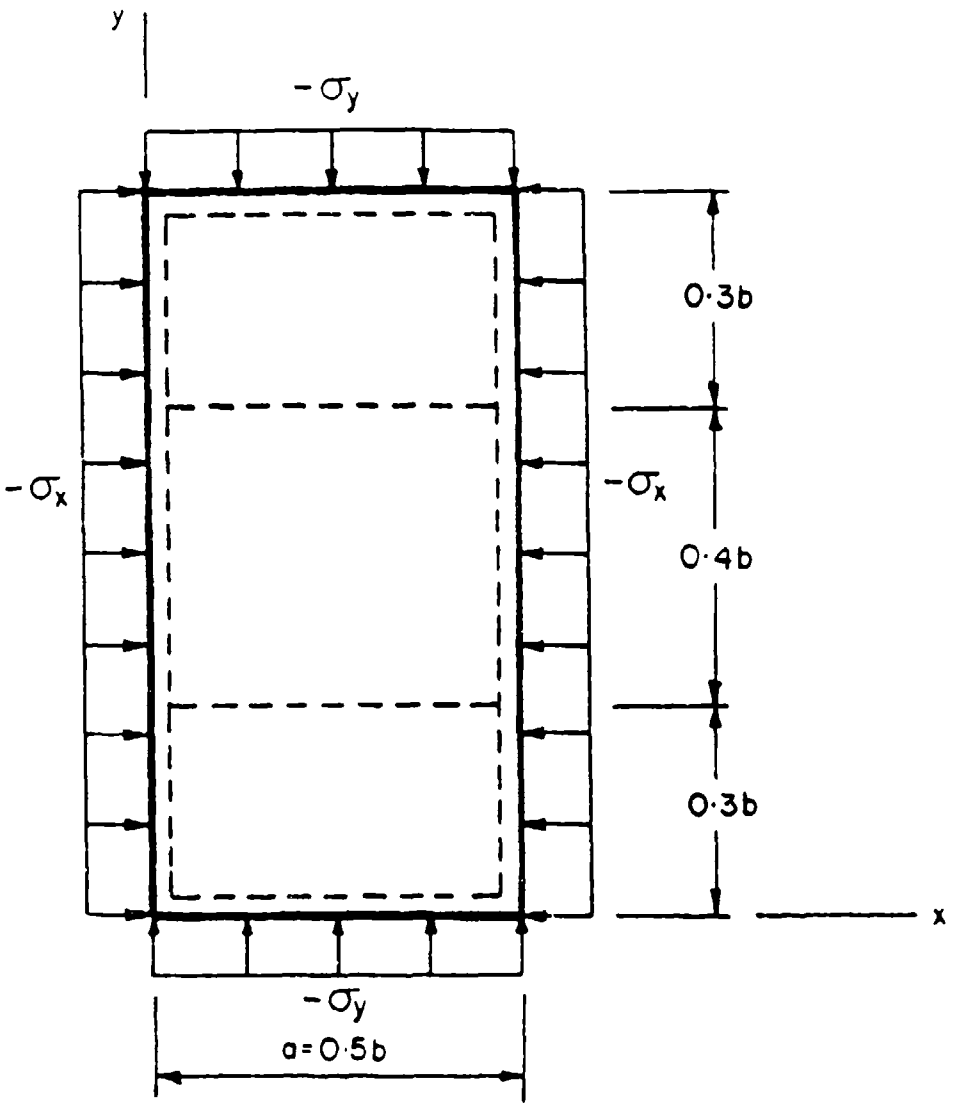

Figure 3.15. Continuous SSSS plate with intermediate supports at y = 0.3b and 0.7b; a/b = 0.5.

Table 3.2. Critical buckling parameters K_x/π^2 for an SSSS plate with intermediate supports (see Fig. 3.15).

$\frac{D_{11}}{D_{22}}$	$\sigma_y hb^2/\pi^2 D_{22}$		
	5	0	5
0.5	13.425	22.904	32.203
1.0	15.425	24.904	34.203
2.0	19.425	28.904	38.203

CHAPTER IV. ORTHOTROPIC PLATES - OTHER EDGE CONDITIONS

In the preceding two chapters, orthotropic plates having two opposite edges simply supported were considered, which were seen to include six possible combinations of classical boundary conditions, along with some additional cases where the remaining two edges were elastically supported. It was also seen that exact solutions for buckling problems were possible when the loading consisted of uniform normal stresses. The remaining classical problems may be represented by 15 distinct arrangements of edge conditions [108]. Following the identification system set forth in Chapter I, these may be listed as: CCCC, CCCS, CCCF, CCSS, CCSF, CCFF, CSCF, CSSF, CSFF, CFCF, CFSF, CFFF, SSFF, SFFF and FFFF. As will be seen below, the CCCC plate has received a great deal of attention, whereas relatively little has been done with the other cases. For none of these problems are exact theoretical solutions possible, even in the case of uniform normal buckling stresses, and approximate methods must be used.

Dickinson [109] generalized a method which was developed by Warburton [110] to determine the free vibration frequencies of isotropic rectangular plates having all 21 possible combinations of boundary conditions to orthotropic plates subjected to uniform inplane stresses. The method is a development of one first suggested by Rayleigh [111], whereby a reasonable mode shape is assumed and substituted into the proper energy functionals to determine the eigenvalue for the problem. In the case of buckling the total potential function is defined by Equations 2.2-2.4, and setting $V = 0$ determines the buckling load. The mode shapes are assumed to be the products of the eigenfunctions of vibrating beams; for example, for a CSCF plate, the products of CC and SF beam functions would be used. In addition to satisfying the boundary

conditions for the plate (although not exactly in the case of a free edge), the eigenfunctions are orthogonal over the plate dimensions, which reduces the numerical complexity of the calculations. The method has been demonstrated to be quite accurate for plate vibrations [112], but should be less accurate for plate buckling, for beam buckling mode shapes are somewhat different than beam vibration mode shapes (except when both ends are simply supported). Following the procedure described above, Dickinson [109] arrived at the following general formula for the determination of plate buckling loads:

$$\frac{K_x}{\pi^2}\left[J_x+\left(\frac{\sigma_y}{\sigma_x}\right)\left(\frac{a}{b}\right)^2 J_y\right] = G_x\left(\frac{b}{a}\right)^2\left(\frac{D_{11}}{D_{22}}\right)+ G_y\left(\frac{a}{b}\right)^2 + \frac{2(D_{12}+2D_{66})}{D_{22}} H_x H_y + 4\frac{D_{66}}{D_{22}}(J_x J_y - H_x H_y) \tag{4.1}$$

where K_x is defined by Equation 2.11, G_x, H_x and J_x are functions determined from Table 4.1 according to the conditions at $x = 0$ and $x = a$, and G_y, H_y and J_y are obtained by replacing x and y and m by n in Table 4.1. The integers m (and n) used in Table 4.1 are <u>not</u> the half-wave numbers used in previous chapters, but rather the number of nodal lines, including clamped or supported edges, perpendicular to x (or y). If m-1 in Table 4.1 is replaced by m (and n-1 by n) then, in the case of SSSS boundary conditions, Equation 4.1 agrees exactly with Equation 2.24 for the buckling due to biaxial loading.

Figure 4.1 (taken from [8]) is a useful set of curves governing the buckling of <u>isotropic</u> plates which are uniaxially loaded, and have the loaded edges either clamped or simply supported. The other two edges are either CC, CS, CF, SS and SF (i.e., all combinations except FF). Variation of the buckling parameter K_x/π^2 (see Equation 2.11) with a/b is seen, along with the number of longitudinal half-waves in the

Table 4.1. Coefficients in Equations 4.1 for buckling loads of plates with arbitrary boundary conditions.

Boundary conditions at—	m	G_s	H_s	J_s
SS[a], SS[b]	2, 3, 4, . . .	$m-1$	$(m-1)^2$	$(m-1)^2$
C[a], C[b]	2	1.506	1.248	1.248
C[a], C[b]	3, 4, 5, . . .	$m-\frac{1}{2}$	$\left(m-\frac{1}{2}\right)^2\left[1-\frac{2}{\left(m-\frac{1}{2}\right)\pi}\right]$	$\left(m-\frac{1}{2}\right)^2\left[1-\frac{2}{\left(m-\frac{1}{2}\right)\pi}\right]$
F[a], F[b]	0	0	0	0
	1	0	0	$12/\pi^2$
	2	1.506	1.248	5.017
F[a], F[b]	3, 4, 5, . . .	$m-\frac{1}{2}$	$\left(m-\frac{1}{2}\right)^2\left[1-\frac{2}{\left(m-\frac{1}{2}\right)\pi}\right]$	$\left(m-\frac{1}{2}\right)^2\left[1+\frac{6}{\left(m-\frac{1}{2}\right)\pi}\right]$
C[a], SS[b]	2, 3, 4, . . .	$m-\frac{3}{4}$	$\left(m-\frac{3}{4}\right)^2\left[1-\frac{1}{\left(m-\frac{3}{4}\right)\pi}\right]$	$\left(m-\frac{3}{4}\right)^2\left[1-\frac{1}{\left(m-\frac{3}{4}\right)\pi}\right]$
F[a], SS[b]	1	0	0	$5/\pi^2$
F[a], SS[b]	2, 3, 4, . . .	$m-\frac{3}{4}$	$\left(m-\frac{3}{4}\right)^2\left[1-\frac{1}{\left(m-\frac{3}{4}\right)\pi}\right]$	$\left(m-\frac{3}{4}\right)^2\left[1+\frac{3}{\left(m-\frac{3}{4}\right)\pi}\right]$
C[a], F[b]	1	0.597	−0.0870	0.471
	2	1.494	1.347	3.284
F[a], F[b]	3, 4, 5, . . .	$m-\frac{1}{2}$	$\left(m-\frac{1}{2}\right)^2\left[1-\frac{2}{\left(m-\frac{1}{2}\right)\pi}\right]$	$\left(m-\frac{1}{2}\right)^2\left[1+\frac{2}{\left(m-\frac{1}{2}\right)\pi}\right]$

[a] $x=0$.
[b] $x=a$.

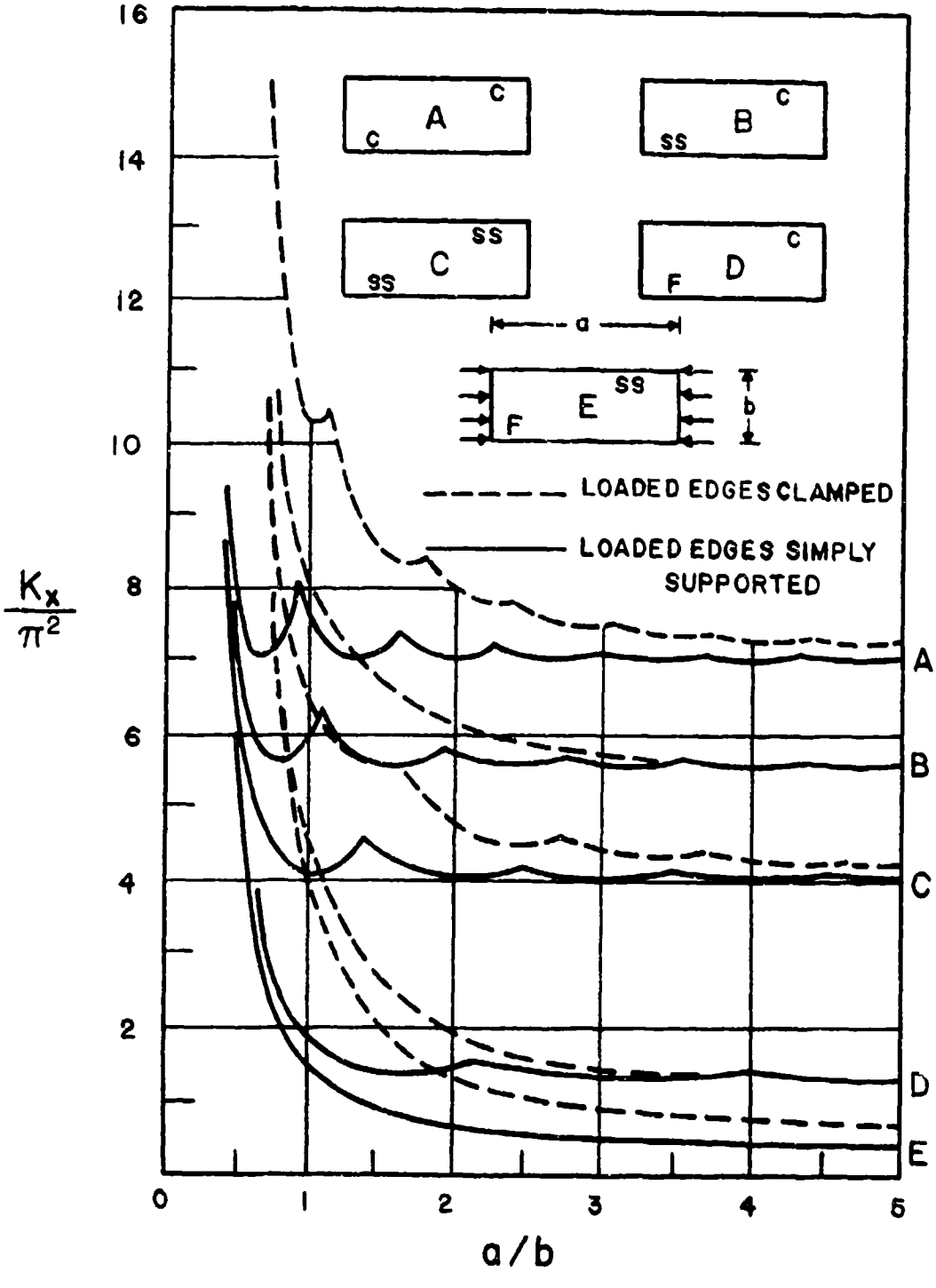

Figure 4.1. Buckling parameters for uniaxially loaded isotropic plates.

mode shape for each case. While the curves are only for a particular case of an orthotropic plate ($D_{11}/D_{22} = 1$, $(D_{12}+2D_{66})/D_{22} = 1$), they are useful in predicting trends in critical loads and mode shapes as boundary conditions are varied. The data shown previously in Figure 3.2 is consistent with Figure 4.1.

4.1. CCCC

Brunelle and Oyibo [58,59] solved the problem of the uniaxially loaded (σ_x = constant, $\sigma_y = \tau_{xy} = 0$) CCCC orthotropic plate, and expressed the buckling parameter k_o (see Equation 3.18) in terms of a reduced aspect ratio parameter and a single orthotropic stiffness parameter D* (see Equation 2.53). This relationship is plotted in Figure 4.2.

Wittrick [57] showed that the uniaxial buckling load for CCCC orthotropic plates can be determined from the single curve arising from isotropic plate analysis. This is shown as curve (d) in Figure 3.2. For this graph, k is defined by Equation 3.17, with C = 2.46, and λ is defined by Equation 2.31 with σ_y set equal to zero.

The uniaxially loaded CCCC plate was also analyzed by Brukva [82]. The Galerkin method was used along with the displacement function

$$w = \left(\cos\frac{m-1}{a}\pi x - \cos\frac{m+1}{a}\pi x\right)\left(1 - \cos\frac{2\pi y}{b}\right) \tag{4.2}$$

to determine approximate formulas for the buckling parameter K_x (see Equation 2.11). For one half-wave (m = 1) the value was found to be

$$\frac{K_x}{\pi^2} = 4\left(\frac{b}{a}\right)^2 C_1 + \frac{8}{3}C_2 + 4\left(\frac{a}{b}\right)^2 \tag{4.3}$$

whereas for m = 2,3,...

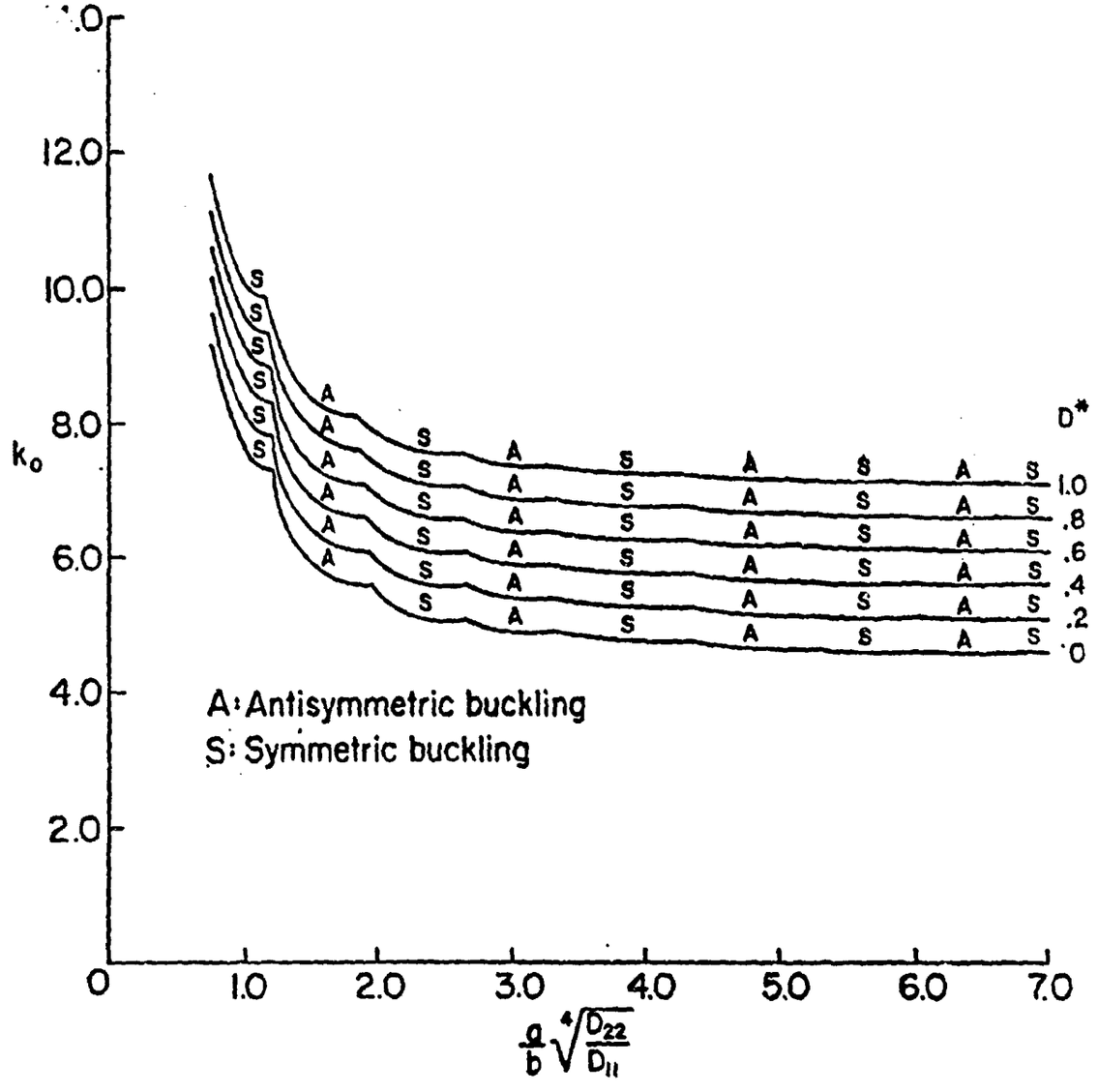

Figure 4.2. Uniaxial buckling parameters for CCCC orthotropic plates.

$$\frac{K_x}{\pi^2} = \frac{(m-1)^4+(m+1)^4}{(m-1)^2+(m+1)^2}\left(\frac{b}{a}\right)^2 C_1 + \frac{8}{3}C_2 + \frac{10.66}{(m-1)^2+(m+1)^2}\left(\frac{a}{b}\right)^2 \qquad (4.4)$$

The ranges of aspect ratio having one, two or three half-waves in the critical mode shape were found to be:

$$\frac{a}{b} < 1.11\sqrt[4]{C_1} \quad , \text{ for } m = 1$$

$$1.11\sqrt[4]{C_1} < \frac{a}{b} < 1.78\sqrt[4]{C_1} \quad , \text{ for } m = 2$$

$$1.78\sqrt[4]{C_1} < \frac{a}{b} < 2.48\sqrt[4]{C_1} \quad , \text{ for } m = 3$$

Baharlou [101] used the Ritz method with 25 algebraic polynomial terms to analyze CCCC orthotropic plates having the following parameters: $a/b = 1$, $C_1 = 10$, $C_2 = 1$ (see Equations 2.16). He obtained buckling parameters for uniaxial compression, biaxial hydrostatic ($\sigma_x = \sigma_y$) compression and uniform shear. These are seen in Table 4.2, where K_x and K_s are as given by Equations 2.11 and 2.35a, respectively. The values given are all close upper bounds to the exact solutions.

A number of other researchers have also investigated the buckling of uniaxially loaded, CCCC orthotropic plates [32,83,85,87,91,112-114].

Housner and Stein [68,69] used a finite difference energy method (see description in Section 2.3) to analyze the buckling of CCCC plates subjected to uniform shear stress. Numerical results for buckling parameters k_s are given in Table 4.3 for wide ranges of the aspect ratio and stiffness parameters B and θ, respectively, which are defined in Equations 2.40. These data are also plotted in Figure 4.3, and may be compared with results for SSSS plates given earlier in Table 2.6 and

Table 4.2. Buckling parameters for CCCC orthotropic square plates; $C_1=10$, $C_2=1$.

Uniaxial loading $\frac{K_x}{\pi^2}$	Hydrostatic loading $\frac{K_x}{\pi^2}$	Shear loading $\frac{K_s}{\pi^2}$
46.25	16.75	47.03

Table 4.3. Shear buckling parameters k_s for CCCC orthotropic plates (see Equations 2.40 for definitions).

θ	B	k_s	θ	B	k_s
0.2	1.0	32.56	1.25	1.0	13.87
	0.8	26.31		0.8	11.68
	0.6	22.21		0.6	10.46
	0.4	18.91		0.4	9.39
	0.2	17.34		0.2	8.80
	0.1	17.31		0.1	8.98
	0	17.13		0	8.45
0.4	1.0	21.63	1.667	1.0	12.91
	0.8	17.92		0.8	10.90
	0.6	15.43		0.6	9.80
	0.4	13.62		0.4	8.86
	0.2	12.64		0.2	8.34
	0.1	12.89		0.1	8.58
	0	12.51		0	7.93
0.6	1.0	17.86	2.5	1.0	11.93
	0.8	14.89		0.8	10.11
	0.6	13.06		0.6	9.07
	0.4	11.60		0.4	8.31
	0.2	10.64		0.2	7.84
	0.1	10.95		0.1	8.12
	0	10.69		0	7.32
0.8	1.0	15.94	5.0	1.0	10.94
	0.8	13.34		0.8	9.31
	0.6	11.84		0.6	8.33
	0.4	10.55		0.4	7.74
	0.2	9.99		0.2	7.33
	0.1	10.16		0.1	7.66
	0	9.63		0	6.72
1.0	1.0	14.81	∞	1.0	9.92
	0.8	12.44		0.8	8.48
	0.6	11.08		0.6	7.57
	0.4	9.89		0.4	6.97
	0.2	9.27		0.2	6.79
	0.1	9.11		0.1	7.17
	0	8.99		0	6.11

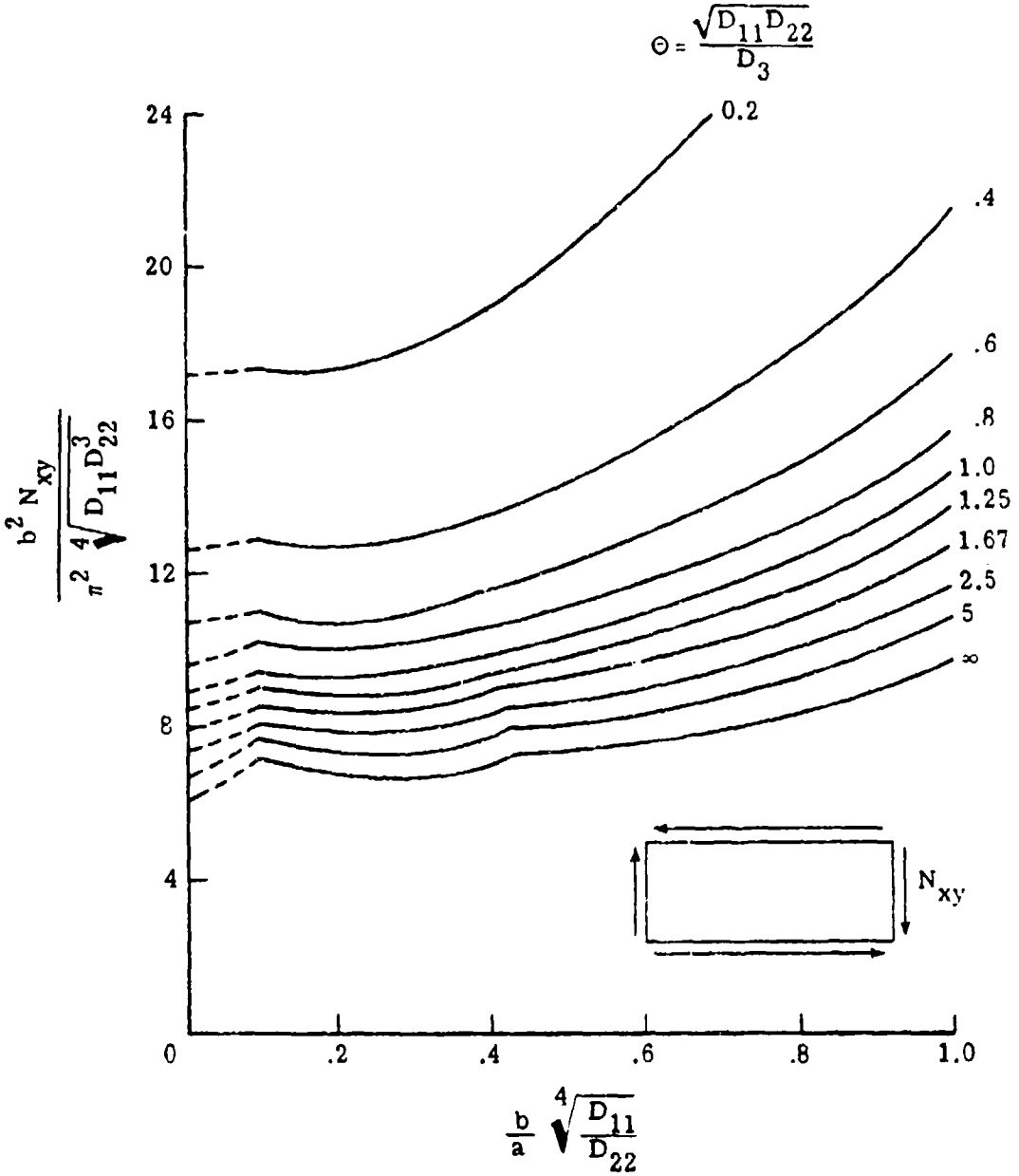

Figure 4.3. Shear buckling parameters for CCCC orthotropic plates.

Figure 2.8. It is seen that the critical mode shape changes occur more clearly for CCCC than for SSSS plates.

Another set of useful results for the CCCC plate loaded in shear was obtained by Smith [75]. This is shown in Figure 4.4. Here the load parameter k_s (see Equation 2.42b) is plotted versus the stiffness and aspect ratio parameters, $1/\theta$ and B, respectively (see Equations 2.42a). The case of shear loading was also studied by a few others [32, 72,115,116].

4.2. CCCS

CCCS orthotropic plates having the edges x = 0,a subjected to a uniaxial loading (σ_x = constant, $\sigma_y = \tau_{xy} = 0$) were analyzed by Brukva [82]. The Galerkin method was used along with the displacement function

$$w = \left(\cos\frac{m-1}{a}\pi x - \cos\frac{m+1}{a}\pi x\right)\left(\cos\frac{\pi y}{2b} - \cos\frac{3\pi y}{2b}\right) \tag{4.5}$$

An approximate value for the buckling parameter K_x (see Equation 2.11) was determined for m = 1 (one half-wave) to be

$$\frac{K_x}{\pi^2} = 4C_1\left(\frac{b}{a}\right)^2 + 2.5C_2 + 1.92\left(\frac{a}{b}\right)^2 \tag{4.6}$$

whereas for m = 2,3,...

$$\frac{K_x}{\pi^2} = \frac{(m-1)^4+(m+1)^4}{(m-1)^2+(m+1)^2}\left(\frac{b}{a}\right)^2 C_1 + 2.5\,C_2 + \frac{5.12}{(m-1)^2+(m+1)^2}\left(\frac{a}{b}\right)^2 \tag{4.7.}$$

The ranges of aspect ratio having one or two half-waves in the critical mode shape were found to be:

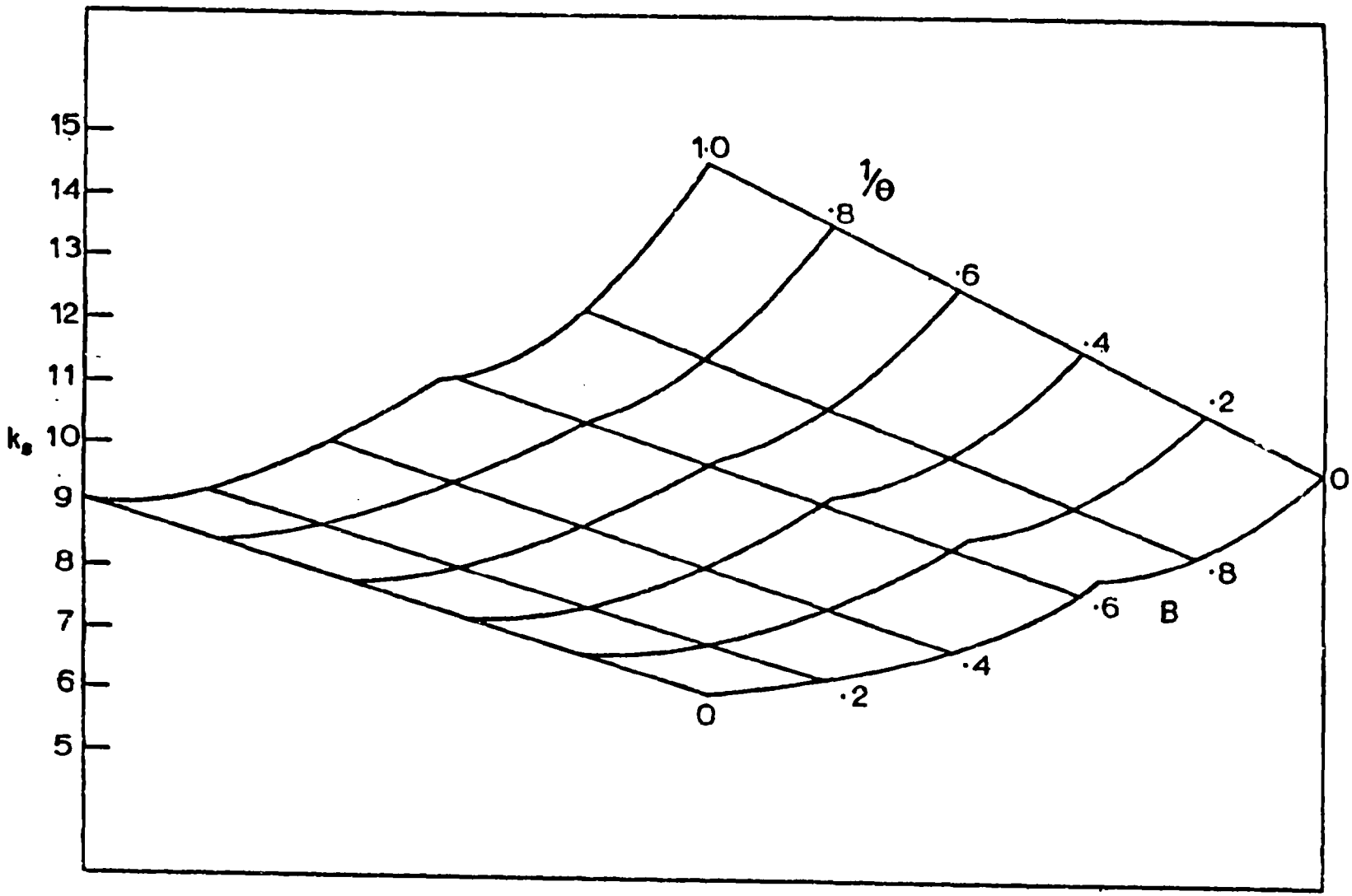

Figure 4.4. Buckling parameter k_s for CCCC plates loaded in shear.

$$\frac{a}{b} < 1.31\sqrt[4]{C_1} \quad , \text{ for } m = 1$$

$$1.31\sqrt[4]{C_1} < \frac{a}{b} < 2.15\sqrt[4]{C_1} \quad , \text{ for } m = 2$$

The same problem was also analyzed by Shuleshko [96] using the "reduction method" to obtain an approximate solution.

The case when the edge $x = a$ is simply supported, and the other edges are clamped (a CCSC plate) was also treated by Brukva [82]. In this case the displacement function

$$w = \left(\cos\frac{2m-1}{2a}\pi x - \cos\frac{2m+1}{2a}\pi x\right)\left(1 - \cos\frac{2\pi y}{b}\right) \tag{4.8}$$

was used. An approximate value of K_x was found to be:

$$\frac{K_x}{\pi^2} = 0.25\,\frac{(2m-1)^4+(2m+1)^4}{(2m-1)^2+(2m-1)^2}\left(\frac{b}{a}\right)^2 C_1 + 2.67\,C_2 + \frac{42.66}{(2m-1)^2+(2m+1)^2}\left(\frac{a}{b}\right)^2 \tag{4.9}$$

The ranges of aspect ratio having one or two half-waves in the critical mode shape were found to be:

$$\frac{a}{b} < 1.01\sqrt[4]{C_1} \quad , \text{ for } m = 1$$

$$1.01\sqrt[4]{C_1} < \frac{a}{b} < 1.64\sqrt[4]{C_1} \quad , \text{ for } m = 2$$

4.3. CCSS

CCSS orthotropic plates having the edges $x = 0,a$ subjected to uniaxial loading (σ_x = constant, $\sigma_y = \tau_{xy} = 0$) were analyzed by Brukva [82].

The Galerkin method was used along with the displacement function

$$w = \left(\cos \frac{2m-1}{2a}\pi x - \cos \frac{2m+1}{2a}\pi x\right)\left(\cos \frac{\pi y}{2b} - \cos \frac{3\pi y}{2b}\right) \qquad (4.10)$$

An approximate value for the buckling parameter K_x (see Equation 2.11) was determined to be:

$$\frac{K_x}{\pi^2} = 0.25\,\frac{(2m-1)^4+(2m+1)^4}{(2m-1)^2+(2m+1)^2}\left(\frac{b}{a}\right)^2 C_1 + 2.5\,C_2 + \frac{20.5}{(2m-1)^2+(2m+1)^2}\left(\frac{a}{b}\right)^2 \qquad (4.11)$$

The ranges of aspect ratio having one, two or three half-waves in the critical mode shape were found to be:

$$\frac{a}{b} < 1.21\sqrt[4]{C_1} \quad , \text{ for } m = 1$$

$$1.21\sqrt[4]{C_1} < \frac{a}{b} < 1.97\sqrt[4]{C_1} \quad , \text{ for } m = 2$$

$$1.97\sqrt[4]{C_1} < \frac{a}{b} < 2.76\sqrt[4]{C_1} \quad , \text{ for } m = 3$$

4.4. Other Edge Conditions

The case of the CFCF plate subjected to uniaxial compression along the clamped edges was examined by Viswanathan, Soong and Miller [92]. A set of experiments was conducted on 24 specimens made of combinations of titanium, adhesive and boron composite material. Theoretical values were obtained by taking results for the SFSF plate and multiplying by four (as in isotropic beam theory). Difficulty in experimentally achieving perfect clamping conditions also resulted in the use of a "modified length" between the clamped edges in an effort to achieve better correlation between experiment and theory.

Simitses and Giri [117] analyzed SSSS plates having rotational constraints along all four edges for uniaxial loading conditions (σ_x = constant, $\sigma_y = \tau_{xy} = 0$). Let the rotational spring stiffness per unit length along the edges x = 0,a be β_1, whereas along y = 0,b it is β_2 (corresponding to k_r in Equation 3.49). The modified Galerkin method (i.e., using additional line integrals the edges to account for the moment conditions not being exactly satisfied) was used, with transverse displacements assumed in the form

$$w(x,y) = a_m \sin\frac{m\pi x}{a} \sin\frac{\pi y}{b} + \sum_{i=0}^{\infty} b_i \left[\cos\frac{i\pi x}{a} - \cos\frac{(i+2)\pi x}{a}\right]\left(1 - \cos\frac{2\pi y}{b}\right) \tag{4.12}$$

The modes separated into symmetric and antisymmetric classes with respect to the x-direction, and numerical results were obtained [117] with third order determinants (i.e., two terms retained in the summation shown in Equation 4.12). Numerical results for the nondimensional buckling parameter $K_x(D_{11}/D_{22})/\pi^2$ (see Equation 2.11) are presented in Table 4.4 for plates having $G_{xy}/E_x = 0.4$, $\nu_{xy} = 0.7$, for various values of $E_x/E_y (= D_{11}/D_{22})$, a/b, $\beta_1 a/D_{11}$ and $\beta_2 a/D_{11}$. The plate stiffness ratio $2(D_{12}+2D_{66})/D_{11}$ is related to the elastic constants by

$$\frac{D_{12}+2D_{66}}{D_{11}} = \nu_{yx} + 2\frac{G_{xy}}{E_{xx}}\left(1 - \frac{E_{yy}}{E_{xx}}\nu_{xy}^2\right) \tag{4.13a}$$

$$E_{xx}\,\nu_{yx} = E_{yy}\,\nu_{xy} \tag{4.13b}$$

The numerical data given is aimed at application to folding cartons made of paperboard. The displacement functions used above were criticized by

Table 4.4. Buckling parameter $K_x(D_{11}/D_{22})\pi^2$ for uniaxially loaded SSSS orthotropic plates having rotational edge constraints. (G_{xy}/E_{xx}=0.4, ν_{xy}=0.7). Numbers in parentheses are numbers of half-waves in the x direction.

(a) $\beta_1 a/D_{11} = 0$

$\frac{D_{11}}{D_{22}}$	$\frac{a}{b}$	$\beta_2 a/D_{11}$				
		0	1	10	100	1000
4.0	0.5	5.816(1)	6.017(1)	7.629(1)	10.364(3)	15.466(3)
	1.0	3.004(1)	3.383(1)	5.286(1)	6.776(3)	7.259(3)
	1.5	2.761(1)	3.302(1)	4.739(2)	6.107(1)	6.207(1)
	2.0	3.004(1)	3.195(2)	4.203(2)	5.254(2)	5.428(2)
3.0	0.5	5.889(1)	6.089(1)	7.703(1)	10.558(3)	15.640(3)
	1.0	3.139(1)	3.520(1)	5.487(1)	7.247(3)	7.664(3)
	1.5	3.000(1)	3.550(1)	4.857(2)	6.444(2)	6.808(2)
	2.0	3.139(2)	3.331(2)	4.397(2)	5.626(2)	5.836(2)
2.0	0.5	6.033(1)	6.233(1)	7.850(1)	10.946(3)	15.990(3)
	1.0	3.408(1)	3.791(1)	5.875(1)	8.097(1)	8.460(1)
	1.5	3.477(1)	4.039(1)	5.088(2)	6.893(2)	7.333(2)
	2.0	3.408(1)	3.602(2)	4.763(2)	6.347(2)	6.630(2)
1.0	0.5	6.466(1)	6.666(1)	8.290(1)	12.113(3)	17.036(3)
	1.0	4.216(1)	4.605(1)	6.961(1)	10.139(1)	10.698(1)
	1.5	4.556(2)	4.704(2)	5.755(2)	8.189(2)	8.886(2)
	2.0	4.216(2)	4.413(2)	5.663(3)	7.619(3)	8.375(3)

Table 4.4. (Continued)

(b) $\beta_1 a/D_{11} = 1$

$\frac{D_{11}}{D_{22}}$	$\frac{a}{b}$	$\beta_2 a/D_{11}$				
		0	1	10	100	1000
4.0	0.5	7.299(1)	7.466(1)	8.812(1)	11.219(3)	15.622(3)
	1.0	3.383(1)	3.716(1)	5.399(1)	6.810(3)	7.259(3)
	1.5	2.935(1)	3.439(1)	4.822(2)	6.107(1)	6.207(1)
	2.0	3.102(2)	3.282(2)	4.235(2)	5.255(2)	5.428(2)
3.0	0.5	7.372(1)	7.539(1)	8.888(1)	11.412(3)	15.796(3)
	1.0	3.520(1)	3.856(1)	5.607(1)	7.277(3)	7.664(3)
	1.5	3.175(1)	3.692(1)	4.943(2)	6.448(2)	6.808(2)
	2.0	3.237(2)	3.419(2)	4.433(2)	5.627(2)	5.836(2)
2.0	0.5	7.518(1)	7.686(1)	9.039(1)	11.797(3)	16.144(3)
	1.0	3.791(1)	4.134(1)	6.010(1)	8.101(1)	10.698(1)
	1.5	3.653(1)	4.189(1)	5.180(2)	6.898(2)	7.333(2)
	2.0	3.237(1)	3.692(2)	4.806(2)	6.348(2)	6.630(2)
1.0	0.5	7.956(1)	8.124(1)	9.493(1)	12.951(3)	17.184(3)
	1.0	4.605(1)	4.961(1)	7.132(1)	10.145(1)	10.698(1)
	1.5	4.731(2)	4.871(2)	5.862(2)	8.197(2)	8.886(2)
	2.0	4.316(2)	4.507(2)	5.731(3)	7.627(3)	8.375(3)

Table 4.4. (Continued)

(c) $\beta_1 a/D_{11} = 10$

$\frac{D_{11}}{D_{22}}$	$\frac{a}{b}$	$\beta_2 a/D_{11}$				
		0	1	10	100	1000
4.0	0.5	13.580(1)	13.622(1)	13.969(1)	14.994(3)	16.554(3)
	1.0	5.286(1)	5.399(1)	6.058(1)	6.999(3)	7.264(3)
	1.5	4.057(1)	4.331(1)	5.346(2)	6.110(1)	6.207(1)
	2.0	3.766(2)	3.873(2)	4.472(2)	5.263(2)	5.428(2)
3.0	0.5	13.681(1)	13.722(1)	14.072(1)	15.172(3)	16.722(3)
	1.0	5.487(1)	5.607(1)	6.318(1)	7.417(1)	7.668(3)
	1.5	4.353(1)	4.657(1)	5.496(2)	6.484(2)	6.808(2)
	2.0	3.923(2)	4.037(2)	4.700(2)	5.637(2)	5.836(2)
2.0	0.5	13.880(1)	13.923(1)	14.278(1)	15.527(3)	17.057(3)
	1.0	5.875(1)	6.010(1)	6.823(1)	8.132(1)	8.460(1)
	1.5	4.913(1)	5.265(1)	5.788(2)	6.941(2)	7.334(2)
	2.0	4.227(2)	4.352(2)	5.128(2)	6.361(2)	6.630(2)
1.0	0.5	14.476(1)	14.520(1)	14.892(1)	16.590(3)	18.060(3)
	1.0	6.961(1)	7.132(1)	8.228(1)	10.194(1)	10.698(1)
	1.5	5.920(2)	6.003(2)	6.609(2)	8.264(2)	8.887(2)
	2.0	5.095(2)	5.243(2)	6.241(3)	7.691(3)	8.376(3)

Table 4.4. (Continued)

(d) $\beta_1 a/D_{11} = 100$

$\frac{D_{11}}{D_{22}}$	$\frac{a}{b}$	$\beta_2 a/D_{11}$				
		0	1	10	100	1000
4.0	0.5	17.913(1)	17.913(1)	17.921(1)	17.986(1)	18.105(3)
	1.0	7.028(1)	7.031(1)	7.054(1)	7.176(1)	7.292(3)
	1.5	5.845(1)	5.857(1)	5.938(1)	6.132(1)	6.207(1)
	2.0	5.077(2)	5.084(2)	5.134(2)	5.317(2)	5.429(2)
3.0	0.5	18.056(1)	18.057(1)	18.065(1)	18.130(1)	18.261(3)
	1.0	7.388(1)	7.391(1)	7.417(1)	7.552(1)	7.691(1)
	1.5	6.456(1)	6.470(1)	6.528(2)	6.656(2)	6.812(2)
	2.0	5.412(2)	5.420(2)	5.481(2)	5.702(2)	5.837(2)
2.0	0.5	18.343(1)	18.344(1)	18.352(1)	18.419(1)	18.572(3)
	1.0	8.097(1)	8.101(1)	8.132(1)	8.295(1)	8.464(1)
	1.5	6.964(2)	6.967(2)	6.994(2)	7.149(2)	7.339(2)
	2.0	6.055(2)	6.066(2)	6.149(2)	6.450(2)	6.632(2)
1.0	0.5	19.203(1)	19.204(1)	19.212(1)	19.284(1)	19.505(3)
	1.0	10.139(1)	10.145(1)	10.194(1)	10.446(1)	10.703(1)
	1.5	8.300(2)	8.305(2)	8.348(2)	8.593(2)	8.895(2)
	2.0	7.698(3)	7.704(3)	7.752(3)	8.030(3)	8.385(3)

Table 4.4. (Continued)

(e) $\beta_1 a/D_{11} = 1000$

$\frac{D_{11}}{D_{22}}$	$\frac{a}{b}$	$\beta_2 a/D_{11}$				
		0	1	10	100	1000
4.0	0.5	18.519(1)	18.519(1)	18.519(1)	18.520(1)	18.527(1)
	1.0	7.298(1)	7.298(1)	7.298(1)	7.301(1)	7.313(1)
	1.5	6.181(1)	6.181(1)	6.182(1)	6.190(1)	6.210(1)
	2.0	5.408(2)	5.408(2)	5.409(2)	5.415(2)	5.435(2)
3.0	0.5	18.670(1)	18.670(1)	18.670(1)	18.671(1)	18.678(1)
	1.0	7.688(1)	7.688(1)	7.688(1)	7.691(1)	7.705(1)
	1.5	6.814(1)	6.814(2)	6.815(2)	6.817(2)	6.831(2)
	2.0	5.812(2)	5.812(2)	5.813(2)	5.820(2)	5.844(2)
2.0	0.5	18.972(1)	18.972(1)	18.972(1)	18.972(1)	18.979(1)
	1.0	8.460(1)	8.460(1)	8.460(1)	8.464(1)	8.481(1)
	1.5	7.342(2)	7.342(2)	7.342(2)	7.345(2)	7.362(2)
	2.0	6.598(2)	6.598(2)	6.599(2)	6.609(2)	6.641(2)
1.0	0.5	19.875(1)	19.875(1)	19.875(1)	19.876(1)	19.884(1)
	1.0	10.698(1)	10.698(1)	10.698(1)	10.704(1)	10.729(1)
	1.5	8.899(2)	8.899(2)	8.900(2)	8.904(2)	8.932(2)
	2.0	8.386(3)	8.386(3)	8.387(3)	8.393(3)	8.428(3)

Crouzet-Pascal [118] who said they are only valid when all edges are either simply supported or clamped. The authors did not agree [119] but indicated that the accuracy of the results is questionable only when β_1 and β_2 differ from each other by two orders of magnitude or more.

CHAPTER V. ANISOTROPIC PLATES

Consider next composite plates whose bifurcation buckling is governed by the differential equation (see Appendix);

$$D_{11}\frac{\partial^4 w}{\partial x^4} + 4D_{16}\frac{\partial^4 w}{\partial x^3 \partial y} + 2(D_{12}+2D_{66})\frac{\partial^4 w}{\partial x^2 \partial y} + 4D_{26}\frac{\partial^4 w}{\partial x \partial y^3} + D_{22}\frac{\partial^4 w}{\partial y^4}$$

$$= h(\sigma_x \frac{\partial^2 w}{\partial x^2} + 2\tau_{xy}\frac{\partial^2 w}{\partial x \partial y} + \sigma_y \frac{\partial^2 w}{\partial y^2}) \qquad (5.1)$$

that is, terms containing D_{16} and D_{26}, which involve the bending-twisting coupling, are added to Equation 2.1. This is the classical equation for the buckling of an anisotropic plate. It represents the equilibrium, small amplitude, buckled mode shape of a symmetrically laminated plate which otherwise has no special orientation of the fiber directions of the various plies with respect to each other.

Equation 5.1 also describes an orthotropic plate for which the principal axes (i.e., orthotropy axes) do not align with the xy-coordinate system, which is usually taken in the directions of the edges of a rectangular plate. Thus, although the material is orthotropic, the plate behaves as an anisotropic one, and will be discussed in this chapter.

As discussed by Jones [16] (see pp. 165-166), another important case of symmetrically laminated plates governed by Equation 5.1 is the regular angle-ply laminate having an odd number of plies alternating in the sequence $+\theta, -\theta, +\theta, -\theta, \ldots, +\theta$. Here the bending-twisting stiffness coefficients D_{16} and D_{26} are largest for the smallest number of plies (N=3), and become smaller relative to the other coefficients (D_{11}, D_{22}, D_{12}, D_{66}) as N is increased. Thus, for an angle-ply plate having a large (odd) number of alternating plies, D_{16} and D_{26} may be

quite small. However, as Jones points out, even small D_{16} and D_{26} may cause significantly different results from those cases in which D_{16} and D_{26} are exactly zero.

In Chapters 2 and 3 it was seen that orthotropic plates having two opposite sides simply supported, subjected to uniform inplane normal stresses (σ_x, σ_y), had exact solutions for the buckling loads. The addition of the terms containing D_{16} and D_{26} makes the exact solution of problems for plates of finite dimensions impossible (an exceedingly complex exact solution by Wittrick [120] for infinite strips will be seen later). As it will be seen, results exist for only 4 of the 21 sets of simple boundary conditions (SSSS,SCSC,SFSF,CCCC).

5.1. SSSS

Consider first the SSSS plate loaded either uniaxially or biaxially (Figures 2.1 and 2.3).

Housner and Stein [65] used a finite difference energy method to make parametric studies for angle-ply, graphite-epoxy plates having alternating ($\pm\theta$) plies subjected to uniaxial loading. Individual ply properties were given by:

$$E_1 = 145 \text{ GN/m}^2 \ (21\text{x}10^6 \text{psi})$$
$$E_2/E_1 = 0.1138$$
$$G_{12}/E_1 = 0.03095$$
$$\nu_{12} = 0.31$$

where E_1 and E_2 are the elastic moduli parallel to and transverse to the fibers, respectively; G_{12} is the shear modulus; and ν_{12} is Poisson's ratio relating contraction normal to the fiber direction to extension parallel to the fiber direction. With these ply properties, the aspect ratio and stiffness parameters aB/b and 0, respectively, for the entire

plate related to the plate axes, as defined by Equation 2.40 are as given in Table 5.1. Numerical results were obtained with the assumption that D_{16} and D_{26} are negligible. Variation of the uniaxial compressive buckling parameter $\hat{N}_x$ with fiber orientation ($\pm\theta$) and a/b is seen in Figure 5.1 for SSSS (as well as CCCC) plates, where $\hat{N}_x$ is defined by

$$\hat{N}_x = -\frac{N_x b^2}{E_1 h^3} \tag{5.2}$$

Also appearing on the right hand ordinate of the plot is a circle indicating the corresponding value of $\hat{N}_x$ for an equal weight, isotropic aluminum plate. It is seen that a range of fiber orientations exists for which the buckling strength of the graphite-epoxy panels exceeds that of the comparable aluminum panel with the same aspect ratio and boundary conditions. A similar plot is shown in Figure 5.2 for SSSS (and CCCC) plates subjected to shear loading, where the nondimensional shear buckling parameter $\hat{N}_{xy}$ is defined by

$$\hat{N}_{xy} = \frac{N_{xy} b^2}{E_1 h^3} \tag{5.3}$$

In this case Figure 5.2 shows that the buckling strength of the square graphite-epoxy plate with CCCC edges exceeds that of an aluminum one for all fiber orientations.

Optimum fiber orientations for alternating angle-ply plates with SSSS edge conditions are shown in Figures 5.3 and 5.4 for uniaxial and shear buckling loads, respectively. The compressive buckling curve (Figure 5.3) is seen to have an optimum fiber orientation of 0° for small a/b, increasing rapidly for a/b = 0.56, and lying in the vicinity of 45° for large a/b. In the case of shear buckling (Figure 5.4) the symmetry of the problem requires that the optimum fiber orientation angle θ for a plate of aspect ratio a/b be the complement of the one for aspect ratio b/a. Thus, Figure 5.4 is plotted only for $a/b \geq 1$.

Table 5.1. Parameters for graphite-epoxy, angle-ply plates analyzed by Housner and Stein (θ and B defined by Equations 2.40.

Fiber angles $\pm\theta$(deg)	θ	$\frac{a}{b}$ B
0	3.50	1.722
30	0.511	1.389
45	0.415	1.000
60	0.511	0.720
90	3.50	0.581

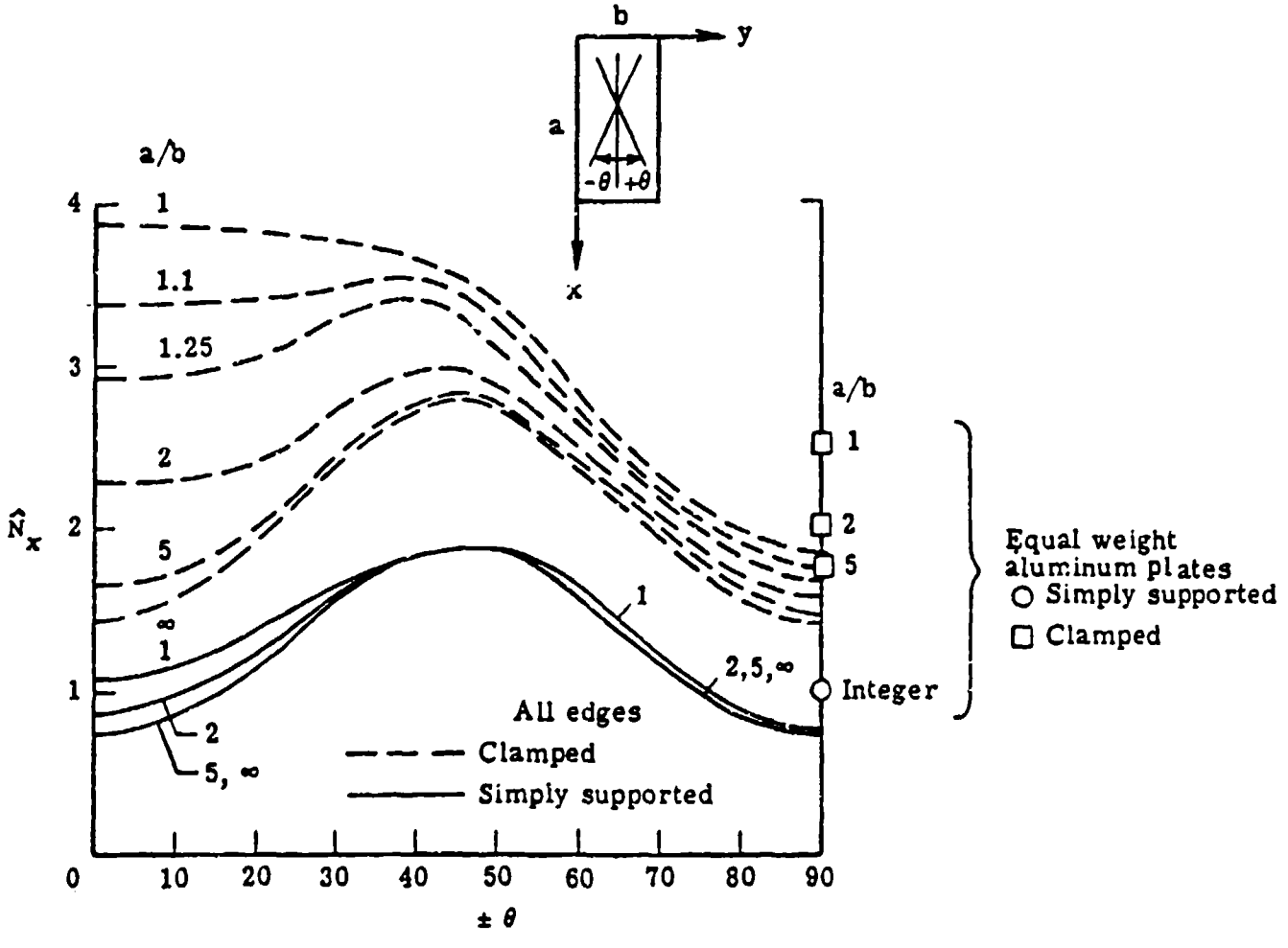

Figure 5.1. Compressive buckling parameters $\hat{N}_x$ for graphite-epoxy, angle-ply plates.

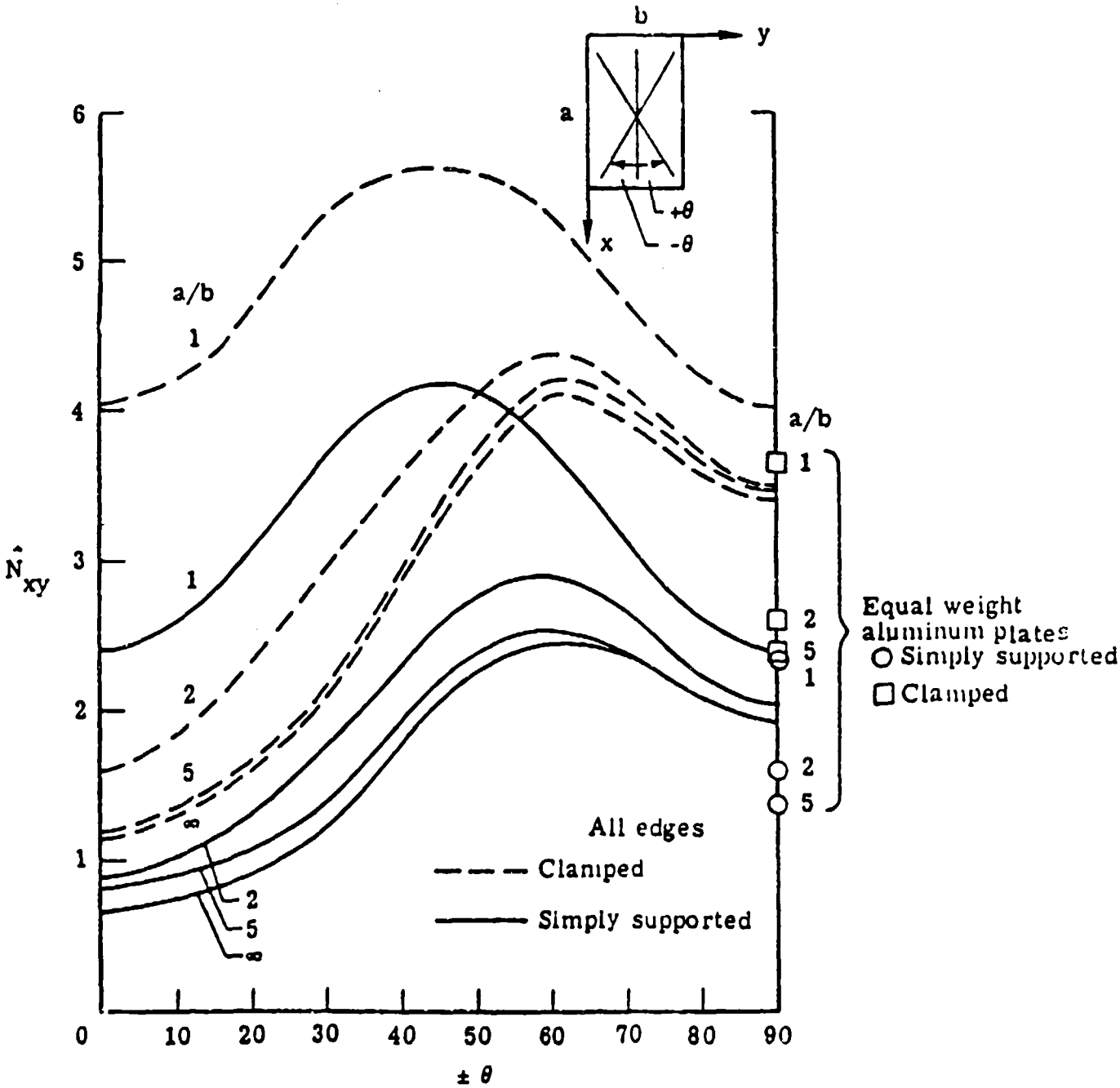

Figure 5.2. Shear buckling parameters $\hat{N}_{xy}$ for graphite-epoxy, angle-ply plates.

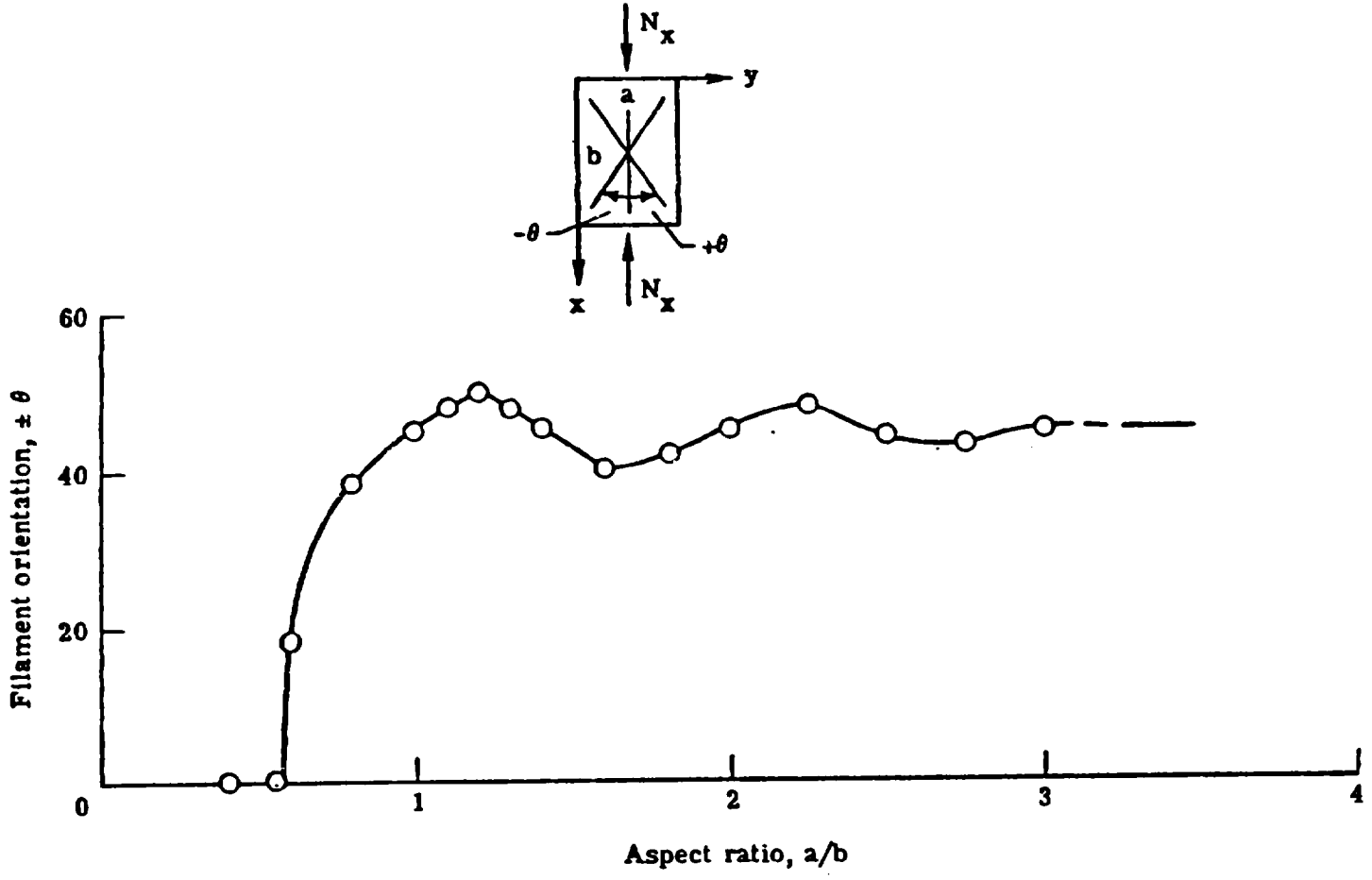

Figure 5.3. Optimum fiber orientations for SSSS, angle-ply plates subjected to uniaxial loading.

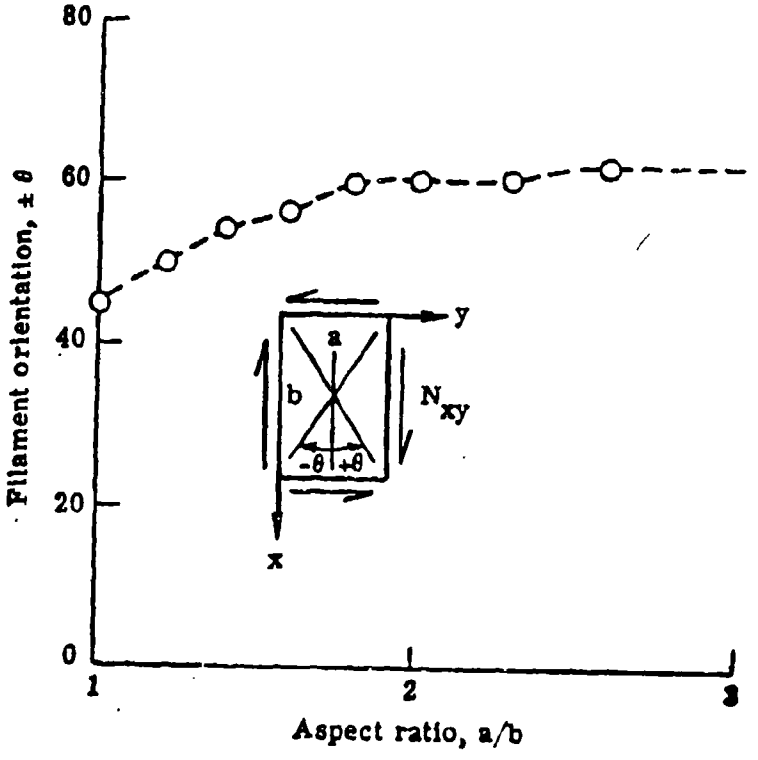

Figure 5.4. Optimum fiber orientations for SSSS, angle-ply plates subjected to shear loading.

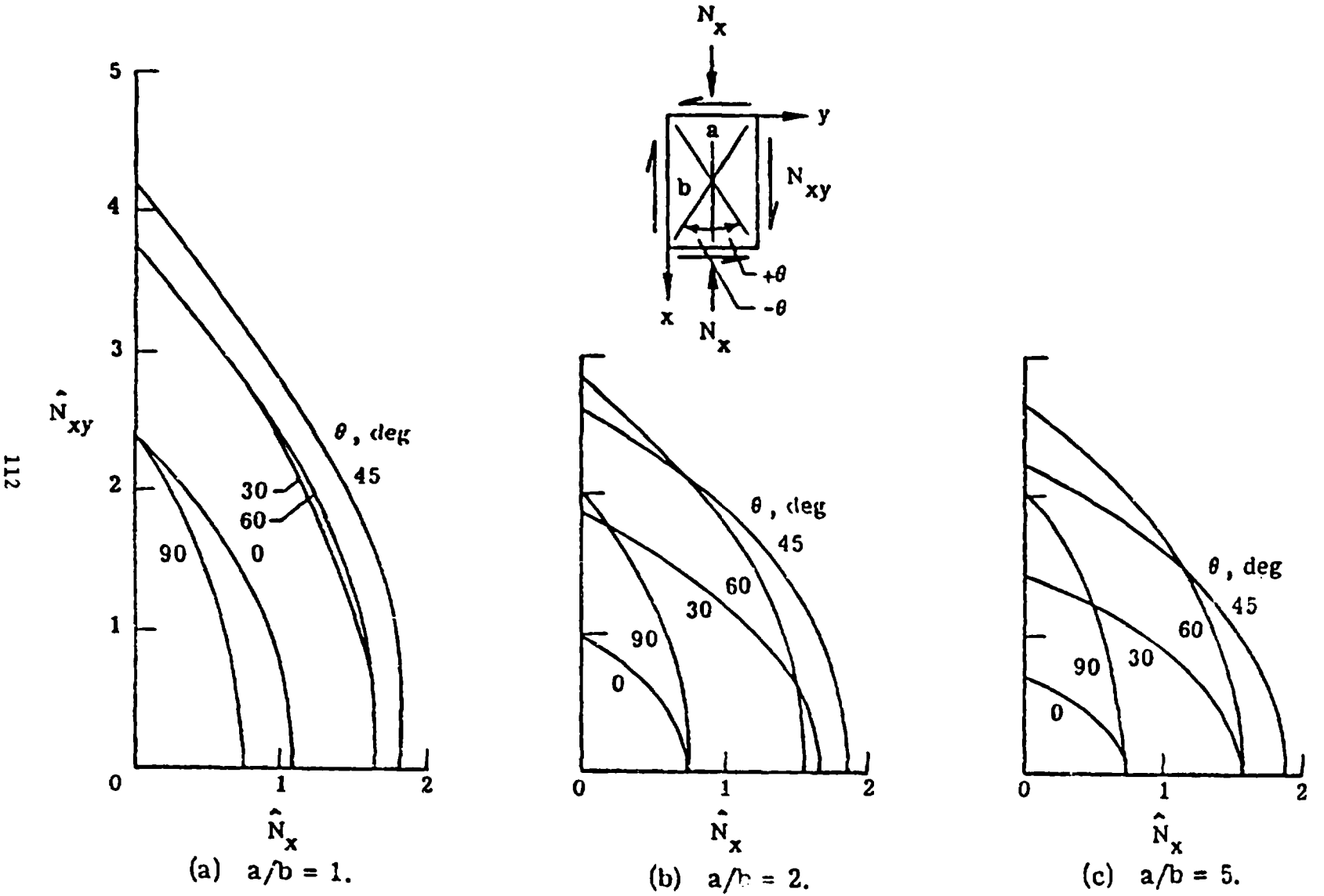

Figure 5.5. Buckling parameters for SSSS, angle-ply plates subjected to combined axial compression and shear.

Housner and Stein [65] also computed and plotted interaction curves for the buckling of alternating angle-ply plates subjected to simultaneous axial compression and shear. Curves for various fiber orientation angles ($\pm\theta$) for SSSS boundary conditions are depicted in Figure 5.5.

Fogg [32] presented an extensive set of numerical results for the compression (uniaxial) and shear buckling of SSSS plates fabricated from T300/5208 graphite-epoxy tape. Results were obtained using a finite element plate analysis program [121]. Calculations were made for two families of laminates: $(45/0/-45/0_N)_S$ and $(45/90/-45,0_N)_S$, where s indicates that the plate is symmetric, having twice the number of plies shown in parentheses, and N indicates the number of 0^o plies immediately adjacent to the midplane on each side. Each ply was 0.005 in thick. For example, the $(45/0/-45/0)_S$ laminate consists of eight plies, arranged 45^o, 0^o, -45^o, 0^o, 0^o, -45^o, 0^o, 45^o, and a total thickness of 0.04 in and a bending stiffness in the x-direction of D_{11} = 53.795 lb-in. A similar laminate having twice as many plies would have D_{11} = $53.795x(2)^3$ = 430.36 lb-in. Laminate orientations, thicknesses and bending stiffnesses of the various anisotropic plates studied are summarized in Table 5.2.

Numerical results for the buckling stress resultants (N) in lb/in for the plates described by Table 5.2 are presented in Table 5.3, along with the complete plate dimensions. The width (b) was taken to be 20 times the thickness (h) in each case. Lengths (a) were set to result in one, two or three half-wave buckles in the mode shape. To evaluate the effect of the D_{16} and D_{26} terms on the buckling loads, the buckling loads of orthotropic plates ($D_{16} = D_{26} = 0$) of infinite length were also computed. These plates are thus designated either "A" or "O" in the second column of results, and the ratio of the anisotropic to the orthotropic buckling loads (N^A/N^O) is also given.

Least squares curve fitting techniques were used to obtain the following empirical formulas for N^A/N^O for the case of <u>uniaxial</u> loading

Table 5.2. Anisotropic laminates analyzed by Fogg

LAMINATE ORIENTATION	h IN	D_{11} LB-IN	D_{12} LB-IN	$D_{16} = D_{26}$ LB-IN	D_{22} LB-IN	D_{66} LB-IN	$\left(\frac{D_{22}}{D11}\right)^{1/4}$
(45/0/-45)s	.03	21.203	7.717	6.373	11.305	8.553	.8545
$(45/-45/0_{1.5})$s	.035	25.633	14.801	5.311	20.860	16.135	.9498
$(45/0/-45/\bar{0})$s	.035	34.976	11.840	8.498	17.478	13.167	.8408
(45/0/-45/0)s	.04	53.795	17.171	10.622	25.516	19.151	.8299
$(45/0/-45/0_2)$s	.05	111.23	31.584	14.871	47.604	35.446	.8088
$(45/0/-45/0_3)$s	.06	202.84	51.208	19.120	78.411	57.874	.7885
$(45/0/-45/0_5)$s	.08	525.87	107.10	27.618	169.55	122.87	.7535
(45/90/-45)s	.03	11.288	7.712	6.373	22.368	8.553	1.1865
(45/90/-45/0)s	.035	17.622	11.830	8.498	36.838	13.167	1.2024
(45/0/-45/90)s (Q)	.04	52.379	17.170	10.622	27.096	19.151	.8481
(45/90/-45/0)s (Q)	.04	26.379	17.156	10.622	55.543	19.151	1.1881
$(45/90/-45/0_2)$s	.05	58.818	31.555	14.871	106.08	35.446	1.1589
$(45/90/-45/0_3)$s	.06	116.43	51.159	19.120	174.82	57.874	1.1070
$(45/90/-45/0_5)$s	.08	345.96	107.00	27.618	370.26	122.97	1.0171

Material is T300/5208 Tape

Table 5.3(a). Uniaxial compression and shear buckling stress resultants (N) of SSSS plates for the laminates of Table 5.2.

Orient.	A/O	Load Type	b in	a in	h in	λ	N lb/in	Ratio N^A/N^O	K MSI	D_{16}	$\bar{D}$	$\frac{D_{16}}{\bar{D}}$	Limit Stress ksi
$(45/0/-45)_s$	O	COMP	.6	∞	.03	∞	2210		29.47	6.373	38.05	.167	32.9
	A	COMP	.6	.702	.03	1	1862	.843	24.83				
	A	COMP	.6	1.404	.03	2	1762	.793	23.36				
	A	COMP	.6	2.106	.03	3	1716	.776	22.87				
	O	SHR	.6	∞	.03	∞	2300		30.67				28.3
	O	SHR	.6	.702	.03	1	4280		57.07				
	A	SHR	.6	.702	.03	1	2173	.608	28.97				
	O	SHR	.6	1.404	.03	2	2791		37.21				
	A	SHR	.6	1.404	.03	2	1405	.503	18.73				
	O	SHR	.6	2.108	.03	3	2568		34.24				
	A	SHR	.6	2.106	.03	3	1233	.480	16.44				
$(45/-45/0_{1.6})_s$	O	COMP	.7	∞	.035	∞	2828		32.32	6.311	69.03	.0769	38.9
	A	COMP	.7	.737		1	2732	.968	31.22				
	A	COMP	.7	1.474	.035	2	2709	.968	30.98				
	A	COMP	.7	2.211	.035	3	2701	.965	30.87				
	O	SHR	.7	∞	.035	∞	3106		35.50				26.2
	O	SHR	.7	.737	.035	1	6094		69.66				
	A	SHR	.7	.737	.036	1	4724	.776	53.99				
	O	SHR	.7	1.474	.035	2	4020		45.94				
	A	SHR	.7	1.474	.035	2	3020	.751	34.61				
	O	SHR	.7	2.211	.035	3	3476		39.73				
	A	SHR	.7	2.211	.035	3	2687	.773	30.71				

Table 5.3(a). (Continued)

Orient.	A/O	Load Type	b in	a in	h in	λ	N lb/in	Ratio N^A/N^O	K MSI	D_{16}	$\bar{D}$	$\frac{D_{16}}{\bar{D}}$	Limit Stress ksi
$(45/0/-45/\bar{0})_s$	O	COMP	.7	∞	.035	∞	2634		28.96	8.498	58.86	.144	38.9
	A	COMP	.7	.833	.035	1	2250	.888	26.71				
	A	COMP	.7	1.665	.035	2	2160	.852	24.69				
	A	COMP	.7	2.498	.035	3	2129	.840	24.33				
	O	SHR	.7	∞	.036	∞	2614		29.87				26.2
	O	SHR	.7	.833	.035	1	4828		55.18				
	A	SHR	.7	.833	.036	1	2845	.589	32.51				
	O	SHR	.7	1.665	.035	2	3165		36.17				
	A	SHR	.7	1.665	.036	2	1852	.585	21.17				
	O	SHR	.7	2.498	.035	3	2920		33.37				
	A	SHR	.7	2.498	.035	3	1632	.559	18.65				
$(45/0/-45/0)_s$	O	COMP	.8	∞	.04	∞	2854		28.54	10.622	86.22	.123	49.69
	A	COMP	.8	.964	.04	1	2627	.920	26.27				
	A	COMP	.8	1.928	.04	2	2664	.896	26.64				
	A	COMP	.8	2.892	.04	3	2530	.886	26.30				
	O	SHR		∞	.04	∞	2924		29.24				23.0
	O	SHR	.8	.964	.04	1	5380		53.80				
	A	SHR	.8	.964	.04	1	3538	.658	36.38				
	O	SHR	.8	1.928	.04	2	3636		36.35				
	A	SHR	.8	1.928	.04	2	2317	.655	23.17				
	O	SHR	.8	2.892	.04	3	3268		32.68				
	A	SHR	.8	2.892	.04	3	2046	.628	20.46				

Table 5.3(a). (Continued)

Orient.	A/O	Load Type	b in	a in	h in	λ	N lb/in	Ratio N^A/N^O	K MSI	D_{16}	$\bar{D}$	$\frac{D_{16}}{\bar{D}}$	Limit Stress ksi
$(45/0/-45/0_2)_s$	O	COMP	1.0	∞	.05	∞	3469		27.67	14.871	161.3	.092	64.67
	A	COMP	1.0	1.236	.05	1	3311	.957	26.49				
	A	COMP	1.0	2.473	.05	2	3263	.943	26.10				
	A	COMP	1.0	3.709	.06	3	3247	.939	26.98				
	O	SHR	1.0	∞	.06	∞	3496						19.8
	O	SHR	1.0	1.236	.05	1	6387		51.10				
	A	SHR	1.0	1.236	.05	1	4814	.754	38.51				
	O	SHR	1.0	2.473	.05	2	4219		33.76				
	A	SHR	1.0	2.473	.05	2	3188	.756	25.60				
	O	SHR	1.0	3.709	.05	3	3914		31.31				
	A	SHR	1.0	3.709	.06	3	2823	.721	22.68				
$(45/0/-45/0_3)_s$	O	COMP	1.20	∞	.06	∞	4017		26.78	19.120	266.4	.072	58.0
	A	COMP	1.20	1.622	.06	1	3916	.975	28.11				
	A	COMP	1.20	3.044	.06	2	3882	.966	26.88				
	A	COMP	1.20	4.566	.06	3	3871	.964	25.81				
	O	SHR	1.20	∞	.06	∞	4007		26.71				17.6
	O	SHR	1.20	1.622	.06	1	7267		48.45				
	A	SHR	1.20	1.622	.06	1	5909	.799	39.39				
	O	SHR	1.20	3.044	.06	2	4829		32.19				
	A	SHR	1.20	3.044	.06	2	3956	.819	26.37				
	O	SHR	1.20	4.566	.06	3	4493		29.95				
	A	SHR	1.20	4.566	.06	3	3508	.781	23.39				

Table 5.3(a). (Continued)

Orient.	A/D	Load Type	b in	a in	h in		N lb/in	Ratio N^A/N^D	K · MSI	D_{16}	$\bar{D}$	$\frac{D_{16}}{\bar{D}}$	Limit Stress ksi
$(45/0/-45/0_5)_s$	D	COMP	1.6	∞	.08	∞	5023		26.12	27.618	577.9	.048	62.15
	A	COMP	1.6	2.123	.08	1	4969	.989	24.85				
	A	COMP	1.6	4.247	.08	2	4960	.985	24.75				
	A	COMP	1.6	6.370	.08	3	4944	.984	24.72				
	D	SHR	1.6	∞	.08	∞	4891		24.46				16.0
	D	SHR	1.6	2.123	.08	1	8785		43.93				
	A	SHR	1.6	2.123	.08	1	7701	.877	38.51				
	D	SHR	1.6	4.247	.08	2	5884		29.42				
	A	SHR	1.6	4.247	.08	2	5245	.891	26.23				
	D	SHR	1.6	6.370	.08	3	5507		27.54				
	A	SHR	1.6	6.370	.08	3	4660	.846	23.30				

Table 5.3(b). Uniaxial compression and shear buckling stress resultants (N) of SSSS plates for the laminates of Table 5.2.

Orient.	A/O	Load Type	b in.	a in.	h in.	λ	N lb/in	Ratio N^A/N^O	K MSI	D_{16}	$\overline{D}$	$\frac{D_{16}}{\overline{D}}$	Limit Stress ksi
$(45/90/-45)_s$	O	COMP	.6	∞	.03	∞	2232		29.76	6.373	43.67	.146	15.1
	A	COMP	.6	.506	.03	1	1874	.840	24.99				
	A	COMP	.6	1.011	.03	2	1863	.835	24.84				
	A	COMP	.6	1.517	.03	3	1858	.832	24.77				
	O	SHR	.6	∞	.03	∞	3234		43.12				28.3
	O	SHR	.6	.506	.03	1	5984		79.79				
	A	SHR	.6	.506	.03	1	3071	.513	40.95				
	O	SHR	.6	1.011	.03	2	3919		52.26				
	A	SHR	.6	1.011	.03	2	2237	.671	29.83				
	O	SHR	.6	1.517	.03	3	3612		48.16				
	A	SHR	.6	1.517	.03	3	2058	.570	27.44				
$(45/90/-45/0)_s$	O	COMP	.7	∞	.035	∞	2564		29.30	8.498	68.8	.124	23.6
	A	COMP	.7	.682	.035	1	2272	.886	26.97				
	A	COMP	.7	1.164	.035	2	2266	.884	25.90				
	A	COMP	.7	1.746	.035	3	2264	.883	26.87				
	O	SHR	.7	∞	.035	∞	3794		43.36				25.6
	O	SHR	.7	.682	.035	1	6981		79.78				
	A	SHR	.7	.682	.035	1	4151	.595	47.44				
	O	SHR	.7	1.164	.035	2	4588		52.43				
	A	SHR	.7	1.164	.035	2	2986	.651	34.13				
	O	SHR	.7	1.746	.035	3	4242		48.48				
	A	SHR	.7	1.746	.035	3	2721	.641	31.10				

Table 5.3(b). (Continued)

Orient.	A/O	Load Type	b in.	a in.	h in.	λ	N lb/in	Ratio N^A/N^O	K MSI	D_{16}	$\overline{D}$	$\frac{D_{16}}{\overline{D}}$	Limit Stress ksi
$(45/0/-45/90)_s$ (Quasi)	O	COMP	.8	∞	.04	∞	2873		28.73	10.622	87.42	.122	38.2
	A	COMP	.8	.843	.04	1	2649	.922	26.49				
	A	COMP	.8	1.887	.04	2	2583	.899	25.83				
	A	COMP	.8	2.830	.04	3	2560	.891	25.60				
	O	SHR	.8	∞	.04	∞	3018		30.18				23.2
	O	SHR	.8	.843	.04	1	6540		65.40				
	A	SHR	.8	.843	.04	1	3668	.662	36.68				
	O	SHR	.8	1.387	.04	2	3647		36.47				
	A	SHR	.8	1.887	.04	2	2442	.870	24.42				
	O	SHR	.8	2.830	.04	3	3376		33.76				
	A	SHR	.8	2.830	.04	3	2141	.634	21.41				
$(45/90/-45/0)_s$ (Quasi)	O	COMP	.8	∞	.04	∞	2902		29.02	10.622	101.78	.104	38.2
	A	COMP	.8	.667	.04	1	2672	.921	26.72				
	A	COMP	.8	1.334	.04	2	2667	.919	26.67				
	A	COMP	.8	2.002	.04	3	2665	.918	26.65				
	O	SHR	.8	∞	.04	∞	4319		43.19				23.2
	O	SHR	.8	.667	.04	1	7902		79.02				
	A	SHR	.8	.667	.04	1	6257	.666	62.57				
	O	SHR	.8	1.334	.04	2	6216		62.16				
	A	SHR	.8	1.334	.04	2	3743	.718	37.43				
	O	SHR	.8	2.002	.04	3	4832		48.32				
	A	SHR	.8	2.002	.04	3	3383	.700	33.83				

Table 5.3(b). (Continued)

Orient.	A/O	Load Type	b in.	a in.	h in.	λ	N lb/in	Ratio N^A/N^O	K MSI	D_{16}	$\bar{D}$	$\frac{D_{16}}{\bar{D}}$	Limit Stress ksi
$(45/90/-45/0_2)_s$	O	COMP	1.0	∞	.05	∞	3581		28.65	14.871	193.99	.0767	38.6
	A	COMP	1.0	.863	.05	1	3438	.960	27.50				
	A	COMP	1.0	1.726	.06	2	3433	.959	27.46				
	A	COMP	1.0	2.589	.05	3	3430	.958	27.44				
	O	SHR	1.0	∞	.05	∞	5264		42.03				20.0
	O	SHR	1.0	.863	.05	1	9504		76.03				
	A	SHR	1.0	.863	.05	1	7277	.766	58.22				
	O	SHR	1.0	1.726	.05	2	6329		50.63				
	A	SHR	1.0	1.726	.05	2	5128	.810	41.02				
	O	SHR	1.0	2.589	.05	3	5896		47.17				
	A	SHR	1.0	2.589	.05	3	4595	.779	36.76				
$(45/90/-45/0_3)_s$	O	COMP	1.2	∞	.06	∞	4244		28.29	19.120	324.8	.059	44.5
	A	COMP	1.2	1.084	.06	1	4150	.978	27.67				
	A	COMP	1.2	2.168	.06	2	4145	.977	27.63				
	A	COMP	1.2	3.252	.06	3	4142	.976	27.61				
	O	SHR	1.2	∞	.06	∞	6064		40.43				17.8
	O	SHR	1.2	1.084	.06	1	10876		72.51				
	A	SHR	1.2	1.084	.06	1	8971	.825	59.81				
	O	SHR	1.2	2.168	.06	2	7293		48.62				
	A	SHR	1.2	2.168	.06	2	6308	.865	42.05				
	O	SHR	1.2	3.252	.06	3	6830		45.53				
	A	SHR	1.2	3.252	.06	3	5640	.826	37.60				

Table 5.3(b). (Continued)

Orient.	A/O	Load Type	b in.	a in.	h in.	λ	N lb/in	Ratio N^A/N^O	K MSI	D_{16}	$\overline{D}$	$\frac{D_{16}}{\overline{D}}$	Limit Stress ksi
$(45/30/-45/0_6)_s$	O	COMP	1.6	∞	.08	∞	5480		27.40	27.618	718.8	.039	61.9
	A	COMP	1.6	1.573	.08	1	5433	.991	27.17				
	A	COMP	1.6	3.146	.08	2	5429	.991	27.15				
	A	COMP	1.6	4.719	.08	3	5427	.990	27.14				
	O	SHR	1.6	∞	.08	∞	7430		37.15				15.1
	O	SHR	1.6	1.573	.08	1	12988		64.94				
	A	SHR	1.6	1.573	.08	1	11611	.894	58.06				
	O	SHR	1.6	3.146	.08	2	8760		43.76				
	A	SHR	1.6	3.146	.08	2	8195	.937	40.98				
	O	SHR	1.6	4.719	.08	3	8148		40.74				
	A	SHR	1.6	4.719	.08	3	7346	.902	36.73				

only [32]:

$$\frac{N^A}{N^O} = 1 - 5.585\left(\frac{D_{16}}{\bar{D}}\right)^{1.995} \quad \text{for } \lambda=1 \tag{5.4a}$$

$$= 1 - 9.588\left(\frac{D_{16}}{\bar{D}}\right)^{2.135} \quad \text{for } \lambda=2 \tag{5.4b}$$

$$= 1 - 9.766\left(\frac{D_{16}}{\bar{D}}\right)^{2.117} \quad \text{for } \lambda=3 \tag{5.4c}$$

where $$\bar{D} = (D_{11}D_{22}^3)^{1/4} + (D_{12}+2D_{66}) \tag{5.5}$$

When the data of Table 5.3 are compared against these curves, most of the values fall within one percent of the curves, with the maximum error being four percent.

Studying Equations 5.4 and 5.5, and Tables 5.2 and 5.3, effects of the bending-twisting coupling coefficient D_{16} (and D_{26}) in changing the buckling loads from those of orthotropic analysis may be seen typically as follows:

1. The buckling loads are always decreased.
2. In the case of uniaxial compression longer plates (larger λ) always have larger decreases.
3. Shear buckling loads are more greatly decreased than those due to uniaxial compression.

Mandell [34,35] conducted an experimental investigation of uniaxial buckling loads for graphite-epoxy and boron-epoxy, angle-ply plates. A description of the plates tested is given in Table 5.4. Plate identification numbers given are those used in [34,35]. A ply layup 4($\pm$60) would indicate a stacking sequence with respect to the load direction (60°, -60°, -60°, 60°), 5($\pm$45) would describe the sequence (45°, -45°, 45°, -45°, 45°) and 20(30) means that 20 plies are all with

Table 5.4. Description of anisotropic plates tested by Mandell

Plate no.	Material	% Fiber by volume	Layup of plies	Dimensions (in)
203a	Thornel-25	40.0	9(±45)	10 x 10 x 0.116
203b	"	"	"	"
208	Thornel-40	60.0	(0,45,45,45,0)	10 x 10 x 0.038
401	Boron	48.2	20(±60)	11 x 11 x 0.110
402	"	"	20(±30)	14 x 11 x 0.110
403a	"	57.0	20(±45)	11 x 11 x 0.110
403b	"	"	"	"
406	"	51.7	20(30)	11 x 11 x 0.106
407	"	"	20(60)	"
408a	"	58.6	20(45)	11 x 11 x 0.095
408b	"	"	20(-45)	"

Table 5.5. Bending stiffnesses (lb.in) for Mandell's anisotropic plates

Plate no.	D_{11}	D_{12}	D_{16}	D_{22}	D_{26}	D_{66}
203	455	326	-100	455	-100	349
208	10.7	6.77	-5.75	94.2	-5.75	8.50
401	480	655	44.6	1943	145	666
402	1943	655	145	480	44.6	666
403	970	782	97.3	970	97.3	799
406	1870	631	923	481	298	644
407	481	631	298	1870	923	644
408	839	671	551	839	551	686

Table 5.6. Stretching stiffnesses (10^3 lb/in) for Mandell's anisotropic plates

Plate no.	A_{11}	A_{12}	A_{16}	A_{22}	A_{26}	A_{66}
203	405.4	290.1	-30.02	405.4	-30.02	310.4
208	532.3	136.8	-132.8	178.3	-132.8	151.2
401	476	649	0	1926	0	661
402	1296	649	0	476	0	661
403	1141	921	0	1141	0	940
406	1996	673	986	513	299	688
407	513	673	299	1996	986	688
408	1115	893	732	1115	732	912

Table 5.7. Uniaxial buckling loads ($-N_x$, lb/in) for Mandell's SSSS anisotropic plates

Plate no.	Experimental	Theoretical
203	313 (283)	292
208	13.8	12.7
401	661	636 600* 666**
402	642	648 616* 665**
403a	582	642 682* 664**
403b	602	642 682* 664**
406	399	515 425* 449**
407	433	589 381* 417**
408a	356	566 406* 412**
408b	372	566 406* 412**

* obtained by the Galerkin method
** obtained by the Ritz method

fibers oriented at 30° with respect to the loading axis. Bending stiffnesses for the plates are given in Table 5.5. The anisotropic character of the plates in bending is clearly seen (D_{16} and D_{26} are not zero). The stretching stiffnesses are listed in Table 5.6. Although the plates are symmetrically laminated, and therefore the stretching stiffnesses do not couple with the buckling problem, the latter table is presented to show that some of the plates are orthotropic in stretching (A_{16} and A_{26} are zero), even though they are anisotropic in bending. More information on these tests is found in Section 2.1.

Table 5.7 lists the experimental buckling loads for the plates described in Table 5.4. Also given are theoretical values obtained by three methods, using the bending stiffness data found in Table 5.5. The first method ignores the D_{16} and D_{26} terms, and uses Equation 2.9 for an orthotropic plate. The second and third methods utilize Galerkin and Ritz formulations, as applied by Chamis [41] and Ashton [42], respectively. Plates 203, 403 and 408 are each listed twice. The two cases (denoted "a" and "b") identify uniaxial loadings in two perpendicular directions. For these plates, different experimental results were found, although the theoretical results are identical for each loading direction. It is interesting to note, contrary to the results of Fogg [32] presented earlier in Table 5.3, addition of D_{16} and D_{26} terms to the analysis does not necessarily decrease the theoretical buckling loads shown in Table 5.7.

Chamis [43,44] used the Galerkin method to analyze the buckling of SSSS anisotropic plates subjected to combinations of compression and shear loading. Two sets of problems were treated. The first set consisted of plates having the fibers all parallel, making an angle θ with respect to the x-axis. The second set were angle-ply plates, having alternating plies at $\pm\theta$ fiber angles. Specifically, the plates were comprised of 20 plies, the top 10 being $\pm\theta$, and the bottom 10 being $\mp\theta$, to preserve symmetry. Bending stiffnesses for the first set are

displayed in Table 5.8, computed using the ply material properties listed in Table 2.7. Critical buckling loads for various loading conditions and sizes of plates for the first set of problems are given in Table 5.9. Stiffnesses and buckling loads for the second set are set forth in Table 5.10 and 5.11. Corresponding results for the same plates having $\theta = 0$ and 90^{o} were given previously in Table 2.9. Comparing Tables 5.8 and 5.10, one observes that the only significant differences between the bending stiffnesses of the two sets of plates is in the bending-twisting coupling terms D_{16} and D_{26}. Additional discussion of the solution procedure may be found in Section 2.4.

Considerable interest has existed in the optimization of fiber orientation to obtain the largest value of critical load. Some work in this direction has already been seen in Figures 5.3 and 5.4. An extensive study for SSSS plates subjected to uniaxial compression (σ_x = constant, $\sigma_y = \tau_{xy} = 0$) was undertaken by Crouzet-Pascal [122] using a finite element method. Three types of laminates were considered, having "severe, medium or mild" orthotropy with respect to the principal material axes of the plate, which in turn are oriented at an angle θ with respect to the sides of the plate. The three types are described by the laminate material properties listed in Table 5.12, where L and T are principal material axes. For $\theta = 0^{o}$, then $E_L = E_x$, $E_T = E_y$, etc. The plate having severe orthotropy consisted of 50 graphite-epoxy plies, all having parallel fibers. Medium orthotropy corresponds to 20 glass-epoxy plies, with parallel fibers. Mild orthotropy stemmed from the reorientation of the layers of the severe orthotropy case, with 14, 14, 14 and 8 layers oriented at 0^{o}, $+45^{o}$, -45^{o} and 90^{o}, respectively relative to the principal material axis.

Optimum material axis orientation versus plate aspect ratio for the laminate having medium orthotropy is shown in Figure 5.6. Results obtained [122] are compared with those of Chao, Koh and Sun [123] for

Table 5.8. Bending stiffnesses (lb.in) for Chamis' parallel-fiber anisotropic plates

Fiber angle θ(deg)	D_{11}	D_{12}	D_{16}	D_{22}	D_{26}	D_{66}
15	2143	172.9	531.4	148.5	44.4	205.3
30	1440	454.0	742.1	228.0	255.1	486.5
45	724.1	594.6	575.8	724.1	575.8	627.0
60	228.0	454.2	255.1	1440	742.1	486.5
75	148.5	172.9	44.4	2143	531.4	205.3

Table 5.9. Buckling loads N_{cr}(lb/in) for Chamis' SSSS parallel fiber anisotropic plates

Plate dimensions (in)	Loading condition $\frac{N_x}{N_{cr}}$	$\frac{N_y}{N_{cr}}$	$\frac{N_{xy}}{N_{cr}}$	Buckling load, N_{cr} θ=15°	θ=30°	θ=45°	θ=60°	θ=75°
5.0x10.0	-1	0	0	949	813	620	403	219
"	0	-1	0	847	1306	1506	1407	876
"	-1	-1	0	623	648	495	322	175
"	-1	0	1	838	661	456	315	193
"	0	-1	1	645	718	635	518	446
"	-1	-1	1	494	510	374	249	159
"	-0.001	0	1	1458*	1238*	980*	808*	667*
10.0x10.0	-1	0	0	328	417	425	344	213
"	0	-1	0	213	344	425	417	328
"	-1	-1	0	164	208	218	208	164
"	-1	0	1	233	223	205	197	164
"	0	-1	1	165	197	205	223	233
"	-1	-1	1	136	146	145	146	136
"	-0.001	0	1	418*	382*	391*	385*	412*
"	-1	-0.75	0	187	236	225	237	178
"	-1	-0.50	0	218	276	262	277	188
"	-1	-0.25	0	262	331	312	322	200
"	-1	0.25	0	436	552	488	353	221
"	-1	0.50	0	654	827	554	386	239
"	-1	1.00	0	1223	970	696	465	280
"	-1	-0.50	0.25	209	232	229	240	179
"	-1	0.50	0.25	563	570	438	342	225
"	-1	-0.50	0.50	196	207	200	213	169
"	-1	0.50	0.50	469	431	348	294	209
20.0x10.0	-1	0	0	219	351	377	327	212
"	0	-1	0	55	101	155	203	237
"	-1	-1	0	44	81	124	162	156
"	-1	0	1	112	135	159	180	175
"	0	-1	1	48	79	114	165	209
"	-1	-1	1	40	66	94	128	123
"	-0.001	0	1	167*	204*	246*	306*	360*
40.0x10.0	-1	0	0	216	336	417	392	268
"	0	-1	0	22	45	91	157	210
"	-1	-1	0	21	42	86	147	163
"	-1	0	1	90	126	183	238	239
"	0	-1	1	22	42	85	149	210
"	-1	-1	1	21	40	80	139	139
"	-0.001	0	1	127*	168*	253*	371*	505*

* values lacking convergence

Table 5.10. Bending stiffnesses (lb.in) for Chamis' angle-ply plates

Fiber angle ±θ(deg)	D_{11}	D_{12}	D_{16}	D_{22}	D_{26}	D_{66}
15	2141	172.7	79.6	148.5	6.7	205.1
30	1439	453.6	111.2	288.6	38.2	486.0
45	723.4	594.0	86.3	723.4	86.3	626.4
60	288.6	453.6	38.2	1439	111.2	486.0
75	148.4	172.7	6.7	2141	79.6	205.1

Table 5.11. Buckling loads N_{cr}(lb/in) for Chamis' SSSS angle-ply plates

Plate dimensions (in)	Loading condition			Buckling load, N_{cr}				
	$\frac{N_x}{N_{cr}}$	$\frac{N_y}{N_{cr}}$	$\frac{N_{xy}}{N_{cr}}$	θ=±15°	θ=±30°	θ=±45°	θ=±60°	θ=±75°
5.0x10.0	-1	0	0	963	854	665	429	226
"	0	-1	0	901	1622	2016	1716	904
"	-1	-1	0	669	683	532	343	181
"	-1	0	1	905	798	621	401	213
"	0	-1	1	786	1271	1402	1054	577
"	-1	-1	1	601	650	506	327	173
"	-0.001	0	1	2290	2823	2571	1772	995
10.0x10.0	-1	0	0	340	450	505	428	226
"	0	-1	0	226	428	505	450	340
"	-1	-1	0	170	225	252	225	170
"	-1	0	1	283	370	414	363	201
"	0	-1	1	201	363	414	370	283
"	-1	-1	1	159	210	235	210	159
"	-0.001	0	1	671	914	1038	914	671
"	-1	-0.75	0	195	258	289	258	190
"	-1	-0.50	0	227	301	338	301	201
"	-1	-0.25	0	273	361	405	361	213
"	-1	0.25	0	454	602	675	458	241
"	-1	0.50	0	681	902	761	491	259
"	-1	1.00	0	1284	1140	888	573	302
"	-1	-0.50	0.25	225	299	334	298	199
"	-1	0.50	0.25	647	849	741	482	255
"	-1	-0.50	0.50	221	292	328	292	196
"	-1	0.50	0.50	579	755	702	464	249
20.0x10.0	-1	0	0	226	429	504	405	225
"	0	-1	0	56	107	166	213	241
"	-1	-1	0	45	86	133	171	167
"	-1	0	1	144	263	351	318	196
"	0	-1	1	53	100	155	200	226
"	-1	-1	1	43	82	127	163	150
"	-0.001	0	1	249	443	643	706	591

two values of a/b. For a/b = 1, both analyses gave the same result. For a/b = 2.5 they differed by approximately two percent. The variation of critical stress with material axis orientation (θ) is depicted in Figure 5.7 for the two cases of a/b = 1 and 2.5 described above. There m indicates the number of half-waves of the buckling mode in the load direction. Transverse to the load the mode shape has one half-wave. The node lines of the mode shapes have been found to rotate with the material axes, and remain approximately normal to the stiffer material axis over the whole range of orientation [42]. The results of similar studies [122] for the plates having mild and severe orthotropy are seen in Figures 5.8 through 5.10.

A number of other optimization studies have been made for SSSS anisotropic plates [28,34,68,101,124-135]. Optimization under biaxial loading conditions was treated by Bert and Chen [125] and by Lukoshevichyus [131]. Biaxial loading combined with shear was dealt with by Schmit and Farshi [133].

The case of the infinitely long anisotropic plate <u>simply supported</u> along its two edges (y = 0,b) and subjected to combined longitudinal (σ_x), transverse (σ_y), shear (τ_{xy}) and inplane bending (see Equation 2.43) was analyzed by Wittrick [120]. Critical values of the parameter K_L are given in Table 5.13 as the parameters Ω^2 and K_S^2 are varied, for the case of no bending stress. The parameters are defined as follows:

$$K_L = \frac{-\sigma_x hb^2}{Q\pi^2 D_{22}} - 2R_{23}K_s + \Omega^2[(1+R_{23}^2)^2 - R_{11}] \qquad (5.6a)$$

$$K_S = -\frac{\tau_{xy} hb^2}{Q\pi^2 D_{22}} + 2\Omega^2(R_{23}+R_{23}^3-R_{13}) \qquad (5.6b)$$

Table 5.12. Principal axis material properties of plates analyzed by Crouzet-Pascal

Type of plate	$E_L x10^{-6}$ (psi)	$E_T x10^{-6}$ (psi)	$G_{LT} x10^{-6}$ (psi)	ν_{LT}
Severe orthotropy	18.5	1.6	0.65	0.25
Medium orthotropy	7.8	2.6	1.25	0.25
Mild orthotropy	7.64	5.87	3.00	0.409

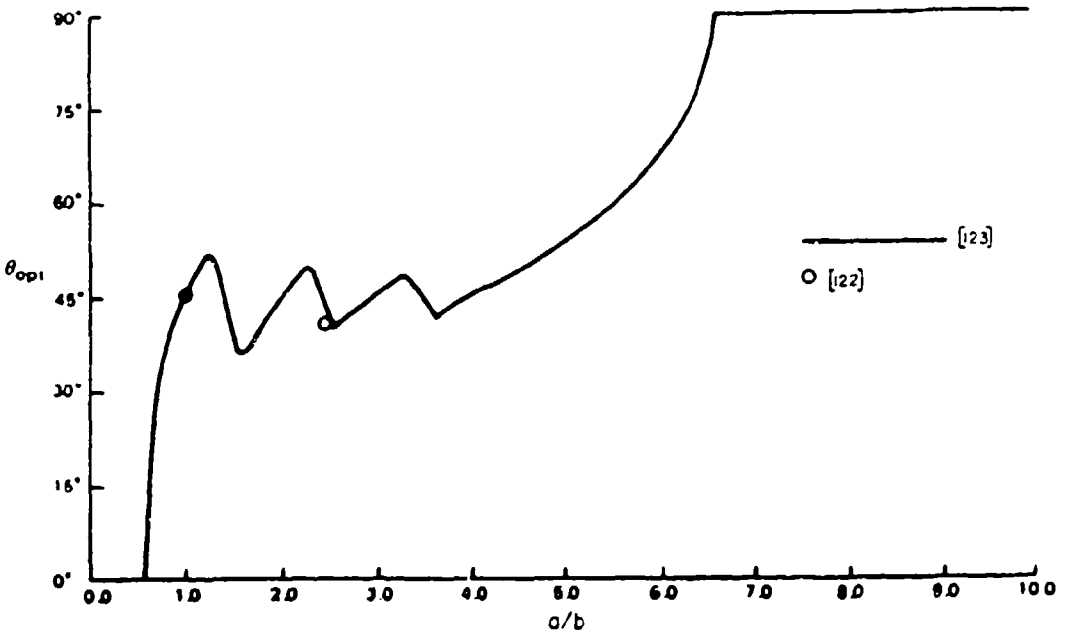

Figure 5.6. Optimum material axis orientation versus aspect ratio for a uniaxially loaded SSSS plate (unidirectional, medium orthotropy laminate).

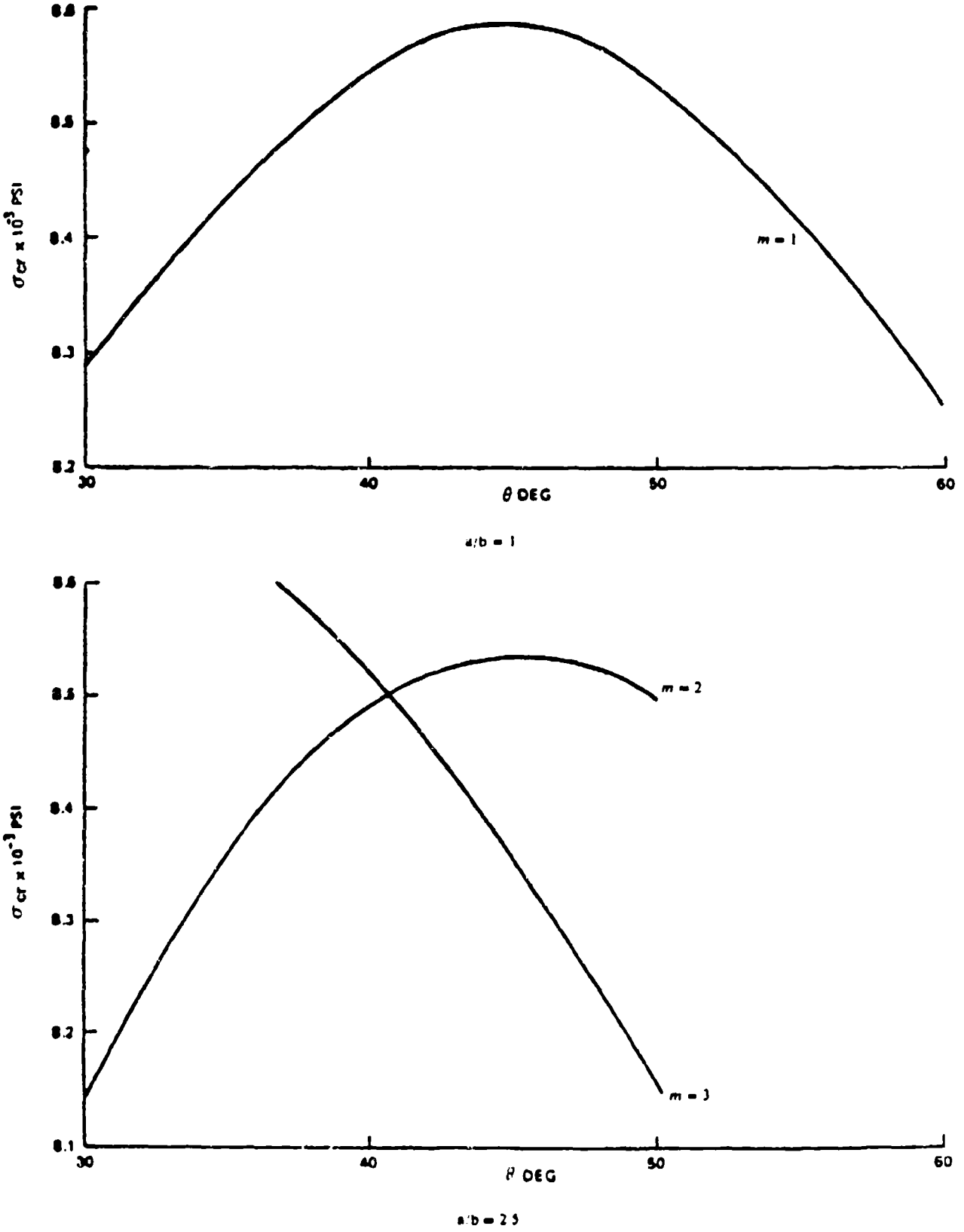

Figure 5.7. Variation of critical stress with material axis orientation, corresponding to a/b = 1 and 2.5 in Figure 5.6 (unidirectional, medium orthotropy laminate).

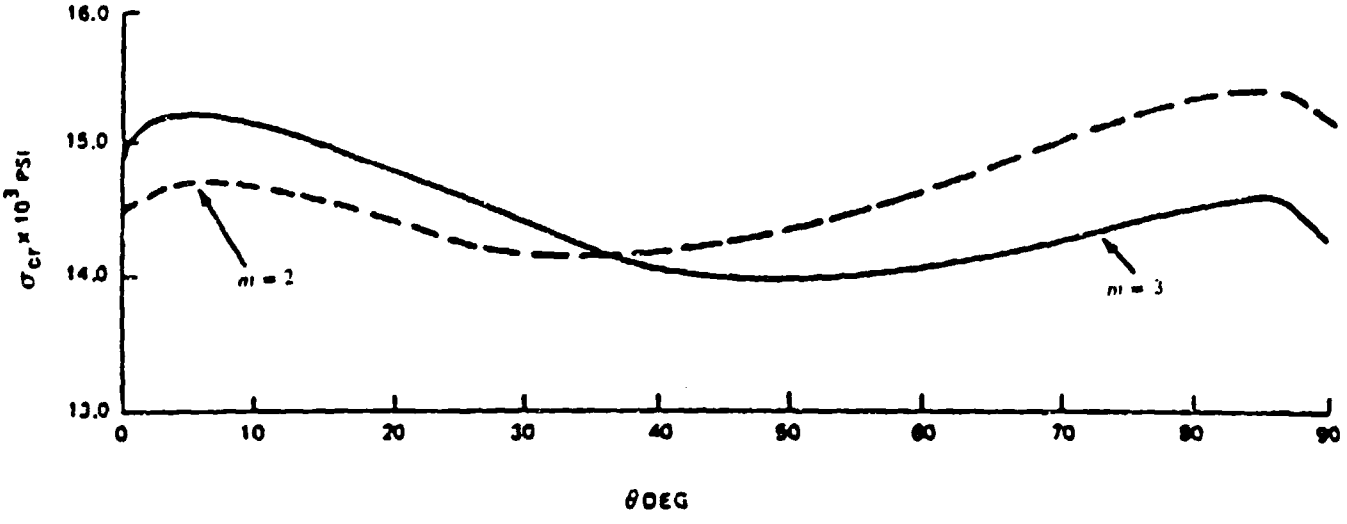

Figure 5.8. Variation of critical stress with material axis orientation, a/b = 2.5 (angle-ply, mild orthotropy laminate).

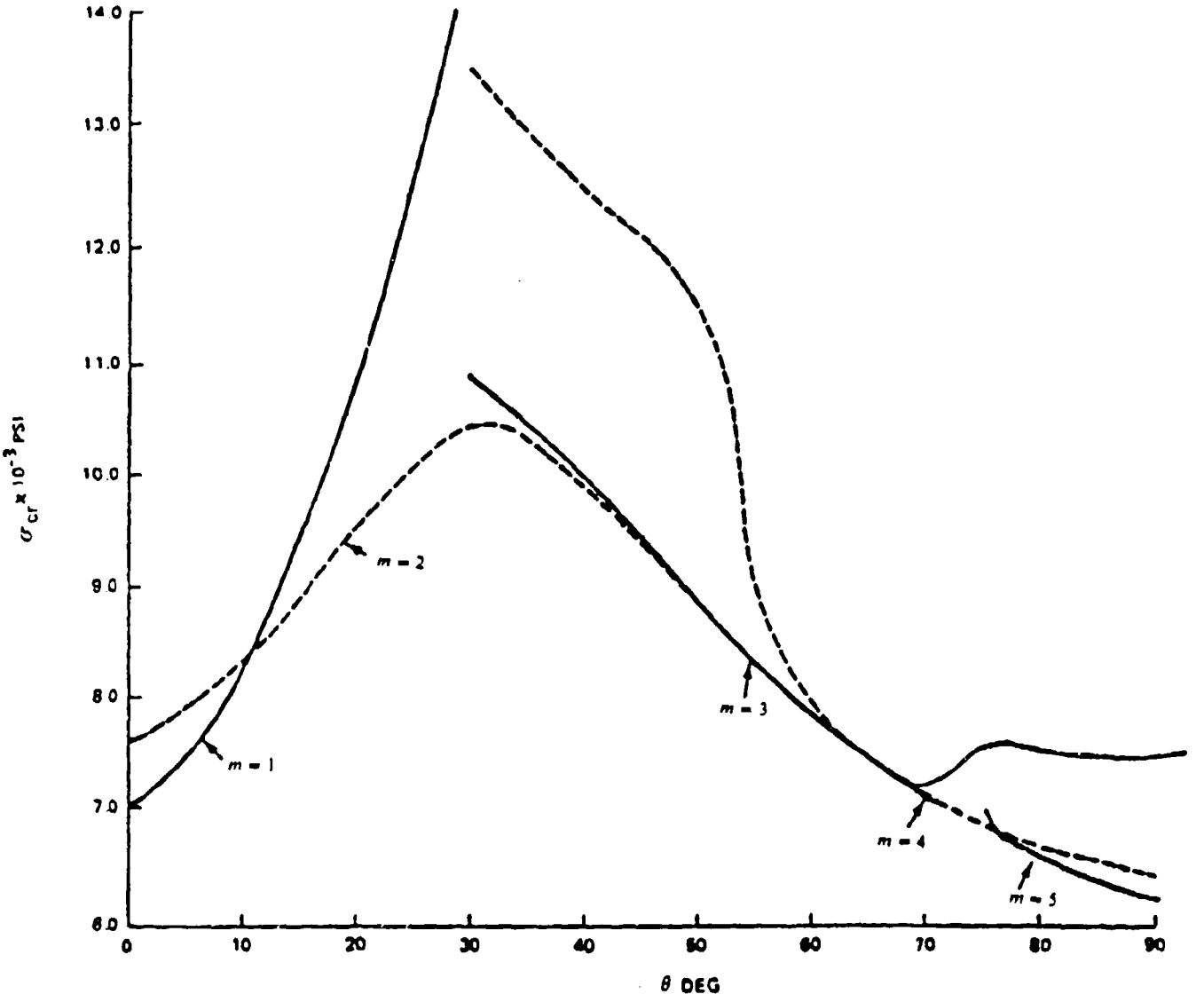

Figure 5.9. Variation of critical stress with material axis orientation, a/b = 2.5 (unidirectional, severe orthotropy laminate).

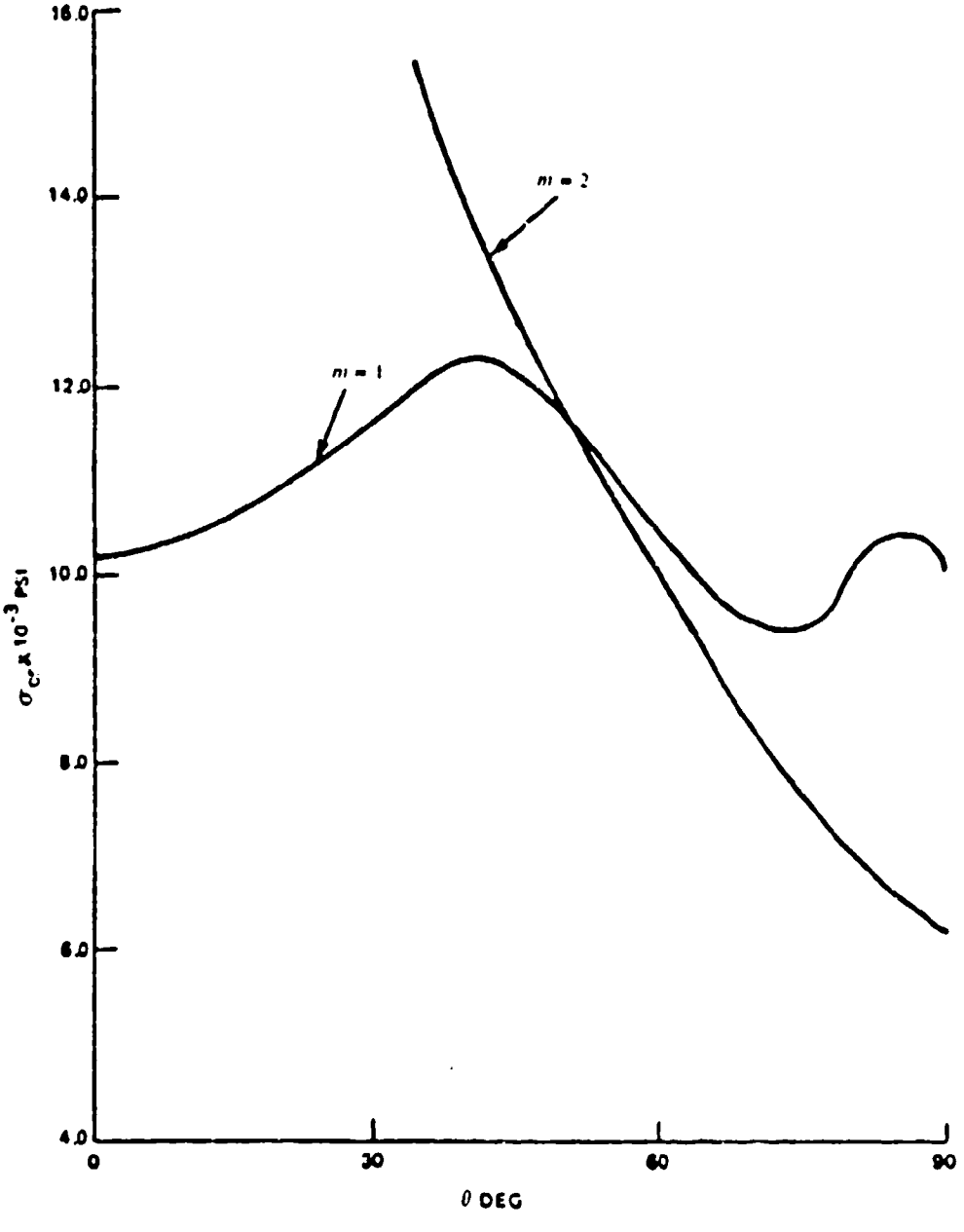

Figure 5.10. Variation of critical stress with material axis orientation, a/b = 1 (unidirectional, severe orthotropy laminate).

$$\Omega^2 = Q\left(\frac{b}{\lambda}\right)^2 \tag{5.6c}$$

where

$$R_{11} = \left(\frac{D_{11}}{D_{22}}\right)Q^{-2} \quad , \quad R_{13} = \left(\frac{D_{16}}{D_{22}}\right)Q^{-3/2} \quad , \quad R_{23} = \left(\frac{D_{26}}{D_{22}}\right)Q^{-1/2}$$

$$Q = D_{22} - 3\left(\frac{D_{26}}{D_{22}}\right)^2 + \frac{\lambda^2 \sigma_y h}{2\pi^2 D_{22}}$$

with λ being the longitudinal half-wavelength and σ_x and σ_y taken positive in tension, as elsewhere in the present work. The infinite strip having its principal material axis oriented at 45° with respect to the simply supported sides, subjected to uniaxial compression or shear, was also treated by Thielemann [136,137].

In addition to those references listed previously in this section, many others are available which consider the buckling of SSSS anisotropic plates [14,26,45,101,138-149], most of them dealing with uniaxial loading conditions only. Sarkisyan and Movsisyan [144] demonstrated how the perturbation method may be used, where the zeroeth order perturbation is the orthotropic plate. Therefore, for small D_{16} and D_{26}, the first order perturbation will be an accurate representation of an anisotropic plate. Whitney [147,148] demonstrated the rapid convergence of the series method for anisotropic problems. Ashton and Waddoups [138] showed that the buckling load of a $\pm$45° angle-ply plate may either decrease or increase when loaded in shear, depending upon whether τ_{xy} is positive or negative, respectively.

5.2. SCSC

Ashton and Love [112] conducted a set of experimental tests on

Table 5.13. Critical values of K_L for buckling of a simply supported, infinite strip subjected to σ_x, σ_y and σ_{xy}.

K_s^2 =	0	5	10	15	20	25	30	35
Ω^2 = 0.2	7.200	6.305	5.417	4.537	3.665	2.798	1.939	1.086
0.3	5.633	4.771	3.919	3.077	2.243	1.418	0.601	−0.208
0.4	4.900	4.069	3.249	2.440	1.641	0.852	0.072	−0.700
0.5	4.500	3.697	2.906	2.128	1.360	0.602	−0.145	−0.884
0.6	4.267	3.490	2.726	1.975	1.236	0.507	−0.212	−0.922
0.7	4.129	3.376	2.638	1.912	1.198	0.495	−0.198	−0.882
0.8	4.050	3.321	2.605	1.903	1.212	0.533	−0.137	−0.797
0.9	4.011	3.303	2.610	1.929	1.260	0.601	−0.047	−0.685
1.0	4.000	3.312	2.639	1.978	1.329	0.691	0.062	−0.557
1.2	4.033	3.383	2.746	2.122	1.508	0.906	0.312	−0.272
1.4	4.114	3.497	2.893	2.300	1.719	1.147	0.584	0.030
1.6	4.225	3.638	3.062	2.498	1.945	1.400	0.865	0.337
1.8	4.356	3.795	3.246	2.708	2.179	1.659	1.148	0.643
2.0	4.500	3.964	3.439	2.924	2.418	1.920	1.430	0.947
2.2	4.655	4.141	3.638	3.144	2.659	2.181	1.710	1.247
2.4	4.817	4.324	3.841	3.366	2.899	2.440	1.987	1.541
2.6	4.985	4.511	4.046	3.589	3.140	2.697	2.261	1.831
2.8	5.157	4.701	4.253	3.813	3.379	2.952	2.531	2.116
3.0	5.333	4.893	4.461	4.036	3.618	3.205	2.798	2.397
3.4	5.694	5.284	4.880	4.482	4.090	3.704	3.322	2.945
3.8	6.063	5.678	5.299	4.925	4.557	4.193	3.834	3.478
4.2	6.438	6.076	5.718	5.366	5.018	4.674	4.334	3.998
4.6	6.817	6.475	6.137	5.804	5.474	5.148	4.826	4.507
5.0	7.200	6.876	6.555	6.239	5.925	5.616	5.309	5.005

SCSC plates loaded uniaxially, where the clamped edges were loaded and the simply supported edges were unloaded (σ_y = constant, $\sigma_x = \tau_{xy} = 0$). A total of 20 boron-epoxy laminates were evaluated. Layers of epoxy-bonded boron fibers (Narmco 5505 prepreged type) were combined in directions located with reference to a 0° axis of plate symmetry as indicated in Table 5.14. Material properties of typical plies were: $E_1 = 31 \times 10^6$psi, $E_2 = 2.7 \times 10^6$psi, $G_{12} = 0.75 \times 10^6$psi, $\nu_{12} = 0.28$. Nineteen of the twenty plates were symmetrically laminated (Plate 2 was unsymmetric). Plates 1, 3, 4 and 20 had principal material axes aligned with the plate edges (i.e., orthotropic), the others behaved as anisotropic plates. Plate 11 had 12 plies, plates 15 and 16 had 16 plies, and the others all had 20 plies. Thicknesses varied no more than two percent throughout the plates. Plate dimensions were 10x10 inches within the loading frame, except for plate 11, which measured 10x5 inches. Plate edges had layers of Teflon tape attached to reduce undesirable, secondary inplane forces due to friction, which was found to be very important -- without it, the induced stress resultant N_y was as much as 50 percent of the applied stress resultant, causing buckling loads to be reduced by one-fourth to one-third. The presence of induced secondary stresses was observed by strain gages.

Critical buckling loads were determined by the Southwell method [40]. These are listed in Table 5.15 [112]. Two tests were conducted for each plate. The first test had the zero degree material reference axis aligned with the load. Then each plate (except number 11) was rotated 90° and the tests were repeated. Results from both sets of tests are seen in Table 5.15. Further details about the testing procedure and observations may be obtained from [112].

Sandorff [150] and Baharlou [101] studied a set of SCSC plates with uniaxial load applied to the clamped edges (σ_y = constant, $\sigma_x = \tau_{xy} = 0$). The plates were made of graphite-epoxy, with individual

Table 5.14, Boron-epoxy plate tested by Ashton and Love

Plate no	Description	Layer number										Average thickness (inches)
		1	2	3	4	5	6	7	8	9	10	
1	Orthotropic	0	90	0	90	0	90	0	90	0	90	0.115
2	Unsymmetric	+45	+45	+45	+45	+45	+45	+45	+45	+45	+45	0.112
3	Orthotropic	Same as plate 1										0.102
4	"	"	"	"	"							0.091
5	"	All 20 layers at 0										0.098
6	Anisotropic	All 20 layers at 45										0.105
7	"	Same as plate 6										0.097
8	"	+45	-45	+45	-45	+45	-45	+45	-45	+45	-45	0.102
9	"	Same as plate 8										0.110
10	"	All 20 layers at 30										0.110
11	"	+45	-45	+45	-45	+45	-45					0.063
12	"	0	0	+45	-45	0	0	+45	-45	0	0	0.112
13	"	+30	-30	+30	-30	+30	-30	+30	-30	+30	-30	0.111
14	"	Same as plate 13										0.111
15	"	0	+45	90	-45	0	+45	90	-45			0.085
16	"	Same as plate 15										0.084
17	"	0	0	+30	-30	0	0	+30	-30	0	0	0.107
18	"	Same as plate 17										0.107
19	"	Same as plate 10										0.106
20	Orthotropic	Same as plate 5										0.103

Table 5.15. Experimental uniaxial buckling loads (lb) for SCSC plates corresponding to Table 5.14.

Plate no.	Load orientation	
	0^{o}	90^{o}
1	11,300	9,600
2	5,400	5,610
3	9,500	9,000
4	7,400	7,200
5	12,400	4,350
6	5,600	6,100
7	4,650	5,600
8	8,600	8,400
9	9,900	9,600
10	8,950	5,200
11	3,650	—
12	14,700	7,550
13	12,700	7,600
14	12,650	7,750
15	6,100	5,100
16	5,400	4,800
17	14,200	5,400
18	13,200	5,900
19	7,700	4,760
20	13,700	4,200

Table 5.16. Uniaxial buckling stress resultants $-N_y$ (lb/in) for SCSC anisotropic plates (σ_y = constant, $\sigma_x = \tau_{xy} = 0$).

Dimensions a x b (in)	Experimental results [150]	Theoretical results	
		Sandorff [150]	Baharlou [101]
3.003x9.625	4530 4290	5185	5070
2.503x9.625	5910 5740	7249	7004
2.003x9.625	8140 8360	10,760	10,460

plies having the following properties: $E_1 = 19.0 \times 10^6$psi, $E_2 = 1.5 \times 10^6$psi, $G_{12} = 0.80 \times 10^6$psi, $\nu = 0.30$. The laminate orientation was $(0/45/0/0/-45/0)_{2S}$. The plates all had the same length in the loaded direction (b = 9.625 in) and the same thickness (h = 0.1232 in). Three plate widths were considered (a = 3.003, 2.503, 2.003 in). Buckling stress resultants (lb/in) for the three plates are given in Table 5.16. It is seen that as the width of the plate (a) is decreased from 3.003 in to 2.003 in, the difference between the two sets of theoretical results and the experimental data becomes quite significant.

Several other publications dealing with the buckling of SCSC anisotropic plates have appeared [26,151-153].

5.3. SFSF

In Table 5.17 are listed the experimental buckling loads obtained by Mandell [34,35] for SFSF anisotropic plates having the simply supported edges subjected to uniaxial loading. The plates are those described previously in Section 5.1 (Tables 5.4-5.6). Theoretical results in all cases were calculated on the assumption that the plate bends as a simply supported beam having no transverse curvature or twist (see description of analysis in Section 3.6). Theoretical results obtained by the Ritz method developed by Ashton [42] are also given for several of the plates in Table 5.17.

5.4. CCCC

Ashton [42] investigated the effect of varying θ upon the uniaxial (σ_x = constant, $\sigma_y = \tau_{xy} = 0$) buckling loads of parallel fiber composite plates, as the angle (θ) between the principal material axes and the plate edges is varied. The Ritz method was used, with assumed displacements taken as the product of vibrating beam functions. The material

Table 5.17. Uniaxial buckling loads ($-N_x$, lb/in) for Mandell's SFSF anisotropic plates

Plate no.	Experimental	Theoretical
203a	33.8	44.9
203b	34.7	44.9
208	8.27	9.30
401	30.3	37.8
		34.3**
402	137	161
		150**
403a	53	70.6
		60.8**
403b	45	170.6
		160.8**
406	89	150
		132**
407	30.1	35.1
		30.0**
408a	41.6	79.6
		51.8**
408b	34.2	70.6
		51.8**

** obtained by the Ritz method

properties taken in the direction of principal axes were: $E_L/E_T = 10$, $G_{LT}/E_T = 0.25$, $\nu_{LT} = 0.3$. Numerical results for the nondimensional buckling parameter $-\sigma_x hb^2/D_{\phi\phi}$ are shown in Table 5.18 for a/b = 1 and 2, and for a variation of θ between zero and ninety degrees. Results are also given for an "orthotropic solution" for a/b = 1, wherein the D_{16} and D_{26} bending stiffnesses are omitted. The results for the square plate are also plotted in Figure 5.11. It is seen that neglect of the D_{16} and D_{26} terms yields results which are considerably too high for θ in the vicinity of 45°. The orthotropic analysis also corresponds to an angle-ply plate having an infinite number of plies alternating at $\pm\theta$, and practical laminates will yield results which fall between the two curves of Figure 5.11. The node lines (lines of zero displacement) for the critical mode shapes are shown in Figure 5.12. For orthotropic plates, these lines are parallel to (or nearly parallel to) the edges, but for anisotropic plates they are not.

Experimental results for the buckling of uniaxially loaded CCCC plates were obtained by Ashton and Love [112]. These are given in Table 5.19. For information concerning the plates tested, see Table 5.14 and Section 5.1.

Uniaxial and shear buckling parameters $\hat{N}_x$ and $\hat{N}_{xy}$ for angle-ply, graphite-epoxy plates having CCCC edges, as obtained by Housner and Stein [65] were presented in Figures 5.1 and 5.2, respectively. Optimum fiber orientations for such plates and loadings may be seen in Figures 5.13 and 5.14, which may be compared with similar curves for SSSS plates which appeared as Figures 5.3 and 5.4. Interaction curves for buckling due to simultaneous axial compression and shear are seen in Figure 5.15. $\hat{N}_x$ and $\hat{N}_{xy}$ are defined by Equations 5.1 and 5.2, respectively.

The buckling of CCCC anisotropic plates subjected to uniaxial compressive loads was also studied by Ashton and Waddoups [138], using

Table 5.18. Critical buckling loads ($-\sigma_x hb^2/D_{\phi\phi}$) for parallel-fiber CCCC anisotropic plates.

$\frac{a}{b}$	Principal material axis orientation, θ (degrees)							
	0	15	26.6	30	45	60	75	90
1	45.20	39.47	——	29.94	25.35	23.69	21.39	19.65
	45.20*	44.72*	——	43.51*	42.26*	35.37*	24.16*	19.65*
2	25.53	25.19	22.00	——	20.08	18.50	17.75	17.35

* Values from orthotropic analysis (setting $D_{16} = D_{26} = 0$).

Table 5.19. Experimental uniaxial buckling loads (lb) for CCCC plates corresponding to Table 5.14.

Plate no.	Load orientation	
	0^{o}	90^{o}
1	15,500	15,200
2	6,150	6,560
3	13,900	12,200
4	10,300	10,200
5	12,000	4,900
6	6,840	7,150
7	5,800	6,100
8	10,700	10,100
9	12,100	11,700
10	9,800	8,200
11	4,550	——
12	17,600	10,600
13	13,600	9,500
14	13,900	9,800
15	6,950	6,250
16	6,850	6,600
17	15,400	6,700
18	15,500	7,350
19	8,700	6,500
20	14,900	5,880

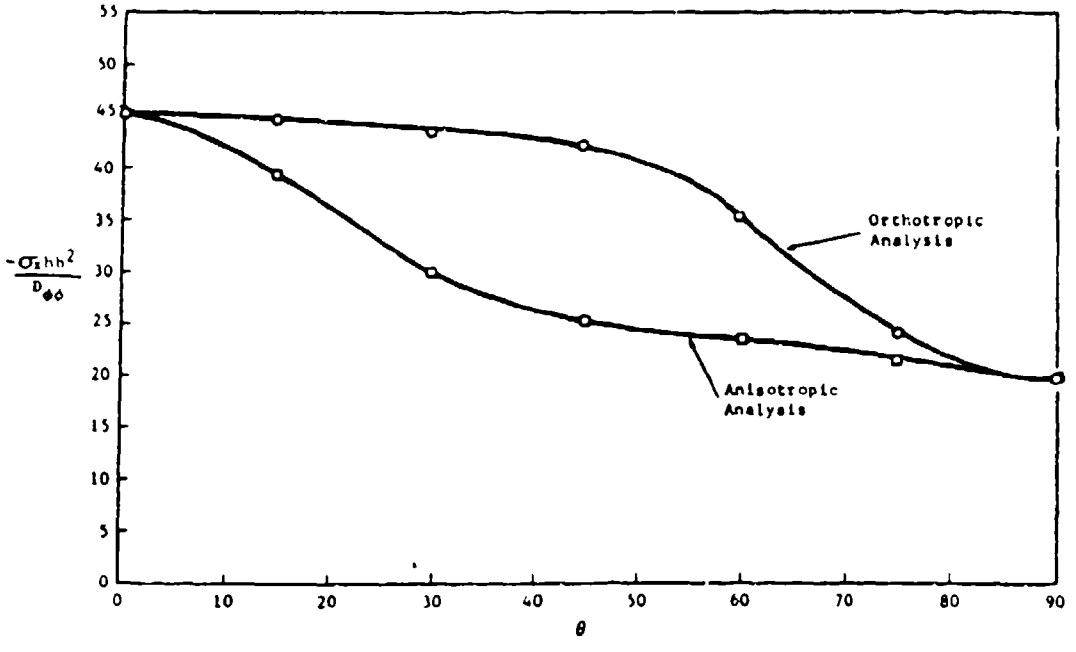

Figure 5.11. Comparison of anisotropic and orthotropic solutions for uniaxial buckling of a parallel-fiber CCCC plate.

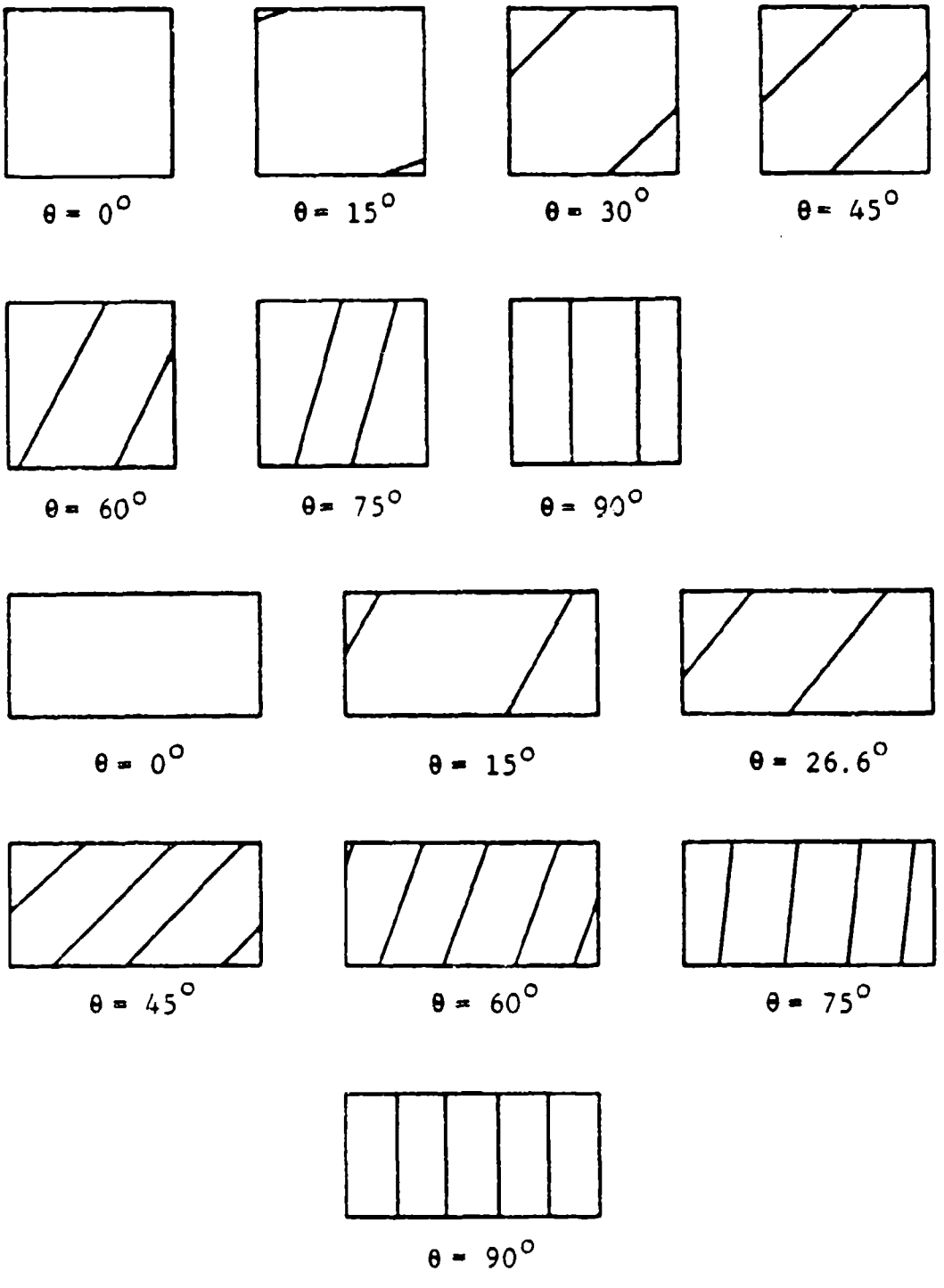

Figure 5.12. Node lines for the buckled anisotropic CCCC plates corresponding to Table 5.18.

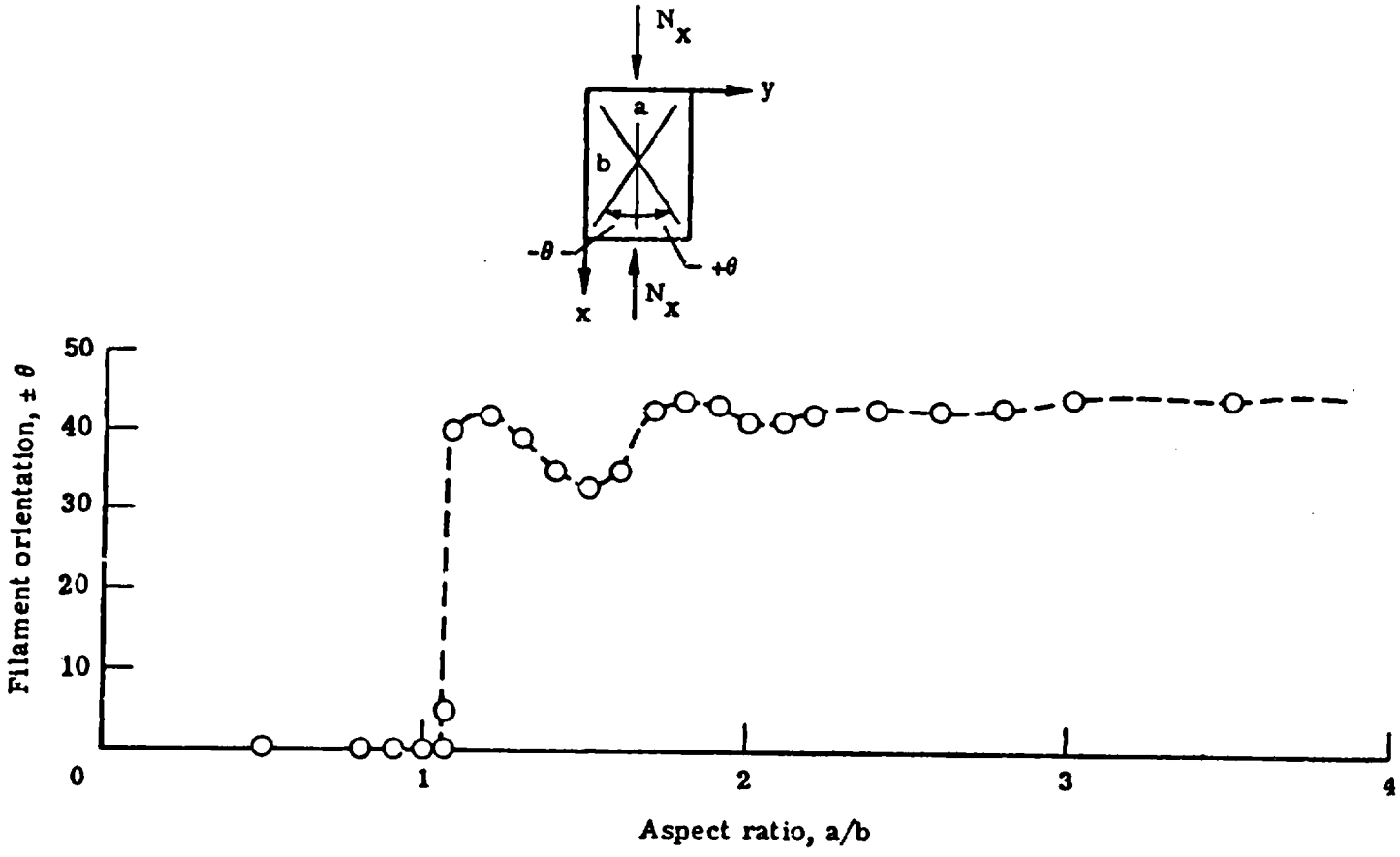

Figure 5.13. Optimum filament orientation for the uniaxial buckling of a CCCC plate.

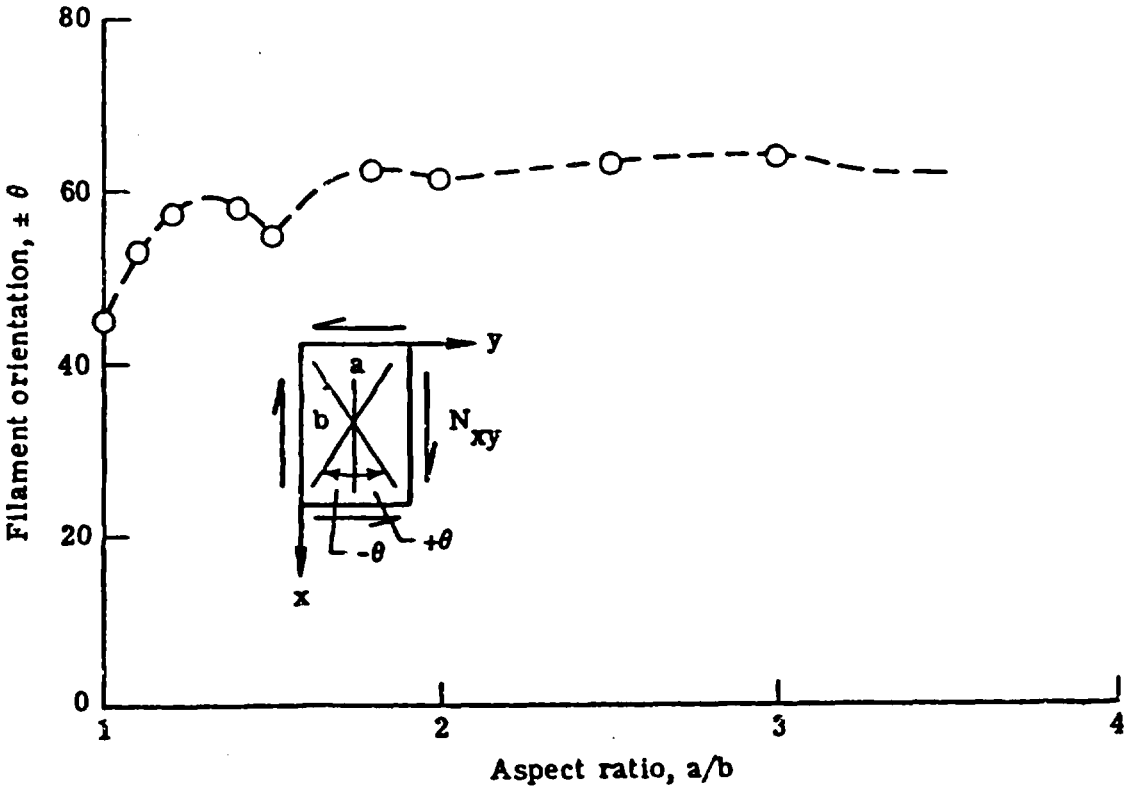

Figure 5.14. Optimum filament orientation for the uniaxial shear of a CCCC plate.

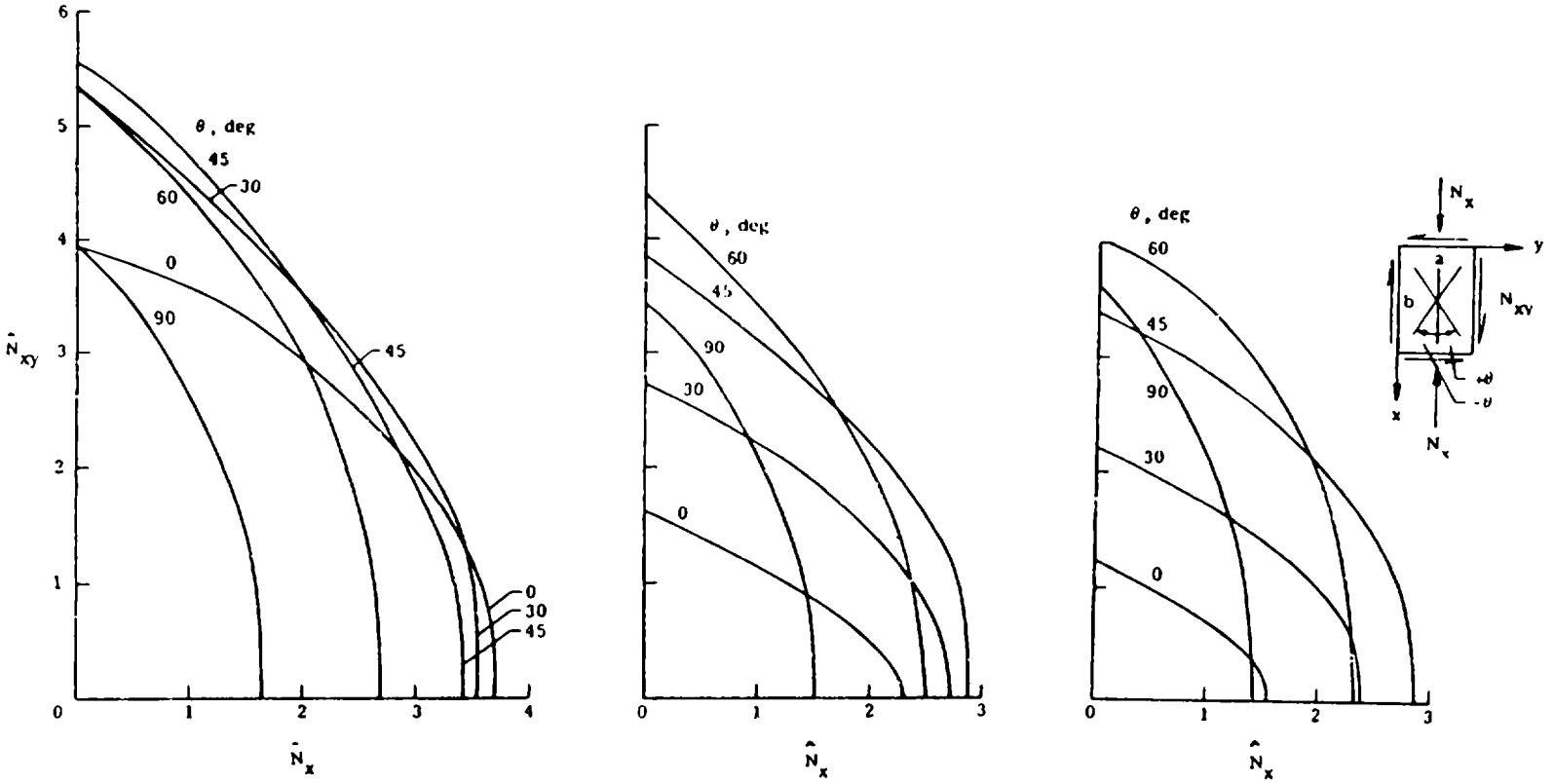

(a) a/b = 1. (b) a/b = 2. (c) a/b = 5.

Figure 5.15. Buckling parameters for CCCC angle-ply plates subjected to combined axial compression and shear.

the Ritz method with beam functions, and by Green and Hearmon [26] and Whitney [154,155], using a series (or superposition) method with trigonometric functions. Fraser and Miller [156,157] analyzed these problems for uniaxial compression and shear loading by means of the Ritz method with trigonometric functions and Lagrange multipliers.

The case of the infinitely long anisotropic plate clamped along its two edges (y = 0,b) and subjected to combined longitudinal (σ_x), transverse (σ_y), shear (τ_{xy}) and inplane bending (see Equation 2.43) was analyzed by Wittrick [120]. Critical values of the parameter K_L are given in Table 5.20 as the parameters Ω^2 and K_S^2 are varied, for the case of no bending stress. The parameters are defined in Equations 5.6. The infinite strip having its principal material axis oriented at 45° with respect to the clamped sides, subjected to uniaxial compression or shear, was also treated by Thielemann [136,137].

5.5. ELASTIC EDGE CONSTRAINTS

Symmetrically laminated angle-ply plates having all their edges elastically restrained against rotation were analyzed by Housner and Stein [65]. Uniaxial compression and shear buckling parameters $\hat{N}_x$ and $\hat{N}_y$, as defined by Equations 5.1 and 5.2 are plotted in Figures 5.16 through 5.21, respectively. The rotational spring constant k_r used in the abscissas relates the rotational moment to the change in slope at each edge by

$$M_n = k_r \frac{\partial w}{\partial n} \tag{5.7}$$

where n is the direction of the normal to the edge. The springs are uniformly distributed along all four edges. The other edge condition is w = 0. Thus, $k_r = 0$ and ∞ correspond to SSSS and CCCC plates, respectively.

Table 5.20. Critical values of K_L for buckling of a clamped, infinite strip with $K_B=0$.

K_S^2 =	0	10	20	30	40	50	60	70	80	90
Ω^2 = 0.2	28.381	27.103	25.832	24.567	23.309	22.058	20.812	19.573	18.340	17.113
0.3	19.914	18.666	17.427	16.198	14.978	13.766	12.563	11.367	10.180	9.000
0.4	15.728	14.509	13.302	12.106	10.920	9.745	8.579	7.423	6.276	5.138
0.5	13.256	12.065	10.887	9.721	8.568	7.426	6.295	5.175	4.064	2.964
0.6	11.641	10.476	9.325	8.189	7.065	5.954	4.855	3.768	2.691	1.624
0.7	10.514	9.375	8.251	7.141	6.046	4.964	3.894	2.837	1.790	0.754
0.8	9.694	8.579	7.479	6.396	5.327	4.272	3.230	2.200	1.181	0.174
0.9	9.078	7.985	6.910	5.851	4.807	3.777	2.760	1.756	0.764	−0.217
1.0	8.604	7.534	6.482	5.445	4.425	3.419	2.426	1.446	0.478	−0.479
1.2	7.943	6.915	5.904	4.911	3.934	2.971	2.022	1.086	0.162	−0.751
1.4	7.527	6.537	5.565	4.611	3.673	2.749	1.839	0.942	0.057	−0.817
1.6	7.263	6.309	5.374	4.455	3.552	2.664	1.789	0.927	0.077	−0.763
1.8	7.102	6.181	5.279	4.393	3.523	2.667	1.824	0.994	0.175	−0.634
2.0	7.012	6.123	5.251	4.396	3.556	2.729	1.916	1.114	0.324	−0.456
2.2	6.975	6.114	5.271	4.444	3.632	2.833	2.046	1.271	0.507	−0.247
2.4	6.976	6.143	5.326	4.526	3.739	2.965	2.204	1.453	0.713	−0.017
2.6	7.007	6.200	5.409	4.632	3.870	3.120	2.381	1.654	0.936	0.228
2.8	7.062	6.279	5.511	4.758	4.018	3.290	2.573	1.867	1.170	0.482
3.0	7.136	6.376	5.630	4.899	4.180	3.472	2.776	2.089	1.412	0.743
3.4	7.328	6.609	5.904	5.212	4.531	3.862	3.202	2.552	1.910	1.276
3.8	7.562	6.881	6.212	5.556	4.910	4.273	3.647	3.028	2.418	1.815
4.2	7.827	7.180	6.544	5.919	5.304	4.698	4.101	3.511	2.929	2.354
4.6	8.115	7.498	6.892	6.296	5.709	5.130	4.560	3.996	3.440	2.889
5.0	8.420	7.831	7.252	6.682	6.121	5.567	5.021	4.481	3.947	3.420

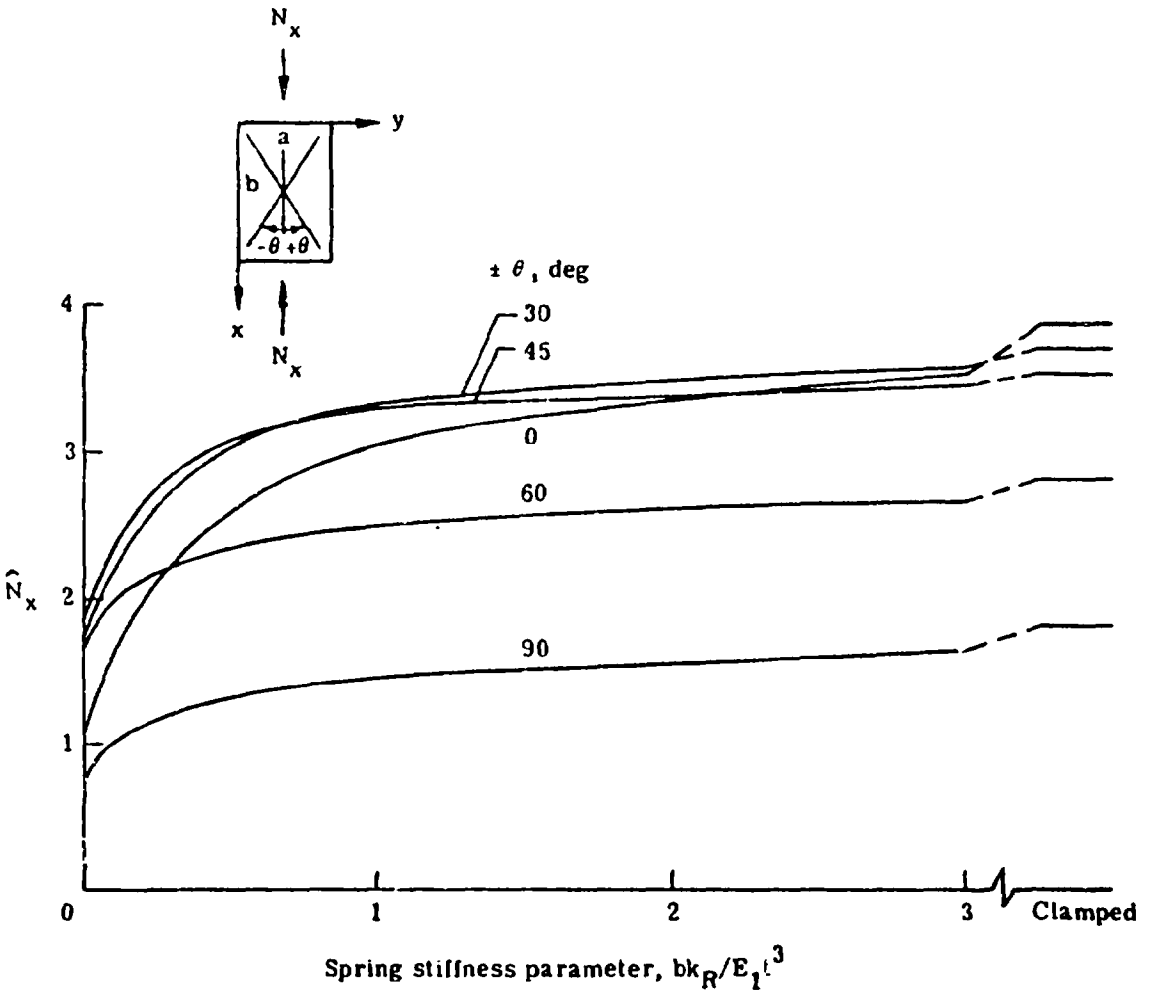

(a) a/b = 1.

Figure 5.16. Uniaxial compression buckling parameters for rotationally constrained, angle-ply plates (a/b = 1).

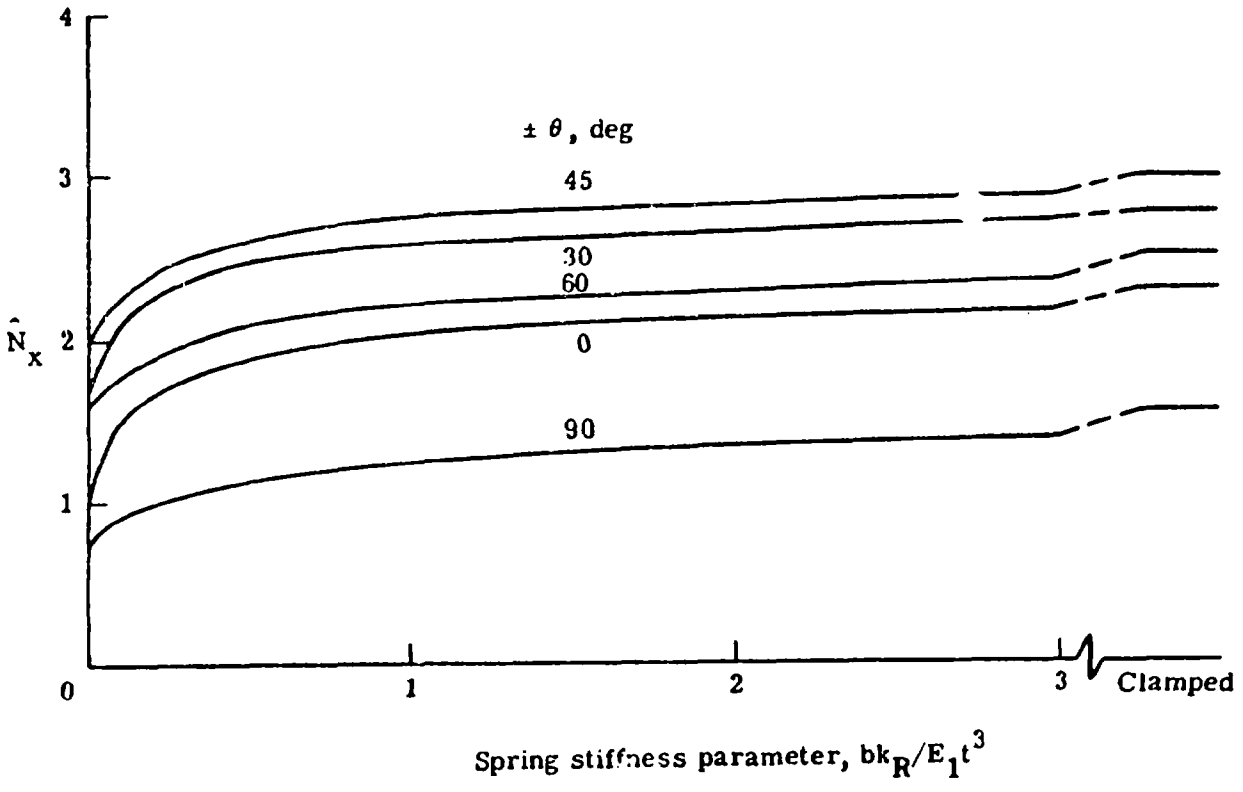

(b) a/b = 2.

Figure 5.17. Uniaxial compression buckling parameters for rotationally constrained, angle-ply plates (a/b = 2).

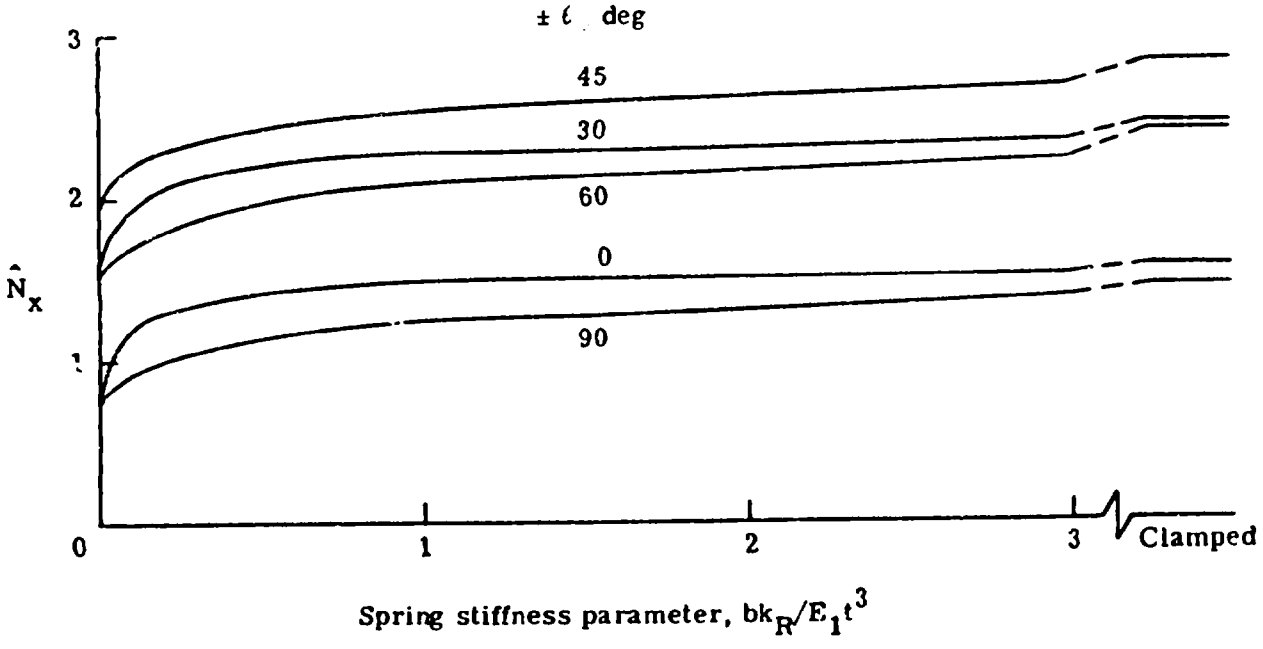

(c) a/b = 5.

Figure 5.18. Uniaxially compression buckling parameters for rotationally constrained, angle-ply plates (a/b = 5).

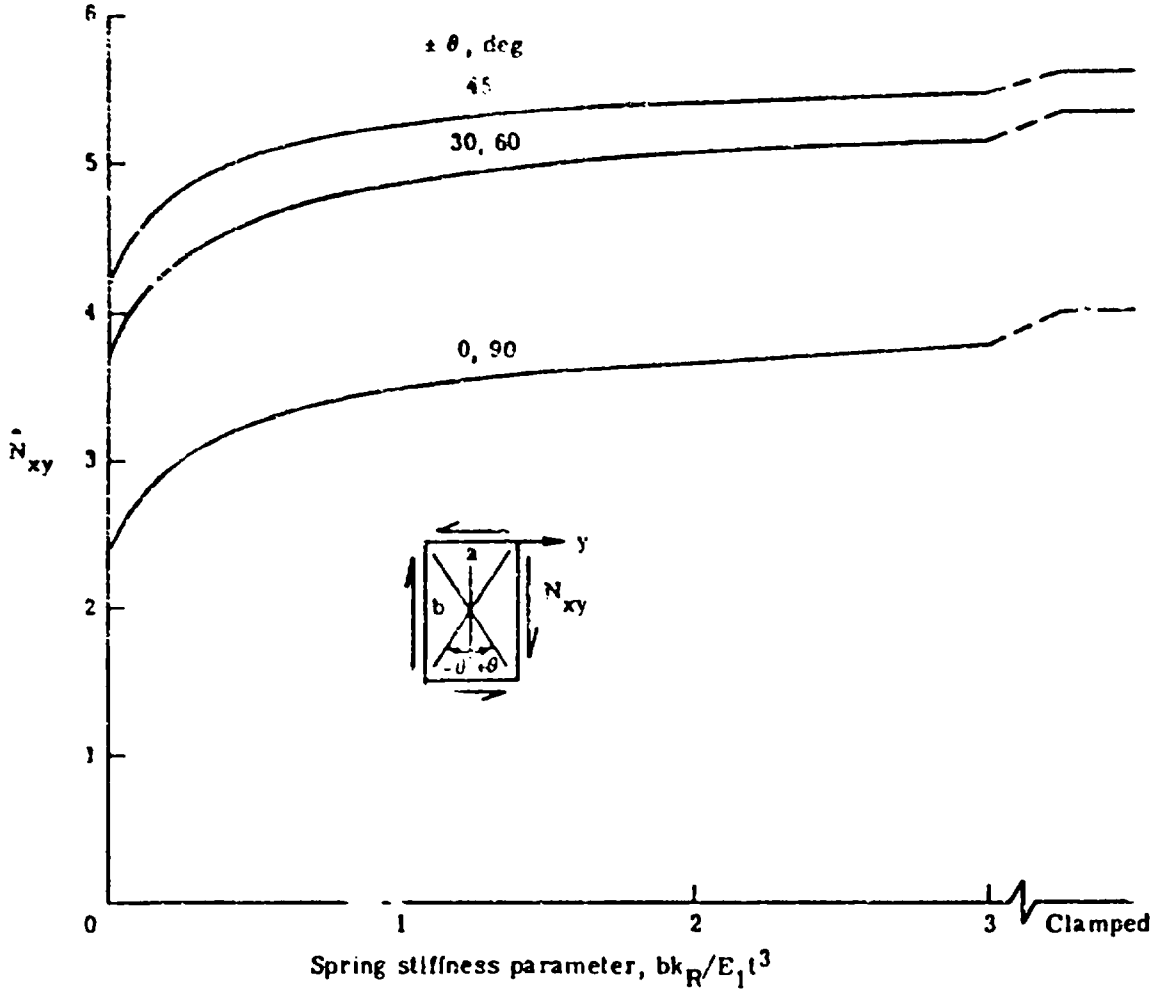

(a) a/b = 1.

Figure 5.19. Shear buckling parameters for rotationally constrained, angle-ply plates (a/b = 1).

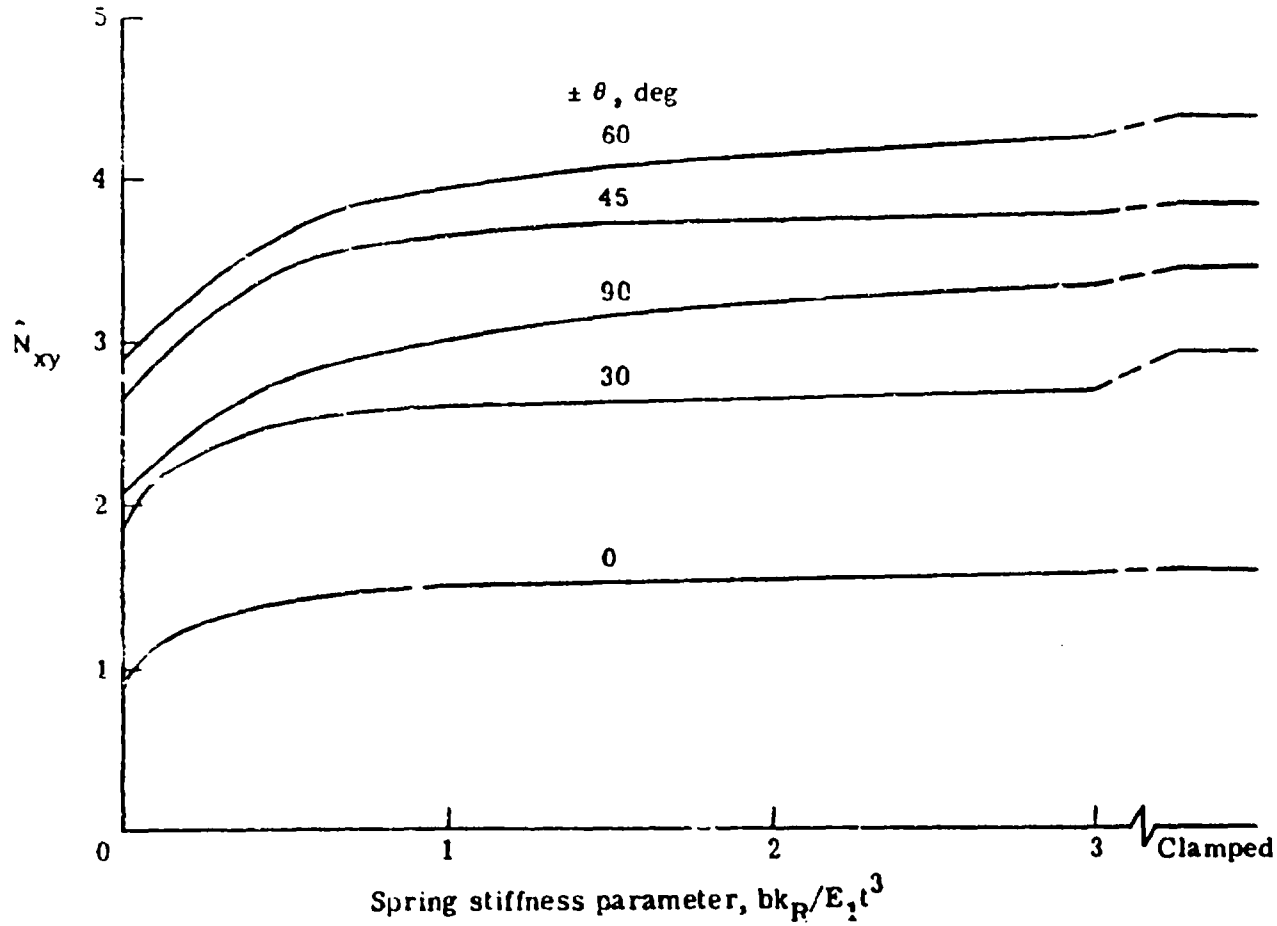

(b) a/b = 2.

Figure 5.20. Shear buckling parameters for rotationally constrained, angle-ply plates (a/b = 2).

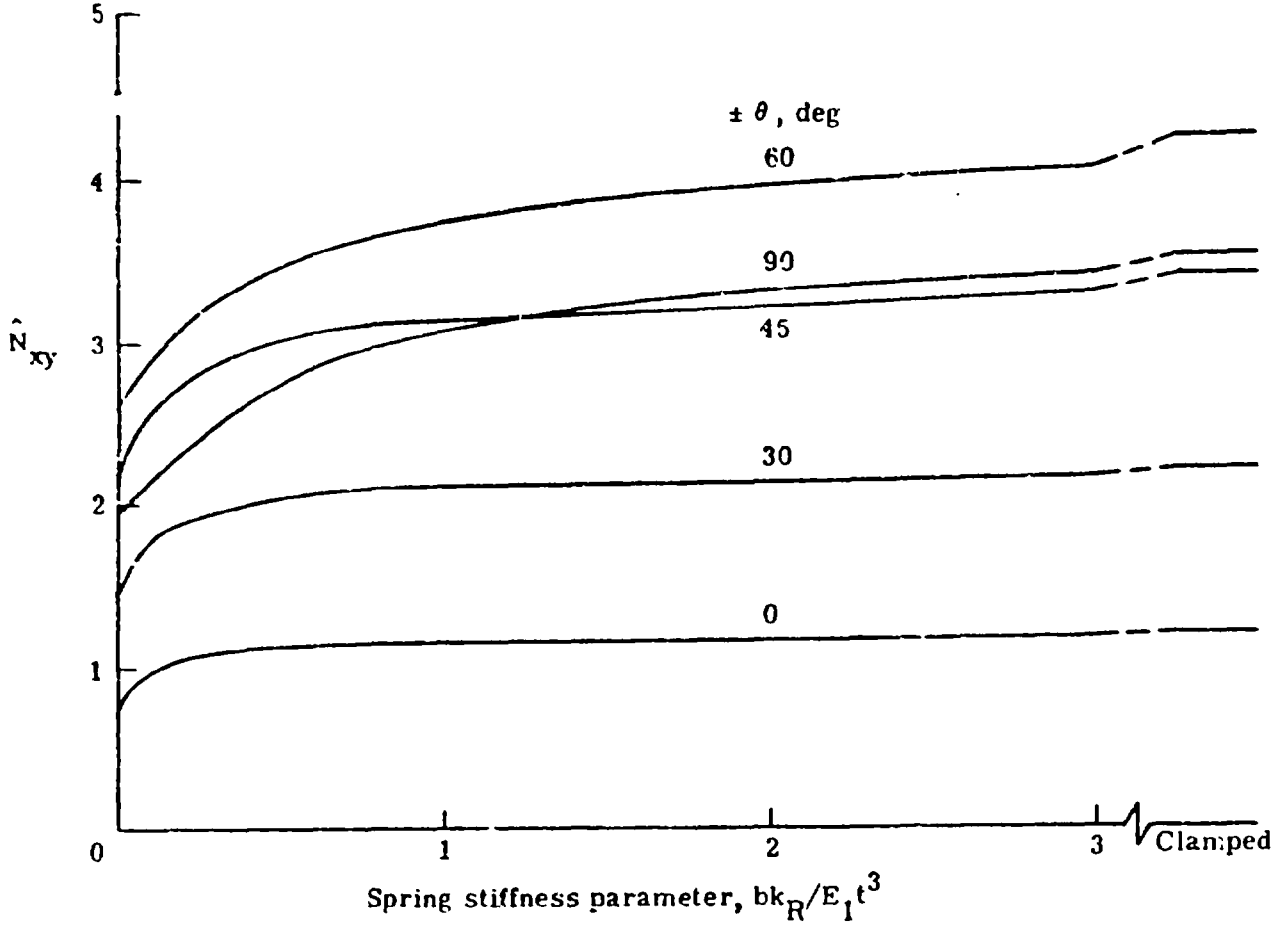

(c) a/b = 5.

Figure 5.21 Shear buckling parameters for rotationally constrained, angle-ply plates (a/b = 5).

CHAPTER VI. UNSYMMETRIC LAMINATES

In general, laminated composite plates will be fabricated with ply arrangements which are not necessarily symmetrical with respect to the midplane of the plate. This situation may arise either in a general stacking sequence, or in certain special ones. An example of the latter configuration is the cross-ply plate having an even number of equal thickness plies, which is an antisymmetrical laminate. Examples of symmetrical, antisymmetrical and more generally unsymmetrical cross-ply layups are shown in Figure 6.1 [158]. The adjective "regular" denotes equal thickness plies.

The equations governing the bifurcation buckling of an unsymmetrical laminate are derived in the Appendix, and may be expressed in terms of the displacements in matrix operator form as

$$\begin{bmatrix} L_{11} & L_{12} & L_{13} \\ L_{21} & L_{22} & L_{23} \\ L_{31} & L_{32} & (L_{33}-F) \end{bmatrix} \begin{Bmatrix} u \\ v \\ w \end{Bmatrix} = \begin{Bmatrix} 0 \\ 0 \\ 0 \end{Bmatrix} \tag{6.1}$$

where the L_{ij} are differential operators representing the plate stiffness, defined in the Appendix by Equations A.21; F is a differential operator representing the inplane stress resultants (N_x, N_y, N_{xy}), defined by Equation A.22; u and v are inplane displacements of the midplane during buckling in the x and y directions; and w is the transverse displacement. It is important to note that u and v are not the inplane displacements which occur with increasing inplane stress resultants, but rather the additional displacements which arise when the buckling load is reached and the plate is deformed in a buckled mode shape of infinitesimal amplitude. These additional inplane displacements characterize the bending-stretching coupling which exists in the deformation of an unsymmetrical laminate. In Equation 6.1 the bending-stretching coupling is induced by

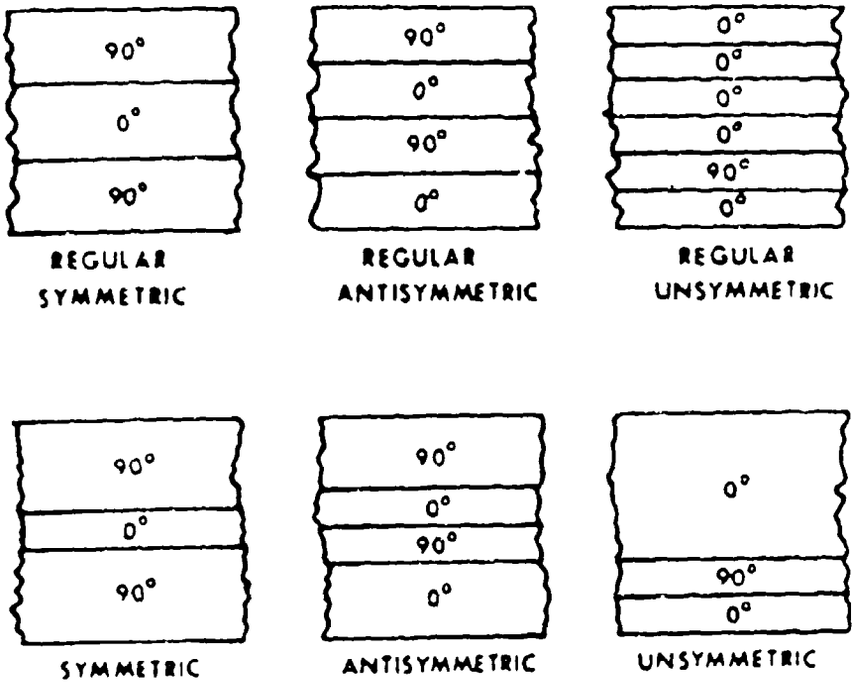

Figure 6.1. Examples of symmetrical, antisymmetrical and unsymmetrical cross-ply laminates.

the operators $L_{13}(=L_{31})$ and $L_{23}(=L_{32})$, which vanish only when the B_{ij} bending-stretching stiffness coefficients (see Equation A.8) are all zero. Then the plate buckling problem reduces to $(L_{33}-F)w = 0$, which is Equation 5.1 previously given for the anisotropic plate.

Equations 6.1 are an eighth order set of differential tions which closely resemble the form of shell buckling equatio , ch are also of eighth order. (Indeed, the coupling between bending and stretching is what links together the two sets of fourth order equations which would otherwise exist for a shell.) Since the equations are of eighth order, four boundary conditions must be specified along each edge to define the problem physically, and to generate a proper mathematical eigenvalue problem.

The first satisfactory theory incorporating bending-stretching effects into the deformations of laminated plates was developed by Reissner and Stavsky [20,159]. This was done for the special case of an antisymmetrical, angle-ply plate, for which $B_{11} = B_{12} = B_{22} = B_{66} = 0$, which leaves B_{16} and B_{26} terms to cause the coupling. Governing equations for the buckling equilibrium position were expressed in terms of w and an Airy stress function (ϕ). Transverse equilibrium and inplane compatibility conditions were then used to generate an eighth order set of equations equivalent to those of Equations A.32 and A.33.

Existence of the bending-stretching coupling in unsymmetrical laminates was questioned (c.f., [159,160]) at the time of the development of the new theory more than two decades ago. But, since then, the effects have been demonstrated and quantified, both theoretically and experimentally. The primary effect is to decrease the stiffness of a plate; therefore, in the case of buckling, critical loads are reduced. As it will be subsequently seen, the effect is strongest when only a small number of plies is used, and decreases as the number increases.

An approximate theory was suggested by Chamis [43] and Ashton [162] for simplifying problems involving unsymmetrical laminates. It replaces the eighth order set of Equations 6.1 by that of anisotropic plate theory, Equation 5.1, where the bending stiffness coefficients D_{ij} are replaced by the "reduced bending stiffness" coefficients D^*_{ij} as given by the last of Equations A.31. The boundary conditions are also reduced in number from four to two, and the resulting solutions are independent of the degree of inplane constraint. Comparisons of results obtained using the "reduced stiffness" versus ones using the complete stiffness matrix show varying degrees of agreement [14,34,162-164] indicating that the approximate theory is not accurate for all problems.

6.1. SSSS

For an unsymmetrically laminated plate, the meaning of a "simply supported" edge is not clear. Assuming that, as in classical plate theory, the edge must have zero transverse displacement and bending moment, there remain yet four possible combinations of "simple" (i.e., not elastically restrained) boundary conditions, depending upon the inplane constraints, viz.

$$\begin{aligned} &S1 : w = M_n = u_n = u_t = 0 \\ &S2 : w = M_n = N_n = u_t = 0 \\ &S3 : w = M_n = u_n = N_{nt} = 0 \\ &S4 : w = M_n = N_n = N_{nt} = 0 \end{aligned} \tag{6.2}$$

where n and t are used to designate directions normal and tangent to a boundary, respectively. The bending moment (M_n), normal stress (N_n) and shear stress (N_{nt}) resultants at edges x = constant or y = constant are related to the displacement components by Equations A.38.

Two closed form, exact solutions are available for unsymmetrically laminated plates subjected to uniform, biaxial stresses (σ_x = constant,

σ_y = constant, $\tau_{xy} = 0$) [165,166]. One is for cross-ply plates having S2 boundary conditions along all edges; the other is for angle-ply plates having S3 edges.

For unsymmetrical cross-ply laminates, $A_{16} = A_{26} = B_{16} = B_{26} = D_{16} = D_{26} = 0$ (antisymmetrical lamination simplifies the problem further, with $A_{11}=A_{22}$, $D_{11}=D_{22}$, $B_{11}=-B_{22}$, and $B_{12}=B_{66}=0$). For plates of this type having S2 conditions at $x = 0,a$ and $y = 0,b$ the exact solution takes the form

$$u = A \cos \frac{m\pi x}{a} \sin \frac{n\pi y}{b}$$

$$v = B \sin \frac{m\pi x}{a} \cos \frac{n\pi y}{b} \qquad (6.3)$$

$$w = C \sin \frac{m\pi x}{a} \sin \frac{n\pi y}{b}$$

with $m,n = 1,2,\ldots$ The similarity of unsymmetrically laminated plate equations and shell equations remarked upon earlier in this chapter is again seen in Equations 6.3, for these are the displacement functions yielding exact solutions for either (a) shallow shells of arbitrary (but uniform) curvature and rectangular planform, with shear diaphragm support conditions along all four edges (cf. [167]), or (b) closed circular cylindrical shells having shear diaphragm supports on the ends (cf. [168], p. 43). Substituting Equations 6.3 into Equation 6.1 yields

$$\begin{bmatrix} C_{11} & C_{12} & C_{13} \\ C_{21} & C_{22} & C_{23} \\ C_{31} & C_{32} & C_{33}+(N_x\alpha^2+N_y\beta^2) \end{bmatrix} \begin{Bmatrix} A \\ B \\ C \end{Bmatrix} = \begin{Bmatrix} 0 \\ 0 \\ 0 \end{Bmatrix} \qquad (6.4)$$

where

$$
\begin{aligned}
C_{11} &= A_{11}\alpha^2 + A_{66}\beta^2 \\
C_{22} &= A_{22}\beta^2 + A_{66}\alpha^2 \\
C_{33} &= D_{11}\alpha^4 + 2(D_{12}+2D_{66})\alpha^2\beta^2 + D_{22}\beta^4 \\
C_{12} &= C_{21} = (A_{12}+A_{66})\alpha\beta \\
C_{13} &= C_{31} = B_{11}\alpha^3 + (B_{12}+2B_{66})\alpha\beta^2 \\
C_{23} &= C_{32} = (B_{12}+2B_{66})\alpha^2\beta + B_{22}\beta^3
\end{aligned}
\tag{6.5}
$$

$$
\alpha = \frac{m\pi}{a} \quad , \quad \beta = \frac{n\pi}{b}
$$

For a nontrivial solution, the determinant of the coefficient matrix of Equation 6.4 must be set equal to zero, yielding the solution for buckling stresses (N_x and N_y are positive in tension):

$$
-N_x\alpha^2 - N_y\beta^2 = C_{33} + \frac{2C_{12}C_{13}C_{23} - C_{11}C_{23}^2 - C_{22}C_{13}^2}{C_{11}C_{22} - C_{12}^2} \tag{6.6}
$$

It is seen that for a symmetrical laminate ($B_{ij} = 0$), the right-hand-side of Equation 6.6 reduces to C_{33}, and the equation is the same as Equation 2.22 for the biaxially loaded, orthotropic plate having SSSS edge conditions. For parametric studies, it may be desirable to recast Equation 6.6 in terms of nondimensional parameters, as was done in changing Equation 2.22 to 2.24. Once the eigenvalues (nondimensional buckling parameters) are found from Equation 6.6, the eigenfunctions (buckled mode shapes) are found in the usual manner for an eigenvalue problem; that is, an eigenvalue is substituted back into Equation 6.4, and the

eigenvector (A/C, B/C) which determines the eigenfunction is obtained by solving any two of the three linear equations represented by Equation 6.4.

Jones [158] obtained numerical results for antisymmetrical and unsymmetrical cross-ply laminates having S2 edge conditions, subjected to uniaxial loads. Figure 6.2 shows the variation of $N_x b^2/\pi^2 D_{22}$ with a/b for representative graphite/epoxy plates ($E_1/E_2 = 40$, $G_{12}/E_2 = 0.5$, $\nu_{12} = 0.25$) having 2, 4, 6 and an infinite number of layers. The results for an antisymmetrical laminate become the same as those for an orthotropic plate as the number of layers goes to infinity (for B_{11}, the only remaining bending-stretching stiffness coefficient, then goes to zero). Figure 6.2 shows that for a/b = 1, neglect of the B_{ij} for a two-layer plate will result in an orthotropic solution for the buckling load which is about three times the correct value. As the number of layers increases, the antisymmetrical solution rapidly approaches the orthotropic solution, indicating a rapid decrease in B_{11}. For four and six layers, the orthotropic solution for a/b = 1 is in error by 19 and 8 percents, respectively [158]. It is interesting to note in Figure 6.2 that the values of a/b where the minimum buckling loads occur, are unchanged as the number of layers changes. The same may be said for the locations of the cusps, where the buckled mode shape changes from m to m + 1 half-waves. The values of $N_x b^2/\pi^2 D_{22}$ for a/b = 1 are 0.7481, 1.7783, 1.9691 and 2.1218 for 2, 4, 6 and ∞ layers, respectively. Identically the same values occur for a/b = 2 and 3.

Figure 6.3 [158] shows the variation in uniaxial buckling load with E_1/E_2 for plates having $G_{12}/E_2 = 0.5$, $\nu_{12} = 0.25$ and a/b = 1. The loading parameter is plotted in the normalized form N_x/N_o, where N_o is the critical load for the orthotropic plate. These results may be used to demonstrate, for example, that the orthotropic solution for a two-layer, antisymmetrically laminated square plate is approximately 75 percent too high. However, for six layers it is only 5 percent too high [158].

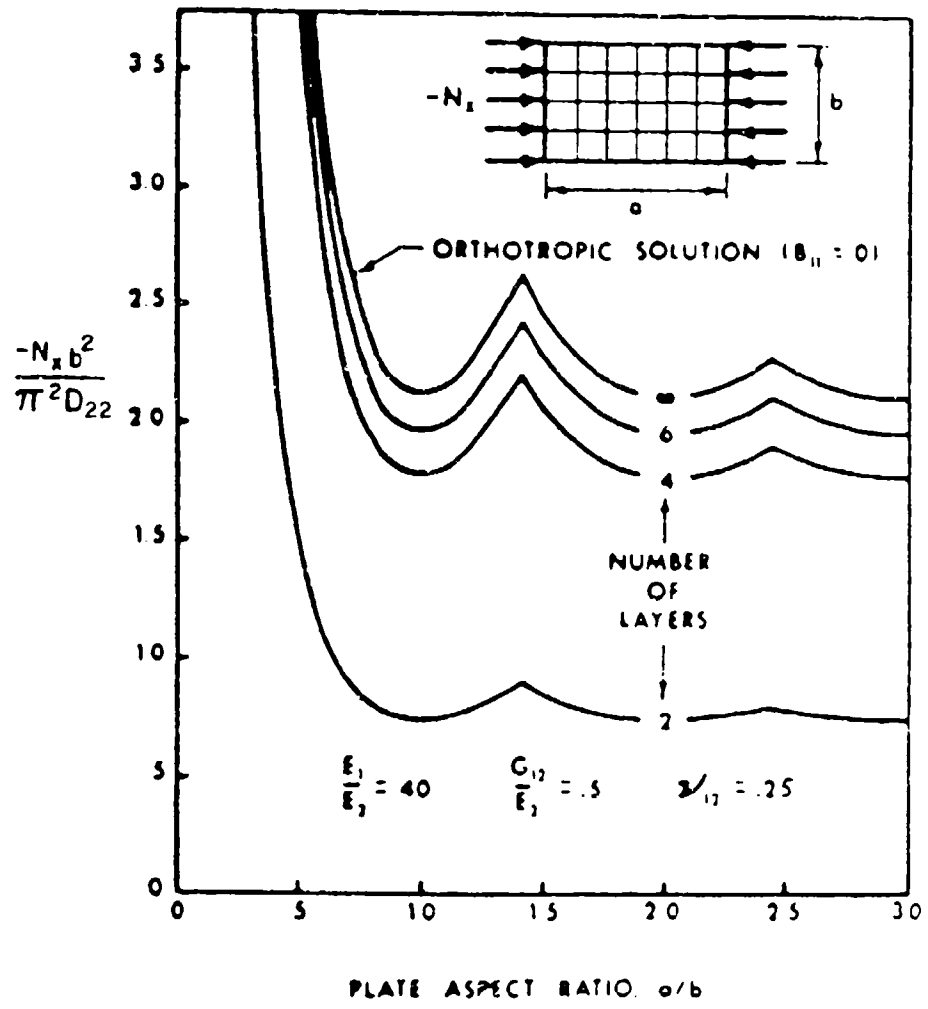

Figure 6.2. Comparison of antisymmetrical and orthotropic solutions with varying a/b for uniaxially loaded, cross-ply plates having 52 edge conditions.

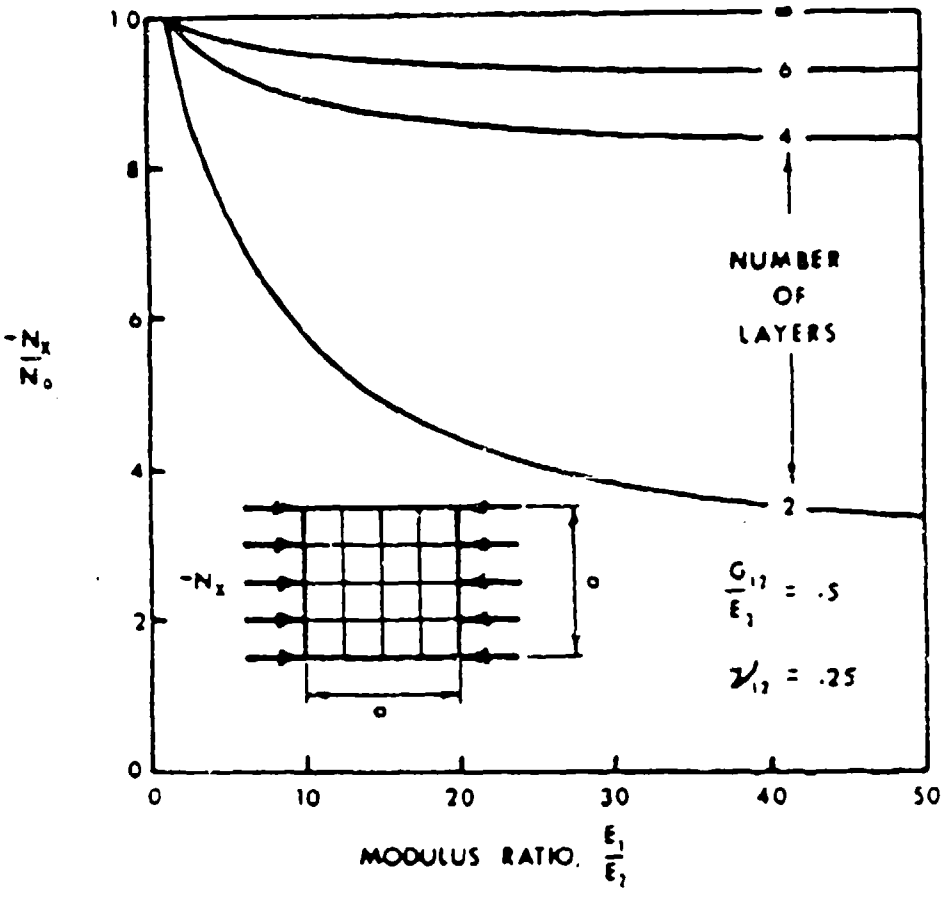

Figure 6.3. Comparison of antisymmetrical and orthotropic solutions with varying E_1/E_2 for uniaxially loaded, cross-ply plates having S2 edge conditions (a/b = 1).

Results were also obtained by Jones [158] for an unsymmetrically laminated cross-ply plate having S2 edge conditions for the case of a laminate having the fibers in the second layer from the bottom oriented 90° and the fibers in all other layers oriented at 0° to the direction of loading (x-axis). Thus, for a constant thickness laminate, the 90° layer becomes thinner and moves to the bottom of the laminate as the number of layers increases (see Figure 6.4). The buckling parameter $-N_x b^2/E_2 h^3$ versus number of layers is plotted in Figures 6.5 and 6.6 for graphite/epoxy and boron/epoxy plates, respectively. In both cases, $a/b = 2$. In both figures, one comparison is made with the buckling load for a parallel-fiber laminate having 0° fiber orientation, and another is with an orthotropic solution (setting all $B_{ij} = 0$). The discontinuity observed for the latter curve in Figure 6.6 is due to a mode shape change. In the case of three layers, the laminate is symmetrical, and the exact solution coincides with the orthotropic solution. It is particularly important to note that in both Figures 9 and 10, but especially in the former case where $E_1/E_2 = 40$, the exact solution approaches the orthotropic solution with increasing number of layers much more slowly than was seen previously for the antisymmetrical laminates (Figures 6.1 and 6.2). Significant differences are seen to exist even with 40 layers.

For antisymmetrical angle-ply laminates, $A_{16} = A_{26} = D_{16} = D_{26} = B_{11} = B_{22} = B_{12} = 0$ (cf. [16], pp. 169-170). For plates of this type having S3 boundary conditions (see Equations 6.2) at $x = 0,a$ and $y = 0,b$ and biaxial loading the exact solution takes the form [165,166]

$$u = A \sin \frac{m\pi x}{a} \cos \frac{n\pi y}{b}$$

$$v = B \cos \frac{m\pi x}{a} \sin \frac{n\pi y}{b} \qquad (6.7)$$

$$w = C \sin \frac{m\pi x}{a} \sin \frac{n\pi y}{b}$$

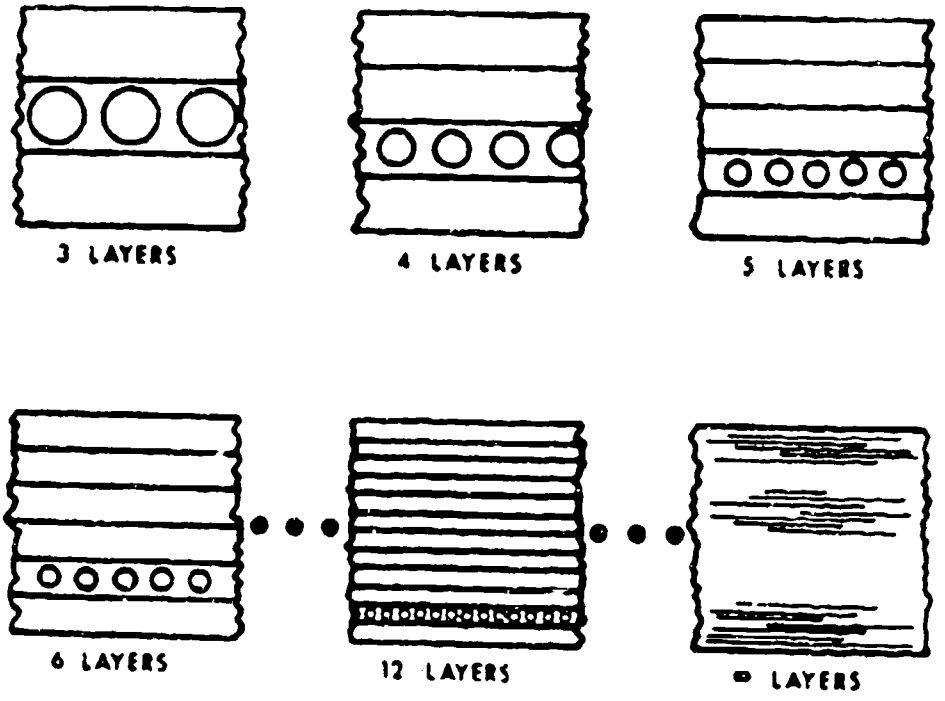

Figure 6.4. Unsymmetrical laminate having one 90° layer located second from the bottom.

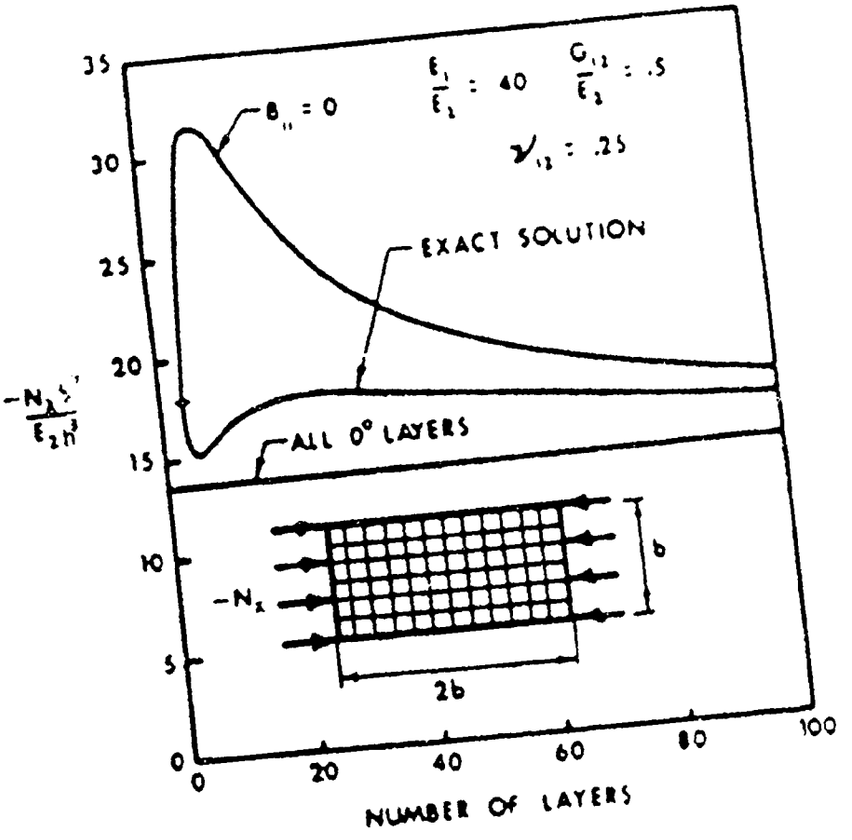

Figure 6.5. Comparison of unsymmetrical, orthotropic and parallel-fiber solutions for graphite/epoxy, cross-ply plates having S2 edges and the layups shown in Figure 6.4.

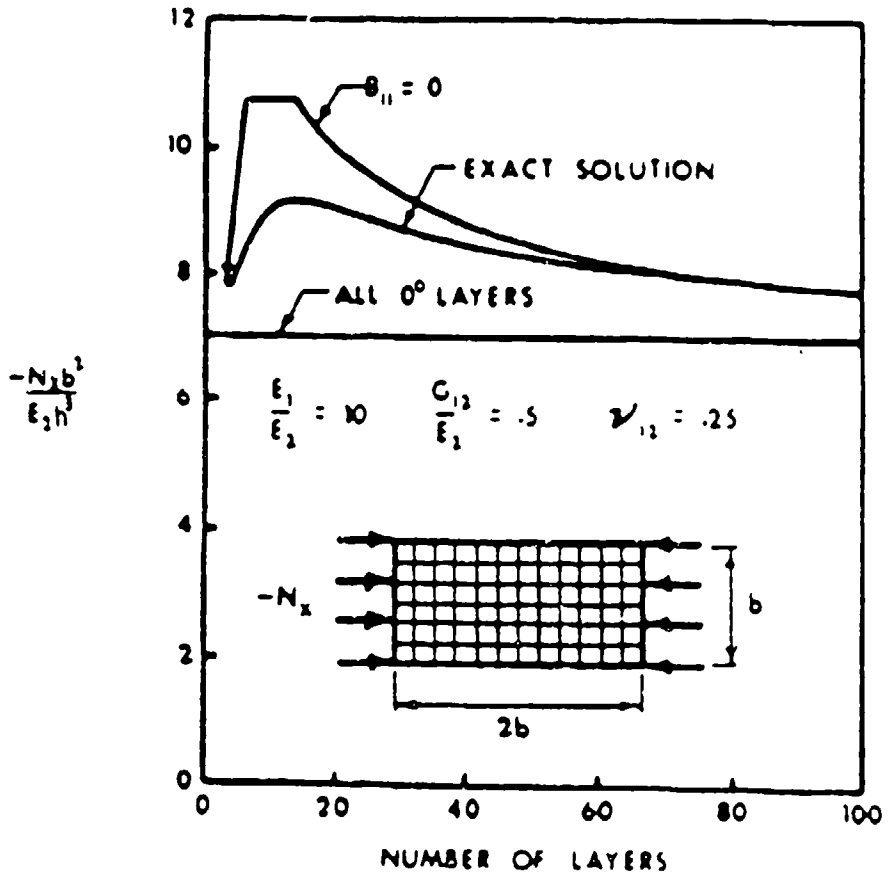

Figure 6.6. Comparison of unsymmetrical, orthotropic and parallel-fiber solutions for boron/epoxy, cross-ply plates having S2 edges and the layups shown in Figure 6.4.

Substituting Equations 6.7 into 6.1 again yields a set of algebraic equations which may be written in the matrix form of Equation 6.4, where now

$$
\begin{aligned}
C_{11} &= -(A_{11}\alpha^2+A_{66}\beta^2) \\
C_{22} &= -(A_{22}\beta^2+A_{66}\alpha^2) \\
C_{33} &= D_1\alpha^4 + 2(D_{12}+2D_{66})\alpha^2\beta^2 + D_{22}\beta^4 \\
C_{12} &= C_{21} = -(A_{12}+A_{66})\alpha\beta \\
C_{13} &= C_{31} = 3B_{16}\alpha^2\beta + B_{26}\beta^3 \\
C_{23} &= C_{32} = B_{16}\alpha^3 + 3B_{26}\alpha\beta^2 \\
\alpha &= \frac{m\pi}{a} \quad , \quad \beta = \frac{n\pi}{b}
\end{aligned}
\tag{6.8}
$$

The critical buckling stress resultants are given by Equation 6.6, where now the C_{ij} are defined by Equations 6.8. It was also shown [165,166,169] that the buckling stress may be written as

$$
\begin{aligned}
-\sigma_x h = \frac{\pi^2}{a^2\left[m^2+n^2\left(\frac{\sigma_y}{\sigma_x}\right)R^2\right]} &\{D_{11}m^4 + 2(D_{12}+2D_{66})m^2n^2R^2 + D_{22}n^4R^4 \\
&- \frac{1}{J_6}[J_4m^2(B_{16}m^2+3B_{26}n^2R^2) + J_5n^2R^2(3B_{16}m^2+B_{26}n^2R^2)]\}
\end{aligned}
\tag{6.9}
$$

where

$$J_4 = (A_{11}m^2+A_{66}n^2R^2)(B_{16}m^2+3B_{26}n^2R^2)$$
$$- (A_{12}+A_{66})(3B_{16}m^2+B_{26}n^2R^2)n^2R^2$$

$$J_5 = (A_{66}m^2+A_{22}n^2R^2)(3B_{16}m^2+B_{26}n^2R^2)$$
$$- (A_{12}+A_{66})(B_{16}m^2+3B_{26}n^2R^2)m^2$$

$$J_6 = (A_{11}m^2+A_{66}n^2R^2)(A_{66}m^2+A_{22}n^2R^2)$$
$$- (A_{12}+A_{66})^2m^2n^2R^2$$

with $R = a/b$.

Jones, Morgan and Whitney [170] obtained numerical results for antisymmetrical angle-ply laminates using the above exact solution. The buckling parameter $-N_xb^2/E_2h^2$ is plotted versus lamination angle (θ) for uniaxial and hydrostatic ($N_x = N_y$ = constant, $N_{xy} = 0$) compression in Figures 6.7 and 6.8, respectively, for the case of a square plate, with $E_1/E_2 = 40$, $G_{12}/E_2 = 0.5$ and $\nu_{12} = 0.25$ (corresponding to graphite/epoxy material with $E_1 = 30\text{x}10^6$psi, $E_2 = 0.75\text{x}10^6$psi, $G_{12} = 0.375\text{x}10^6$psi, $\nu = 0.25$). Corresponding data are also given in Tables 6.1 and 6.2. Comparisons are made for plates having 2, 4, 6 and infinite layers, the last case corresponding to an orthotropic plate (B_{ij} all zero). It is seen for both types of loadings that the optimum lamination angle is $\theta = 45^o$, and the error in using orthotropic analysis for the antisymmetrically laminated plate is very large for $\theta = 45^o$, being 211 percent for both types of loading. Chen and Bert [169] and Hayashi [126,127] also determined the optimum angle for maximum uniaxial buckling load to be $\theta = 45^o$ for a series of antisymmetrically laminated angle-ply plates with S3 boundary conditions.

Consider next the antisymmetrically laminated angle-ply plate having S4 edge conditions (see Equation 6.2) all around. This problem was solved

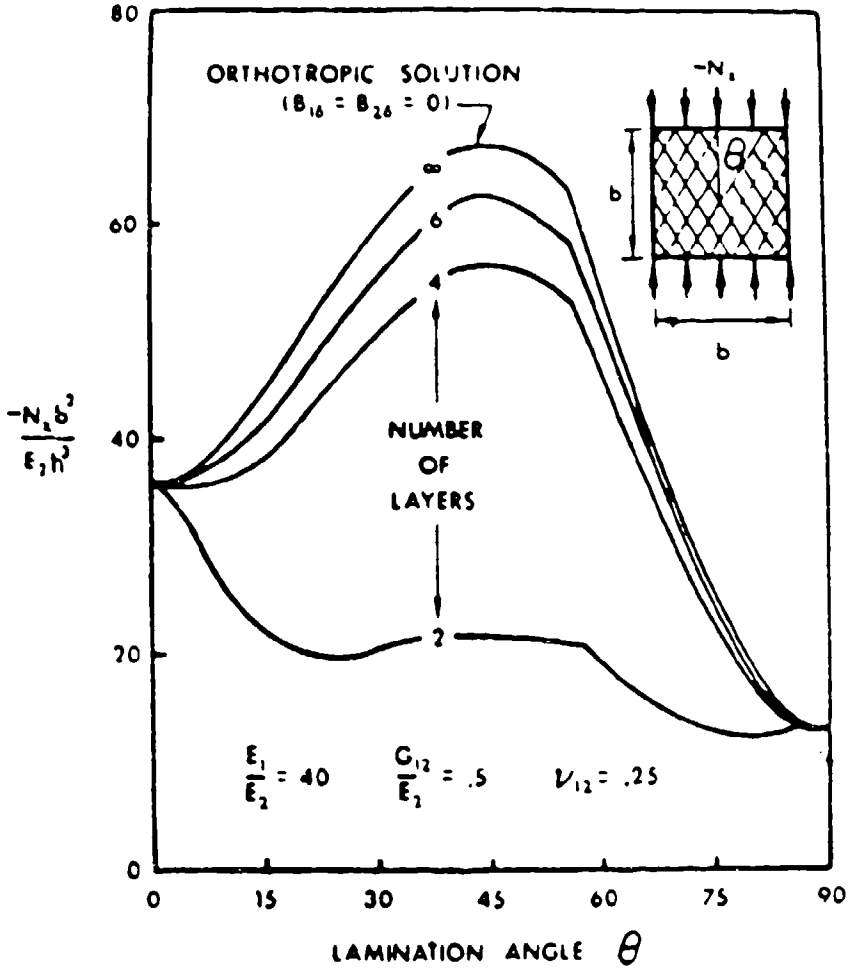

Figure 6.7. Comparison of antisymmetrical and orthotropic solutions with varying lamination angle for uniaxially loaded, angle-ply plates having S3 edge conditions (a/b = 1).

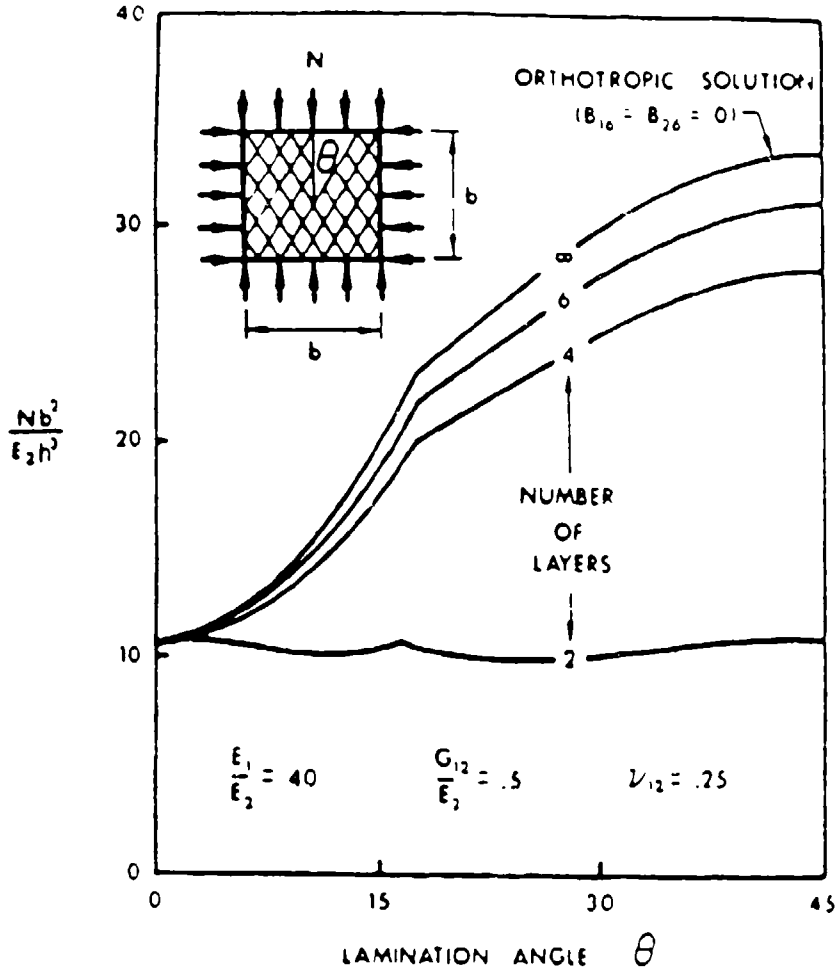

Figure 6.8. Comparions of antisymmetrical and orthotropic solutions with varying lamination angle for biaxially loaded, angle-ply plates having S3 edge conditions (a/b = 1).

Table 6.1. Uniaxial buckling loads for square antisymmetrically laminated graphite/epoxy plates (corresponding to Fig. 6.7).

θ	$-N_x b^2/E_2 h^3$			
	Number of Layers			
	2	4	6	∞ =(Orthotropic)
0	35.831	35.831	35.831	35.831
15	21.734	38.253	41.313	43.760
30	20.441	49.824	55.265	59.619
45	21.709	56.088	62.455	67.548
60	19.392(m=2)	45.434(m=2)	50.257(m=2)	54.115(m=2)
75	12.915(m=2)	22.075(m=2)	23.772(m=2)	25.129(m=2)
90	13.132(m=3)	13.132(m=3)	13.132(m=3)	13.132(m=3)

Table 6.2. Biaxial buckling loads for square antisymmetrically laminated graphite/epoxy plates (corresponding to Fig. 6.8).

θ	$-N_x b^2/E_2 h^3$			
	Number of Layers			
	2	4	6	∞ =(Orthotropic)
0	10.871	10.871	10.871	10.871
15	10.332	17.660	19.017	20.103
30	10.220	24.912	27.[illegible]3	29.809
45	10.854	28.044	31.[illegible]27	33.774

for the case of uniaxial loading [165,171] using the series method (cf. [26]) with trigonometric displacement functions. Numerical results were obtained for square plates having 2, 4 and ∞ layers having lamination angles of $\pm 45^{\circ}$. These are shown in Figure 6.9, where the nondimensional loading parameter N_x/N_o is plotted versus E_1, E_2, where N_o is the critical load for the orthotropic plate. The remaining material parameters are $G_{12}/E_2 = 0.5$ and $\nu_{12} = 0.25$. Figure 6.9 closely resembles Figure 6.3 (for uniaxially loaded, antisymmetric, cross-ply laminates with S2 edge conditions), showing a large difference between the correct, antisymmetric solution and the orthotropic solution (obtained by omitting all B_{ij}). Figures 6.3 and 6.9 are applicable to a variety of laminated composites, such as glass-epoxy, boron-epoxy, graphite-epoxy and plywood.

Mandell and Kicher [34,35,172] conducted an experimental investigation of uniaxial buckling loads for graphite-epoxy (Thornel), boron-epoxy and fiberglass-epoxy, unsymmetrically laminated plates. A description of the plates tested is given in Table 6.3. Plate identification numbers given are those used in [34,35,172]. A ply layup 4(0,90) describes the stacking sequence 0°, 0°, 0°, 0°, G, 90°, 90°, 90°, 90°, where "G" signifies a glue layer. To avoid initial warping from cooling during the fabrication process, such plates were made of two symmetrically laminated sub-plates which were bonded together with a room-temperature curing adhesive. Stretching, bending and coupling stiffnesses for the plates are given in Tables 6.4-6.6. From the description of the edge constraints [34,35,172] it appears that S4 boundary conditions (see Equation 6.2) were closely approximated on all edges. More information on these tests is found in Section 2.1.

Table 6.7 lists the experimental buckling loads for the plates described in Table 6.3. Also given are theoretical values obtained by four methods, using the stiffness data found in Tables 6.4 and 6.5. The first method ignores the D_{16} and D_{26} terms, as well as all B_{ij}, and uses

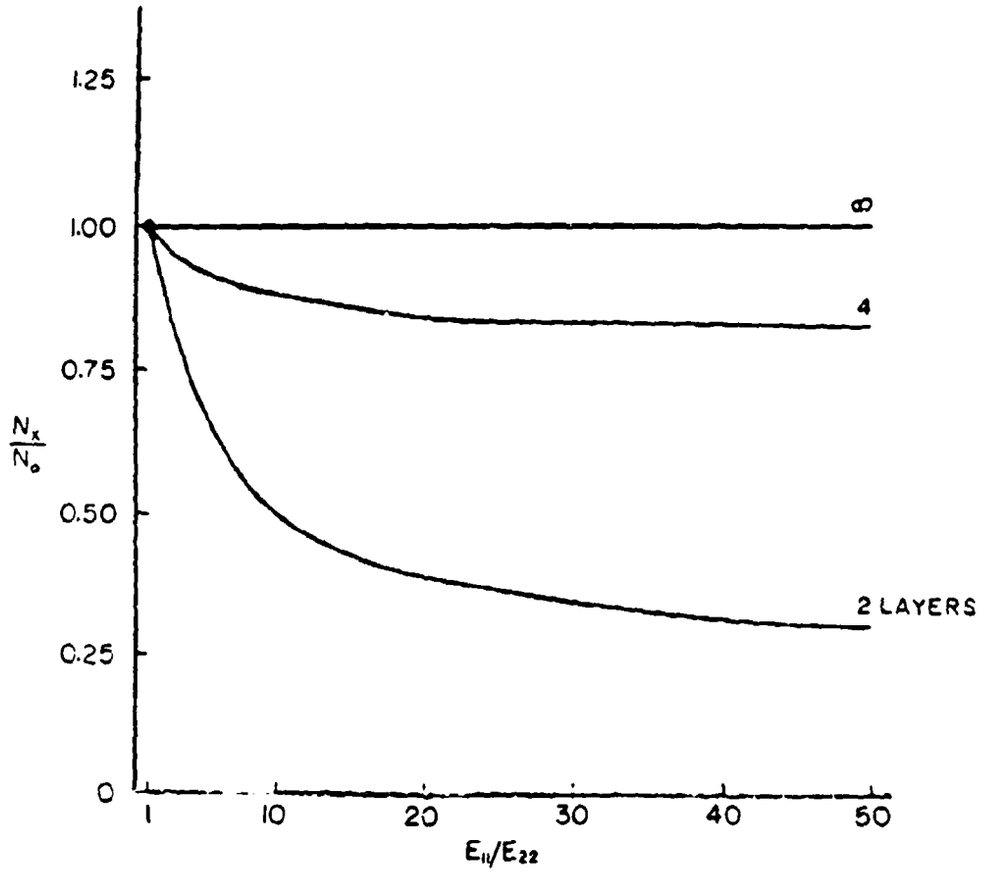

Figure 6.9. Uniaxial buckling loads for antisymmetric, angle-ply laminates having SSSS (S4) edge supports (a/b = 1, $\theta = \pm 45^{o}$).

Table 6.3. Description of unsymmetrically laminated plates tested by Mandell

Plate no.	Material	% Fiber by volume	Layup of plies	Dimensions (in)
209a	Thornel-40	50.0	(0,0,90,90)	10x10x0.091
209b	"	"	(90,90,0,0)	"
409a	Boron	49.1	10(45),10(-45)	11x11x0.109
409b	"	"	10(-45),10(45)	"
501	Fiberglass	44.0	(90,+45,-45,90)	10x10x0.103
502	"	"	(0,-45,+45,0)	"
503	"	"	(45,90,-90,-45)	10x10x0.108
504	"	"	(-45,0,0,45)	"
505	"	"	(90,25,-25,90)	10x10x0.103
506	"	"	(0,-25,25,0)	"
507	"	"	(25,90,-90,-25)	10x10x0.085
508	"	"	(-65,0,0,65)	"
509a	"	"	4(0),4(90)	10x10x0.090
509b	"	"	4(90),4(0)	"

Table 6.4. Bending stiffnesses (lb,in) for Mandell's unsymmetrically laminated plates

Plate no.	D_{11}	D_{12}	D_{16}	D_{22}	D_{26}	D_{66}
209	631	19.1	0	631	0	34.5
409	1011	842	0	1011	0	854
501	139	47.8	0	440	0	59.5
502	440	47.8	0	139	0	59.5
503	229	120	0	272	0	133
504	272	120	0	229	0	133
505	156	43.9	0	431	0	55.6
506	431	43.9	0	156	0	55.6
507	208	49.5	0	113	0	56.9
508	113	49.5	0	208	0	56.9
509	242	30.4	0	242	0	40.1

Table 6.5. Stretching stiffnesses (10^3 lb/in) for Mandell's unsymmetrically laminated plates

Plate no.	A_{11}	A_{12}	A_{16}	A_{22}	A_{26}	A_{66}
209	863.3	27.46	0	863.3	0	48.15
409	1021	850	0	1021	0	862
501	195.8	88.23	0	385.2	0	101.1
502	385.2	88.23	0	195.8	0	101.1
503	198.0	88.98	0	387.4	0	101.8
504	387.4	88.98	0	198.0	0	101.8
505	275.0	69.87	0	342.7	0	82.78
506	342.7	69.87	0	275.0	0	82.78
507	246.3	62.22	0	307.8	0	74.06
508	330.0	42.05	0	330.0	0	55.09
509	330.0	42.05	0	330.0	0	55.09

Table 6.6. Coupling stiffnesses (10^3 lb) for Mandell's unsymmetrically laminated plates

Plate no.	B_{11}	B_{12}	B_{16}	B_{22}	B_{26}	B_{66}
209	-18.33	0	0	18.33	0	0
409	0	0	19.9	0	19.9	0
501	0	0	0.6215	0	0.6215	0
502	0	0	-0.6215	0	-0.6215	0
503	0	0	1.953	0	1.953	0
504	0	0	-1.953	0	-1.953	0
505	0	0	0.7632	0	0.1889	0
506	0	0	-0.1889	0	-0.7632	0
507	0	0	1.721	0	0.4259	0
508	0	0	-0.4259	0	-1.721	0
509	-4.546	0	0	4.546	0	0

Table 6.7. Uniaxial buckling loads ($-N_x$, lb/in) for Mandell's SSSS unsymmetrically laminated plates

Plate no.	Experimental	Theoretical
209a	72.1	142 71.5* 74.2** (77.0)
209b	73.7	142 71.5* 74.2** (77.0)
409a	347	745 376* 357** (391)
409b	394	745 376* 357** (391)
501	120	90.2 100*
502	102	90.2 100*
503	113	126 111* 102**
504	108	126 111* 102**
505	101	88.4 99.0*
506	88	88.4 99.0*
507	57.3	64 53* 52.9*
508	68.8	64 53* 52.9*
509a	63.7	69.5 53* 55.4**
509b	72.7	69.5 53* 55.4**

* obtained by Galerkin method
** obtained by Ritz method, using reduced bending stiffness matrix
( ) obtained by geometrically nonlinear finite element method

Equation 2.9 for an orthotropic plate. The second method is the Galerkin formulation, as applied by Chamis [41] to anisotropic plates, not accounting for the B_{ij} terms. The third method is the Ritz procedure developed by Ashton [42], which accounts for the D_{16} and D_{26} terms, and deals with bending-stretching coupling by means of the reduced stiffness method. The last method is a finite element technique developed by Monforton [173]. Plates 209, 409 and 509 are each listed twice. The two cases (denoted "a" and "b") identify uniaxial loadings in two perpendicular directions. For these plates, different experimental results were found, although the theoretical results are identical for each loading direction.

Additional experimental results for uniaxial buckling loads of SSSS, unsymmetrically laminated plates were obtained by Chailleux, Hans and Verchery [174-176]. Tests were conducted on nearly-square, angle-ply plates made of boron fibers in an aluminum matrix. Buckling loads were obtained by two methods: (1) static tests using the Southwell [40] plot, and (2) vibration tests, to determine the load at which the frequency approaches zero. Three sets of static test results were employed (labelled P_w, P_{k1} and P_{k2} in Table 6.8), where measurements of the transverse displacement (w) and the curvatures in the loaded (κ_1) and unloaded (κ_2) directions were made. P_D identifies the dynamically measured load in Table 6.8. Plates were loaded by a framework which gave a uniform density of in-plane forces along two opposite edges. It appears that S4 edge conditions (see Equation 6.2) were closely approximated along all four edges. Test specimens were alternating angle-ply layups, having two or four plies, as described in Table 6.8, with the exception of one cross-ply case. In all cases the volume ratio of fibers was approximately 55 percent.

Unsymmetrical cross-ply plates subjected to <u>shear</u> loading ($\sigma_x = \sigma_y = 0$, τ_{xy} = constant) were also analyzed by Whitney [177]. Displacements were assumed in the form of double summations of the terms on the

Table 6.8. Buckling loads (kg) for uniaxially loaded, SSSS plates with boron fibers in an aluminum matrix.

Ply layup	No.of plies	Thickness (mm)	a x b (mm)	Critical loads (kg)			
				P_w	P_{K1}	P_{K2}	P_D
$0\text{-}90^\circ$	2	1.54	218x222	623	580	578	651
$\pm 15^\circ$	4	0.96	182x179	430	417	507	812
$\pm 30^\circ$	4	0.99	183x181	368	369	371	384
$\pm 45^\circ$	2	1.35	181x174	758	648	680	786
$\pm 60^\circ$	4	0.99	184x179	383	—	389	391
$\pm 75^\circ$	4	0.96	183x179	652	735	652	724

right-hand-sides of Equations (6.3), with m,n = 1,2,... Thus, S2 boundary conditions are satisfied exactly. The first two of Equations (6.1) are satisfied exactly by substituting u, v, w into them to express A_{mn} and B_{mn} in terms of C_{mn}. The last of Equations (6.1) is satisfied as closely as desired by using the Galerkin method. This procedure was followed [117] to get numerical values of buckling loads for the case when a/b = 1, $\nu_{12} = 0.25$ and $G_{12}/E_{22} = 0.5$. These results are seen in Figure 6.10, where the ratio $\tau_{xy}/(\tau_{xy})_o$ is plotted versus E_{11}/E_{22} for laminates having 2, 4 and ∞ layers. There $(\tau_{xy})_o$ is the critical buckling stress for an orthotropic plate, obtained either by setting $B_{ij}=0$, or by taking an infinite number of plies in the laminate. Results obtained by using the reduced bending stiffness method (see discussion preceding Section 6.1) were found to agree with those from the Galerkin method within three significant figures.

A procedure similar to the one described above was followed by Hui [178] to determine additional data for the shear buckling loads of S2 cross-ply plates. It was shown that, similar to isotropic plates, the buckling modes separate into to symmetric and unsymmetric classes, with the critical (i.e., lowest) buckling load changing from one class to the other as a/b is varied. Curves of the nondimensional buckling parameter $\tau_{xy}b^2/Eh^2$ versus a/b are displayed in Figures 6.11, 6.12 and 6.13 for graphite-epoxy ($E_1/E_2 = 40$, $G_{12}/E_2 = 0.33$, $\nu_1 = 0.22$) and glass-epoxy ($E_1/E_2 = 3$, $G_{12}/E_2 = 0.5$, $\nu_{12} = 0.25$) cross-ply plates having 2, 4 or plies.

Hirano [179,180] followed the Galerkin procedure that Whitney [177] used (see above) to make optimization studies for unsymmetrical, angle-ply laminates subjected to shear [179] and combined compression and shear [180]. Several other references are also available which treat the buckling of SSSS unsymmetrical laminates [101,145,181-187].

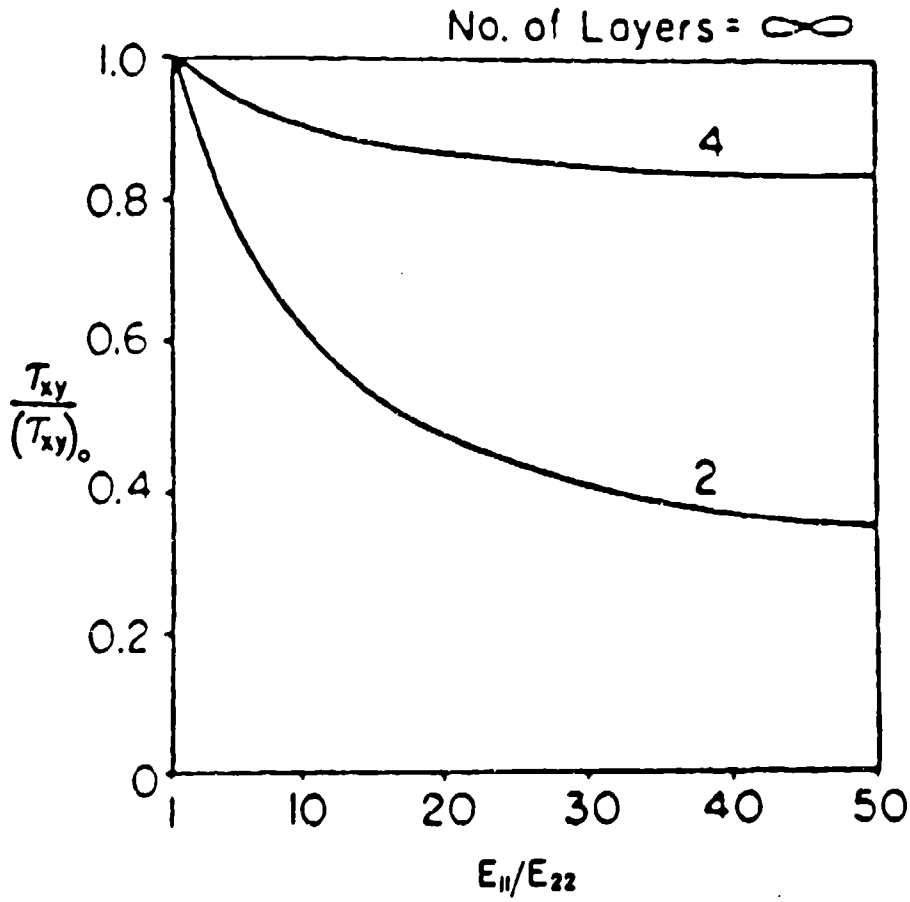

Figure 6.10. Shear buckling loads for antisymmetric, cross-ply laminates having SSSS (S2) edge supports (a/b = 1, $G_{12}/E_{22} = 0.5, \nu_{12} = 0.25$).

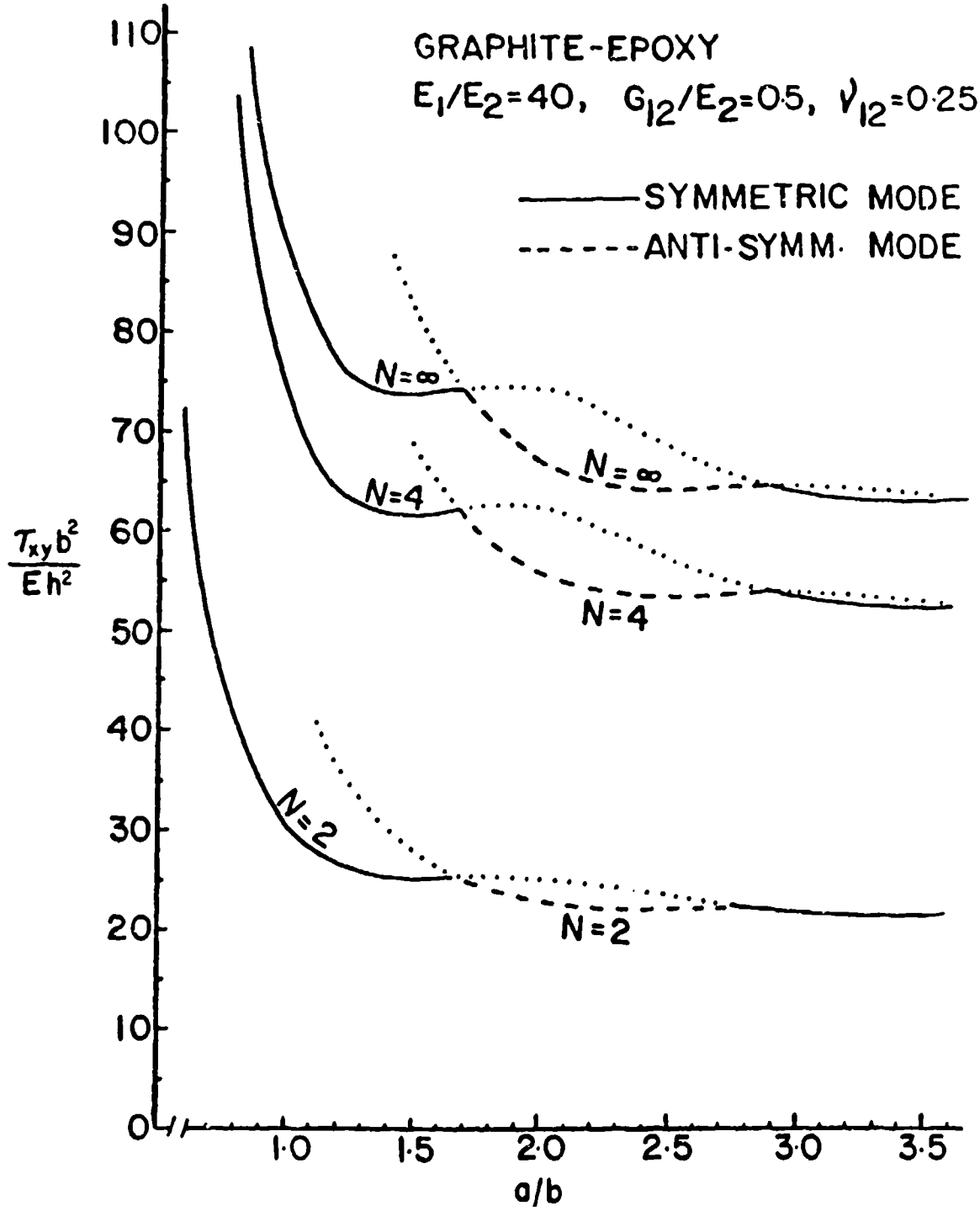

Figure 6.11. Shear buckling parameters for antisymmetric, cross-ply, SSSS (S2), graphite-epoxy plates.

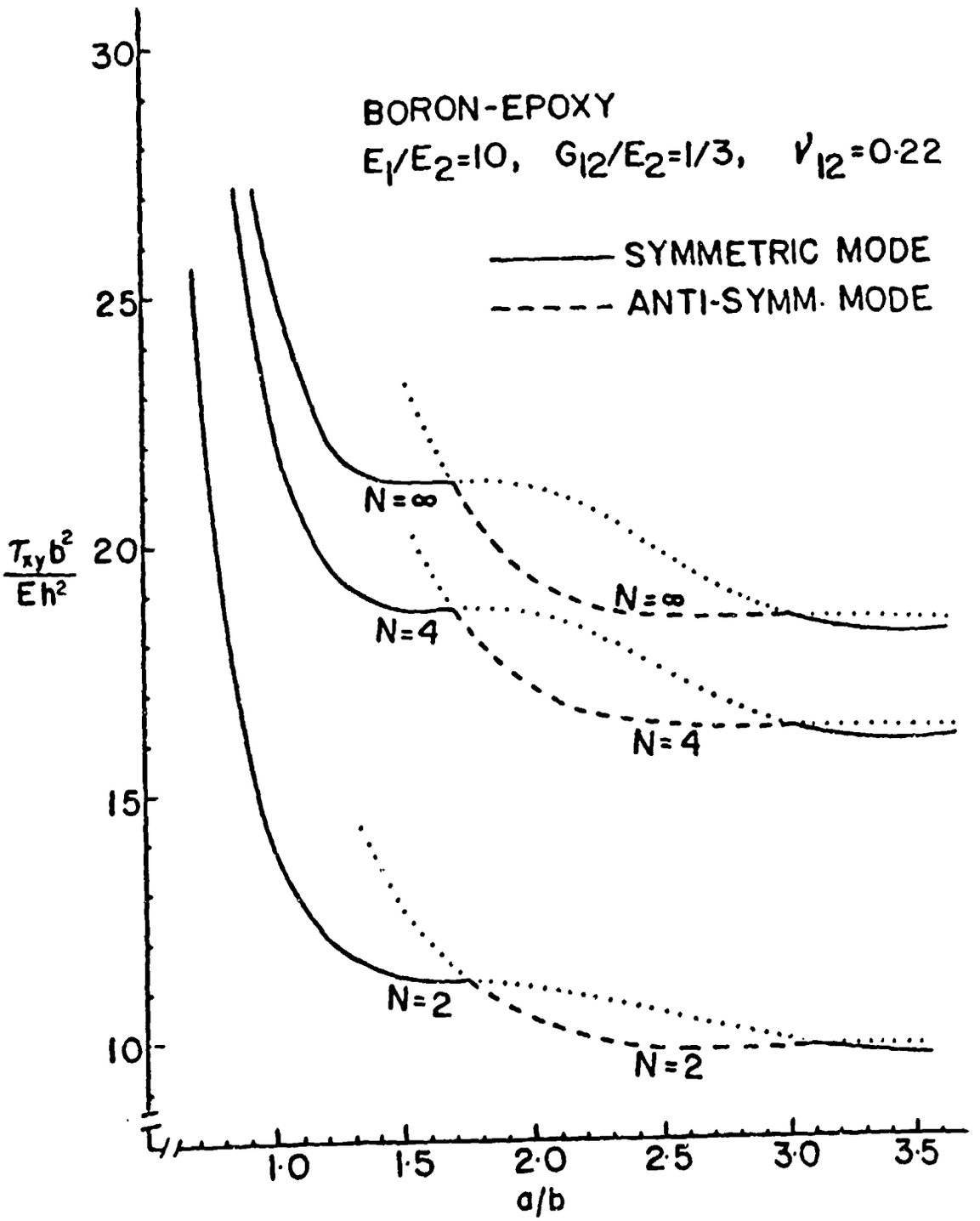

Figure 6.12. Shear buckling parameters for antisymmetric, cross-ply, SSSS (S2), boron-epoxy plates.

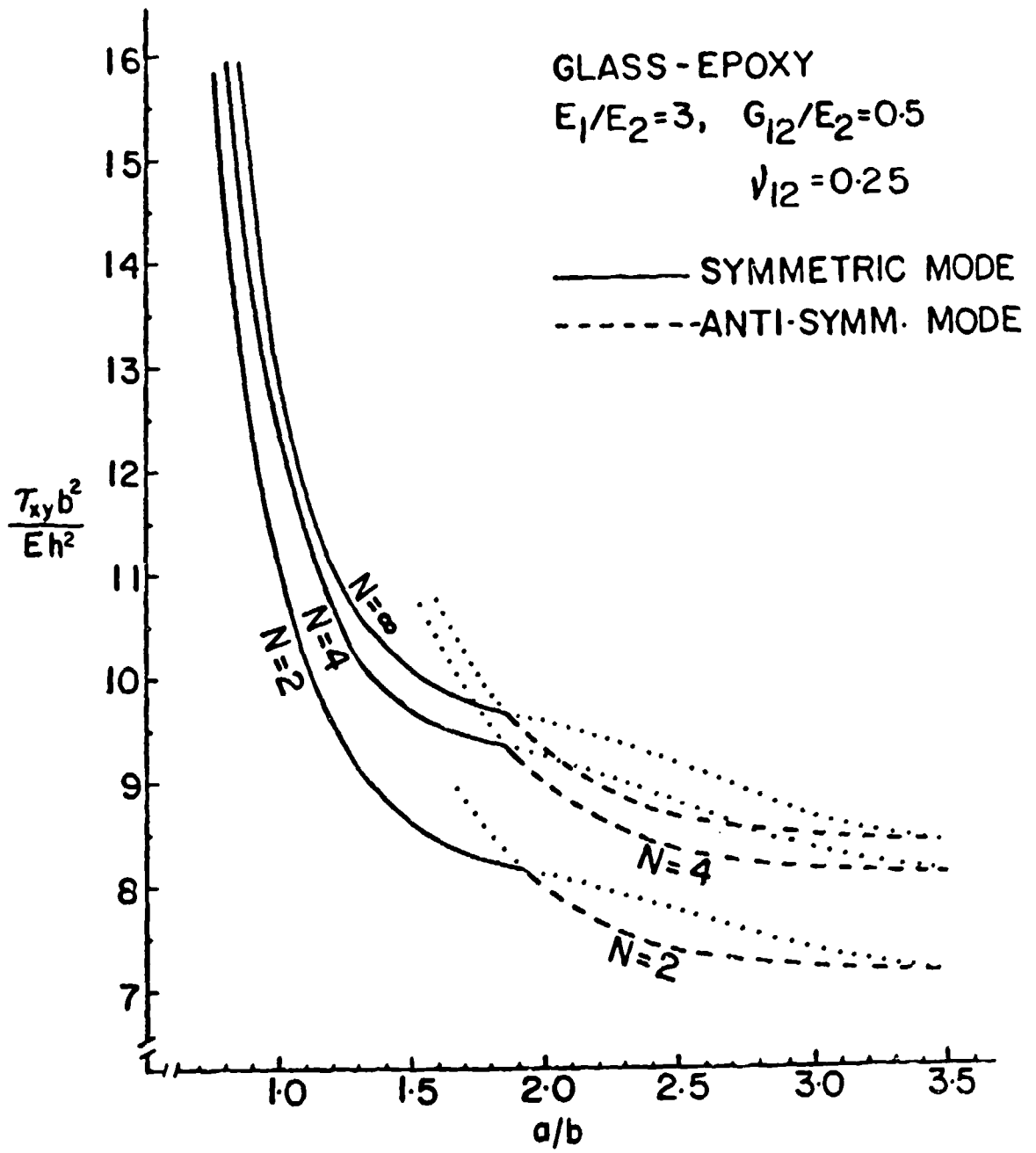

Figure 6.13. Shear buckling parameters for anytisymmetric, cross-ply, SSSS (82), glass-epoxy plates.

6.2. SFSF

In Table 6.9 are listed the experimental buckling loads obtained by Mandell and Kicher [34,35,172] for SFSF unsymmetrically laminated plates having the simply supported edges subjected to uniaxial loading. The plates are those described previously in Section 6.1 (Tables 6.3-6.6). Theoretical results in all cases were calculated on the assumption that the plate bends as a simply supported beam having no transverse curvature or twist (see description of analysis in Section 3.6). Additional theoretical results obtained by the Ritz method using the reduced bending stiffness matrix, as developed by Ashton [42], are also given for most of the plates in Table 6.9.

Chailleux, Hans and Verchery [174-176] also obtained experimental, uniaxial buckling loads of SFSF plates (loaded edges with S4 conditions). Tests were conducted on nearly-square, angle-ply plates made of boron fibers in an aluminum matrix, as described previously in Section 6.1. Numerical results are given in Table 6.10, which may be compared with results given previously in Table 6.8 for SSSS plates (and where additional plate data is available).

Theoretical and experimental results for the buckling of uniaxially loaded SFSF laminates composed of boron-epoxy and titanium layers were found by Viswanathan, Soong and Miller [92].

6.3. CCCC

In the case of clamped edges, the transverse displacement and normal slopes are everywhere zero. However, permitting various degrees of constraint in the inplane directions gives rise to four sets of boundary conditions, in a manner similar to that used for simply supported edges (see Section 6.1), viz

Table 6.9. Uniaxial buckling loads ($-N_x$, lb/in) for Mandell's SFSF unsymmetrically laminated plates

Plate no.	Experimental	Theoretical
209a	20.7	62.3 23.7**
209b	19.7	62.3 23.7**
409a	38.5	70.6 42.7**
409b	36.1	70.6 42.7**
501	13.7	15.4
502	36.6	43.4
503	18.3	22.5 18.9**
504	23.0	26.8 23.2**
505	12.5	15.4
506	39.1	42.6
507	12.8	20.5 16.6**
508	9.51	11.2 10.9**
509a	15.4	23.9 17.6**
509b	15.3	23.9 17.6**

** obtained by the Ritz method, using reduced bending stiffness matrix

Table 6.10. Buckling loads (kg) for uniaxially loaded, SFSF plates with boron fibers in an aluminum matrix (see Table 6.8 for other data).

Ply layup	Critical loads (kg)		
	P_w	P_{K1}	P_D
$0\text{-}90^\circ$	175	175	185
$\pm 15^\circ$	86.2	85.1	119
$\pm 30^\circ$	-	80.4	-
$\pm 45^\circ$	153	148.5	153
$\pm 60^\circ$	54.3	54.3	57.4
$\pm 75^\circ$	-	-	-

$$
\begin{aligned}
&\text{C1:} \quad w = \frac{\partial w}{\partial n} = u_n = u_t = 0 \\
&\text{C2:} \quad w = \frac{\partial w}{\partial n} = N_n = u_t = 0 \\
&\text{C3:} \quad w = \frac{\partial w}{\partial n} = u_n = N_{nt} = 0 \\
&\text{C4:} \quad w = \frac{\partial w}{\partial n} = N_n = N_{nt} = 0
\end{aligned}
\tag{6.10}
$$

Whitney [163,164] extended the series method used previously to analyze SSSS(S4) plates [165,171] (see Section 6.1) to clamped edge conditions. In this manner data was obtained for the buckling of biaxially loaded ($\sigma_x = \sigma_y$ = constant, $\tau_{xy} = 0$), $\pm 45^\circ$ angle-ply, square plates with C1 edge conditions. Figure 6.14 shows the variation of $-\sigma_x h a^2/E_{22}h^2$ with E_{11}/E_{22} for plates haing 2, 4 and ∞ layers. The other material properties used apparently were $G_{12}/E_{22} = 0.5$ and $\nu_{12} = 0.25$. Additional data are given in Tables 6.11 and 6.12 for cross-ply and $\pm 45^\circ$ angle-ply plates, respectively, having two layers with $E_{11}/E_{22} = 40$, $G_{12}/E_{22} = 0.5$ and $\nu_{12} = 0.25$, for C1, C2 and C3 types of edge constraints, and five aspect ratios. Results from using orthotropic plate analysis with reduced bending stiffnesses (see discussion preceding Section 6.1) are also presented. It appears that the results of Tables 6.11 and 6.12 violate a fundamental principle of mechanics; viz, that the addition of constraints should only increase (or leave unchanged) the buckling load of a system.

Some numerical results for uniaxially loaded, CCCC plates were obtained by Chia and Prabhakara [15,181] as part of a postbuckling analysis of unsymmetrical laminates. The Galerkin method was used, with displacements taken as the products of beam functions. Results are shown in Table 6.13 for a set of cross-ply and angle-ply ($\pm 45^\circ$) plates, each composed of four graphite-epoxy plies ($E_{11}/E_{22} = 40$, $G_{12}/E_2 = 0.5$, $\nu_{12} = 0.25$). These data were attained by using 9 terms of the double infinite series of displacement functions. Zhang and Mathews [188] subsequently showed that the results from the Galerkin method are very sensitive to the number of significant figures kept in the computation of the beam functions. Results given by them in Table 6.13 were achieved carrying 15 significant

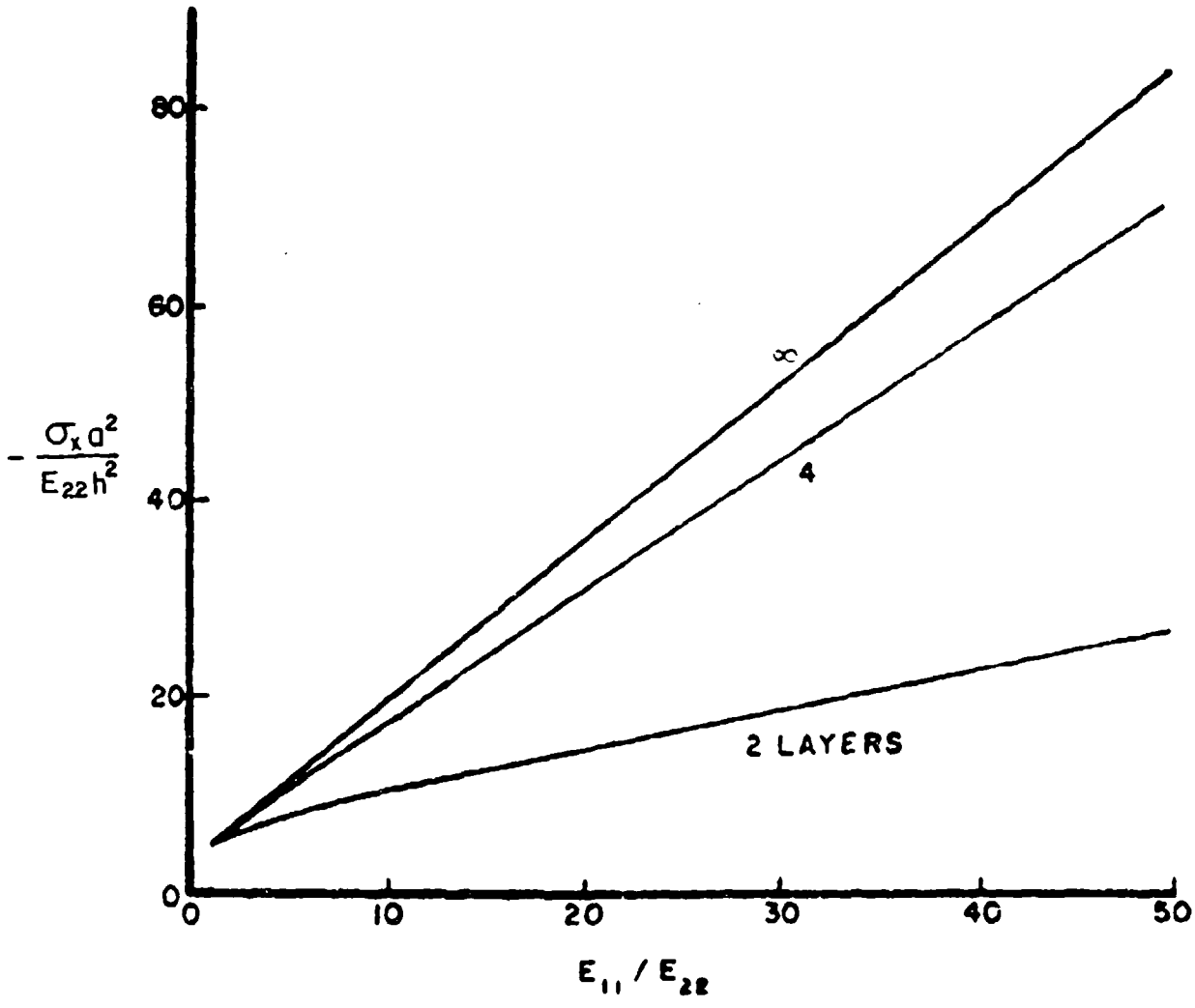

Figure 6.14. Buckling parameters for biaxially-loaded CCCC (C1), unsymmetrically laminated, square, angle-ply plates.

Table 6.11. Buckling parameters $-\sigma_x a^2/E_{22}h^2$ for biax[illegible] loaded CCCC cross-ply plates having two

$\frac{a}{b}$	Edge conditions		
	C1	C2	Reduced bending stiffness
1	23.450	22.697	23.068
2	11.360	11.352	11.352
3	6.313	6.315	6.315
4	4.967	4.968	4.968
5	4.977	4.977	4.977

Table 6.12. Buckling parameters $-\sigma_x a^2/E_{22}h^2$ for biaxially-loaded CCCC $\pm 45^\circ$ angle-ply plates having two layers.

$\frac{a}{b}$	Edge conditions		
	C1	C2	Reduced bending stiffness
1	26.002	26.592	24.765
2	24.655	27.767	21.889
3	25.147	27.873	23.686
4	23.168	25.790	22.867
5	22.664	22.960	22.658

Table 6.13. Critical uniaxial buckling parameters $-\sigma_x b^2/E_{22}h^2$ for CCCC graphite-epoxy plates having four layers.

Laminate description	$\frac{a}{b}$	Source of results [15,181]	[188]
cross-ply	1.0	112.65 (1)	109.90
	1.5	87.74 (2)	-
	2.0	76.83 (3)	-
$\pm 45^o$ angle-ply	1.0	113.67 (1)	106.87
	1.5	95.73 (2)	-
	2.0	89.86 (3)	-

*values in parentheses are the number of half-waves of the mode shape in the load (x) direction

figures in the beam function parameters, whereas Chia and Prabhakara [151,181] had used six significant figures.

CHAPTER VII. COMPLICATING EFFECTS

In this chapter, more complicated bifurcation buckling problems for laminated composite plates will be taken up. The complicating effects will be seen to include: internal holes, shear deformation, sandwich plates having laminated composite layers combined with other materials, localized buckling, nonlinear stress-strain relationships and hygrothermal effects. Stiffeners will be discussed in Chapter IX.

7.1. INTERNAL HOLES

Marshall [189] took up the problem of the buckling of a uniaxially loaded, rectangular plate of dimensions axb containing a central, circular hole of radius r (see Figure 7.1). All edges along the rectangular boundary were simply supported, whereas the circular boundary was free. Test plates were made of unidirectional glass cloth embedded in a polyester resin matrix, yielding orthotropic plates having the following properties: $E_x = 3.1$ GN/m^2, $E_y = 10.4$ GN/m^2, $G_{xy} = 2.14$ GN/m^2, $\nu_{xy} = 0.30$. Theoretical results were obtained by assuming the following internal stresses:

$$\sigma_x = \frac{\sigma_o}{2} z^2[\cos 2\theta + (2-3z^2)\cos 4\theta]$$

$$\sigma_y = \frac{\sigma_o}{2} \{2 + z^2[3\cos 2\theta - (2-3z^2)\cos 4\theta]\} \qquad (7.1)$$

$$\tau_{xy} = \frac{\sigma_o}{2} z^2[-\sin 2\theta + (2-3z^2)\sin 4\theta]$$

where $z = r_o/r$. The buckling problem was solved by means of the Ritz method, with the buckled mode shape assumed in the form:

$$w = \cos\frac{\pi x}{a}\cos\frac{\pi y}{b} + Be^{-c\left(\frac{x^2}{a^2}+\frac{y^2}{b^2}\right)} \qquad (7.2)$$

The first term of Equation 7.2 describes the overall mode shape, whereas the second term accounts for localized displacements in the vicinity of

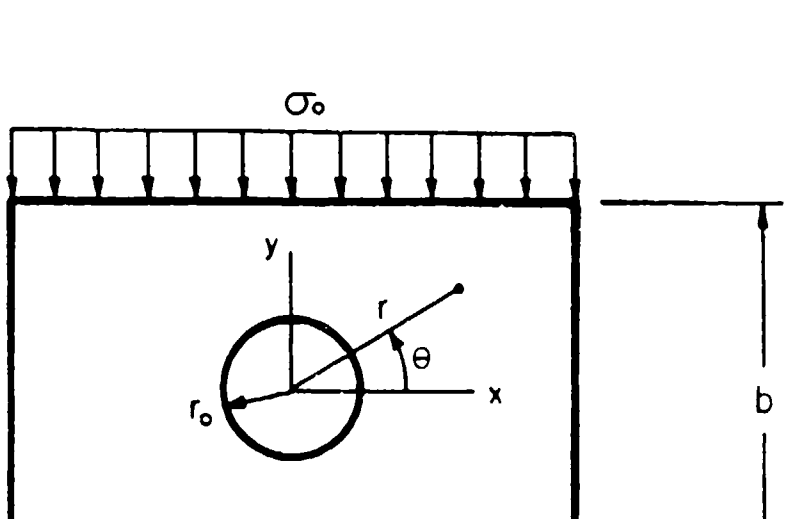

Figure 7.1. Uniaxially loaded plate with a central, circular hole.

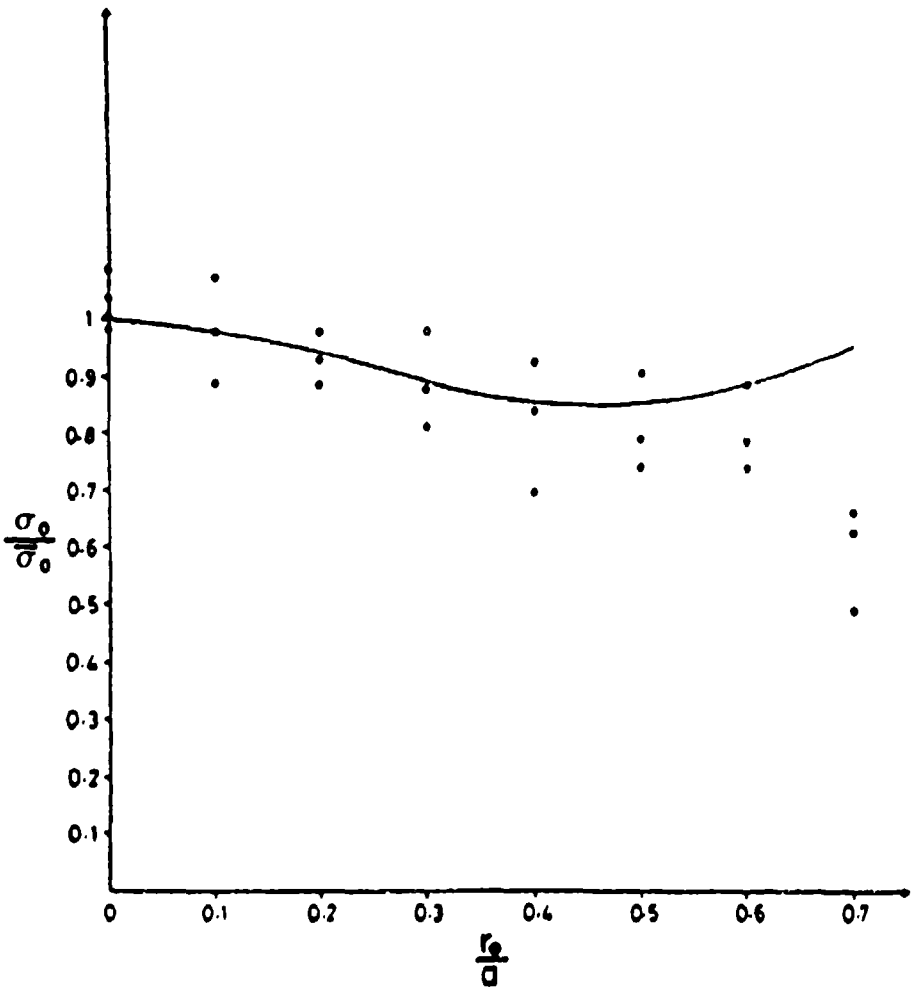

Figure 7.2 Critical uniaxial buckling stress ratio for SSSS orthotropic plates with holes.

the hole [189]. B and C are constants determined by the minimizing process. Numerical data were obtained for square plates (250 mm x 250 mm x 1.9 mm) having $r_o/a = 0, 0.1,\ldots,0.7$. These are shown in Figure 7.2. There the continuous curve represents the result of the theoretical analysis and the data points show the results of experiments conducted on three test specimens. The ordinate $\sigma_o/\bar{\sigma}_o$ is the ratio the critical buckling stress to that of the plate not having a hole.

The buckling of laminated composite square plates having central, circular holes was also studied by Martin [190,191].

7.2. SHEAR DEFORMATION

Classical plate theory is based upon the Kirchhoff hypothesis: "Normals to the midplane of the undeformed plate remain straight and normal to the midplane during deformation." This assumption therefore ignores the transverse shear deformation. Consideration of shear deformation results in added flexibility, which becomes significant as the plate thickness increases relative to its length and width.

A quantitative theory which accurately provides the necessary correction to provide for shear deformation has been available for thick beams for at least 60 years. Generalization of isotropic plate theory to include shear deformation was carried out by Reissner [192,193] 40 years ago. More recently, Ziegler [194] showed that the effects of the inplane deformation immediately prior to buckling are of the same order of magnitude as, and in some cases even more than, the transverse shear deformation.

In thick plate theory one may express the total slopes of the deformed midsurface at a typical point as

$$\frac{\partial w}{\partial x} = \psi_x + \phi_x$$

$$\frac{\partial w}{\partial y} = \psi_y + \phi_y \qquad (7.3)$$

where ψ_x and ψ_y are the rotations in the x and y directions (i.e., rotations about the y and x axes), respectively, due to bending and ϕ_x and ϕ_y are the slope changes due to shear. Shear deformation theory requires a solution in terms of three independent variables, each of which is a function of the two independent variables (x,y). The dependent variables are typically taken to be w and either ψ_x and ψ_y or ϕ_x and ϕ_y, with the remaining two variables determined by Equations 7.3. The resulting set of governing differential equations is of sixth order, which requires specification of three boundary conditions per edge. This is in contrast with classical plate theory and with beam theory (with or without shear deformation) which only require fourth order equations and two boundary conditions per edge. Further generalization to unsymmetrical laminates, with the ensuing additional coupling between bending and stretching, would result in a tenth order set of equations, as one finds for thick, isotropic shells.

A major contribution to the analysis of laminated composite, thick plates is the book by Ambartsumyan, which was translated from the Russian in 1970 [13]. Recently, Bert [195] made an excellent analysis of various thick plate theories as applied to laminated composite materials.

One set of differential equations governing the equilibrium of an orthotropic plate in its small displacement, buckled configuration may be adapted from pages 39 and 198 of the book by Ambartsumyan [13]. They may be written as

$$D_{11}\frac{\partial^3 w}{\partial x^3} + (D_{12}+2D_{66})\frac{\partial^3 w}{\partial x \partial y^2} - \frac{h^2}{10}\left[\frac{1}{G_{13}}\ D_{11}\left(\frac{\partial^2 \phi_x}{\partial x^2} + D_{66}\frac{\partial^2 \phi_x}{\partial y^2}\right)\right.$$
$$\left. + \frac{1}{G_{23}}(D_{11}+D_{66})\frac{\partial^2 \phi_y}{\partial x \partial y}\right] + \frac{h^3}{12}\phi_x = 0 \qquad (7.4a)$$

$$D_{22}\frac{\partial^3 w}{\partial y^3} + (D_{12}+2D_{66})\frac{\partial^3 w}{\partial x^2 \partial y} - \frac{h^2}{10}\left[\frac{1}{G_{23}}\left(D_{22}\frac{\partial^2 \phi_y}{\partial y^2} + D_{66}\frac{\partial^2 \phi_y}{\partial x^2}\right)\right.$$
$$\left. + \frac{1}{G_{13}}(D_{12}+D_{66})\frac{\partial^2 \phi_x}{\partial x \partial y}\right] + \frac{h^3}{12}\phi_y = 0 \qquad (7.4b)$$

$$\frac{h^3}{12}\left(\frac{\partial \phi_x}{\partial x} + \frac{\partial \phi_y}{\partial y}\right) + N_x\frac{\partial^2 w}{\partial x^2} + 2N_{xy}\frac{\partial^2 w}{\partial x \partial y} + N_y\frac{\partial^2 w}{\partial y^2} = 0 \qquad (7.4c)$$

where the D_{ij} are as used in previous chapters, and where G_{13} and G_{23} are the shear moduli relating the transverse stresses and strains. It is seen that classical, orthotropic plate theory, governed by Equation 2.1, results when the shear stiffnesses G_{13} and G_{23} are set equal to infinity, and Equations 7.4a and 7.4b are substituted into Equation 7.4c.

An exact solution to Equations 7.4 may be obtained in the case when $N_{xy} = 0$ and the plate is simply supported along all four edges. The corresponding boundary conditions are:

$$\text{Along } x = 0,a \ : \ w = M_x = \phi_y = 0$$
$$\text{Along } y = 0,b \ : \ w = M_y = \phi_x = 0 \qquad (7.5)$$

It is remarked that since, for example, $w = 0$ along $x = 0$ implies that $\partial w/\partial y = 0$ along $x = 0$, as well, then $\phi_y = 0$ along $x = 0$ implies that $\psi_y = 0$, as well. Thus, along all edges, not only are the total tangential slopes zero, but both the shear and bending parts of total

tangential slopes are each zero for the boundary conditions of Equations 7.5. Equations 7.5 are exactly satisfied by assuming the functions

$$\begin{aligned} \phi_x &= A \cos \frac{m\pi x}{a} \sin \frac{n\pi y}{b} \\ \phi_y &= B \sin \frac{m\pi x}{a} \cos \frac{n\pi y}{b} \\ w &= C \sin \frac{m\pi x}{a} \sin \frac{n\pi y}{b} \end{aligned} \tag{7.6}$$

with m, n = 1, 2,... Substituting Equations 7.6 into Equations 7.4, one obtains (generalized from p. 200, [13])

$$\sigma_x h \left(\frac{m}{a}\right)^2 + \sigma_y h \left(\frac{n}{b}\right)^2 = -\pi^2 \left[D_{11}\left(\frac{m}{a}\right)^4 + 2(D_{12}+2D_{66}) \left(\frac{m}{a}\right)^2\left(\frac{n}{b}\right)^2 + D_{22}\left(\frac{n}{b}\right)^4 \right] \frac{1+K_1}{1+K_2} \tag{7.7}$$

where

$$\begin{aligned} K_1 = \frac{\pi^2 h^2}{10} \left(\frac{1}{G_{23}} \frac{m^2}{a^2} + \frac{1}{G_{13}} \frac{n^2}{b^2}\right) \Bigg[\left(D_{11} \frac{m^2}{a^2} + D_{66} \frac{n^2}{b^2}\right) \\ \times \left(D_{66} \frac{m^2}{a^2} + D_{22} \frac{n^2}{b^2}\right) - (D_{12}+D_{66})^2 \left(\frac{m}{a}\right)^2\left(\frac{n}{b}\right)^2 \Bigg] \\ \div \left[D_{11}\left(\frac{m}{a}\right)^4 + 2(D_{12}+2D_{66}) \left(\frac{m}{a}\right)^2\left(\frac{n}{b}\right)^2 + D_{22}\left(\frac{n}{b}\right)^4 \right] \end{aligned} \tag{7.8a}$$

$$K_2 = \frac{\pi^2 h^2}{10}\left[\frac{1}{G_{13}}\left(D_{11}\frac{m^2}{a^2} + D_{66}\frac{n^2}{b^2}\right) + \frac{1}{G_{23}}\left(D_{66}\frac{m^2}{a^2} + D_{22}\frac{n^2}{b^2}\right)\right]$$

$$+ \frac{1}{G_{13}G_{23}}\frac{\pi^4 h^4}{100}\left[\left(D_{11}\frac{m^2}{a^2} + D_{66}\frac{n^2}{b^2}\right)\left(D_{66}\frac{m^2}{a^2} + D_{22}\frac{n^2}{b^2}\right)\right. \tag{7.8b}$$

$$\left. - (D_{12}+D_{66})^2\left(\frac{m}{a}\right)^2\left(\frac{n}{b}\right)^2\right]$$

It is observed that in the case of no shear deformation, G_{13} and G_{23} are infinite, $K_1 = K_2 = 0$, and Equation 7.7 is the same as Equation 2.22 for a classical orthotropic plate.

Ambartsumyan [13] made parametric studies for the uniaxial buckling loads (σ_x = constant, $\sigma_y = \tau_{xy} = 0$) resulting from Equation 7.7 for variations of the following material modulus ratios:

$$k_1 = \frac{E_1}{E_2} \quad , \quad k_2 = \frac{E_1}{G_{12}} \quad , \quad k_3 = \frac{E_1}{G_{13}} = \frac{E_2}{G_{23}} \tag{7.9}$$

For uniaxial loading, critical loads occur always with n = 1. Nondimensional buckling parameters $-\sigma_x b^2/\pi^2 D_{11}$ are listed in Table 7.1 for various combinations of k_1, k_2, k_3 and a/b, with h/b taken as 0.1. The column with $k_3 = 0$ corresponds to classical theory (neglecting shear deformation). Also listed in Table 7.1 are the minimum values of $-\sigma_x b^2/\pi^2 D_{11}$, and the corresponding a/b where they occur. It is seen that the buckling parameters all decrease with increasing k_3.

Whitney [196] extended Ambartsumyan's [13] work to accommodate laminated plates having layers with fibers not all parallel to the plate edges. The exact solution used in Equation 7.6 was found to be valid for SSSS angle-ply plates having large numbers of layers. Numerical

Table 7.1. Buckling parameters $-\sigma_x b^2/\pi^2 D_{11}$ for uniaxially loaded, SSSS orthotropic plates with shear deformation (h/b = 0.1).

(a) $k_1 = k_2 = 5.0$, $\nu_{12} = 0.3$

$\frac{a}{b}$	k_3			
	0	2.0	5.0	10.0
0.35	9.093	7.682	6.241	4.763
0.65	3.357	3.144	2.873	2.516
0.95	2.194	2.105	1.984	1.816
1.25	1.858	1.799	1.716	1.596
1.65	1.817	1.769	1.700	1.598
1.95	1.929	1.881	1.814	1.712
2.25	2.116	2.066	1.995	1.889
2.55	2.360	2.306	2.230	2.115
min.	1.5954*	1.4820*	1.4629*	1.4336*
	1.8000	1.7488	1.6770	1.5694

* values of a/b where minimum buckling load occurs.

(b) $k_1 = k_2 = 2.0$, $\nu_{12} = 0.3$

$\frac{a}{b}$	k_3			
	0	2.0	5.0	10.0
0.25	18.241	13.263	9.440	6.392
0.45	7.250	6.335	5.335	4.234
0.75	4.269	3.978	3.610	3.130
0.95	3.769	3.569	3.305	2.944
1.25	3.631	3.481	3.277	2.986
1.45	3.737	3.599	3.411	3.137
1.75	4.068	3.936	3.754	3.485
2.15	4.738	4.601	4.411	4.126
min.	1.1892*	1.1588*	1.1151*	1.0475*
	3.6241	3.4657	3.2469	2.9264

* values of a/b where minimum buckling load occurs.

(c) $k_1 = 0.5$, $k_2 = 1.0$, $\nu_{21} = 0.3$

$\frac{a}{b}$	k_3			
	0	2.0	5.0	10.0
0.25	20.545	14.915	10.570	7.115
0.35	12.828	10.576	8.371	6.212
0.55	8.331	7.519	6.561	5.412
0.75	7.323	6.826	6.196	5.372
1.05	7.532	7.167	6.683	6.008
1.25	8.185	7.844	7.384	6.728
1.45	9.101	8.763	8.301	7.634
1.55	9.641	9.300	8.832	8.151
min.	0.8409*	0.8036*	0.7489*	0.6605*
	7.2484	6.8026	6.1964	5.3267

* value of a/b where minimum buckling load occurs.

(d) $k_1 = 0.2$, $k_2 = 1.0$, $\nu_{21} = 0.3$

$\frac{a}{b}$	k_3			
	0	2.0	5.0	10.0
0.25	20.840	15.547	11.291	7.784
0.35	13.304	11.239	9.135	6.987
0.55	9.346	8.601	7.691	6.552
0.65	9.007	8.435	7.708	6.751
0.85	9.525	9.087	8.507	7.696
0.95	10.149	9.734	9.177	8.385
1.15	11.897	11.489	10.931	10.119
1.25	12.981	12.565	11.991	11.150
min.	0.6688*	0.6386*	0.5937*	0.5177*
	9.0001	8.4329	7.6577	6.5377

* values of a/b where minimum buckling load occurs.

results were found for the uniaxial buckling of a square plate with $\pm 45^{\circ}$ angle-ply stacking sequence and with $E_1/E_2 = 40$, $G_{12}/E_2 = 0.6$, $G_{23}/E_{22} = 0.5$, $\nu_{12} = 0.25$. Variation of the buckling load parameter $-\sigma_x a^2/E_2 h^2$ with the thickness ratio, a/h, is shown in Figure 7.3. It is seen that the buckling load for a/h = 20 is considerably less with shear deformation theory (SDT) than with classical plate theory (CPT). Furthermore, the shear deformation effect is much more significant for the laminated composite plate than it would be for an isotropic plate.

Vinson and Smith [197] derived an expression for the strain energy of an orthotropic plate, considering the effects of shear deformation, which can be put into the following form:

$$V_S = \frac{1}{2} \iint_A \left\{ \left[D_{11} \left(\frac{\partial \psi_x}{\partial x} \right)^2 + 2D_{12} \frac{\partial \psi_x}{\partial x} \frac{\partial \psi_y}{\partial y} + D_{22} \left(\frac{\partial \psi_y}{\partial y} \right)^2 \right] + D_{66} \left[\left(\frac{\partial \psi_x}{\partial y} \right)^2 + 2 \frac{\partial \psi_x}{\partial y} \frac{\partial \psi_y}{\partial x} + \left(\frac{\partial \psi_y}{\partial x} \right)^2 \right] + \frac{5}{12} h \left[G_{13} \phi_x^2 + G_{23} \phi_y^2 \right] \right\} dA \tag{7.10}$$

From Equations 7.3 it is seen that when shear deformation is excluded ($\phi_x = \phi_y = 0$), Equation 7.10 reduces to the bending strain energy of an orthotropic plate, given by Equation 2.3. (In the limit, for example, as G_{13} increases, ϕ_x vanishes, with the product $G_{13}\phi_x$ remaining finite and proportional to the shear stress, and $G_{13}\phi_x^2$ therefore vanishing.) Thus, Equation 7.10 together with the potential energy due to inplane forces, Equation 2.4, is useful for analyzing the buckling of orthotropic plates with arbitrary edge conditions by Rayleigh-Ritz methods when shear deformation is included.

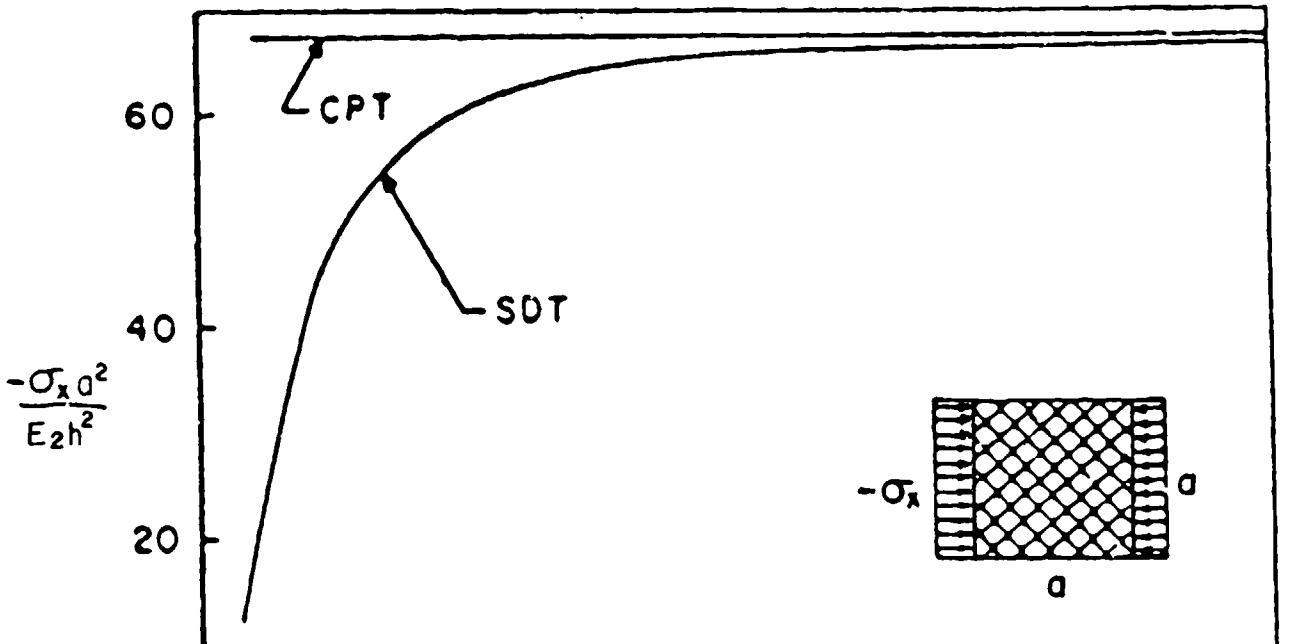

Figure 7.3. Buckling of a uniaxially loaded, SSSS, $\pm 45^{\circ}$ angle-ply, square plate having an infinite number of layers, with and without shear deformation.

In using Rayleigh-Ritz methods with Equation 7.10 the typical procedure would be to specify three sets of functions, either w, ϕ_x, ϕ_y or w, ψ_x, ψ_y, with Equations 7.3 providing the required relationships among them. Vinson and Smith [197] derived additional, approximate relationships among these functions from considerations of beam behavior with shear deformation present. These are:

$$\psi_x = \frac{\partial w}{\partial x} + \frac{h^2}{10}\frac{E_1}{G_{13}}\left(1 + \frac{6N_x}{5G_{13}h}\right)$$
$$\psi_y = \frac{\partial w}{\partial y} + \frac{h^2}{10}\frac{E_2}{G_{23}}\left(1 + \frac{6N_y}{5G_{23}h}\right) \qquad (7.11)$$

Substituting Equations 7.3 and 7.11 into Equation 7.10 results in a lengthy, but manageable, expression for V_S in terms of the single dependent variable w(x,y). The detailed form of this functional is given in [197].

Using the approximate strain energy functional described above, along with the displacement function given by Equation (2.8), numerical results were calculated for SSSS orthotropic plates made of unidirectional boron fibers (56% in volume) embedded in an epoxy matrix [197]. The corresponding orthotropic elastic moduli are:

$$E_1 = 32.5\times10^6\text{psi}\ ,\ E_2 = 1.84\times10^6\text{psi}$$
$$G_{12} = G_{13} = 0.642\times10^6\text{psi}\ ,\ G_{23} = 0.361\times10^6\text{psi}$$
$$\nu_{12} = 0.256,\ \nu_{21} = 0.0146.$$

It was found that the differences between buckling loads according to classical and shear deformation theories were small for thickness ratios h/a = 0.02 and 0.01, but became significant for thicker plates. Critical loads occurred for n = 1. Numerical results for the buckling parameter $\sigma_x\pi^2/G_{13}$ are presented in Table 7.2 and Figure 7.4 for h/a = 0.1, and in

Table 7.2. Uniaxial buckling parameters $-\sigma_x \pi^2/G_{13}$ for SSSS orthotropic plates with and without shear deformation (h/a = 0.1).

Classical theory	Shear deformation theory	$\frac{a}{b}$	m
4.15	2.76	0.33	1
4.22	2.80	0.5	1
4.78	3.32	1	1
5.45	3.92	1.28	1
6.28	4.95	1.50	1
9.60	9.20	2	1
—	4.64	1	2
—	4.70	1.28	2
—	4.73	1.50	2
—	5.08	2.00	2
—	5.35	2.25	2
—	5.53	2.40	2
—	5.37	1.28	3
—	5.38	1.50	3
—	5.40	2	3
—	5.44	2.4	3
—	5.45	3	3
—	5.46	4	3

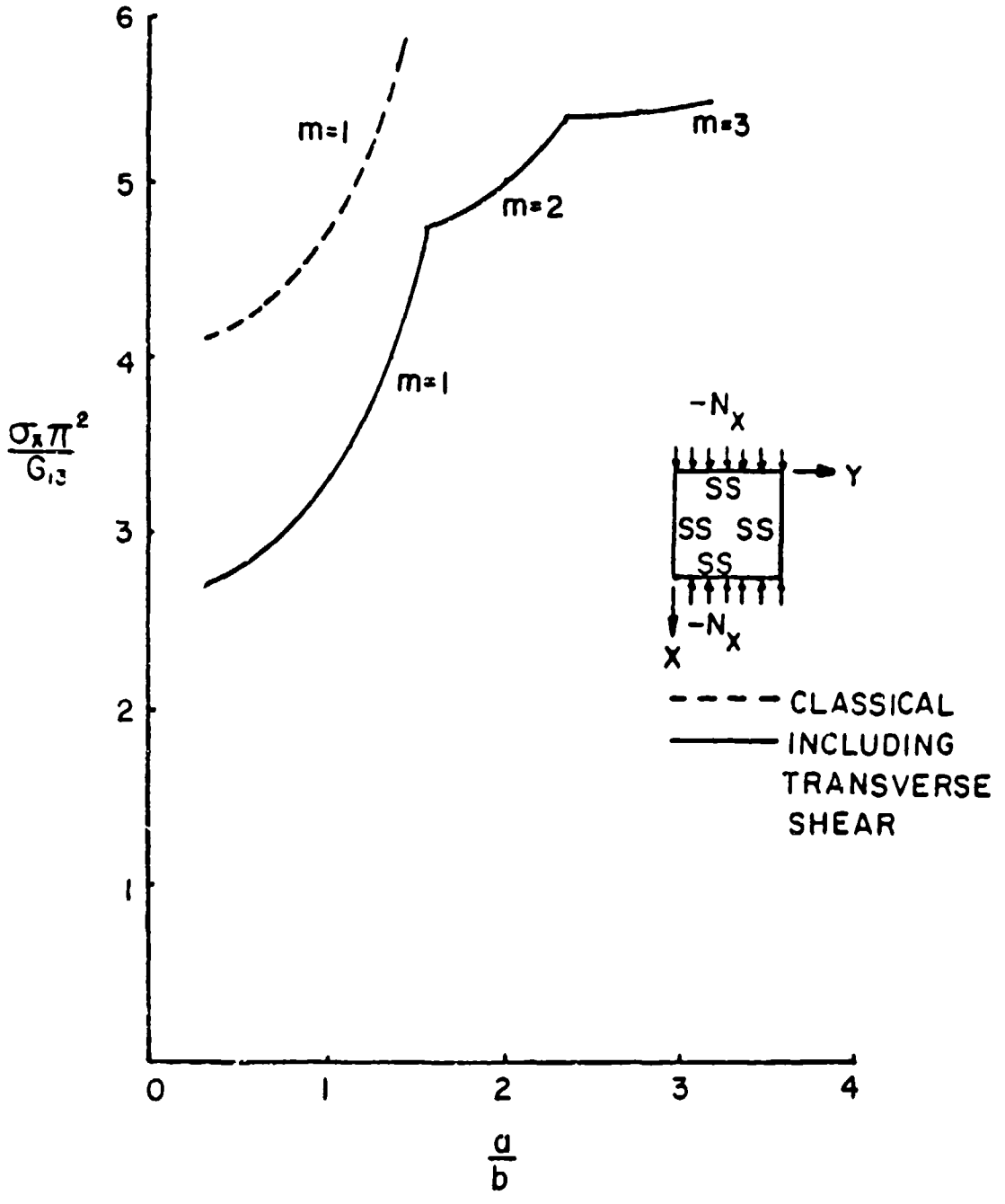

Figure 7.4. Uniaxial buckling parameters for SSSS orthotropic plates with and without shear deformation (h/a = 0.1).

Table 7.3. Uniaxial buckling parameters $-\sigma_x \pi^2/G_{13}$ for SSSS orthotropic plates with and without shear deformation (h/a = 0.04).

Classical theory	Shear deformation theory	$\frac{a}{b}$	m
.658	.615	0.33	1
.669	.625	0.5	1
.756	.712	1	1
1.518	1.482	2	1
4.268	4.231	3	1
2.678	2.051	1	2
3.022	2.343	2	2
3.958	3.244	3	2
6.034	5.124	4	2
6.649	6.200	4.2	2
6.795	4.144	3	3
7.978	4.654	4	3
8.311	6.160	4.2	3
8.494	6.669	4.3	3
8.648	7.640	4.4	3

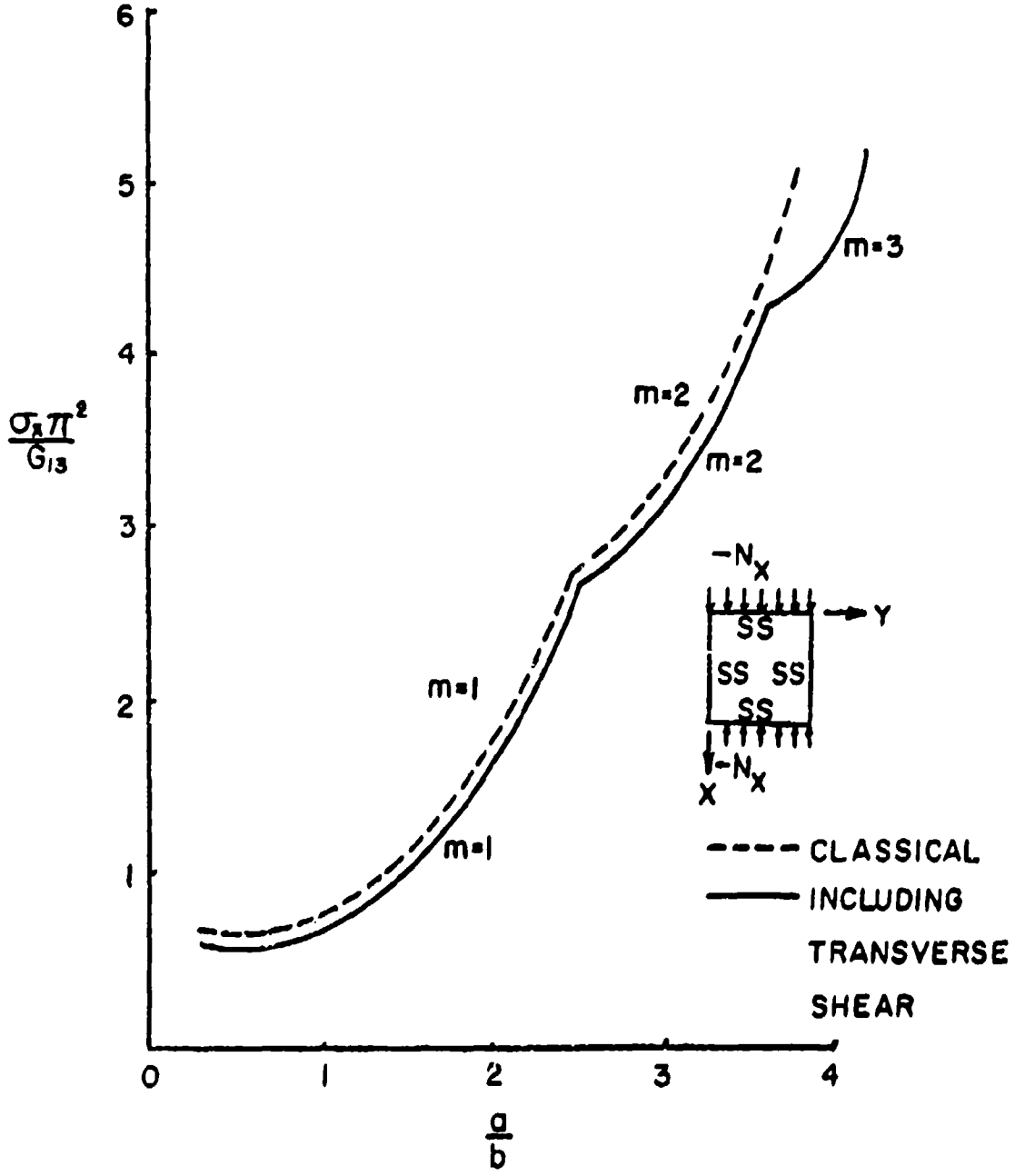

Figure 7.5. Uniaxial buckling parameters for SSSS orthotropic plates with and without shear deformation (h/a = 0.04).

Table 7.3 and Figure 7.5 for h/a = 0.04. Additional results are also available for h/a = 0.02 and 0.01 [197].

Exact solutions of the three-dimensional elasticity equations for the buckling of cross-ply laminates having four edges simply supported are also possible. These were obtained by Srinivas, Joga Rao and Rao [198,199] and by Noor [200]. It was determined that shear deformation theory gave accurate results for thickness/width ratios of at least 0.3. An example of the type of results found may be observed in Figure 7.6 where the uniaxial buckling load parameter $-\sigma_x b^2/E_2 h^2$ is plotted versus a/b for plates having even numbers of layers (NL), thereby yielding unsymmetrical laminates, and h/a = 0.1. Material properties used for each layer were: $E_1/E_2 = 30$, $G_{12}/E_2 = 0.6$, $G_{13}/E_2 = 0.5$, and $\nu_{12} = 0.25$. The curves of Figure 7.6 show very close agreement between the shear deformation theory (SDT) and elasticity solution values. However, the classical plate theory (CPT) differs considerably especially for NL = 4 or greater. On the other hand, for symmetrically laminated plates the error in classical plate theory was found to decrease as NL increases.

Turvey [201] incorporated the reduced stiffness method (see Chapter VI) into shear deformation plate theory for unsymmetrical laminates, thereby arriving at a sixth order set of governing differential equations. Comparison with Noor's [200] three dimensional results for SSSS plates showed close agreement of uniaxial buckling loads for square plates having h/b = 0.1. At least two other references also deal with the buckling of SSSS plates, including shear deformation effects [202,203].

Vinson and Smith [197] followed the approximate procedure described earlier in this section to solve uniaxial buckling problems (σ_x = constant, $\sigma_y = \tau_{xy} = 0$) for SCSC orthotropic plates having shear deformation. A buckling mode shape was assumed in the form

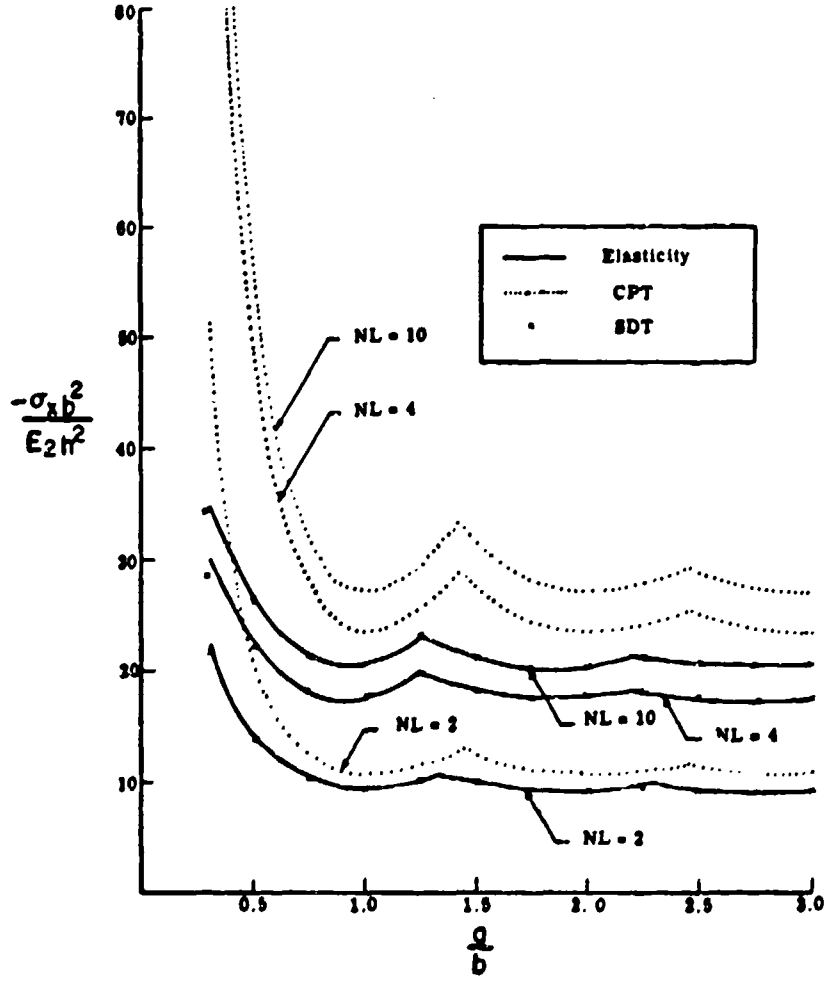

Figure 7.6. Comparison of exact elasticity, classical plate theory (CPT) and shear deformation theory (SDT) solutions for uniaxially loaded, SSSS cross-ply laminates.

$$w(x,y) = c_{mn} \sin \frac{m\pi x}{a} \left(1 - \cos \frac{2n\pi y}{b}\right) \tag{7.12}$$

Numerical results were presented for boron-epoxy plates as described earlier in this section, and are given in Table 7.4 and Figure 7.7 for h/a = 0.1, in Table 7.5 and Figure 7.8 for h/a = 0.04, and in Tables 7.6 and 7.7 for h/a = 0.02 and 0.01, respectively. It is seen that shear deformation effects are more significant for the SCSC plate than for the SSSS plate (see previously), being quite significant even for the relatively thin plate having h/a = 0.02.

Sandorff [150,204] conducted tests on a series of ten, 16-ply, graphite-epoxy laminates having SCSC edges. The specimens had dimensions: h = 0.081 in, b = 9.625 in, with the length (a) varying from 1.75 to 3.00 in. Thus, the short, clamped edges were loaded, and the long edges were simply supported. Experimental buckling loads were found which were considerably less (approx. 25 per cent) than those predicted by shear deformation theory.

Results for the uniaxially loaded SCSS orthotropic plate were also obtained by Vinson and Smith [197] using the approximate method described earlier in this section. A buckling mode shape was assumed in the form

$$w(x,y) = c_m \sin \frac{m\pi x}{a} \left(2y^4 - 3by^3 + b^3y\right) \tag{7.13}$$

Numerical results were presented for boron-epoxy plates as described earlier in this section, and are given in Table 7.8 and Figure 7.9 for h/a = 0.1, in Table 7.9 and Figure 7.10 for h/a = 0.04, and in Table 7.10 for h/a = 0.02. Classical and shear deformation plate theories agreed quite closely for h/a = 0.01 [197].

SSSF orthotropic plates with uniaxial loading were also analyzed by Vinson and Smith [197] using the approximate method described earlier in this section. A buckling mode shape was assumed in the form

Table 7.4. Uniaxial buckling parameters $-\sigma_x \pi^2/G_{13}$ for SCSC orthotropic plates with and without shear deformation (h/a = 0.1).

Classical theory	Shear deformation theory	$\frac{a}{b}$	m
4.15	2.84	0.33	1
4.32	2.95	0.5	1
5.90	4.30	1	1
8.41	6.60	1.28	1
11.77	11.00	1.50	1
16.47	5.40	0.33	2
–	5.43	0.5	2
–	5.45	1	2
–	5.58	1.28	2
–	5.65	1.50	2
–	5.84	1.75	2
37.63	5.75	1	3
–	5.77	1.28	3
–	5.79	1.50	3
–	5.80	1.75	3
–	5.83	2	3
–	6.55	2.75	3

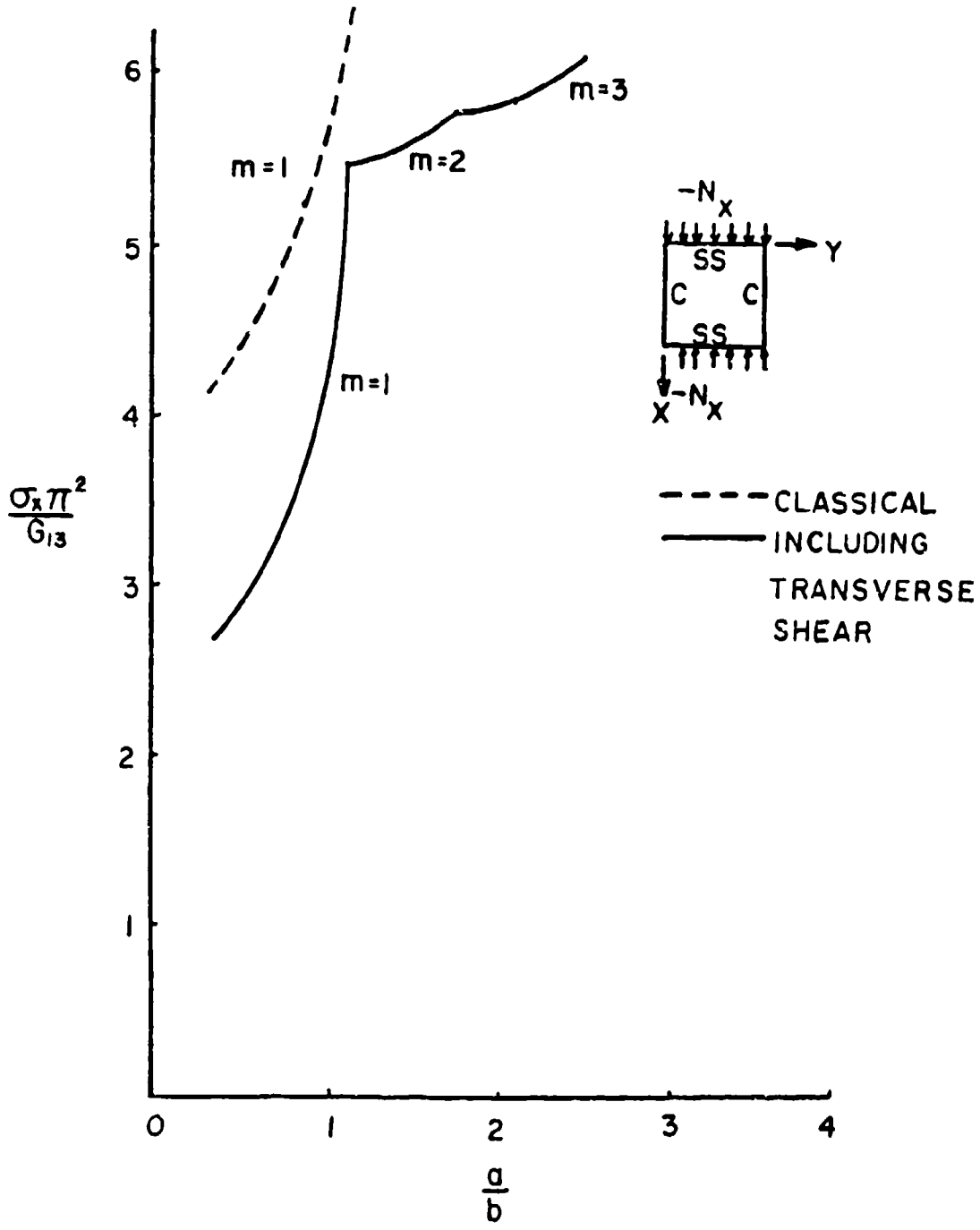

Figure 7.7. Uniaxial buckling parameters for SCSC orthotropic plates with and without shear deformation (h/a = 0.1).

Table 7.5. Uniaxial buckling parameters $-\sigma_x \pi^2/G_{13}$ for SCSC orthotropic plates with and without shear deformation (h/a = 0.04).

Classical theory	Shear deformation theory	$\frac{a}{b}$	m
.6688	.6233	0.33	1
.6919	.6490	0.5	1
.9497	.8878	1	1
4.2236	3.7641	2	1
17.6561	14.2650	3	1
2.7681	2.1091	1	2
3.7988	2.9783	2	2
5.1604	4.1026	2.5	2
7.5105	6.0227	3	2
8.1292	8.1340	3.1	2
16.8944	15.6564	4	2
6.0205	3.4805	1	3
6.6364	3.9571	2	3
7.3565	4.5944	2.5	3
8.5428	6.0289	3	3
8.8511	6.6599	3.1	3

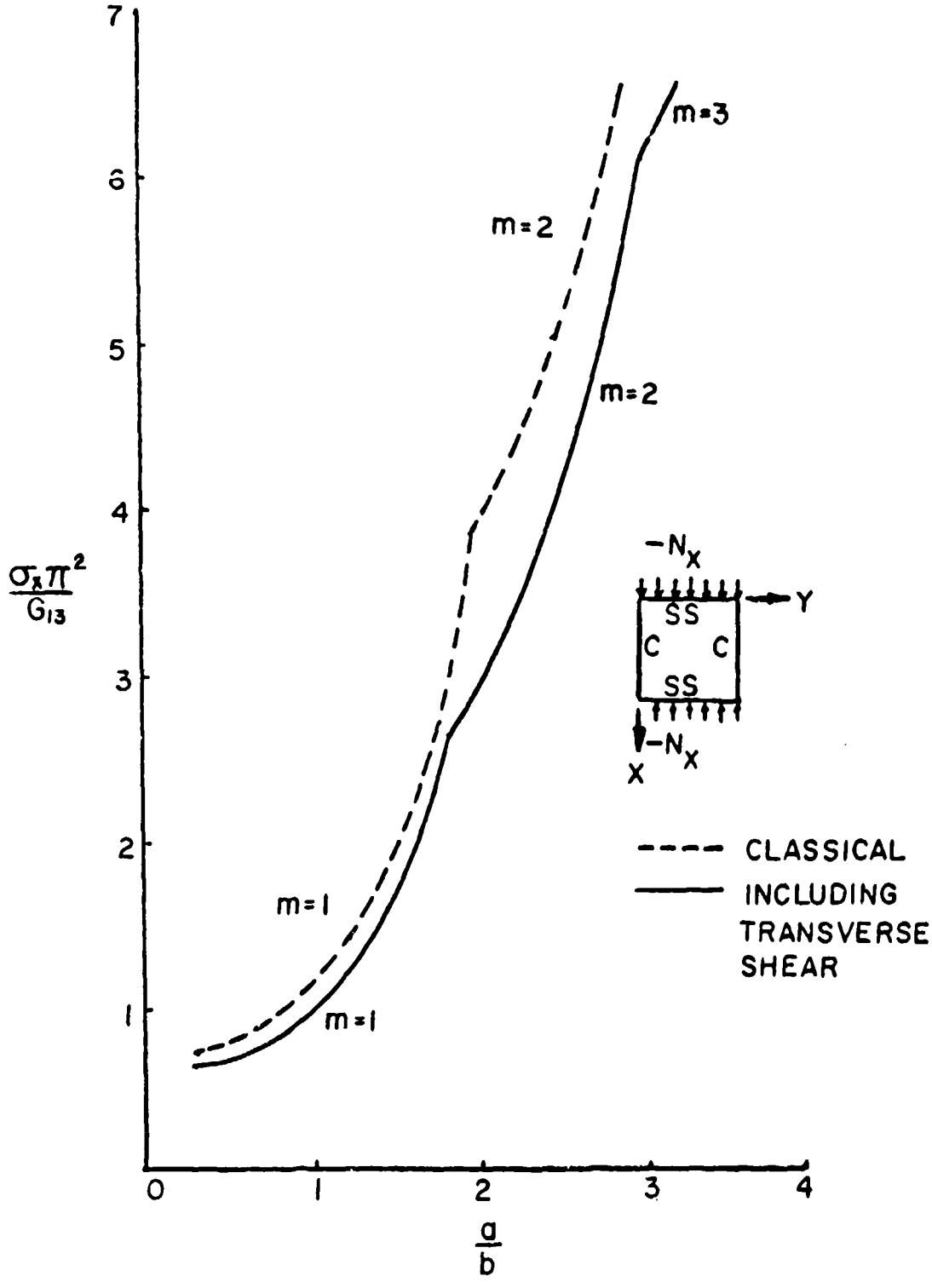

Figure 7.8. Uniaxial buckling parameters for SCSC orthotropic plates with and without shear deformation (h/a = 0.04).

Table 7.6. Uniaxial buckling parameters $-\sigma_x \pi^2/G_{13}$ for SCSC orthotropic plates with and without shear deformation (h/a = 0.02).

Classical theory	Shear deformation theory	$\frac{a}{b}$	m
.167	.163	0.33	1
.238	.234	1	1
1.058	.978	2	1
4.426	4.110	3	1
13.342	11.755	4	1
.692	.645	1	2
.950	.901	2	2
1.881	1.734	3	2
4.234	3.681	4	2
8.946	7.648	5	2
1.658	1.423	2	3
2.134	1.847	3	3
3.264	2.828	4	3
5.506	4.646	5	3
9.446	8.952	6	3

Table 7.7. Uniaxial buckling parameters $-\sigma_x \pi^2/G_{13}$ for SCSC orthotropic plates with and without shear deformation (h/a = 0.01).

Classical theory	Shear deformation theory	$\frac{a}{b}$	m
.04330	.04320	0.5	1
.05936	.05916	1	1
.2640	.2628	2	1
1.1034	1.0854	3	1
.1730	.1708	1	2
.2374	.2362	2	2
.4694	.4637	3	2
1.0558	1.0296	4	2
2.2584	2.1854	5	2
.5342	.5154	3	3
.8117	.7871	4	3
1.3815	1.3131	5	3
2.3750	2.2176	6	3
3.9811	3.6416	7	3

Table 7.8. Uniaxial buckling parameters $-\sigma_x \pi^2/G_{13}$ for SCSS orthotropic plates with and without shear deformation (h/a = 0.1).

Classical theory	Shear deformation theory	$\frac{a}{b}$	m
4.0736	2.8089	0.33	1
4.1733	2.8879	0.5	1
5.0930	3.7133	1.00	1
5.9305	4.8019	1.2	1
6.2702	5.3300	1.26	1
—	4.9992	1.00	2
—	5.0994	1.2	2
—	5.1902	1.26	2
—	5.2845	1.30	2
—	5.8102	1.50	2
—	5.7150	1.00	3
—	5.7180	1.30	3
—	5.7200	1.50	3
—	5.9200	2.00	3

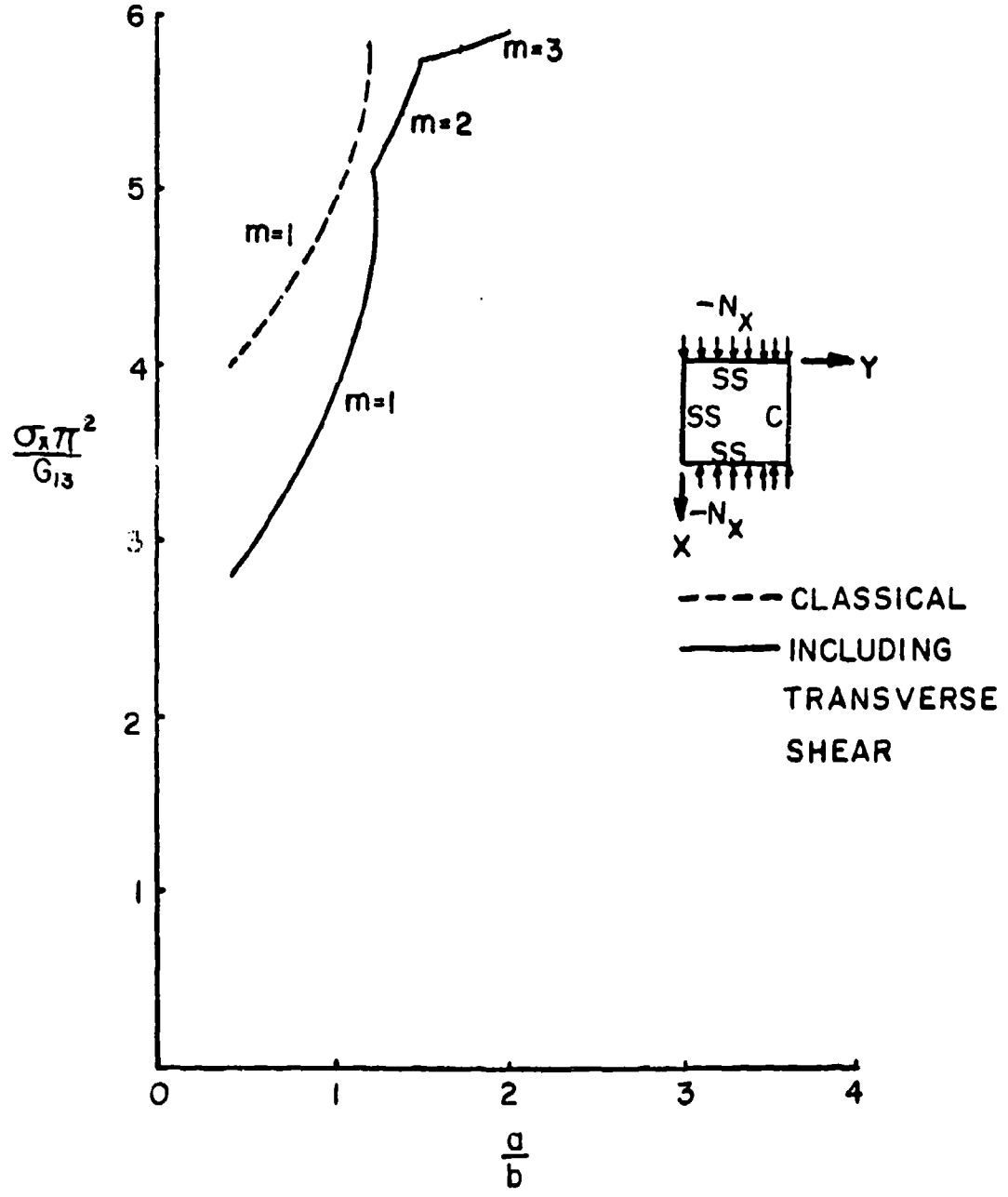

Figure 7.9. Uniaxial buckling parameters for SCSS orthotropic plates with and without shear deformation (h/a = 0.1).

Table 7.9. Uniaxial buckling parameters $-\sigma_x \pi^2/G_{13}$ for SCSS orthotropic plates with and without shear deformation (h/a = 0.04).

Classical theory	Shear deformation theory	$\frac{a}{b}$	m
.6622	.6177	0.33	1
.6863	.6255	0.5	1
.8165	.7437	1	1
2.4410	2.4226	2	1
8.8285	8.6127	3	1
3.2660	2.6505	2	2
5.1655	4.8650	3	2
5.4792	5.2780	3.1	2
6.1333	6.0120	3.3	2
6.7370	6.7012	3.4	2
7.3472	5.3040	3	3
7.5123	5.6500	3.1	3
7.8838	6.4445	3.3	3
8.6020	6.6982	3.4	3

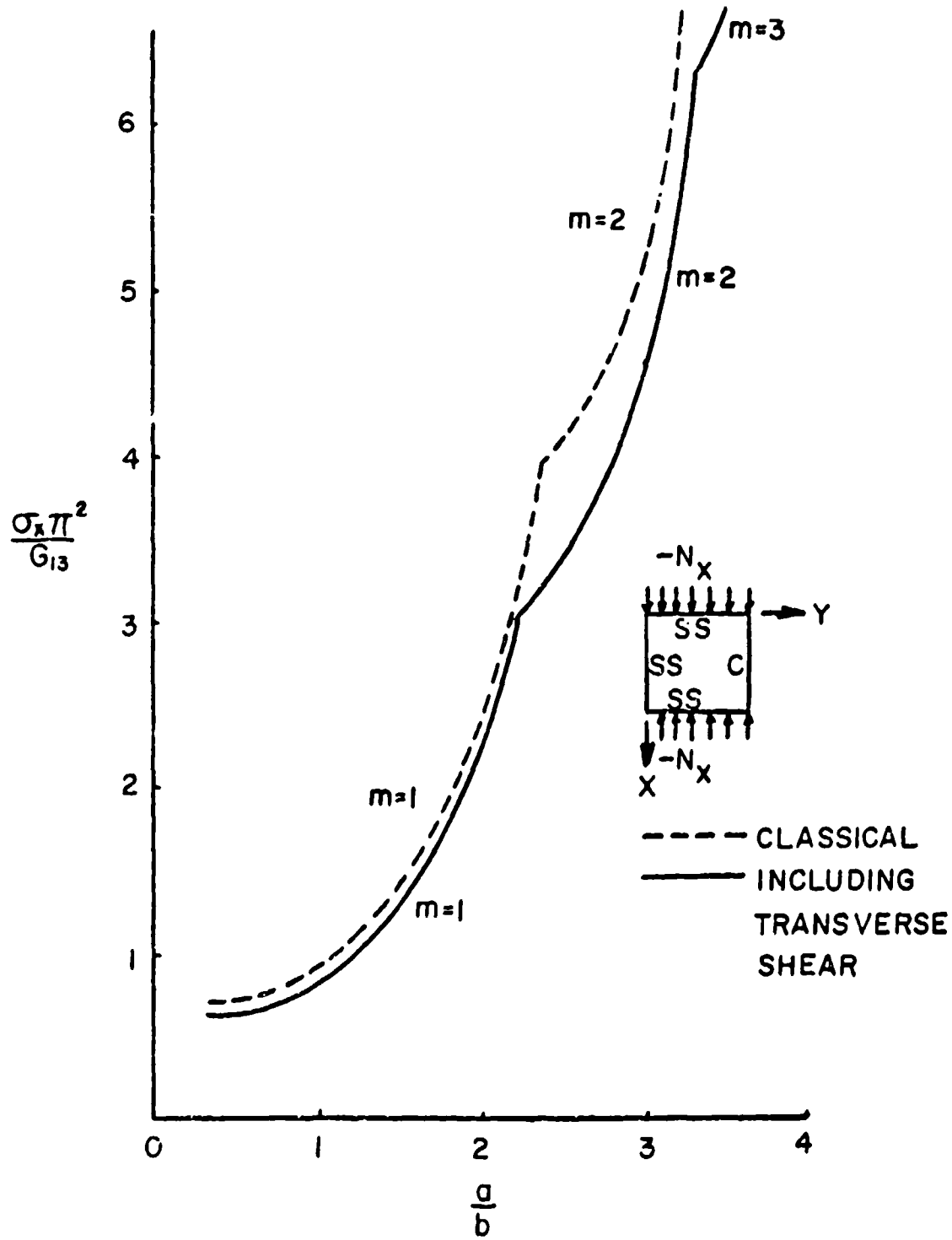

Figure 7.10. Uniaxial buckling parameters for SCSS orthotropic plates with and without shear deformation (h/a = 0.04).

Table 7.10. Uniaxial buckling parameters $-\sigma_x \pi^2/G_{13}$ for SCSC orthotropic plates with and without shear deformation (h/a = 0.02).

Classical theory	Shear deformation theory	$\frac{a}{b}$	m
.1628	.1624	0.33	1
.1668	.1660	0.5	1
.2036	.2030	1	1
.6080	.6078	2	1
2.1980	2.1970	3	1
.8144	.7819	2	2
1.2860	1.2659	3	2
2.4256	2.4056	4	2
4.7086	4.6875	5	2
1.8288	1.6239	3	3
2.4084	2.2305	4	3
3.5136	3.4669	5	3
5.4186	5.2174	6	3

Table 7.11. Uniaxial buckling parameters $-\sigma_x \pi^2/G_{13}$ for SSSF orthotropic plates with and without shear deformation (h/a = 0.1).

Classical theory	Shear deformation theory	$\frac{a}{b}$	m
.173	.171	0.33	2
.260	.256	1	2
1.045	1.028	3	2
1.631	1.380	0.33	20
1.720	1.451	1	20
2.500	2.132	3	20
4.871	3.940	0.33	60
4.958	4.040	1	60
5.750	5.100	3	60

Table 7.12. Uniaxial buckling parameters $-\sigma_x \pi^2/G_{13}$ for SSSF orthotropic plates with and without shear deformation (h/a = 0.04).

Classical theory	Shear deformation theory	$\frac{a}{b}$	m
.00694	.00695	0.33	2
.01042	.0105	1	2
.0417	.0418	3	2
.0654	.0652	0.33	20
.0689	.0687	1	20
.100	.0996	3	20
.1954	.1917	0.33	60
.1989	.1950	1	60
.230	.225	3	60

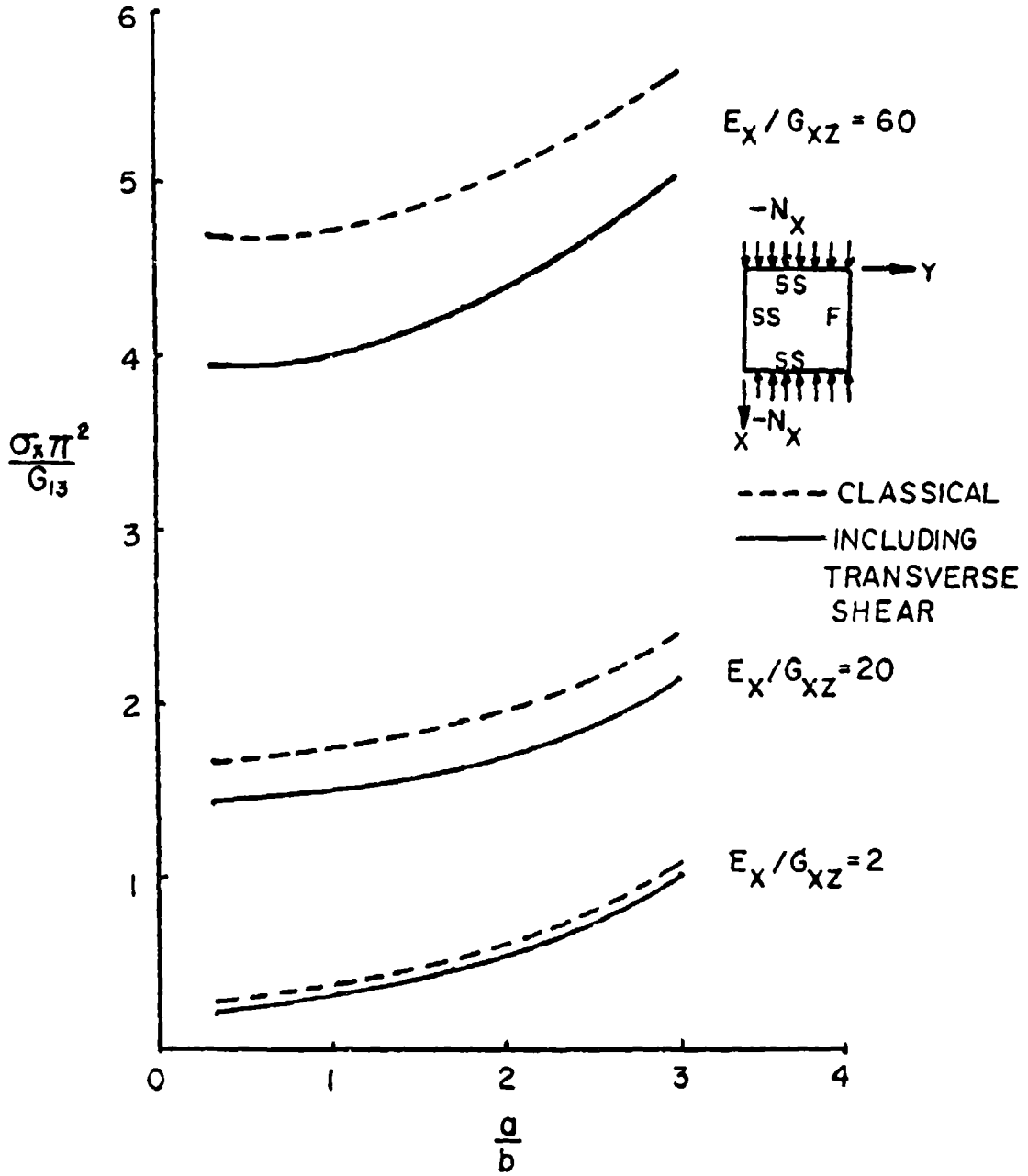

Figure 7.11. Uniaxial buckling parameters for SSSF orthotropic plates with and without shear deformation (h/a = 0.1).

$$w(x,y) = c_m y \sin \frac{m\pi x}{a} \tag{7.14}$$

Critical loads were found to occur always with m = 1. Buckling parameters were calculated for unidirectional composites and were found to depend upon only one material modulus ratio: E_1/G_{13}. Numerical results for $\sigma_x \pi^2/G_{13}$ are listed in Tables 7.11 and 7.12 for h/a = 0.1 and 0.04, respectively for a/b = 0.33, 1, 3 and E_1/G_{13} = 2, 20, 60. Data for h/a = 0.1 are also plotted in Figure 7.11. No significant differences between classical and shear deformation theories were found for h/a = 0.02 or 0.01.

Some data for the buckling of CCCC plates including the effects of shear deformation were obtained by Davenport and Bert [205-207] as part of a shell analysis, but no direct comparisons with classical plate theory were made. Results for SFSF plates including shear deformation effects are also available [32,208,209]. Other buckling studies for laminated composite plates with shear deformation include [210-212].

7.3. SANDWICH PLATES WITH SOFT CORES

The use of sandwich plates consisting of orthotropic or anisotropic face sheets separated by core material has become widespread, for such plates are capable of providing lightweight construction. For decades plywood has been used for the face sheets. More recently the fiber composites have been used, especially for aerospace applications. Core materials may be considered as either homogeneous (e.g., foam) or heterogeneous (e.g., hexagonal or honeycomb cells, or corrugated).

Early experimental work to determine buckling loads was conducted by Boller [213] on sandwich plates having glass-cloth laminate face sheets and either end-grain balsa or cellular cellulose acetate cores. Various edge conditions were considered. Experimental results were compared

with theoretical values given by formulas derived by March and Smith [214]. Modifications were made in the formulas to account for shear deformation in the cores. These and more recent references [215-218] are indicative of the considerable amount of work on buckling of laminated composite sandwich plates which has taken place at the U.S. Forest Products Laboratory.

Pearce and Webber [219-221] made a theoretical and experimental study of uniaxially loaded, SSSS sandwich plates composed of fiber-reinforced, face sheets and honeycomb cores. A set of differential equations was derived, and numerical results were obtained for a square plate having face sheets composed of $\pm 45^{\circ}$ angle-ply laminates and a honeycomb core of aluminum. It was shown in a specific example that a sandwich plate having carbon fiber-reinforced face sheets would only need to weigh approximately one-half as much as one using aluminum face sheets to fail at the same buckling load.

Vinson and Shore [222] analyzed the buckling of sandwich plates made of a web-core construction (see Figure 7.12) using orthotropic materials. Three types of instability were considered:

1. Overall plate buckling
2. Local face buckling in the region from A to B (Figure 7.12)
3. Web element buckling.

Optimization studies were conducted with faces and cores made of different materials. It was shown that optimum design occurs when the weight of the core material is half that of the facing material, and that boron-epoxy and graphite-epoxy materials provide lower weight designs than do other materials.

Housner and Stein [68] proposed a simple correction in orthotropic or anisotropic plate buckling loads to accommodate sandwich plates. This requires only multiplying the critical stress by $[1-(t/h)^3]$, where t is

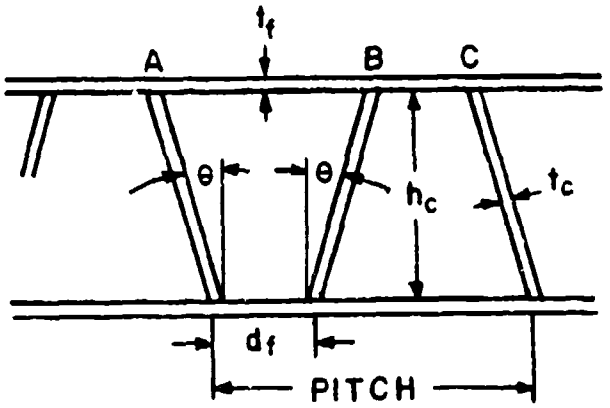

Figure 7.12. Cross-section of web-core construction.

the thickness of the core and h is the total thickness of the plate. This correction factor is based upon the following assumptions:

1. The plate is symmetrically laminated.
2. Bending-twisting coupling is negligible (i.e., each layer has the same fiber orientation angle (θ), except for sign).
3. The core carries no load and undergoes no shear deformation (or its shear modulus is negligibly small).

It was pointed out that for the second assumption to be valid, "it may be necessary that t/h to be nearly unity, and that the amount of material in either cover oriented in the $+\theta$ and $-\theta$ directions be equal."

Hyer and Hagaman [223] conducted buckling tests on sandwich plates having face sheets composed of layers of woven fabric, and cores made of Hexcel glass-reinforced polymide honeycomb. The plates were loaded uniaxially, with the loaded edges clamped and the other edges either simply supported or free.

Zubchaninov [224] analyzed the stability of three-layer plates having a central layer of metal sandwiched between glass-reinforced plastic outer layers. An example is presented for a rectangular plate in pure shear.

A number of other references are also available dealing with the buckling of sandwich plates made of laminated composites [225-232].

7.4. LOCAL INSTABILITY

The effects of delamination and delamination growth upon the buckling of composite plates were examined by several researchers [233-235]. Delamination is the result of either imperfection in the manufacturing process, or is due to developments during the life of the laminate, such as impact by foreign objects. Delaminations may cause a reduction in the overall

stiffness of the plate, thereby reducing its buckling loads. Further, delaminations may grow, depending upon the loading and the toughness of the material. Clark [231] also considered the buckling of laminates having discontinuous bonding.

Harris, Crisman and Nordby [225-227] studied the local instability of sandwich plates having facings made of fibrous composite plies. Four types of instability were discussed [226]. These included:

1. Overall plate buckling.
2. Shear crimping
3. Dimpling, or intercellular buckling
4. Face-wrinkling.

These types of buckling are illustrated in Figure 7.13. Face-wrinkling may occur with either an inward or outward displacement of the face sheet relative to the core. Outward buckling involves either a tensile failure of the bond between the core and the facing, or a tensile failure within the core. Inward buckling may be accompanied by compression failure in the core. Face-wrinkling is typically analyzed either by treating the face sheets as beams on elastic foundations, or by a quasi-elasticity approach. Experimental results were obtained for sandwich plates of two types: (1) fiberglass face sheets with aluminum, honeycomb cores and (2) plywood face sheets with foam cores. It was pointed out that experimental results are typically lower than theoretically predicted values, and that this may be due to initial waviness (i.e., deviation from flatness) of the face sheets [226]. The local instability failure of sandwich plates having composite face sheets was also treated by Fogg (see pp. 5-0 to 5-13 in [32]), Pearce and Webber [219-221], and Vinson and Shore [222](see Section 7.3).

Biot [237] studied the localized edge buckling of a laminated composite plate. The theory developed to deal with this problem included couple stresses and stress-gradient dependence of the strain. This theory was subsequently extended to more general laminated plate analysis [238].

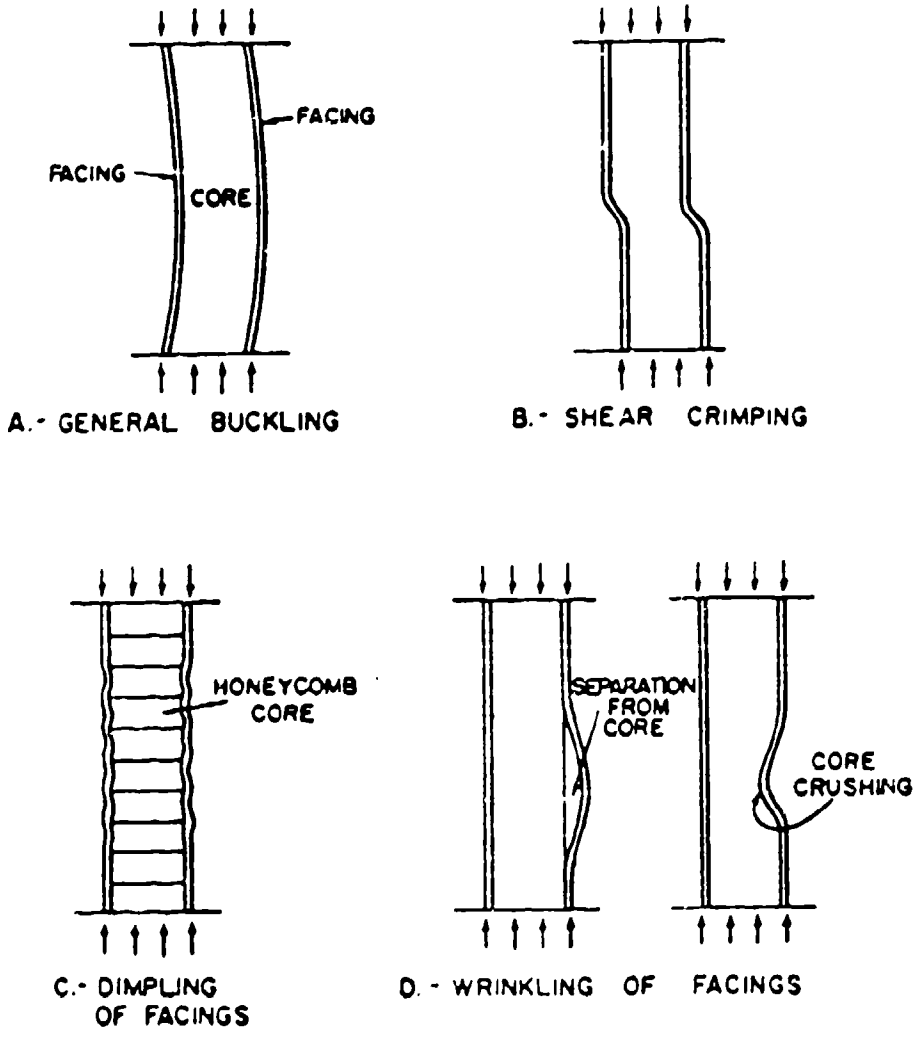

Figure 7.13. Types of buckling failure for soft-core sandwich plates.

7.5. INELASTIC MATERIALS

This section will consider laminate composites made of materials which are not linearly elastic.

The buckling of cross-ply plates with nonlinear stress-strain variation was analyzed by Morgan and Jones [239]. The nonlinear behavior was characterized by assuming

$$E_{ij} = A\left[1 - B\left(\frac{U}{U_o}\right)^C\right] \tag{7.15}$$

for each of the material moduli, where A, B, and C are constants to be determined experimentally for each material. U is the strain energy density, given by the integrand of Equation A.41, and U_o is a constant used to nondimensionalize U. Typical stress-strain curves for fiber-reinforced composite materials are shown in Figure 7.14. The equations of equilibrium for the buckled configuration (Equations 6.1) in the most general case of an unsymmetrical laminate) are satisfied incrementally by an iterative numerical procedure as the plate undergoes buckling deformation.

Numerical results were obtained for SSSS, cross-ply laminated plates composed of boron-epoxy, graphite-epoxy and boron-aluminum materials [239]. The constants A, B, C associated with each composite material to be used in Equation 7.15 are listed in Table 7.13. The values of inplane Poisson's ratio (ν_{12}) used were 0.225, 0.38 and 0.275, respectively. Values of σ^* listed for a few of the material moduli in Table 7.13 are limiting values of stress beyond which Equation 7.15 is no longer valid. At such a point on the stress-strain curve a linear extension is added having a slope given by the value of E^* in Table 7.13.

Figure 7.15 shows the nondimensional buckling stress resultant N_x as a function of plate thickness for SSSS plates consisting of a single

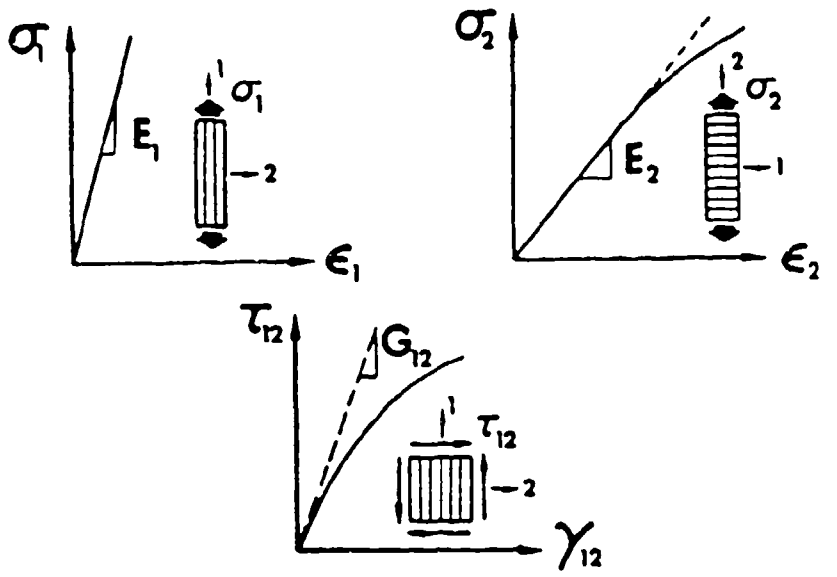

Figure 7.14. Typical stress-strain curves for fiber-reinforced composite materials [239].

Table 7.13. Constants used in Equation 7.15.

Material	Modulus	A (GN/m^2)	B	C	σ^* (KN/m^2)	E^* (GN/m^2)
Boron-epoxy	E_1	208	0	1	-	-
	E_2	19.8	0	1	-	-
	G_{12}	5.52	0.0628	0.462	64.1	0.331
Graphite-epoxy	E_1	159	0	1	-	-
	E_2	8.76	0	1	-	-
	G_{12}	6.72	0.00144	1.13	88.3	0.779
Boron-aluminum	E_1	210	0.00008	1.042	1380	165
	E_2	186	0.05814	0.723	155	25.0
	G_{12}	0.154	-399	-0.676	-	-

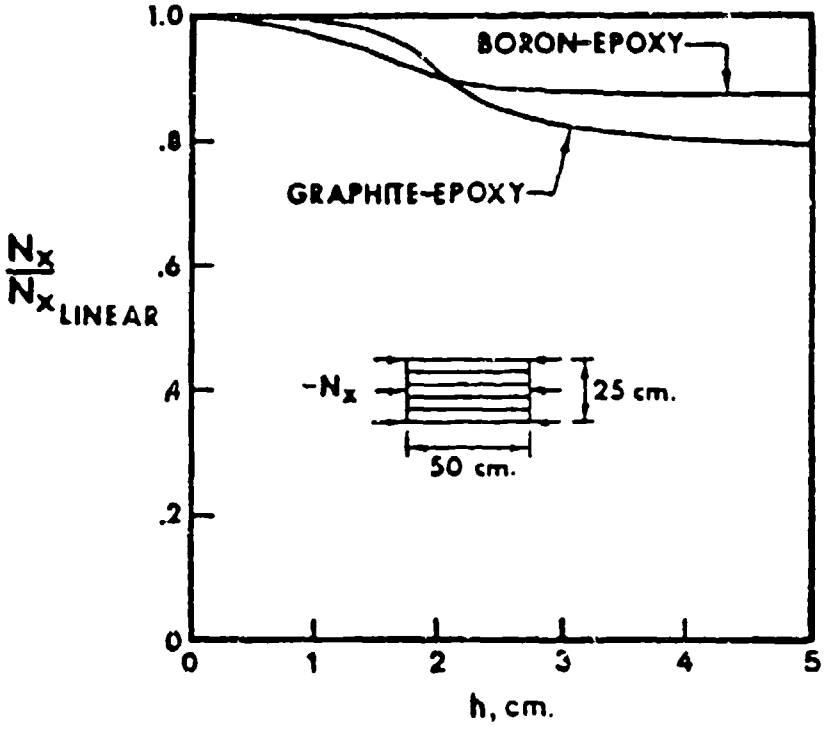

Figure 7.15. Ratio of nonlinear to linear elastic buckling loads for boron-epoxy and graphite-epoxy, SSSS, unidirectional laminates.

ply, with the loading along the direction of the fibers [239]. N_x is divided by the value of N_x which would exist for a linearly elastic material (obtained by setting B = 0 in Equation 7.15 for all moduli). This ratio is seen to decrease from 0.95 to 0.87 for a boron-epoxy laminate as h increases from 1 cm to 3 cm. For graphite-epoxy, the corresponding ratios are 0.98 and 0.79. The buckling loads increase as h increases for both the linear and nonlinear elastic materials. Similar plots are shown in Figure 7.16 for a unidirectional boron-aluminum laminate. The total nonlinearity effect is observed to be stronger for this material than for those in Figure 7.15, the ratio of buckling stress for the nonlinear material to that of the linear material being only 0.35 for h = 1 cm. In addition, the effects of nonlinearities of each modulus taken separately is depicted. The shear nonlinearity is most significant for thicknesses less than 1 cm; however, the nonlinearity in E_2 is most important for h > 1 cm. For three layer ($0^o/90^o/0^o$), cross-ply laminates similar behavior was found, with essentially no dependence upon aspect ratio (a/b) [239].

For unsymmetrically laminated, cross-ply plates made of boron-epoxy, the effect of nonlinearity in modulus was found to be small. However, for boron-aluminum laminates very significant effects were uncovered, as may be seen in Figure 7.17 [239]. The linearly elastic buckling loads with 2, 4 and an infinite number of layers are very close to each other and are shown on a single curve in Figure 7.17 because E_1/E_2 is small, causing small bending-stretching coupling. However, E_1/E_2 increases with load for the nonlinear case, causing the corresponding curves in Figure 7.17 to be much lower. Finally, the variation in $-N_x b^2/E_2 h^3$ with number of layers in a boron-epoxy, unsymmetrically laminated, cross-ply plate is shown in Figure 7.18, considering coupled (exact) and uncoupled (orthotropic), and linear modulus and nonlinear modulus solutions.

Hahn [240] in an earlier paper analyzed the buckling of $\pm 45^o$ angle-ply plates having nonlinear stress-strain relationships. The elastic

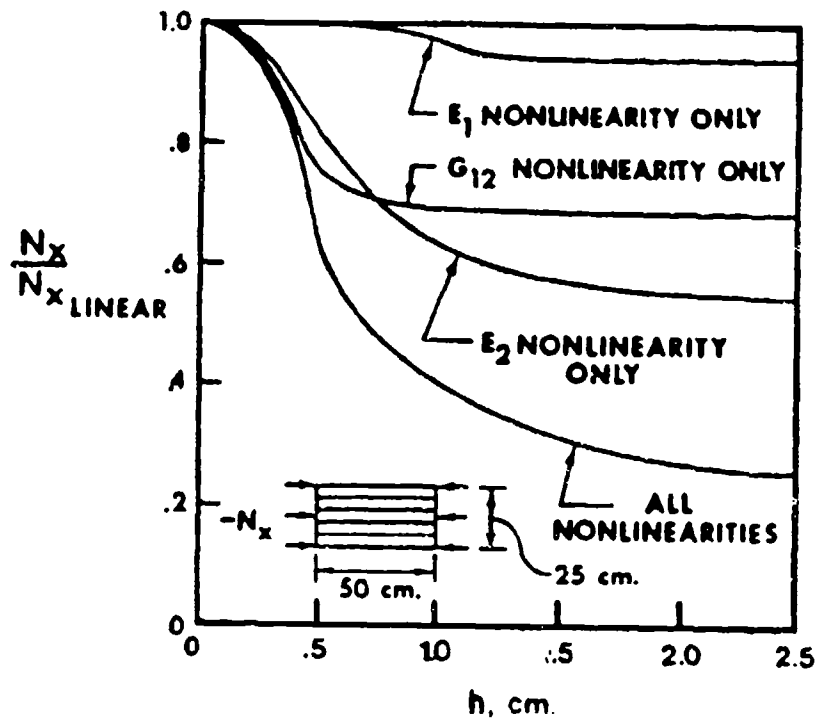

Figure 7.16. Ratio of nonlinear to linear elastic buckling loads for boron-aluminum, SSSS, unidirectional laminates.

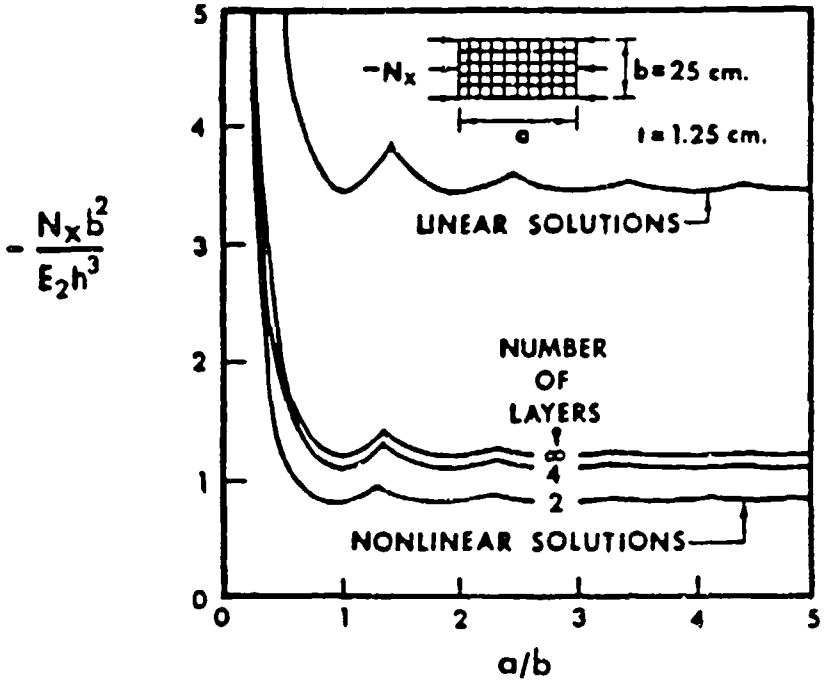

Figure 7.17. Uniaxial buckling loads of unsymmetric, SSSS, cross-ply, boron-aluminum plates.

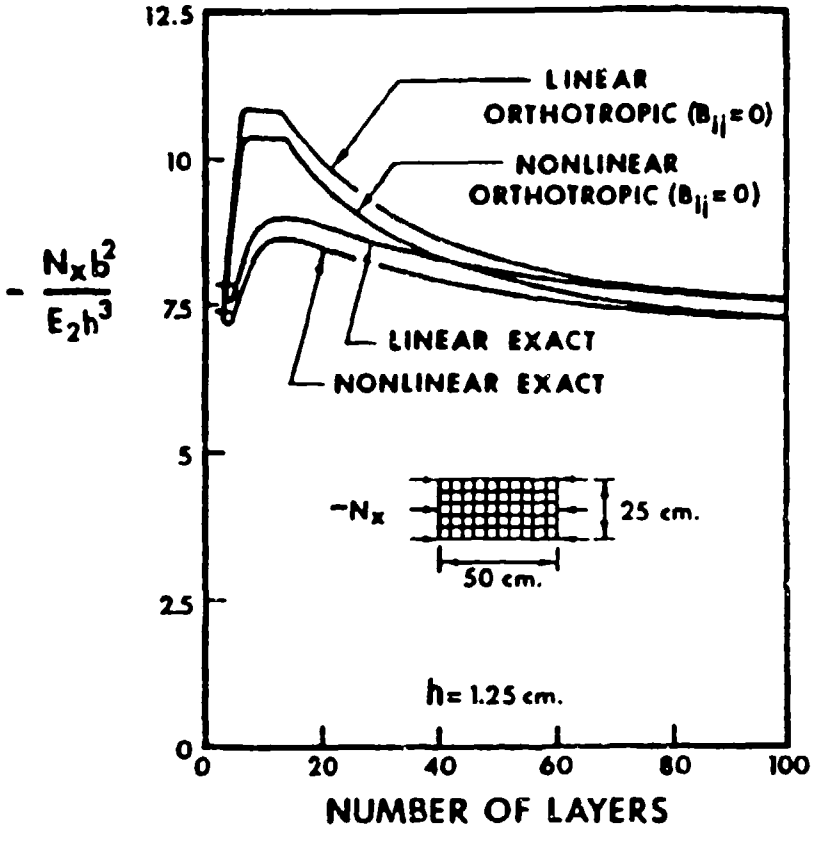

Figure 7.18. Uniaxial buckling loads of unsymmetric, SSSS, cross-ply, boron-epoxy plates.

moduli were assumed to vary quadratically. In one example for a symmetrically laminated, SSSS plate a small decrease in buckling load due to the nonlinearity was found. Another paper which deals with the buckling of a boron-epoxy plate having nonlinear stress-strain equations is that by Durocher and Palazotto [241,242].

Teters [243] used flow theory to describe the plastic properties of orthotropic plates undergoing buckling. Shear deformation effects were also included, which were found to be important if E_1/G_{13} is large. For $E_1/G_{13} = 60$ and $a/b = 20$, inclusions of shear deformation decreased the critical stress by 45 percent.

7.6. HYGROTHERMAL EFFECTS

Two effects of the external environment may cause significant internal strains, thereby affecting buckling loads -- hygroscopic (i.e., moisture absorption) and thermal. Both moisture absorption and temperature increase serve to expand a plate causing internal compressive stresses due to edge restraints or differential expansion. These effects in the laminated composite plate buckling problem apparently were first jointly taken up by Whitney and Ashton [244].

An interesting situation was found to develop in plates using graphite fibers, for these fibers have negative values of thermal expansion coefficient in the axial direction. It was found that certain orientations of angle-ply layups for graphite-epoxy plates having certain inplane boundary constraints can be buckled by lowering the temperature rather than raising it [244]. This may be seen in Figure 7.19 which is for a plate of aspect ratio (a/b) of 3 clamped at two opposite edges and free at the other two edges. The nondimensional buckling temperature change $\alpha_m(\Delta T)(b/h)^2$ is plotted versus angle-ply orientation angle (θ), where α_m is the thermal expansion coefficient of the matrix material, and ΔT is the temperature

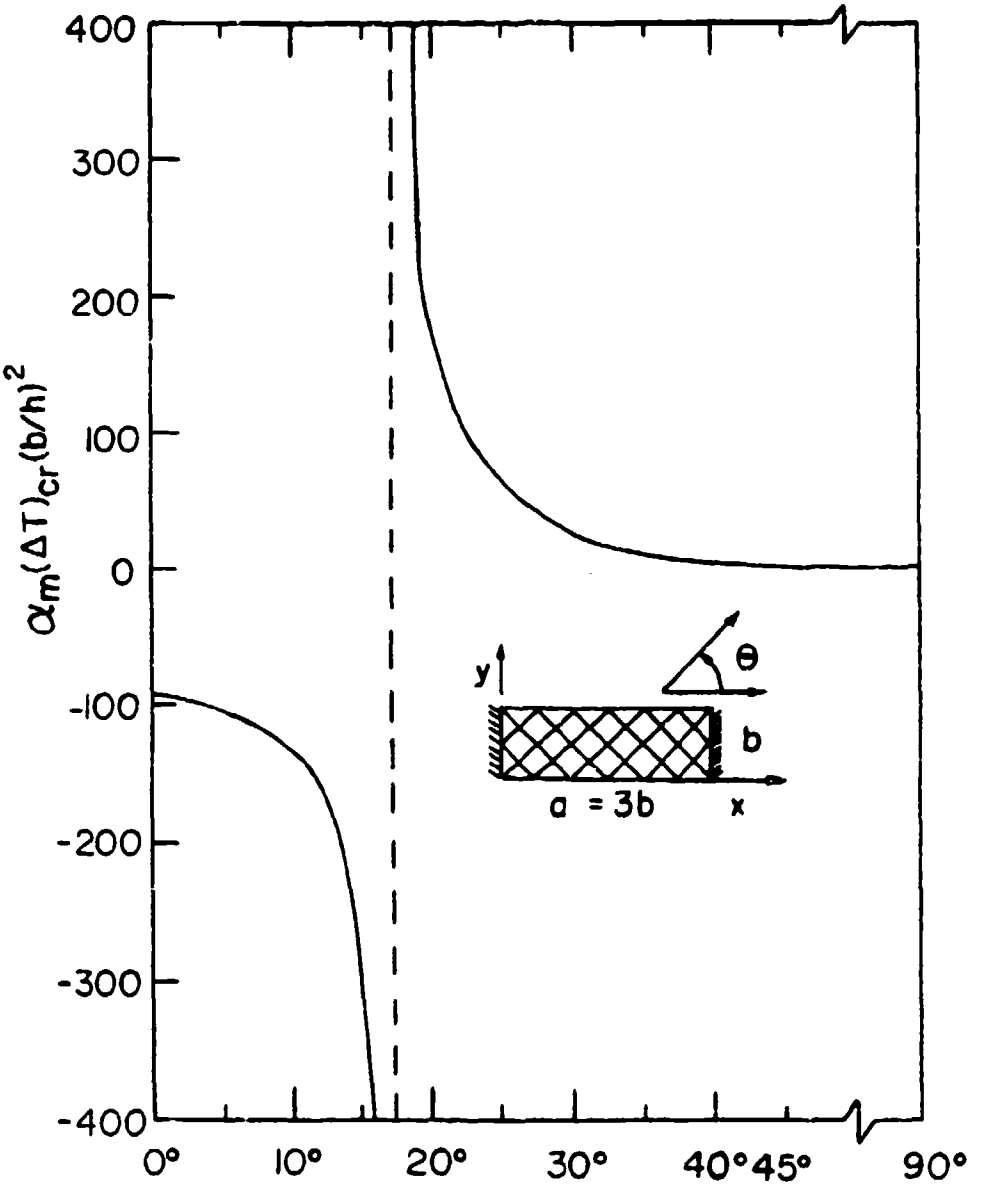

Figure 7.19. Thermal buckling of a CFCF symmetrically laminated, graphite-epoxy plate.

increase. The plate is composed of 4 layers symmetrically stacked ($+\theta$, $-\theta$, $-\theta$, $+\theta$), and is subjected to a uniform temperature rise. For fiber orientations $0^{\circ} \leq \theta < 17.5^{\circ}$, the laminate has a negative coefficient of thermal expansion relative to the x-axis, and a temperature decrease is required to cause buckling. For $\theta = 17.5^{\circ}$, the effective coefficient of thermal expansion in the x-direction disappears, and the plate cannot buckle by either increasing or decreasing the temperature. For $17.5^{\circ} < \theta \leq 90^{\circ}$ buckling may be caused only by raising the temperature. It was shown that plates constrained along all four edges could only buckle with temperature increase [244].

Hygrothermal effects were also studied by Flaggs and Vinson [245-247]. A general set of governing differential equations and energy functionals was derived for symmetrically or unsymmetrically laminated plates with shear and transverse normal deformation effects also included. The Ritz method was used to solve for buckling loads of plates having S3 simply supported (see Equations 6.2) or C3 clamped (see Equations 6.10) edge conditions. Displacements in the form of Equations 6.7 were chosen for the SSSS plates, whereas the w displacement component was changed for CCCC plates. A parametric study was made for symmetrically and unsymmetrically laminated, graphite-epoxy, angle-ply plates showing the simultaneous effects of temperature change and moisture absorption upon uniaxial buckling stress resultants. Numerical results for the SSSS and CCCC plates are shown in Figures 7.20 and 7.21, respectively. In both cases a symmetric $[0, 45, -45, 90]_{4S}$ ply orientation was used, $a = b = 12$ in, and $h = 0.176$ in. The uniaxial buckling stress resultant $-N_x$ is shown plotted versus temperature and moisture absorption (M). Considerable additional numerical results may be found in [246].

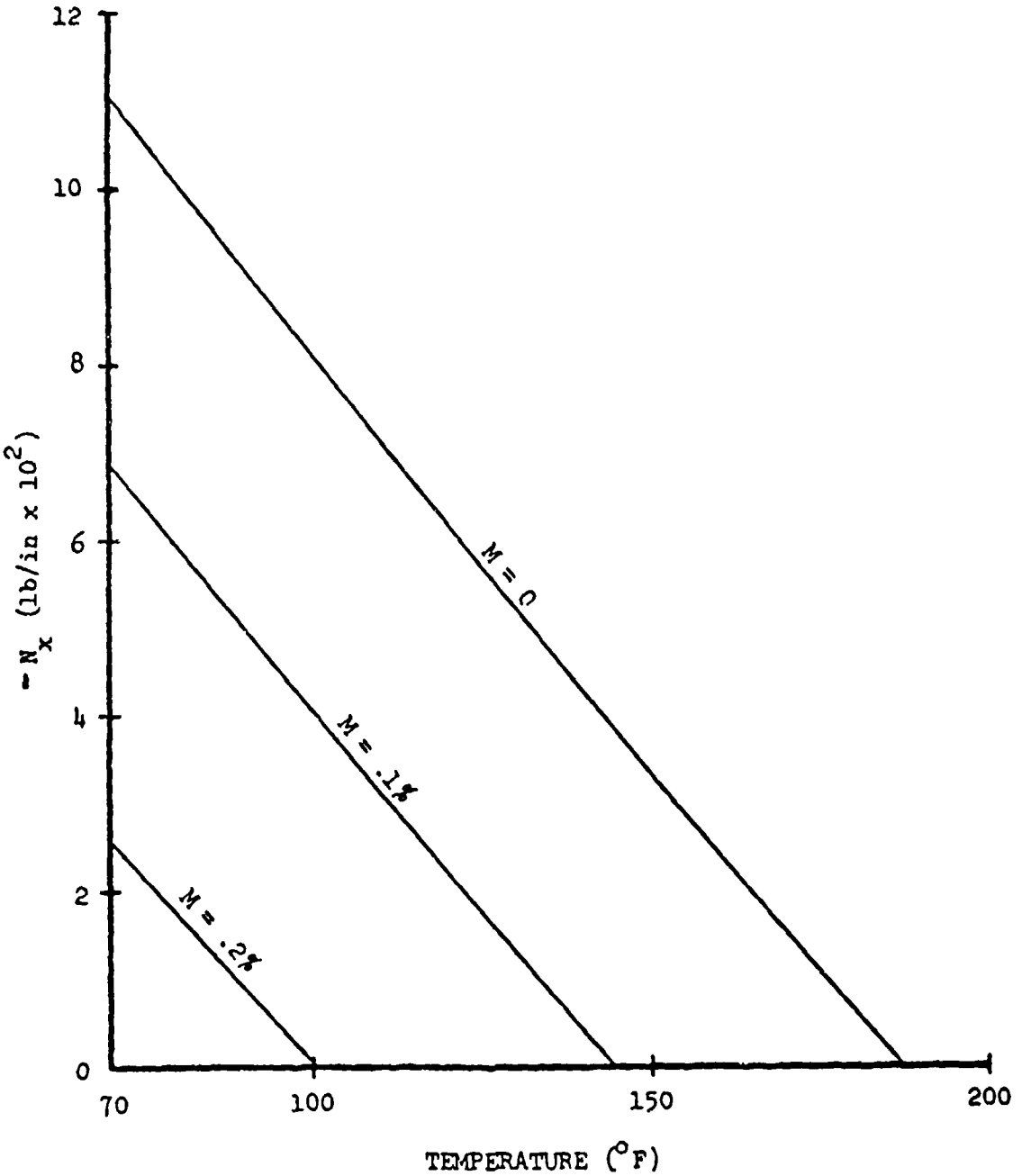

Figure 7.20. Hygrothermal effects upon the uniaxial buckling stress resultant of an SSSS plate.

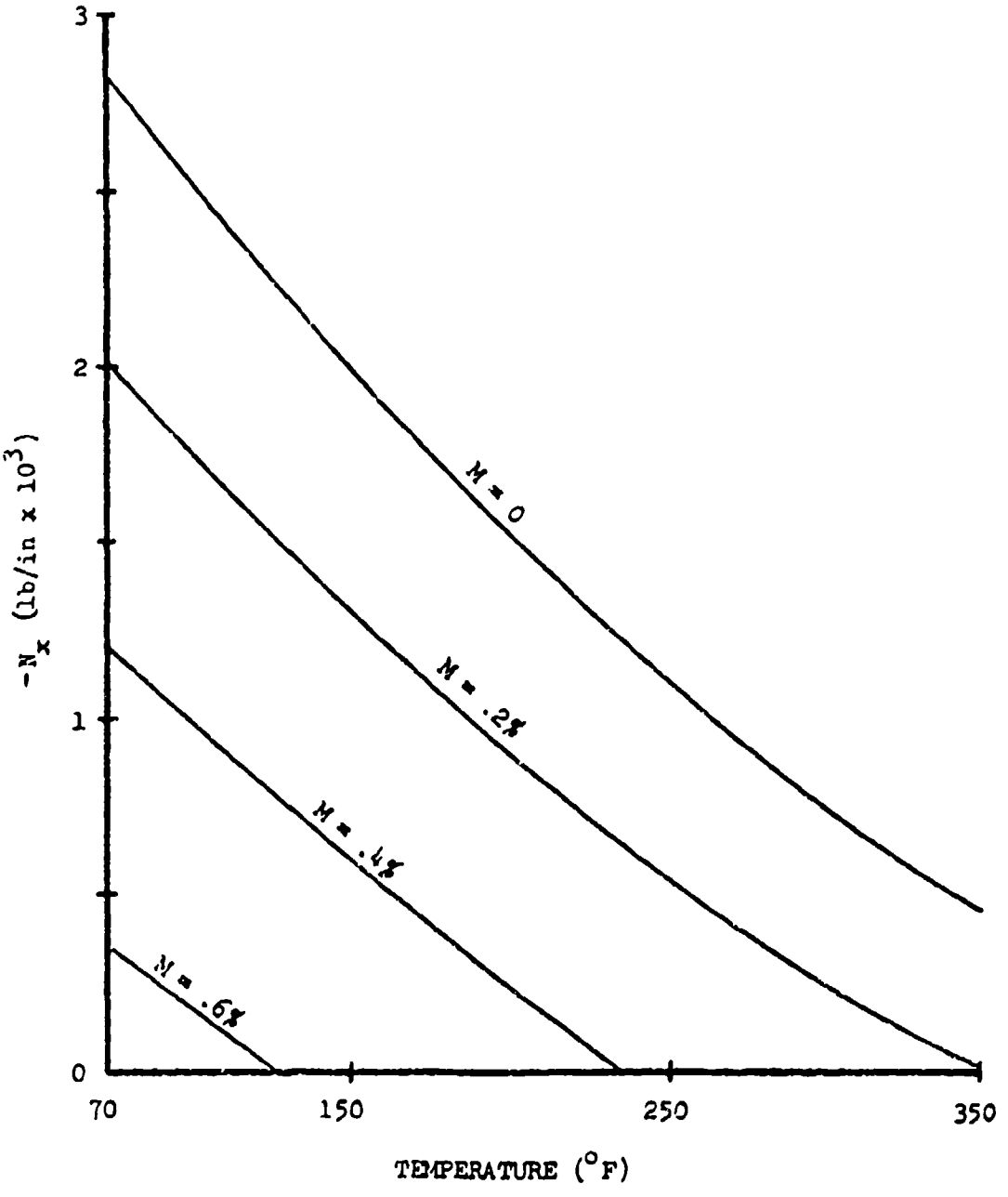

Figure 7.21. Hygrothermal effects upon the uniaxial buckling stress resultant of a CCCC plate.

CHAPTER VIII. POSTBUCKLING AND IMPERFECTIONS

As discussed in Chapter I (Figure 1.1), a linear, bifurcation buckling analysis establishes the critical value of loading for a particular plate. However, plates are typically capable of carrying considerable additional load before the collapse (or crippling, or ultimate) load is reached. In some cases this is even several times as much as the critical load, although this capability has been found to be less pronounced for laminated composite plates than for metal plates. Theoretical analysis of postbuckling behavior of plates is nonlinear, even though the transverse displacements considered may be only "moderately large" (i.e., on the order of a few times the plate thickness). The initial nonlinearity is due to additional inplane strains (and stresses) caused by the transverse displacements. Additional geometrical or material nonlinearities may arise during larger transverse displacements after buckling, but these are typically not considered in theoretical postbuckling analyses.

Imperfections considered are typically geometrical in nature. In the case of a plate, they are usually measures of deviation from flatness. Thus, for example, a SSSS plate may have an initial bow which may be represented by a half-sine-wave in each direction, where w_o is the imperfection amplitude. The application of compressive loads in the flat reference plane defined by the four plate edges causes a change in the displacement, no matter how small the load. Thus, a curve of the type V in Figure 1.1 may be followed with increasing load, with no "buckling load" readily apparent. As w_o decreases, curve V approaches curves I and IV and becomes kinked in the vicinity of the bifurcation buckling load. Also, as depicted in the figure, as the transverse displacement amplitudes become very large, the imperfection and postbuckling solutions become the same. Two other types of situations where this type of behavior occur are: (1) eccentricity due to loads not applied in the elastic midplane, and (2) transverse loads acting simultaneously with inplane loads.

These problems all are equilibrium problems, in contrast with classical bifurcation buckling problems, which are eigenvalue problems.

The behavior of plates with geometrical imperfections may be studied with either linear or nonlinear analysis, depending upon the relative magnitude of the transverse displacement which will be permitted. For example, small displacement analysis of plates with imperfection in flatness may be carried out by linear, shallow shell theory.

An excellent book by Chia [15] is available which provides a complete theory for dealing with the large displacement behavior of laminated composite plates, including orthotropic, anisotropic and unsymmetrical laminates. Numerous example problems are also solved therein for plates undergoing transverse loading, postbuckling, imperfection behavior and free vibrations.

8.1. EQUATIONS FOR POSTBUCKLING ANALYSIS

After buckling, a plate may undergo transverse displacement which is relatively large in comparison with the thickness. In this case the midplane strains given by Equations A.4 are generalized to include additional terms which account for stretching due to w:

$$\varepsilon_x^o = \frac{\partial u_o}{\partial x} + \frac{1}{2}\left(\frac{\partial w}{\partial x}\right)^2$$

$$\varepsilon_y^o = \frac{\partial v_o}{\partial y} + \frac{1}{2}\left(\frac{\partial w}{\partial y}\right)^2 \qquad (8.1)$$

$$\gamma_{xy}^o = \frac{\partial v_o}{\partial x} + \frac{\partial u_o}{\partial y} + \frac{\partial w}{\partial x}\frac{\partial w}{\partial y}$$

The added terms, which contain w, are seen to be nonlinear. The curvature changes remain related to w by Equations A.5. In using Equations 8.1

one realizes that they represent a first order correction to the classical linear theory, and that the added terms are those deemed the most significant corrections. For very large displacements, additional nonlinear terms would be required in both Equations 8.1 and A.5.

Substituting Equations 8.1, A.4, A.5 and A.8 into Equations A.12, and deleting the pressure components p_x, p_y and q acting along the plate surface the following set of equations of equilibrium ensue [15], expressed in terms of displacements:

$$\begin{bmatrix} L_{11} & L_{12} & L_{13} \\ L_{21} & L_{22} & L_{23} \\ L_{31} & L_{32} & L_{33} \end{bmatrix} \begin{Bmatrix} u \\ v \\ w \end{Bmatrix} = \frac{\partial w}{\partial x} \begin{Bmatrix} L_{11}w \\ L_{12}w \\ L_{13}w \end{Bmatrix} + \frac{\partial w}{\partial y} \begin{Bmatrix} L_{21}w \\ L_{22}w \\ L_{23}w \end{Bmatrix} + \begin{Bmatrix} 0 \\ 0 \\ \psi \end{Bmatrix} \tag{8.2}$$

where the 0 subscripts have been dropped from the displacements, but the displacements are understood to refer to the plate midplane, where the linear differential operators are defined by Equations A.21, and

$$\begin{aligned} \psi = {} & [\frac{\partial u}{\partial x} + \frac{1}{2}(\frac{\partial w}{\partial x})^2]L_7 w + [\frac{\partial v}{\partial y} + \frac{1}{2}(\frac{\partial w}{\partial y})^2]L_8 w \\ & + [\frac{\partial v}{\partial x} + \frac{\partial u}{\partial y} + \frac{\partial w}{\partial x}\frac{\partial w}{\partial y}]L_9 w - 2(B_{12}-B_{66})[(\frac{\partial^2 w}{\partial x \partial y})^2 \\ & + 2(B_{12}-B_{66})[\frac{\partial^2 w}{\partial x^2}\frac{\partial^2 w}{\partial y^2} - (\frac{\partial^2 w}{\partial x \partial y})^2] \end{aligned} \tag{8.3}$$

with

$$L_7 = A_{11}\frac{\partial^2}{\partial x^2} + 2A_{16}\frac{\partial^2}{\partial x \partial y} + A_{12}\frac{\partial^2}{\partial y^2}$$

$$L_8 = A_{12}\frac{\partial^2}{\partial x^2} + 2A_{26}\frac{\partial^2}{\partial x \partial y} + A_{22}\frac{\partial^2}{\partial y^2}$$

$$L_9 = A_{16}\frac{\partial^2}{\partial x^2} + 2A_{66}\frac{\partial^2}{\partial x \partial y} + A_{26}\frac{\partial^2}{\partial y^2} \qquad (8.4)$$

It is observed that the left-hand-side of Equations 8.2 consists of linear terms as in the classical bifurcation buckling problem, and that the right-hand-side contains only nonlinear terms which arise from the inplane stresses.

Equations 8.2 form an eighth order set of differential equations which govern the postbuckling equilibrium shape of a generally laminated (e.g., unsymmetrical) composite plate, with transverse shear deformation neglected. Certain simplifications are possible for symmetrical laminates. In one case, when the plate may be treated as anisotropic (e.g., angle-ply), all $B_{ij} = 0$, which results in $L_{13} = L_{31} = L_{23} = L_{32} = 0$, and some simplification in Equation 8.3. Further, for a plate which may be considered orthotropic (e.g., cross-ply) then, in addition, $A_{16} = A_{26} = D_{16} = D_{26} = 0$. Detailed simplified forms are given by Chia [15]. It is important to note, however, that even for symmetric laminates Equations 8.2 remain coupled by means of the nonlinear terms and that a system of eighth order, nonlinear, differential equations must be dealt with.

The nonlinear, postbuckling solution differs from the classical, linear buckling solution in a fundamental way in that the former results from an <u>equilibrium</u> problem, whereas the latter is for an <u>eigenvalue</u> problem. In both cases the governing differential equations are homogeneous. However, in the latter the boundary conditions are also homogeneous, whereas in the former they are not. Moreover, for the postbuckling problem

either the inplane stresses or the inplane displacements are prescribed along the edges, and analysis of the postbuckling problem typically entails solving for w(x,y) in terms of these edge values.

Formulation of the postbuckling problem for symmetrical and unsymmetrical laminated plates in terms of w and an Airy stress function is also available in detail in [15]. In the case of a homogeneous, isotropic plate the equations reduce to the well known ones originally derived by von Karman [248]:

$$\nabla^4\phi = E\left[\left(\frac{\partial^2 w}{\partial x \partial y}\right)^2 - \frac{\partial^2 w}{\partial x^2}\frac{\partial^2 w}{\partial y^2}\right]$$

$$D\nabla^4 w = h\left[\frac{\partial^2 w}{\partial x^2}\frac{\partial^2 \phi}{\partial y^2} + \frac{\partial^2 w}{\partial y^2}\frac{\partial^2 \phi}{\partial x^2} - 2\frac{\partial^2 w}{\partial x \partial y}\frac{\partial^2 \phi}{\partial x \partial y}\right] \qquad (8.5)$$

where ϕ is the Airy stress function and ∇^4 is the biharmonic differential operator.

8.2. POSTBUCKLING RESULTS

Prabhakara and Chia [15,249] analyzed the postbuckling behavior of orthotropic plates which represented parallel-fiber configurations made of glass, boron or graphite fibers embedded in epoxy resin. Numerical values of the moduli ratio and ν_{12} for the plates are listed in Table 8.1, as well as for an isotropic comparison plate. The critical values of uniaxial buckling stress are also given. The Galerkin method was used to obtain numerical results for SSSS plates subjected to uniform, biaxial stress. The transverse displacement (w) was taken in the form of a double Fourier sine series, and the stress function as the double sum of the products of beam functions. The variation of σ_x/σ_{cr} with w_c/h for square plates made of the four materials is shown in Figure 8.1, where σ_{cr} is the critical uniaxial buckling stress, w_c is the plate

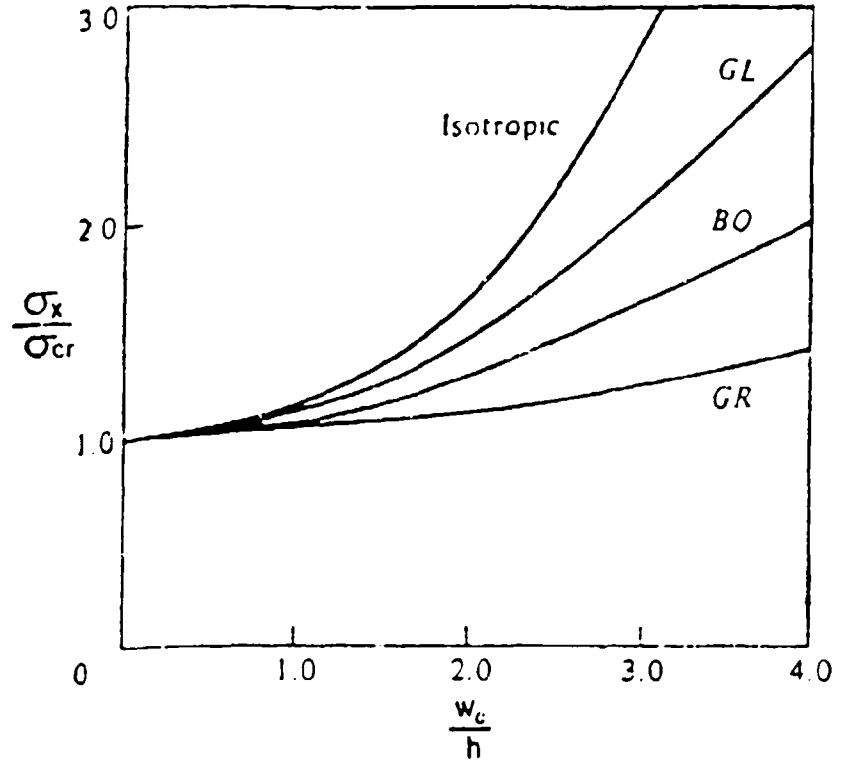

Figure 3.1. Postbuckling uniaxial stress-deflection curves for isotropic and orthotropic, SSSS plates (a/b = 1).

Table 8.1. Orthotropic SSSS plates analyzed by Prabhakara and Chia.

Material	$\frac{E_1}{E_2}$	$\frac{G_{12}}{E_1}$	ν_{12}	$-\frac{\sigma_x b^2}{\pi^2 E_1 h^2}$
Isotropic	-	-	0.316	0.3704
Glass-epoxy	3	0.1667	0.25	0.1943
Boron-epoxy	10	0.0333	0.22	0.1069
Graphite-epoxy	40	0.0150	0.25	0.0916

Table 8.2. Orthotropic SSSS plates analyzed by Chandra and Bavisu Raju.

Plate	E_f^*	E_x^*	E_y^*	G_{xy}^*	ν_{yx}	ν_{xy}
A	2	1.887	1.577	0.6123	0.3	0.251
B	5	3.761	1.648	1.061	0.3	0.211
C	10	7.068	3.578	1.409	0.3	0.152
D	20	14.13	4.282	1.714	0.3	0.0909
E	50	36.39	4.788	1.959	0.3	0.0394
F	100	69.66	5.071	2.062	0.3	0.0218
G	2	1.577	1.887	0.6123	0.251	0.3
H	5	1.648	3.761	1.061	0.211	0.3
I	10	3.578	7.068	1.409	0.152	0.3
J	20	4.282	14.13	1.714	0.0909	0.3
K	50	4.788	36.39	1.959	0.0394	0.3
L	100	5.071	69.66	2.062	0.0218	0.3

deflection at its center, and where GL, BO and GR identify the glass, boron, and graphite fiber plates, respectively. It may be observed that, for a given percent increase in axial compressive stress beyond the buckling stress, the laminated composite plates all require greater deflection than the isotropic ones with the graphite-epoxy exhibiting the greatest increase in w_c/h. Similar curves are also available for a/b = 1.5 and 2 [249], and their slopes were found to increase with increasing a/b.

Chandra and Bavasa Raju [250] carried out a postbuckling analysis of SSSS orthotropic plates by means of expanding each of the displacement components (u,v,w) in terms of a power series of a perturbation parameter. Substituting them into the equations of equilibrium for the postbuckled state yields an infinite set of linear differential equations, the first three equations of which correspond to classical, bifurcation buckling theory, which may be called the zeroeth approximation to the nonlinear analysis. First and second order approximations were obtained and added to the zeroeth one to represent the postbuckling solution. The solution procedure was applied to a number of example problems for uniaxially loaded, parallel-fiber plates having the elastic moduli listed in Table 8.2. Longitudinal fiber moduli (E_f) are also given. Thus, plates A-F have their fibers parallel to the load, whereas plates G-L have their fibers transverse to the load. Load - end shortening curves for the plates of Table 8.2 are depicted in Figures 8.2-8.5 for $\lambda = mb/a = 1$, 1.33, 2 and ∞, where m is the number of half-waves in the x-direction. In these figures P/P_o is plotted versus Δ/Δ_o, where P is the load, P_o is the buckling load, Δ is the end-shortening displacement, and Δ_o is the value of Δ at buckling. A curve for an isotropic plate is also shown for comparison. For a/b = 1 (Figure 8.2), P/P_o for plates A-D and the isotropic plate are all the same.

The "effective widths" of the plates of Table 8.2 were also calculated [250] for the case of mb/a = 1. The ratio b_e/b is plotted versus

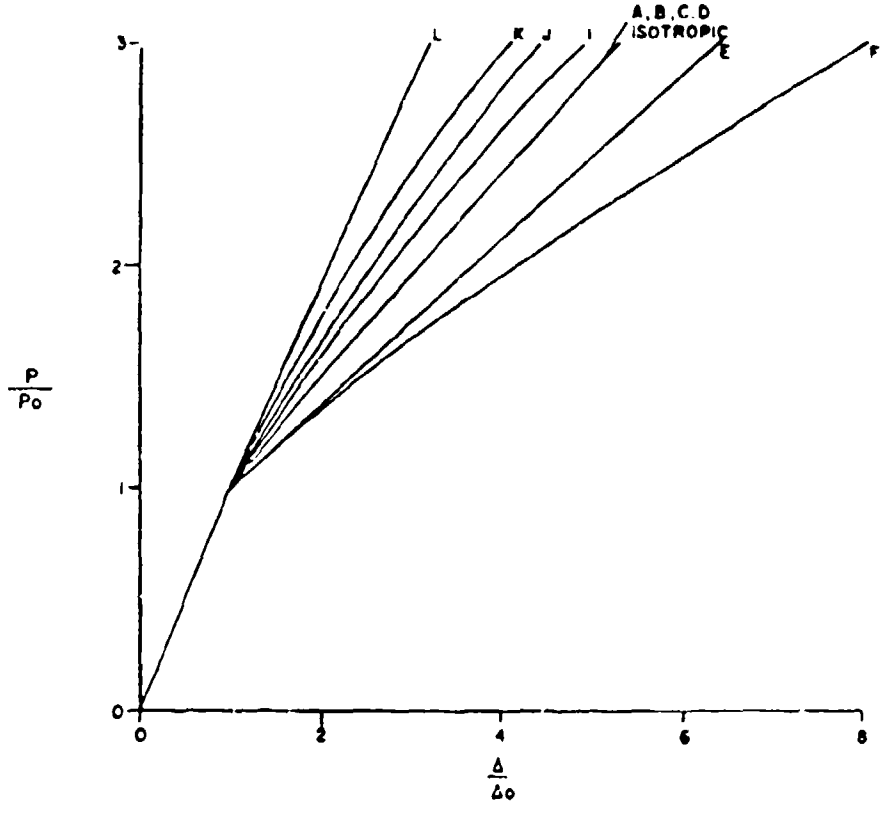

Figure 8.2. Load-shortening curves for the plates of Table 8.2 (mb/a = 1).

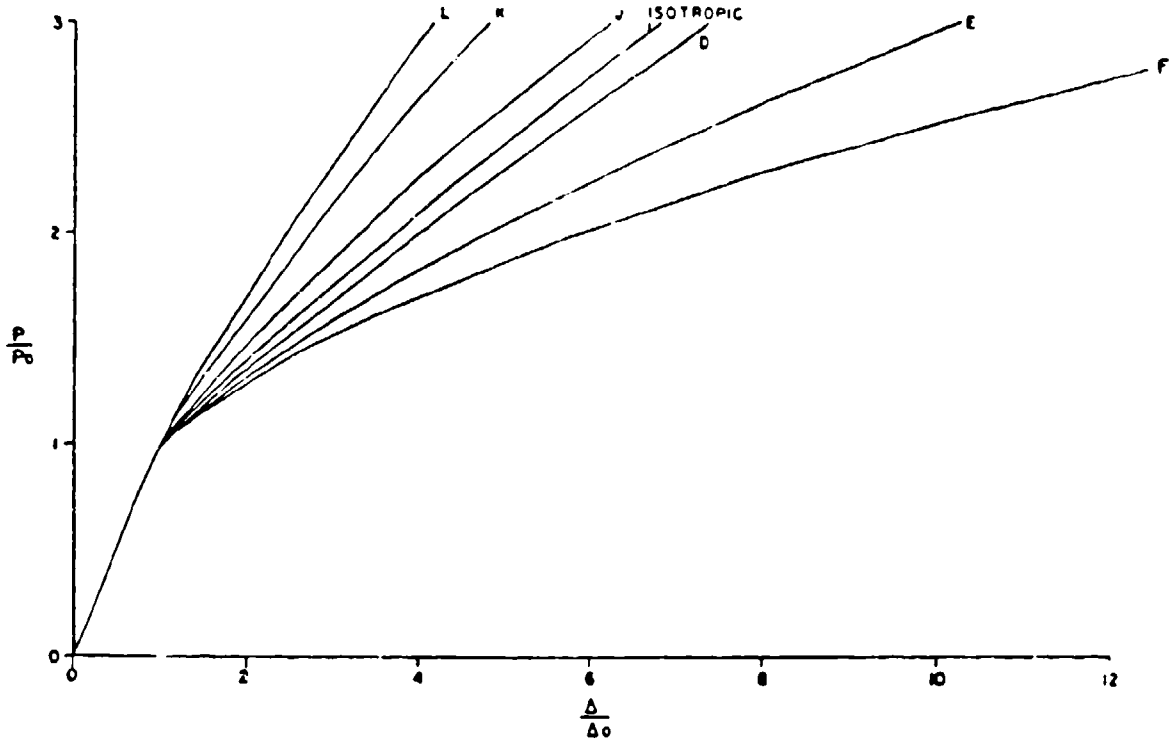

Figure 8.3. Load-shortening curves for the plates of Table 8.2 (mb/a = 1.33).

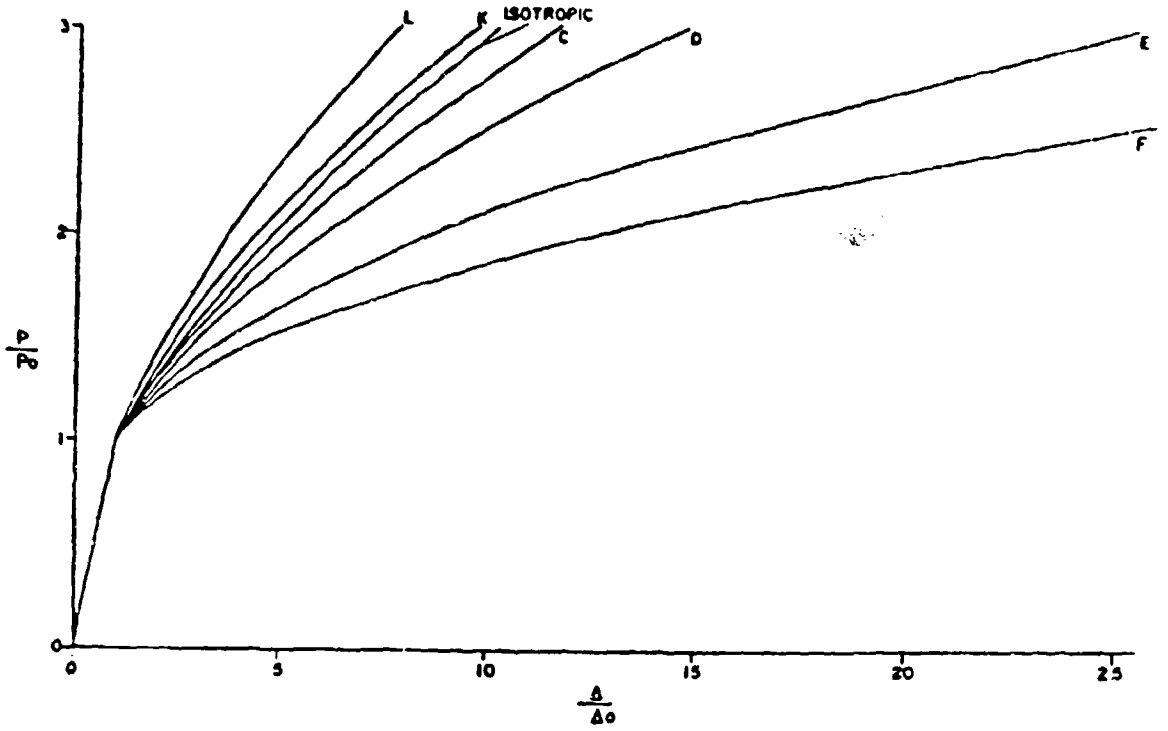

Figure 8.4. Load-shortening curves for the plates of Table 8.2. (mb/a = 2).

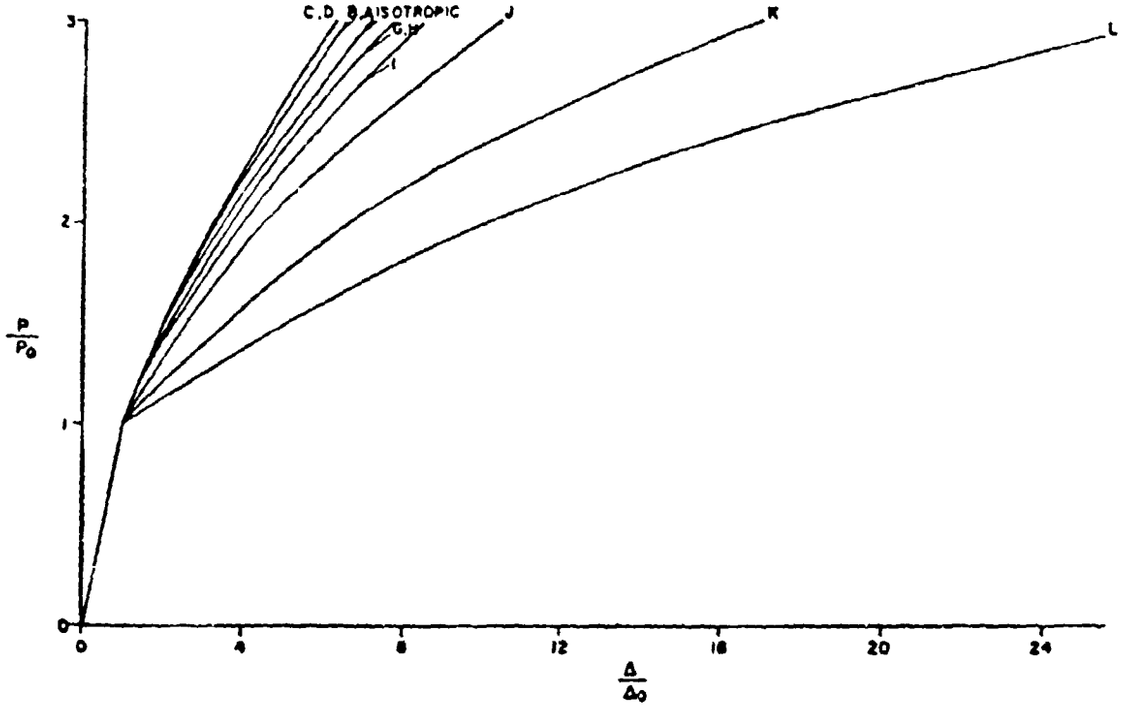

Figure 8.5. Load-shortening curves for the plates of Table 8.2 (mb/a = ∞).

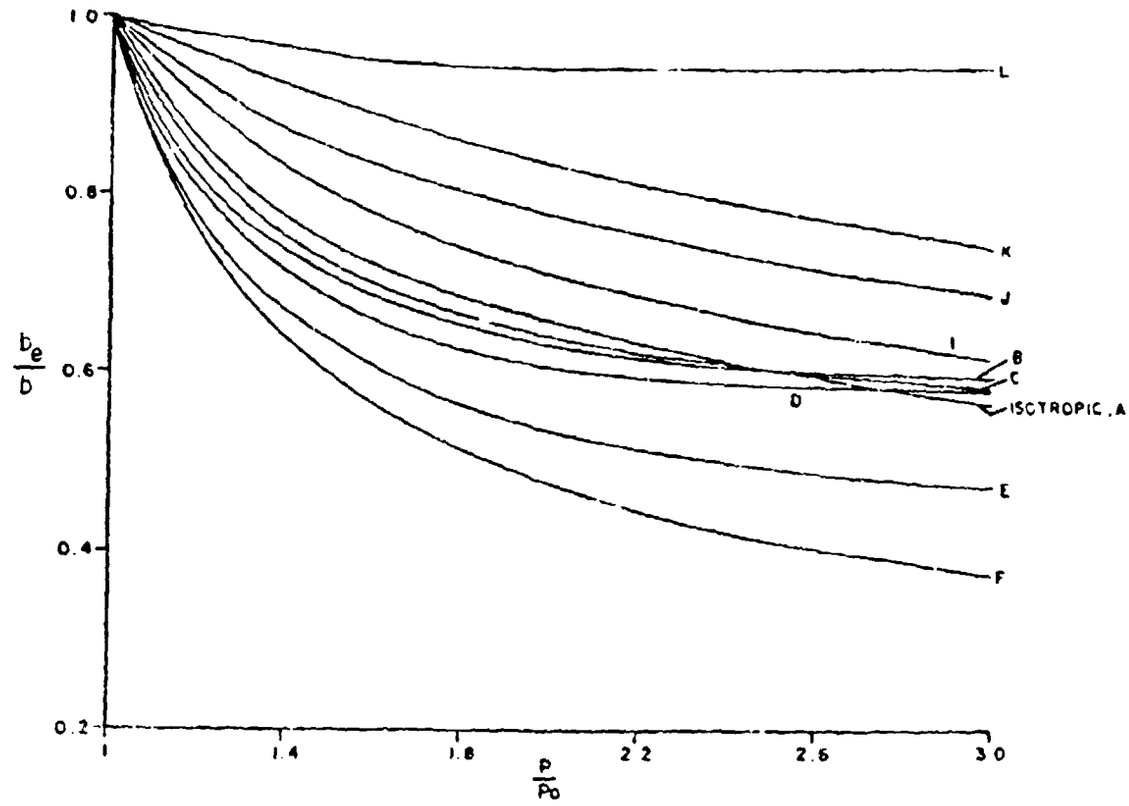

Figure 8.6. Effective widths during postbuckling for the plates of Table 8.2 (mb/a = 1).

P/P_o in Figure 8.6, where b_e is the effective width. This is a concept suggested by von Karman, Sechler and Donnell [251] to describe the portions of the plate width which carry the loading during postbuckling, assuming that the ends are shortened by uniform displacements (rather than uniform stresses). Figure 8.6 shows that when $P/P_o = 3$, the effective widths of plates having large D_{11}/D_{22} ratios (e.g., plate F) have $b_e/b < 0.5$, whereas those with small D_{11}/D_{22} (e.g., plate L) have b_e/b nearly unity.

The postbuckling behavior of CCCC orthotropic plates subjected to uniaxial loads was also studied by Chia and Prabhakara [15,113]. The nonlinear problem was solved by the Galerkin method, with both w and ϕ expressed as infinite series of the products of beam vibration eigenfunctions. Results were obtained for plates of various parallel-fiber composite and isotropic materials, as described previously in Table 8.1, except that G_{12}/E_2 was taken as 0.2 and 0.0125 for glass-epoxy and graphite-epoxy plates, respectively. Nondimensional uniaxial stresses $-\sigma_x b^2/E_2 h^2$ versus w_c/h for various aspect ratio ($\lambda = a/b$) plates may be seen in Figure 8.7. The critical buckling loads, which correspond to $w_c/h = 1$ in Figure 8.7 are listed in Table 8.3.

Postbuckling studies of anisotropic SSSS and CCCC plates were conducted by Prabhakara and Chia [15,252]. Numerical results were obtained for two cases of square, graphite-epoxy plates: (1) $\pm 45^o$ angle-ply plates loaded in hydrostatic compression ($\sigma_x = \sigma_y$ = constant, $\tau_{xy} = 0$) and (2) parallel-fiber plates having various fiber axis orientations (θ) with respect to a uniaxial loading direction. Material modulus ratios are those listed in Table 8.1, except $G_{12}/E_2 = 0.0125$. Postbuckling results are depicted in Figures 8.8 and 8.9, respectively. In the first case, results are seen for $n = 1,3,5$ and infinite numbers of layers. In these figures, w_c/h is plotted versus $-\sigma_x b^2/E_2 h^2$. For the CCCC plate with $n = 5$ in Figure 8.8, $-\sigma_x b^2/E_2 h^2 = 57.5$; whereas for the SSSS plate with $\theta = 15^o$ in Figure 8.9, it is 31.7.

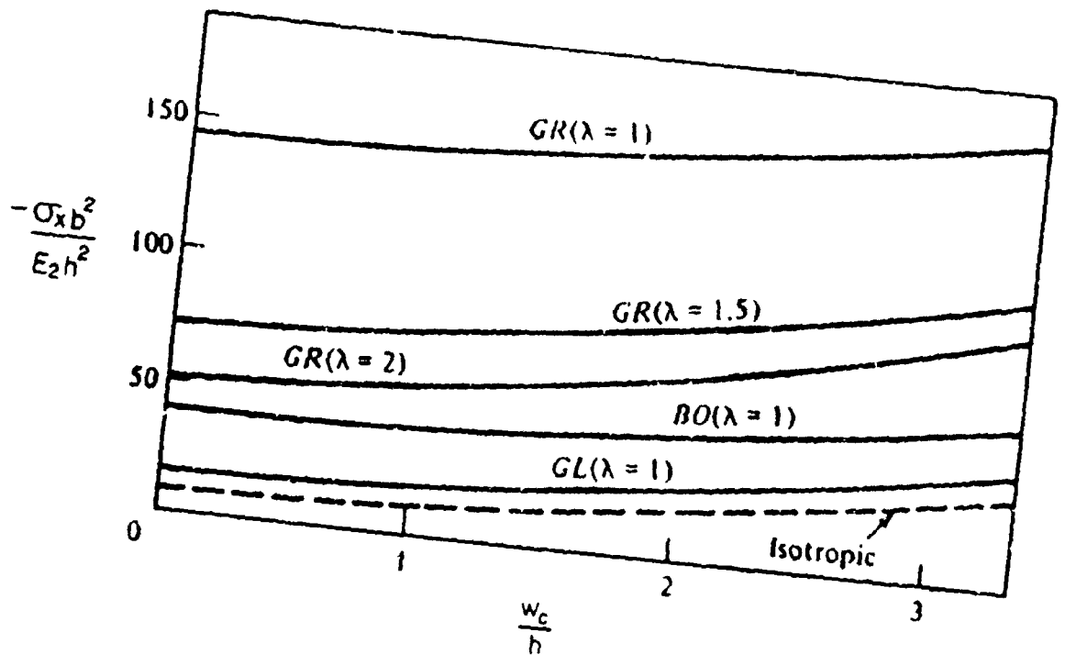

Figure 8.7. Postbuckling load-deflection curves for CCCC, uniaxially loaded, isotropic and orthotropic plates.

Table 8.3. Nondimensional critical buckling stresses for the curves of Figure 8.7.

Material	λ (=a/b)	$-\frac{\sigma_x b^2}{E_2 h^2}$
Isotropic	1.0	9.481
Glass-epoxy	1.0	16.20
Boron-epoxy	1.0	38.07
Graphite-epoxy	1.0	137.65
" "	1.5	68.30
" "	2.0	48.01

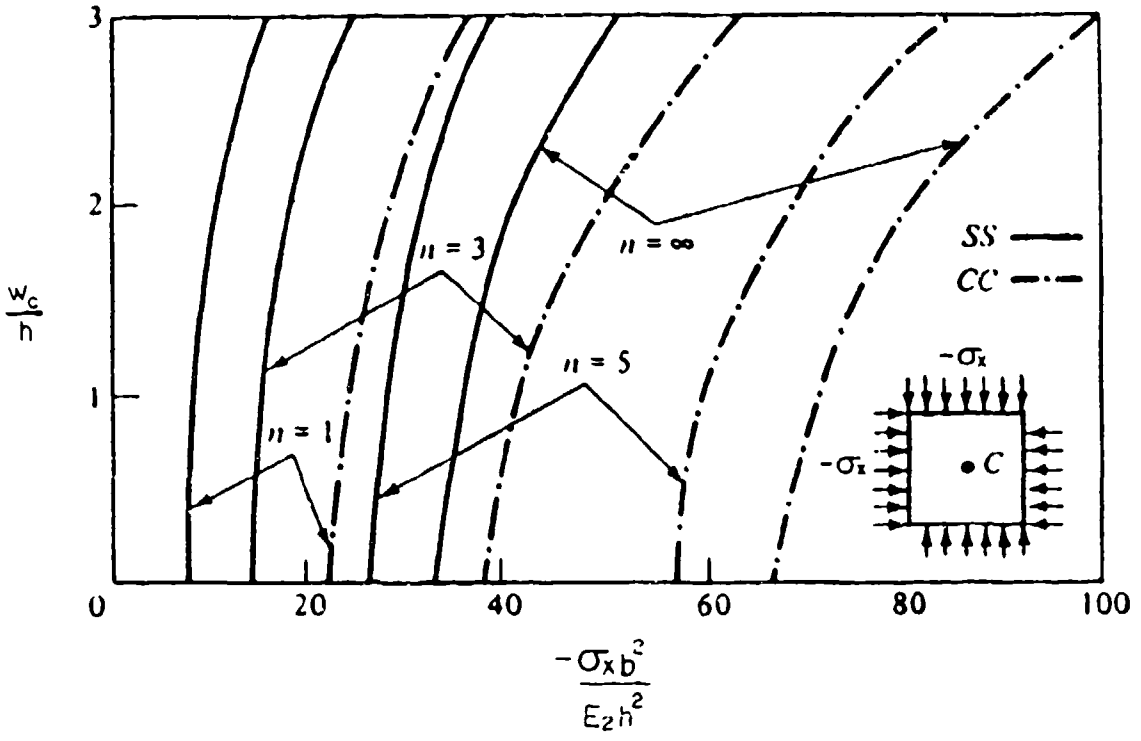

Figure 8.8. Postbuckling deflection-load curves for anisotropic ($\pm 45^\circ$ angle-ply), graphite-epoxy plates (a/b = 1).

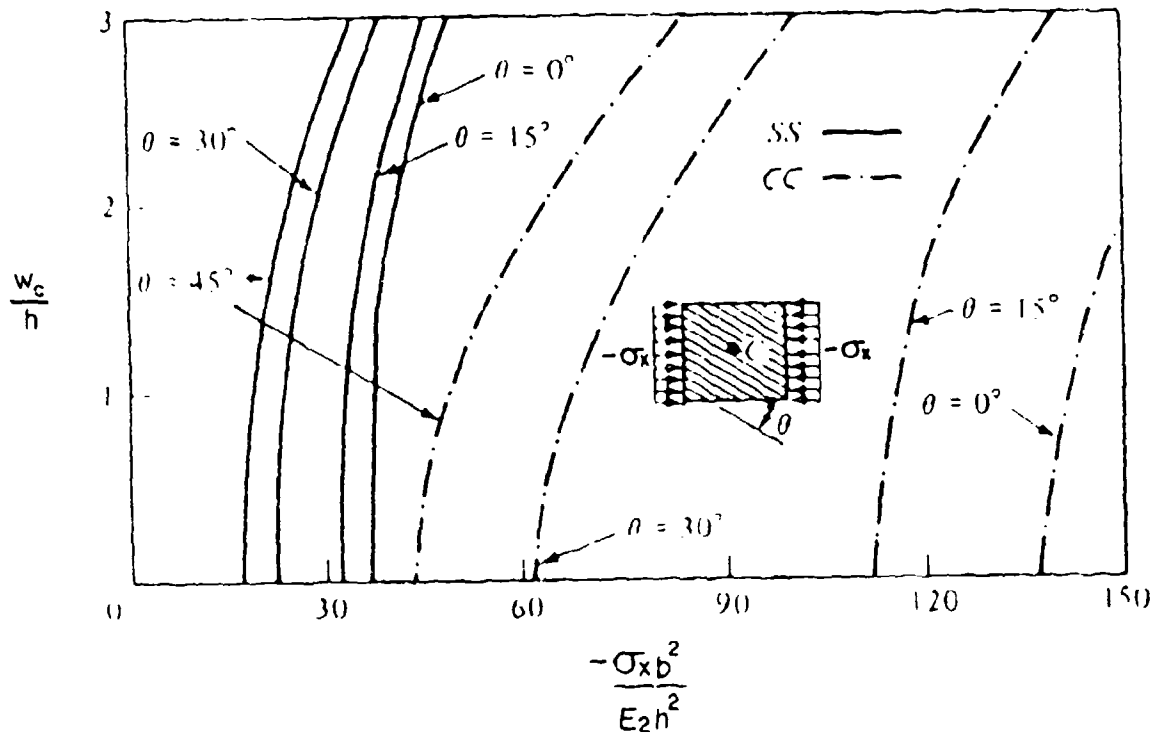

Figure 8.9. Postbuckling deflection-load curves for anisotropic (parallel-fiber), graphite-epoxy plates (a/b = 1).

Noor, Mathers and Anderson [253] discussed how taking into account the symmetry of the problem (geometrical configuration and deflection pattern) may reduce computational time significantly in postbuckling analysis of laminated composite plates. Both symmetric and unsymmetric laminates were considered. Shear deformation effects were also included in the study. Numerical results for the postbuckling behavior of biaxially loaded graphite-epoxy plates were presented, including both load-transverse displacement and load-shortening curves.

Turvey and Wittrick [254,255] examined the postbuckling of SSSS, unsymmetrically laminated, carbon-epoxy, square plates made up of two, angle-ply layers. Load-shortening curves were plotted for three plates having $\theta = \pm 30^{o}, \pm 45^{o}, \pm 60^{o}$. These are shown in Figure 8.10, where u_o is the inplane, end - shortening displacement in the direction of the loading. For each plate, two points of bifurcational buckling and two postbuckling branches are seen. The lower one in each case is for the complete, unsymmetrical analysis, retaining B_{ij} coupling stiffness terms. The upper one corresponds to an orthotropic analysis obtaining by setting all $B_{ij} = 0$. It is observed that, although the buckling stresses are greatly affected by the bending-stretching coupling, the postbuckling stiffnesses are unaffected by it. Load-displacement curves were also determined for symmetrically laminated, CCCC, anisotropic plates loaded in shear, comparing the effects of neglecting or including the bending-twisting stiffnesses (D_{16},D_{26}) in the postbuckling analyses [254,255].

Postbuckling analysis of unsymmetrically laminated, SSSS plates was carried out by Chia and Prabhakara [15,181]. Results were determined for glass-epoxy, boron-epoxy and graphite-epoxy plates having moduli ratios as given in Table 8.1, except $G_{12}/E_1 = 0.0125$ was used for graphite-epoxy. Load-deflection curves for 4-layer, $\pm 45^{o}$ angle-ply, square plates are depicted in Figure 8.11. The loading is uniaxial, except for the graphite-epoxy plate (GR) which is also subjected to hydrostatic compression

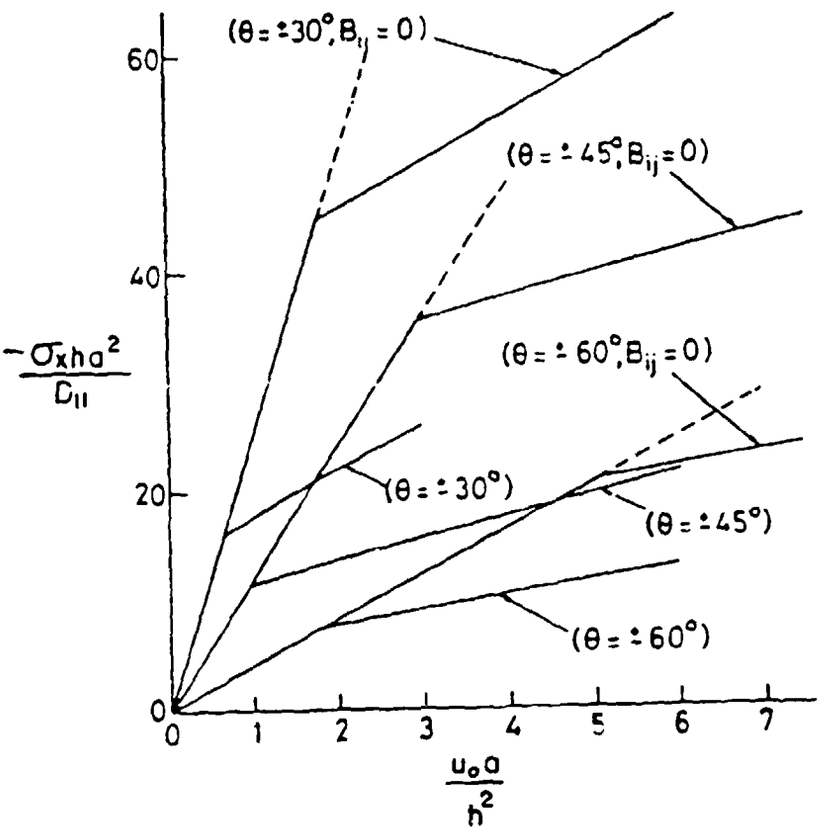

Figure 8.10. Load-shortening curves for SSSS, 2-layer, angle-ply plates.

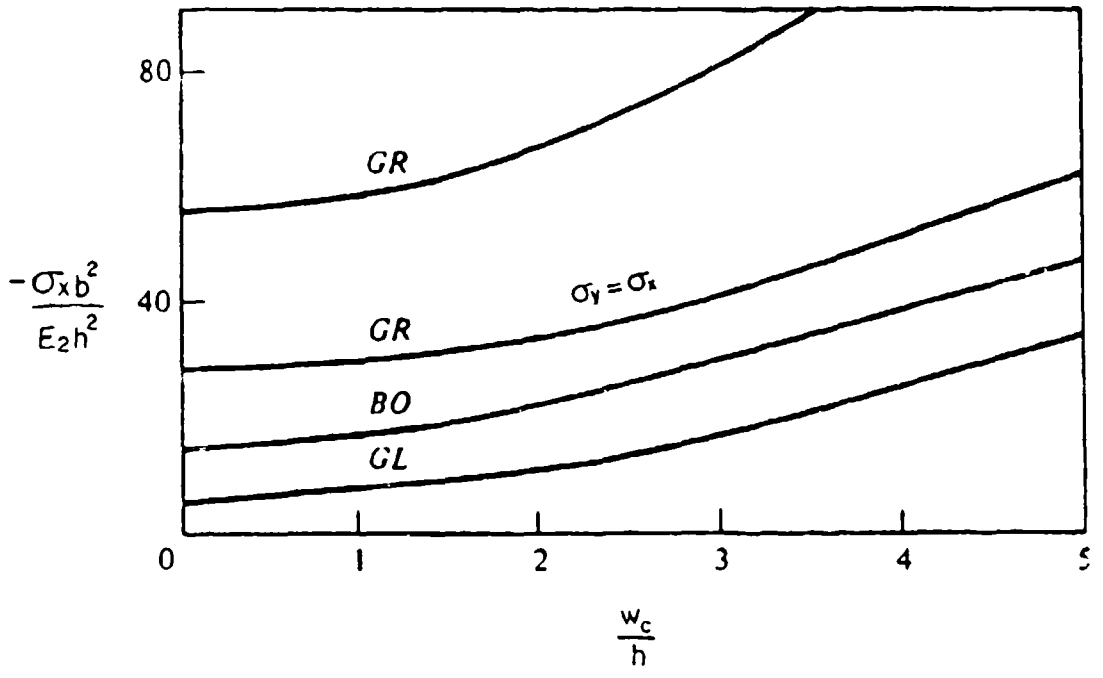

Figure 8.11. Postbuckling load-deflection curves for SSSS, uniaxially and biaxially loaded, unsymmetrically laminated, 4-layer, $\pm 45^{\circ}$ angle-ply plates (a/b = 1).

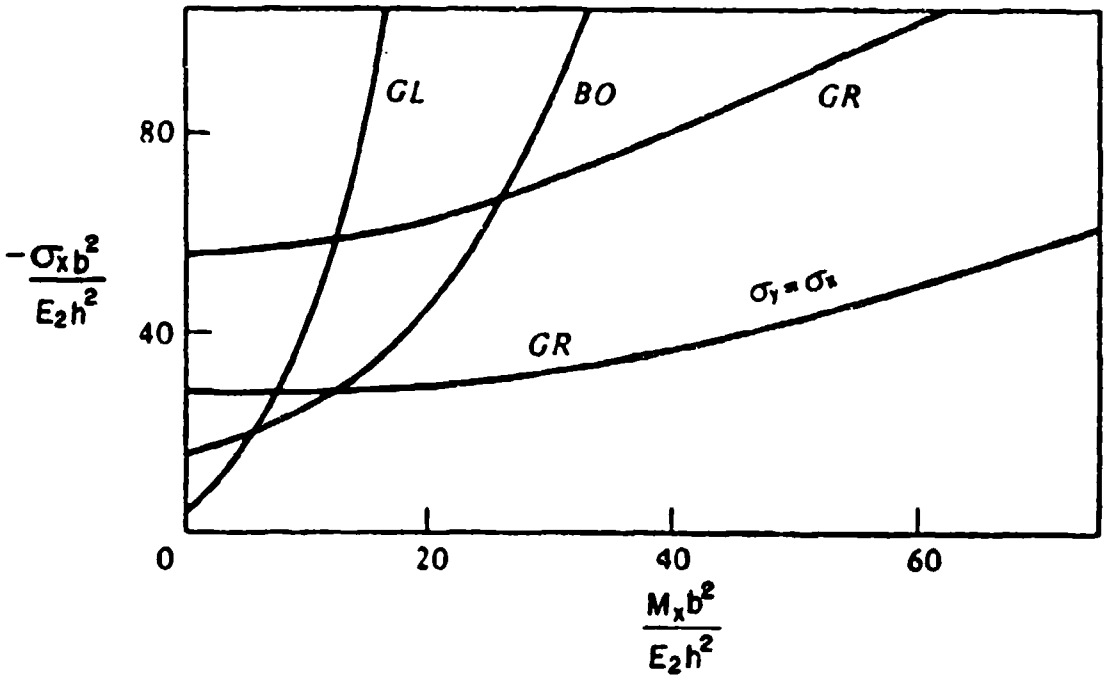

Figure 8.12. Nondimensional bending moments at the centers of the buckled plates of Figure 8.11.

($\sigma_x = \sigma_y$ = constant, $\tau_{xy} = 0$). Bending moments at the centers of the plates in their postbuckled configurations are shown in Figure 8.12. Postbuckling analysis of SSSS angle-ply plates was also carried out by Harris [182].

Prabhakara [256] and Chia [15] also considered unsymmetrically laminated, SSSS, cross-ply plates having 2, 4, 6 and an infinite number of layers of graphite-epoxy material. Critical uniaxial buckling loads were presented which agreed with those determined by Jones [158]. However, the load-deflection curves presented, resulting from both linear and nonlinear analysis, showed "bending of the plate even in the pre-buckling range, owing to the existence of coupling" [256]. This is contrary to the above-mentioned bifurcation buckling results. These curves are shown in Figure 8.13 for square plates having the graphite-epoxy modulus properties listed in Table 8.1, except $G_{12}/E_1 = 0.0125$. The buckling stress parameters listed for the plates of Figure 8.13 were given as [15]: $-\sigma_x b^2/E_2 h^2 = 12.6282, 30.0301, 33.2527, 35.8307$ for $n = 2, 4, 6, \infty$ layers, respectively.

Postbuckling load-deflection curves were also obtained by Chia and Prabhakara [15,181] for CCCC, unsymmetrical, cross-ply plates with graphite-epoxy layers having the same material properties described above for Figure 8.13. These curves are presented in Figure 8.14. Similar curves for uniaxially loaded glass-epoxy, boron-epoxy and graphite-epoxy plates and hydrostatically loaded ($\sigma_x = \sigma_y$) graphite-epoxy plates having four layers are seen in Figure 8.15. Glass-epoxy and boron-epoxy material properties are listed in Table 8.1.

Comparison of load-deflection curves for 4-layer, $\pm 45^\circ$ angle-ply, graphite-epoxy plates having a/b = 1.5 subjected to uniaxial compression (σ_x = constant, $\sigma_y = \tau_{xy} = 0$) may be made between CCCC and SSSS edge conditions in Figure 8.16 [15,181]. In this case, the buckling mode

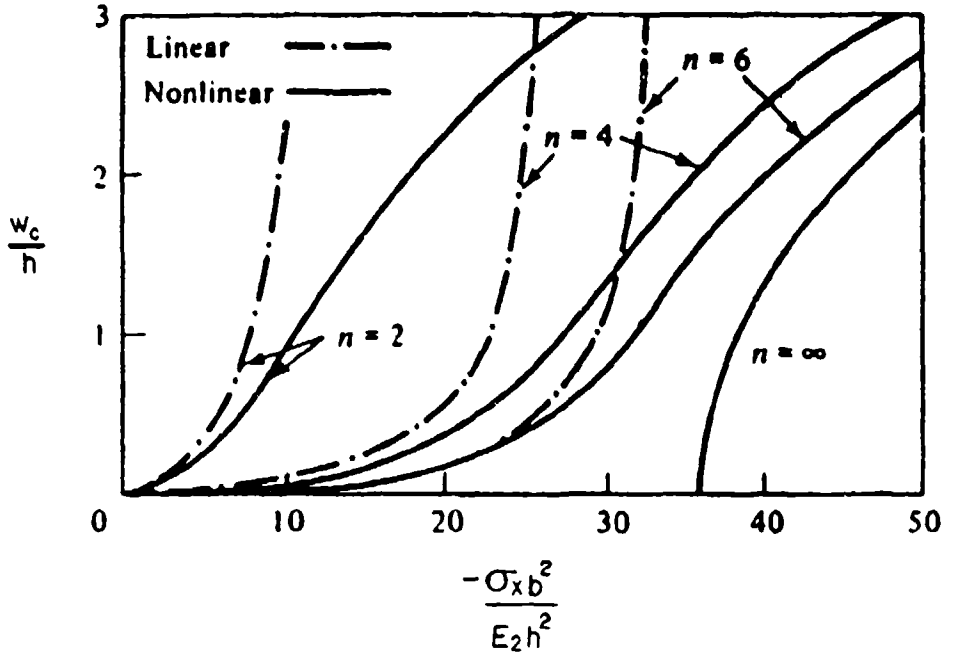

Figure 8.13. Displacement-load curves for SSSS, unsymmetrically laminated, cross-ply plates (a/b = 1).

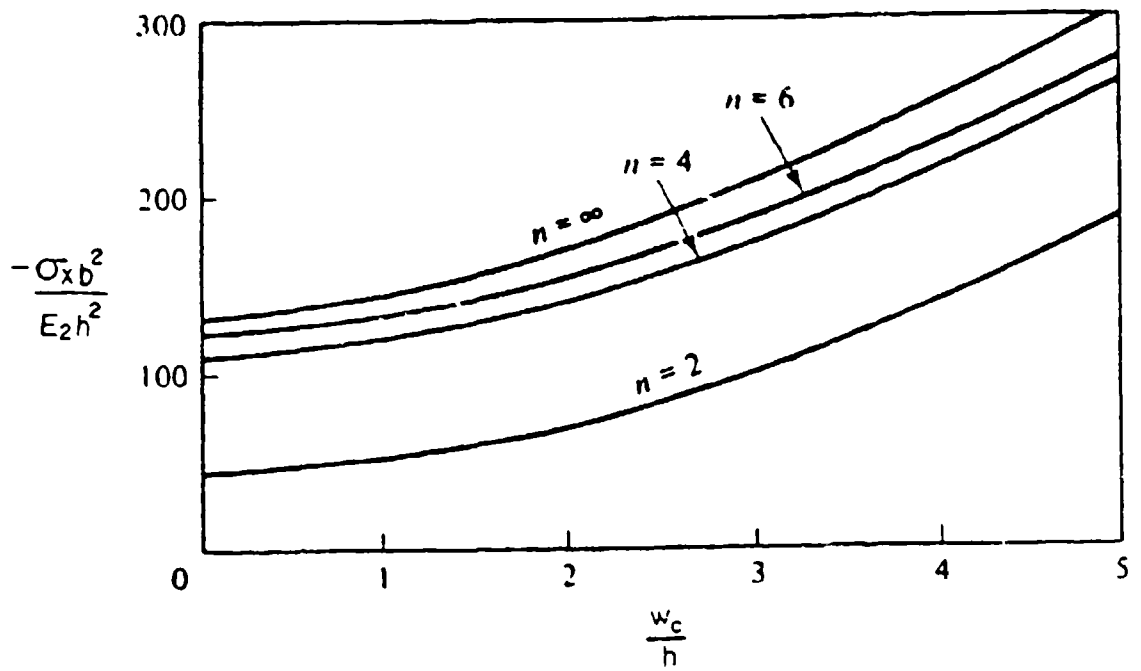

Figure 8.14. Postbuckling load-deflection curves for CCCC, unsymmetrically laminated, cross-ply plates (a/b = 1).

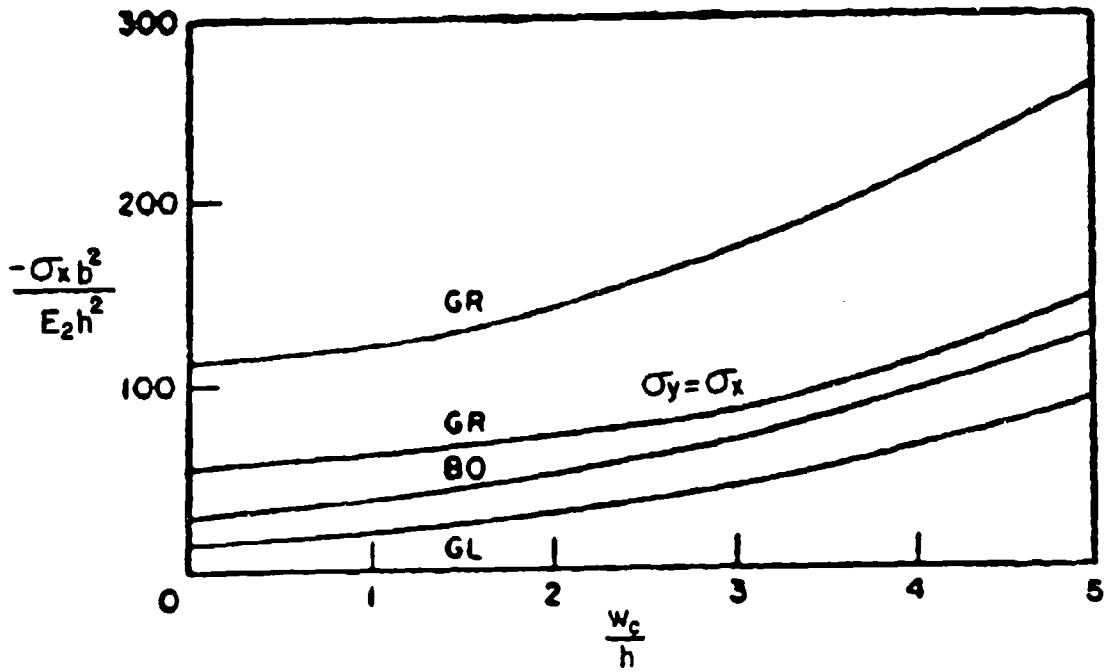

Figure 8.15. Comparison of postbuckling curves for CCCC, unsymmetrically laminated, cross-ply plates of various materials (a/b = 1).

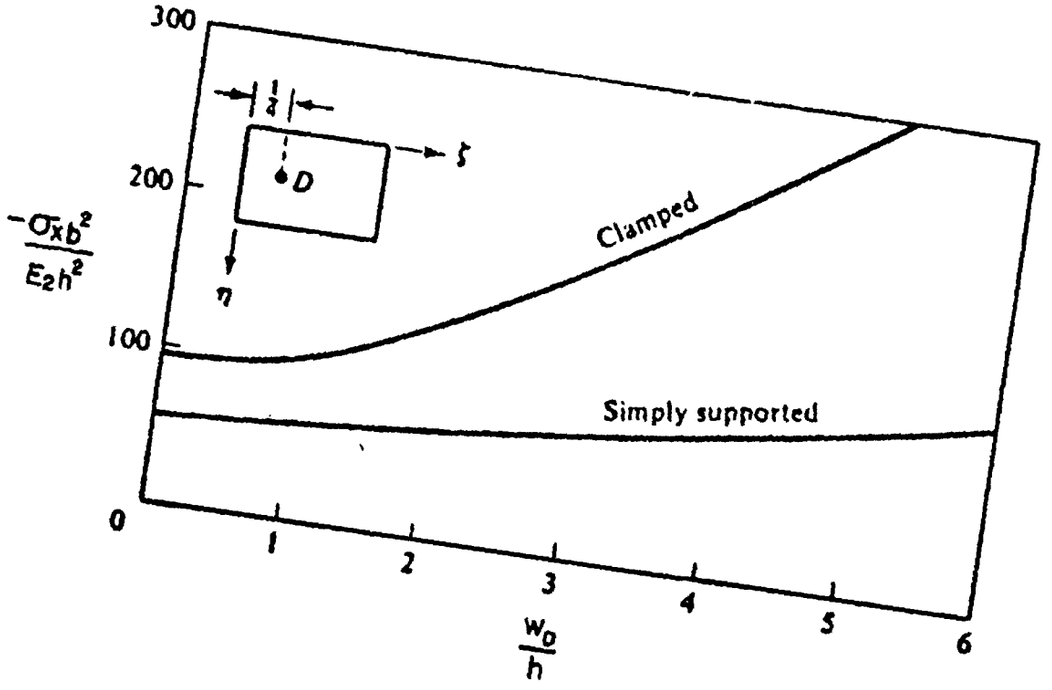

Figure 8.16. Comparison of postbuckling curves for CCCC and SSSS, 4-layer, $\pm 45^{\circ}$ angle-ply, graphite-epoxy, non-square (a/b = 1.5) plates under uniaxial compression.

shape has two half-waves in the x-direction, and the displacement is therefore calculated at $x = a/4$, $y = b/2$.

Prabhakara and Kennedy [186] made a study of the postbuckling behavior of unsymmetrically laminated, angle-ply plates loaded in shear ($\sigma_x = \sigma_y = 0$, τ_{xy} = constant). Results were obtained for glass-epoxy, boron-epoxy and graphite-epoxy laminates having layer moduli given by Table 8.1, except that $G_{12}/E_1 = 0.0125$ for graphite-epoxy. Deflection-load curves for various plates are shown in Figures 8.17-8.20, where w_c is the deflection at the center of the plate. In Figure 8.17 $\pm 45^o$ angle-ply, SSSS, square plates having two layers are considered. The effect of number of layers (n) for graphite-epoxy plates are seen in Figure 8.18. Results from both linear and nonlinear analyses are shown. Figure 8.19 shows the influence of orientation angle, θ, on the curves for two- and four-layer, graphite-epoxy, SSSS square plates. The effect of aspect ratio ($\lambda = a/b$) for $\pm 45^o$, four-layer, graphite-epoxy, SSSS and CCCC plates is described by Figure 8.20.

Hui [178] considered the initial postbuckling behavior of antisymmetrically laminated, SSSS, cross-ply plates subjected to uniform inplane shear stress. He showed that the initial mode of buckling for non-square plates is asymmetric.

An extensive experimental program to study the buckling, postbuckling and crippling (i.e., ultimate failure) of graphite-epoxy and boron-aluminum laminated composite plates has been conducted by Spier, Klouman and Wang [257-263]. The plates typically were uniaxially loaded, with the loaded edges clamped, and the other two either simply supported or with one edge simply supported and the other free (i.e., CSCS or CSCF with σ_x = constant, $\sigma_y = \tau_{xy} = 0$). These plates were also used to represent a section of a stiffening element. An example of a load - end shortening plot made for two CSCF, graphite-epoxy specimens of nearly identical

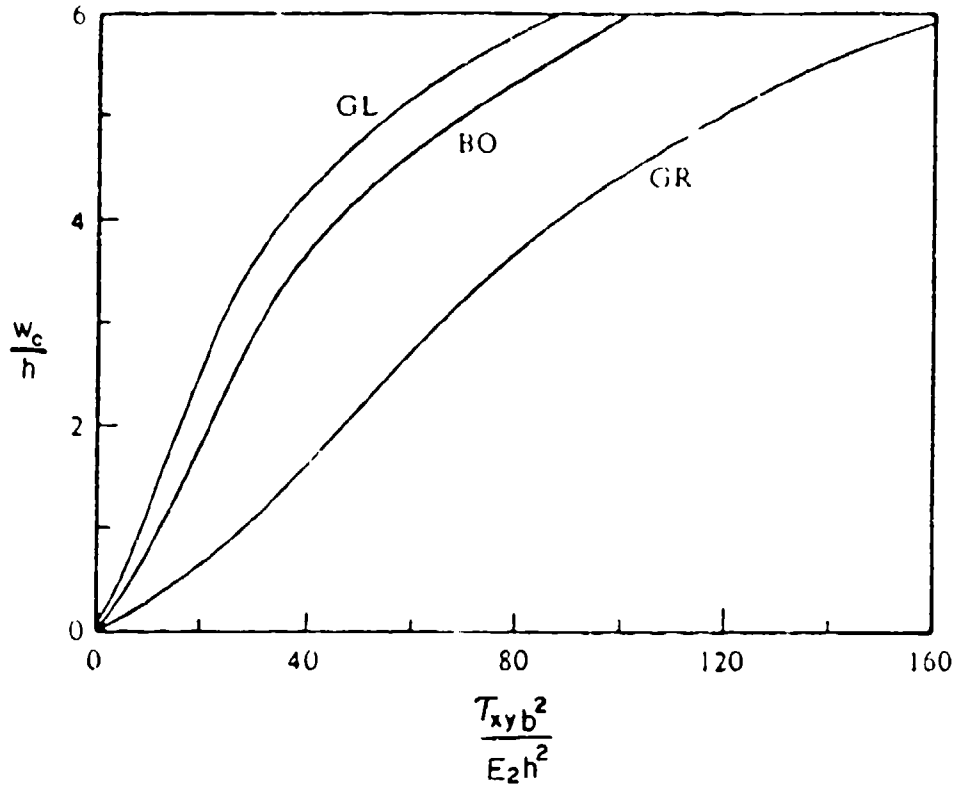

Figure 8.17. Deflection-load curves for shear-loaded, $\pm 45^{\circ}$ angle-ply, SSSS plates having two layers (a/b = 1).

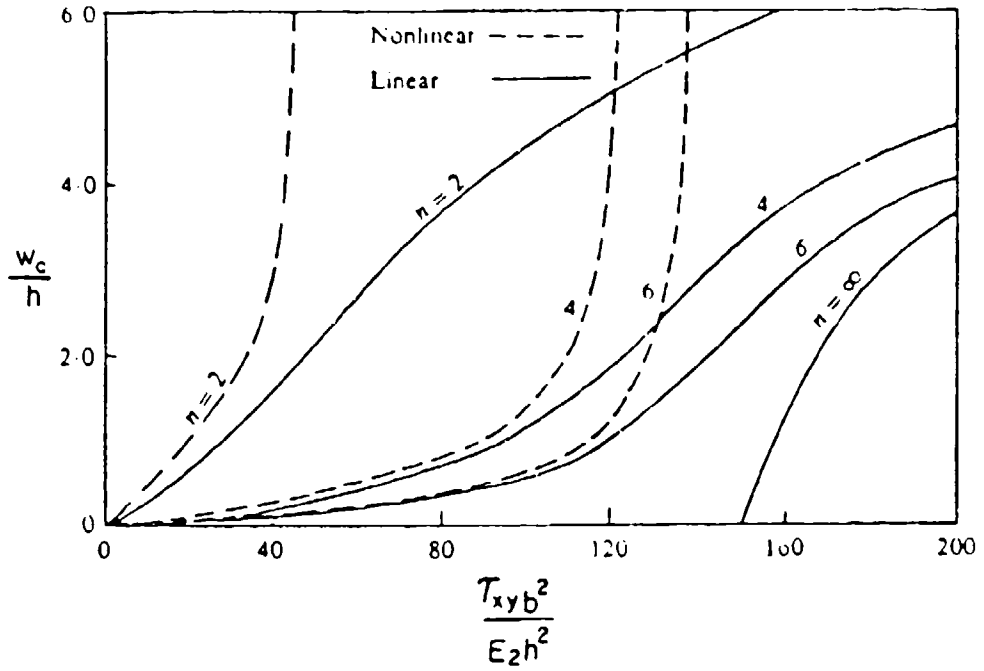

Figure 8.18. Deflection-load curves for shear-loaded, $\pm 45^{o}$ angle-ply, SSSS, graphite-epoxy plates (a/b = 1).

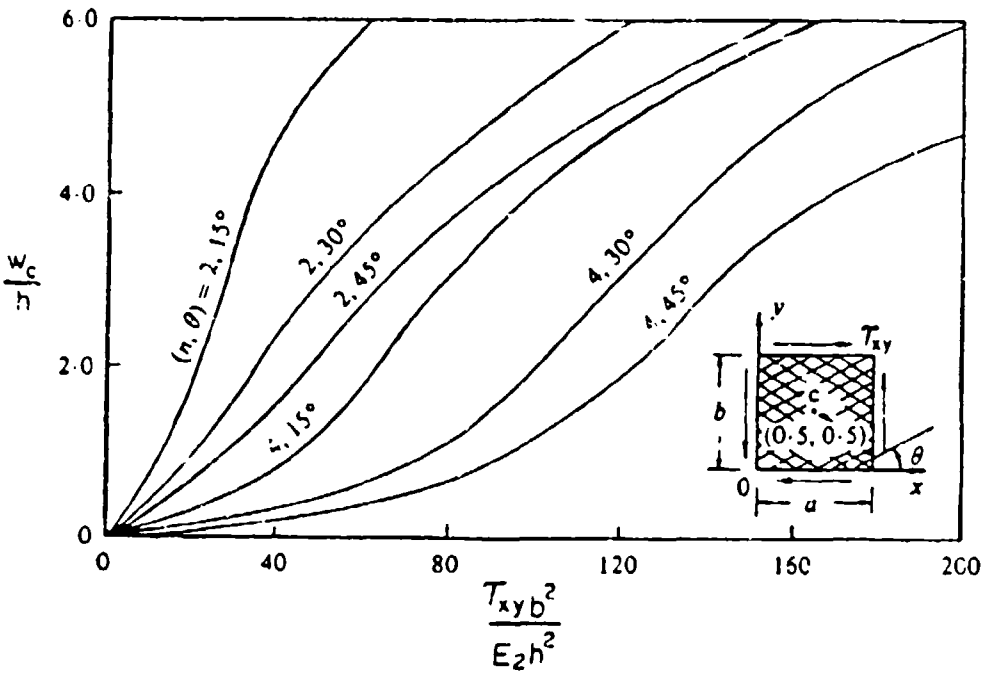

Figure 8.19. Deflection-load curves for shear-loaded $\pm\theta$, angle-ply, SSSS, graphite-epoxy plates (a/b = 1).

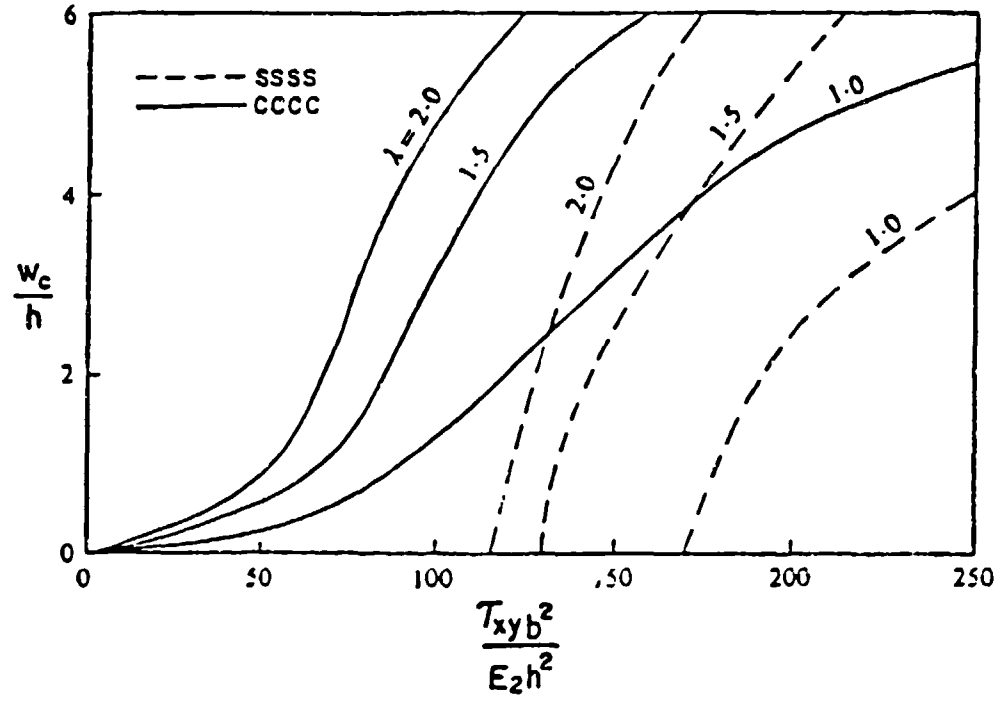

Figure 8.20. Deflection-load curves for shear-loaded $\pm 45^{\circ}$, four-layer, graphite-epoxy plates.

dimensions with a/b = 4.5 is shown in Figure 8.21 [260]. The sudden drop in loading for one of the specimens was due to a jump from a two half-wave displacement pattern to one having three half-waves. For both graphite-epoxy and boron-aluminum composites, experimental crippling loads were found to be considerably less than theoretically predicted values [258,263].

A postbuckling analysis of SESF orthotropic plates subjected to uniaxial loading was made by Banks and Rhodes [264]. The elastically constrained unloaded edge had rotational restraint. This type of plate may represent the flange of a composite channel section.

An experimental study of the postbuckling behavior of CCCC laminated plates loaded in shear was carried out by Kaminski and Ashton [265,266]. Nine boron-epoxy plates having cross-ply and angle-ply orientations were tested. A subsequent theoretical correlation with these results was made by Shariffi [87]. Experimental results for this type of problem were also obtained by Kobayashi, Sumihara and Kihara [267] and compared with theory.

Postbuckling studies of laminated composite plates with holes have also been carried out. Ter-Emmanuil'yan [268] examined a SFSF, orthotropic, square plate having a central square hole. Starnes and Rouse [269] made an experimental investigation of SCSC, graphite-epoxy plates (σ_y = constant, $\sigma_x = \tau_{xy} = 0$) with circular holes. Knauss, Starnes and Henneke [270] also considered circular holes.

A considerable amount of additional research on the postbuckling behavior of laminated composite plates may be found in the literature [38,173,191,271-299].

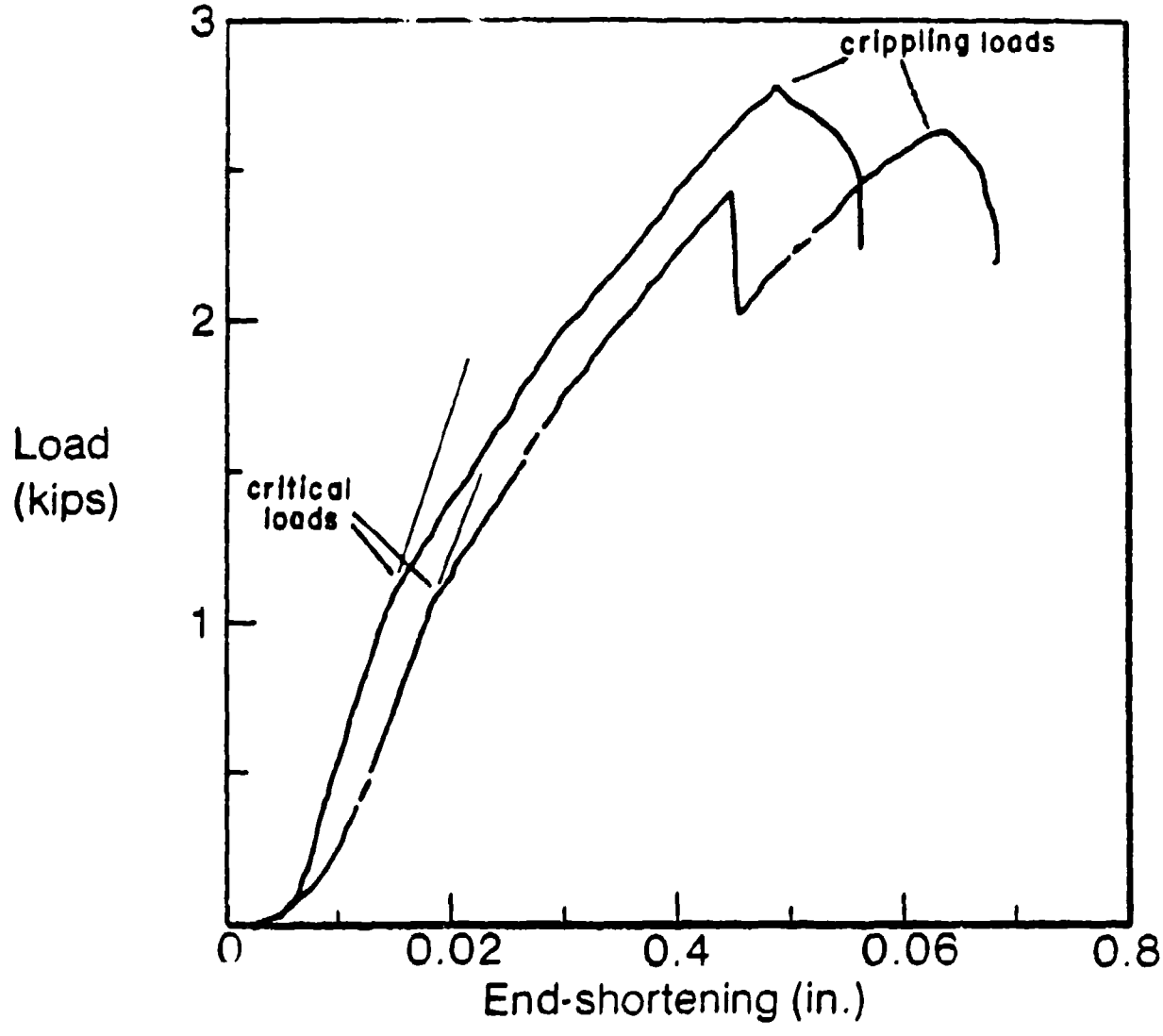

Figure 8.21. Experimental load-end shortening curves for uniaxially loaded CSCF graphite epoxy plates.

8.3. IMPERFECTION ANALYSIS

Bhattacharya [300] made a study of symmetrically laminated, cross-ply plates having initial imperfections subjected to uniaxial loading (σ_y = constant, $\sigma_x = \tau_{xy} = 0$). The plate edges were taken to be simply supported with elastic rotational constraint (cf., Equation 3.49). The governing equations were taken in the forms using the transverse displacement (w) and the Airy stress function (ϕ), and may be written as

$$A_{22}^* \frac{\partial^4 \phi}{\partial x^4} + (2A_{12}^* + A_{66}^*) \frac{\partial^4 \phi}{\partial x^2 \partial y^2} + A_{11}^* \frac{\partial^4 \phi}{\partial y^4}$$

$$= \left(\frac{\partial^2 w}{\partial x \partial y}\right)^2 - \frac{\partial^2 w}{\partial x^2} \frac{\partial^2 w}{\partial y^2} + 2 \frac{\partial^2 \bar{w}}{\partial x \partial y} \frac{\partial^2 w}{\partial x \partial y} - \frac{\partial^2 \bar{w}}{\partial x^2} \frac{\partial^2 w}{\partial y^2} - \frac{\partial^2 \bar{w}}{\partial y^2} \frac{\partial^2 w}{\partial x^2} \tag{8.6a}$$

$$D_{11}^* \frac{\partial^4 w}{\partial x^4} + (2D_{12}^* + D_{66}^*) \frac{\partial^4 w}{\partial x^2 \partial y^2} + D_{22}^* \frac{\partial^4 w}{\partial y^4}$$

$$= \frac{\partial^2 \phi}{\partial y^2} \frac{\partial^2}{\partial x^2}(\bar{w} + w) + \frac{\partial^2 \phi}{\partial x^2} \frac{\partial^2}{\partial y^2}(\bar{w} + w) - 2 \frac{\partial^2 \phi}{\partial x \partial y} \frac{\partial^2}{\partial x \partial y}(\bar{w} + w) \tag{8.6b}$$

where $\bar{w}$ is the initial transverse displacement due to the imperfection, w is the additional transverse displacement due to the applied load, and the A_{ij}^* and D_{ij}^* are coefficients arising from a partial inversion of the stiffness relationships (see Equation A.30). Equations (8.6) are seen to be similar to Equations A.32 and A.33, with the following modifications:

1. $A_{16}^* = A_{26}^* = B_{ij} = 0$, to specialize to the orthotropic form for a symmetrically laminated, cross-ply plate.

2. Nonlinear bending-stretching terms of the type found in Equations 8.5 are added to the right-hand-sides.

3. Additional linear terms appear on the right-hand-sides to account for the effects of the initial imperfection.

An approximate solution to Equations 8.6 was assumed [300] in the form of double series of the products of beam vibration eigenfunctions for both ϕ and w, and $\bar{w}$ was also assumed in this form. The Galerkin method was used to provide numerical results.

Results were obtained for square plates composed of five layers, having equal rotational constraints along all four edges [300]. Figures 8.22 and 8.23 show plots of the nondimensional uniaxial loading parameter $-\sigma_y a^2/4A_{22}h$ versus w_c/h, where w_c is the displacement at the center, for carbon fiber reinforced plastic (CFRP) and glass fiber reinforced plastic (GFRP) plates, respectively. Ratios $E_L/E_T = 7.6$ and 2.0 were used for CFRP and GFRP plates, respectively, and $G_{LT}/E_T = 0.4$, $\nu_{LT} = 0.3$ were used for both plates. Two sets of curves are shown in each figure, corresponding to zero and small ($w_c/h = 0.1$) imperfections. For each set, curves are drawn corresponding to various rotational stiffness parameters K ($= ak_r/2A_{22}h^2$), and k_r is the rotational stiffness defined by Equation 3.49. For $K = 0$, the plate is SSSS; for $K = \infty$, it is CCCC.

The effects of load eccentricity were considered by Sallam and Simitses [301]. Uniform, uniaxial, inplane stresses $-\sigma_x$ were applied with an eccentricity (e, measured positive in the positive z-direction) to unsymmetrically laminated, SSSS, $\pm 45^\circ$ angle ply, graphite-epoxy plates. The same material properties used by Chia and Prabhakara [15,181] in their postbuckling studies (see Section 8.3) were assumed ($E_{11} = 30\text{x}10^6$psi, $E_{22} = 0.75\text{x}10^6$psi, $G_{12} = 0.375\text{x}10$ psi, $\nu_{12} = 0.25$). Load-deflection curves were plotted for two- and four-layer plates having $a/b = 1$ or 2,

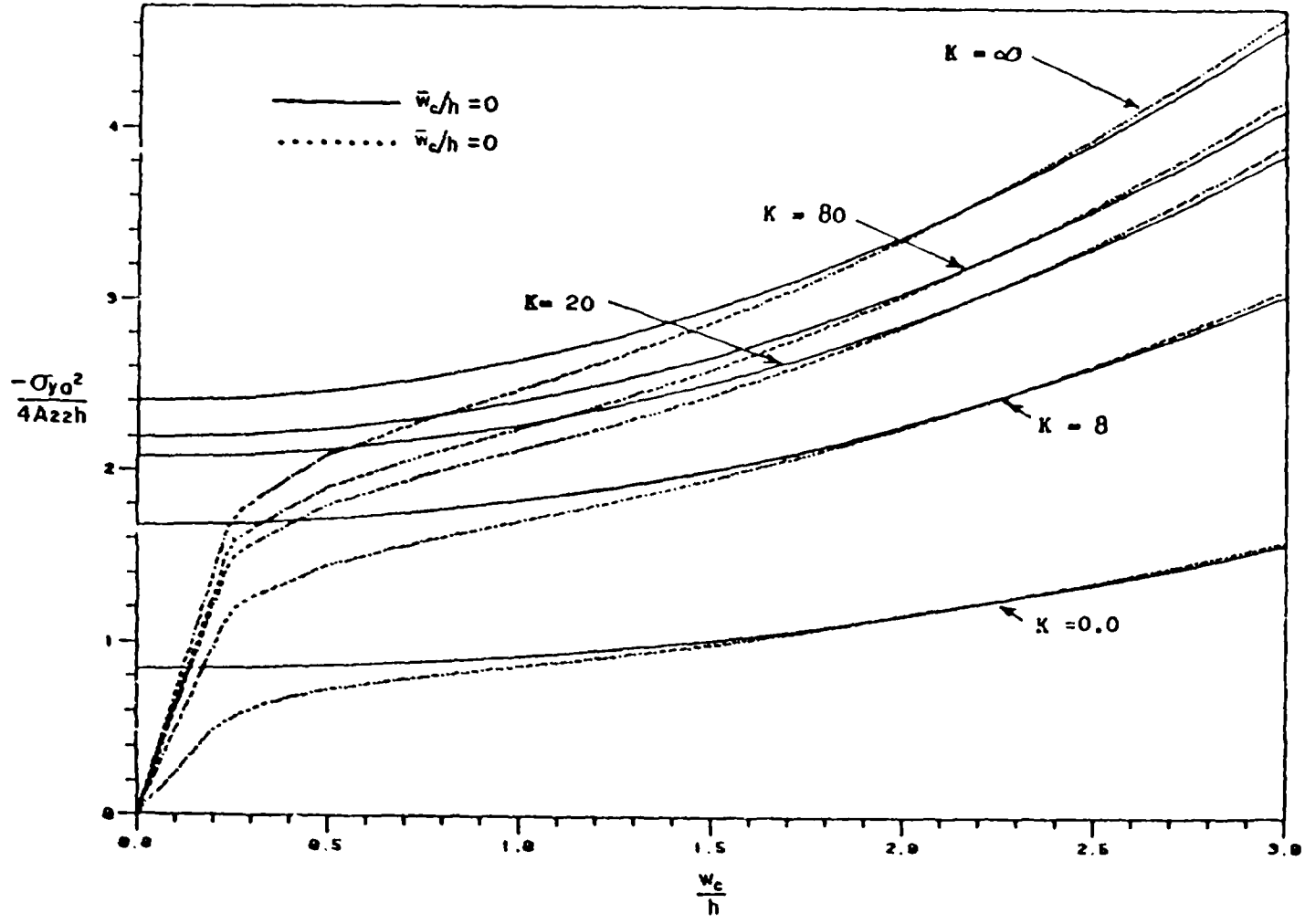

Figure 8.22. Load-deflection curves for cross-ply, CFRP plates having rotational edge constraints (a/b = 1).

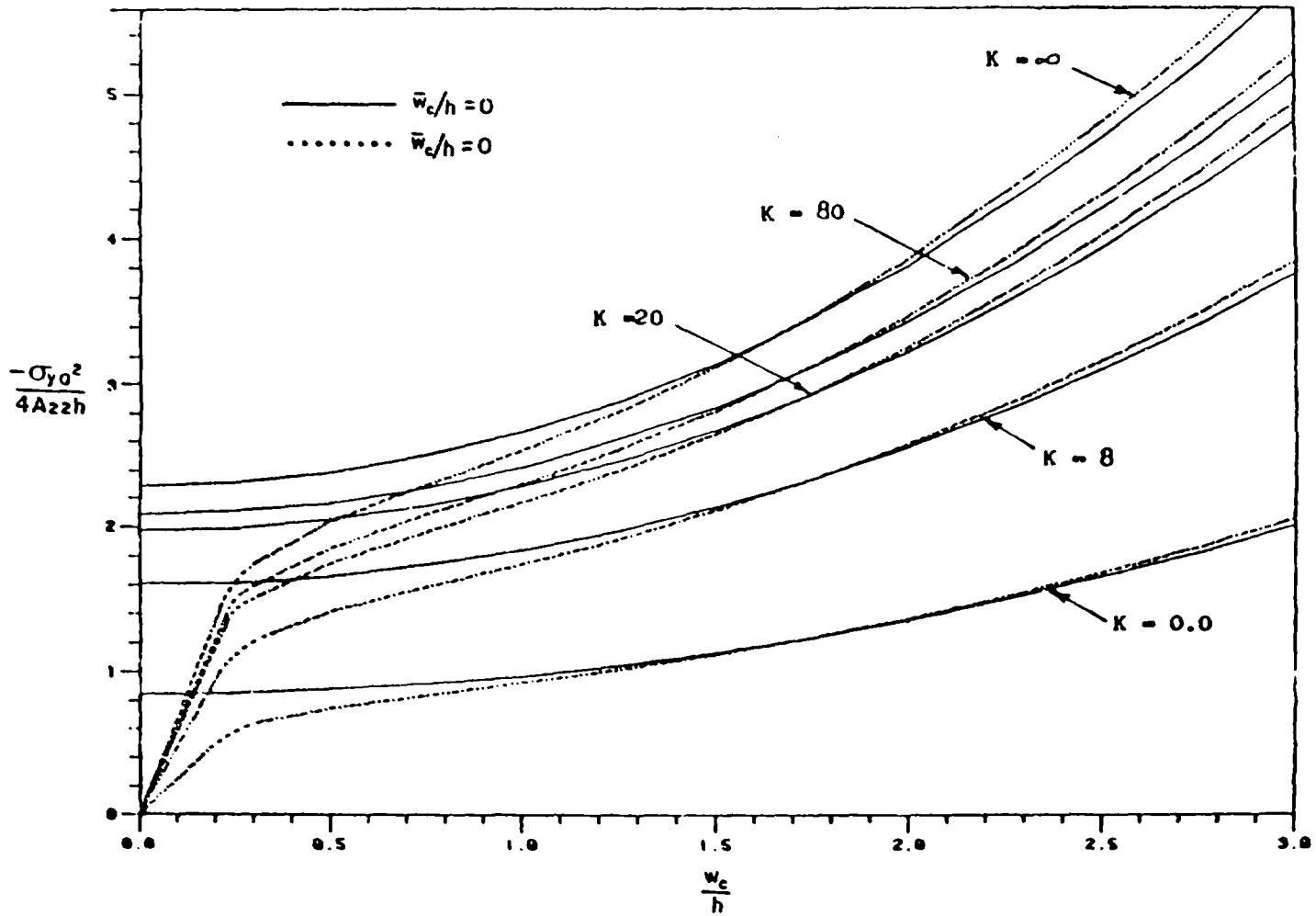

Figure 8.23. Load-deflection curves for cross-ply, GFRP plates having rotational edge constraints (a/b = 1).

and values of e/h varying from 0 to 0.1. These are shown in Figures 8.24 through 8.27, where w_c is the transverse deflection of the center of the plate. In Figure 8.26 the results of Chia and Prabhakara [15,181] are also shown for e = 0.

Inasmuch as it is impossible to fabricate plates which are perfectly flat, test specimens will always have some initial imperfection. Southwell [40] derived a very useful formula for estimating both the critical load and the amplitude of the imperfection from experimentally determined data. It is extendable to laminated composite plates. Let w_o be the displacement of the plate at any point in the unloaded condition (usually measured at the plate center or at a point of maximum anticipated displacement) - that is, the imperfection amplitude. Let Δ be the additional deflection at the same point resulting from the inplane load, P. It can be shown that Δ/P can be linearly related to Δ by the equation

$$\frac{\Delta}{P} = \left(\frac{1}{P_{cr}}\right)\Delta + \frac{w_o}{P_{cr}} \tag{8.7}$$

Thus if the experimental data is plotted on a graph having Δ/P as ordinate and Δ as abscissa, and a best-fit straight line is drawn through the data, then the reciprocal of the slope of the line is P_{cr}, and the intercept with the abscissa is $-w_o$.

Mandell [34] obtained load-displacement data for each of the numerous composite plates he tested (see Tables 2.1, 5.4, 6.3) for both SSSS and SFSF edge conditions and made Southwell plots (Δ/P versus Δ) for each case. A representative one for plate 201 - a graphite-epoxy, cross-ply laminate (see Table 2.1) - is shown in Figure 8.28. Also shown in the same figure are theoretical and experimental curves of P versus Δ. The theoretical curve was obtained by the nonlinear finite element method developed by Monforton [173], assuming no geometrical imperfection.

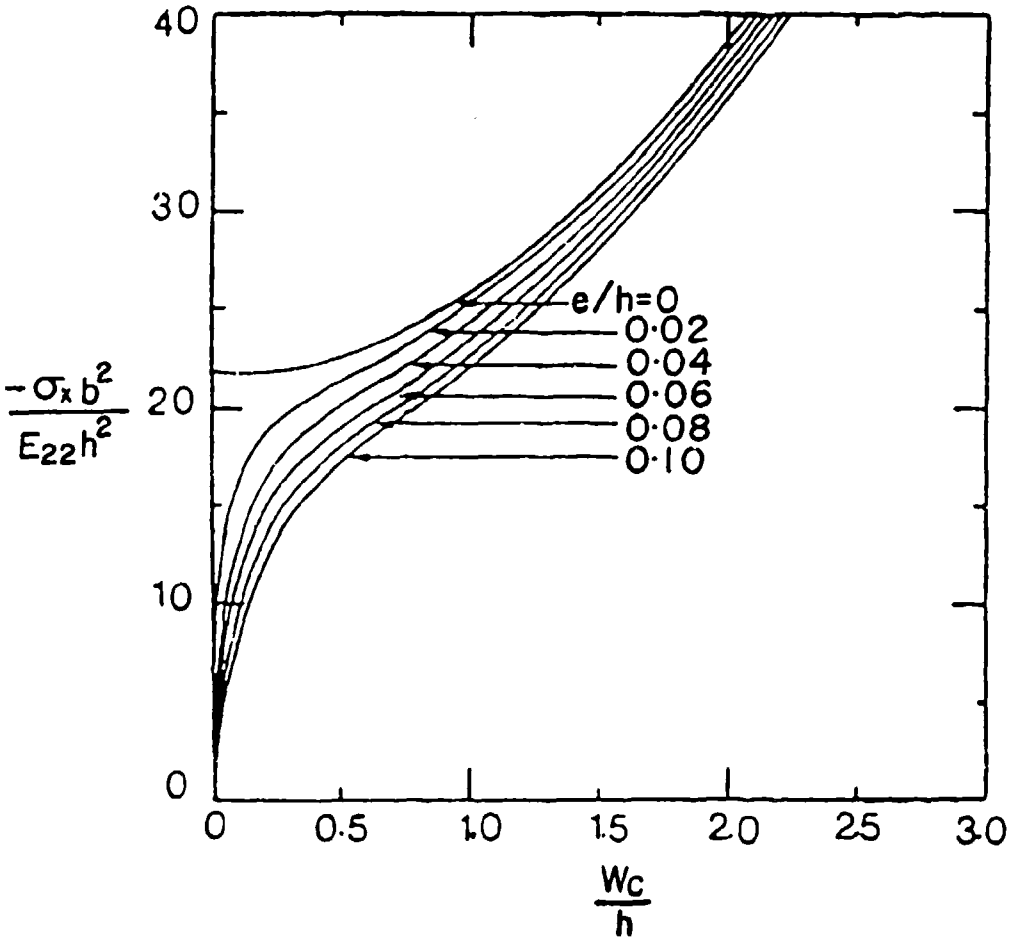

Figure 8.24. Load-displacement curves for eccentrically loaded, two-layer, SSSS, angle-ply plates (a/b = 1).

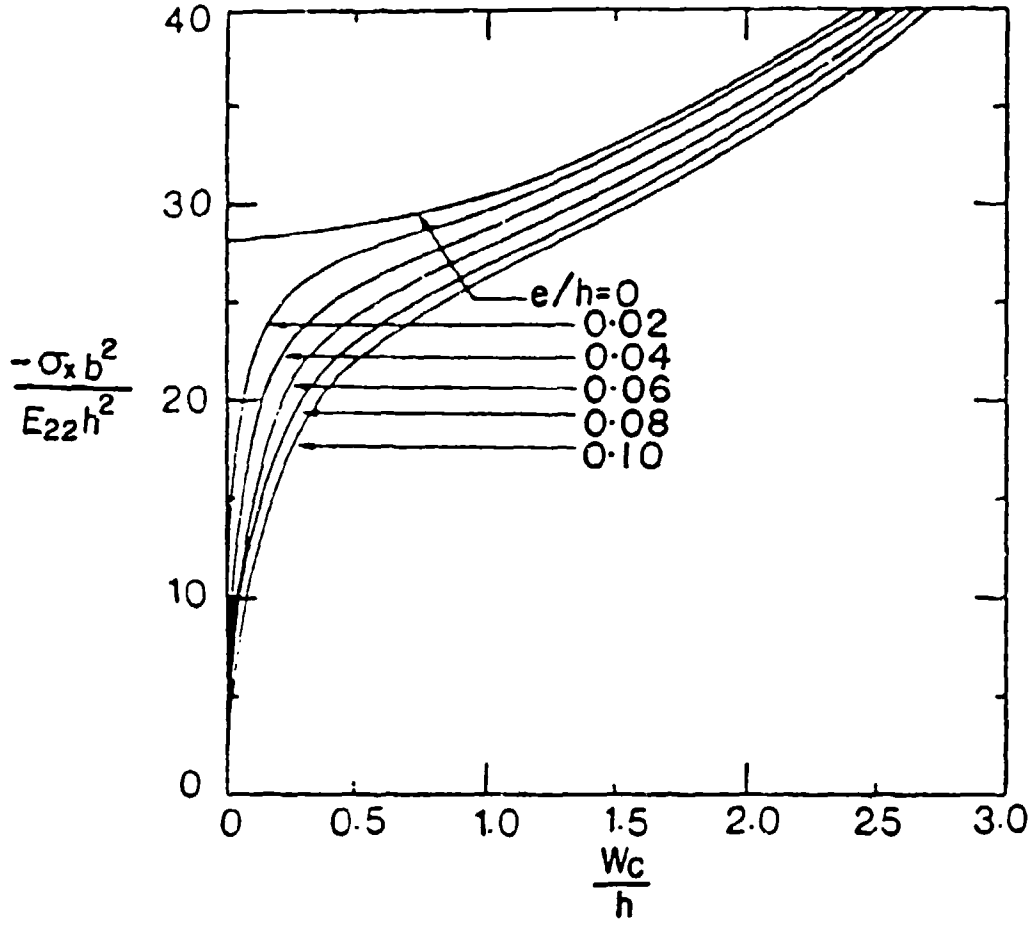

Figure 8.25. Load-displacement curves for eccentrically loaded, two-layer, SSSS, angle-ply plates (a/b = 1).

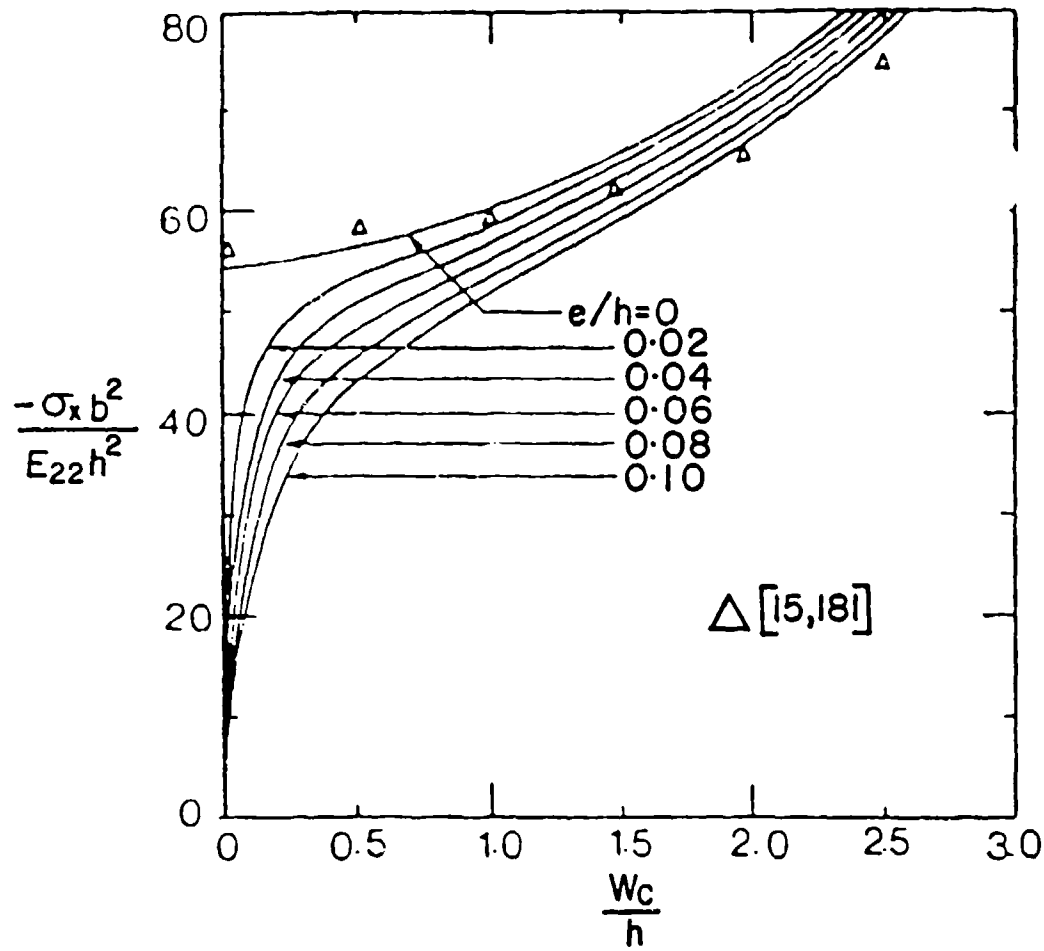

Figure 8.26. Load-displacement curves for eccentrically loaded, four-layer, SSSS, angle-ply plates (a/b = 1).

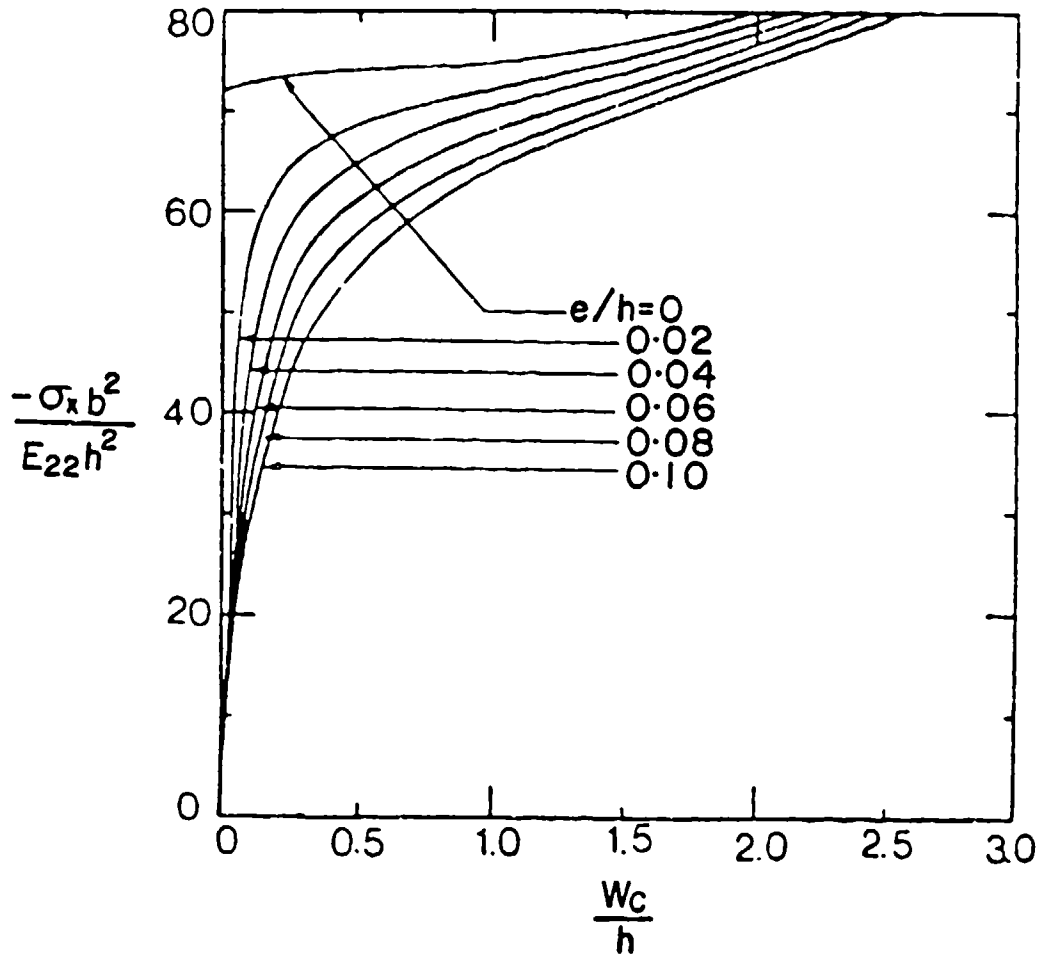

Figure 8.27. Load-displacement curves for eccentrically loaded, four-layer, SSSS, angle-ply plates (a/b = 2).

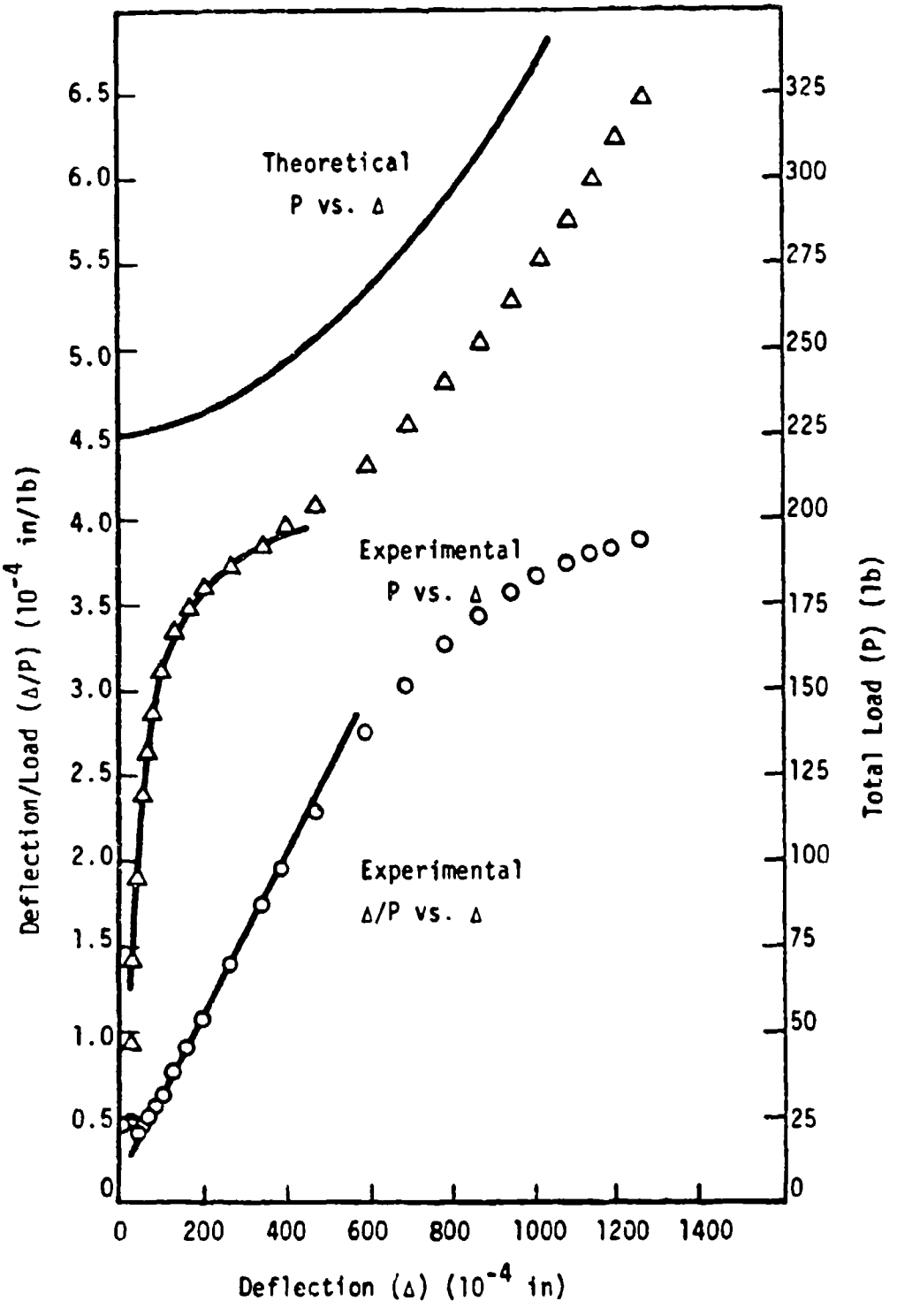

Figure 8.28. Southwell plot and load-displacement curves for Mandell's plate 201 (SSSS).

Banks [302] conducted postbuckling experiments on unidirectional fiber, SSSS, orthotropic plates made of glass reinforced plastic. Large deflection results and postbuckling stress distributions were obtained for plates subjected to uniaxial loading consisting of constant in-plane displacement. Experimental results were compared with theoretical curves for initial imperfection amplitudes $w_o/h = 0$ and 0.5. Banks, Harvey and Rhodes [303] made a study of alternative methods of expressing the inplane boundary conditions during the moderately large deflections of uniaxially loaded composite plates having geometric imperfections. Giri and Simitses [304] analyzed the behavior of an SSSS anisotropic plate under the simultaneous action of inplane and transverse loads. Aalami and Chapman [305] treated similar problems for orthotropic plates.

The effect of sign in the imperfection (i.e., positive or negative initial curvature) upon the initial postbuckling behavior was examined by Hui [306]. It was shown that, in certain circumstances, the initial postbuckling behavior will be unstable (i.e., negative slope in the load-displacement curve) rather than the customary stable form.

Meffert, Derek and Menges [307] considered the creep deformation of SSSS laminated composite plates with initial imperfections subjected to uniaxial compression. The creep effect was accounted for by assuming an exponential decay of the elastic moduli with time.

CHAPTER IX. STIFFENED PLATES

Stiffened plates typically consist of plates having attached stiffeners lying parallel to one of the edges. They are usually designed to provide additional stiffness in the direction of primary, uniaxial loading. Stiffeners may be of a variety of shapes, for example, I, Z, T, J, hat, box, angle, blade or sandwich blade. Examples of four of these shapes are seen in Figure 9.1 [308]. The stiffeners may be integrally fabricated with a plate, or may be attached. A plate may also be stiffened by preforming it into corrugations.

The buckling modes of a stiffened plate (or panel) may be quite complex, even under relatively simple loading conditions such as uniaxial, uniform compression. The presence of bending/twisting and/or bending/stretching coupling due to laminate layup serves to complicate the modes further. The buckling modes may be generally classified as overall or local, depending upon the wave lengths of the patterns. Williams and Stein [309] divided the classification of buckling modes of open-section stiffened panels into local, twisting and column buckling modes. Examples f - a repeating section of a J-stiffened plate are shown in Figure 9.2. These modes involve either relatively independent or strongly coupled displacements of the plate sections (skins) and stiffening elements (webs). The "column" mode corresponds to one dimensional buckling of each repeating section essentially independent of the adjacent sections.

To deal with local buckling modes it is at least necessary to subdivide the stiffened structure into a series of rectangular plates joined to the stiffeners by proper continuity conditions. This allows local buckling between the stiffeners. Further refinement consists of subdividing the stiffeners as well into plate elements, which accounts for the possibility of very localized buckling within stiffener segments. Presumably, this latter refinement also more accurately represents the stiffeners of the entire plate structure.

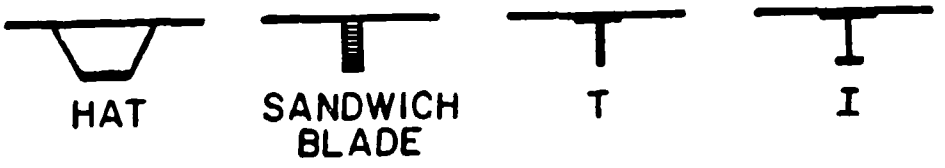

Figure 9.1. Typical plate stiffening elements.

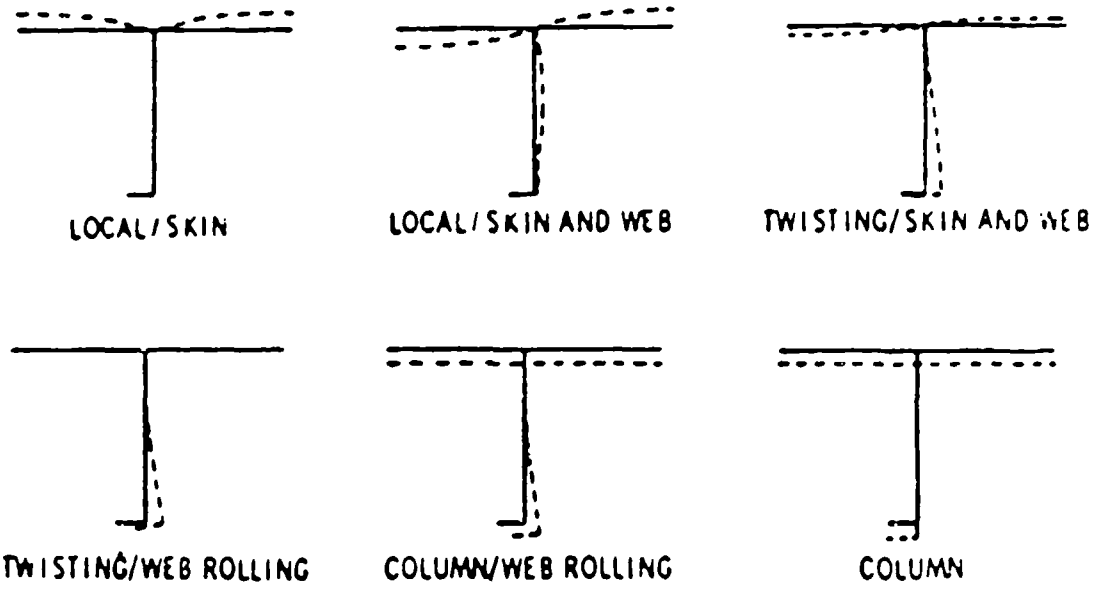

Figure 9.2. Characteristic buckling modes of J-stiffened plates.

However, to deal with the refined buckling investigation described above, complex computer programs (codes) are necessary. Listed below are four relatively widely used codes capable of buckling analysis of laminated composite plates with stiffeners, along with literature sources. These sources may consist of publications describing the theoretical background, user's manuals or applications to specific problems.

1. BUCLASP (Buckling of Laminated Stiffened Plates) - References 92, 93, 309-315.
2. NASTRAN (NASA Structural Analysis) - References 311, 318
3. STAGS - References 308, 309, 319, 320
4. VIPASA (Vibration and Instability of Plate Assemblies, including Shear and Anisotropy) - References 308, 309, 321-326.

These buckling analysis codes sometimes are used as parts of larger optimization procedures leading to efficient designs. Compared with metallic stiffened plates, the number of design parameters which may be varied is significantly greater.

The information given below is intended to give some samples of the large amount of information which is available for the buckling of laminated composite plates having a large variety of possible stiffeners. The reader is referred to the individual publications for details such as plate and stiffener detailed dimensions, laminate layups, etc.

Williams et al. [308] made a comparison of bifurcation buckling loads obtained with various computer codes for a blade-stiffened SSSS composite plate. The configuration analyzed consisted of a 7.6 cm square plate with six stiffeners. Combined shear and longitudinal compression (in the direction of the stiffeners) loading was applied. Interaction curves for critical combinations of shear and longitudinal stress resultants are shown in Figure 9.3. The two distinct data points were obtained by

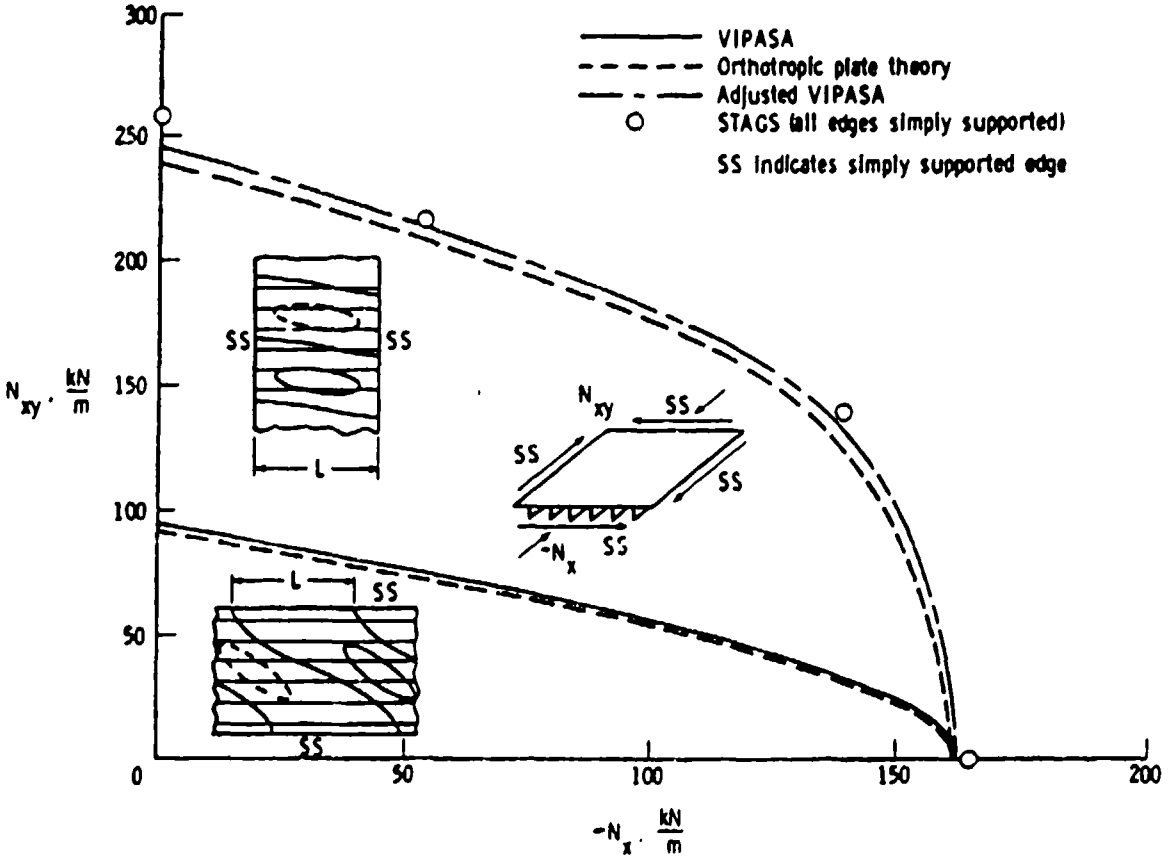

Figure 9.3. Comparison of theoretical buckling loads from various analyses for a blade-stiffened plate subjected to combined longitudinal compression and shear loading.

an accurate, two-dimensional analysis using the STAGS code for the square plate. The VIPASA code was also utilized. This code is one-dimensional (i.e., two opposite edges are simply supported, exact solutions similar in form to those described in Section 3.1 are used, and boundary conditions may be specified only on the two edges parallel to the stiffeners) and is therefore more economical than STAGS. The solid (lower) curve shows the interaction curve obtained with VIPASA with the plate having its side edges simply supported. The dashed, lower curve was also obtained with VIPASA, where the stiffeners were "smeared" out to represent an orthotropic plate. The same orthotropic plate was then analyzed with the two edges perpendicular to the stiffeners being simply suppported, yielding the upper dashed curve. The large difference between these curves shows the importance of correctly representing the boundary conditions on the edges normal to the stiffening. Finally, an "adjusted" VIPASA curve is depicted in Figure 9.3, which results from applying a correction factor obtained from comparing the lower two curves to the upper dashed one.

An interesting set of curves showing the relative structural efficiency of various types of stiffened plates to withstand uniaxial buckling loads may be seen in Figure 9.4 [308]. The mass index (W/AL), which is the mass per unit area of stiffened plate divided by the plate length, is plotted versus the load index (N_x/L). The PASCO [327] code was used to optimize the various designs. It is seen from Figure 9.4 that the blade- and I-stiffened plates give nearly the same results and are least efficient of the graphite-epoxy constructions. Honeycomb sandwich-blade-stiffened plates are seen to be approximately 20 percent lighter. The lightest design employed graphite-epoxy, hat-stiffened plates. These latter plates weighed 60 percent less than aluminum hat-stiffened plates, which are also included in Figure 9.4. A similar plot for blade-stiffened, graphite-epoxy plates designed for specific ratios of combined in-plane loads is shown in Figure 9.5. These were 76 cm square plates. The optimum

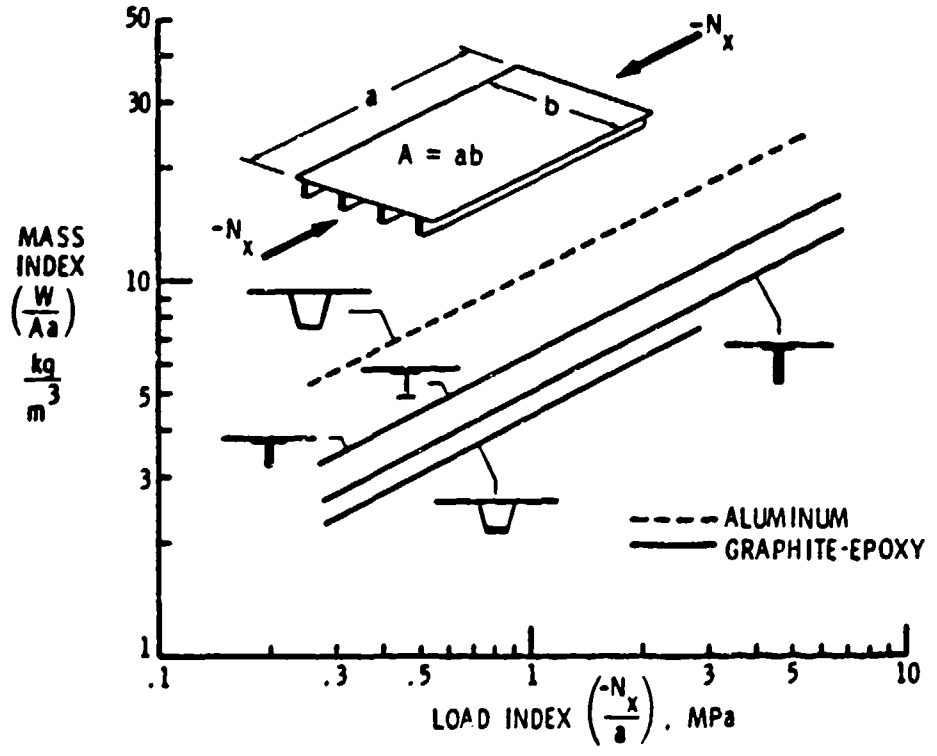

Figure 9.4. Structural efficiencies of various stiffened plate configurations.

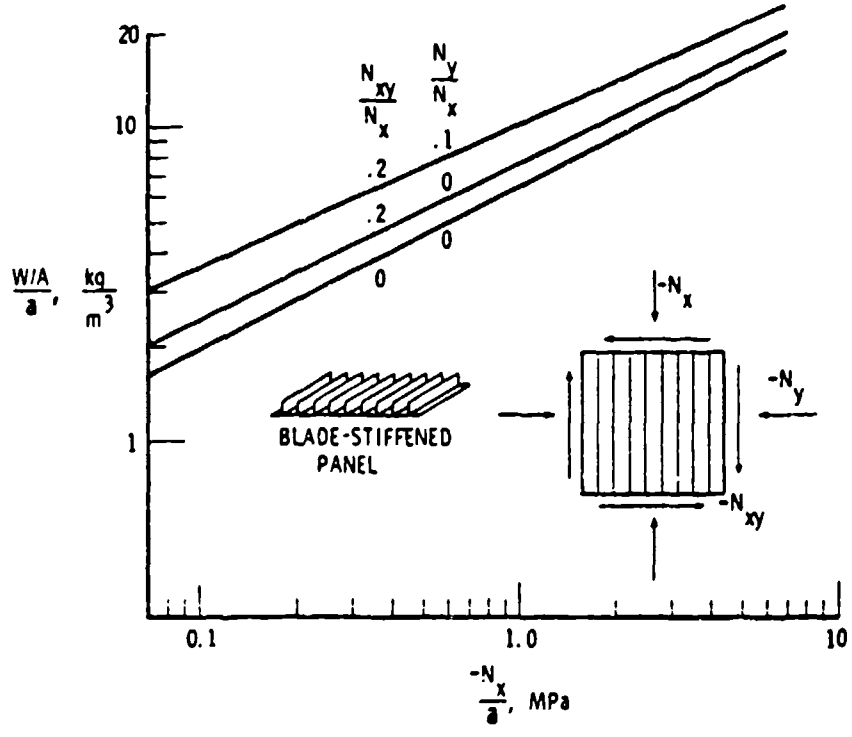

Figure 9.5. Structural efficiencies of graphite-epoxy, blade-stiffened plates.

number of stiffeners varied with loading from 16 to lightly-loaded plates (N_x/L = 0.07 to 0.10 MPa) to 8 for heavily-loaded plates (N_x/L = 5 to 7 MPa).

Wittrick and Williams [120,326] developed a procedure for obtaining exact solutions for the buckling of anisotropic, stiffened plates which became known as the VIPASA computer code. This analysis permits the use of anisotropic (but symmetrically laminated) plates and arbitrary (but constant) components of combined (σ_x, σ_y, τ_{xy}) inplane stress. Plates and stiffeners are made up of component plate segments, each joined together by appropriate continuity conditions.

Recently, Wittrick and Horsington [325] set forth an accurate procedure for analyzing the buckling of stiffened composite plates which circumvents two of the limitations of the VIPASA code:

1. When the component plates of the structure carry shear as well as compression, only the local buckling modes may be found.
2. Typical stiffened-plate assemblies require using 1300 to 2000 rectangular plate elements, leading to characteristic determinants of order 8000 to 21,000.

The procedure is based upon the Ritz method and assumes displacements for SSSS plates in the form of Equation 2.40. The resulting computer code was called CASIOPEIA (Compression And Shear Instability of Orthotropic Panels), and was found to yield accurate results for six stiffened panels previously analyzed by NASA using an extremely expensive finite element method.

Viswanathan, Soong and Miller [92,93] developed the method for analyzing stiffened composite plates which resulted in the BUCLASP code [310]. Correlations with buckling tests were made for hat- and angle-stiffened, composite plates, as well as isotropic honeycomb, sandwich plates reinforced internally with boron composite strips.

Structural efficiency studies were made by Williams and Mikulas [317] on graphite-epoxy plates having hat-stiffened and open corrugation configurations. From the theoretical results, selected configurations were fabricated and tested to study local and overall buckling characteristics. Experimental results were obtained for 23 plates critical in local buckling and six critical in overall buckling and were compared with theoretical data obtained using the BUCLASP-2 code. Theoretical studies indicated potential weight savings of up to 50% for similar configurations made of aluminum. Another similar set of theoretical efficiency studies with J- and blade-stiffened, graphite-epoxy plates was made by Williams and Stein [309]. STAGS, BUCLASP-2 and VIPASA codes were used in the analysis.

Agarwal and Davis [328] used a structural synthesis technique to determine optimum hat-stiffened, graphite-epoxy compression panel designs. Buckling loads and mode shapes were calculated with the BUCLASP-2 code. Optimization results showed a 50-percent weight savings over optimized aluminum panels.

Bushnell [329] demonstrated the PANDA code by comparisons with the results of Williams and Stein [309] for a blade-stiffened composite plate.

Theoretical analysis and experimental testing of a boron-aluminum laminate with closely spaced stiffeners was reported by Spier [330]. It was necessary to analyze the laminate material in its inelastic range. This design was found to yield weight savings of 34 and 42 percents over equivalent aluminum-alloy and titanium alloy designs, respectively.

Stein and Housner [69] analyzed the shear buckling of an SSSS orthotropic plate having a single central stiffener which is interrupted by a break.

Mass optimization studies for uniaxially loaded, stiffened, composite plates were made by Stein and Williams [311]. In particular, sandwich-blade stiffeners were employed, in which the webs of the blade stiffeners are composed of high strength composite material bonded to a low-density core such as aluminum honeycomb. This has the effect of increasing the critical twisting and local buckling strains without appreciably increasing the total structural mass. An analysis method was developed which was compared with BUCLASP 2 and NASTRAN codes on sample problems.

A procedure for designing uniaxially stiffened plates made of composite material and subjected to combined inplane buckling loads was described by Stroud, Agranoff and Anderson [324]. The procedure is based upon the VIPASA code. Complex, local buckling modes as well as overall buckling were considered.

Stroud and Agranoff [331] developed a procedure for analyzing hat-stiffened and corrugated composite plates subjected to uniaxial (in the direction of the stiffeners) compression and shear loadings. Numerous curves were plotted showing the structural efficiency of such plates as stiffener and plate thicknesses are varied.

The effect of one-dimensional (bow-type) imperfection on the inplane load carrying capacity of graphite-epoxy, blade-stiffened plates was studied by Stroud, Anderson and Hennessy [332]. The VIPASA code was modified to permit the imperfection analysis. The effects of bow-type imperfections are also discussed in [308].

Turvey and Wittrick [333] made comparisons of the buckling stresses of CFRP composite plates having open (blade), closed (box) and Z-type stiffeners with those of corresponding aluminum plates. Comparisons for troughed (corrugated) plates were also made.

Chiu [334] considered the buckling of uniaxially loaded CFCF laminated composite plates having attached stiffeners composed of both metal and composite portions. Theoretical and experimental results were compared. Because the buckling loads predicted theoretically were much higher than test results, a simplified method to accommodate plastic behavior of the metal beyond the yield point was developed.

Experimental and theoretical studies of the shear buckling of a graphite-epoxy plate having J-stiffeners in its interior and along its edges were made by Davis [335]. Theoretical calculations were made with the VIPASA code.

Gunnink, Vogelsang and Schijve [336,337] studied the buckling of orthotropic plates made of ARALL (Aramide Reinforced Aluminum Laminates) having Z-stiffeners.

Hui and Hansen [338] took up the buckling of square, antisymmetric, angle-ply plates with stiffeners attached to unloaded edges, while the loaded edges are simply supported.

Buckling and postbuckling static tests of shear-loaded graphite-epoxy plates were conducted by Ostrom [339]. Integral J-stiffeners were located internally, parallel to the plate edges. The postbuckling behavior of multibay composite shear webs was explored by Agarwal [272]. Hat and I stiffeners were added to graphite-epoxy plates to form the webs. Both theoretical and experimental results were obtained. Composite shear webs were found to have significant postbuckling strength. Several other postbuckling studies for stiffened composite plates have been reported [191,260,340-346].

Symmetrically laminated SSSF plates having integral blade and Y-stiffeners were considered by Lackman and Ault [99]. Weight optimization studies were conducted for uniaxial loading.

Kicher and Martin (see [191], pp. 206-209, and [190]) investigated the buckling and postbuckling of SSSS symmetrically laminated plates with circular holes, with or without stiffeners around the hole periphery. Both theoretical and experimental data were obtained.

The vast majority of references in this chapter dealing with stiffened, orthotropic or anisotropic plates are aimed at aerospace structures. One also finds buckling analysis of such configurations found for bridge decks [347] and ships [348].

Other references taking up the buckling of composite plates with stiffeners are [34,349-367].

CHAPTER X. BUCKLING OF CYLINDRICAL SHELL PANELS

This chapter is devoted to the bifurcation buckling of laminated composite panels having curvature. Such configurations are properly called "shells" (although one sees the term "curved plate" sometimes used in the non-academic literature). Indeed, a plate may be considered to be a special case of a shell having zero curvature.

General shells are described by three components of curvature along every point giving rise to a wide variety of shell configurations (e.g., circular cylindrical, noncircular cylindrical, conical, spherical, ellipsoidal, hyperbolic paraboloidal). The present work will limit itself to circular cylindrical shells which is, by far, the case most frequently studied in the literature (more has been written for these shells than all other types together), and which is particularly important for laminated composites.

Moreover, the present work will be limited to shell panels - that is, open rather than closed cylindrical shells. Such a panel is depicted in Figure 10.1. The shell has radius R, axial length a, projected width b, rise c and thickness h. A shell, like a plate, is mathematically a two dimensional configuration, its behavior being characterized completely by its middle surface. Thus, two coordinates attached to the middle surface described its deflected (e.g., buckled) shape. For the circular cylindrical shell these are the axial (or longitudinal) coordinate (x) and the circumferential coordinate (θ), as shown in Figure 10.1. For the latter, the arc length $y = R\theta$ is sometimes substituted.

Isotropic shells are governed by eighth order sets of differential equations which describe the configuration displaced in an equilibrium state. Laminated composite shells also yield eighth order sets of equations, although they are algebraically somewhat more complicated due to the

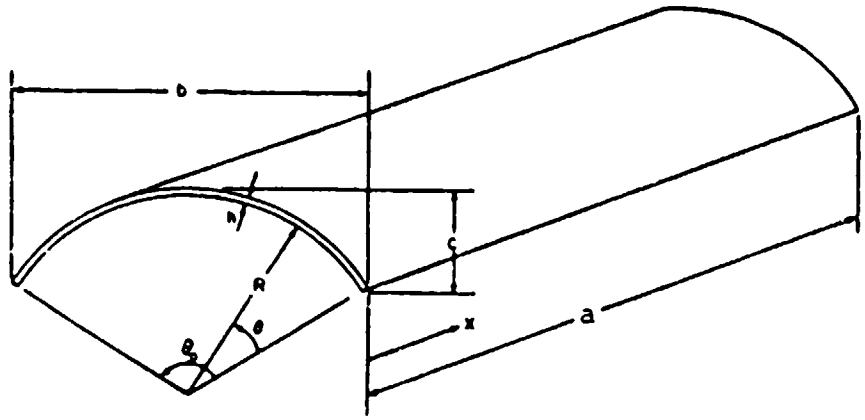

Figure 10.1. Circular cylindrical shell panel.

relatively large number of stiffness coefficients involved (for an isotropic shell there are only two). Thus, four boundary conditions must be specified along each edge to completely define a problem.

One set of boundary conditions deserves special mention. This is the shear diaphragm (also called "simply supported" or "freely supported" in the literature). For the unsymmetrically laminated plate they were called S2 conditions (see Equation 6.2). For such conditions on all four edges and uniform axial and/or circumferential loading, an exact solution for buckling of orthotropic (i.e., cross-ply or unidirectional plies parallel to the edges) is available. This is given by Equations 6.3, where now u and v are tangential displacements in the x and y (or θ) directions, respectively, and w is the transverse (or normal) displacement component. Interestingly enough, exact solutions are also theoretically possible when only two opposite edges (either straight or curved ones) have shear diaphragm conditions (cf., pp. 83-85, [168]), but the algebraic complexity is so overwhelming as to make a properly convergent approximate solution more desirable. Furthermore, the case when the two straight edges have shear diaphragm supports (and included angle $\theta_o = \pi/n$ radians, with n an integer) is identical to that of a <u>closed</u> circular cylindrical shell buckling into a mode shape having two or more circumferential half-waves.

No attempt will be made in this work to present a <u>derivation</u> of shell buckling equations for laminated composites. The procedure is quite intricate and can lead to various final forms of equations depending upon assumptions which must be made at various stages of the process. For a careful exposition of the steps and assumptions involved in deriving shell <u>vibration</u> equations, the reader is referred to Chapter 1 of Reference [168]. Buckling equations (or shell vibration equations with initial stresses present) are even more complicated, for they require consideration of infinitesimal displacements from a previous, loaded equilibrium state.

10.1. CYLINDRICAL SHELL BUCKLING EQUATIONS

The equations governing the equilibrium, buckling or vibration of a homogeneous, isotropic, thin plate are uniformly agreed upon by essentially all academicians. For laminated, composite plates essential agreement is also found, even in the case of unsymmetrical laminates where bending-stretching coupling exists. However, the situation is different for shells. Equations for the bifurcation buckling of a circular cylindrical shell may be written in matrix form as

$$[L]\{u\} = \{0\} \tag{10.1}$$

where $\{u\}$ is the vector consisting of the three displacement components, and $[L]$ is a matrix differential operator containing two parts; i.e.

$$[L] = [L^S] - [L^i] \tag{10.2}$$

$[L^S]$ represents the stiffness of the shell, whereas $[L^i]$ results from the initial stresses (prior to buckling). $[L^S]$ can take many forms, depending upon assumptions made in deriving thin shell theories, even for an isotropic shell (cf. [168], pp. 32-34), and the results for buckling loads may differ significantly depending upon the theory used. DiGiovanni and Dugundji [368] (see also [168], pp. 188-189) developed $[L^S]$ matrices for anisotropic, circular cylindrical shells for several of the most widely used theories. It is also found that the initial stress matrices $[L^i]$ will differ, depending upon the assumptions made in deriving the various theories (cf. [168], pp. 232-234).

Viswanathan, Tamekuni and Baker [369,370] developed a theory for the buckling of laminated composite, cylindrical shells. In examining their equations of equilibrium for the buckled state, it is found that the stiffness matrix may be expressed as the sum of two parts, i.e.,

$$[L^s] = [L^{s1}] + \frac{1}{R}[L^{s2}] \tag{10.3}$$

where $[L^{s1}]$ is a matrix operator having elements defined in the Appendix by Equations A.21, and the elements of $[L^{s2}]$ are

$$L_{11}^{s2} = 0$$

$$L_{22}^{s2} = \left(-4B_{66} + \frac{4D_{66}}{R}\right)\frac{\partial^2}{\partial x^2} + \left(-6B_{26} + \frac{4D_{26}}{R}\right)\frac{\partial^2}{\partial x \partial y} - \left(2B_{22} + \frac{D_{22}}{R}\right)\frac{\partial^2}{\partial y^2}$$

$$L_{33}^{s2} = 2B_{12}\frac{\partial^2}{\partial x^2} + 4B_{26}\frac{\partial^2}{\partial x \partial y} + 2B_{22}\frac{\partial^2}{\partial y^2} + \frac{A_{22}}{R}$$

$$L_{12}^{s2} = L_{21}^{s2} = -2B_{16}\frac{\partial^2}{\partial x^2} - \left(B_{12} + 2B_{66}\right)\frac{\partial^2}{\partial x \partial y} - B_{26}\frac{\partial^2}{\partial y^2} \tag{10.4}$$

$$L_{13}^{s2} = L_{31}^{s2} = -A_{12}\frac{\partial}{\partial x} - A_{26}\frac{\partial}{\partial y}$$

$$L_{23}^{s2} = L_{32}^{s2} = \left(-A_{26} + \frac{2B_{26}}{R}\right)\frac{\partial}{\partial x} + \left(-A_{22} + \frac{B_{22}}{R}\right)\frac{\partial}{\partial y} + 2D_{16}\frac{\partial^3}{\partial x^3} + \left(D_{12} + 4D_{66}\right)\frac{\partial^3}{\partial x^2 \partial y} + 4D_{26}\frac{\partial^3}{\partial x \partial y^2} + D_{22}\frac{\partial^3}{\partial y^3}$$

It is observed that Equation 10.3 yields the differential operator $[L^{s1}]$ for unsymmetrically laminated composite plates as the curvature (1/R) approaches zero. Elements of the initial stress matrix operator were found to be [370]:

$$L_{11}^{i} = -N_y\frac{\partial^2}{\partial y^2}$$

$$L_{22}^{i} = -N_x\frac{\partial^2}{\partial x^2} + \frac{N_y}{R^2}$$

$$L_{33}^{i} = N_x\frac{\partial^2}{\partial x^2} + 2N_{xy}\frac{\partial^2}{\partial x \partial y} + N_y\frac{\partial^2}{\partial y^2}$$

$$L^i_{12} = L^i_{21} = N_{xy}\left(\frac{\partial^2}{\partial x^2} + \frac{\partial^2}{\partial y^2}\right)$$

$$L^i_{13} = L^i_{31} = -\frac{N_{xy}}{R}\frac{\partial}{\partial y} \qquad (10.5)$$

$$L^i_{33} = L^i_{32} = \frac{N_{xy}}{R}\frac{\partial}{\partial x} + \frac{N_y}{R}\frac{\partial}{\partial y}$$

with N_x and N_y positive in tension. In Equations 10.5 it is observed that L^i_{13} and L^i_{23} become zero as 1/R approaches zero, which yields Equation 5.1 in the case of a symmetrically laminated flat plate; however, for the unsymmetric laminate, other elements of Equations 10.5 do not vanish and the result is not consistent with Equation A.20.

10.2. NUMERICAL RESULTS

Soldatos and Tzivnidis [371] derived a Donnell-type cylindrical shell theory for the analysis of cross-ply laminates. An exact solution was presented for the buckling of a shell panel supported by shear diaphragms on all four edges and subjected to uniform axial and/or circumferential stresses. Numerical results are shown in Figure 10.2 for the case of an unsymmetric laminate having one 90° layer with circumferentially directed fibers located second from the bottom (see Figure 6.4) which had been studied by Jones [158] for a flat plate (see Section 6.1). The circumferential stress buckling parameter $-N_y\bar{b}^2/E_2h^2$ (where $\bar{b}$ is the circumferential curved width of the panel) is plotted versus the included angle ($\theta_o = \bar{b}/R$), which is a measure of the shell shallowness, for a/b = 1, a/h = 20, and for a graphite-epoxy material having $E_2/E_1 = 40$, $G_{12}/E_2 = 0.5$ and $\nu_{12} = 0.25$. Figure 10.2 shows that all the unsymmetrically laminated panels have more circumferential buckling resistance than the one having all 0° layers (i.e., all fibers directed axially). However, the 3 layer configuration, which is a symmetric laminate, is seen to buckle at larger loads than all the unsymmetric laminates.

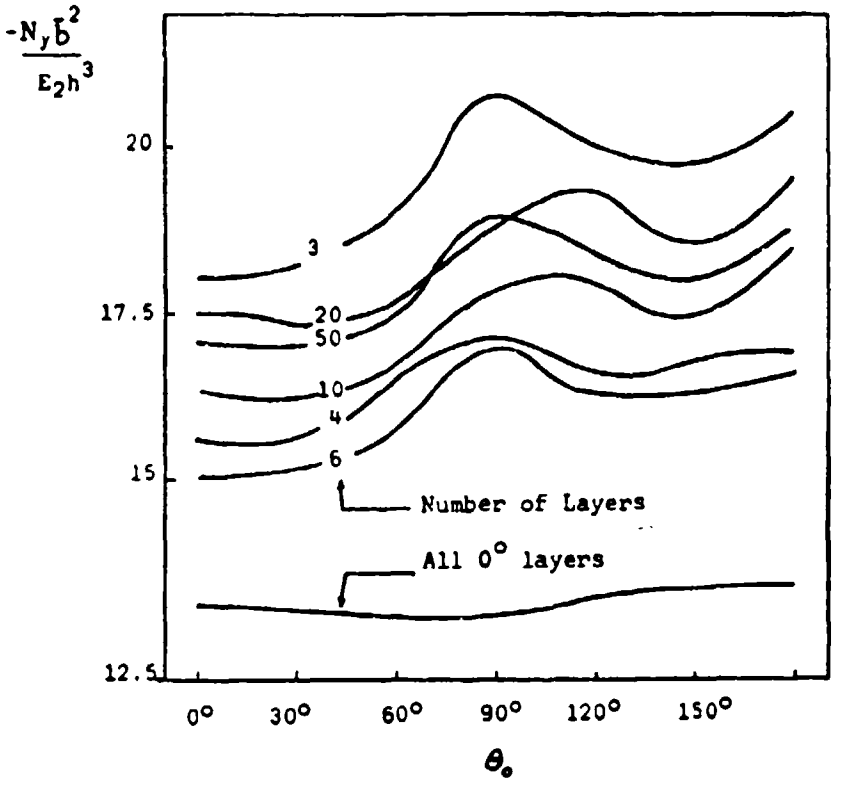

Figure 10.2. Circumferential buckling parameters for shear-diaphragm supported, cross-ply shell panels.

Viswanathan, Tamekuni and Baker [369,370] conducted extensive parametric studies of the influences of curvature and inplane boundary conditions on the buckling of symmetrically laminated, boron/epoxy shell panels of infinite length. The panels contained eight layers $(0/90^{o}/+45^{o}/-45^{o})_{s}$, each layer being 0.014 cm thick, yielding a total thickness of 0.112 cm. Composite material properties used were: $E_{11} = 20.7 \times 10^{10} N/m^2$ $(30.0 \times 10^{6} psi)$, $E_{22} = 1.86 \times 10^{10} N/m^2$ $(2.7 \times 10^{6} psi)$, $G_{12} = 0.48 \times 10^{10} N/m^2$ $(0.7 \times 10^{6} psi)$ and $\nu_{12} = 0.21$. All panels were 25.4 cm (10 in) in projected planform width, b (see Figure 10.3). Six possible combinations of inplane boundary conditions along the straight edges were investigated (Figure 10.3). The out-of-plane boundary conditions were clamped ($w = \partial w/\partial x = 0$). The curvature parameter $\bar{b}^2/Rh$ was varied between 1 and 1000, where $\bar{b}$ is the circumferential arc length.

Critical values of the axial stress resultant N_x are shown in Figure 10.4 [370]. Numbers designating the curves correspond to the inplane boundary condition code listed in Figure 10.3. Variation of circumferential buckling stress resultant N_y with $\lambda/\bar{b}$, where λ is the axial half-wave length of the buckle pattern is depicted in Figure 10.5 for $\bar{b}^2/Rh = 300$. Abrupt changes in the curves occur where the buckling mode shape changes drastically. Results from using a Donnell-type shell theory deviate significantly from the more accurate analysis for large $\lambda/\bar{b}$. Figure 10.6 shows a more abrupt change in the vicinity of $\lambda/\bar{b} = 100$ for a shell panel having boundary condition type 4 and $\bar{b}^2/Rh = 1$. Variation of N_y with $\bar{b}^2/Rh$ for various edge conditions is seen in Figure 10.7. Changes in shear stress resultant N_{xy} with $\lambda/\bar{b}$ are depicted in Figure 10.8 for $\bar{b}^2/Rh = 700$ with boundary condition type 3. Curves for all six types of boundary conditions listed in Figure 10.3 are shown in Figure 10.9, where critical N_{xy} is plotted versus $\bar{b}^2/Rh$. Curves similar to Figures 10.4, 10.7 and 10.9 are seen for <u>combined</u> stresses, $-N_x = N_{xy}$ (Figure 10.10), $-N_y = N_{xy}$ (Figure 10.11), $N_x = N_y$ (Figure 10.12) and $N_x = N_y = -N_{xy}$ (Figure 10.13). Tabulated values of the critical buckling loads and the associated

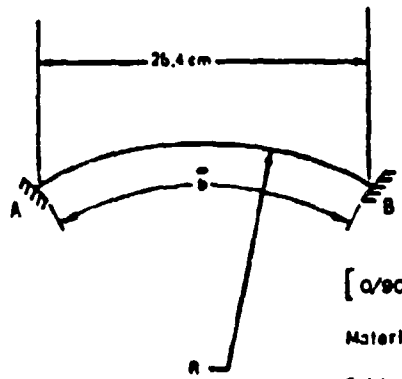

$[0/90/+45/-45]_s$

Material: boron/epoxy

Thickness of each lamina: 0.014 cm

Total thickness h = 0.112 cm

Boundary condition code	Inplane boundary conditions on clamped edge A	Inplane boundary conditions on clamped edge B
1	$u = v = 0$	$u = v = 0$
2	$v = N_{xy} = 0$	$v = N_{xy} = 0$
3	$u = N_y = 0$	$u = N_y = 0$
4	$N_y = N_{xy} = 0$	$N_y = N_{xy} = 0$
5	$u = N_y = 0$	$u = v = 0$
6	$N_{xy} = N_y = 0$	$N_{xy} = v = 0$

Figure 10.3. Boundary conditions along straight edges of shell panels analyzed by Viswanathan, Tamekuni and Baker.

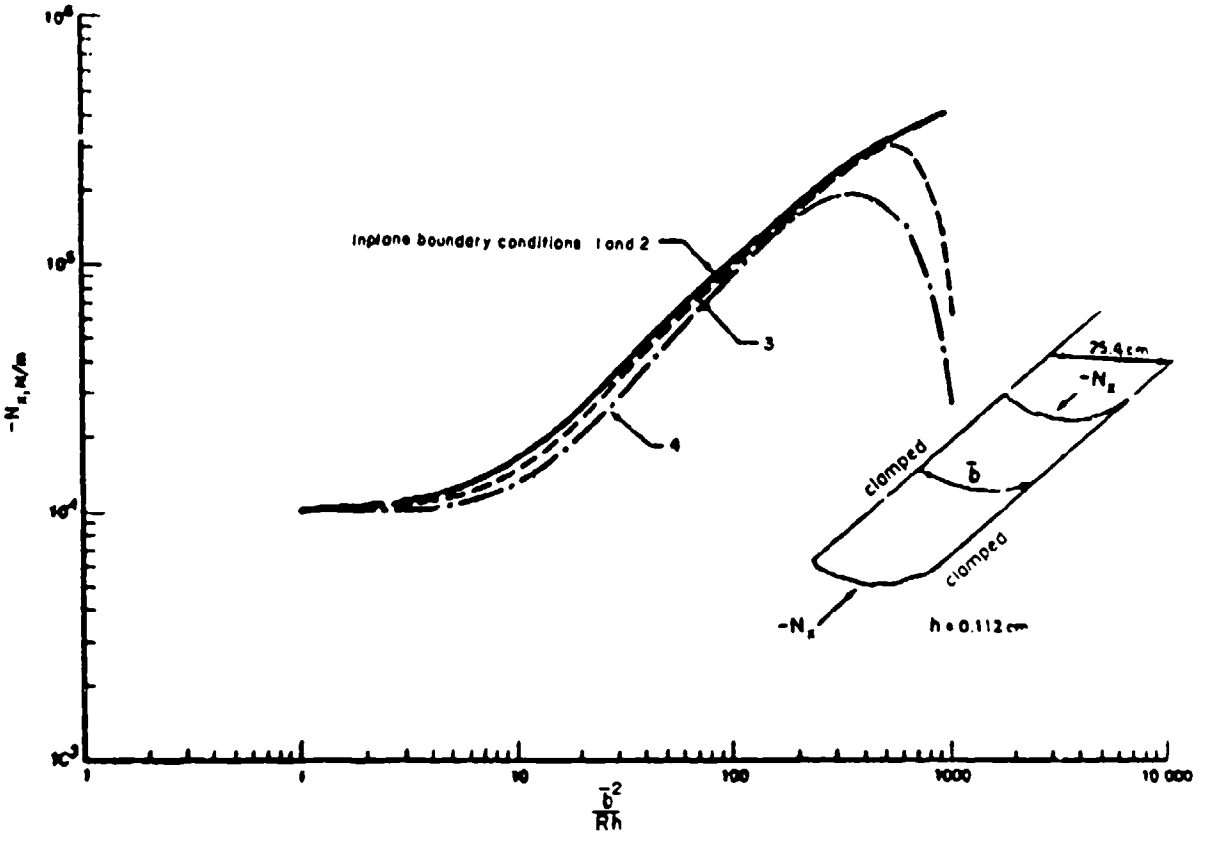

Figure 10.4. Variation of N_x with curvature parameter for shell panels of Figure 10.3.

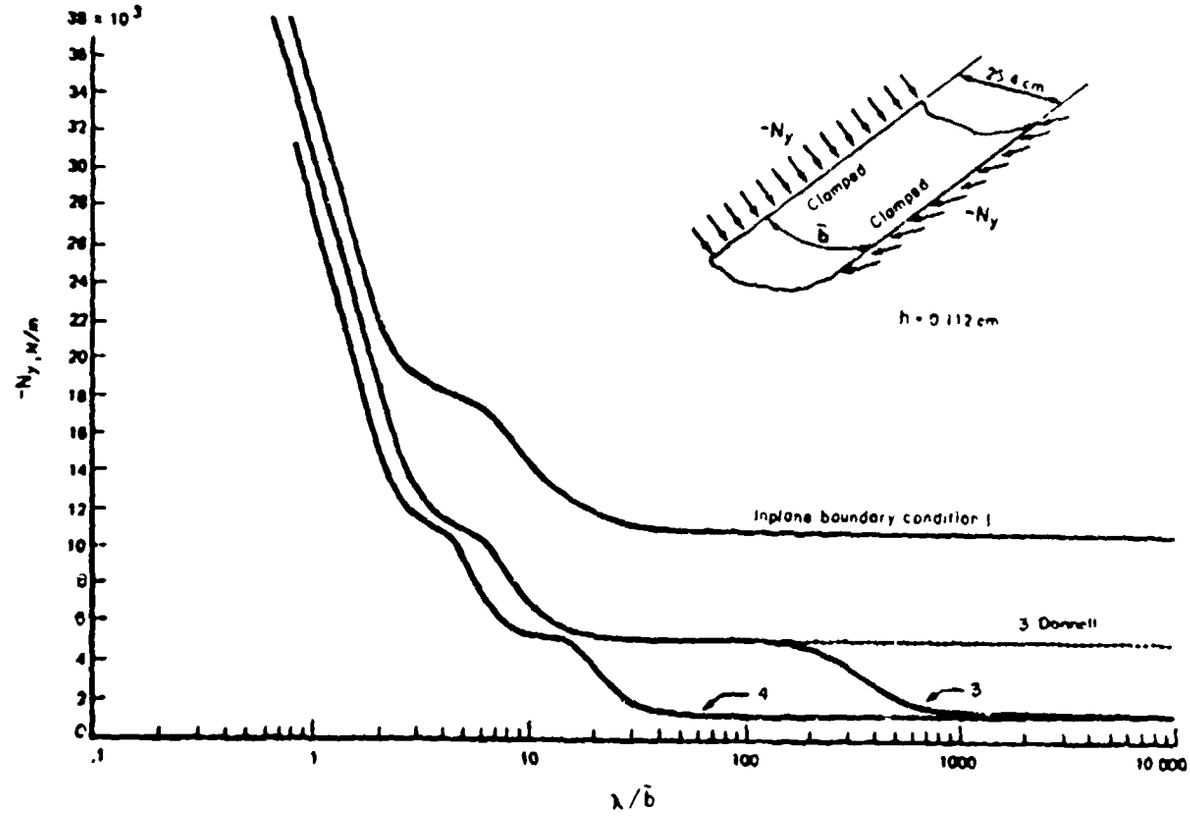

Figure 10.5. Variation of N_y with axial half-wave length (λ) for $\bar{b}^2/Rh = 300$.

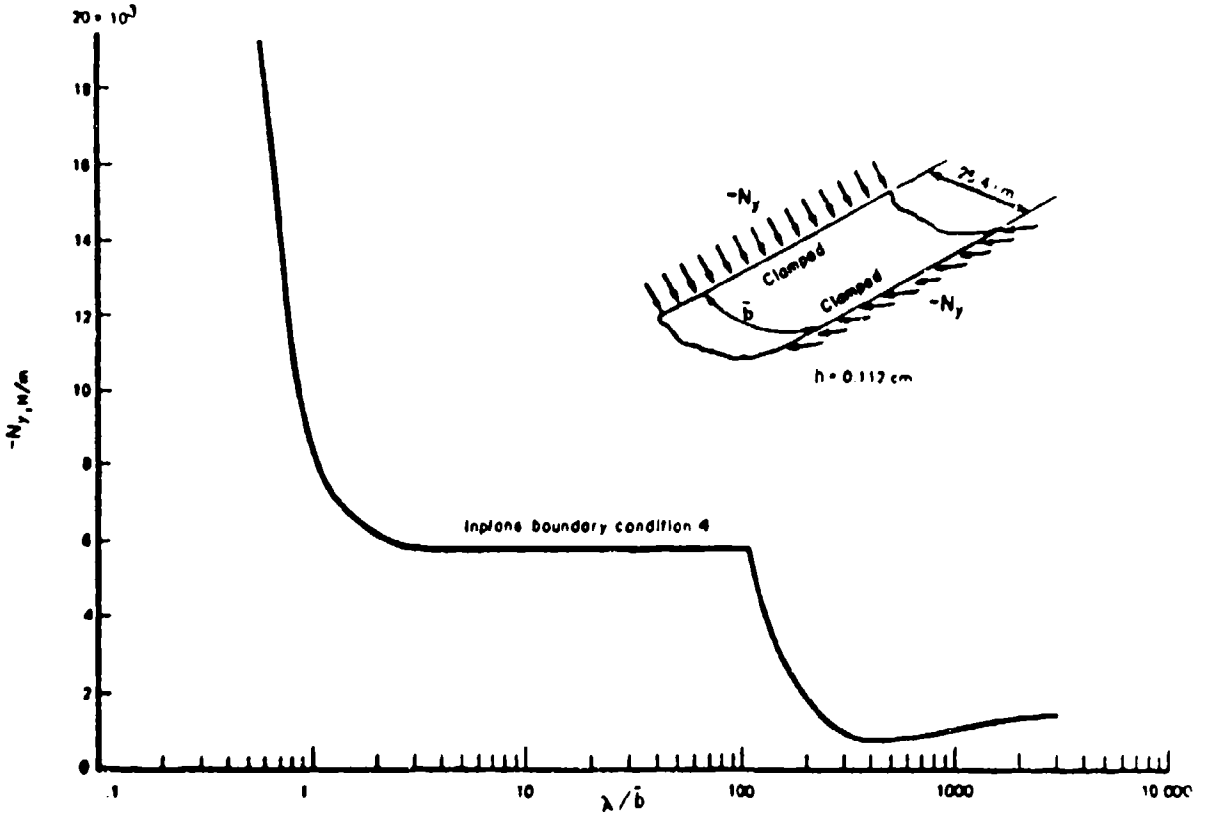

Figure 10.6. Variation of N_y with axial wave-length (λ) for $\bar{b}^2/Rh = 1$.

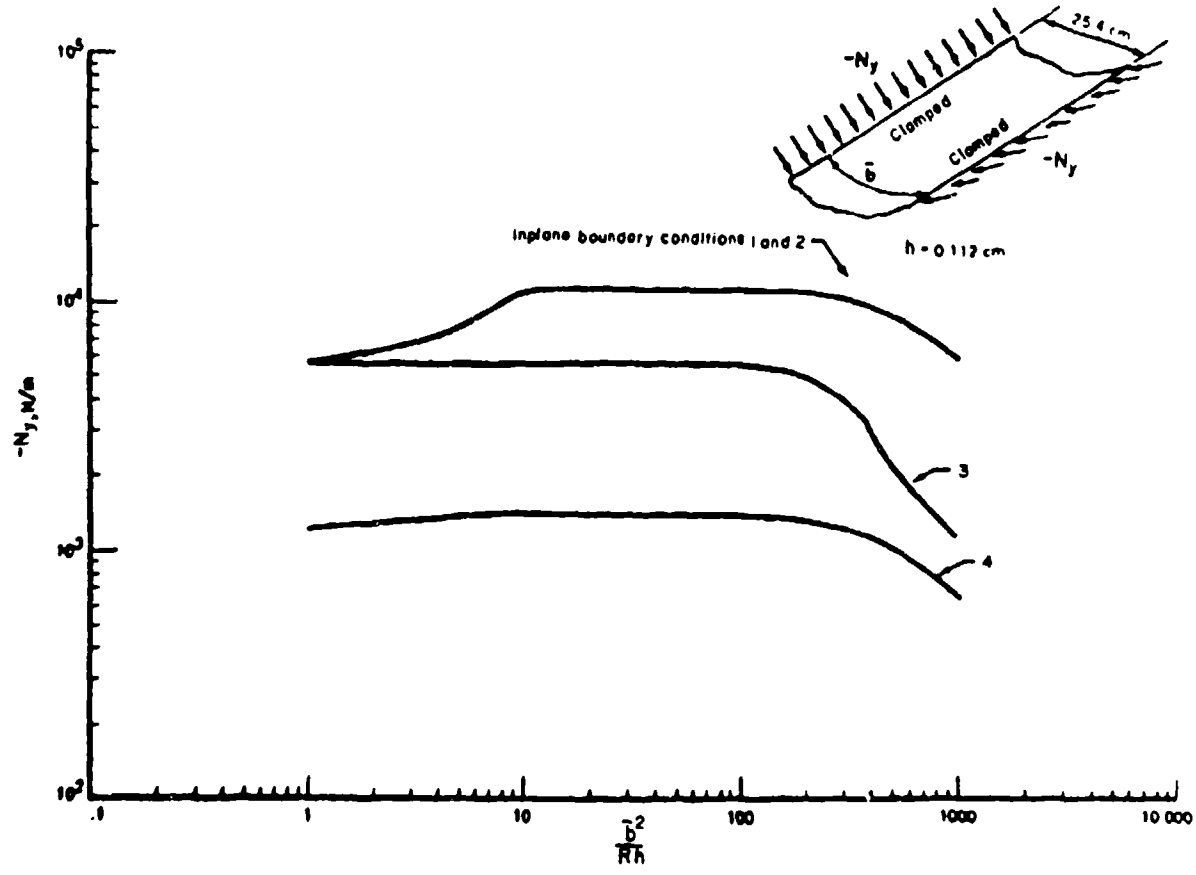

Figure 10.7. Variation of N_y with curvature parameter.

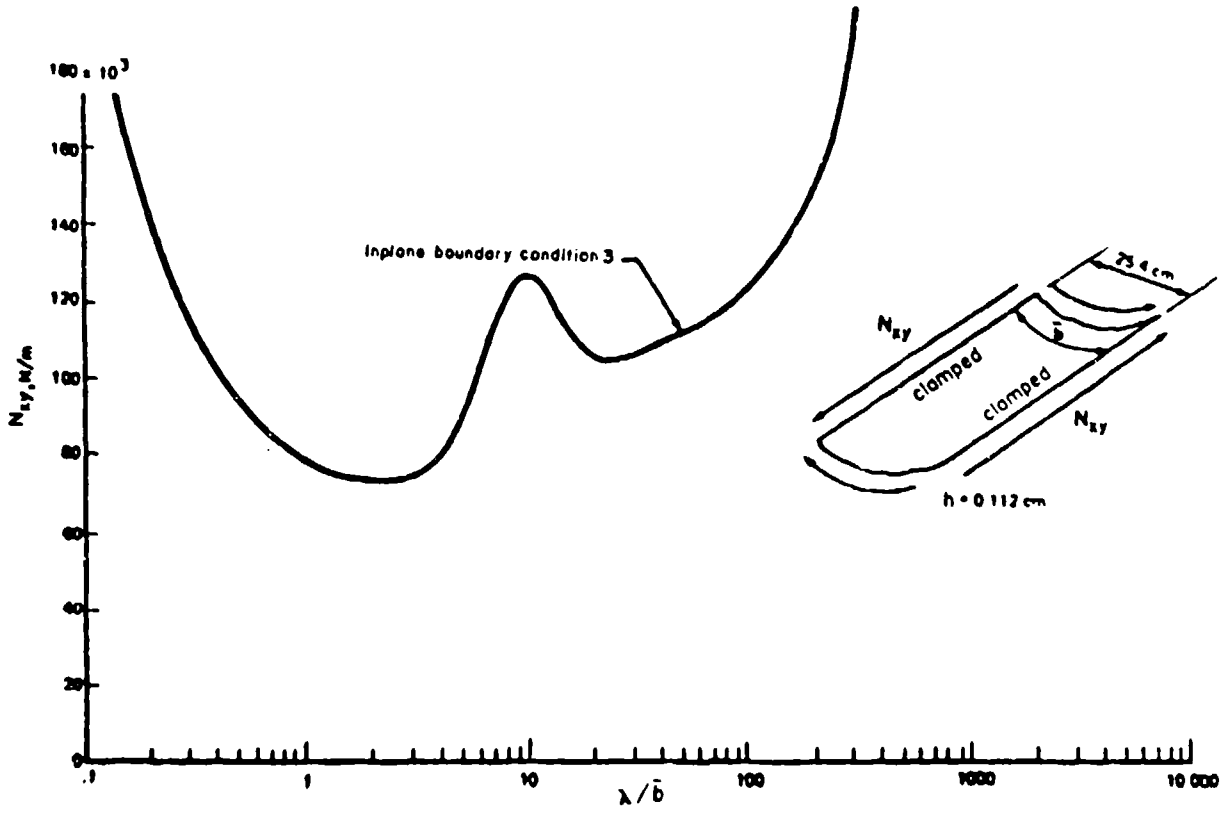

Figure 10.8. Variation of N_{xy} with axial half-wave length (λ) for $\bar{b}^2/Rh = 700$.

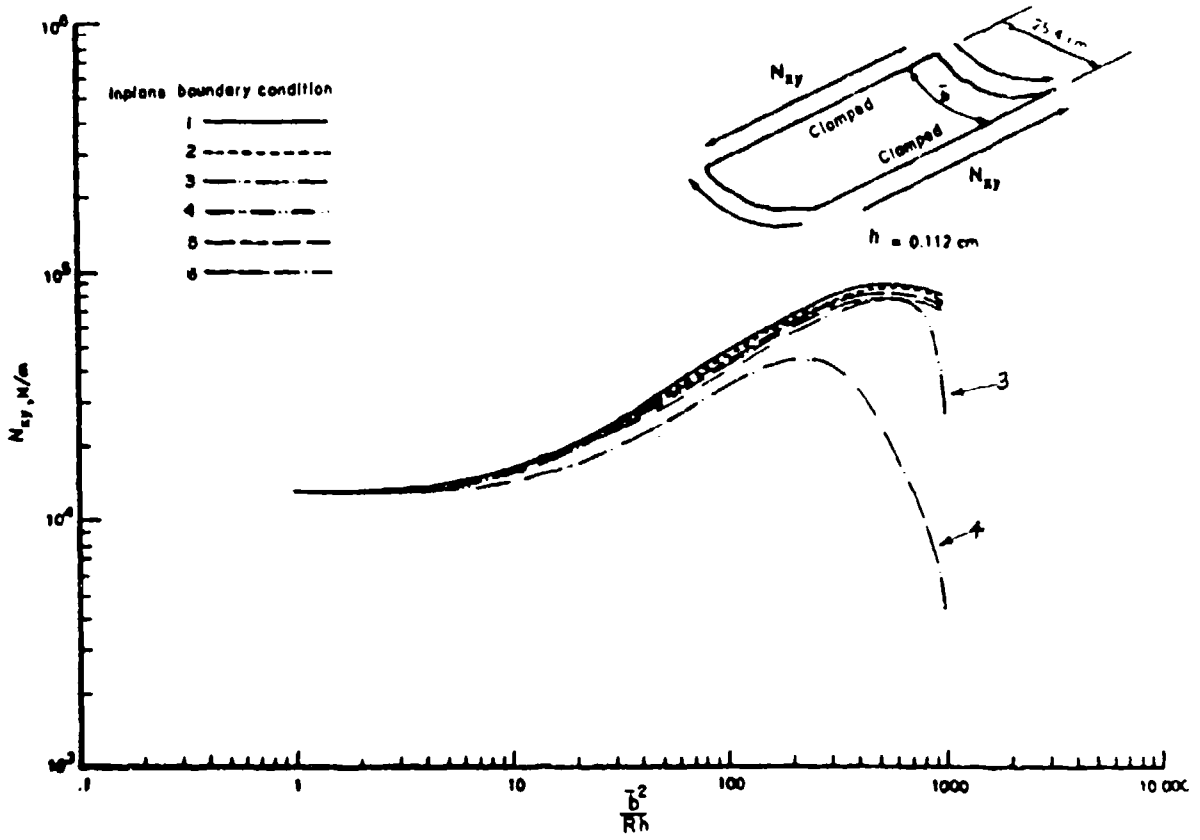

Figure 10.9. Variation of N_{xy} with curvature parameter.

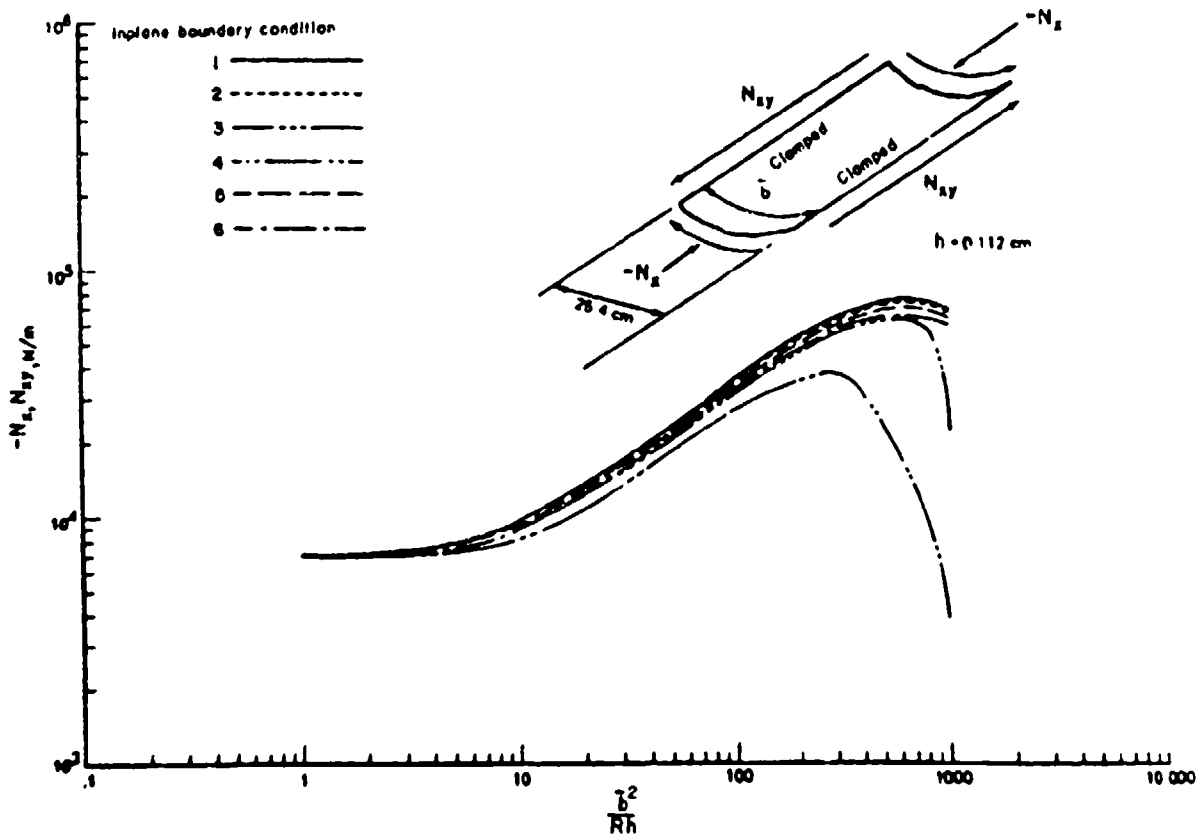

Figure 10.10. Combined stress buckling parameters ($-N_x = N_{xy}$).

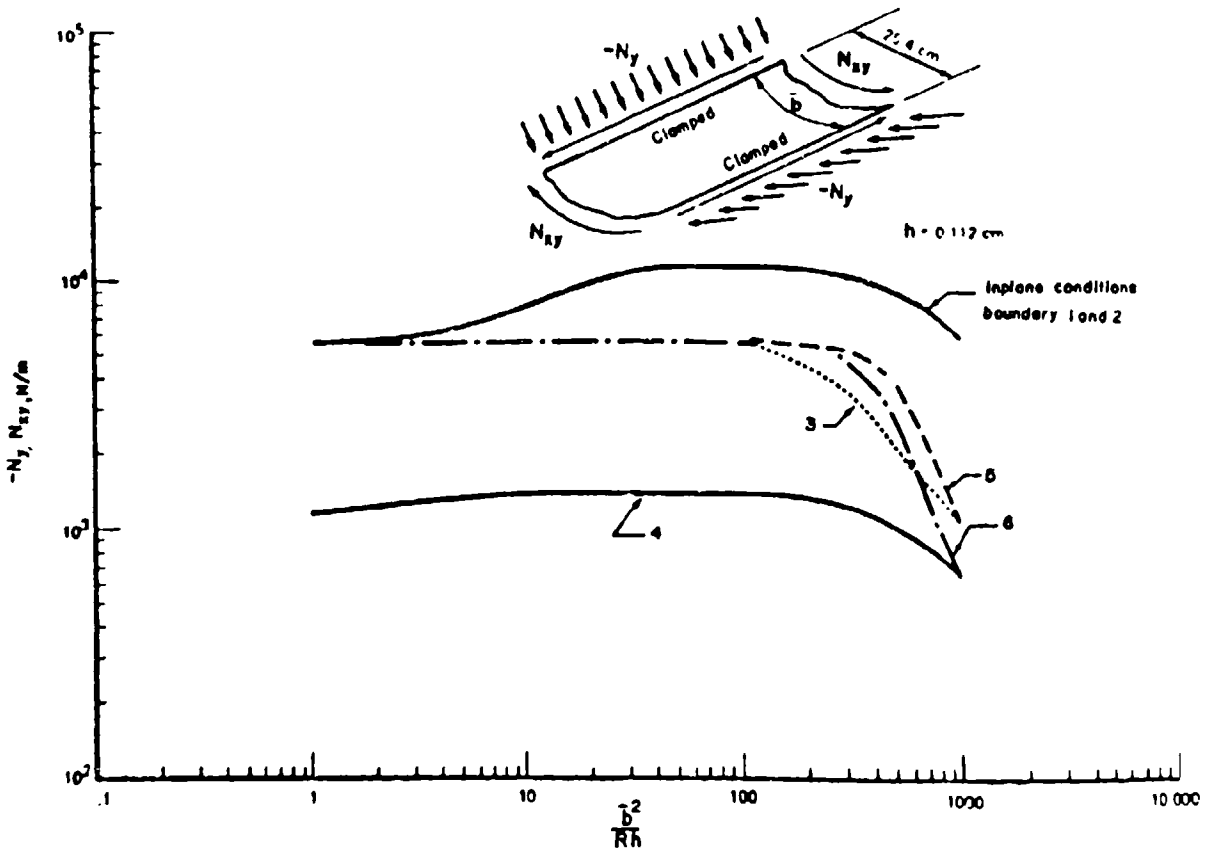

Figure 10.11. Combined stress buckling parameters ($-N_y = N_{xy}$).

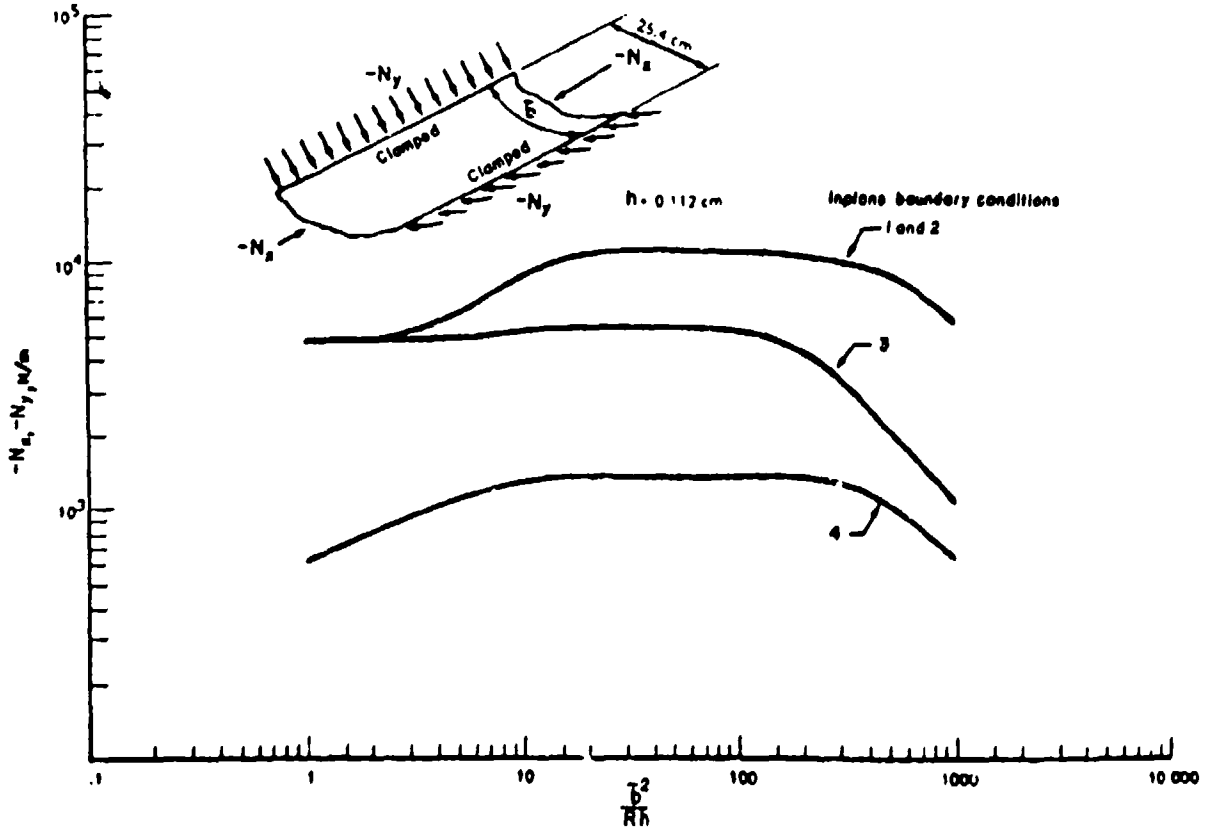

Figure 10.12. Combined stress buckling parameters ($N_x = N_y$).

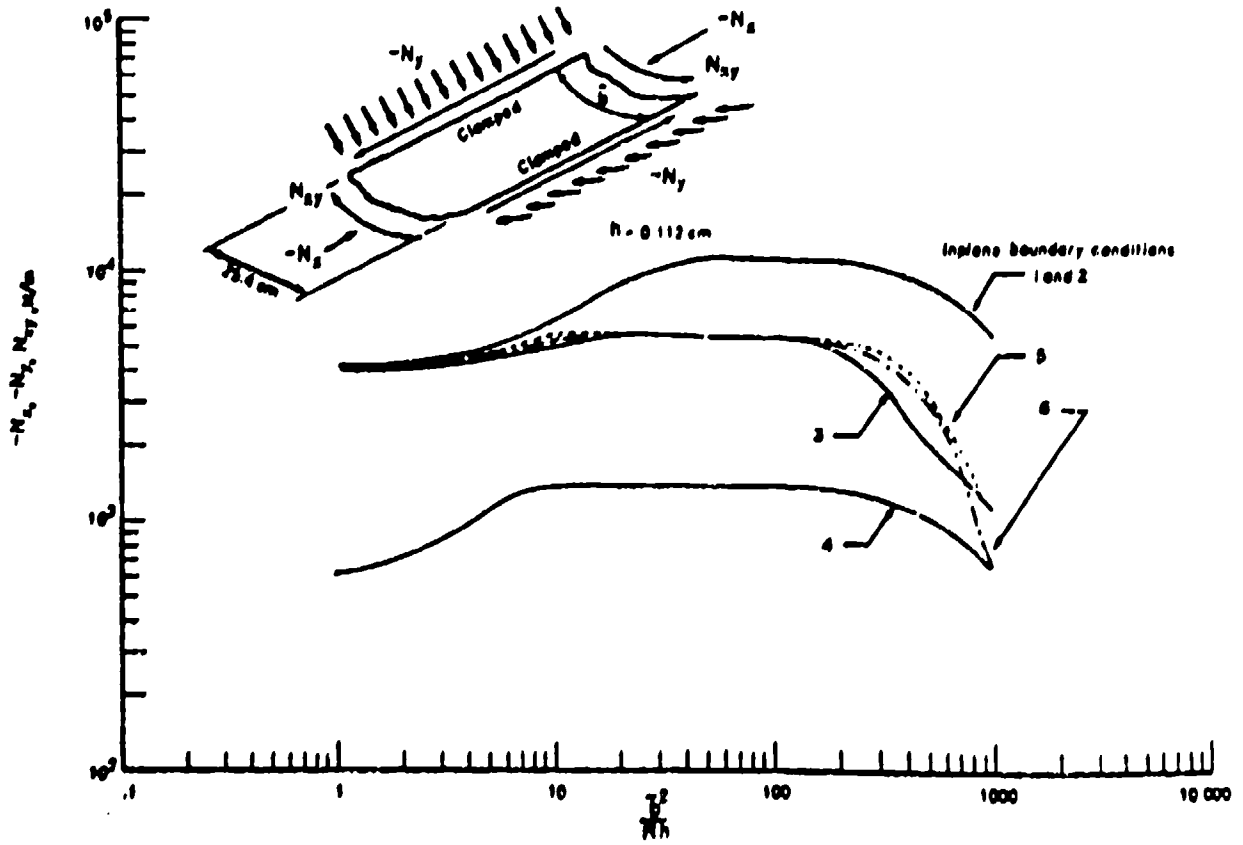

Figure 10.13. Combined stress buckling parameters ($N_x = N_y = -N_{xy}$).

values of $\lambda/\bar{b}$ are also given in [370] corresponding to Figures 10.4-10.13.

In addition to the results described above, data are also plotted in [370] for other laminated composite shell panels of boron-epoxy, boron-aluminum, high modulus graphite-epoxy and borsic-aluminum materials. The analysis methods leading to BUCLASP-3, a computer code capable of determining buckling loads for heated, stiffened, laminated composite shell panels was described by Viswanathan and Tamekuni [314]. Biaxially loaded, stiffened composite shell panels also received particular attention [315,316,372].

Becker, Palazotto and Khot [373-375] conducted a theoretical and experimental investigation of the buckling of a set of 8-ply laminated, graphite-epoxy, cylindrical shell panels subjected to axial compressive loading. The curved edges were clamped and the straight edges had five types of boundary conditions, varying between completely clamped and completely free. Three types of symmetric ply layups were used, as described in Table 10.1. Material properties were determined experimentally to be: $E_1 = 20.5\times10^6$psi, $E_2 = 1.3\times10^6$psi, $G_{12} = 0.75\times10^6$psi, $\nu_{12} = 0.335$. Numerical results for bifurcation buckling were obtained by the STAGS-C computer code, which utilizes two-dimensional finite-difference approximations of the total potential energy of the system for a/b = 1.5, 1 and 0.75, with a/R = 1 and R/h = 300. Values for $-N_x a^2/E_1 h^3$ are listed in Table 10.1. Two types of clamped (C1 and C4) and simply supported (S1 and S4) boundary conditions were employed on the straight edges, as defined by Equations (6.2) and (6.10). As expected, the buckling loads in Table 10.1 for the C1 and S1 straight edge support conditions are larger than those for the C4 and S4 conditions, respectively. One configuration (12x16, $(\pm45)_{2S}$) shows contrary data, which was attributed to be the result of an incorrect bifurcation analysis [374]. Experimental results for six of the configurations are presented in Chapter 11. From the

Table 10.1. Axial buckling load parameters $-N_x a^2/E_1 h^3$ for a series of 8-ply shell panels.

Size, a x b (in)	Straight edge B.C.	Ply layup $(\pm 45)_{2s}$	$(90,\pm 45,0)_s$	$(90,0)_{2s}$
12x8	C1	68.8	58.2	50.3
	C4	44.1	46.0	36.7
	S1	66.0	57.5	49.2
	S4	40.8	45.7	32.0
	free	12.0	14.5	10.7
12x12	C1	54.5	52.6	40.3
	C4	43.0	45.6	34.4
	S1	52.3	52.1	39.6
	S4	42.9	45.4	33.3
	free	12.8	15.1	11.4
12x16	C1	40.7	49.5	36.0
	C4	42.6	45.2	33.5
	S1	38.9	49.3	35.8
	S4	42.5	45.2	33.1
	free	12.8	15.2	11.5

entire study it was concluded that [374] the boundary conditions had the greatest influence on the buckling load, followed by the aspect ratio and, finally, the ply orientation.

Davenport and Bert [205-207] investigated the buckling of sandwich shell panels subjected to combined shear and axial compressive loads. Both facing and core materials were assumed to be orthotropic. CCCC and SSSS edge conditions were treated. The problems were solved by the Galerkin method using assumed displacements which were the sums of products of trigonometric functions.

Wilkens [376] provided extensive experimental results for the buckling of graphite-epoxy laminated composite shell panels having clamped (loaded) circular edges and either clamped or simply supported straight edges. Experimental buckling loads were determined by the Moire grid shadow and Southwell methods. Theoretical values were also calculated using the Ritz method [377]. Tests were conducted on 72 panels having R = 12 in, a = 12 in, $\bar{b} = R\theta_o = 8$ in and $100 \leq R/h \leq 400$. Although thickness deviations were measured, which in some panels were considerable, no attempt was made to measure imperfections due to deviation from cylindrical curvature. Experimentally determined buckling loads were typically found to be considerably less ($\approx$ 20-50 percent) than the theoretical values.

Extensive data was also given by Fogg [32] for the buckling of graphite-epoxy shear panels loaded in axial compression or shear. Sandwich panels were also investigated.

Zhang and Matthews [188,378] derived a set of governing equations for buckling of arbitrarily laminated cylindrical shells expressed in terms of the transverse displacement (w) and an Airy stress function (Ψ). Problems for shell panels having all edges clamped and subjected to axial and/or shear loads were solved by means of the Galerkin method,

using products of beam vibration eigenfunctions to represent both w and ϕ. The importance of using double precision in the calculation of the beam functions was demonstrated. Extensive numerical results were obtained for panels having $a/\bar{b} = 1$, $a/R = 0.5$ and $R/h = 200$, where $\bar{b} = R\theta_o$ is the circumferential arc length. The materials typically used in the parameter study was boron-epoxy, with $E_1/E_2 = 10$, $G_{12}/E_2 = 0.3$ and $\nu_{12} = 0.3$.

Numerical results for the axial buckling load of angle-ply panels having 20 plies are shown in Figure 10.14. Two types of layups are considered: (1) alternate plies ($\pm\theta$) and (2) unidirectional plies ($+\theta$). Variation of $-N_x b^2/E_2 h^3$ with the layup angle θ (measured from the x-axis) is shown for both the shell panel and a flat plate ($R = \infty$). For the alternating angle-ply layup the shell shows maximum buckling loads at <u>two</u> values of θ, approximately 20^o and 70^o. The change in buckling load with decreasing curvature for various numbers of plies is depicted in Figure 10.15. The effect of fiber orientation upon <u>shear</u> buckling loads is seen in Figure 10.16 for shell panels having unidirectional layups ($+\theta$). Curves for both positive and negatively directed shear loads are shown for three curvatures. Change in sign for the shear load may also be interpreted as change from $+\theta$ to $-\theta$ in fiber orientation for a given shear load. It is observed in Figure 10.15 that this change of sign causes considerable change in shear buckling loads. It was further found [188] that this effect was less pronounced for symmetric ($\pm\theta$) angle-ply layups, and it decreased as the number of plies was increased. For antisymmetrical layups the direction of shear loading was found to have essentially no influence on the critical load.

Figures 10.17-10.19 are interaction curves showing critical combinations of axial and shear loads which cause buckling [3-30]. In each case $\bar{N}_x$ is plotted versus $\bar{N}_{xy}$, where $\bar{N}_x$ is the ratio of the critical compressive axial load with shear to that without shear and $\bar{N}_{xy}$ is the ratio of the critical shear load with compression to that without compression.

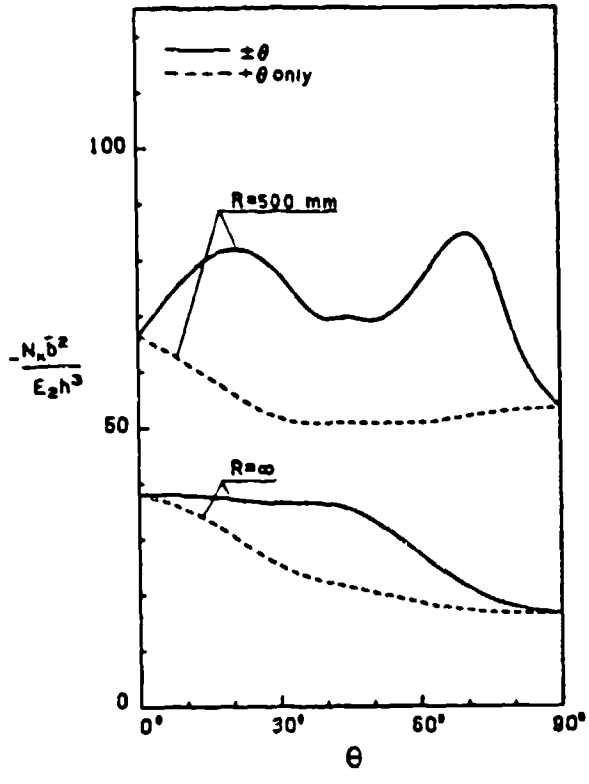

Figure 10.14. Axial buckling loads of CCCC, angle-ply shell panels ($a/\bar{b} = 1$, $a/R = 0.5$, $R/h = 2000$).

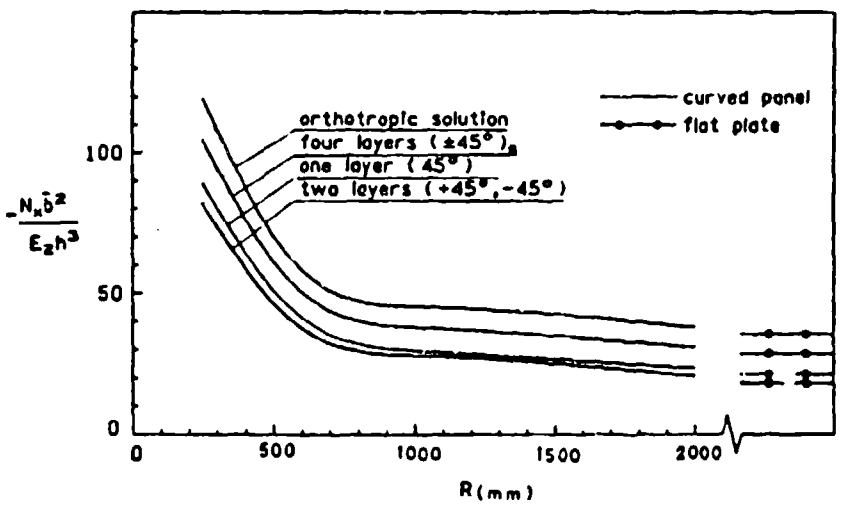

Figure 10.15. Variation of axial buckling load with decreasing curvature (CCCC, $a/\bar{b} = 1$, $a/h = 2000$, $a = 250$ mm).

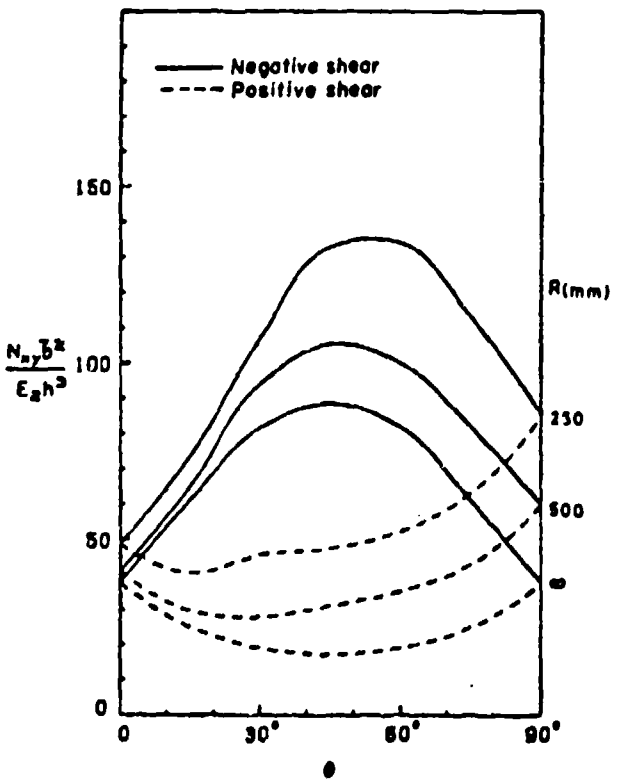

Figure 10.16. Effect of shear loading direction upon the critical buckling loads of CCCC shells having unidirectional layups ($a/\bar{b} = 1$, $a/R = 0.5$, $R/h = 2000$).

Curves for both positive and negative shear are drawn. In Figure 10.17 the curvature is varied for a shell panel with unidirectional fibers ($\theta = +45^{o}$). Figure 10.18 examines the effects of various types of layups (R/h = 2000). Figure 10.19 shows curves for three types of materials - graphite-epoxy and glass-epoxy, in addition to the previous boron-epoxy - for $\theta = +45^{o}$ unidirectional layups (R/h = 2000). Elastic constants for the materials are listed in Table 10.2.

Figures 10.20-10.23 show the results of a study made to compare the effects of clamped versus shear diaphragm (simply supported) edge conditions [188]. Figure 10.20 is for the unidirectional layup (compare with Figure 10.14) with varying fiber orientation. In Figure 10.21 the number of layers (n) in symmetric and antisymmetric angle-ply layups ($\pm$ 45^{o}) is varied. The effects of varying the aspect ratio ($a/\bar{b}$) in the case of positive shear loading are seen in Figure 10.22. Finally, Figure 10.23 shows interaction curves for shell panels having two opposite edges clamped and the other two simply supported, loaded in combined axial compression and shear. These panels have $\pm$45^{o} symmetric angle-ply layups with four layers, and the data may be compared with that for the CCCC case shown previously in Figure 10.18.

Baharlou [101] considered the buckling of a two-layer, cross-ply, SSSS shell panel subjected to axial compression and showed that, even for relatively deep panels (b/R = 0.5) the critical load is virtually unaffected by the stacking sequence (i.e., whether the ply with circumferential fibers is outer or inner).

Knutsson [379] tested an integrally stiffened, graphite-epoxy shell panel with the ends clamped and the sides supported. Good correlation was found between the theoretical and experimental buckling load.

Durlofsky and Mayers [210,211] developed a theory for the buckling of generally laminated, cylindrical shell panels including the effects

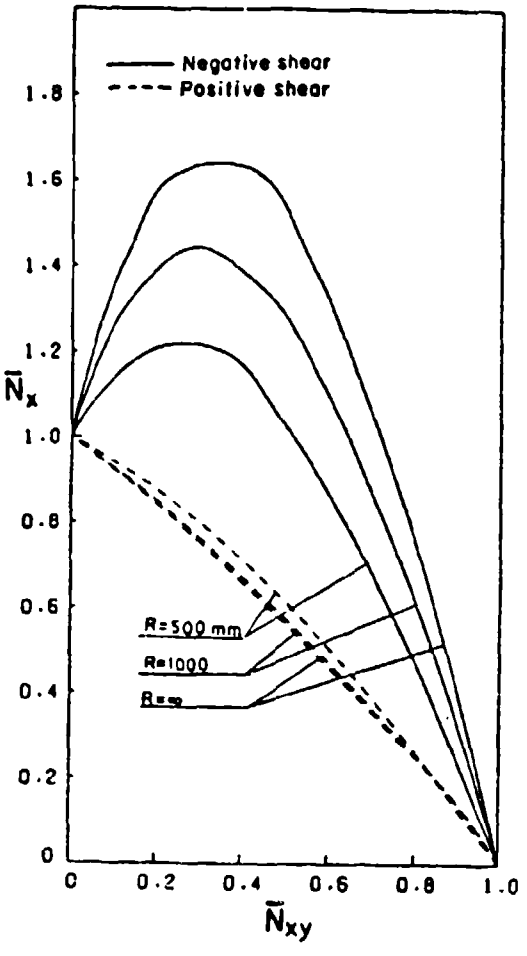

Figure 10.17. Compression-shear interaction curves for CCCC, unidirectionally laminated ($\theta = 45^{o}$), shell panels with various curvatures ($a/\bar{b} = 1$).

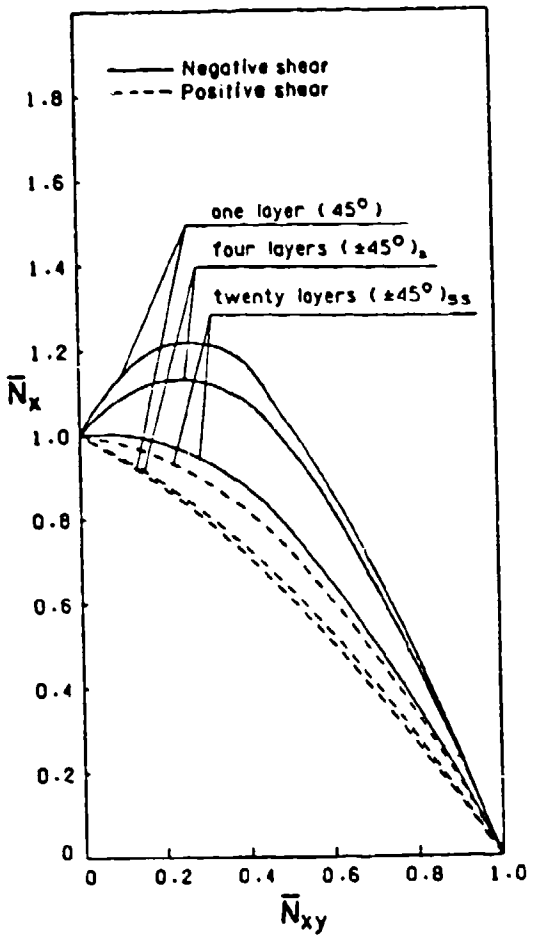

Figure 10.18. Compression-shear interaction curves for CCCC shell panels with various layups ($a/\bar{b} = 1$, $a/R = 0.5$, $R/h = 2000$).

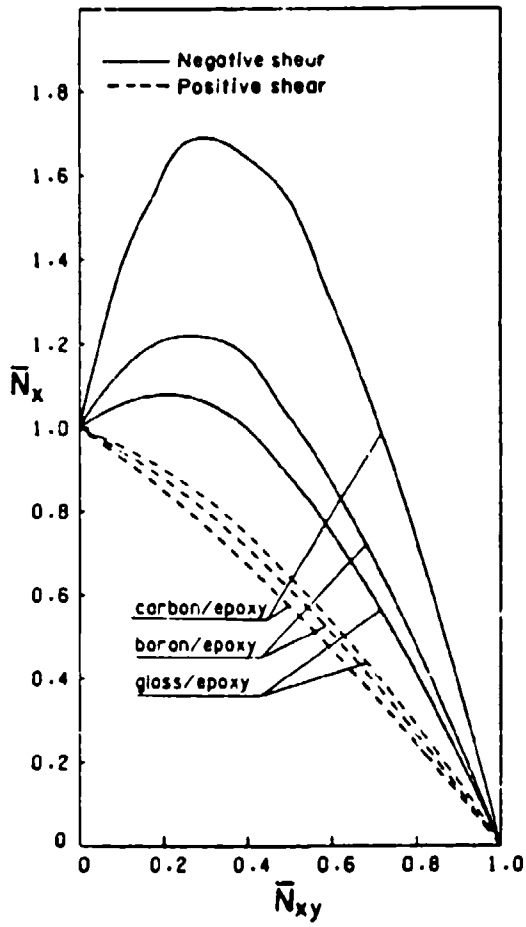

Figure 10.19. Compression-shear interaction curves for CCCC, unidirectionally laminated ($\theta = 45^{\circ}$), shell panels of various materials ($a/\bar{b} = 1$, $a/R = 0.5$, $R/h = 2000$).

Table 10.2. Elastic constants used by Zhang and Matthews.

Material	Moduli (GN/m^2)			ν_{12}
	E_1	E_2	G_{12}	
Boron-epoxy	206.9	20.7	5.2	0.3
Graphite-epoxy	206.9	5.2	2.6	2.6
Glass-epoxy	53.8	17.9	8.9	8.9

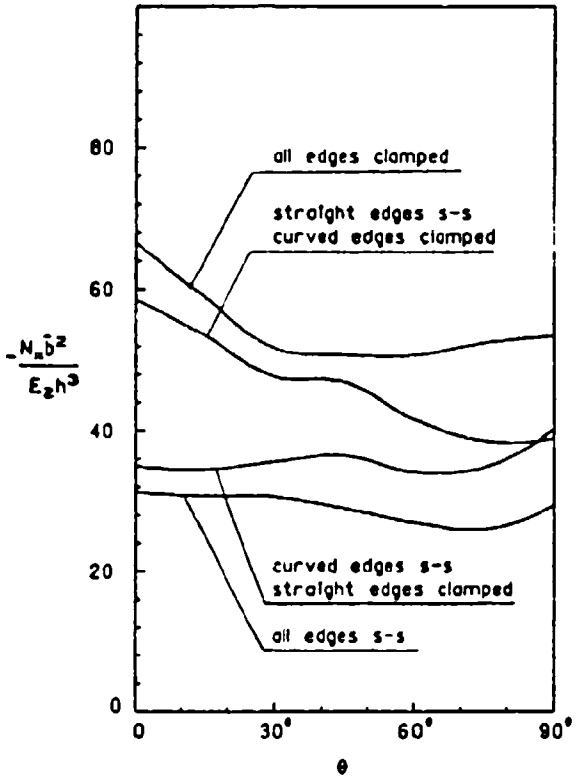

Figure 10.20. Comparison of uniaxial buckling loads for clamped and simply supported edge conditions ($a/\bar{b} = 1$, $a/R = 0.5$, $R/h = 2000$).

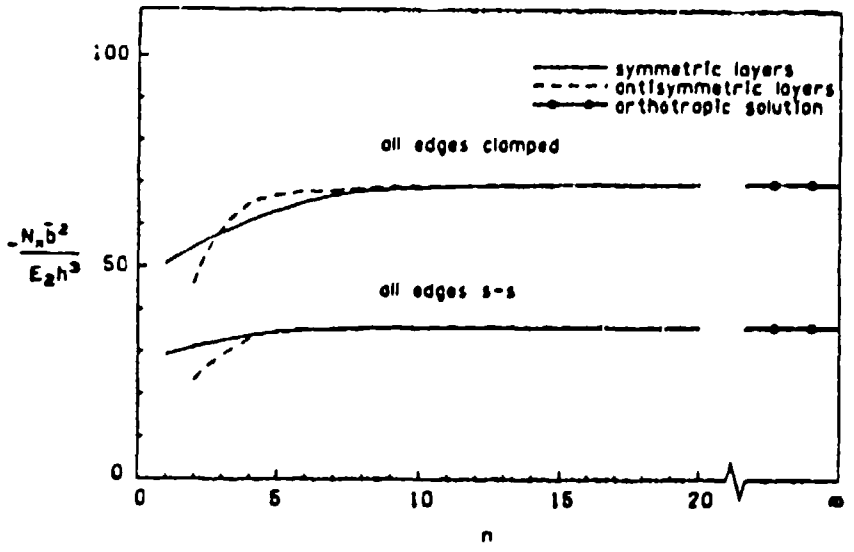

Figure 10.21. Comparison of uniaxial buckling loads with varying number of layers in angle-ply ($\pm 45^{\circ}$) layups ($a/\bar{b} = 1$, $a/R = 0.5$, $R/h = 2000$).

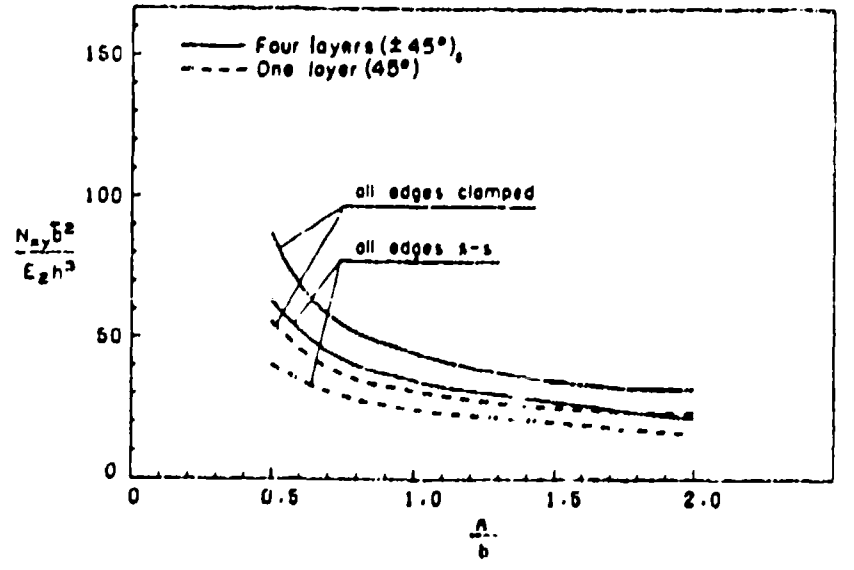

Figure 10.22. Comparison of positive shear buckling loads with aspect ratio for various shell panels ($a/R = 0.5$, $R/h = 2000$).

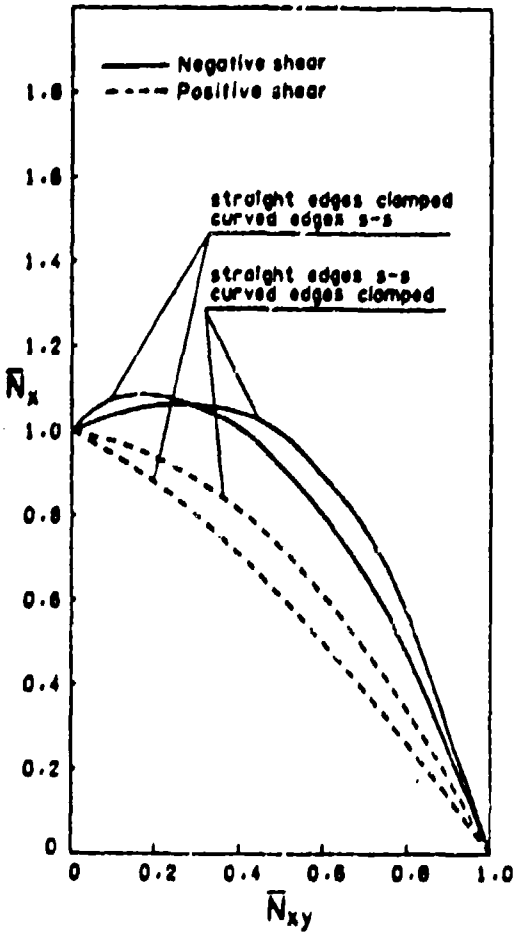

Figure 10.23. Compression-shear interaction curves for SCSC shell panels having symmetric angle-ply ($\pm 45^{\circ}$) layups ($a/\bar{b} = 1$, $a/R = 0.5$, $R/h = 2000$).

of shear deformation. Application was made to an SSSS panel carrying axial compression. It was shown that the shear deformation effects may be significant.

Buckling as a special case of a free vibration analysis (when the frequency becomes zero) was the approach used by Fortier [380] and by Sinha and Rath [381]. The former used the Ritz method with assumed solutions in the form of products of beam vibration eigenfunctions to analyze symmetrically laminated, cross ply and $\pm 45^{\circ}$ angle ply shell panels having four types of edge conditions, subjected to axial compression. The latter treated SSSS, arbitrarily laminated, cross-ply panels for which an exact solution is possible.

CHAPTER XI. POSTBUCKLING AND IMPERFECTIONS IN SHELL PANELS

Relatively few references are available which treat the postbuckling behavior of cylindrical shell panels, or which consider the effects of geometric imperfections (i.e., deviations from the perfect cylindrical surface) upon the load-deflection characteristics. Postbuckling studies for shell panels are particularly important because, unlike plates, their load-carrying capacities may decrease after the bifurcation buckling loads are reached. Furthermore, the presence of small imperfections may cause large displacements to occur at loads well below the buckling loads.

11.1. POSTBUCKLING STUDIES

Zhang and Matthews [378,382] developed a set of coupled equilibrium and compatibility equations governing the postbuckling behavior of arbitrarily laminated, cylindrical shell panels. These nonlinear equations were solved by the Galerkin procedure for the case of SSSS panels subjected to axial compression. Normal displacements were assumed as the sum of the products of sine functions and the squares of sine functions, whereas the Airy stress function was taken as a sum of products of vibrating beam eigenfunctions. Applying the Galerkin method led to an infinite set of algebraic cubic equations. A truncated set of these nonlinear equations was solved by an iterative scheme.

Parameter studies were made for boron-epoxy panels ($E_1/E_2 = 10$, $G_{12}/E_2 = 0.3$, $\nu_{12} = 0.3$) having either unidirectional plies with fibers oriented at 45^o with the longitudinal axis, or angle-ply ($\pm 45^o$) layups [382]. The panels were subjected to axial compression. $a/\bar{b}$ was set at unity ($\bar{b} = R\theta_o$ is the circumferential width), and the circumferential width to thickness ratio ($\bar{b}/h$) was set at 100. Figure 11.1 depicts the postbuckling behavior of a shell panel having a curvature parameter $\bar{b}^2/Rh = 25$ compared with that of a corresponding flat plate for panels

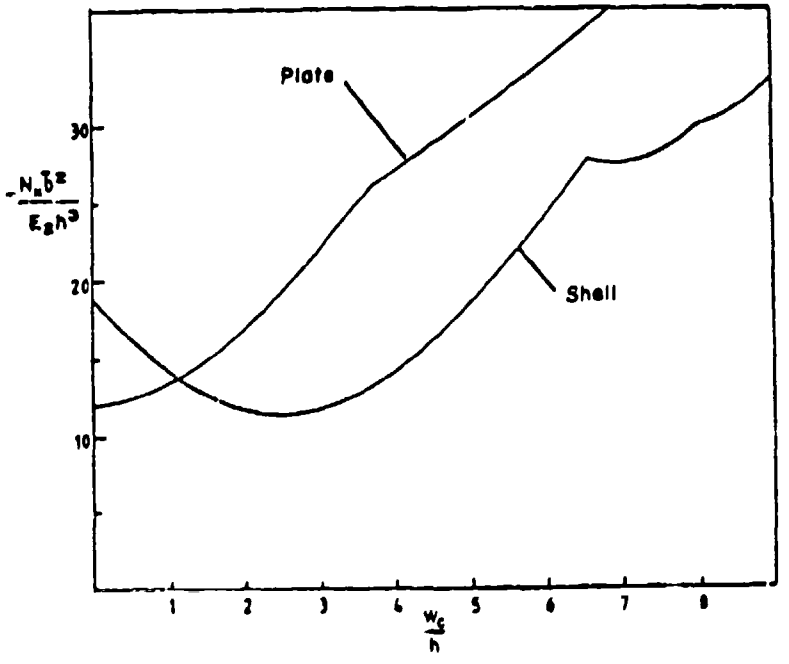

Figure 11.1. Postbuckling load-deflection curves for SSSS boron-epoxy panels with unidirectional fibers at $\theta = 45^{\circ}$.

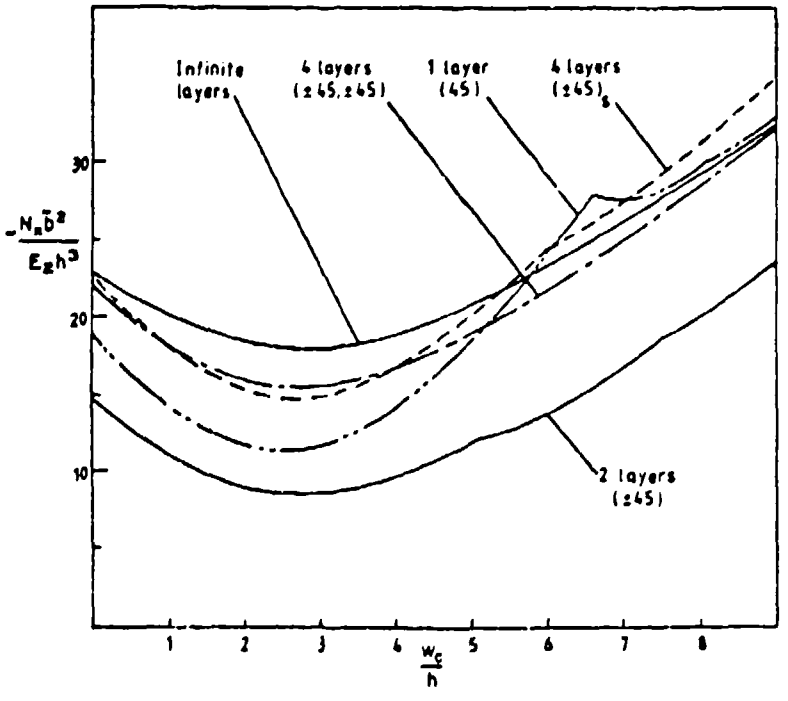

Figure 11.2. Postbuckling load-deflection curves for SSSS boron-epoxy shell panels with various ply layups.

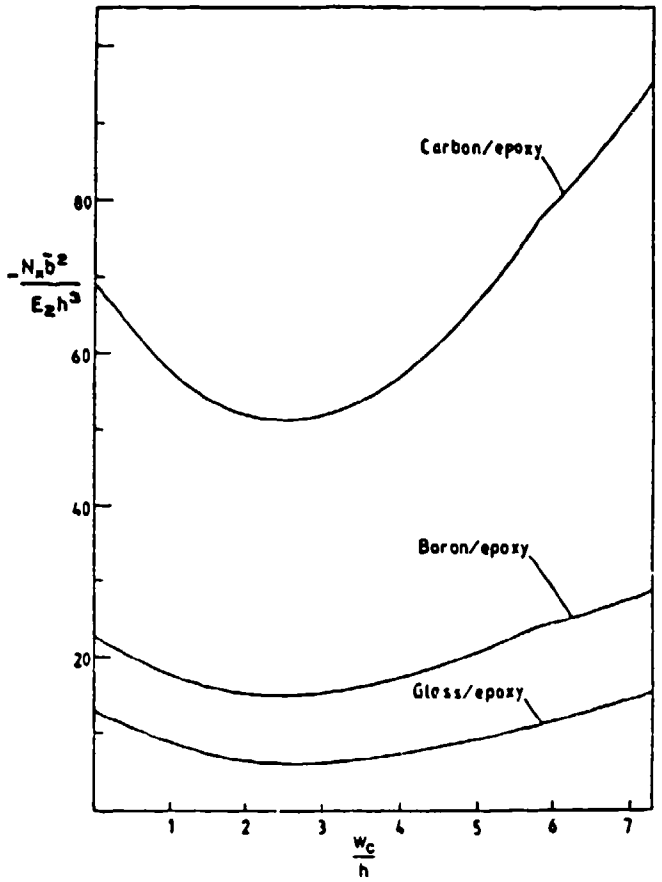

Figure 11.3. Postbuckling load-defection curves for SSSS shell panels of various materials with a symmetric four-layer, angle-ply layup.

having unidirectional fibers. The nondimensional load $-N_x\bar{b}^2/E_2h^3$ is shown plotted versus the ratio of the center deflection to the thickness (w_c/h). As for isotropic panels, the presence of curvature is seen to increase the bifurcation buckling load, as shown on the ordinate axis. However, unlike the plate, which has a monotonically increasing load-deflection curve in the postbuckling region, the shell panel exhibits an initial drop in load before increasing. In a physical situation, a jump across may occur before the bifurcation load is reached. The cusps occurring in the curves of Figure 11.1 correspond to abrupt changes in the postbuckled mode shapes as one follows an equilibrium path of minimum loading.

Figure 11.2 shows the influence of ply layup on the postbuckling behavior of the shell panel. Two of the curves are for antisymmetrical, angle-ply laminates having two and four layers [382]. One is for a symmetrical, angle-ply laminate with four layers. The two-layer, antisymmetrical layup is seen to yield not only the lowest buckling load, but also the lowest postbuckling equilibrium curve. Figure 11.3 describes postbuckling curves for symmetrically laminated, four ply shell panels made of three sets of materials - carbon-epoxy, boron-epoxy and glass-epoxy. Elastic constants used are given in Table 10.2. Additional results are given in [382] for the variations in membrane force and bending moment at selected points on a boron-epoxy shell panel.

Tests were reported by Becker, Palazotto and Khot [373-375] for a set of shell panels which were clamped along their curved edges and had either S4 or free straight edge boundary conditions. Results for axial compressive buckling loads were obtained for six configurations as indicated in Table 11.1 (experimental values listed are the average of the results found using two specimens for each configuration). The shell panels are described further in Section 10.2. Table 11.1 shows that the theoretical, bifurcation buckling loads obtained were from 23

Table 11.1. Comparison of theoretical and experimental values of $-N_x a^2/E_1 h^3$ for a series of 8-ply shell panels.

Panel description	Type of result	Ply layup $(\pm 45)_{2S}$	Ply layup $(90,\pm 45,0)_S$	Ply layup $(90,0)_{2S}$
12x12 S4 straight edges	Bifurcation analysis	42.9	45.4	33.3
	Nonlinear collapse analysis	32.5	32.5	29.5
	Experimental	28.5	25.0	24.5
12x16 free straight edges	Bifurcation analysis	12.8	15.2	11.5
	Experimental	9.8	11.3	8.3

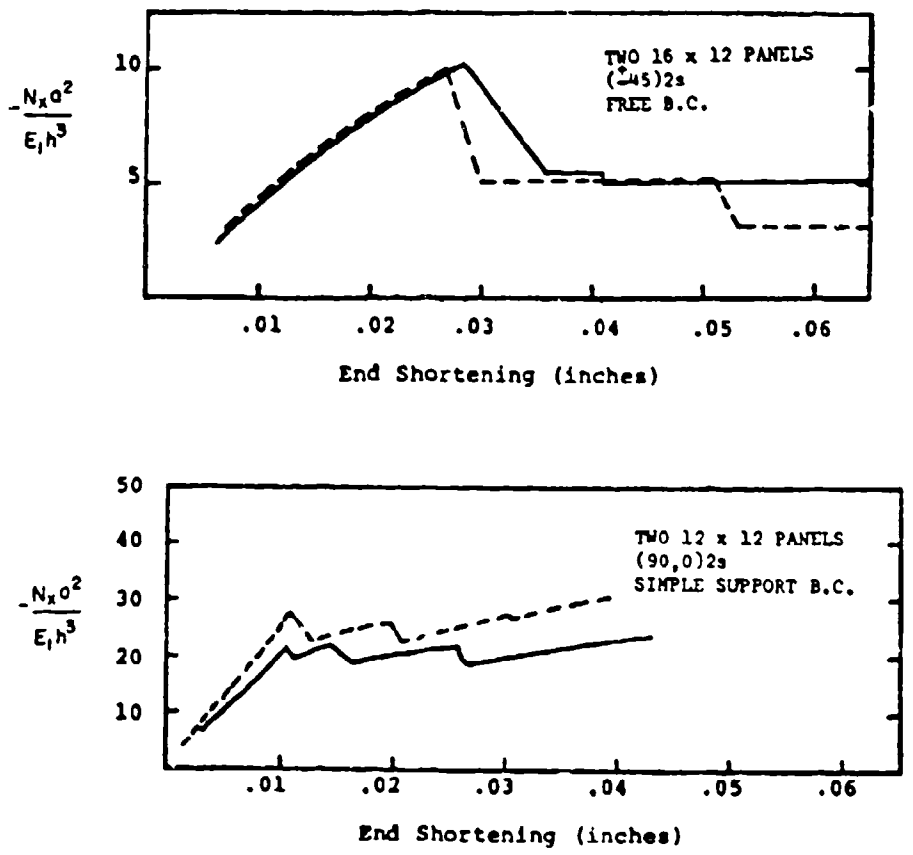

Figure 11.4. Experimentally determined end-shortening curves for two of the shell configurations of Table 11.1.

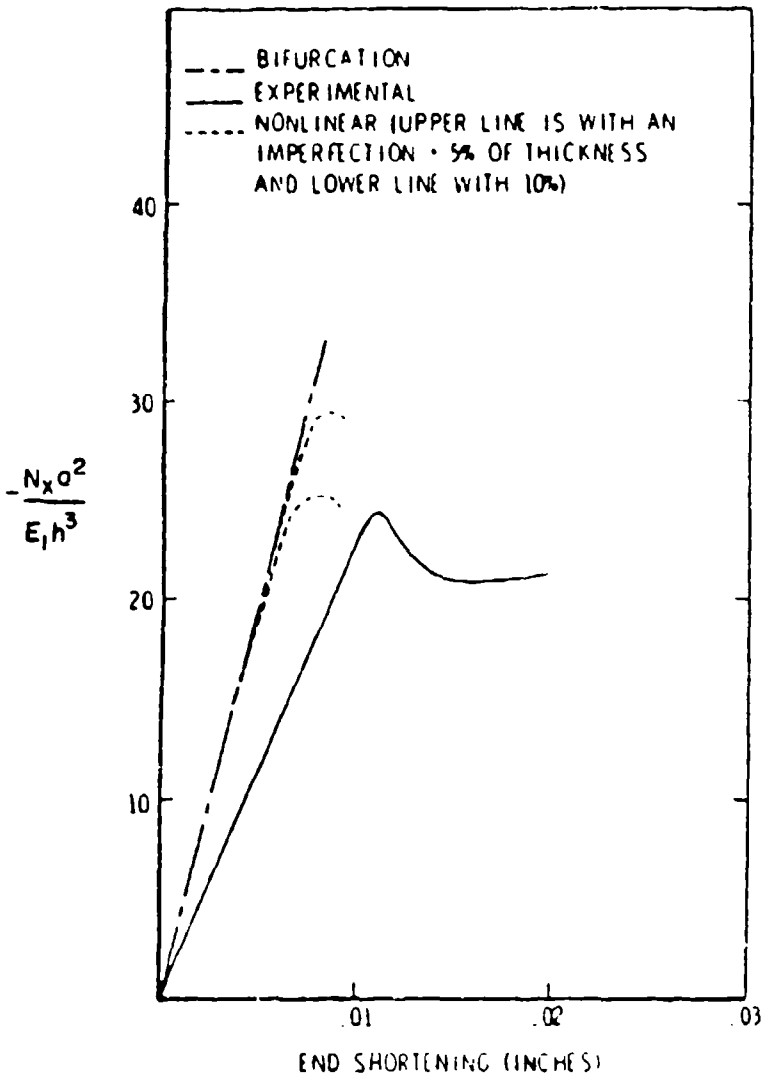

Figure 11.5. Comparison of theoretical and experimental end-shortening curves for the 12x12$(90,0)_{2S}$ panels of Table 11.1.

to 34 percent greater than the experimental loads, except for the (90, $\pm$45, 0)$_S$ 12 x 12 panel, which was 45 percent larger. It was thought that the latter large disagreement was primarily due to improper fixture alignment during the test. Typical experimental end shortening curves are depicted in Figure 11.4. The curves show abrupt drops, which correspond to abrupt changes in mode shapes. Nonlinear collapse analyses were also made for the 12x12 panels by means of the STAGS-C computer code.

The nonlinear collapse analysis was accomplished by introducing a small imperfection in the form of a transverse point load at the center of a panel. The magnitude of this load was chosen so as to produce a transverse displacement (w) of approximately five percent of the panel thickness when the axial compression is zero. Theoretical and experimental load-shortening curves for the 12 x 12 $(90,0)_{2S}$ panels with S4 straight edges may be compared in Figure 11.5.

Agarwal [383] reported the results of a theoretical and experimental study of the postbuckling behavior of hat-stiffened, composite shell panels loaded in axial compression. It was found that the panels exhibited considerable postbuckling strength, reaching ultimate loads of approximately five times their bifurcation buckling loads. Furthermore, it was shown that 92 percent of the total buckling load was carried in or near the stiffeners, and thus the postbuckling strength may be determined by calculating the crippling strength of the stiffeners alone. The postbuckling behavior of stiffened, composite panels loaded in axial compression was also taken up by Hinkle, Sorensen and Garrett [384].

Monforton and Schmit [173,292] presented a finite element method capable of dealing with the geometric nonlinearity existing in the postbuckling analysis of shell panels. Shell panels having composite face sheets and sandwich cores were also considered.

11.2. IMPERFECTIONS

Bauld, Khot and Sathyamoorthy [385-387] developed a computer code to determine bifurcation buckling loads and the nonlinear load-deflection characteristics of cylindrical shell panels having initial imperfections, general loading conditions and arbitrary boundary conditions. The method used finite differences together with the total potential energy of the system. It was demonstrated [385,386] on axially loaded, boron-epoxy panels having a = 6 in, b = 4 in and R = 25 in. The edges had variations of simply supported conditions, with S4 along the straight edges and the (loaded) curve edges having S1 at one end and S2 at the other (see Equation 6.2). All panels had four plies and a total thickness of 0.024 in. Material properties for the plies were: $E_1 = 40 \times 10^6$psi, $E_2 = 4.5 \times 10^6$psi, $G_{12} = 1.5 \times 10^6$psi, $\nu_{12} = 0.25$.

Figure 11.6 [386] shows the effect of laminate layup on the load-deflection curves for four different layups. The total axial load (lb) is plotted versus the average transverse deflection (w, in). The uppermost curve (labelled 1) is the nonlinear analysis result for a symmetrically laminated panel having (-45, +45, +45, -45) fiber orientations. The linear, bifurcation analysis yielded a critical load of 510 lb. It is of interest that transverse deflections should arise for this case from the nonlinear analysis. Membrane stretching-shear coupling does not exist for this case. Curves 2 and 3 are for antisymmetric laminates, (+45, -45, +45, -45) and (+45, +45, -45, -45), respectively. For these configurations the membrane stretching-shear coupling and the bending-twisting coupling are both zero ($A_{16} = A_{26} = D_{16} = D_{26} = 0$), but the bending-stretching coupling is not zero ($B_{ij} \neq 0$). Comparing the laminates for curves 2 and 3, the latter has twice as much bending-stretching coupling, therefore it is the less stiff configuration. The bottom curve in Figure 11.6 is for an unsymmetrical laminate (0, 30, 45, 60). All three types of coupling are present, and the stiffness is further reduced.

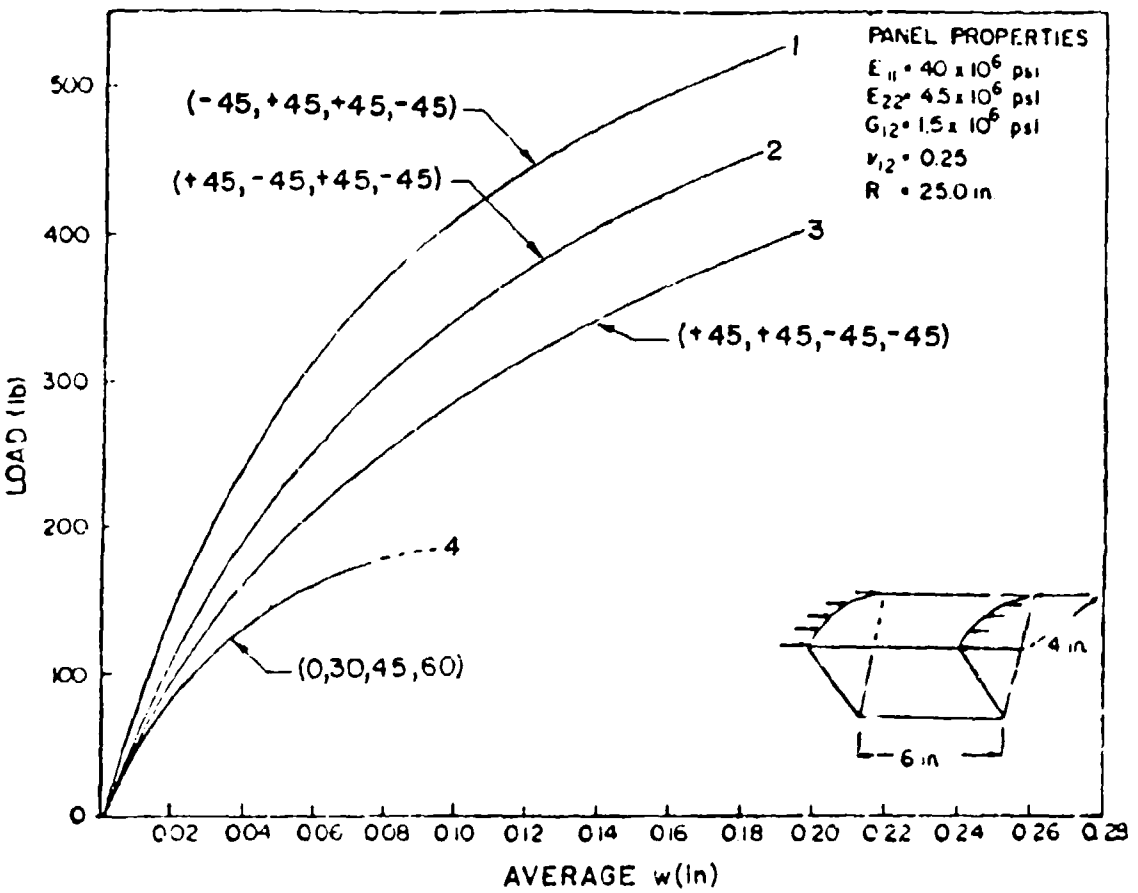

Figure 11.6. Load-deflection curves for shell panels having various layups and axial loading.

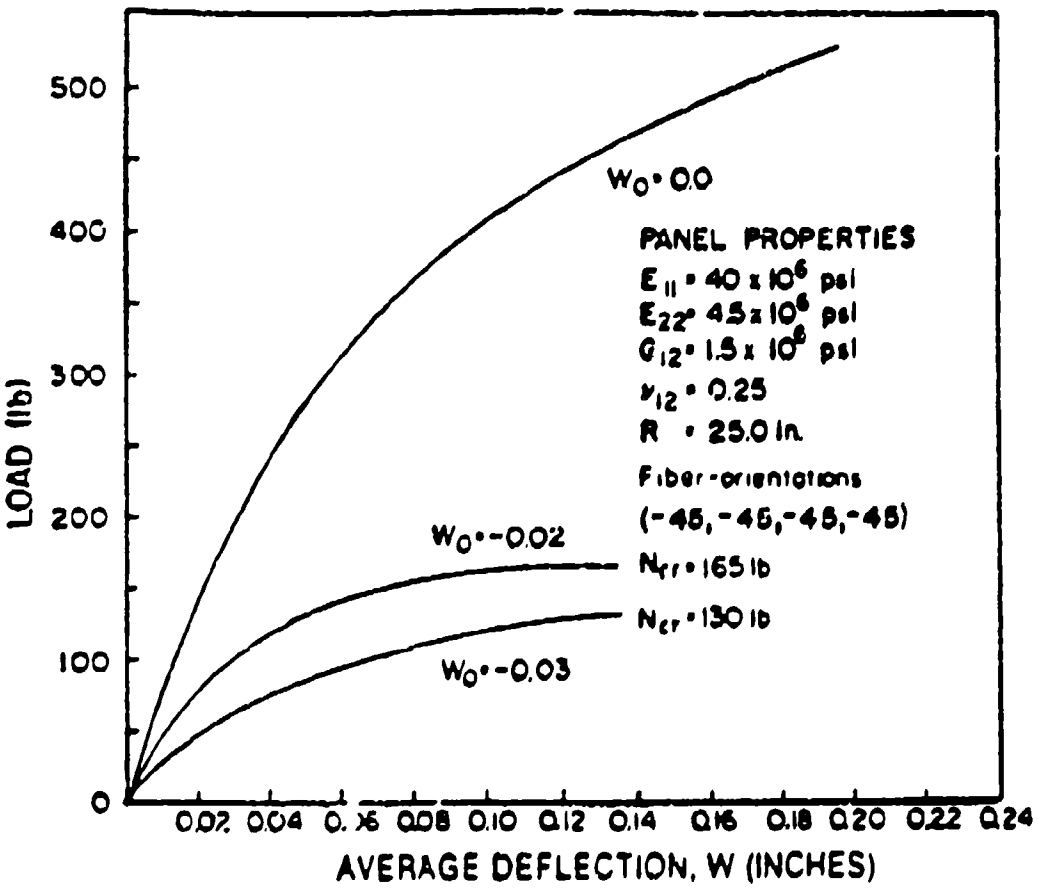

Figure 11.7. Effect of initial imperfections on load deflection curves for an axially loaded, symmetrically laminated shell panel.

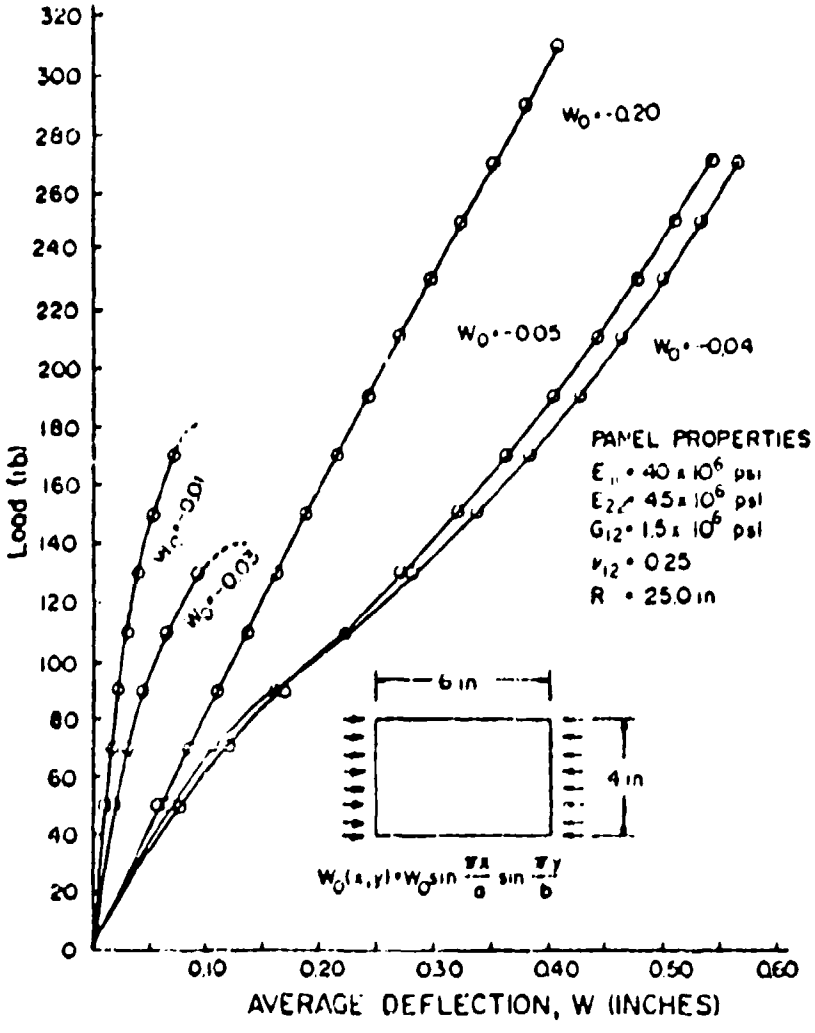

Figure 11.8. Effect of initial imperfections on load-deflection curves for an axially loaded, unsymmetrically laminated shell panel.

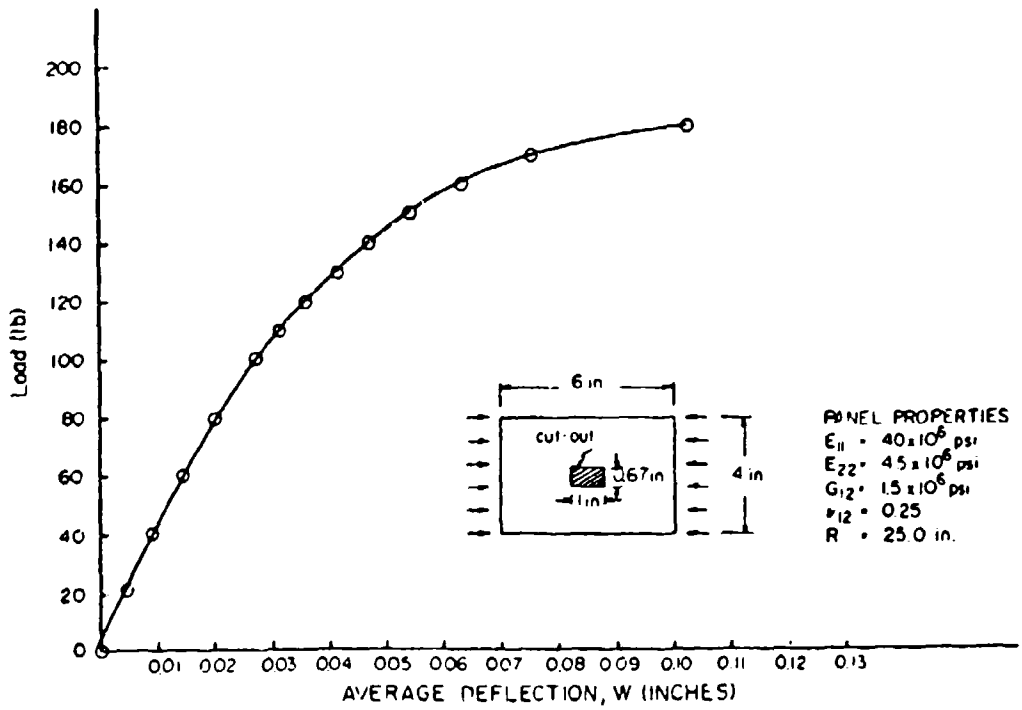

Figure 11.9. Load-deflection curve for an unsymmetrically laminated shell panel having a rectangular cutout.

Figures 11.7 and 11.8 [386] demonstrate the effects of initial geometric imperfections on the load-deflection curves for the symmetric (-45, +45, +45, -45) and unsymmetric (0, 30, 45, 60) laminates, respectively, which were described in the preceding paragraph. The imperfection shape is a half-sine wave in each direction, with an amplitude w_o. It is interesting to note that, for a given axial load, increased magnitude of imperfection causes increased deflection for the symmetric laminate; however, for the unsymmetric laminate, a maximum appears to occur for $|w_o| = 0.05$ (i.e., twice the shell thickness). For large imperfection magnitude in the latter case ($|w_o| = -0.20$), an essentially linear load-deflection curve is observed in Figure 11.8.

The effect of a centrally located, rectangular cutout on the load-deflection curve of the unsymmetrically (0, 30, 45, 60) laminated shell panel is seen in Figure 11.9 [386]. A limit load (maximum value of curve) was found to be 185 lb, compared with 190 lb for the panel without the small cutout.

Hui [388] used Koiter's [389] approach to study the initial postbuckling behavior of cross-ply, symmetrically laminated SSSS shell panels subjected to axial compression. Geometric imperfections were included in the analysis. Assuming an imperfection shape having the same form as the buckling mode shape (Equation 6.3), it was shown that the load-transverse displacement relationship may be expressed as

$$a^* \xi^2 + (1 - \bar{\sigma}_x) = \bar{\sigma}_x \bar{\xi} \tag{11.1}$$

where $\xi = w_c/h$ and $\bar{\xi} = w_o/h$ are the nondimensional amplitudes of the transverse displacement and the imperfection, respectively, $\bar{\sigma}_x$ is the ratio of the applied axial stress to the critical, bifurcation buckling stress, and a^* is a parameter depending upon the geometric and material properties of the shell panel. Figure 11.10 is a plot of Equation 11.1

for $a^* = 0.670$, which corresponds to an isotropic, homogeneous shell panel having $\nu = 0.3$, $a/\bar{b} = 1$ and $\psi = 1$, where $\bar{b} = R\theta_o$ (see Figure 10.1) is the circumferential arc length, and ψ is a shallowness parameter defined by

$$\psi = \frac{\bar{b}}{2\pi}\sqrt[4]{\frac{12(1-\nu_{12}^2)}{R^2h^2}} \tag{11.2}$$

The asymmetric equilibrium paths shown in Figure 11.10 are all stable for positive $\bar{\xi}$ (i.e., deviation from the perfect circular cylindrical surface by outward bulging). However, for negative $\bar{\xi}$ (inward bulging), the equilibrium paths become unstable as ξ increases, and the panel is imperfection sensitive. For a flat plate, a^* is zero, Equation 11.1 yields a horizontal straight line for $\bar{\xi} = 0$, and the equilibrium paths are symmetric about $\bar{\xi} = 0$.

Figure 11.11 [388] presents values of the a^* parameter as a function of ψ, for shell panels with $a/\bar{b} = 1$ having an infinite number of layers and composed of five materials: isotropic, glass-epoxy, boron-epoxy, graphite-epoxy I and graphite-epoxy II. The elastic modulus ratios for the materials are listed in Table 11.2. It is seen in Figure 11.11 that laminated composite shells having large E_1/E_2 (e.g., graphite-epoxy II) are less imperfection sensitive (i.e., smaller a^*). Figure 11.12 gives values of a^* for graphite-epoxy I panels having $a/\bar{b} = 0.7$, 1.0, 1.4 and numbers of layers (N) = 3, 5, ∞. It is seen that for the shorter panels ($a/\bar{b} = 0.7$) imperfection sensitivity increases with increasing N, whereas for longer panels ($a/\bar{b} = 1.4$), it decreases with increasing N.

Bauld and Khot [390,391] made a study of the buckling behavior of laminated composite, cylindrical shell panels having initial imperfections. The curved edges were loaded in compression and the straight edges were

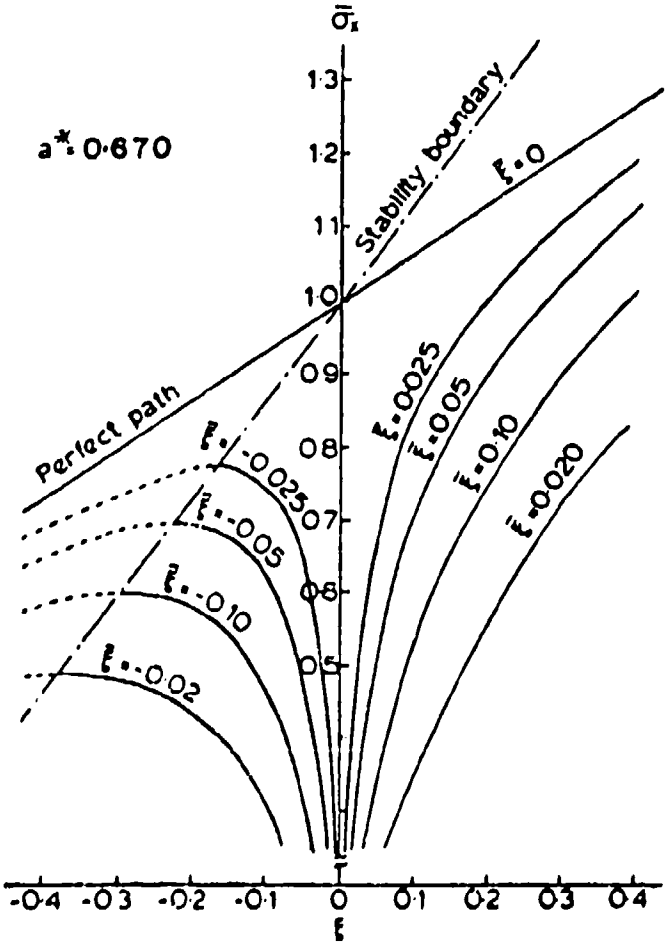

Figure 11.10. Load-transverse deflection curves for isotropic, SSSS shell panels having imperfections.

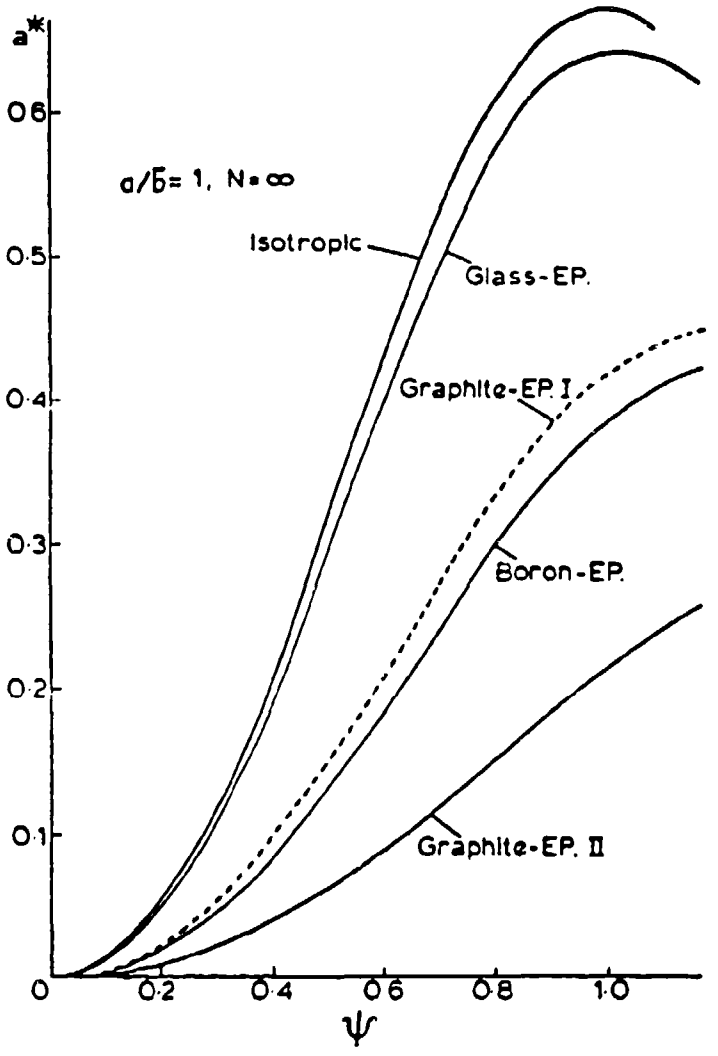

Figure 11.11. Imperfection sensitivity versus shallowness parameter for orthotropic, cross-ply shell panels ($a/\bar{b} = 1$).

Table 11.2. Elastic modulus ratios used by Hui.

Material	$\frac{E_1}{E_2}$	$\frac{G_{12}}{E_2}$	ν_{12}
Isotropic	1.0	0.385	0.30
Glass-epoxy	3.0	0.500	0.25
Boron-epoxy	10.0	0.333	0.22
Graphite-epoxy I	15.8	0.577	0.34
Graphite-epoxy II	40.0	0.500	0.25

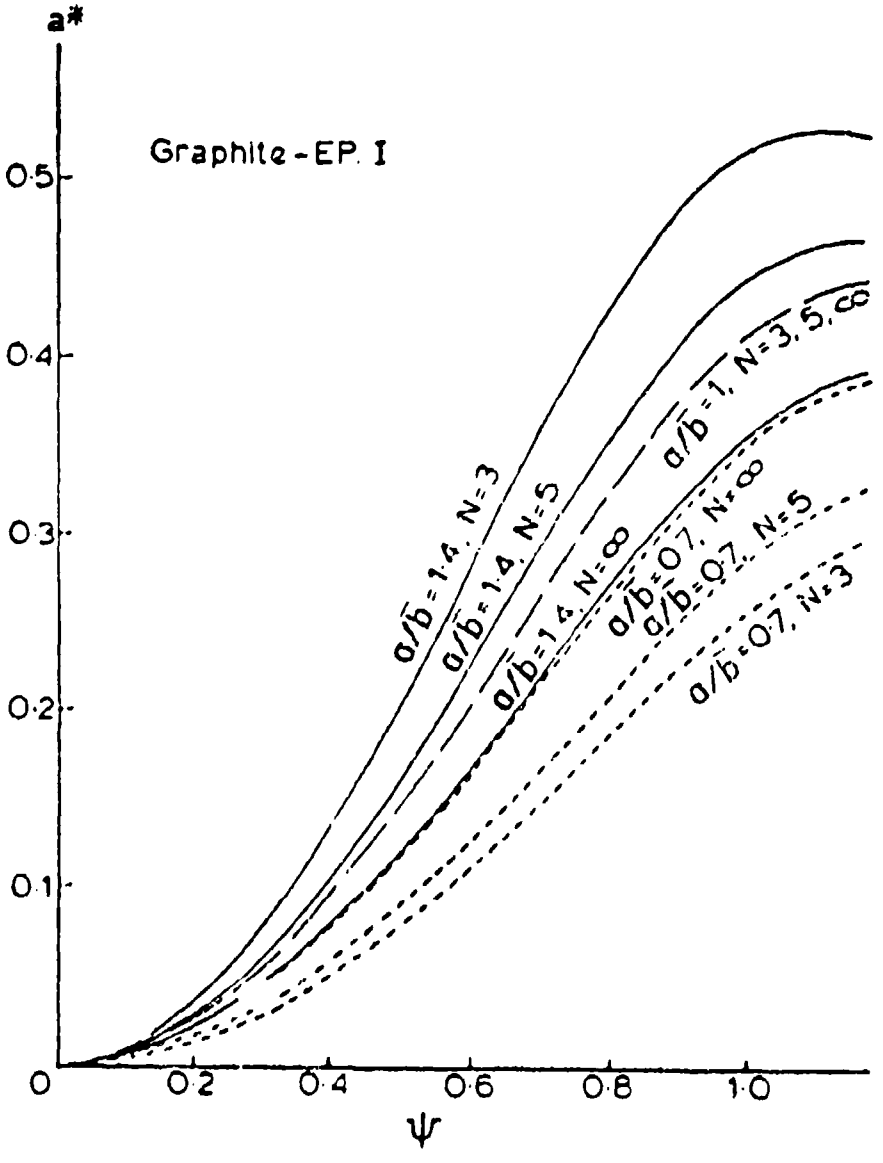

Figure 11.12. Imperfection sensitivity versus shallowness parameter for symmetrically laminated, cross-ply, graphite-epoxy I shell panels.

either simply supported or free. Both theoretical and experimental results were obtained. Theoretical data were calculated using the finite difference, energy computer code previously developed 385-387 .

The initial study [390] was for a set of four panels consisting of eight layers of graphite-epoxy, symmetrically laminated in a $(0/90)_{2s}$ layup. Dimensions were: a = 16 in, b = 8 in, R = 12 in, h = 0.038 in (see Figure 10.1). Composite material properties were: $E_1 = 20.5 \times 10^6$psi, $E_2 = 1.3 \times 10^6$psi, $G_{12} = 0.75 \times 10^6$psi and $\nu_{12} = 0.335$. The imperfection (deviation from a perfect, circular cylindrical surface) for each test specimen was measured mechanically by means of a special fixture. For the two test specimens used with free straight edges, imperfection data was fit to the imperfection function

$$\bar{w} = w_o(1 + \cos \frac{2\pi x}{a}) \tag{11.3}$$

where x is measured from the center of the panel. Figure 11.13 shows load - end shortening curves determined from tests on the two specimens, as well as three analytical curves obtained using w_o = 0, 0.005, 0.010 (in) as imperfection amplitudes in Equation 11.3. Corresponding theoretical curves are seen in Figure 11.14 for the load plotted versus the least squares average of the transverse displacement (w) computed over the shell surface. Figure 11.15 shows the load-shortening curves for two CSCS test specimens. Theoretical limit loads of 2522 and 4311 lb were determined, depending upon whether the circumferential displacement at the straight edges was not or was constrained, respectively. Curves showing the load plotted versus average transverse displacement for the two types of straight edge conditions may be seen in Figures 11.16 and 11.17. The importance of the circumferential displacement along the straight edges is evident from these plots.

Subsequent investigation of ten additional test specimens was made [391]. All ten had the dimensions: a = 16 in, b = 12 in, R = 12 in, h =

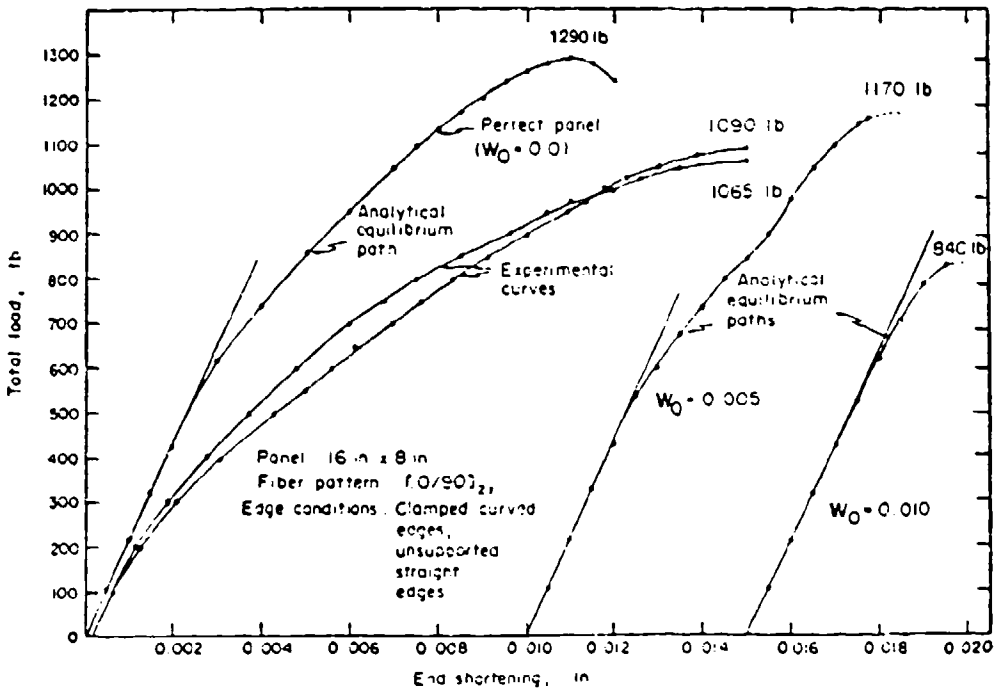

Figure 11.13. Load-end shortening curves for axially loaded CFCF, 16x8, shell panels having geometric imperfections.

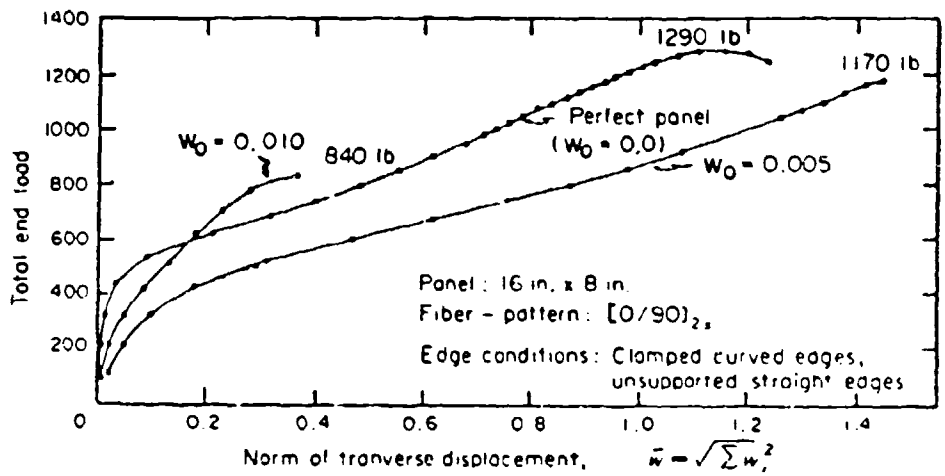

Figure 11.14. Theoretical load-transverse displacement curves corresponding to Figure 11.13.

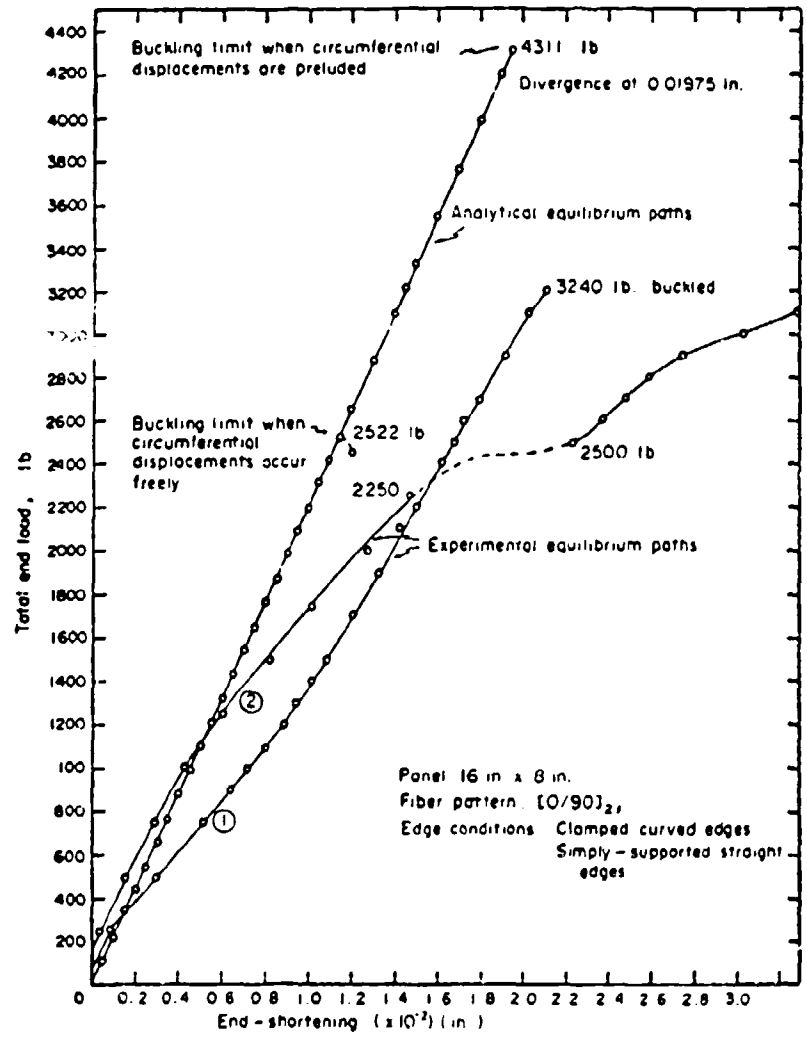

Figure 11.15. Load-end shortening curves for axially loaded, 16x8, shell panels.

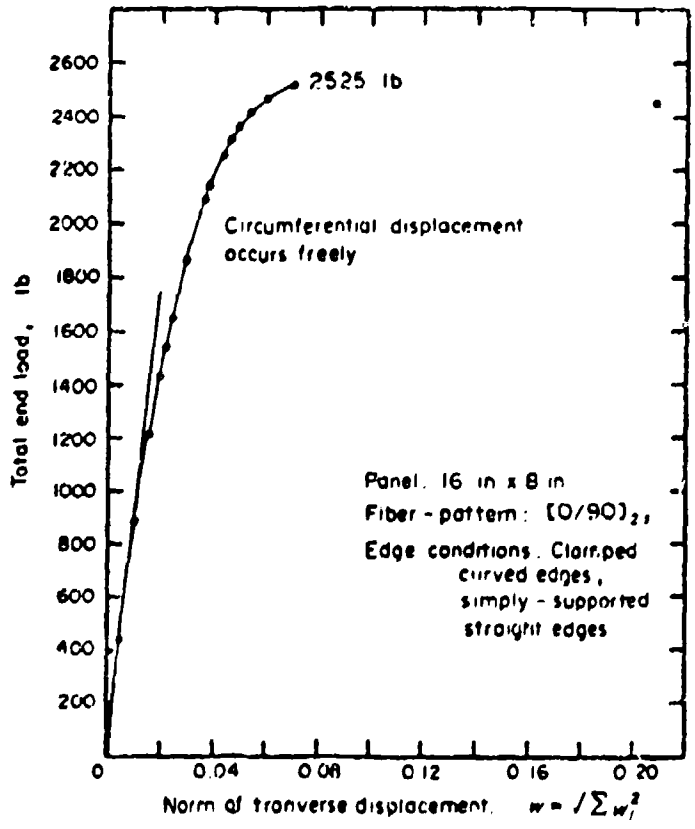

Figure 11.16. Theoretical load-transverse displacement curves corresponding to Figure 11.12 (straight edges not constrained circumferentially).

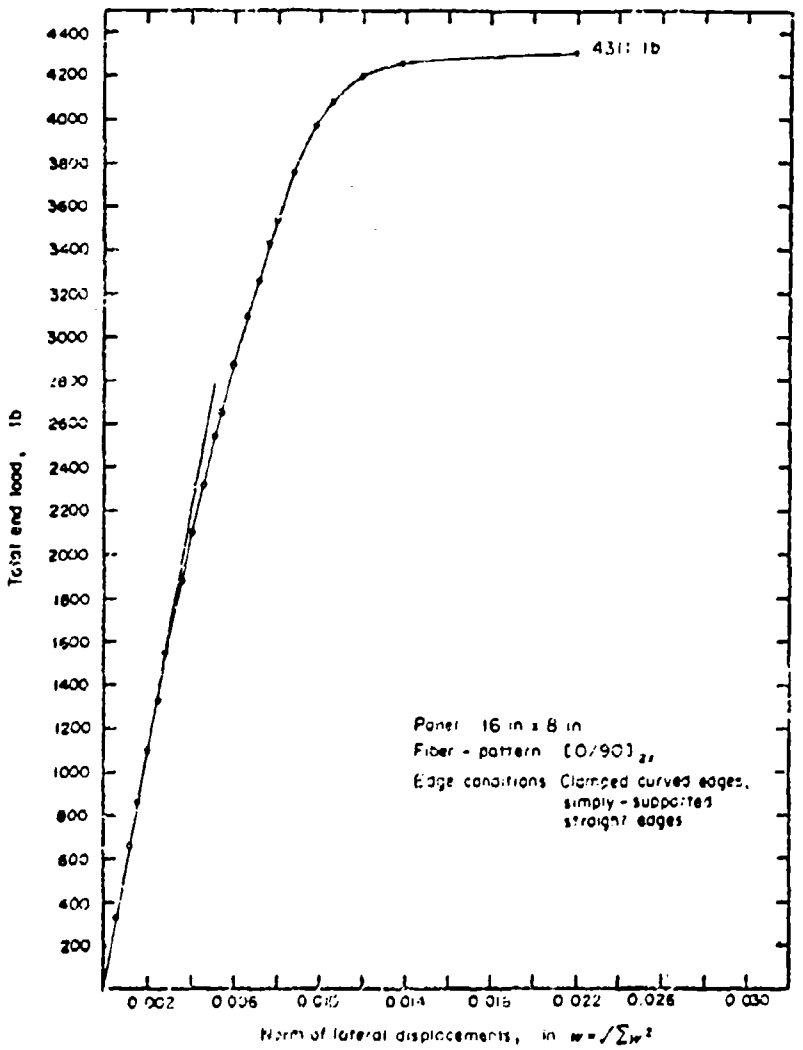

Figure 11.17. Theoretical load-displacement curves corresponding to Figure 11.12 (straight edges constrained circumferentially).

0.038 in (thus, only the width was different from the preceding specimens described earlier). Shell panels were fabricated with eight plies having the same boron-epoxy material described above. Five panels having simply supported straight edges had a $(0/+45/-45/90)_s$ layup and five others with free straight edges had a $(0/90)_{2s}$ layup. Initial imperfection data was measured for one CSCS panel and one CFCF panel and is shown in Figure 11.18. This data was used as the basis for subsequent theoretical calculations. The effects of axial load upon end shortening and average transverse displacement for the CSCS panels are shown in Figures 11.19 and 11.20, respectively. Two theoretical curves are shown in each figure, corresponding to straight edges with or without restraint of the circumferential displacements. Theoretical and experimental end-shortening curves for the CFCF panel are seen in Figure 11.21. Two theoretical curves for the average transverse displacement are given in Figure 11.22. The solid one results from using the measured imperfection data. The dashed curve arose from a previous study [392] which showed it to be the limiting case when the imperfection magnitude is decreased. Figures 11.23 and 11.24 compare the transverse displacements of lines taken along the shell generators (i.e., axial lines) located at the straight edges and the centerline, respectively, for the CFCF shell panel having the measured imperfection subjected to various axial loads. It is seen that the free edges deflect considerably more than the centerline.

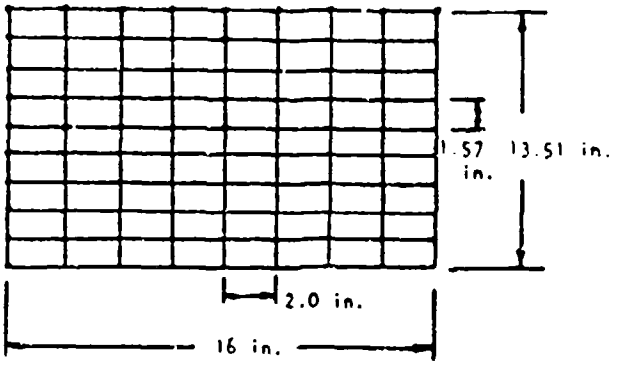

CSCS Panel

0.000	0.000	0.000	0.000	0.000	0.000	0.000	0.000	0.000
0.000	0.001	0.000	-0.003	-0.007	-0.009	-0.009	-0.006	0.000
0.000	0.000	-0.001	-0.003	-0.004	-0.007	-0.006	-0.007	0.000
0.000	-0.002	-0.001	0.000	-0.004	-0.006	-0.006	-0.007	0.000
0.000	0.001	-0.001	0.000	-0.004	-0.007	-0.004	-0.004	0.000
0.000	0.000	-0.001	-0.002	-0.003	-0.007	-0.004	-0.005	0.000
0.000	0.002	0.004	0.005	0.002	0.000	-0.002	-0.004	0.000
0.000	0.006	0.012	0.012	0.010	0.007	0.004	0.000	0.000
0.000	0.000	0.000	0.000	0.000	0.000	0.000	0.000	0.000

CFCF Panel

0.000	-0.006	-0.009	-0.009	-0.011	-0.012	-0.013	-0.013	0.000
0.000	-0.003	-0.005	-0.005	-0.008	-0.010	-0.010	-0.008	0.000
0.000	0.002	0.001	-0.002	-0.005	-0.006	-0.006	-0.007	0.000
0.000	-0.001	-0.001	-0.003	-0.006	-0.008	-0.007	-0.007	0.000
0.000	-0.001	-0.001	-0.005	-0.007	-0.009	-0.009	-0.006	0.000
0.000	-0.003	-0.002	-0.006	-0.007	-0.007	-0.008	-0.008	0.000
0.000	0.000	0.000	-0.003	-0.004	-0.007	-0.006	-0.005	0.000
0.000	0.007	0.009	0.007	0.002	-0.002	-0.003	-0.006	0.000
0.000	0.010	0.014	0.012	0.008	0.002	-0.004	-0.009	0.000

Figure 11.18. Measured initial transverse imperfections (in) for CSCS and CFCF shell panels.

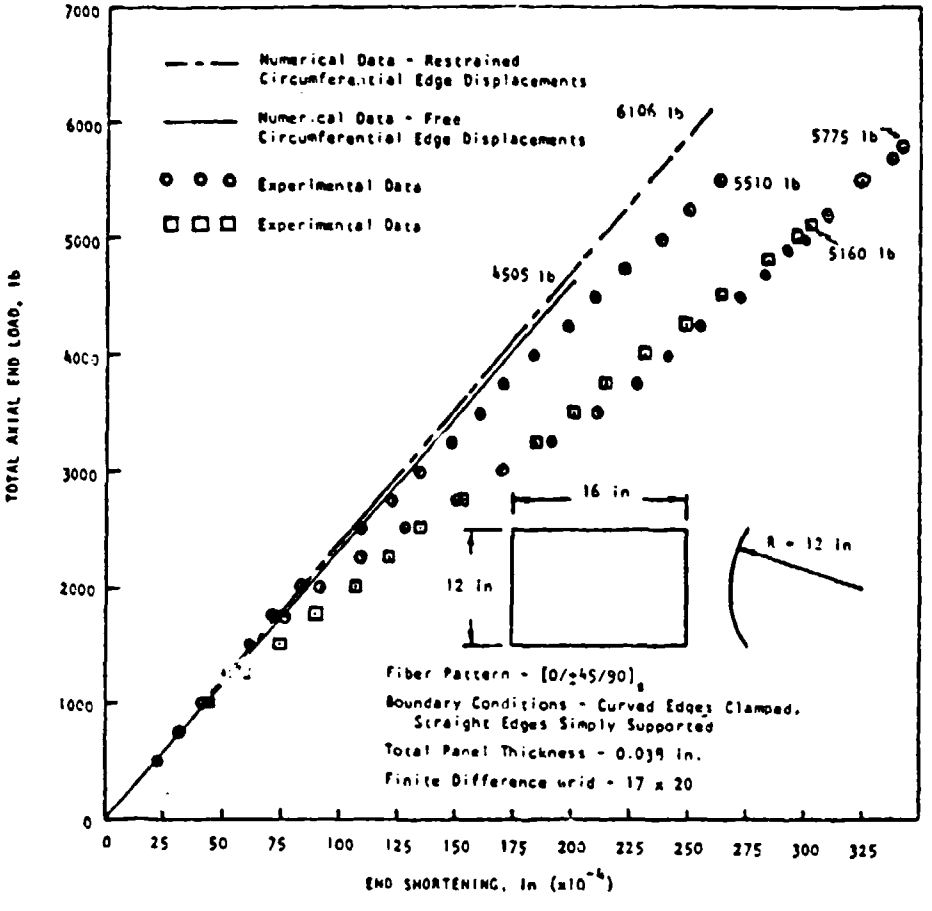

Figure 11.19. Theoretical and experimental load - end shortening results for axially loaded, 16x12, CSCS shell panels.

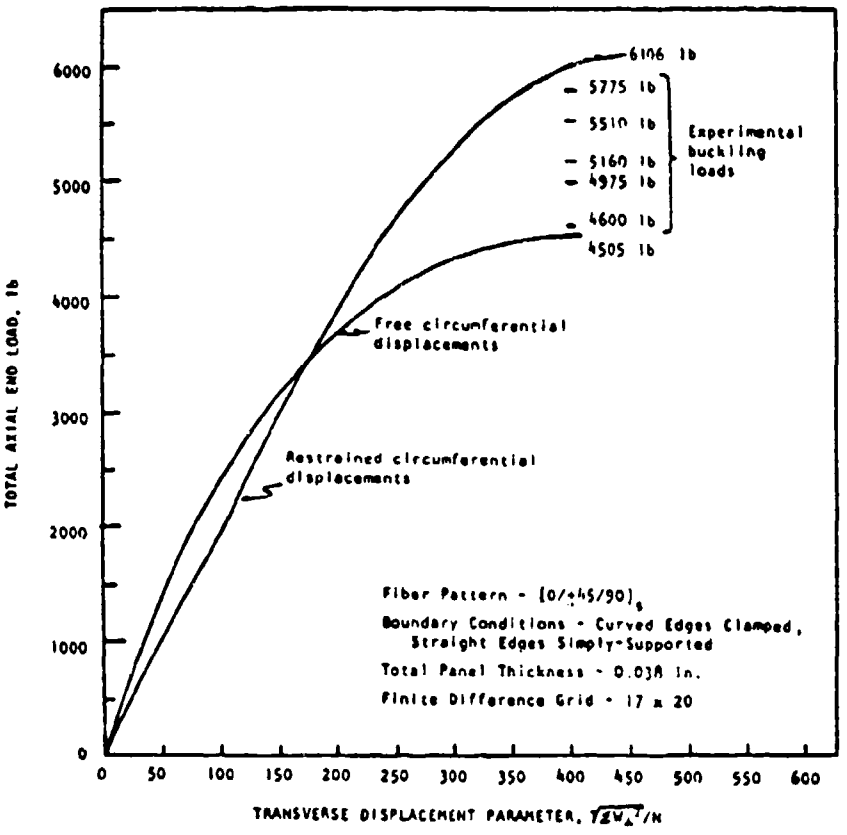

Figure 11.20. Theoretical load - transverse displacement curves for axially loaded, 16x12, CSCS shell panels.

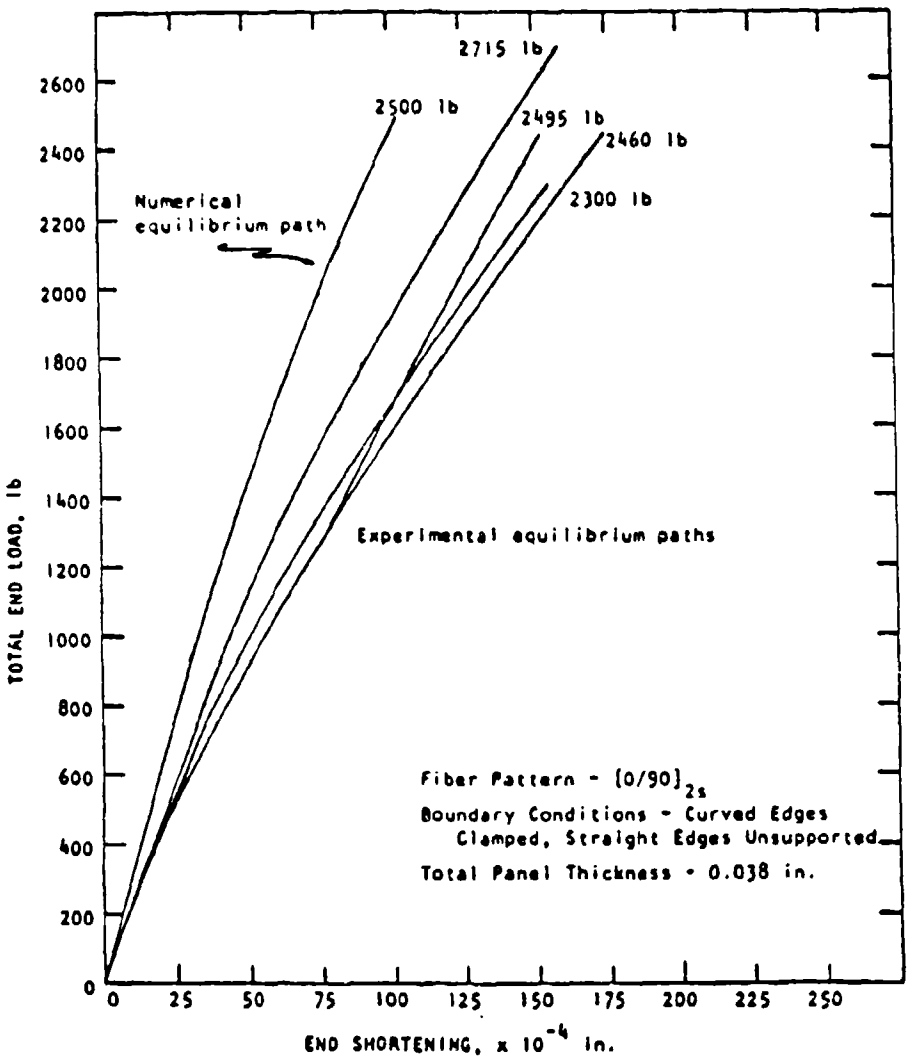

Figure 11.21. Theoretical and experimental load - end shortening curves for axially loaded, CFCF shell panels.

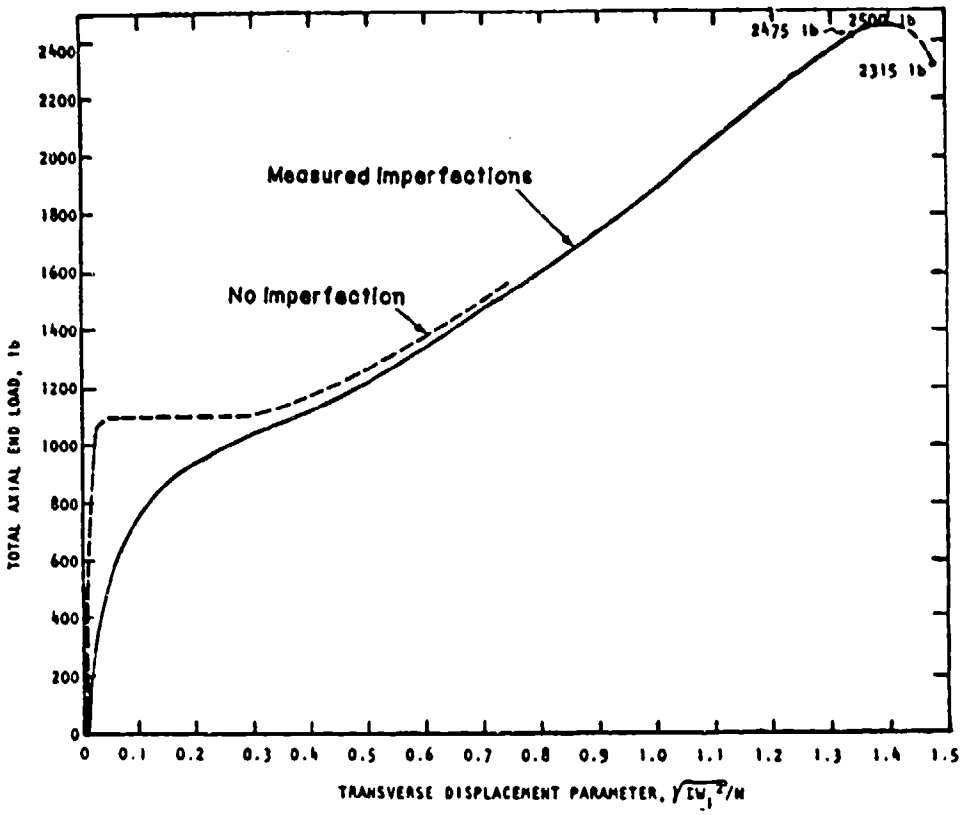

Figure 11.22. Theoretical load - transverse displacement curves for axially loaded, 16x12, CFCF shell panels.

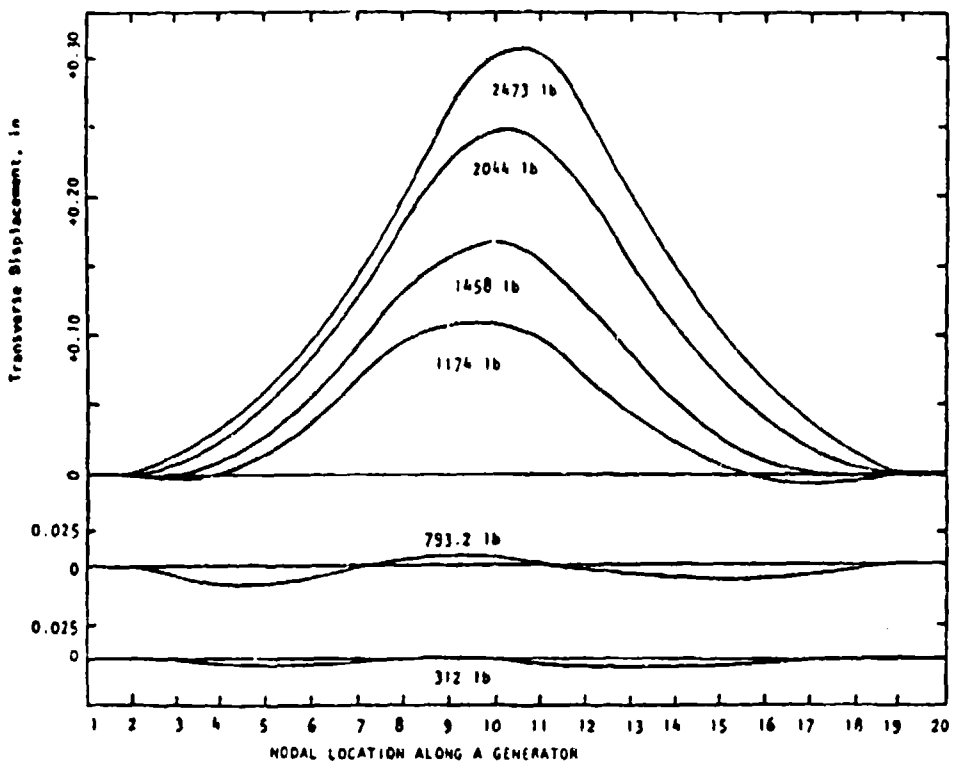

Figure 11.23. Theoretical transverse displacements of the straight edge generator of a CFCF shell panel with imperfections.

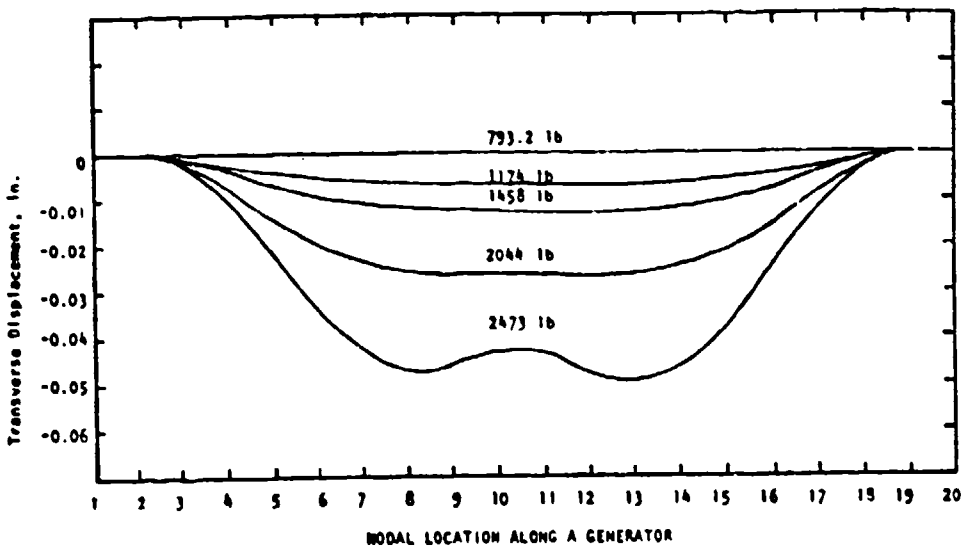

Figure 11.24. Theoretical transverse displacements of the centerline generator of a CFCF shell panel with imperfections.

REFERENCES

1. Bryan, G. H., "On the Stability of a Plane Plate Under Thrusts in its Own Plane, with Applications to the "Buckling" of the Sides of a Ship", Proc. London Mathematical Society, Vol. 22, pp. 54-67 (1981).

2. Timoshenko, S. P. and Gere, J. M., Theory of Elastic Stability, Second Edition, McGraw-Hill Book Co., 541 pp. (1961).

3. Volmir, A. S., Stability of Elastic Systems (in Russian), Gosudarstvennoye Izdatelstvo, Moscow, 879 pp. (1963). Also available in English as Foreign Technology Div. translation MT 64-335 (AD No. 628 508), 1028 pp. (1965).

4. Volmir, A.S., Stability of Deformable Systems (in Russian), Izdatyelstvo "Nauka", Moscow, 984 pp. (1967).

5. Ziegler, H., Principles of Structural Stability, Blaisdell Publishing Co., 150 pp. (1968).

6. Simitses, G. J., An Introduction to the Elastic Stability of Structures, Prentice-Hall, Inc., 253 pp. (1976).

7. Brush, D. O. and Almroth, B. O., Buckling of Bars, Plates and Shells, McGraw-Hill Book Co., 379 pp. (1975).

8. Gerard, G. and Becker, H., "Handbook of Structural Stability. Part I - Buckling of Flat Plates", NACA TN 3781, 102 pp. (1957).

9. Bulson, P. S., The Stability of Flat Plates, Chatto and Windus, Ltd., London, 470 pp. (1970).

10. Column Research Committee of Japan, Handbook of Structural Stability, Corona Publishing Co., Ltd., Tokyo, 1064 pp. (1971).

11. Johns, D. J., "Shear Buckling of Isotropic and Orthotropic Plates: A Review", Aeronautical Research Council, London, Reports and Memoranda, No. 3677, 34 pp. (1971).

12. Leissa, A. W., "Advances and Trends in Plate Buckling Research", Proc. Symp. on Advances and Trends in Structures and Solid Mechanics, Washington, D.C., Oct. 4-7 (1982).

13. Ambartsumyan, S. A., Theory of Anisotropic Plates, Technomic Publishing Co., Stamford, Conn. (1970).

14. Ashton, J. E. and Whitney, J. M., Theory of Laminated Plates, Technomic Publishing Co., Stamford, Conn., 153 pp. (1970).

15. Chia, C.-Y., Nonlinear Analysis of Plates, McGraw-Hill Book Co., 422 pp. (1980).

16. Jones, R. M., Mechanics of Composite Materials, Scripta Book Co., Washington, D.C., 355 pp. (1975).

17. Lekhnitskii, S. G., Anisotropic Plates, Second Edition, translated from the Russian by S. W. Tsai and T. Cheron, Gordon and Breach Science Publishers, Inc., 534 pp. (1968).

18. Vinson, J. R. and Chou, T. W., Composite Materials and Their Use in Structures, Applied Science Publishers, Ltd., London, 438 pp. (1975).

19. Dong, S. B., Pister, K. S. and Taylor, R. L., "On the Theory of Laminated Anisotropic Shells and Plates", Journal of the Aeronautical Sciences, Vol. 29. pp. 969-975 (1962).

20. Reissner, E. and Stavsky, Y., "Bending and Stretching of Certain Types of Heterogeneous Aeolotropic Elastic Plates", Trans. ASME, Journal of Applied Mechanics, Vol. 9, pp. 402-408 (1961).

21. Bergmann, S. and Reissner, H., "Neuere Probleme aus der Flugzeugstatik. Ueber die Knickung von Wellblechstreifen bei Schubbeanspruchung", Z.F.M., Vol. 20 (1929).

22. Schmieden, C., "Das Ausknicken versteifter Bleche unter Schubbeanspruchung", Z.F.M., Vol. 21 (1930).

23. Gerard, G. and Becker, H., "Handbook of Structural Stability. Part VII. - Strength of Thin-Wing Construction", Technical Note, NACA TN D-162, 83pp. (1959).

24. Baiabukh, L. I., "Stability of Plywood Sheets" (in Russian), Tekhnika Vozdushnogo Flota (1937).

25. March, H., "Buckling of Flat Plywood Plates in Compression, Shear, or Combined Compression and Shear", Forest Products Lab., Madison, Wis.,Rept. No. 1316 (1942).

26. Green, A. E. and Hearmon, R. F. S., "The Buckling of Flat Rectangular Plywood Plates", Philosophical Magazine, Series 7, Vol. 36, p. 659 (1945).

27. Almroth, B. O., "Design of Composite Material Structures for Buckling - An Evaluation of the State-of-the-Art", Wright Patterson Air Force Base, Technical Report AFWAL-TR-81-3102, 66 pp. (1981).

28. Bert, C. W., "Optimal Design of Composite-Material Panels for Business Aircraft", Presented at the Society of Automative Engineers Business Aircraft Meeting, Wichita, Kansas, Mar.29 -April 1, 1977, 13 pp. (1977).

29. Bert. C. W. and Francis, P. H., "Composite Material Mechanics: Structural Mechanics", AIAA Journal, Vol. 12, No. 9, pp. 1173-1186 (1974).

30. Leissa, A. W., "Advances in Vibration, Buckling and Postbuckling Studies on Composite Plates", Composite Structures, (Proc. First Inter. Conf.. on Compos. Struct., Paisley, Scotland, Sept. 16-18, 1981), Edited by I.H. Marshall, Applied Science Publishers, pp. 312-334 (1981).

31. Leissa, A. W., "Buckling of Composite Plates", Composite Structures, Vol. 1, pp. 51-66 (1983).

32. Fogg, L., "Stability Analysis of Laminated Materials", State of the Art Design and Analysis of Advanced Composite Materials, Lockheed California Company, Sessions I and II, 162 pp. (1981).

33. Leissa, A. W. and Vagins, M., "The Design of Orthotropic Materials for Stress Optimization", International Journal of Solids and Structures, Vol. 14, pp. 517-526 (1978).

34. Mandell, J. F., "An Experimental Study of the Buckling of Anisotropic Plates", M.S.Thesis (and Report No. 23), Case Western Reserve University, Division of Solid Mechanics, Structures and Mechanical Design, 315 pp. (June, 1968).

35. Mandell, J. F., "An Experimental Investigation of Anisotropic Fiber Reinforced Plastic Plates", Technical Report, AFML TR 68-281 (1968).

36. Hoff, N. J., Boley, B. A. and Coan, J. M., "The Development of a Technique for Testing Stiff Panels in Edgewise Compression", Proc. Society of Experimental Stress Analysis, Vol. 5, No. 2, pp. 14-24 (1948).

37. Dekker, J., Kuipers, J., et al., "Buckling Strength of Plywood. Results of Tests and Design Recommendations", Heron, (Delft), Vol. 23, No. 4, pp. 5-59 (1978).

38. Knutsson, L., "Theoretical and Experimental Investigation of the Buckling and Post-Buckling Characteristics of Flat CFRP Panels Subjected to Compression", Aeronautical Research Institute of Sweden, Stockholm, Structures Dept., Report No.: FFA-TN-HU-1934, 26 pp. (Aug. 1978).

39. Willey, B. T., "Instability of Glass Fiber Reinforced Plastic Panels under Axial Compression", Stanford Univ., California, Dept. of Aeronautics and Astronautics, Technical Report, Contract: DA-44-177-AMC-115(T), 62 pp. (Sept. 1971).

40. Southwell, R. V., "On the Analysis of Experimental Observations in Problems of Elastic Stability", Proc. Royal Society, London, Series A, Vol. 135, p. 601 (1932).

41. Chamis, C. C., "Micro and Structural Mechanics and Structural Synthesis of Multilayered Filamentary Composite Panels", Case Western Reserve University, Rept. No. SMSMDD 9, Contract No. AF33(615)-3112 (1967).

42. Ashton, J. E., "Anisotropic Plate Analysis", General Dynamics Corp., Research and Engineering Rept. FZM-4899, 161 pp. (Oct. 1967).

43. Chamis, C. C., "Buckling of Anisotropic Composite Plates", Proc. ASCE, Journal of the Structural Division, Vol. 95 (ST 10), pp. 2119-2139 (1969).

44. Chamis, C. C., "Buckling of Anisotropic Plates, Closure and Errata", Proc. ASCE, Journal of the Structural Division, Vol 97, pp. 960-962 (1971).

45. Chamis, C. C., "Theoretical Buckling Loads of Boron/Aluminum and Graphite/Resin Fiber-Composite Anisotropic Plates", Technical Note, NASA TN D-6572, 36 pp. (Dec. 1971).

46. Chamis, C. C., "Buckling of Boron/Aluminum and Graphite/Resin Fiber Composite Panels", Proc. Natl. SAMPE Conf. on Space Shuttle Materials (1971).

47. Das, Y. C., "Buckling of Rectangular Orthotropic Plates", Applied Scientific Research (A), Vol. II, pp. 97-103 (1962).

48. Engineering Sciences Data Unit., London, England, "Buckling of Flat Rectangular Orthotropic Plates (Computer Program)", ESDU-73003, 32 pp. Mar. 1973).

49. Gerard, G. "Minimum Weight Analysis of Orthotropic Plates Under Compressive Loading", Journal of Aerospace Sciences, Vol. 27, No. 64, pp. 21-26,64 (1960).

50. Hudson, R. A., Giri, J. and Simitses, G. J., "Buckling Performance of Folding Cartons", Tappi, Vol. 62, No. 10, pp. 95-98 (1979).

51. Linsenmann, D. R., "Stability of Plates of Composite Materials", AIAA 13th Aerospace Sciences Meeting, Pasadena, Calif., 20-22 Jan. (1975).

52. Pflüger, A., "The Buckling of Anisotropic Rectangular Plates. (Zum Beulproblem der anisotropen Rechteckplatte)" (in German), Ingenieur-Archiv, Vol. 16, No. 2, pp. 111-120 (1947).

53. Samuelson, A., Vestergren, P., Knutsson, L., Wangberg, K. G. and Gamziukas, V., "Stability and Ultimate Strength of Carbon Fiber Reinforced Plastic Panels", "Advances in Composite Materials". Pergamon Press, Headington Hill Hall, Oxford, England, (Proc. 3rd Intern. Conf. on Composite Materials, Paris, France, 26-29 Aug. (1980))

54. Tsay, C. S. and Reddy, J. N., "Bending, Stability and Free Vibrations of Thin Orthotropic Plates by Simplified Mixed Finite Elements", Journal of Sound and Vibration, Vol. 59, No. 2, pp. 307-311 (1978).

55. Yamana, M., "On the Elastic Stability of Aeroplane Structures" (in Japanese), J. Faculty of Engineering, Univ. of Tokyo, Vol. 20 (1933).

56. Zizicas, G. A., "Stability of Thin Anisotropic Elastic Plates", Ph.D.Dissertation, Univ. of California, Los Angeles, Calif. (1952).

57. Wittrick, W. H., "Correlation Between Some Stability Problems for Orthotropic and Isotropic Plates under Bi-Axial and Uni-Axial Direct Stress", Aeronautical Quarterly, Vol. 4 (Part 1), pp. 83-92 (1952).

58. Brunelle, E. J. and Oyibo, G. A., "Generic Buckling Curves for Specially Orthotropic Rectangular Plates", AIAA Journal, (Aug. 1983).

59. Oyibo, G. A., "The Use of Affine Transformations in the Analysis of Stability and Vibrations of Orthotropic Plates", Ph.D.Thesis, Rensselaer Polytechnic Institute, Troy, N.Y. (1981).

60. Harris, G. Z., "The Buckling of Orthotropic Rectangular Plates, including the Effect of Lateral Edge Restraint", International Journal of Solids and Structures, Vol. 11, No. 7/8, pp. 877-885 (1975).

61. Schmieden, C., "Das Ausknicken eines Plattenstreifens unter Schub- und Druckkraften", Zeitschrift fur Angewandte Mathematik, Vol. 15 (1935).

62. Seydel, E., "Contribution to the Problem of Buckling of Reinforced Plates by Tangential Stresses", (in German), DVL-Bericht Luftfahrtforschung, Vol. 8, No. 2, p. 71. (1930). English translation also available as NACA TM-602.

63. Seydel, E., "Schubknickversuche mit Wellblechtafeln", Jahrbuch DVL, R. Oldenburg, Berlin, p. 233 (1931).

64. Seydel, E., "Ausbeul-Schublast rechteckiger Platten (Zahlen, Beispiele und Versuchsergebnisse)", Zeitschrift für Flugtechnik und Motorluftsch., Vol. 24 (1933).

65. Seydel, E., "Buckling of Rectangular Isotropic or Orthogonal-Anisotropic Plates under Shear Stresses", NASA TT F-16240, (Transl. from Ingenieur-Archiv.)

66. Stavsky, Y. and Hoff, N. J., "Mechanics of Composite Structures, Chapter 1", in Composite Engineering Laminates, Editor: A. G. H. Dietz, MIT Press, pp. 5-59 (1969).

67. Southwell, R. V. and Skan, S. W., "On the Stability under Shearing Forces of a Flat Elastic Strip", Proc. Royal Society of London, Series A, Vol. 105, pp. 582-607 (1924).

68. Housner, J. M. and Stein, M., "Numerical Analysis and Parametric Studies of the Buckling of Composite Orthotropic Compression and Shear Panels", Technical Note, NASA TN D-7996, 103 pp. (Oct. 1975).

69. Stein M. and Housner, J. M., "Application of a Trigonometric Finite Difference Procedure to Numerical Analysis of Compressive and Shear Buckling of Orthotropic Panels", Computers & Structures, Vol. 9, No. 1, pp. 17-25 (1978).

70. Anon., "Structural Optimization of Six Different Types of Rectangular Plates Subjected to Combined Shear and Biaxial Compressive Loading", Lockheed-California Company, Rept. LR 21662 (1968).

71. Davenport, O. B. an Bert, C. W., "Buckling of Orthotropic, Curved, Sandwich Panels Subjected to Shear Edge Loads", Journal of Aircraft, Vol. 9, No. 7, pp. 477-480 (1972).

72. Libove, C., "Buckling of Orthotropic Plates", 4th edition of Structural Stability Research Council, "Guide to Stability Design Criteria for Metal Structures", 10 pp. (1981).

73. Sekeriy-Tsenkovich, Proc. 5th International Congress of Aeronautics (The Hague, Netherlands), Vol. 2, pp. 1071-1080 (1930).

74. Sekerzh-Zch'kovich, "Calculating the Stability of Plywood Sheets as an Anisotropic Plate" (in Russian), Trudy Ts AGI, No. 76 (1931).

75. Smith, R. C. T., "The Buckling of Plywood Plates in Shear", Australian C.S.I.R., Aeronautical Research Labs (Melbourne), Rept. SM 51 (1946).

76. Vestergren, P., "A Theoretical and Experimental Investigation of the Buckling Behaviour of Rectangular CFRP Panels Subjected to Shear Loading", Aeronautical Research Institute of Sweden, Stockholm, Rept. FFA HU-1818 (1977).

77. Sandorff, P. E., "Design of Structural Models with Application to Stiffened Panels Under Combined Shear and Compression", Journal of Aeronautical Sciences, Vol. 23, pp. 623-632 (1956).

78. Zahn, J. J. and Romstad, K. M., "Buckling of Simply Supported Plywood Plates under Combined Edgewise Bending and Compression", U.S. Forest Service, Research Paper FPL 50, 20 pp. (Dec. 1965).

79. Thierauf, G., "An Elementary Method for Calculation of Buckling Values for Orthotropic and Isotropic Rectangular Plates. (Ein elementarer Weg zur Berechnung von Beulwerten orthotroper und isotroper Rechteckplatten)" (in German), Ph.D.Thesis, Technische Hochschule München (West Germany), No. 1, 77 pp. (Jan. 1969).

80. Knoepke, K.-H., "Contribution to the Calculation of the Buckling Loads of Plate Strips with Heat Stresses Variable Across the Width of the Plate" (in German), Deutsche Forschungsanstalt für Luft- und Raumfahrt, Brunswick (West Germany), Institut für Flugzeugbau, DLR-FB-68-33, 31 pp. (May 1968).

81. Nowacki, W., "On Stability Problems of an Orthotropic Plate" (in French), Archives of Mechanics Stosowanej, Vol. 2, No. 3, pp. 169-182 (1950).

82. Brukva, N. F., "Stability of Rectangular Orthotropic Plates", (in Russian), Prikladnaya Mekhanika, Vol. 4, No. 3, pp. 77-85 (1968).

83. Anon., "Buckling of Orthotropic Plates (Corrugated Plate Applications)", Bell Aerosystems, Rept. 7-60-941001 (1961).

84. Bowen, D. V. and Ayers, K. B., "Buckling and Failure of Metal Faced CFRP Sheets in Compression", Composites, Vol. 6, No. 2, pp. 69-74 (1975).

85. Dale, F. A. and Smith, R. C. T., "Grid Sandwich Panels in Compression", Australian Council for Aeronautics, Melbourne, Rept. ACA-16 (April 1945).

86. Mazzolani, F. M. and Visconti, I. C., "Stability of Composite Plates" (in Italian), Aerotecnica Missili e Spazio, Vol. 53, No. 4, pp. 261-276 (1974).

87. Sharifi, P., "Nonlinear Buckling Analysis of Composite Shells", AIAA Journal, Vol. 13, pp. 729-734 (1975).

88. Shuleshko, P., "Reduction Method for Buckling Problems of Orthotropic Plates", Aeronautical Quarterly, Vol. 8, pp. 145-156 (1957).

89. Smith, R. C. T., "The Buckling of Flat Plywood Plates in Compression", Australian Council for Aeronautics, Melbourne, Rept. ACA-12 (Dec. 1944).

90. Soni, S. R. and Amba Rao, C. L., "Vibrations of Orthotropic Rectangular Plates Under Inplane Forces", Computers & Structures, Vol. 4, No. 5, pp. 1105-1115 (1974).

91. Suarez, J. A., "Advanced Composite Wing Structures - Stability Analysis of Advanced Filamentary Composite Panels", Grumman Aircraft Engineering Corp., Tech. Rept. AC-SM-8087 (1970).

92. Viswanathan, A. V., Soong, T. C. and Miller, R. E., Jr., "Buckling Analysis for Axially Compressed Flat Plates, Structural Sections, and Stiffened Plates Reinforced with Laminated Composites", Contractor Report, NASA CR-1887, 75 pp. (Nov. 1971).

93. Viswanathan, A. V., Soong, T. C. and Miller, R. E., Jr., Buckling Analysis for Structural Sections and Stiffened Plates Reinforced With Laminated Composites", International Journal of Solids and Structures, Vol. 8, No. 3, pp. 347-367 (1972).

94. Garashchuk, I. N., Zamula, G. N. and Prikazchikov, V. G., "Numerical Solution of Plate-Stability Problems", Soviet Applied Mechanics, Vol. 14, No. 5, pp. 86-91 (1978).

95. Leissa, A. W., "The Free Vibration of Rectangular Plates", Journal of Sound and Vibration, Vol. 31, pp. 257-293 (1973).

96. Shuleshko, P., "Solution of Buckling Problems by Reduction Method", Proc. ASCE, Journal of the Engineering Mechanics Division, Vol. 90, pp. 147-169 (1964).

97. Massey, C., "The Elastic Buckling of Orthotropic Rectangular Plates", Institution of Engineers, Australia, Civil Engineering Trans., Vol. 13, No. 1, pp. 63-65 (1971).

98. Holston, A., Jr., "Buckling of Orthotropic Plates with one Free Edge", AIAA Journal, Vol. 8, No. 7, pp. 1352-1354 (1970).

99. Lackman, L. M. and Ault, R. M., "Minimum-Weight Analysis of Filamentary Composite Wide Columns", Journal of Aircraft, Vol. 5, No.2, pp. 184-190 (1968).

100. Anon., "Advanced Composite Wing Structures; Preliminary Analysis and Optimization Methods", Grumman Aircraft Engrg. Corp., Technical Report, AC-SM-7843 (1968).

101. Baharlou, B., "Vibration and Buckling of Laminated Composite Plates with Arbitrary Edge Conditions", Ph.D.Dissertation, Ohio State University, 141 pp. (1985).

102. Banks W. M. and Rhodes, J., "The Buckling Behaviour of Reinforced Plastic Box Sections", Proc. 12th Reinforced Plastics Congress, Brighton, Sussex, England, pp. 85-88 (1980).

103. Halstead, D. W., Tripp, L. L., Tamekuni, M. and Baker, L. L., "BUCLAP2: A Computer Program for Instability Analysis of Laminated Long Plates Subjected to Combined Inplane Loads", Contractor Report, NASA CR-132299, 96 pp. (Aug. 1973).

104. Oeverli, V. and Viswanathan, A. V., "BUCLAP - A Computer Program for Uniaxial Compressive Buckling Loads of Orthotropic Laminated Plates", Contractor Report, NASA CR-111869 (1971).

105. Schultz, H.-G., "Zum Stabilitätsproblem elastisch eingespannter orthotroper Platten", Stahlbau, Vol. 32, pp. 22-25 (1963).

106. Sakata, T., "A Reduction Method for Vibrating and Buckling Problems of Orthotropic Continuous Plates", Journal of Sound and Vibration, Vol. 49, No. 1, pp. 45-52 (1976).

107. Nowacki, W., "Bending and Buckling of Certain Types of Continuous Orthotropic Plates (Flexion et Flambage d'un certain type de plaques continues orthotropes)" (in French), Publ. Intern. Assoc. Bridge Struct. Engrg., 3rd Congress, prelim. publ., pp. 519-530 (1948).

108. Leissa, A. W., Vibration of Plates, NASA SP-160, U.S. Govt. Printing Office, Washington, D.C., 353 pp. (1969).

109. Dickinson, S. M., "The Buckling and Frequency of Flexural Vibration of Rectangular Isotropic and Orthotropic Plates Using Rayleigh's Method", Journal of Sound and Vibration, Vol. 61, No. 1, pp. 1-8 (1978).

110. Warburton, G. B., "The Vibration of Rectangular Plates", Proc. of the Institut of Mechanical Engineers, Vol. 168, pp. 371-384 (1954).

111. Leissa, A. W., "The Free Vibration of Rectangular Plates", Journal of Sound and Vibration, Vol. 31, pp. 257-293 (1973).

112. Ashton, J. E. and Love, T. S., "Experimental Study of the Stability of Composite Plates", Journal of Composite Materials, Vol. 3, pp. 230-242 (1969).

113. Chia, C. Y. and Prabhakara, M. K., "Nonlinear Analysis of Orthotropic Plates", Journal of Mechanical Engineering Science, Vol. 17, No. 3, pp. 133-138 (1975).

114. Srinivasan, R. S. and Ramachandran, S. V., "Stability of Generally Orthotropic Skew Plates", Technical Notes, Proc. ASCE, Journal of the Engineering Mechanics Division, Vol. 102, No. 3, pp. 569-572 (1976).

115. Mar, J. W. and Lagace, P. A., "Design Technology of Advanced Composites", Technical Report, AFWAL TR-82-4178, 57 pp. (Nov. 1982).

116. Marquis, W. A., "Fatigue Behavior of Graphite/Epoxy Plates Under Shear Buckling", S.M.Thesis, Dept. of Aeronautics and Astronautics, Mass.Inst.Tech. (1982).

117. Simitses, G. J. and Giri, J., "Buckling of Rotationally Restrained Orthotropic Plates Under Uniaxial Compression", Journal of Composite Materials, Vol. 11, pp. 345-364 (1977).

118. Crouzet-Pascal, J., "Comment on Buckling of Rotationally Restrained Orthotropic Plates Under Uniaxial Compression", Journal of Composite Materials, Vol. 12, pp. 215-218 (1978).

119. Simitses, G. J. and Giri, J., "Response to Dr. Crouzet-Pascal's Comment", Journal of Composite Materials, Vol. 12, pp. 218-219 (1978).

120. Wittrick, W. H., "Rationalization of Anisotropic Buckling Problems", "Contributions to the Theory of Aircraft Structures", Van der Neut Anniversary Vol., Delft University Press, pp. 359-377 (1972).

121. Anon., "A Displacement-Type Finite Element Analysis of Bifurcation Buckling of Rectangular Plates Based on a Conforming Finite Element", Lockheed-California Co., Rept. LR 23841 (1970).

122. Crouzet-Pascal, J., "Buckling Analysis of Laminated Composite Plates", Fibre Science and Technology, Vol. 11, pp. 413-446 (1978).

123. Chao, C. C., Koh, S. L. and Sun, C. T., "Optimization of Buckling and Yield Strengths of Laminated Composites", AIAA Journal (Synoptic), Vol. 13, No. 9, pp. 1131-1132 (1975). Full paper available from NTIS as N75-19370, 33 pp. (May 1974).

124. Chao, C. C., "Optimization of Strength and Stability of Laminated Composites", Ph.D.Thesis, Purdue University, 170 pp. (1974).

125. Bert, C. W. and Chen, T. L. C., "Optimal Design of Composite-Material Plates ot Resist Buckling Under Biaxial Compression", Trans. Japan Soc., Composite Materials (JSCM), Vol. 2, No. 1, pp. 7-10 (1976).

126. Hayashi, T., "Optimum Design of Cross- and Angle-Plied Laminated Composite Plates Under Compression", Composite Materials and Structures (Japan), Vol. 3, No. 2, pp. 18-20 (1974).

127. Hayashi, T., "Optimization for Elastic Buckling Strength of Fiber-Reinforced Composite Structures - Columns, Plates and Cylinders", Proc. 1974 Symp. on Mechanical Behavior of Materials, Kyoto, Japan, 21-24 August (1974).

128. Kominar, V. A., "Stability of a Rectangular Glass-Plate" (in Russian), Bulletin of the All-Union Scientific Research Institute of Rail Transport, Moscow, Vol. 2, pp. 35-38 (1967).

129. Kominar, V. A., "Influence of the Reinforcement Pattern on the Stability of a Rectangular Glass-Plastic Plate" (in Russian), Mekhanika Polymerov, Vol. 6, pp. 1136-1139 (1967).

130. Konishi, D. Y. and Lee, K. J., "Strength and Stability Optimization of an Unstiffened Panel Under Multiple Inplane Loads", Ch. 1.8, Advanced Composites Design Guide, 3rd Ed., Air Force Materials Lab., WPAFB, Ohio (1973).

131. Lukoshevichyus, R. S., "Minimizing the Mass of Reinforced Rectangular Plates Compressed in Two Directions in a Manner Conductive Toward Stability", Polymer Mechanics, Vol. 12, No. 6, pp. 929-933 (1977).

132. Rothwell, A., "Optimum Fibre Orientations for the Buckling of Composite Materials", Fibre Science and Technology, Vol. 2, pp. 111-122 (1969).

133. Schmit, L. A., Jr. and Farshi, B., "Optimum Design of Laminated Fibre Composite Plates", International Journal for Numerical Methods in Engineering, Vol. 11, No. 4, pp. 623-640 (1977).

134. Tashkandi, M. A., "Optimum Design of Laminated Fiber Composite Plates", Ph.D.Thesis, California University, Los Angele, 123 pp. (1976).

135. Verette, R. M., "Stiffness, Strength and Stability Optimization of Laminated Composites", Northrop Aircraft Corp., Hawthorne, Calif., Report NOR-70-138,(1970).

136. Thielemann, W., "Contribution to the Problem of Buckling of Orthotropic Plates, With Special Reference to Plywood", Technical Memorandum, NACA TM-1263, 122 pp. (Aug. 1950).

137. Thielemann, W., "Buckling of Anisotropic Plate Strips" (in German), Deutsche Versuchsanstalt Luftfahrt E.V., Report No. 16, 70 pp (June 1956).

138. Ashton, J. E. and Waddoups, M. E., "Analysis of Anisotropic Plates", Journal of Composite Materials, Vol. 3, pp. 148-165 (1969).

139. Davis, J. G. and Zender, G. W., "Compressive Behavior of Plates Fabricated from Glass Filaments and Epoxy Resin", Technical Note, NASA TN-D-3918 (1968).

140. Movsisyan, L. A. and Peshtmaldzhyan, D. V., "On the Equations of Stability and Vibrations of Anisotropic Plates" (in Russian), Izvestiya Akademii Nauk Armyanskoi SSR, Mekhanika, Vol. 26, No. 6, pp. 18-28 (1973).

141. Petrov, Yu. P., "Calculating Flexure and Stability of Rec' and Nonrectangular Anisotropic Plates by the Differential Difference Method", WPAFB, Foreign Technology Div., Rept. 23-461-70, 23 pp. (Oct. 1970).

142. Prachuktam, S., "Static, Vibration, and Stability Analyses of Anisotropic Plates", Ph.D.Thesis, The University of Akron, 200 pp. (1974).

143. Robinson, J. C. and Blackburn, C. L., "Evaluation of a Hybrid, Anisotropic, Multilayered, Quadrilateral Finite Element", NASA TP-1236, 28 pp. (Aug. 1978).

144. Sarkisyan, V. S. and Movsisyan, L. A., "A Method for Determining the Critical Loads on Anisotropic Plates", Soviet Engineering Journal, Vol. 5, No. 4, pp. 600-602 (1965).

145. Sawyer, J. W., "Flutter and Buckling of General Laminated Plates", Journal of Aircraft, Vol. 14, No. 4, pp. 387-393 (1977).

146. Silberstein, J. P. O. and Smith, R. C. T., "3-Ply Flat Panels in End Compression at 45° to the Grain", Division of Aeronautics, C.S.I.R. Australia, Rept. S. M. 42, (1944).

147. Whitney, J. M., "Analysis of Anisotropic Rectangular Plates", AIAA Journal, Vol. 10, No. 10, pp. 1344-1345 (1972).

148. Whitney, J. M., "On the Analysis of Anisotropic Rectangular Plates", WPAFB, Air Force Materials Lab., Rept. AFML-TR-72-76, 24 pp. (Aug. 1972).

149. Wiggenraad, J. F. M., "A Finite Element Model, to Study the Buckling Behavior of General Orthotropic, Midplane Symmetric and Elastic Plates", National Lucht-en Ruimtevaartlaboratorium, The Netherlands, Technical Report, NLR TR 77062 U, 14 pp. (1977).

150. Sandorff, P. E., Lockheed-California Company, Private communication, (May 14, 1984).

151. Ashton, J. E. and Love, T. S., "Shear Stability of Laminated Anisotropic Plates", Composite Materials: Testing an Design, ASTM STP 460, pp. 352-361 (1969).

152. Freiberger, W., Shaw, F. S., Silberstein, J. P. O. and Smith, R. C. T., "Plywood Panels in End Compression: Flat Panels with Grain at Various Angles to Direction of Loading", Australian Council for Aeronautics, No. 30, pp. 3-35 (Jan. 1947).

153. Ringelstetter, L. A., "Buckling Tests of Flat Plywood Plates in Compression with Face Grain 45° to Load - Loaded Edges Clamped, Others Simply Supported", Forest Products Lab. Rept. No. 1316-J., 7 pp. (1949).

154. Whitney, J. M., "Fourier Analysis of Clamped Anisotropic Plates", Trans. ASME, Journal of Applied Mechanics, Series E, Vol. 38, No. 2, pp. 530-532 (1971).

155. Whitney, J. M., "Fourier Analysis of Clamped Anisotropic Plates", Wright-Patterson AFBML, Ohio, Technical Rept. AFML-TR-70-281, 17 pp. (Feb. 1971).

156. Fraser, H. Jr., "Bifurcation Type Buckling of Generally Orthotropic Plates", Ph.D.Dissertation, University of Illinois (1968).

157. Fraser, H. R., Jr. and Miller, R. E., "Bifurcation Type Buckling of Generally Orthotropic Clamped Plates", AIAA Journal, Vol. 8, No. 4, pp. 707-712 (1970).

158. Jones, R. M., "Buckling and Vibration of Unsymmetrically Laminated Cross-Ply Rectangular Plates", AIAA Journal, Vol. 11, No. 12, pp. 1626-1632 (1973).

159. Stavsky, Y., "On the Theory of Heterogeneous Anisotropic Plates", Doctoral Thesis, Massachusetts Institute of Technology, Cambridge, Mass. (1959).

160. Smith, C. B. (Forest Products Laboratory), Letter to E. Reissner (1961).

161. Broutman, L. J., Haslett, W. H., Krokosky, E. M., Roy, J. R. and McGarry, F. J., "Investigation of Mechanics of Reinforced Plastics", Aeronautical Systems Div., WPAFB, WADD-TR-60-746, Pt. II (1962).

162. Ashton, J. E., "Approximate Solutions for Unsymmetrical Laminated Plates", Journal of Composite Material, Vol. 3, pp. 189-191 (1969).

163. Whitney, J. M., "Bending, Vibrations, and Buckling of Laminated Anisotropic Rectangular Plates", Wright Patterson AFBML, Ohio, Technical Rept. AFML-TR-70-75, 35 pp. (Aug. 1970).

164. Whitney, J. M., "The Effect of Boundary Conditions of the Response of Laminated Composites", Journal of Composite Materials, Vol. 4, pp. 192-203 (1970).

165. Whitney, J. M., "A Study of the Effects of Coupling Between Bending and Stretching on the Mechanical Rehavior of Layered Anisotropic Composite Materials", Ph.D.Dissertation, Ohio State University (1968), also Tech. Rept. AFML-TR-68-330, 80 pp. (Apr. 1969).

166. Whitney, J. M. and Leissa, A. W., "Analysis of Heterogeneous Anisotropic Plates" Trans. ASME, Journal of Applied Mechanics, Vol. 36, No. 2, pp. 261-266 (1969).

167. Leissa, A. W. and Kadi, A. S., "Curvature Effects on Shallow Shell Vibrations", Journal of Sound and Vibration, Vol. 16, pp. 173-187 (1971).

168. Leissa, A. W., Vibration of Shells, NASA SP-288, U.S.Govt. Printing Office, 428 pp. (1973).

169. Chen, T. L. C. and Bert, C. W., "Design of Composite-Material Plates for Maximum Uniaxial Compressive Buckling Load", Proc. of the Oklahoma Academy of Science, Vol. 56, pp. 104-107 (1976).

170. Jones, R. M., Morgan, H. S., Whitney, J. M., "Buckling and Vibration of Antisymmetrically Laminated Angle-Ply Rectangular Plates", Trans. ASME, Journal of Applied Mechanics, Vol. 12, pp. 1143-1144 (1973).

171. Whitney, J. M. and Leissa, A. W., "Analysis of a Simply Supported Laminated Anisotropic Rectangular Plate", AIAA Journal, Vol. 8, No. 1, pp. 28-33 (1970).

172. Kicher, T. P. and Mandell, J. F., "A Study of the Buckling of Laminated Composite Plates", AIAA Journal, Vol. 9, No. 4, pp. 605-613 (1971).

173. Monforton, G. R., "Discrete Element Finite Displacement Analysis of Anisotropic Sandwich Shells", Ph.D.Thesis, Case Western Reserve University (1970).

174. Chailleux, A., Hans, Y. and Verchery, G., "Experimental Study of the Buckling of Laminated Composite Columns and Plates", International Journal of Mechanical Sciences, Vol. 17, No. 8, pp. 489-498 (1975).

175. Chailleux, A. and Hans, Y., Internal Report No. 007, ENSTA (Paris) (1972).

176. Verchery, G., Internal Report No. 010, ENSTA (Paris) (1973).

177. Whitney, J. M., "Shear Buckling of Unsymmetrical Cross-Ply Plates", Journal of Composite Materials, Vol. 3, pp. 359-363 (1969).

178. Hui, D., "Shear Buckling of Anti-Symmetric Cross-Ply Rectangular Plates", Fibre Science and Technology, Vol. 21, pp. 327-340 (1984).

179. Hirano, Y., "Optimum Design of Laminated Plates Under Shear", Journal of Composite Materials, Vol. 13, pp. 329-334 (1979).

180. Hirano, Y., "Stability Optimization of Laminated Composite Plates", Tokyo University Japan, Inst. of Space and Aeronautical Science, ISAS-579, Vol. 45, No. 4. Also NASA CR-163456, 19 pp. (July 1980).

181. Chia, C. Y. and Prabhakara, M. K., "Postbuckling Behavior of Unsymmetrically Layered Anisotropic Rectangular Plates", Trans. ASME, Journal of Applied Mechanics, Vol. 41, pp. 155-162 (1974).

182. Harris, G. Z., "The Buckling and Post-Buckling Behavior of Composite Plates under Biaxial Loading", International Journal of Mechanical Sciences, Vol. 17, No. 3, pp. 187-202 (1975).

183. Jones, R. M., "Mechanics of Composite Materials with Different Moduli in Tension and Compression", Southern Methodist University, Dallas, Texas, Dept. of Civil and Mech. Engineering, Grant: AF-AFOSR-2532-73, Project: AF-9782, 41 pp. (July 1975).

184. Jones, R. M., "Mechanics of Composite Materials with Different Moduli in Tension and Compression", Southern Methodist University, Dallas, Texas, Dept. of Civil and Mech. Engineering, Grant: AF-AFOSR-2532-73, Project: AF-9782, 48 pp (July 1974).

185. Kicher, T. P., "Predicting Structural Behavior of Composites", Proc. 26th Annual Tech. Conf. of the Society of the Plastic Industry, Inc. (1971).

186. Prabhakara, M. K. and Kennedy, J. B., "Nonlinear Behaviour of Unsymmetric, Angle-Ply, Rectangular Plates under In-Plane Edge Shear", Journal of Mechanical Engineering Science, Vol. 21, No. 3, pp. 205-214 (1979).

187. Sawyer, J. W., "Flutter of Laminated Plates in Supersonic Flow", Technical Memorandum, NASA TM X-72800 (1975).

188. Zhang, Y. and Matthews, F. L., "Initial Buckling of Curved Panels of Generally Layered Composite Materials", Composite Structures, Vol. 1, pp. 3-30 (1983).

189. Marshall, I. H., Little, W. and El Tayeby, M. M., "The Stability of Composite Panels with Holes", Proc. Reinforced Plastics Congress, Brighton, U.K., pp. 139-141 (1984).

190. Martin, J., "Buckling and Postbuckling of Laminated Composite Square Plates with Reinforced Central Circular Holes", Ph.D.Thesis, Case Western Reserve University, Solid Mechanics Division (Jan. 1972).

191. Nara, H. R., "Interface and Mechanics Research in Fiber Reinforced Composites", Case Western Reserve University, Cleveland, Ohio, Technical Rept. AFML-TR-71-260, 278 pp. (March 1972).

192. Reissner, E., "On the Theory of Bending of Elastic Plates", Journal of Mathematical Physics, Vol. 23, pp. 184-191 (1944).

193. Reissner, E., "The Effect of Transverse Shear Deformation on the Bending of Elastic Plates", Trans. ASME, Journal of Applied Mechanics, Vol. 12, pp. A69-A77 (1945).

194. Ziegler, H., "The Influence of Inplane Deformations on the Buckling Loads of Isotropic Elastic Plates", Ingenieur-Archiv, Vol. 53, pp. 61-72 (1983).

195. Bert, C. W., "A Critical Evaluation of New Plate Theories Applied to Laminated Composites", Proc. Symp. on Mechanics of Composite Materials, ASME (1983). Also University of Oklahoma, School of Aerospace, Mech. and Nuclear Engrg, Rept. No. OU-AMNE-83-3, 24 pp. (1983).

196. Whitney, J. M., "The Effect of Transverse Shear Deformation on the Bending of Laminated Plates", Journal of Composite Materials, Vo. 3, pp. 534-547 (1969).

197. Vinson, J. R. and Smith, A. P, Jr., "The Effect of Transverse Shear Deformation on the Elastic Stability of Plates of Composite Materials", Technical Report, AFOSR TR-75-1628, 77 pp. (March 1975).

198. Srinivas, S., Joga Rao, C. V. and Rao, A. K., "Some Results from an Exact Analysis of Thick Laminates in Vibration and Buckling", Trans. ASME, Journal of Applied Mechanics, Vol. 37, pp. 868-870 (1970).

199. Srinivas, S. and Rao, A. K., "Bending, Vibration and Buckling of Simply Supported Thick Orthotropic Rectangular Plates and Laminates", International Journal of Solids and Structures, Vol. 6, No. 11, pp. 1463-1481 (1970).

200. Noor, A. K., "Stability of Multilayered Composite Plates", Fibre Science and Technology, Vol. 8, No. 2, pp. 81-89 (1975).

201. Turvey, G. J., "Biaxial Buckling of Moderately Thick Laminated Plates", Journal of Strain Analysis, Vol. 12, No. 2, pp. 89-96 (1977).

202. Ambartsumuyan, S. A. and Khachatryan, A. A., "On Stability and Vibration of Anisotropic Plates", Izvestiya Academii Nauk SSSR, Otdel. Tekhn. Nauk, Mekhan. i Mashinostr. (1960).

203. Bert, C. W. and Chang, S., "Shear-Flexible Orthotropic Plates Loaded in Plane", Proc. ASCE, Journal of Engineering Mechanics Division, pp. 1499-1509 (Dec. 1972).

204. Sandorff, P. E., "Experimental Mechanics", Lockheed-California Company, Technical Note, 26 pp. (Feb. 1, 1985).

205. Davenport, O. B., "Buckling of Orthotropic, Curved, Sandwich Panels Subjected to Edge Shear and Axial Compression", M.S.Thesis, University of Oklahoma (1972).

206. Davenport, O. B. and Bert, C. W., "Buckling of Orthotropic, Curved, Sandwich Panels Subjected to Edge Shear Loads", Journal of Aircraft, Vol. 9, pp. 477-480 (1972).

207. Davenport, O. B. and Bert, C. W., "Buckling of Orthotropic, Curved, Sandwich Panels in Shear and Axial Compression", Journal of Aircraft, Vol. 10, No. 10, pp. 632-634 (1973).

208. Fogg, L. D., Griffin, C. F., Jackson, A. C., and Pearson, J. P., "Advanced Composite Structural Methods - Analytical Procedures of Computer Programs", Lockheed-California Company, Rept. LR 27334 (1975).

209. Sandorff, P. E., "Compression an Column Buckling Testing of Composits", Lockheed-California Company, Report LR 27980 (1977).

210. Durlofsky, H., "The Effects of Interlaminar Shear on the Bending and Buckling of Fiber-Reinforced, Composite, Flat and Curved Plates", Ph.D.Thesis, Stanford University, 78 pp. (1971).

211. Durlofsky, H. and Mayers, J., "The Effects of Interlaminar Shear on the Bending and Buckling of Fiber-Reinforced Composite Flat and Curved Panels", USAAVLABS Report 71-10 (1971).

212. Show-wen, Y. and Keh-chih, H., "An Approximate Theory for Elastic Orthotropic Plates with Transverse Shear Deformations" (in Chinese), Acta Mech. Sinica, Vol. 6, No. 4, pp. 304-320 (Dec. 1963).

213. Boller, K. H., "Buckling Loads of Flat Sandwich Panels in Compression", Forest Products Lab., Madison, Wis., Repts No. 1525-A, pp. 1-53 (Feb. 1947), No. 1525-B, pp. 1-25 (Sept. 1947), No. 1525-C, pp. 1-16 (Sept. 1947), No. 1525-D, pp. 1-15 (Sept. 1947), No. 1525-E, pp. 1-10 (Mar. 1948).

214. March, H. W. and Smith, C. B., "Buckling Loads of Flat Sandwich Panels in Compression - Various Types of Edge Conditions", Forest Products Lab., Madison, Wis., Rept. No. 1525 (March 1945).

215. March, H. W., "Sandwich Construction in the Elastic Range", Symp. on Structural Sandwich Construction, ASTM Spec.Tech.Publ., No. 118, pp. 32-45 (1952).

216. Norris, C. B., "Compressive Buckling Curves for Simply Supported Sandwich Panels with Glass-Fabric-Laminate Facings and Honeycomb Cores", Forest Products Lab., Madison, Wis., Rept. No. 1867, 18 pp. (Dec. 1958).

217. Jenkinson, P. M. and Kuenzi, E. W., "Buckling Coefficients for Flat, Rectangular Sandwich Panels with Corrugated Cores under Edgewise Compression", Forest Products Lab., Madison, Wis., Rept. No. ESRP-FPL-25, 19 pp (May 1965).

218. Kuenzi, E. W., "Buckling Coefficients for Simply Supported, Flat Rectangular Sandwich Panels Under Biaxial Compression", Forest Products Lab., Madison, Wis., Rept. No. FPL 135 (1970).

219. Pearce, T. R. A., "The Stability of Simply-Supported Sandwich Panels with Fibre Reinforced Faceplates", Ph.D.Thesis, Bristol Univ., England, Dept. of Aeronautical Engrg, 220 pp. (Sep. 1973).

220. Pearce, T. R. A. and Webber, J. P. H., "Buckling of Sandwich Panels with Laminated Face Plates", Aeronautical Quarterly, Vol. 23., No. 2, pp. 148-160 (1972).

221. Pearce, T. R. A. and Webber, J. P. H., "Experimental Buckling Loads of Sandwich Panels with Carbon Fiber Faceplates", Aeronautical Quarterly, Vol. 24, No. 4, pp. 295-312 (1973).

222. Vinson, J. R. and Shore, S., "Minimum Weight Web-Core Sandwich Panels Subjected to Uniaxial Compression", Journal of Aircraft, Vol. 8, No. 11, pp. 843-847 (1971).

223. Hyer, M. W. and Hagaman, J. A., "The Structural Behavior of a Graphite-Polymide Honeycomb Sandwich Panel with Quasi-Isotropic Face Sheets and an Orthotropic Core", Contractor Report, NASA-CR-163297, 124 pp. (June 1979).

224. Zubchaninov, V. G., "Elastoplastic Stability of Glass-Reinforced Plastic Plates with a Central Metal Layer", Polymer Mechanics, Vol. 5, No. 5, pp. 802-807 (1072).

225. Harris, B. J., "Strength Properties and Relationships Associated with Various Types of Fiberglas Reinforced Facing Sandwich Structures", University of Oklahoma Research Institute, Norman, Okla., Rept. No. 1386-16 (1964).

226. Harris, B. J. and Crisman, W. C., "Face-Wrinkling Mode of Buckling of Sandwich Panels", Proc. ASCE, Journal of Engineering Mechanics Division, Vol. 91, EM 3, pp. 93-111 (1965).

227. Harris, B. J. and Nordby, G. M., "Local Failure of Plastic-Foam Core Sandwich Panels", Proc. ASCE, Journal of the Structural Division, pp. 585-610 (1969).

228. Lackman, L. M. and Konishi, D. Y., "Advanced Composites Data for Aircraft Structural Design. Volume II: Structural Element Behavior -Test and Analytical Determination", North American Rockwell Corp., Los Angeles, Calif., Final Technical Rept., Contract: F33615-68-C-1489, 344 pp. (March 1972).

229. Lackman, L. M., Lin, T. H., Konishi, D. Y. and Davidson, J. W., "Advanced Composites Data for Aircraft Structural Design. Vol. III. Theoretical Methods", Air Force Materials Lab., Rept. No. AFML-TR-70-58.

230. Luckin-Smith, R. H. and Thomas, D. J., "Intercell Buckling of Honeycomb-Core Sandwich Panels", Bristol University, England, Dept. of Aeronautical Engrg, Rept. No. BU-174, 53 pp. (June 1974).

231. Stehlin, P. and Holsteinson, L., "Minimum Weight Design of Orthotropic Sandwich Panels Loaded in Compression and Shear", Aeronautical Research Institute of Sweden, Stockholm, Rept. No. FAA-122, 75 pp. (Jan. 1971).

232. Suarez, J. A., Whiteside, J. E. and Hadcock, R. N., "The Influence of Local Failure Modes on the Compressive Strength of Boron/Epoxy Composites", Proc. 2nd Conf. on Composite Materials: Testing and Design, Amer. Soc. for Testing and Materials, ASTM STP 497 (1972).

233. Konishi, D. Y. and Johnson, W. R., "Fatigue Effects of Delamination and Strength Degradation in Graphite/Epoxy Laminates", Composite Materials: Testing and Design, Amer. Soc. for Testing and Materials, ASTM STP 674, S. W. Tsai, editor, pp. 597-619 (1979).

234. Simitses, G. J. and Sallam, S., "Delamination Buckling and Growth of Flat Composite Structural Elements", AFOSR Technical Report, 74 pp. (1984).

235. Shivakumar, K. N. and Whitcomb, J. D., "Buckling of a Sublaminate in a Quasi-Isotropic Composite Laminate", Technical Memorandum, NASA TM-85755 (1984).

236. Clark, L. G., "General Small Deflection Theory of Elastic Bending and Buckling of Laminated Plates", Proc. 4th Midwest. Conf. on Solid Mechanics, Austin, Texas, Sept. 1959, Austin, Tex. Univ. Press, pp. 127-151 (1959).

237. Biot, M. A., "Edge Buckling of a Laminated Medium", International Journal of Solids and Structures, Vol. 4, No. 1, pp. 125-137 (1968).

238. Biot, M. A., "Buckling and Dynamics of Multilayered and Laminated Plates under Initial Stress", International Journal of Solids and Structures, Vol. 10, No. 4, pp. 419-451 (1974).

239. Morgan, H. S. and Jones, R. M., "Buckling of Rectangular Cross-Ply Laminated Plates with Nonlinear Stress-Strain Behavior", Trans. ASME, Journal of Applied Mechanics, Vol. 46, No. 3, pp. 637-643 (1979).

240. Hahn, H. T., "Nonlinear Behavior of Laminated Composites", Journal of Composite Materials, Vol. 7, No. 2, pp. 257-271 (1973).

241. Durocher, L. L. and Palazotto, A. N., "Elastic Plastic Buckling of Anisotropic Plates", ASCE National Structural Engineering Meeting, Preprint 1997, pp. 1-23 (1973).

242. Durocher, L. L. and Palazotto, A. N., "Instability of Plastically Anisotropic Rectangular Plates", Development in Theoretical and Applied Mechanics, (Proc. 8th Southeast. Conf. on Theoretical and Applied Mechanics, Blacksburg, VA., April 29-30, 1976, Vol. 8, pp. 123-137 (1976).

243. Teters, G. A., "The Effect of Transverse Shear Upon the Buckling Stability of Inelastic Orthotropic Plates", Polymer Mechanics, Vol. 1, No. 2, pp. 100-102 (1965).

244. Whitney, J. M. and Ashton, J. E., "Effect of Environment on the Elastic Response of Layered Composite Plates", AIAA Journal, Vol. 9, pp. 1708-1713 (1971).

245. Flaggs, D. L., "Elastic Stability of Generally Laminated Composite Plates Including Hygrothermal Effects", M.S.Thesis, Dept. of Mechanical and Aerospace Engineering, University of Delaware (1978).

246. Flaggs, D. L. and Vinson, J. R., "Elastic Stability of Generally Laminated Composite Plates Including Hygrothermal Effects", Technical Report, AFOSR TR 78-1349, 68 pp. (July 1977).

247. Flaggs, D. and Vinson, J. R., "Hygrothermal Effects on the Buckling of Laminated Composite Plates", Fibre Science and Technology, Vol. 11, pp. 353-365 (1978).

248. Von Kármán, Th., "Festigkeitsprobleme im Maschinenbau", Encyklopädie der Mathematischen Wissenschaften, Vol. 4, pp. 311-385 (1910).

249. Prabhakara, M. K. and Chia, C. Y., "Post-Buckling Behaviour of Rectangular Orthotropic Plates", Journal of Mechanical Engineering Science, Vol. 15, No. 1, pp. 25-33 (1973).

250. Chandra, R. and Bavasu Raju, B., "Postbuckling Analysis of Rectangular Orthotropic Plates", International Journal of Mechanical Sciences, Vol. 15, pp. 81-97 (1973).

251. Von Kármán, Th., Sechler, E. E. and Donnell, L. H., "Trans. ASME", Vol. 54, p. 53 (1932).

252. Prabhakara, M. K. and Chia, C. Y., "Postbuckling of Angle-Ply and Anisotropic Plates", Ingenieur-Archiv, Vol. 45, No. 2, pp. 131-139 (1976).

253. Noor, A. K., Mathers, M. D. and Anderson, M. S., "Exploiting Symmetries for Efficient Postbuckling Analysis of Composite Plates", AIAA Journal, Vol. 15, No. 1, pp. 24-32 (1977).

254. Turvey, G. J., "A Contribution to the Elastic Stability of Thin-Walled Structures Fabricated from Isotropic and Orthotropic Materials", Ph.D.Thesis, Dept. of Civil Engineering, University of Birmingham (1971).

255. Turvey, G. J. and Wittrick, W. H., "The Large Deflection and Post-Buckling Behavior of Some Laminated Plates", Aeronautical Quarterly, Vol. 24, No. 2, pp. 77-86 (1973).

256. Prabhakara, M. K., "Post-Buckling Behaviour of Simply-Supported Cross-Ply Rectangular Plates", Aeronautical Quarterly, Vol. 27, No. 4, pp. 309-316 (1976).

257. Spier, E. E., "Crippling Analysis of Unidirectional Boron/Aluminum Composites in Compression Structures", Paper pres. at Air Force Conf. on Fibrous Composites in Flight Vehicle Design, Dayton, Sept. 1972, 12 pp. (1972).

258. Spier, E. E., "Stability of Graphite/Epoxy Structures with Arbitrary Symmetrical Laminates", Experimental Mechanics, Vol. 18, Vol. 11, pp. 401-408 (1978).

259. Spier, E. E., "On Experimental Versus Theoretical Incipient Buckling of Narrow Graphite/Epoxy Plates in Compression", AIAA/ASME/AHS, 21st Structures, Structural Dynamics and Materials Conf., Seattle, Washington, 12-14 May, 1980, Paper No: AIAA-80-0686-CP, pp. 187-193 (1980).

260. Spier, E. E., "Local Buckling, Postbuckling, and Crippling Behavior of Graphite-Epoxy Short Thin Walled Compression Members", Naval Air Systems Command, Final Technical Report, NASC-N00019-80-C-0174, 148 pp. (July 1981).

261. Spier, E. E. and Klouman, F. L., "Post-Buckling Behavior of Graphite/Epoxy Laminated Plates and Channels", Proc. Army Symp. on Solid Mechanics, Bass River, Mass., 17 pp. (1976).

262. Spier, E. E. and Klouman, F. L., "Empirical Crippling Analysis of Graphite/Epoxy Laminated Plates", American Society for Testing and Materials, Special Technical Publication, No. 617, pp. 255-271 (1977).

263. Spier, E. E. and Wang, G., "On Buckling of Unidirectional Boron/Aluminum Stiffeners - A Caution to Designers", Journal of Composite Materials, Vol. 9, No. 4, pp. 347-360 (1975).

264. Banks, W. M. and Rhodes, J., "The Instability of Composite Channel Sections", Proc. 4th ICCM, Tokyo, 9 pp (1982).

265. Kaminski, B. E., "Development of Engineering Data for Advanced Composite Materials. Volume III. Anisotropic Plate Characterization Bending, Dynamics, Stability", General Dynamics, Fort Worth, Texas, Technical Rept., Contract: F33615-68-C-1474, 337 pp. (Aug. 1970).

266. Kaminski, B. E. and Ashton, J. E., "Diagonal Tension Behavior of Boron-Epoxy Shear Panels", Journal of Composite Materials, Vol. 5, pp. 553-558 (1971).

267. Kobayashi, S., Sumihara, K. and Koyama, K., "Shear Buckling Strengths of Graphite-Epoxy Laminated Panels", Proc. Japan-U.S. Conf. on Composite Materials, Tokyo, 1981, pp. 436-445 (1981).

268. Ter-Emmanuil'yan, N. Ya., "Stability of an Orthotropic Flexible Square Plate Weakened by a Square Opening", Polymer Mechanics, Vol. 7, pp. 425-429 (1971).

269. Starnes, J. H., Jr. and Rouse, M., "Postbuckling and Failure Characteristics of Selected Flat Rectangular Graphite-Epoxy Plates Loaded in Compression", AIAA/ASME/ASCE/AHS, 22nd Structures, Structural Dynamics, and Materials Conference, Atlanta, Georgia, April 6-8, 1981, AIAA Paper No. 81-0543, 12 pp. (1981).

270. Knauss, J. F., Starnes, J. H., Jr. and Henneke, E. G., II, "The Compressive Failure of Graphite/Epoxy Plates with Circular Holes", Contractor Report, NASA CR-157115 (1978).

271. Agarwal, B. L., "Design Methodology and Life Analysis of Post-buckled Metal and Composite Panels", Northrop Corp., Aircraft Division, Technical Operating Report, Analytical Methods Selection, 51 pp. (1982).

272. Agarwal, B. L., "Postbuckling Behavior of Composite Shear Webs", AIAA Journal, Vol. 19, No. 7, pp. 933-939 (1981).

273. Anderson, R. E., "A Variational Theorem for Laminated Composite Plates of Nonlinear Materials and Applications to Postbuckling", Ph.D.Thesis, Stanford University, California, 206 pp. (1979).

274. Anderson, R. E. and Mayers, J., "Effects of Non-Linear Material Behavior on Postbuckling Stiffness of Laminated Composite Plates", AIAA Paper 79-1806 (1979).

275. Banks, W. M., "Post-Buckling Behavior of Composite Panels", Proc. Conf. on Composite Materials, Geneva, Switzerland, Vol. 2, pp. 272-293 (1975).

276. Banks, W. M., "Application Potential of Reinforced Plastic Plates", Proc. 31st Annual Conf., SPI Reinforced Plastic/Composites Institute (1976).

277. Banks, W. M., "A Contribution to the Geometric Nonlinear Behaviour of Orthotropic Plates", Ph.D.Thesis, University of Strathclyde, Scotland (1977).

278. Banks, W. M. and Harvey, J. M., "Experimental Study of Stability Problems in Composite Materials", Contrib. to Stability Problems in Engineering Structure and Components, Editors: T. H. Richards and P. Stanley, Applied Science Publishers (1979).

279. Banks, W. M. and Rhodes, J., "A Parametric Study of the Buckling of Composite Sections", Proc. 13th Reinforced Plastics Congress, Brighton, Sussex, England, Supplement, pp. 19-20 (1982).

280. Bhatia, N. M., "Postbuckling Fatigue Behavior of Advanced Composite Shear Panels", Proc. of the Army Symp. on Solid Mechanics, 1976 - Composite Materials, The Influence of Failure on Design, Army Materials and Mechanics Research Center, Watertown, Mass., Rept. MS 76-3 (1976).

281. Butakova, L. G., "Stability of a Flexible Orthotropic Plate with Free Edges", Polymer Mechanics, Vol. 2, No. 4, pp. 361-367 (1966).

282. Chan, D. P., "An Analytical Study of the Postbuckling of Laminated, Anisotropic Plates", Ph.D.Thesis, Case Western Reserve University, Cleveland, Ohio (1971).

283. Chanc ., R., uckling Analysis of Crossply Laminated Plates", AIAA Journal, Vol. , No. 10, pp. 1388-1389 (1975).

284. Feng, M., "Postbuckling Analysis of Laminated Plates", Lockheed-California Company, Rept. LR 29323 (1980).

285. Harris, G. Z., "Buckling and Post-Buckling of Orthotropic Laminated Plates", AIAA/ASME/SAE, 16th Structures, Structural Dynamics and Materials Conf., Denver, Col., 27-29 May, 1975, Paper No. 75-813 (1975). See also AIAA J., Vol. 14, pp. 1505-1506 (1976).

286. Harris, G. Z., "Instability of Laminated Composite Plates", Proc. AGARD Conf., No. 112, Paper 14(1973).

287. Ho, T., "Post-Buckling of Kevlar/Epoxy Composite Shear Panels", Proc. 5th DOD/NASA Conf. on Fibrous Composites in Structural Design; New Orleans, La. (1981).

288. Islam, M. T., "Buckling and Post-Buckling Strength of Anisotropic Plates", Ph.D.Thesis, Case Western Reserve University, Div. of Solid Mechanics, Structures and Mechanical Design, 162 pp. (Sept. 1971).

289. Kobayashi, S, Sumihara, K. and Kihira, M., "Compressive Buckling Strengths of CFRP Laminated Panels (Part 1)" (in Japanese, English abstract), Journal of Japan Society of Aeronautical and Space Sciences, Vol. 28, pp. 293-301 (1980).

290. Noor, A. K., "Post-Buckling Analysis of Composite Plates", AIAA/ASME/SAE, 17th Structures, Structural Dynamics and Materials Conf., King of Prussia, Penn., 5-7 May (1976).

291. Pimm, J. H., "Advanced Composite Tension Field Tests and Evaluation", Proc. 24th National SAMPE Symposium and Exhibition, May 8-10 (1979).

292. Schmit, L. A., Jr. and Monforton, G. R., "Finite Deflection Discrete Element Analysis of Sandwich Plates and Cylindrical Shells with Laminated Faces", AIAA Journal, Vol. 8, No. 8, pp. 1454-1461 (1970).

293. Schultz, H.-G., "Postbuckled Strength of Orthotropic Plates" (in German), Jahrbuch der Schiffbautechnischen Gesellschaft, Vol. 56, pp. 182-200 (1964).

294. Shankar, P., "Postbuckling Analysis of Laminated, Anisotropic Plates Using Successive Bifurcations", Ph.D.Thesis, Case Western Reserve University, 134 pp. (1973).

295. Stein, M., "Postbuckling of Long Orthotropic Plates in Combined Shear and Compression", Proc. 24th Structures, Structural Dynamics and Materials Conf. (AIAA Paper No. 83-0876) (1983).

296. Sumihara, K. and Kobayashi, S., "Compressive Buckling Strengths of CFRP Laminated Panels (Part 2)" (in Japanese, English abstract), Journal of Japan Society of Aeronautical and Space Sciences, Vol. 29, pp. 216-227 (1981).

297. Vestergren, P., "Theoretical and Experimental Investigation of the Buckling and Post-Buckling Characteristics of Flat Carbon Fibre Reinforced Plastic (CFRP) Panels Subjected to Compression or Shear Loads", 11th Intern. Council of the Aeronautical Sciences Congress, Lisbon, Portugal, 10-16 Sept. (1978).

298. Vestergren, P. and Knutsson, L., "Theoretical and Experimental Investigation of the Buckling and Postbuckling Characteristics of Flat Carbon Fiber Reinforced Plastic Panels Subjected to Compression or Shear Loads", Proc. 11th Intern. Council of the Aeronautical Sciences, Lisbon, Portugal (1978).

299. Yusuff, S., "Large Deflection Theory for Orthotropic Rectangular Plates Subjected to Edge Compression", Trans. ASME, Journal of Applied Mechanics, Vol. 19, pp. 446-450 (1952).

300. Bhattacharya, A. P., "Note on the Postbuckling Analysis of Cross-Ply Laminated Plates with Elastically Restrained Edges and Initial Curvatures", Journal of Structural Mechanics, Vol. 10, No. 3, pp. 359-372 (1982-83).

301. Sallam, S. and Simitses, G. J., "Nonlinear Analysis of Laminated, Antisymmetric Flat Plates Subjected to Eccentric Compression", Composite Structures, Vol. 2, pp. 273-281 (1984).

302. Banks, W. M., "Experimental Study of the Nonlinear Behaviour of Composite Panels", Proc. 3rd Intern. Conf. on Composite Materials, Paris, 1980, pp. 372-386 (1980).

303. Banks, W. M., Harvey, J. M. and Rhodes, J., "The Non-Linear Behaviour of Composite Panels with Alternative Membrane Boundary Conditions on the Unloaded Edges", Proc. 2nd Intern. Conf. on Composite Materials, Toronto, April, 1978, pp. 316-336 (1978).

304. Giri, J. and Simitses, G. J., "Deflection Response of Asymmetric, Layered Simply Supported Plates to Combined Loads", Fibre Science and Technology, Vol. 13, pp. 225-242 (1980).

305. Aalami, B. and Chapman, J. C., "Large Deflection Behaviour of Rectangular Orthotropic Plates Under Transverse and In-Plane Loads", Proc. ICE, Vol. 42, pp. 347-382 (1969).

306. Hui, D., "Imperfection Sensitivity of Axially Compressed Laminated Flat Plates Due to Bending-Stretching Coupling", International Journal of Solids and Structures, Vol. 21 (1985).

307. Meffert, B., Derek, H. and Menges, G., "Stress Deformation Behavior of Orthotropic Plates with Initial Curvature Made of Glass Fiber-Reinforced Unsaturated Polyester Plastics (GFUP) Under Uniaxial Load in the Plane of the Plate", (in German), Bauingenieur, Vol. 52, No. 6, pp. 211-216 (1977).

308. Williams, J. G., Anderson, M. S., Rhodes, M. D., Starnes, J. H, Jr., and Stroud, W. J., "Recent Developments in the Design Testing and Impact-Damage Tolerance of Stiffened Composite Panels", in: Fibrous Composites in Structural Design, Plenum Publishing Corp., New York, pp. 259-291 (1980).

309. Williams, J. G. and Stein, M., "Buckling Behavior and Structural Efficiency of Open-Section Stiffened Composite Compression Panels", AIAA Journal, Vol. 14, No. 11, pp. 1618-1626 (1976).

310. Oeverli, V. and Viswanathan, A. V., "BUCLASP - A Computer Program for Uniaxial Compressive Buckling Loads of Orthotropic Laminated Stiffened Plates", Contractor Rept., NASA CR-111871 (1971).

311. Stein, M. and Williams, J. G., "Buckling and Structural Efficiency of Sandwich-Blade Stiffened Composite Compression Panels", Technical Paper, NASA-TP-1269, 40 pp. (Sept. 1978).

312. Tripp, L. L., Tamekuni, M. and Viswanathan, A. V., "User's Manual - BUCLASP 3, A Computer Program for Stresses and Buckling of Heated Composite Stiffened Panels and Other Structures", Contractor Rept., NASA CR-112228, 221 pp. (March 1973).

313. Tripp, L. L., Tamekuni, M. and Viswanathan, A. V., "User's Manual - BUCLASP 2, A Computer Program for Instability Analysis of Biaxially Loaded Composite Stiffened Panels and Other Structures", Contractor Rept., NASA CR-112226, 172 pp. (March 1973).

314. Viswanathan, A. V. and Tamekuni, M., "Analysis for Stresses and Buckling of Heated Composite Stiffened Panels and Other Structures", Contractor Rept., NASA CR-112227, 83 pp. (March 1973).

315. Viswanathan, A. V. and Tamekuni, M., "Elastic Buckling Analysis for Composite Stiffened Panels and Other Structures Subjected to Biaxial Inplane Loads", Contractor Rept., NASA CR-2216, 88 pp. (Sept. 1973).

316. Viswanathan, A. V., Tamekuni, M. and Tripp, L. L., "Elastic Stability of Biaxially Loaded Longitudinally Stiffened Composite Structures", AIAA Journal, Vol. 11, pp. 1553-1559 (1973).

317. Williams, J. G. and Mikulas, M. M., Jr., "Analytical and Experimental Study of Structurally Efficient Composite Hat-Stiffened Panels Loaded in Axial Compression", AIAA Paper No. 75-754. Also Technical Memorandum, NASA TM X-72813, 21 pp. (Jan. 1976).

318. Anon., "The NASTRAN User's Manual (Level 16.0)", NASA SP-222(03) (1976).

319. Almroth, B. O. and Brogan, F. A., "The STAGS Computer Code", Contractor Rept., NASA CR-2950 (1978).

320. Almroth, B. O., Brogan, F. A. and Marlow, M. B., "Collapse Analysis for Shells of General Shape. Volume I, Analysis", Air Force Flight Dynamics Lab, WPAFB, Ohio, AFFDL-TR-71-8 (1972).

321. Anderson, M. S., Hennessy, K. W. and Heard, W. L., Jr., "Addendum to Users Guide to VIPASA (Vibration and Instability of Plate Assemblies Including Shear and Anisotropy", Technical Memorandum, NASA TM X-73914 (1976).

322. Anderson, M. S., Hennessy, K. W. and Stroud, W. J., "Users Guide to a Computer Code for Optimization of a Panel with Arbitrary Cross Section Subject to Inplane and Lateral Loads and Temperature", Technical Memorandum, NASA TM-74064 (1977).

323. Plank, R. J. and Williams, F. W., "Critical Buckling of Some Stiffened Panels in Compression, Shear and Bending", Aeronautical Quarterly, Vol. 25, pp. 165-179 (1974).

324. Stroud, W. J., Agranoff, N. and Anderson, M. S., "Minimum-Mass Design of Filamentary Composite Panels Under Combined Loads: Design Procedure Based on a Rigorous Buckling Analysis", Technical Note, NASA TN D-8417, pp. 1-38 (July 1977).

325. Wittrick, W. H. and Horsington R. W., "Buckling and Vibration of Composite Folded-Plate Structures of Finite Length in Combined Shear and Compression", Proc. Royal Society of London, Vol. A392, pp. 107-144 (1984).

326. Wittrick, W. H. and Williams, F. W., "Buckling and Vibration of Anisotropic or Isotropic Plate Assemblies under Combined Loadings", International Journal of Mechanical Sciences, Vol. 16, pp. 209-239 (1974).

327. Anderson, M. S. and Stroud, W. J., "A General Panel Sizing Computer Code and Its Application to Composite Structural Panels", AIAA/ASME, 19th Structures, Structural Dynamics and Materials Conf., AIAA Paper No. 78-467, pp. 14-22 (1978).

328. Agarwal, B. and Davis, R. C., "Minimum-Weight Designs for Hat-Stiffened Composite Panels Under Uniaxial Compressions", Technical Note, NASA TN D-7779, 44 pp. (1974).

329. Bushnell, D., "Panel Optimization with Integrated Software (POIS), Vol. I. - PANDA - Interactive Program for Preliminary Minimum Weight Design", Lockheed Missiles and Space Company, Inc., Rept. AFWAL-81-3073, Vol. I, 253 pp. (1981).

330. Spier, E. E., "Inelastic Analysis and Testing of a Boron/Aluminum Composite Stiffened Panel", Proc. Air Force Conf. on Fibrous Composites in Flight Vehicle Design, Dayton, Ohio, 43 pp. (1974).

331. Stroud, W. J. and Agranoff, N., "Minimum-Mass Design of Filamentary Composite Panels under Combined Loads: Design Procedure Based on Simplified Buckling Equations", Technical Note, NASA TN D-8257, 49 pp. (Oct. 1976).

332. Stroud, W. J., Anderson, M. S. and Hennessy, K. W., "Effect of Bow-Type Initial Imperfection on the Buckling Load and Mass of Graphite-Epoxy Blade-Stiffened Panels", Technical Memorandum, NASA TM-74063, 25 pp. (1977).

333. Turvey, G. J. and Wittrick, W. H., "The Influence of Orthotropy on the Stability of Some Multi-Plate Structures in Compression", AIAA Journal, Vol. 24, 8 pp. (Feb. 1973).

334. Chiu, K. D., "Stability of Orthotropic Stiffened Composite Plates", Proc. ASCE, Journal of the Engineering Mechanics Division, Vol. 98, EM 5, pp.1253-1271 (1972).

335. Davis, R. C., "Stress Analysis and Buckling of J-Stiffened Graphite-Expoxy Panel", Technical Paper, NASA TP-1607, 20 pp. (Feb. 1980).

336. Gunnink, J. M., "Overall Buckling of Specially Orthotropic Z-Stiffened Panels - Part 1: Theory", Delft University of Technology, Dept. of Aerospace Engineering, Report LR-351, 36 pp. (April 1982).

337. Gunnink, J. W., Vogelesang, L. B. and Schijve, J., "Application of a New Hybrid Material (ARALL) in Aircraft Structures", Delft University of Technology, Dept. of Aerospace Engineering Delft, The Netherlands, ICAS-82-2.6.1, pp. 990-1000 (1982).

338. Hui, D. and Hansen, J. S., "Effect of Stringer Torsional Rigidity on Buckling of Integrally Stiffened Angle Ply Plates", Fibre Science and Technology, Vol. 16, pp. 39-43 (1982).

339. Ostrom, R. B., "Post-Buckling Fatigue Behavior of Flat, Stiffened Graphite/Epoxy Panels under Shear Loading", Lockheed-California Company, Burbank, Calif., Final Report, NADC-78137-60, 60 pp. (May 1981).

340. Bhatia, N. M. and Van Putten, D., "Post-Buckling Behavior of Cross-Stiffened Advanced Composite Panel Under Combined Loads", Proc. 5th DOD/NASA Conf. on Fibrous Composites in Structural Design, New Orleans, La. (1981).

341. Dickson, J. N. and Biggers, S. B., "Design and Analysis of a Stiffened Composite Fuselage Panel", Contractor Rept., NASA CR-159302, 51 pp. (Aug. 1980).

342. Dickson, J. N., Biggers, S. B. and Wang, J. T. S., "A Preliminary Design Procedure for Composite Panels with Open Section Stiffeners Loaded in the Post Buckling Range", Advances in Composite Materials, Pergamon Press, Headington Hill Hall, Oxford, England, (Proc. 3rd Intern. Conf. on Composite Materials, Paris, France, 26-29 August (1980).

343. Dickson, J. N., Cole, R. T. and Wang, J. T. S., "Design of Stiffened Composite Panels in the Post-Buckling Range", Fibrous Composites in Structural Design, Edited by Lenoe, E. M., Oplinger, D. W. and Burke, J. J., Plenum Press, New York (1980).

344. Renieri, M. P. and Garrett, R. A., "Postbuckling Behavior of Flat Stiffened Graphite/Epoxy Shear Panels", McDonnell Aircraft Co., St. Louis, Mo., MCAIR Rept. No. 81-015. Also Proc. 5th DOD/NASA Conf. on Fibrous Composites in Structural Design, New Orleans, La. (1981).

345. Spier, E. E., "Crippling/Column Buckling Analysis and Test of Graphite/Epoxy Stiffened Panels", AIAA/ASME/SAE, 16th Structures, Structural Dynamics and Materials Conf., Denver, Col., 27-29 May (1975). Also AIAA Paper 75-753, 16 pp. (1975).

346. Stein, M. and Starnes, J. H., Jr., "Numerical Analysis of Stiffened Shear Webs in the Post-Buckling Range", in Numerical Solution of Nonlinear Structural Problems, ASME, Applied Mechanics Division, Vol. 6, pp. 211-223 (1973).

347. Djubek, J., "Orthotropic Rectangular Webs in Compression", Stavebnicky Casopis, Vol. 23, No. 10, pp. 782-792 (1975).

348. Smith, C. S., "Buckling Problems in the Design of Fiberglass-Reinforced Plastic Ships", Journal of Ship Research, Vol. 16, No. 3, pp. 174-190 (1972).

349. Anon., "Buckling Analysis for Axially Compressed Flat Plates, Structural Sections, and Stiffened Plates Reinforced with Laminated Composites", Contractor Report, NASA CR-1887.

350. Heebink, T. B., March, H. W., Norris, C. B., Smith, C. B. and Ringelstetter, L. A., "Buckling of Stiffened Flat Plywood Plates in Compression", Forest Products Lab., Madison, Wis., Repts. No. 1553, pp. 1-33 (June 1946), No. 1553-A, pp. 1-22 (Nov. 1946), No. 1553-B, pp. 1-52 (May 1947).

351. Ieremia, M., "Buckling of Rectangular Orthotropic Plates", (in German), Revue Roumaine des Sciences Techniques, Série de Mécanique Appliquée, Vol. 22, No. 6, pp. 917-940 (1977).

352. Ieremia, M., "Buckling of Rectangular Orthotropic Plates. II" (in German), Revue Roumaine des Sciences Techniques, Série de Mécanique Appliquée, Vol. 23, No. 2, pp. 229-248 (1978).

353. Krumweide, G. C. and Spier, E., "Development and Test of a Graphite/Epoxy Wingbox", Proc. 3rd NASA/USAF Conf. on Fibrous Composites in Flight Vehicle Design, Williamsburg, Va., Nov. 1975, pp. 1-26 (1975).

354. Massonnet, C., Mazy, G. and Tanghe, A., "General Theory of the Buckling of Orthotropic, Rectangular Plates, Clamped or Freely Supported at the Edges, Provided with Stiffeners, Parallel to the Edges, Having Considerable Flexural and Torsional Rigidities", Université de Liège. Publication No. 71, pp. 223-262 (1960).

355. Mikulas, M. M., Jr., Bush, H. G. and Rhodes, M. D., "Current Langley Research Center Studies on Buckling and Low-Velocity Impact of Composite Panels", Proc. 3rd Conf. on Fibrous Composites in Flight Vehicle Design, Williamsburg, Va. (1975).

356. Norris, C. B., Kommers, W. J. and McKinnon, P. F., "Critical Buckling Strength of Stiffened Flat Plywood Plates in Compression and Shear - Closely Spaced Stiffeners", Forest Products Lab., Madison, Wis., Rept. No. 1800, pp. 1-38 (1948).

357. Norris, C. B. and Ringelstetter, L. A., "Buckling of Stiffened Flat Plywood Plates in Compression - a Single Stiffener Parallel to Stress, Face Grain of Plywood at 45 Deg. to its Edges", Forest Products Lab., Madison, Wis., Rept. No. 1553-C, pp. 1-13 (Oct. 1948).

358. Okada, H., Kitaura, K.-i., Fukumoto, Y., "Buckling Strength of Stiffened Plates Containing One Longitudinal or Transverse Girder Under Compression", Bull. Univ. Osaka Prefecture, Series A, Engrg & Nat. Sci., Vol. 20, No. 2, pp. 287-306 (1971).

359. Peterson, J. P., "Structural Efficiency of Aluminum Multiweb Beams and Z-Stiffened Panels Reinforced With Filamentary Boron-Epoxy Composites", Technical Note, NASA TN D-5856 (1970).

360. Reed, D. L., "Laminated Sandwich Panel Analysis", General Dynamics, Convair Aerospace Division, Rept. FZM-5590 (1971).

361. Richards, D. M., "Optimum Design of Fibre-Reinforced Compression Panels", College of Aeronautics, Rept. No. Aero. 209, Cranfield, U.K. (1969).

362. Ringelstetter, L. A. and Norris, C. B., "The Effect of a Stiffener on the Maximum Load of Flat Plywood Plates in Edgewise Compression, with the Face Grain at 0° and 90° to the Load", Forest Products Lab., Madison, Wis., Rept. No. 1553-D, 7 pp. (July 1949).

363. Sanbongi, S. , Toda, S. and Nakai, E., "Buckling Strength of CFRP-Stiffened Panel" (in Japanese), Journal of Japan Society for Aeronautical and Space Sciences, Vol. 30, No. 338, pp. 127-133 (1982).

364. Smith, C. S., Journal of Ship Research, Vol. 12, p. 249 (1968).

365. Stroud, W. J., Greene, W. H. and Anderson, M. S., "Buckling Loads of Stiffened Panels Subjected to Combined Longitudinal Compression and Shear: Results Obtained with PASCO, EAL and STAGS Computer Programs", Technical Paper, NASA TP-2215, 77 pp. (1984).

366. Wagner, H. and Pattabiraman, J., "Buckling of Eccentrically Stiffened Rectangular Plates Subjected to Linearly Varying Longitudinal Compression" (in English), Zeitschrift fur Flugwissenschaften, Vol. 21, No. 4, pp. 131-140 (1973).

367. Williams, J. G. and Martin, M. M., Jr., "Analytical Experimental Study of Structurally Efficient Composite Hat-Stiffened Panels Loaded in Axial Compression, Technical Memorandum, NASA TM X-72813, 23 pp. (Jan. 1976).

368. DiGiovanni, P. R. an Dugundji, J., "Vibrations of Freely Supported Orthotropic Circular Cylindrical Shells Under Internal Pressure" AFOSR Rept. 65-0640, ASRL TR 112-4 (1965).

369. Viswanathan, A. V., Tamekuni, M. and Baker, L. L., "Buckling Analysis for Anisotropic Laminated Plates under Combined Inplane Loads", 25th Intern. Astronautical Congress, Amsterdam, Netherlands, 30 Sept.-5 Oct. 1974, 11 pp. (1974).

370. Viswanathan, A. V., Tamekuni, M. and Baker, L. L., "Elastic Stability of Laminated, Flat and Curved, Long Rectangular Plates Subjected to Combined Inplane Loads", Contractor Rept., NASA CR-2330, 68 pp. (June 1974).

371. Soldatos, K. P. and Tzivanidis, G. J., "Buckling and Vibration of Cross-Ply Laminated Circular Cylindrical Shell Panels", Zeitschrift fur Angewandte Mathematik und Physik (ZAMP), Vol. 33, pp. 229-240 (1982).

372. Viswanathan, A. V., "Elastic Stability of Laminated, Flat and Curved, Long Rectangular Plates Subjected to Combined Inplane Loads", 25th Intern. Astronautical Congress, Amsterdam, Netherlands, 30 Sept.-5 Oct. (1974).

373. Becker, M. L., "Analytical/Experimental Investigation of the Instability of Composite Cylindrical Panels", M.Sc.Thesis, U.S.Air Force Institute of Technology, Dayton, Ohio (1979).

374. Becker, M. L., Palazotto, A. N. and Khot, N. S., "Instability of Composite Panels", Journal of Aircraft, Vol. 18, pp. 739-743 (1981).

375. Becker, M. L., Palazotto, A. N. and Khot, N. S., "Experimental Investigation of the Instability of Composite Cylindrical Panels", Experimental Mechanics, Vol. 22, pp. 372-376 (1982).

376. Wilkins, D. J., "Compression Buckling Tests of Laminated Graphite-Epoxy Curved Panels", AIAA Journal, Vol. 13, pp. 465-470 (1975).

377. Wilkins, D. J., "Anisotropic Curved Panel Analysis", General Dynamics, Convair Aerospace Division, Rept. FZM-5567 (1973).

378. Zhang, Y., Ph.D.Thesis, University of London (1982).

379. Knutsson, L. "Manufacture of a Stiffened CFRP Panel and an Experimental Evaluation of its Buckling Characteristics", Aeronautical Research Institute of Sweden, Stockholm, Structures Dept., Rept. FFA-HE-1971, 31 pp. (1977).

380. Fortier, R. C., "Transverse Vibrations Related to Stability of Curved Anisotropic Plates", AIAA Journal, Vol. 11, No. 12, pp. 1782-1783 (Dec. 1973).

381. Sinha, P. K. and Rath, A. K., "Vibration and Buckling of Cross-Ply Laminated Circular Cylindrical Panels", Aeronautical Quarterly, Vol. 26, No. 3, pp. 211-218 (Aug. 1975).

382. Zhang, Y. and Matthews, F. L., "Postbuckling Behaviour of Curved Panels of Generally Layered Composite Materials", Composite Structures, Vol. 1, pp. 115-135 (1983).

383. Agarwal, B. L., "Postbuckling Behavior of Composite-Stiffened Curved Panels in Compression", Experimental Mechanics, Vol. 22, pp. 231-236 (1982).

384. Hinkle, T. V., Sorensen, J. P. and Garrett, R. A., "Compression Post-Buckling Behavior of Stiffened Curved Graphite/Epoxy Panels", Proc. 5th DOD/NASA Conf. on Fibrous Composites in Structural Design, New Orelans, LA (1981).

385. Bauld, N. R., Jr. and Satyamurthy, K., "Collapse Load Analysis for Plates and Panels" Clemson University, Clemson, SC, Final Technical Rept. AFFDL-TR-79-3038, 209 pp. (May 1979).

386. Satyamurthy, K., Khot, N. S. and Bauld N. R., Jr., "An Automated, Energy-Based, Finite-Difference Procedure for the Elastic Collapse of Rectangular Plates and Panels", Computers & Structures, Vol. 11, No. 3, pp. 239-249 (1980).

387. Satyamurthy, K., "Collapse Load Analysis for Plates and Panels", Ph.D.Thesis, Clemson University, Clemson, SC, 101 pp. (1979).

388. Hui, D., "Asymmetric Postbuckling of Symmetrically Laminated Cross-Ply, Short Cylindrical Panels under Compression", Composite Structures, Vol. 3, pp. 81-95 (1985).

389. Koiter, W. T., "The Effect of Axisymmetric Imperfections on the Buckling of Cylindrical Shells Under Axial Compression", Proc. K. Ned. Akad. Wet., Amsterdam, Ser. B, Vol. 6 (1963). Also: Lockheed Missiles and Space Co., Rept. 6-90-63-86 (1963).

390. Bauld, N. R., Jr. and Khot, N. S., "A Numerical and Experimental Investigation of the Buckling Behavior of Composite Panels", Computers and Structures, Vol. 15, pp. 393-403 (1982).

391. Khot, N. S. and Bauld, N. R., Jr., "Further Comparison of the Numerical and Experimental Buckling Behaviors of Composite Panels", Computers and Structures, Vol. 17, pp. 61-68 (1983).

392. Bauld, N, R., Jr., "Experimental and Numerical Analysis of Axially Compressed Circular Cylindrical Fiber-Reinforced Panels with Various Boundary Conditions", Air Force Flight Dynamics Lab., Technical Rept. AFWAL-TR-81-3158 (1982).

APPENDIX. PLATE BUCKLING EQUATIONS

The theory required to analyze the buckling of laminated composite plates is considerably more complicated than that of classical, homogeneous, isotropic plate theory. This is particularly true for unsymmetrically laminated plates because of the coupling which exists between bending and stretching.

The purpose of this Appendix is to provide in one convenient place the basic equations needed to analyze plate bifurcation buckling, including a summary of the steps required in their derivation. At the same time, the notation and conventions used throughout this monograph are established.

To keep the presentation reasonably short, not all the details are presented. In particular, the steps required to integrate the stress and moment resultant equations over the plate thickness, Equations A.6 and A.7, to obtain the stiffness relationships, Equation A.8, are explained, but not carried out in detail. These steps may be found in several well known texts [A.1-A.4].

A.1. PLATE STIFFNESS EQUATIONS

Classical plate theory is governed by the Kirchhoff hypothesis: Normals to the midplane remain straight and normal as the plane deforms into a surface. Let the x and y axes of a rectangular coordinate system lie in the midplane, and the z axis in the direction of the plate thickness. Then the kinematical behavior of the plate described by the Kirchhoff hypothesis may be expressed by the following relationships:

$$u = u_o - z \frac{\partial w}{\partial x}$$
$$v = v_o - z \frac{\partial w}{\partial y} \qquad \text{(A.1)}$$

where u, v, w are displacement components of a typical point in the plate, and u_o, v_o are inplane displacements at a point of the midplane. Furthermore, u_o, v_o and w are functions only of x and y.

Using the strain-displacement equations of classical plane elasticity theory,

$$\varepsilon_x = \frac{\partial u}{\partial x} , \quad \varepsilon_y = \frac{\partial v}{\partial y} , \quad \gamma_{xy} = \frac{\partial v}{\partial x} + \frac{\partial u}{\partial x} \qquad \text{(A.2)}$$

where ε_x , ε_y are the inplane normal strains, and γ_{xy} is the inplane, engineering (i.e., not tensorial) shear strain, Equation A.1 may be re-written as

$$\varepsilon_x = \varepsilon_x^{\,o} - zK_x$$
$$\varepsilon_y = \varepsilon_y^{\,o} - zK_y \qquad \text{(A.3)}$$
$$\gamma_{xy} = \gamma_{xy}^{\,o} - zK_{xy}$$

where $\varepsilon_x^{\,o}$, $\varepsilon_y^{\,o}$ and $\gamma_{xy}^{\,o}$ are the midplane strains, and K_x, K_y and K_{xy} are the curvature changes of the midplane during deformation. These quantities are also functions of x and y only, and are given by

$$\varepsilon_x^{\,o} = \frac{\partial u_o}{\partial x} , \quad \varepsilon_y^{\,o} = \frac{\partial v_o}{\partial y} , \quad \gamma_{xy}^{\,o} = \frac{\partial v_o}{\partial x} + \frac{\partial u_o}{\partial y} \qquad \text{(A.4)}$$

$$K_x = \frac{\partial^2 w}{\partial x^2} , \quad K_y = \frac{\partial^2 w}{\partial y^2} , \quad K_{xy} = 2 \frac{\partial^2 w}{\partial x \partial y} \qquad \text{(A.5)}$$

The inplane stress resultants N_x, N_y, N_{xy} (forces per unit length) and moment resultants M_x, M_y, M_{xy} (moments per unit length) are obtained by carrying out the force and moment integrals through the thickness; that is,

$$N_x = \int_{-h/2}^{h/2} \sigma_x dz$$

$$N_y = \int_{-h/2}^{h/2} \sigma_y dz \qquad \text{(A.6)}$$

$$N_{xy} = \int_{-h/2}^{h/2} \tau_{xy} dz$$

$$M_x = \int_{-h/2}^{h/2} \sigma_x z dz$$

$$M_y = \int_{-h/2}^{h/2} \sigma_y z dz \qquad \text{(A.7)}$$

$$M_{xy} = \int_{-h/2}^{h/2} \tau_{xy} z dz$$

where σ_x and σ_y are the inplane normal stresses and τ_{xy} is the inplane shear stress. The positive senses of the stress and moment resultants (including the transverse shear stress resultants, Q_x and Q_y) are shown in Figures A.1 and A.2. For laminated plates, the integrations required by Equations A.6 and A.7 must be carried out piecewise (i.e. stepwise) from layer to layer. Furthermore, for typical lamina consisting of

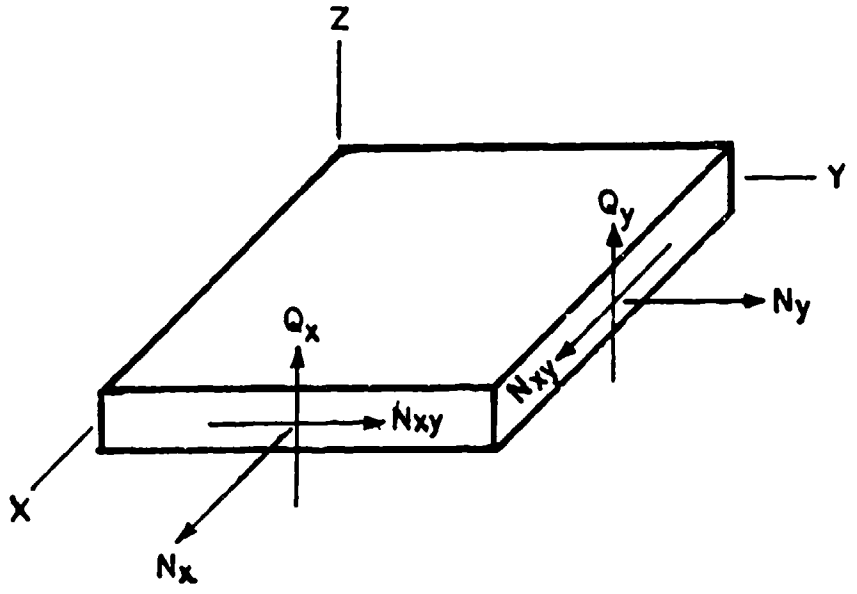

Figure A.1. Positive stress resultants.

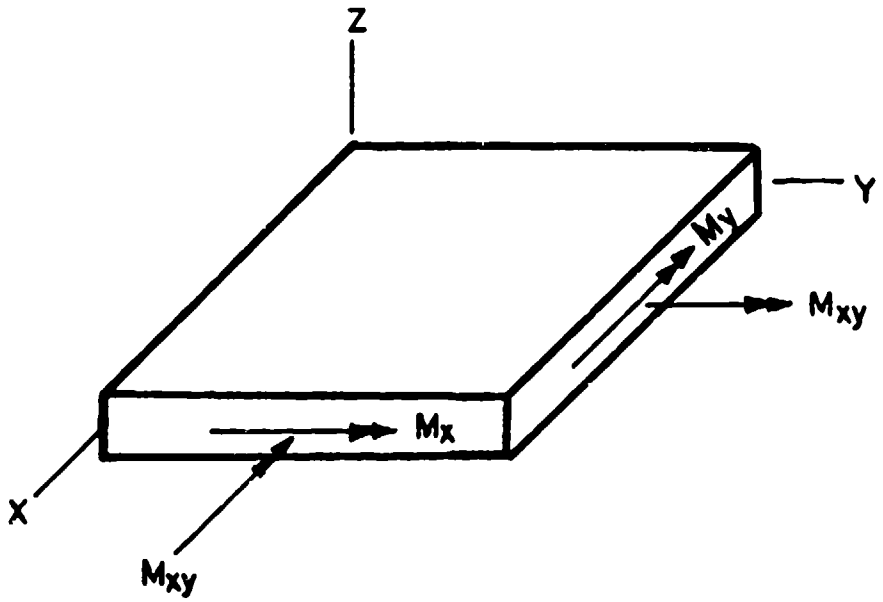

Figure A.2. Positive moment resultants.

parallel fibers imbedded in a matrix material, with the fibers lying at an angle θ with respect to the x-axis of the plate, the orthotropic stress-strain relationships for the lamina must be transformed tensorially to be consistent with the plate axes. The details of these somewhat complicated calculations may be found elsewhere (cf. [A.1, A.2, A.3]) and will not be elaborated upon here. Carrying out these calculations, one is able to relate the stress and moment resultants to the midplane strains and curvature changes as follows:

$$\left[\begin{array}{c} N_x \\ N_y \\ N_{xy} \\ \hline M_x \\ M_y \\ M_{xy} \end{array}\right] = \left[\begin{array}{ccc:ccc} A_{11} & A_{12} & A_{16} & B_{11} & B_{12} & B_{16} \\ A_{12} & A_{22} & A_{26} & B_{12} & B_{22} & B_{26} \\ A_{16} & A_{26} & A_{66} & B_{16} & B_{26} & B_{66} \\ \hdashline B_{11} & B_{12} & B_{16} & D_{11} & D_{12} & D_{16} \\ B_{12} & B_{22} & B_{26} & D_{12} & D_{22} & D_{26} \\ B_{16} & B_{26} & B_{66} & D_{16} & D_{26} & D_{66} \end{array}\right] \left[\begin{array}{c} \varepsilon_x^o \\ \varepsilon_y^o \\ \gamma_{xy}^o \\ \hline -K_x \\ -K_y \\ -K_{xy} \end{array}\right] \tag{A.8}$$

where A_{ij}, B_{ij} and D_{ij} are stiffness coefficients arising from integrals of the following forms:

$$\begin{aligned} A_{ij} &= \int_{-h/2}^{h/2} C_{ij}\, dz \\ B_{ij} &= \int_{-h/2}^{h/2} C_{ij}\, z\, dz \\ D_{ij} &= \int_{-h/2}^{h/2} C_{ij}\, z^2 dz \end{aligned} \tag{A.9}$$

with C_{ij} being constants which change from layer to layer during the

integrations. It is observed that, not only is the 6 x 6 stiffness matrix of Equation A.8 symmetric, but the 3 x 3 submatrices A_{ij}, B_{ij} and C_{ij} are also symmetric.

It is important to understand the implications of the stiffness coefficients in Equation A.8. The B_{ij} coefficients cause coupling between bending and stretching at the plate during transverse displacements. As can be seen from the second of Equations A.9, these coefficients vanish if the C_{ij} are even functions of z. This occurs when the laminate is symmetric (in thickness, fiber orientation and material properties) with respect to the plate midplane.

Another type of coupling is seen by the existence of the A_{16}, A_{26}, B_{16}, B_{26}, D_{16}, D_{26} coefficients. These coefficients indicate extension-shear and/or bending-twisting coupling during the plate deformation. This coupling vanishes for cross-ply lay-ups (i.e., fiber orientations of adjacent lamina all lie along parallel or perpendicular axes). Further discussions of coupling may be found in several excellent references [A.1-A.5].

A.2. GOVERNING DIFFERENTIAL EQUATIONS

Consider a plate which, due to pressure components (p_x, p_y, q in the x, y, z directions, respectively) and inplane stress resultants (N_x, N_y, N_{xy}), has undergone bending. Summing forces in the x, y and z directions on a infinitesimal plate element yields the following equations of equilibrium, respectively:

$$\frac{\partial N_x}{\partial x} + \frac{\partial N_{xy}}{\partial y} - Q_x \frac{\partial w}{\partial x} + p_x = 0$$

$$\frac{\partial N_{xy}}{\partial x} + \frac{\partial N_y}{\partial y} - Q_y \frac{\partial w}{\partial y} + p_y = 0 \qquad \text{(A.10)}$$

$$\frac{\partial Q_x}{\partial x} + \frac{\partial Q_y}{\partial y} + N_x \frac{\partial^2 w}{\partial x^2} + 2N_{xy} \frac{\partial^2 w}{\partial x \partial y} + N_y \frac{\partial^2 w}{\partial y^2} + q = 0$$

Summing moments about axes parallel to the y and x coordinates yields, respectively,

$$Q_x = \frac{\partial M_x}{\partial x} + \frac{\partial M_{xy}}{\partial y}$$

$$Q_y = \frac{\partial M_{xy}}{\partial x} + \frac{\partial M_y}{\partial y} \qquad \text{(A.11)}$$

The transverse shear forces Q_x and Q_y, as well as the slopes $\partial w/\partial x$ and $\partial w/\partial y$, are typically small in the first two of Equations A.10. Taking advantage of this, and substituting Equations A.11, Equations A.10 become

$$\begin{aligned}
&\frac{\partial N_x}{\partial x} + \frac{\partial N_{xy}}{\partial y} + p_x = 0 \\
&\frac{\partial N_{xy}}{\partial x} + \frac{\partial N_y}{\partial y} + p_y = 0 \\
&\frac{\partial^2 M_x}{\partial x^2} + 2\frac{\partial^2 M_{xy}}{\partial x \partial y} + \frac{\partial^2 M_y}{\partial y^2} + N_x \frac{\partial^2 w}{\partial x^2} + 2N_{xy}\frac{\partial^2 w}{\partial x \partial y} \\
&\qquad + N_y \frac{\partial^2 w}{\partial y^2} + q = 0
\end{aligned} \qquad \text{(A.12)}$$

Let us now consider each of the functions represented in Equations A.12, except for w and the body forces, to be composed of two parts - an <u>initial</u> part which exists before the onset of buckling, and an additional part which is due to <u>buckling</u>. Let these two parts be denoted by the superscripts "i" and "b". That is,

$$N_x = N_x^i + N_x^b \quad , \quad \text{etc.}$$

$$M_x = M_x^i + M_x^b \quad , \quad \text{etc.} \qquad \text{(A.13)}$$

It is assumed that the plate remains flat before buckling; i.e.,

$$w = w^b \tag{A.14}$$

and further that no additional body forces are added during buckling; i.e.,

$$p_x = p_x^i \quad , \quad p_y = p_y^i \quad , \quad q = q^i \tag{A.15}$$

At the onset of buckling, but before it takes place, Equations A.12 reduce to

$$\begin{aligned} &\frac{\partial N_x^i}{\partial x} + \frac{\partial N_{xy}^i}{\partial y} + p_x^i = 0 \\ &\frac{\partial N_{xy}^i}{\partial x} + \frac{\partial N_y^i}{\partial y} + p_y^i = 0 \\ &\frac{\partial^2 M_x^i}{\partial x^2} + 2\frac{\partial^2 M_{xy}^i}{\partial x \partial y} + \frac{\partial^2 M_y^i}{\partial y^2} + q^i = 0 \end{aligned} \tag{A.16}$$

Substituting Equations A.13, A.14 and A.15 into Equations A.12 and subtracting Equations A.16 results in

$$\begin{aligned} &\frac{\partial N_x^b}{\partial x} + \frac{\partial N_{xy}^b}{\partial y} = 0 \\ &\frac{\partial N_{xy}^b}{\partial x} + \frac{\partial N_y^b}{\partial y} = 0 \\ &\frac{\partial^2 M_x^b}{\partial x^2} + 2\frac{\partial^2 M_{xy}^b}{\partial x \partial y} + \frac{\partial^2 M_y^b}{\partial y^2} + N_x^i \frac{\partial^2 w}{\partial x^2} + 2N_{xy}^i \frac{\partial^2 w}{\partial x \partial y} + N_y^i \frac{\partial^2 w}{\partial y^2} = 0 \end{aligned} \tag{A.17}$$

wherein the three terms

$$N_x^b \frac{\partial^2 w}{\partial x^2} + 2N_{xy}^b \frac{\partial^2 w}{\partial x \partial y} + N_y^b \frac{\partial^2 w}{\partial y^2} \tag{A.18}$$

are considered small relative to the ... ee terms of the third of Equations A.17, and have been dropped ... Because, in general, N_x^b, N_{xy}^b and N_y^b are functions of w, the three terms in expression (A.18) are each nonlinear, and it is therefore imperative that they be dropped in order for the buckling problem to be reasonably tractable.

Before proceeding further with the buckling equations, it is worthwhile to study further the meaning of Equations A.16 for the prebuckled state. Since $w^i = 0$, then $K_x^i = K_y^i = K_{xy}^i = 0$. Substituting the prebuckled forms of Equations A.4 and A.8 into Equations A.16 yields

$$\frac{\partial}{\partial x}\left[A_{11}\frac{\partial u^i}{\partial x} + A_{12}\frac{\partial v^i}{\partial y} + A_{16}\left(\frac{\partial v^i}{\partial x} + \frac{\partial u^i}{\partial y}\right)\right] + \frac{\partial}{\partial y}\left[A_{16}\frac{\partial u^i}{\partial x} + A_{26}\frac{\partial v^i}{\partial y} + A_{66}\left(\frac{\partial v^i}{\partial x} + \frac{\partial u^i}{\partial y}\right)\right] + p_x^i = 0 \tag{A.19a}$$

$$\frac{\partial}{\partial x}\left[A_{16}\frac{\partial u^i}{\partial x} + A_{26}\frac{\partial v^i}{\partial y} + A_{66}\left(\frac{\partial v^i}{\partial x} + \frac{\partial u^i}{\partial y}\right)\right] + \frac{\partial}{\partial y}\left[A_{12}\frac{\partial u^i}{\partial x} + A_{22}\frac{\partial v^i}{\partial y} + A_{26}\left(\frac{\partial v^i}{\partial x} + \frac{\partial u^i}{\partial y}\right)\right] + p_y^i = 0 \tag{A.19b}$$

$$\frac{\partial^2}{\partial x^2}\left[B_{11}\frac{\partial u^i}{\partial x} + B_{12}\frac{\partial v^i}{\partial y} + B_{16}\left(\frac{\partial v^i}{\partial x} + \frac{\partial u^i}{\partial y}\right)\right] + 2\frac{\partial^2}{\partial x \partial y}\left[B_{16}\frac{\partial u^i}{\partial x} + B_{26}\frac{\partial v^i}{\partial y} + B_{66}\left(\frac{\partial v^i}{\partial x} + \frac{\partial u^i}{\partial y}\right)\right] + \frac{\partial^2}{\partial y^2}\left[B_{12}\frac{\partial u^i}{\partial x} + B_{22}\frac{\partial v^i}{\partial y} + B_{26}\left(\frac{\partial v^i}{\partial x} + \frac{\partial u^i}{\partial y}\right)\right] + q^i = 0 \tag{A.19c}$$

where, for simplicity, the subscript "o" has been dropped from the displacements. For a <u>symmetrically</u> laminated plate, all the B_{ij} are zero. Then Equation A.19c yields $q^i = 0$. For given values of the initial, tangential, body force components p_x^i and p_y^i, and given values of u^i and v^i

and/or their derivatives (i.e., inplane stresses) on the plate boundaries, one could solve Equations A.19a and A.19b for the displacement field u^i and v^i and, if desired, the corresponding initial stress field.

For an <u>unsymmetrically</u> laminated plate, the B_{ij} are not all zero, and the solutions for u^i and v^i can be substituted into Equation A.19c to determine what transverse pressure distribution q^i, together with boundary moments and transverse forces, must be applied in order that the plate remain flat. In the case that the initial, inplane stresses (and strains) are constant or linearly varying with respect to x and y, all terms except q^i vanish in Equation A.19c, with the result that no initial, transverse pressure is needed for the plate to remain flat. Equations A.8 and A.11 show that constant initial strains give rise to constant edge moments, and that linearly varying initial strains require linearly varying moments and constant transverse shear forces for equilibrium at the edges.

One convenient manner to represent the equilibrium equations governing the buckled configuration is in terms of the three components of inplane displacement. Substituting Equations A.4, A.5 and A.9 into Equations A.17 yields the equations in matrix form as

$$\begin{bmatrix} L_{11} & L_{12} & L_{13} \\ L_{21} & L_{22} & L_{23} \\ L_{31} & L_{32} & (L_{33}-F) \end{bmatrix} \begin{Bmatrix} u \\ v \\ w \end{Bmatrix} = \begin{Bmatrix} 0 \\ 0 \\ 0 \end{Bmatrix} \qquad \text{(A.20)}$$

where the L_{ij} are differential operators representing the plate stiffness,

$$L_{11} \equiv A_{11}\frac{\partial^2}{\partial x^2} + 2A_{16}\frac{\partial^2}{\partial x\partial y} + A_{66}\frac{\partial^2}{\partial y^2}$$

$$L_{22} \equiv A_{22}\frac{\partial^2}{\partial y^2} + 2A_{26}\frac{\partial^2}{\partial x\partial y} + A_{66}\frac{\partial^2}{\partial x^2}$$

$$L_{33} \equiv D_{11}\frac{\partial^4}{\partial x^4} + 4D_{16}\frac{\partial^4}{\partial x^3\partial y} + 2(D_{12} + 2D_{66})\frac{\partial^4}{\partial x^2\partial y^2}$$
$$+ 4D_{26}\frac{\partial^4}{\partial x\partial y^3} + D_{22}\frac{\partial^4}{\partial y^4} \qquad \text{(A.21)}$$

$$L_{12} = L_{21} \equiv A_{16}\frac{\partial^2}{\partial x^2} + (A_{12} + A_{66})\frac{\partial^2}{\partial x\partial y} + A_{26}\frac{\partial^2}{\partial y^2}$$

$$L_{13} = L_{31} \equiv -B_{11}\frac{\partial^3}{\partial x^3} - 3B_{16}\frac{\partial^3}{\partial x^2\partial y} - (B_{12} + 2B_{66})\frac{\partial^3}{\partial x\partial y^2} - B_{26}\frac{\partial^3}{\partial y^3}$$

$$L_{23} = L_{32} \equiv -B_{16}\frac{\partial^3}{\partial x^3} - (B_{12} + 2B_{66})\frac{\partial^3}{\partial x^2\partial y} - 3B_{26}\frac{\partial^3}{\partial x\partial y^2} - B_{22}\frac{\partial^3}{\partial y^3}$$

and F is a differential operator representing the inplane loading,

$$F \equiv N_x\frac{\partial^2}{\partial x^2} + 2N_{xy}\frac{\partial^2}{\partial x\partial y} + N_y\frac{\partial^2}{\partial y^2} \qquad \text{(A.22)}$$

For simplicity, the superscripts "b" and "i" which were used in Equations A.17 have been dropped. In what follows, and in the main body of the monograph, it will be regarded that u, v, w represent the (infinitesimally) small displacements of the plate <u>during</u> buckling, and that N_x, N_{xy}, N_y represent the inplane forces which exist <u>just before</u> buckling occurs. Equations A.20 are an eighth order set of partial differential equations, similar in form to shell equilibrium equations (cf. [A.6], pp. 32-34). Indeed, the coupling between bending and stretching is responsible for raising the order from four to eight in the present problem, just as the coupling of inextensional and membrane theories raises the order from four to eight in the shell problem.

For symmetrically laminated plates $B_{ij} = 0$ and the L_{13} and L_{23} operators in Equations A.21 are seen to vanish, and the inplane part of

the problem is uncoupled from the transverse part in Equation A.20. The inplane part yields u = v = 0 in the buckled configuration, whereas the transverse displacements are governed by

$$D_{11}\frac{\partial^4 w}{\partial x^4} + 4D_{16}\frac{\partial^4 w}{\partial x^3 \partial y} + 2(D_{12} + 2D_{66})\frac{\partial^4 w}{\partial x^2 \partial y^2} + 4D_{26}\frac{\partial^4 w}{\partial x \partial y^3} + D_{22}\frac{\partial^4 w}{\partial y^4}$$
$$= N_x\frac{\partial^2 w}{\partial x^2} + 2N_{xy}\frac{\partial^2 w}{\partial x \partial y} + N_y\frac{\partial^2 w}{\partial y^2} \qquad \text{(A.23)}$$

Equation A.23 is the same form as the buckling equation for a homogeneous, anisotropic plate. The only difference is in how the stiffness coefficients D_{ij} are calculated.

For symmetrically laminated cross-ply plates there is no coupling between bending and twist, and $D_{12} = D_{16} = 0$. Equation A.23 then specializes to

$$D_{11}\frac{\partial^4 w}{\partial x^4} + 2(D_{12} + 2D_{66})\frac{\partial^4 w}{\partial x^2 \partial y^2} + D_{22}\frac{\partial^4 w}{\partial y^4}$$
$$= N_x\frac{\partial^2 w}{\partial x^2} + 2N_{xy}\frac{\partial^2 w}{\partial x \partial y} + N_y\frac{\partial^2 w}{\partial y^2} \qquad \text{(A.24)}$$

This is the same form as the buckling equation for a homogeneous, orthotropic plate.

If, for example, a cross-ply plate of rectangular shape were fabricated so that its edges were not parallel to the axes of material orthotropy, then a coordinate transformation to provide the proper rotation of axes from the xy material coordinates of Equation A.24 to a set of $x'y'$ coordinates parallel to the plate edges would result in a form similar to Equation A.23. This new form would have six stiffness coefficients D_{11}', D_{16}', D_{12}', D_{66}', D_{26}', D_{22}', but they would be linear combinations of the four material coefficients D_{11}, D_{12}, D_{66}, D_{22}. It is common in the literature to speak of a specially orthotropic plate when

the orthotropic material axes and the rectangular plate edges are parallel. However, this terminology will not be used in the present work, for the word "orthotropic" should be used to describe a property of the material, independent of the shape of the plate (e.g., rectangular) or the orientation of a mathematically convenient coordinate system.

It must be remembered that the stress resultants N_x, N_{xy} and N_y are positive in accordance with the directions shown in Figure A.1. Particularly, compressive N_x or N_y are negative quantities. Although, for the sake of brevity, the stress resultants have been used in the preceding derivation, for the sake of direct engineering application, the stresses are used for the most part elsewhere in this monograph.

For some types of buckling problems where bending-stretching coupling exists it may be desirable to use the inplane stress resultants generated during buckling (i.e., N_x^b, N_y^b, N_{xy}^b) instead of the inplane displacements (u, v) which occur. It is then usually convenient to represent the inplane stress resultants by an Airy stress function (ϕ), with the functions defined by the equations

$$\begin{aligned} N_x^b &= \frac{\partial^2 \phi}{\partial y^2} \\ N_y^b &= \frac{\partial^2 \phi}{\partial x^2} \\ N_{xy}^b &= -\frac{\partial^2 \phi}{\partial x \partial y} \end{aligned} \tag{A.25}$$

If Equations A.25 are substituted into the first two of Equations A.17, it is seen that the latter are identically satisfied. However, since the problem is no longer expressed in terms of inplane displacements, it becomes necessary for the inplane stresses to satisfy the inplane equation of compatibility

$$\frac{\partial^2 \varepsilon_x^{\,o}}{\partial y^2} + \frac{\partial^2 \varepsilon_y^{\,o}}{\partial x^2} - \frac{\partial^2 \gamma_{xy}^{\,o}}{\partial x \partial y} = 0 \qquad \text{(A.26)}$$

where the strains ($\varepsilon_x^{\,o}$, $\varepsilon_y^{\,o}$, $\gamma_{xy}^{\,o}$) are those additional ones arising during buckling, but the superscript "b" is dropped for simplicity.

To utilize Equation A.26, Equation A.8 must be at least partially inverted. Rewriting Equation A.8 in the symbolic form

$$\begin{bmatrix} N \\ M \end{bmatrix} = \begin{bmatrix} A & B \\ B & D \end{bmatrix} \begin{bmatrix} \varepsilon^o \\ -K \end{bmatrix} \qquad \text{(A.27)}$$

where N, M, ε^o and K are 3 x 1 subvectors and A, B and D are the 3 x 3 submatrices delineated in Equation A.8. Multiplying through the first of the two submatrix equations of Equations A.27 by A^{-1}, and solving for ε^o yields

$$\varepsilon^o = A^{-1}N - A^{-1}BK \qquad \text{(A.28)}$$

Substituting Equation A.28 into the second of Equations A.27 results in

$$M = BA^{-1}N - (D-BA^{-1}B)K \qquad \text{(A.29)}$$

and Equations A.28 and A.29 may be written in matrix form [A.4] as

$$\begin{bmatrix} \varepsilon^o \\ M \end{bmatrix} = \begin{bmatrix} A^* & B^* \\ -B^{*T} & D^* \end{bmatrix} \begin{bmatrix} N \\ -K \end{bmatrix} \qquad \text{(A.30)}$$

where B^{*T} is the transpose of the B^* submatrix, and where

$$A^* = A^{-1}, \quad B^* = -A^{-1}B, \quad D^* = D-BA^{-1}B \qquad \text{(A.31)}$$

While A^* and D^* are symmetric submatrices, B^* is, in general, not symmetric. Substituting Equations A.5, A.25 and A.30 into Equation A.26 yields

$$A_{22}^{*}\frac{\partial^4\phi}{\partial x^4} - 2A_{26}^{*}\frac{\partial^4\phi}{\partial x^3\partial y} + (2A_{12}^{*} + A_{66}^{*})\frac{\partial^4\phi}{\partial x^2\partial y^2} - 2A_{16}^{*}\frac{\partial^4\phi}{\partial x\partial y^3} + A_{11}^{*}\frac{\partial^4\phi}{\partial y^4}$$

$$- B_{21}^{*}\frac{\partial^4 w}{\partial x^4} + (B_{61}^{*} - 2B_{26}^{*})\frac{\partial^4 w}{\partial x^3\partial y} - (B_{11}^{*} + B_{22}^{*} - 2B_{66}^{*})\frac{\partial^4 w}{\partial x^2\partial y^2} \qquad \text{(A.32)}$$

$$+ (B_{62}^{*} - 2B_{16}^{*})\frac{\partial^4 w}{\partial x\partial y^3} - B_{12}^{*}\frac{\partial^4 w}{\partial y^4} = 0$$

for the compatibility equation in the buckled state. Similarly, substituting Equations A.5, A.25 and A.30 into Equations A.17 yields

$$B_{21}^{*}\frac{\partial^4\phi}{\partial x^4} + (2B_{26}^{*} - B_{61}^{*})\frac{\partial^4\phi}{\partial x^3\partial y} + (B_{11}^{*} + B_{22}^{*} - 2B_{66}^{*})\frac{\partial^4\phi}{\partial x^2\partial y^2}$$

$$+ (2B_{16}^{*} - B_{62}^{*})\frac{\partial^4\phi}{\partial x\partial y^3} + B_{12}^{*}\frac{\partial^4\phi}{\partial y^4} + D_{11}^{*}\frac{\partial^4 w}{\partial x^4} + 4D_{16}^{*}\frac{\partial^4 w}{\partial x^3\partial y}$$

$$+ 2(D_{12}^{*} + D_{66}^{*})\frac{\partial^4 w}{\partial x^2\partial y^2} + 4D_{26}^{*}\frac{\partial^4 w}{\partial x\partial y^3} + D_{22}^{*}\frac{\partial^4 w}{\partial y^4} \qquad \text{(A.33)}$$

$$= N_x\frac{\partial^2 w}{\partial x^2} + 2N_{xy}\frac{\partial^2 w}{\partial x\partial y} + N_y\frac{\partial^2 w}{\partial y^2}$$

for the equilibrium equation in the buckled state. As in Equations A.22, A.23 and A.24, the superscript "i" has been dropped from N_x, N_y and N_{xy} in Equation A.33, but it must be remembered that these inplane stress resultants exist <u>just before</u> buckling occurs, whereas ϕ is related by Equations A.25 to the additional stress resultants generated by the buckled mode shape. Equations A.32 and A.33 form a set of differential equations of eighth order.

For symmetrically laminated plates $B_{ij} = 0$, and Equations A.32 and A.33 uncouple. Equation A.32 becomes the anisotropic, stress function form of the compatibility equation for plane elasticity, and Equation A.33 reduces to Equation A.23.

A.3. BOUNDARY CONDITIONS

The classical, bifurcation buckling problem for a laminated composite plate requires satisfying the governing differential equations (Section A.2.) and the boundary (or edge) conditions. Both sets of equations are homogeneous, leading to an eigenvalue problem for the eigenvalues (buckling loads) and eigenfunctions (mode shapes). Consistent with the eighth order sets of differential equations which must be satisfied, four boundary conditions must be applied to each edge of the plate. The classical conditions are

$$u_n = 0 \quad \text{or} \quad N_n^b = 0 \tag{A.34a}$$

$$u_t = 0 \quad \text{or} \quad N_{nt}^b = 0 \tag{A.34b}$$

$$w = 0 \quad \text{or} \quad V_n^b = Q_n^b + \frac{\partial M_{nt}}{\partial t} = 0 \tag{A.34c}$$

$$\frac{\partial w}{\partial n} = 0 \quad \text{or} \quad M_n^b = 0 \tag{A.34d}$$

In the above equations the subscripts n and t denote the coordinates normal and tangential to the boundary. The function $Q_n + \partial M_{nt}/\partial t$ is the wellknown Kelvin-Kirchhoff "edge reaction" which must be nullified at a free edge. In addition, at a free rectangular corner (the intersection of two free edges), the point condition $M_{nt} = 0$ must be satisfied. The superscript "b" is added here to the generalized forces to avoid confusing them with the inplane forces (e.g., N_x^i, N_y^i, N_{xy}^i) existing just before buckling.

Equations A.34 may be used to represent any form of "simple" edge condition (e.g., clamped, simply supported, free). More general boundary conditions which are applicable to edges having elastic con-

straints take the forms

$$
\begin{aligned}
N_n^b \pm k_1 u_n &= 0 \\
N_{nt}^b \pm k_2 u_t &= 0 \\
Q_n^b + \frac{\partial M_{nt}}{\partial t} \pm k_3 w &= 0 \\
M_n^b \pm k_4 \frac{\partial w}{\partial n} &= 0
\end{aligned}
\tag{A.35}
$$

Here the constants k_1, k_2, k_3 and k_4 denote the spring stiffnesses of the constraints. Considerable care must be taken to use the proper sign (plus or minus) for the generalized restoring forces supplied by the elastic constraints, depending upon the edge under consideration (cf. [A.7], p. 114).

In some problems inplane forces are applied to free edges of plates. This situation requires special consideration. Figure A.3 shows a plate with free edges loaded by compressive stress resultants (P). In the buckled mode shape the edges have rotated through angles $\pm \psi$. From considerations of internal forces acting an infinitesimal distance inside each edge, it may be seen that

$$
\begin{aligned}
N_x &= -P \cos(\pm\Psi) \\
Q_x + \frac{\partial M_{xy}}{\partial y} &= \pm P \sin(\pm\Psi)
\end{aligned}
\tag{A.36}
$$

With the standard assumptions of classical, linear plate theory, the deflected slopes are small, and $\cos(\pm\psi) \approx 1$ and $\sin(\pm\psi) \approx \pm\partial w/\partial x$. Therefore, Equations A.36 become

$$
\begin{aligned}
N_x &= -P \\
Q_x + \frac{\partial M_{xy}}{\partial y} &= P \frac{\partial w}{\partial x}
\end{aligned}
\tag{A.37}
$$

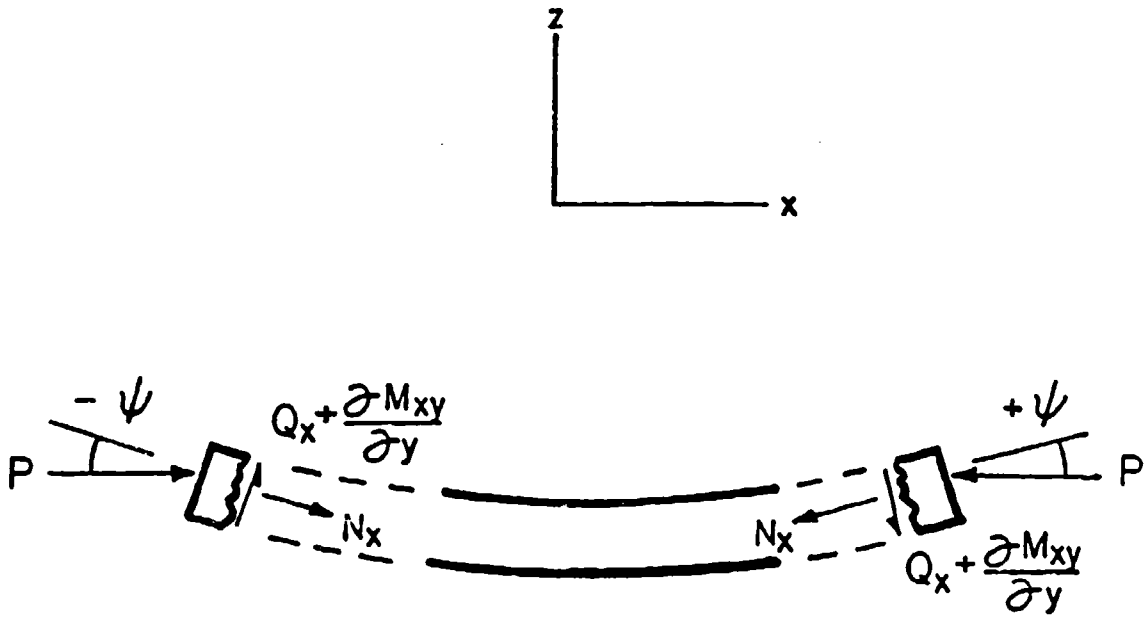

Figure A.3. Inplane stress resultants (P) applied to free edges.

which are the proper conditions to use in solving the problem. Similar conditions exist at free edges y = constant.

In applying the boundary conditions it is useful to have explicit expressions for the various functions used in Equations A.34. For the displacement formulation of the problem they are obtained from Equations A.4, A.5, A.8, A.11 and A.34c.

$$N_x = A_{11}\frac{\partial u}{\partial x} + A_{12}\frac{\partial v}{\partial y} + A_{16}\left(\frac{\partial v}{\partial x} + \frac{\partial u}{\partial y}\right) - B_{11}\frac{\partial^2 w}{\partial x^2} - B_{12}\frac{\partial^2 w}{\partial y^2} - 2B_{16}\frac{\partial^2 w}{\partial x \partial y} \tag{A.38a}$$

$$N_y = A_{12}\frac{\partial u}{\partial x} + A_{22}\frac{\partial v}{\partial y} + A_{26}\left(\frac{\partial v}{\partial x} + \frac{\partial u}{\partial y}\right) - B_{12}\frac{\partial^2 w}{\partial x^2} - B_{22}\frac{\partial^2 w}{\partial y^2} - 2B_{26}\frac{\partial^2 w}{\partial x \partial y} \tag{A.38b}$$

$$N_{xy} = A_{16}\frac{\partial u}{\partial x} + A_{26}\frac{\partial v}{\partial y} + A_{66}\left(\frac{\partial v}{\partial x} + \frac{\partial u}{\partial y}\right) - B_{16}\frac{\partial^2 w}{\partial x^2} - B_{26}\frac{\partial^2 w}{\partial y^2} - 2B_{66}\frac{\partial^2 w}{\partial x \partial y} \tag{A.38c}$$

$$M_x = B_{11}\frac{\partial u}{\partial x} + B_{12}\frac{\partial v}{\partial y} + B_{16}\left(\frac{\partial v}{\partial x} + \frac{\partial u}{\partial y}\right) - D_{11}\frac{\partial^2 w}{\partial x^2} - D_{12}\frac{\partial^2 w}{\partial y^2} - 2D_{16}\frac{\partial^2 w}{\partial x \partial y} \tag{A.38d}$$

$$M_y = B_{12}\frac{\partial u}{\partial x} + B_{22}\frac{\partial v}{\partial y} + B_{26}\left(\frac{\partial v}{\partial x} + \frac{\partial u}{\partial y}\right) - D_{12}\frac{\partial^2 w}{\partial x^2} - D_{22}\frac{\partial^2 w}{\partial y^2} - 2D_{26}\frac{\partial^2 w}{\partial x \partial y} \tag{A.38e}$$

$$M_{xy} = B_{16}\frac{\partial u}{\partial x} + B_{26}\frac{\partial v}{\partial y} + B_{66}\left(\frac{\partial v}{\partial x} + \frac{\partial u}{\partial y}\right)$$
$$- D_{16}\frac{\partial^2 w}{\partial x^2} - D_{26}\frac{\partial^2 w}{\partial y^2} - 2D_{66}\frac{\partial^2 w}{\partial x \partial y} \qquad \text{(A.38f)}$$

$$Q_x = B_{11}\frac{\partial^2 u}{\partial x^2} + 2B_{16}\frac{\partial^2 u}{\partial x \partial y} + B_{66}\frac{\partial^2 u}{\partial y^2} + B_{16}\frac{\partial^2 v}{\partial x^2}$$
$$+ (B_{12} + B_{66})\frac{\partial^2 v}{\partial x \partial y} + B_{26}\frac{\partial^2 v}{\partial y^2} - D_{11}\frac{\partial^3 w}{\partial x^3} \qquad \text{(A.38g)}$$
$$- 3D_{16}\frac{\partial^3 w}{\partial x^2 \partial y} - (D_{12} + 2D_{66})\frac{\partial^3 w}{\partial x \partial y^2} - D_{26}\frac{\partial^3 w}{\partial y^3}$$

$$Q_y = B_{16}\frac{\partial^2 u}{\partial x^2} + (B_{12} + B_{66})\frac{\partial^2 u}{\partial x \partial y} + B_{26}\frac{\partial^2 u}{\partial y^2} + B_{66}\frac{\partial^2 v}{\partial x^2}$$
$$+ 2B_{26}\frac{\partial^2 v}{\partial x \partial y} + B_{22}\frac{\partial^2 v}{\partial y^2} - D_{16}\frac{\partial^3 w}{\partial y^3} - (D_{12} + 2D_{66})\frac{\partial^3 w}{\partial x^2 \partial y} \qquad \text{(A.38h)}$$
$$- 3D_{26}\frac{\partial^3 w}{\partial x \partial y^2} - D_{22}\frac{\partial^3 w}{\partial y^3}$$

$$V_x = B_{11}\frac{\partial^2 u}{\partial x^2} + 3B_{16}\frac{\partial^2 u}{\partial x \partial y} + 2B_{66}\frac{\partial^2 u}{\partial y^2} + B_{16}\frac{\partial^2 v}{\partial x^2}$$
$$+ (B_{12} + 2B_{66})\frac{\partial^2 v}{\partial x \partial y} + 2B_{26}\frac{\partial^2 v}{\partial y^2} - D_{11}\frac{\partial^3 w}{\partial x^3} \qquad \text{(A.38i)}$$
$$- 4D_{16}\frac{\partial^3 w}{\partial x^2 \partial y} - (D_{12} + 4D_{66})\frac{\partial^3 w}{\partial x \partial y^2} - 2D_{26}\frac{\partial^3 w}{\partial y^3}$$

$$V_y = 2B_{16}\frac{\partial^2 u}{\partial x^3} + (B_{12} + 2B_{66})\frac{\partial^2 u}{\partial x \partial y} + B_{26}\frac{\partial^2 u}{\partial y^2} + 2B_{66}\frac{\partial^2 v}{\partial x^2}$$
$$+ 3B_{26}\frac{\partial^2 v}{\partial x \partial y} + B_{22}\frac{\partial^2 v}{\partial y^2} - 2D_{16}\frac{\partial^3 w}{\partial x^3} - (D_{12} + 4D_{66})\frac{\partial^3 w}{\partial x^2 \partial y} \qquad \text{(A.38j)}$$
$$- 4D_{26}\frac{\partial^3 w}{\partial x \partial y^2} - D_{22}\frac{\partial^3 w}{\partial y^3}$$

For the stress function (and transverse displacement) formulation of the problem, the inplane stress resultants are given by Equations A.25; the other useful quantities are obtained from Equations A.5, A.11, A.25, A.30 and A.34c.

$$M_x = -\left(B_{21}^* \frac{\partial^2\phi}{\partial x^2} - B_{61}^* \frac{\partial^2\phi}{\partial x\partial y} + B_{11}^* \frac{\partial^2\phi}{\partial y^2} + D_{11}^* \frac{\partial^2 w}{\partial x^2} + 2D_{16}^* \frac{\partial^2 w}{\partial x\partial y} + D_{12}^* \frac{\partial^2 w}{\partial y^2}\right) \tag{A.39a}$$

$$M_y = -\left(B_{22}^* \frac{\partial^2\phi}{\partial x^2} - B_{62}^* \frac{\partial^2\phi}{\partial x\partial y} + B_{12}^* \frac{\partial^2\phi}{\partial y^2} + D_{12}^* \frac{\partial^2 w}{\partial x^2} + 2D_{26}^* \frac{\partial^2 w}{\partial x\partial y} + D_{22}^* \frac{\partial^2 w}{\partial y^2}\right) \tag{A.39b}$$

$$M_{xy} = -\left(B_{26}^* \frac{\partial^2\phi}{\partial x^2} - B_{66}^* \frac{\partial^2\phi}{\partial x\partial y} + B_{16}^* \frac{\partial^2\phi}{\partial y^2} + D_{16}^* \frac{\partial^2 w}{\partial x^2} + 2D_{66}^* \frac{\partial^2 w}{\partial x\partial y} + D_{26}^* \frac{\partial^2 w}{\partial y^2}\right) \tag{A.39c}$$

$$Q_x = -\left[B_{21}^* \frac{\partial^3\phi}{\partial x^3} + (B_{26}^* - B_{61}^*) \frac{\partial^3\phi}{\partial x^2\partial y} + (B_{11}^* - B_{66}^*) \frac{\partial^3\phi}{\partial x\partial y^2} + B_{16}^* \frac{\partial^3\phi}{\partial y^3} + D_{11}^* \frac{\partial^3 w}{\partial x^3} + 3D_{16}^* \frac{\partial^3 w}{\partial x^2\partial y} + (D_{12}^* + 2D_{66}^*) \frac{\partial^3 w}{\partial x\partial y^2} + D_{26}^* \frac{\partial^3 w}{\partial y^3}\right] \tag{A.39d}$$

$$Q_y = -\left[B_{26}^* \frac{\partial^3\phi}{\partial x^3} + (B_{22}^* - B_{66}^*) \frac{\partial^3\phi}{\partial x^2\partial y} + (B_{16}^* - B_{62}^*) \frac{\partial^3\phi}{\partial x\partial y^2} + B_{12}^* \frac{\partial^3\phi}{\partial y^3} + D_{16}^* \frac{\partial^3 w}{\partial x^3} + (D_{12}^* + 2D_{66}^*) \frac{\partial^3 w}{\partial x^2\partial y} + 3D_{26}^* \frac{\partial^3 w}{\partial x\partial y^2} + D_{22}^* \frac{\partial^3 w}{\partial y^3}\right] \tag{A.39e}$$

$$V_x = -\left[B_{21}^* \frac{\partial^3\phi}{\partial x^3} + (2B_{26}^* - B_{61}^*) \frac{\partial^3\phi}{\partial x^2\partial y} + (B_{11}^* - 2B_{66}^*) \frac{\partial^3\phi}{\partial x\partial y^2} + 2B_{16}^* \frac{\partial^3\phi}{\partial y^3} + B_{11}^* \frac{\partial^3 w}{\partial x^3} + 4D_{16}^* \frac{\partial^3 w}{\partial x^2\partial y} + (D_{12}^* + 4D_{66}^*) \frac{\partial^3 w}{\partial x\partial y^2} + 2D_{26}^* \frac{\partial^3 w}{\partial y^3}\right] \quad \text{(A.39f)}$$

$$V_y = -\left[2B_{26}^* \frac{\partial^3\phi}{\partial x^3} + (B_{22}^* - 2B_{66}^*) \frac{\partial^3\phi}{\partial x^2\partial y} + (2B_{16}^* - B_{62}^*) \frac{\partial^3\phi}{\partial x\partial y^2} + B_{12}^* \frac{\partial^3\phi}{\partial y^3} + 2D_{16}^* \frac{\partial^3 w}{\partial x^3} + (D_{12} + 4D_{66}) \frac{\partial^3 w}{\partial x^2\partial y} + 4D_{26} \frac{\partial^3 w}{\partial x\partial y^2} + D_{22} \frac{\partial^3 w}{\partial y^3}\right] \quad \text{(A.39g)}$$

For non-rectangular plates other forms of u_n, u_t, N_n, N_{nt}, M_n, M_{nt}, Q_n and V_n are needed. These may be obtained by using the vector and tensorial transformation formulas generally available in the standard texts dealing with the theory of elasticity and plate theory (cf., [A.8, A.9]), together with Equations A.38 or A.39.

For symmetric laminates the bending-stretching coupling disappears, and $B_{ij} = 0$ in Equations A.38 and A.39. For cross-ply plates having fibers parallel to the x and y axes, $D_{12} = D_{16} = 0$ in Equations A.38 and A.39.

A.4. ENERGY FUNCTIONALS

The total potential energy of a plate (V) while in equilibrium in a displaced buckling mode is given by

$$V = V_S + V_P + V_{BS} + V_L \quad \text{(A.40)}$$

where V_S, V_B and V_{BS} are the strain energies due to stretching, bending and bending-stretching coupling, respectively, and V_L is the potential due to the applied inplane forces.

Formulation of the buckling problem in terms of the potential energy is useful for at least the following two reasons:

(1) Variational principles may be applied to derive the differential equations of equilibrium and a mathematically consistent set of boundary conditions

(2) The buckling problem may be directly solved by energy methods, such as the widely used Ritz method.

The strain energy in a deformed plate is

$$V = \frac{1}{2} \iiint_{Vol} (\sigma_x \varepsilon_x + \sigma_y \varepsilon_y + \tau_{xy} \gamma_{xy}) d(Vol) \qquad (A.41)$$

where the stresses and strains are those used previously in Section A.1, and the integration is carried out over the volume of the plate. Substituting into Equation A.41 the stress-strain relationships for each lamina, carrying out the tensorial transformations required to express the stresses and strains in terms of a single plate coordinate system (x, y), applying the kinematic conditions of Equations A.3, A.4 and A.5, and integrating over the thickness layer by layer yields [A.4]:

$$\begin{aligned} V_S = \frac{1}{2} \iint_A \Bigg[& A_{11} \left(\frac{\partial u}{\partial x}\right)^2 + 2A_{12} \frac{\partial u}{\partial x} \frac{\partial v}{\partial y} + A_{22} \left(\frac{\partial v}{\partial y}\right)^2 \\ & + 2A_{16} \frac{\partial u}{\partial x} \left(\frac{\partial u}{\partial y} + \frac{\partial v}{\partial x}\right) + 2A_{26} \frac{\partial v}{\partial y} \left(\frac{\partial u}{\partial y} + \frac{\partial v}{\partial x}\right) \\ & + A_{66} \left(\frac{\partial u}{\partial y} + \frac{\partial v}{\partial x}\right)^2 \Bigg] \, dx dy \end{aligned} \qquad (A.42a)$$

$$V_{BS} = -\frac{1}{2}\iint_A \Big[B_{11}\frac{\partial u}{\partial x}\frac{\partial^2 w}{\partial x^2} + 2B_{12}\left(\frac{\partial v}{\partial y}\frac{\partial^2 w}{\partial x^2} + \frac{\partial u}{\partial x}\frac{\partial^2 w}{\partial y^2}\right)$$
$$+ B_{22}\frac{\partial v}{\partial y}\frac{\partial^2 w}{\partial y^2} + 2B_{16}\left(\frac{\partial u}{\partial y}\frac{\partial^2 w}{\partial x^2} + \frac{\partial v}{\partial x}\frac{\partial^2 w}{\partial x^2} + 2\frac{\partial u}{\partial x}\frac{\partial^2 w}{\partial x \partial y}\right) \qquad \text{(A.42b)}$$
$$+ 2B_{26}\left(\frac{\partial u}{\partial y}\frac{\partial^2 w}{\partial y^2} + \frac{\partial v}{\partial x}\frac{\partial^2 w}{\partial y^2} + 2\frac{\partial v}{\partial y}\frac{\partial^2 w}{\partial x \partial y}\right)$$
$$+ 4B_{66}\left(\frac{\partial u}{\partial x} + \frac{\partial v}{\partial y}\right)\frac{\partial^2 w}{\partial x \partial y}\Big]\, dxdy$$

$$V_B = \frac{1}{2}\iint_A \Big[D_{11}\left(\frac{\partial^2 w}{\partial x^2}\right)^2 + 2D_{12}\frac{\partial^2 w}{\partial x^2}\frac{\partial^2 w}{\partial y^2} + D_{22}\left(\frac{\partial^2 w}{\partial y^2}\right)^2$$
$$+ 4D_{16}\frac{\partial^2 w}{\partial x^2}\frac{\partial^2 w}{\partial x \partial y} + 4D_{26}\frac{\partial^2 w}{\partial y^2}\frac{\partial^2 w}{\partial x \partial y} \qquad \text{(A.42c)}$$
$$+ 4D_{66}\left(\frac{\partial^2 w}{\partial x \partial y}\right)^2\Big]\, dxdy$$

where the A_{ij}, B_{ij} and D_{ij} are the plate stiffness coefficients used previously in Equation 8 and the integrals are taken over the area of the plate.

For a symmetric laminate, $B_{ij} = 0$ and consequently the strain energy due to bending-stretching coupling (V_{BS}) vanishes. Then Equation A.42c represents the entire strain energy caused by bending (i.e., changes in curvature), and is of the same form as found for homogeneous, anisotropic plates [A.1]. For a cross-ply laminate, with fibers parallel to the x and y coordinates, $D_{16} = D_{26} = 0$.

The potential energy due to the initial inplane loads is

$$V_L = -\iint_A \left(N_x \varepsilon_x' + N_y \varepsilon_y' + N_{xy}\gamma_{xy}'\right) dxdy \qquad \text{(A.43)}$$

where ε_x' , ε_y' and γ_{xy}' are the midplane strains caused by a transverse displacement field (w). These are given by [A.9]

$$\begin{aligned} \varepsilon_x' &= \frac{1}{2}\left(\frac{\partial w}{\partial x}\right)^2 \\ \varepsilon_y' &= \frac{1}{2}\left(\frac{\partial w}{\partial y}\right)^2 \\ \varepsilon_{xy}' &= \frac{\partial w}{\partial x}\,\frac{\partial w}{\partial y} \end{aligned} \qquad \text{(A.44)}$$

Substituting Equations A.44 into A.43 results in

$$V_L = -\frac{1}{2}\iint_A \left[N_x \left(\frac{\partial w}{\partial x}\right)^2 + N_y \left(\frac{\partial w}{\partial y}\right)^2 + 2N_{xy}\,\frac{\partial w}{\partial x}\,\frac{\partial w}{\partial y} \right] dxdy \qquad \text{(A.45)}$$

A.5. REFERENCES FOR APPENDIX

A.1. Lekhnitskii, S. G., Anisotropic Plates, Second Edition, translated from the Russian by S. W. Tsai and T. Cheron, Gordon and Breach Science Publishers, Inc., 534 pp. (1968).

A.2. Ashton J. E., Halpin, J. C. and Petit, P. H., Primer on Composite Materials: Analysis, Technomic Publishing Co., Inc., 124 pp. (1969).

A.3. Jones, R. M., Mechanics of Composite Materials, Scripta Book Co., Washington, D.C., 355 pp. (1975).

A.4. Ashton, J. E. and Whitney, J. M., Theory of Laminated Plates, Technomic Publishing Co., Stamford, Conn., 153 pp. (1970).

A.5. Reissner, E. and Stavsky, Y., "Bending and Stretching of Certain Types of Heterogeneous Aeolotropic Elastic Plates", Trans. ASME, Journal of Applied Mechanics, Vol. 9, pp. 402-408 (1961).

A.6. Leissa, A. W., Vibration of Shells, NASA SP-288, U.S.Govt. Printing Office, 428 pp. (1973).

A.7. Leissa, A. W., Vibration of Plates, NASA SP-160, U.S.Govt. Printing Office, Washington, D.C., 353 pp. (1969).

A.8. Timoshenko, S. P. and Goodier, J. N., Theory of Elasticity, Third Edition, McGraw-Hill Book Co., 567 pp. (1970).

A.9. Timoshenko, S. and Woinowsky-Krieger, S., Theory of Plates and Shells, Second Edition, McGraw-Hill Book Co., 580 pp. (1959).

U.S. GOVERNMENT PRINTING OFFICE 1985 - 5[illegible]